Research and Technology Highlights

1993

National Aeronautics and
Space Administration
Langley Research Center
Hampton, Virginia 23681-0001

Langley Research Center
*NASA Technical
Memorandum 4575*

FOREWORD

The mission of the NASA Langley Research Center is to increase the knowledge and capability of the United States in a full range of aeronautics disciplines and in selected space disciplines. This mission will be accomplished by performing innovative research relevant to national needs and Agency goals, transferring technology to users in a timely manner, and providing development support to other United States Government agencies, industry, and other NASA centers. This report contains highlights of the major accomplishments and applications that have been made by Langley researchers and by our university and industry colleagues during the past year. The highlights illustrate both the broad range of research and technology (R&T) activities supported by NASA Langley Research Center and the contributions of this work toward maintaining United States leadership in aeronautics and space research. The report also describes some of the Center's most important research and testing facilities. For further information concerning the report, contact Dr. Michael F. Card, Chief Scientist, Mail Stop 110, NASA Langley Research Center, Hampton, Virginia 23681, (804) 864-8985.

Paul F. Holloway
Director

AVAILABILITY INFORMATION

The NASA program office and the corresponding Agency-wide Research and Technology Objectives and Plans (RTOP's) work breakdown structures are listed in the Contents for each research and technology accomplishment. OA designates the Office of Aeronautics; OACT designates the Office of Advanced Concepts and Technology; OSSA designates the Office of Space Science and Applications; OSSD designates the Office of Space Systems Development; and AA designates the Associate Administrator.

The accomplishments are grouped in 10 strategic thrusts including contributions in Critical Technologies, Subsonic Aircraft, High-Speed Civil Transport, High-Performance Military Aircraft, Hypersonic and Transatmospheric Vehicles, Space Transportation, Space Platforms, Space Science, Facilities, and Technology Transfer and Commercial Development. In addition, descriptions are included of some of the most important Aerospace Test Facilities at the NASA Langley Research Center. The use of these facilities in the research described herein is noted in the Contents.

For additional information on any summary, contact the individual identified with the highlight. This individual is generally either a member or a leader of the research group submitting the highlight. Commercial telephone users may dial the listed extension preceded by (804) 86.

CONTENTS

Subsonic Aircraft

High-Speed Civil Transport

High-Performance Military Aircraft

Hypersonic and Transatmospheric Vehicles

Space Transportation

Space Platforms

Space Science

Facilities

Technology Transfer and Commercial Development

Aerospace Test Facilities

Contributing Organizations

TECHNOLOGY TRANSFER ACTIVITIES—FY 1993

The development of new aeronautical technologies and their transfer to American commercial markets have been the major goals of NASA dating back to the founding of its predecessor NACA and the Langley Laboratory in 1917. In that year, the United States had only 23 airplanes, compared to France's 1400, Germany's 1000, Russia's 800, and the United Kingdom's 400. Working with the aviation community in this country to develop and commercialize innovative aircraft designs and technologies through a variety of experimental and theoretical research studies, NACA played a crucial role in the rise of the American aeronautics industry from "worst to first" in the world. Aeronautics exports now provide by far the largest net positive contributor ($30 billion) to our overall balance of payments posture in world trade. Well over half of all world aerospace products are presently manufactured in the United States, providing productive jobs for over a million Americans and sales of about $100 billion.

Despite the strength of our position in this global industry, it cannot be taken for granted. Since the 1970's, America's share of the world aerospace market has fallen by approximately 20 percent because of aggressive competitors in Europe and the Pacific Rim. In response to these challenges, NASA Langley Research Center has dedicated itself to a renewed focus on the transfer of its innovative aerospace technologies to the aeronautical and non-aeronautical commercial marketplaces. Langley is presently undergoing a major reorganization specifically to enhance and streamline its focus on advanced technology and the processes for the transfer of technology to industry for the commercialization of Langley research and technology products. As a visible sign of this renewed focus, the highly successful TOPS (Technology Opportunities Showcase) was held with over 800 attendees from industry, government, and academia on October 19-21, 1993, at Langley. Nearly two hundred Center-developed or Center-supported technologies with commercial potential were exhibited.

Langley Research Center's technology transfer processes are many and varied; often, they begin as a result of personal relationships or initiatives by Langley personnel at technical meetings or through cooperative exchanges. Langley Space Act Agreements involve Boeing, Lockheed, and many other companies, both large and small. These Agreements are similar to the CRADA's used by other government agencies. Under Space Act Agreements, NASA can protect industry results and data from public disclosure for up to 5 years. The Small Business Innovative Research (SBIR) program at Langley funds approximately 50 small businesses across the country each year to show the feasibility of a technology concept; major funding is provided for approximately half of those to go on to prototype construction, a crucial step before commercialization. There were 22 SBIR-developed technologies displayed at TOPS. Langley has always been one of the most active NASA Centers in applying for and acquiring patents for its technology products. In 1993, there were 44 patents awarded at the Center. Langley's Technology Utilization (TU) Office has had a long history of assisting the transfer of hardware and software technology applications through the issuance of Technical Briefs (40 in 1993) and spinoffs, by developing sources of funding support for commercializable developments, and by transferring industry-ready computer codes to the Computer Software Management and Information Center (COSMIC)®. In 1993, Langley published 146 formal NASA reports and 185 journal articles and other publications; there were over 670 presentations by Langley personnel at technical meetings.

There are numerous descriptions throughout this report of technology transfer activities at Langley. This summary presents some of the most interesting examples. One of Langley's collaborative relationships that has high commercial potential involves the Digiray Corporation of San Ramon, California. To improve the resolution of standard dental X-ray photos, Digiray developed a device that shoots through an object with a narrow X-ray, which then registers on a small detector. This innovative approach eliminates most of the scattering that impairs the resolution of standard X-ray photos, but the system is small enough to fit into hard-to-reach places such as the inside of an airplane wing. At a national conference, the head of Langley's Nondestructive Evaluation Sciences Branch saw sample imagery and recognized the potential of the device as a simple and rapid means of detecting aircraft structural fatigue or corrosion, or Space Shuttle material corrosion, fatigue, or erosion. Digiray and Langley have formed a partnership that is expected to lead to the aerospace commercialization of the technology, with possible extra applications such as the X-ray equivalent of a fiber-optic probe for insertion into the body to get stereoscopic X-ray imaging without surgery.

A computational fluid dynamics (CFD) code developed at Langley was used to redesign the engine pylon for the Douglas MD-11 airplane. This cooperative effort resulted in approximately a 0.8-percent reduction in airplane drag, which would translate to a yearly per plane savings in fuel of about $48,000. Verified in Douglas' flight tests, the modifications have been incorporated into the MD-11 aircraft; for the anticipated fleet size (including both new and retrofitted aircraft), the modifications are expected to constitute an annual savings in fuel of about $8,000,000 per year. Douglas has also been working recently with Langley to reduce the drag on the C-17 airplane. Using wind-tunnel tests in the 0.3-Meter Transonic Cryogenic Tunnel, modifications to the wing trailing edge reduced the total drag. The range increase afforded by the drag reduction will be quantified through flight tests. At the same time, National Transonic Facility tests found drag reductions by modifying the design of a previous Langley-developed technology called "winglets". Both of these results will be flight-tested with a C-17. Winglets, wingtip devices mounted at right angles to the wing to reduce drag produced by 3-D effects at the wing's end, have now been incorporated into a number of major transports, including the Boeing 747-400, the McDonnell Douglas C-17, the MD-11, and the Airbus Industries A-330 and A-340. Three new business jets also use winglet technology—the Cessna Citation III, the Gulfstream IV, and the Canadair Challenger.

Developing a technology for mapping waste storage areas and closed nuclear plants has been an important goal in waste-site analysis and cleanup operations. A three-dimensional mapper using coherent laser radar technology has been developed for such inspections; this mapper has high accuracy (better than 0.5 mm), is eye-safe, is immune to lightning effects, and works remotely (up to 15 m). Although it was originally developed for such NASA applications as topographical inspections of the Space Station or the Shuttle thermal protection system, DOE has now requested that the mapper be used in waste-site cleanup studies as well. Another application of coherent laser radar (CLR) technology was developed under a Langley SBIR by Coleman Research Corporation. The CLR Measurement System has the potential to rapidly scan a bridge to determine whether unusual static deflections or rotations have occurred that could be symptomatic of damage or distress. A demonstration was conducted in late 1993 of the system in which a 25-ft beam span was measured under a 200 000-lb load and was compared with the no-load condition to determine the profile change in the girder. The Federal Highway Administration (FHWA) used a standard dial gauge to measure the deflection and compare it with the result from the CLR Measurement System. The center-point deflections were measured at 6.86 mm by the dial and 6.54 mm by the CLR;

very good agreement was also obtained at various points along the girder. The FHWA is interested in the system to assist their research in bridge inspection, repair, and construction techniques.

A microburst is a meteorological phenomenon that occurs in or near thunderstorms involving a blast of high-speed air from above that is often responsible for a potentially dangerous form of wind shear. Large and small aircraft can lose control and crash with little or no warning. Between 1964 and 1985, there were over 26 U.S. airline accidents caused by such wind shears, with 626 fatalities and 200 injuries. The FAA mandated that airlines install some type of wind-shear detection, warning device, or avoidance system by the end of 1993. NASA Langley Research Center has worked with several avionics and airline companies, such as Allied Signal Bendix, Rockwell International, Collins Air Transport Division, and Westinghouse, to develop such predictive systems and has flight-tested prototypes of microwave, infrared, and laser-based devices to detect microburst-induced wind shears. The FAA has extended until 1995 the deadline for airlines to install such equipment because of their cooperative efforts with NASA. Boeing and Airbus are already developing the interfaces and specifications for factory installation of wind-shear radars.

Laboratory simulations of the flux and kinetic energy of atomic oxygen bombardment in low earth orbit have become critically important since the recognition of the major corrosive effect this species has on satellite materials in space. Perhaps the best high-speed atomic oxygen "gun" for spacecraft materials studies was designed and constructed as a Langley Director's Discretionary Fund project. The technology, which uses hot silver foil to dissociate molecular oxygen and an electron source to desorb satellite-speed atomic oxygen from the silver, received an R&D 100 Award for 1993 and is being commercialized by Daco Technologies, Inc. of Florida. One gun has been sold and there are a number of other interested customers.

Some other examples of Langley technology transfer include the SUPRA Scanner, a high-frequency ultrasonic scanner for diagnosing skin conditions and disorders such as burn depth, wound healing progress, and precancerous lesion measurements. The Langley-developed technology was commercialized by TOPOX, Inc. of Pennsylvania. In the area of polymer chemistry, IMITEC has been a very active small business in commercializing Langley-developed polyimides. Other companies that have found commercial applications for Langley polyimides in composites, fibers, optics, bar codes, spin coatings, wires, gaskets, and electronics include DuPont, Lockheed, Northrop, Martin Marietta, IBM, Delco Remy-GM, Barcel, Ford, Motorola, and Cytec (BASF).

The System/Observer/Controller/Identification Toolbox (SOCIT) was developed at NASA Langley Research Center for problems involving spacecraft dynamics, but has now been distributed to over 40 companies, universities, and other government agencies because of such applications as analysis of acoustic data from submarines (Atlantic Aerospace Electronics Corporation), identification of models for control design (Harris Corporation), and system identification of model validation and control (Boeing).

RESEARCH AND
TECHNOLOGY

Critical Technologies

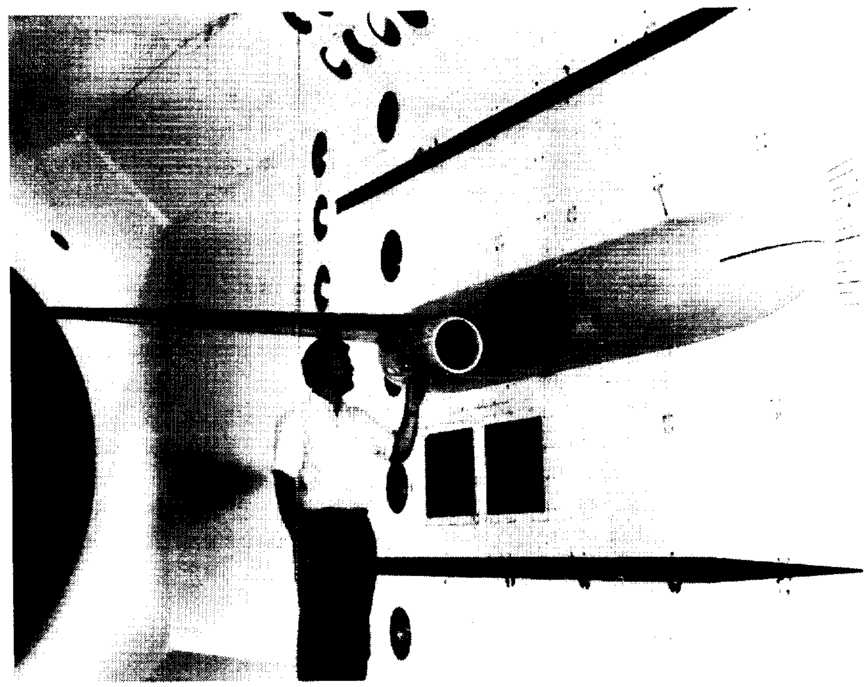

Pioneer the development of innovative concepts and provide the physical understanding and the theoretical, experimental, and computational tools required for the efficient design and operation of advanced aerospace systems

Analysis of Implicit Second-Order Upwind-Biased Stencils

Implicit-difference schemes are desirable when solving the Euler and Navier-Stokes equations because of their unconditional stability. However, standard-difference stencils developed for structured grids do not easily generalize to unstructured grids, and in practice there are time-step limitations that slow the convergence of implicit schemes. To understand this problem, tools for the stability analysis of numerical methods for the Euler and Navier-Stokes equations have been developed and applied to several commonly used upwind-difference stencils.

A Fourier analysis is applied to upwind-difference approximations for the two-dimensional linearized Euler equations. This differs from conventional analysis methods, which are generally applied to a simpler scalar model equation, and allows the examination of the performance of the difference schemes under a wide variety of flow conditions and grid distortions. Codes to perform the Fourier analysis were written in C and using the computer algebra system Mathematica. The analysis is verified by numerical experiments with a recently developed two-dimensional Euler solver.

Several standard structured-grid difference stencils have been examined, as well as a new stencil that is easily generalized to unstructured grids. It was found that the choice of difference stencil has a dramatic effect on the asymptotic stability of the implicit schemes. One of the most popular of the structured-grid difference stencils performs particularly poorly. On the other hand, the new stencil has outstanding stability properties and is less sensitive to high grid aspect ratios. These properties make it well suited for viscous calculations and for multigrid acceleration techniques. The analysis methods developed in this work are general and can be extended to a wide variety of difference stencils and time-marching schemes.
(Thomas W. Roberts, 46804, and Gary P. Warren)
Aeronautics Directorate

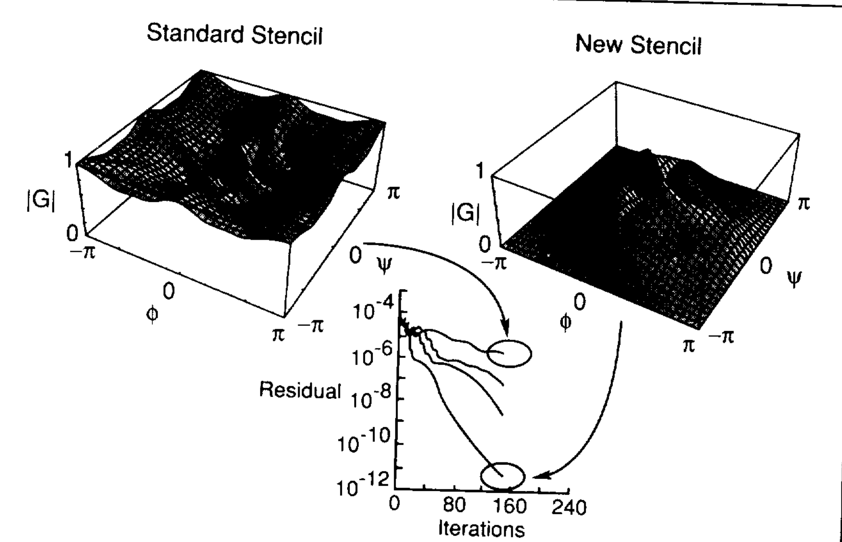

Improved stability of new difference stencil and its effect on convergence of numerical code.

Hot-Film Probe for Use in Hypersonic Flow

Turbulence instrumentation has been developed for hypersonic flows in a collaboration between the Syracuse University Center for Hypersonics and Langley Research Center. The robust microsensor hot-film probe has exhibited an extremely high bandwidth in moderately severe hypersonic flows. Such measurements are important for high-speed civil transport (HSCT) noise reduction efforts, hypersonic facility validation, hypersonic flow physics, and computational fluid dynamics (CFD) validation purposes. Existing

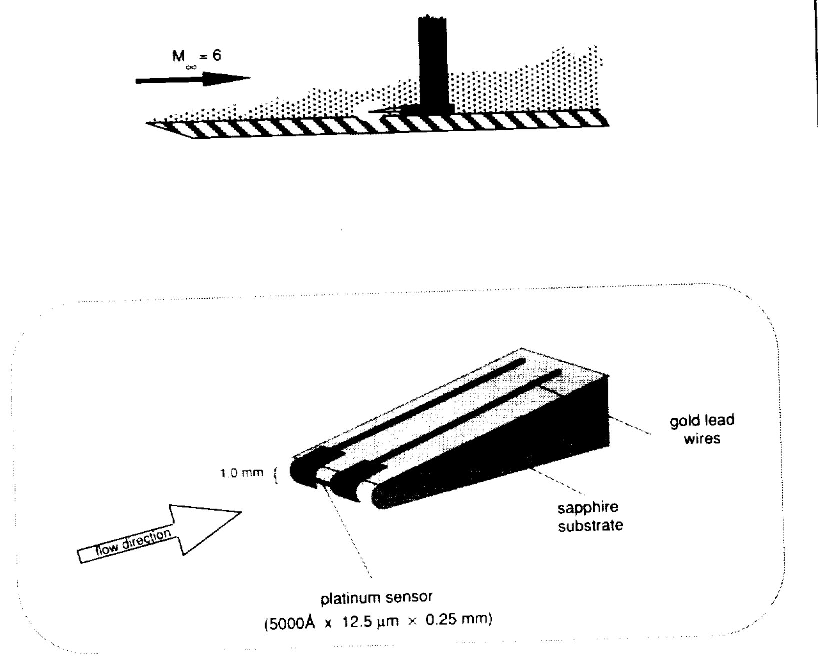

Hot-film probe.

measurement techniques (e.g., hot-wires, laser Doppler velocimeter (LDV)) are insufficient to meet the requirements of high-enthalpy flows, which include elevated stagnation temperatures and high dynamic pressures.

In this newly developed probe, the fragile sensing element of the hot wires is replaced with a thin platinum film (5,000 Å × 12.5 μm × 0.25 mm) deposited along the stagnation line of a wedge-shaped sapphire substrate. This probe represents a significant advancement of an existing concept with optimization through the use of advanced materials and state-of-the-art construction techniques. Microphotolithographic techniques have produced sensor volumes that are 2 orders of magnitude smaller than existing probes. Preliminary tests at Mach 6 indicate excellent durability characteristics. Constant temperature compensation of the probe has produced a typical frequency response of about 750 kHz, which is about 5 times greater than that of existing probes (130 kHz). This is significant since turbulent spectra in hypersonic flows typically exceed 500 kHz. Future work includes the development of several dynamic calibration techniques and detailed flow physics measurements in turbulent boundary layers in the 12-inch Mach 6 High Reynolds Number Tunnel and the 31-inch Mach 10 Tunnel.
**(Mark Sheplak, 44178,
Catherine B. McGinley,
Eric F. Spina, James E. Bartlett,
and Ralph M. Stephens)
Aeronautics Directorate**

Localized Transition and Turbulent Spot Formation on a Flat Plate

Flows that are undergoing transition from laminar to turbulent are notoriously difficult to predict,

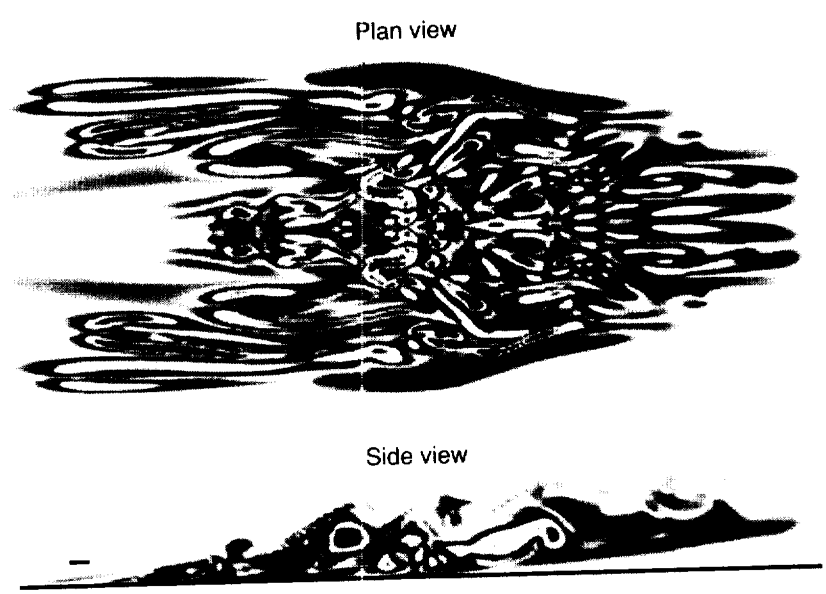

Plan view and side view of vertical vorticity magnitude. Side view includes long horizontal line that represents wall location. Short horizontal line shows location of plan view.

even though a knowledge of the location and extent of the transition region is essential for the accurate calculation of skin friction on aircraft wings, engine nacelles, and gas-turbine blades. Most previous studies of laminar-to-turbulent transition have concentrated on the breakdown of periodic waves in the flow. In contrast, the present research focuses on the evolution of a local disturbance into a turbulent spot. An understanding of the mechanisms involved in this particular transition scenario will enable better transition modeling for a broader range of flow conditions than is presently available.

The nonlinear evolution of the disturbance that was created by fluid injected through a wall slit into a flat-plate boundary layer is computed by direct numerical simulation. All important scales of motion are resolved in the computations.

The injected pulse of fluid initiates the development of a hairpin-shaped vortex. This vortex elongates and then spawns multiple secondary vortices; some of these are aligned with the original vortex, and others are displaced in the spanwise direction. Similar vortices have been observed in the detailed flow-visualization studies done in a water channel at Lehigh University under similar conditions. The direct numerical simulation data provide the necessary details of the instantaneous velocity and the pressure fields to support an earlier hypothesis of vortex formation.

As more vortices form and interact, they develop into a region of highly disturbed flow that resembles a turbulent spot. In the figure, shaded contours of vertical vorticity magnitude illustrate the typical turbulent-spot shape: a downstream pointed arrowhead in the plan view and an overhang region in the side view. Locally averaged skin-friction traces and velocity profiles are neither laminar nor fully turbulent.
(Bart A. Singer, 42316, and Ronald D. Joslin)
Aeronautics Directorate

Numerical Simulation of Variable-Density Compressible Shear Layers

Compressible shear layers play an essential role in the fluid dynamics involved in supersonic combustion. Because of this, the understanding of compressible shear layers plays an important role in the development of scramjet engines used in proposed hypersonic vehicles. Most of the current research has focused on the effect of compressibility alone. It has been found experimentally, as well as theoretically and computationally, that compressibility reduces shear-layer growth rate and mixing efficiency. Relatively little effort has gone into understanding the effect of disparate-mass gas-mixture effects that occur in nitrogen/hydrogen and air/hydrogen shear layers.

The essential difference between compressible and incompressible flows is the ability of pressure gradients arising in high-speed flows to be strong enough to locally compress the fluid. The most simple measure of this compression is the dilatation, or $\nabla \bullet u$, where u is the velocity. Its magnitude is proportional to the rate of change of volume of a local fluid element. Dilatation dynamics play an integral part in the acoustic aspects of high-speed shear layers.

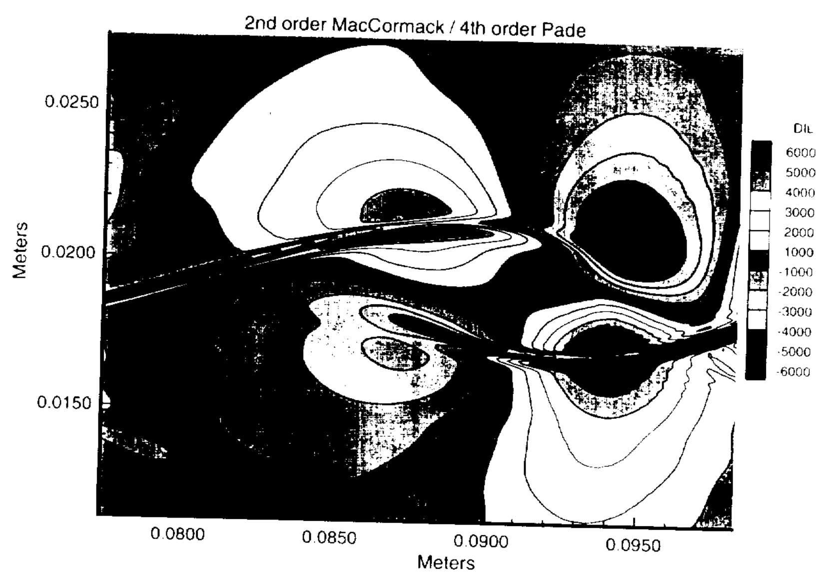

Contours of dilatation field of a nitrogen (lower stream)/hydrogen (upper stream) compressible shear layer at convective Mach number of 0.45.

A representative example of the effect of variable density due to disparate-mass gas mixtures is shown in the figure. This figure shows the outlines of a large spanwise vortex core generated from a two-dimensional Navier-Stokes code developed at NASA Langley. Two features are immediately apparent. First, there appears to be a quadruple-like dilatation structure surrounding the spanwise vortex. The second feature is the striated dilatation pattern found in the braid region that connects successive spanwise vortex cores. This is the effect of variable density. An additional and potentially important effect of this variable density is the fact that the vorticity that mixes the two gases is progressively displaced into the hydrogen stream with increasing density ratio. The lower right dilatation strand is at the species interface. The upper left strand corresponds to a finger of nitrogen being entrained into the predominately hydrogen spanwise vortex core.
(Christopher A. Kennedy, 47968, and Thomas B. Gatski)
Aeronautics Directorate

Noise Generation by Flow Over Cavity

The new field of computational aeroacoustics (CAA) in which the generation of sound by and propagation of sound through a flow field is calculated from first principles is being developed. The techniques necessary have been demonstrated and validated by comparison of numerical solutions with linear analytic and nonlinear multiple-scale analyses of classical acoustic problems.

Acoustic radiation by aircraft wheel well.

As an example of the application of CAA techniques to configurations of aerodynamic interest, the density field produced by flow over a cavity, such as a wheel well in an aircraft, is shown. This density field was computed from the governing Navier-Stokes equations using an acoustic/viscous splitting technique. Lighter areas are regions where the density is higher than the ambient (compressions), while darker areas indicate that the density is lower than the ambient (rarefications). This instantaneous field shows the intense acoustic waves that are produced by this geometry. Further analysis of the time-dependent radiation reveals spectra and directivity patterns that agree with experimental data.

This new capability provides a much better understanding of the sound generated by flows as well as means for its reduction and has important applications, not only for aircraft sources, but also for rail and automotive configurations. Large Eddy Simulation (LES) models are now being incorporated to increase the Reynolds number at which such calculations can be accomplished.
(J. C. Hardin, 43622)
Structures Directorate

Algorithm Development for Multielement Airfoil Computations

The objective of this work is to develop efficient and accurate computational tools for use in analyzing multielement airfoil configurations using the Navier-Stokes equations. The area of high-lift aerodynamics is an important area where advances in technology and better understanding of the relevant flow physics could yield significant improvements in the design and cost effectiveness of future aircraft. The computational analysis of high-lift, multielement devices is difficult, due in part to the complex nature of the geometry and the large number of grid points necessary to adequately resolve the flow field.

An unstructured-grid methodology is employed because of the relative ease with which very complex geometries can be represented. The flow solver is an implicit, upwind-biased algorithm that gains efficiency through multigrid acceleration applied to the flow equations and the turbulence model.

The flow solver has been implemented and tested for various configurations. Extensive comparisons

with experimental data have been conducted for a three-element geometry tested in the Low-Turbulence Pressure Tunnel (LTPT) at NASA Langley Research Center and have been reported in a recent AIAA paper. The results indicated that trends due to variations in Reynolds number as well as slight variations in geometry are well predicted. A sample pressure distribution and a view of the configuration are shown in the figure. Also shown is the convergence of the lift coefficient for the scheme with and without multigrid acceleration. On a grid of 97,000 nodes, the multigrid scheme achieves steady lift in approximately one hour of CPU time on a CRAY-YMP, while the unaccelerated scheme requires approximately 3.5 hours.

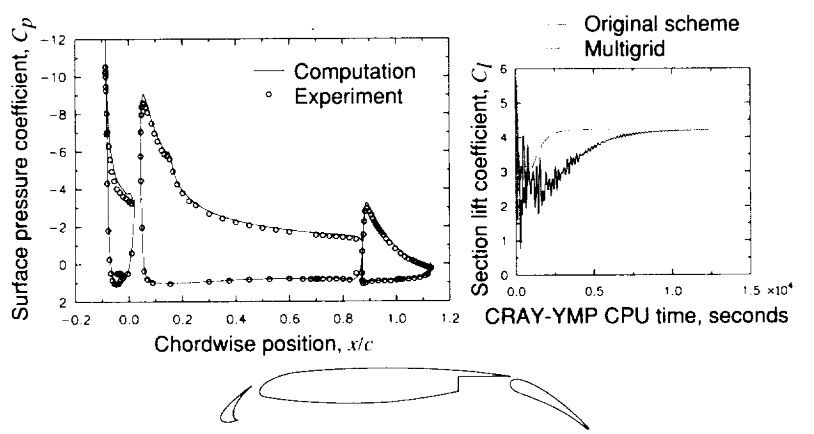

Surface pressure distribution and convergence of section lift coefficient for Douglas three-element airfoil. Free-stream Mach number is 0.2, angle of attack is 16.24°, and Reynolds number is 9×10^6.

As a result of this work, the time required to obtain a Navier-Stokes solution over a multielement airfoil configuration has been significantly reduced.
(Daryl L. Bonhaus, 42293, and W. Kyle Anderson)
Aeronautics Directorate

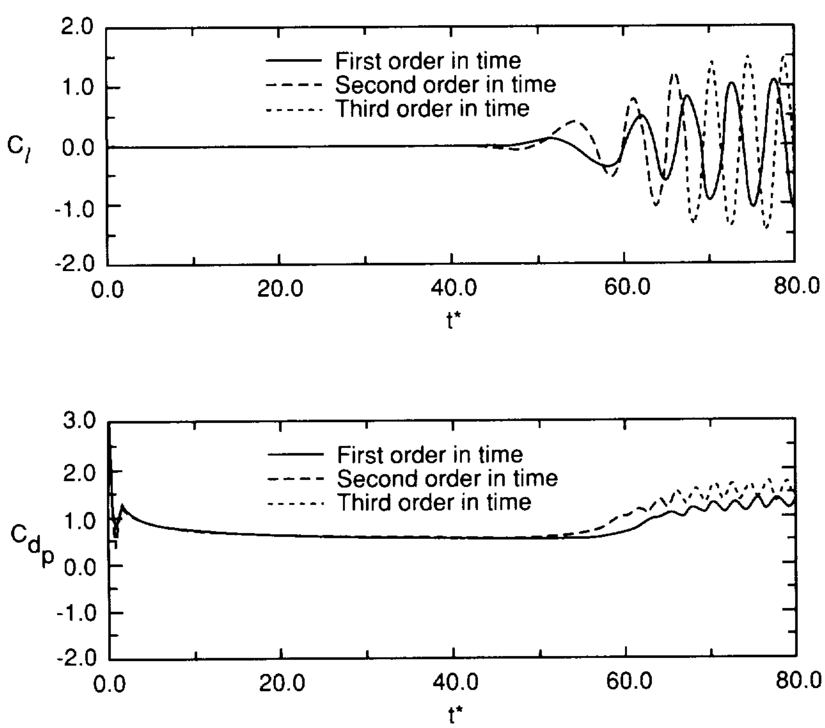

Lift (top) and drag (bottom) histories for impulsively started cylinder.

Efficient Time-Accurate Navier-Stokes Calculations

Although significant progress has been made in the last twenty years in numerically modeling many physical situations with computational fluid dynamics (CFD), most numerical schemes are limited to the prediction of steady flows. However, many physical phenomena (such as separated flows, wake flows, and buffet) are intrinsically unsteady. The present work describes an efficient method for calculating unsteady flows modeled by the unsteady Navier-Stokes equations.

In the present work, the approach taken was to write the unsteady Navier-Stokes equations in a form that is fully implicit in time. The multiblock version of the steady, three-dimensional, thin-layer Navier-Stokes solver, TLNS3D, was modified to iterative-

ly solve the resulting implicit equations at each time step. Discrete operators representing the temporal derivatives can be found that are unconditionally stable when the time operator is approximated to either first or second order. This stability allows the time-step size to be chosen based on the temporal resolution needed in the solution rather than limited by numerical stability requirements as with most other unsteady flow methods.

To demonstrate the capability of the present method, the unsteady flow over an impulsively started, two-dimensional circular cylinder (with a Reynolds number of 1,200 and a Mach number of 0.3) was calculated. The flow is initially symmetric with zero lift as the wake behind the cylinder begins to grow. As the wake continues to grow, it becomes unstable and begins to shed from alternate sides of the cylinder. Time histories of the lift coefficient (C_l) and the drag coefficient based on integrated pressures (C_{dp}) are shown in the accompanying figure. From experimental data and the results of previous global minimum time stepping (GMTS) calculations, the period of the oscillation of C_{dp} is known to be approximately 4 in terms of the nondimensional time t*. To give 40 time steps per period, a time step of $\Delta t^* = 0.1$ was used. A calculation using a first-order discretization of the physical time derivative predicted a Strouhal number of 0.21. Second- and third-order discretizations predicted a Strouhal number of 0.24 compared with the experimentally obtained value of 0.21.

A GMTS calculation required 4,600 steps to reach $\Delta t^* = 2.4$. The present scheme required only 24 physical time steps to reach $\Delta t^* = 2.4$, and a maximum of 20 multigrid cycles at each time step were required to converge C_{dp} to six digits. Therefore, the present scheme required only about 10 percent of the computer time required by GMTS.
(N. Duane Melson, 42227, Harold L. Atkins, and Mark D. Sanetrik) Aeronautics Directorate

Multiblock CFD Codes — A New Paradigm

Significant progress has been made in recent years towards the development of computational fluid dynamics (CFD) codes capable of solving high Reynolds number flows over complex aero-

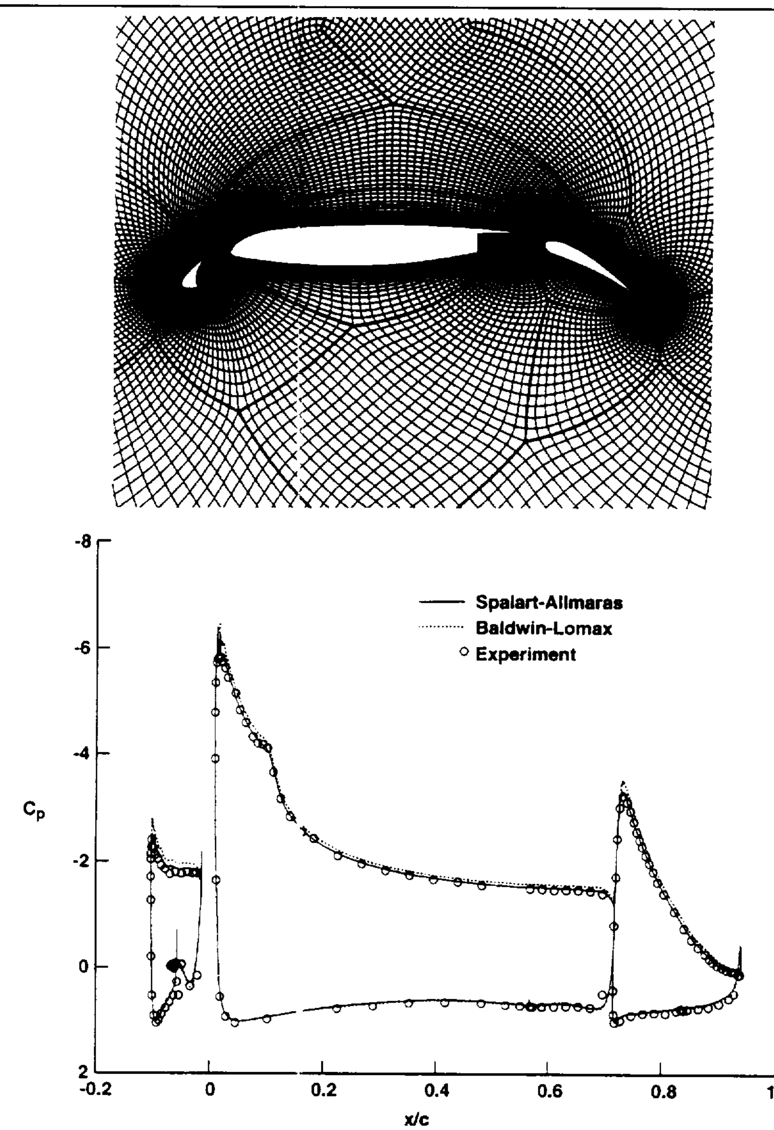

Multiblock computations for Douglas three-element airfoil configuration. Top is partial view of 20-block grid; bottom contains pressure comparisons ($M_\infty = 0.2$; $\alpha = 8.1°$; $Re_c = 9.0 \times 10^6$).

dynamic configurations using multiblock structured grids. However, such codes are not being used to their full potential because of the difficulty associated with generating suitable grids in a timely and automatic manner. In order to reduce the total time required for obtaining flow solutions starting from surface definition, a recently developed automatic blocking procedure, funded under the small business innovative research (SBIR) program at NASA Lewis, is used. One of the most useful features of this new automatic-block structured-grid generation procedure is its ability to generate high-quality computational grids in a batch environment. In addition, small differences in geometry can be accommodated through minor changes in input files developed for geometrically similar configurations.

All essential elements to automate the process of simulating aerodynamic flows over complex configurations have been assembled and applied to a three-dimensional high-lift configuration to demonstrate the feasibility of the entire process. A partial view of the grid employed in these computations is shown in the attached figure. The grids generated by this procedure maintain point continuity and vary smoothly across block interfaces. In addition, grid points are used efficiently through compact grid enrichment by confining the denser grids in high gradient regions of interest. The input files for the multiblock solver are prepared automatically by using the connectivity and grid files created by the grid generator. A field-equation type of turbulent model, namely the Spalart-Allmaras model, is found to give more accurate solutions than the algebraic model of Baldwin-Lomax.

The procedure outlined here is a new paradigm for employing multiblock structured grids, in that it avoids the laborious interactive construction of field grids and allows efficient local clustering of grid points near regions of interest. Such procedures are expected to play a significant role in parametric studies in the aerodynamic design process.

(Veer N. Vatsa, 42236, and Christopher L. Rumsey) Aeronautics Directorate

Sensitivity Derivatives for Multidisciplinary Design Optimization Via Automatic Differentiation

Computer models of diverse systems may be characterized by four traits: the models admit free parameters and produce measures of goodness about a product or process; the system is required to simultaneously satisfy a number of constraints; the product or process consists of subsystems that can be modeled individually; and the measures of goodness are related in complex ways to parameters within the system. The effects of these parameters on the measures of goodness can be quantified by a matrix of terms known as sensitivity derivatives (SD). These derivatives can be approximated by divided differences, obtained exactly by hand differentiation of analytic relationships, or through symbolic manipulators. However, as the size and complexity of the computer models increase, problems arise in obtaining the desired SD matrix; the computational technique of automatic differentiation (AD) addresses these shortcomings.

The AD technique is a powerful computational method for obtaining exact SD from existing computer programs. Argonne National Laboratory and Rice University have developed a precompiler AD tool applicable to FORTRAN programs called ADIFOR. This tool has been easily and quickly applied by NASA Langley researchers to assess its feasibility and computational impact in sensitivity analysis and multidisciplinary design optimization for several different codes: a 3-D multigrid Navier-Stokes flow solver; a structural analysis code; an aircraft performance program; and a potential-flow wing-design code. The ADIFOR tool works quickly and robustly with minimal user intervention; the resulting AD codes have been verified to compute the exact SD in about the same time as that required for other methods or faster. Moreover, the AD codes have been shown to provide reliable SD in cases for which divided differences failed and to offer benefits for parallel problem implementation on distributed-memory machines or networks of workstations.

A recent, highly successful ADIFOR User Training workshop was hosted by NASA Langley and staffed by local, Argonne National Laboratory, and Rice University researchers. It was attended by 49 potential users: 17 industrial, 17 university, and 15 government. Many (29 to date) of the attendees have indicated an interest in using

this technology in their research or applications.
(L. L. Green, 42228, A. Carle, C. H. Bischof, K. J. Haigler, and P. A. Newman)
Aeronautics Directorate

Unstructured Viscous Grid Generation by Advancing-Layers Method

The objective of this research is to formulate a new automated approach for generating unstructured triangular and tetrahedral grids with high-aspect-ratio cells for viscous flow calculation. The approach is based on a new grid-marching strategy referred to as "advancing layers" for constructing highly stretched cells in the boundary-layer region and the "advancing-front" technique for generating equilateral cells in the remaining inviscid-flow region. The new method is conceptually simple but powerful and capable of producing high-quality viscous unstructured grids for complex configurations with ease. The present approach is divided into three separate stages: 1) surface grid generation, 2) construction of high-aspect-ratio cells in the viscous region, and 3) generation of regular (isotropic) cells in the inviscid-flow region. Steps 1 and 3 utilize established methodology encompassed in an existing advancing-front inviscid grid generation code VGRID. The second step proceeds by introducing new grid points in the field along predetermined surface vectors and connecting them to the corresponding faces on the front. The viscous cells are advanced into the field one layer at a time, in contrast to the conventional method in which cells are added in no systematic sequence. The layers continue to advance in the field, while growing in thickness, until a new criterion based on a "spring" analogy determines that two approaching fronts are about to cross or that spacing criteria from a user-prescribed background grid trigger a switch to the conventional advancing-front method. The transition between the two types of grid is both smooth and fully automatic. The fidelity of the new method is demonstrated by generating a viscous grid around a multielement airfoil,

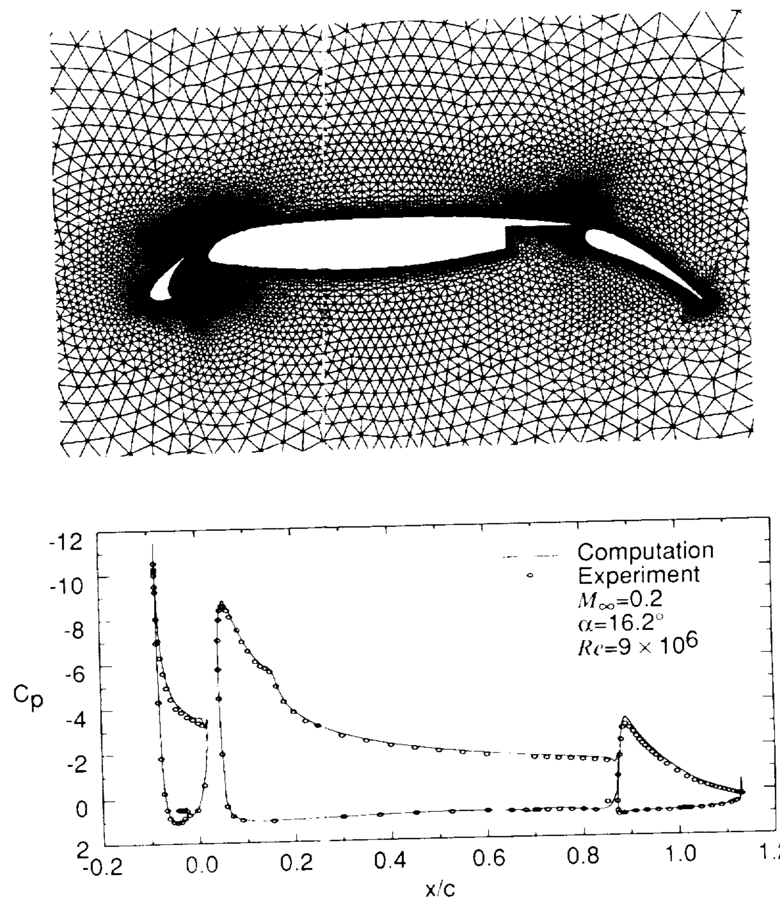

Unstructured viscous grid and flow solution around a multielement airfoil.

shown in the figure, and computing a flow solution. This grid contains 34,987 triangular cells with a first-layer spacing of approximately 7×10^{-6} of the main airfoil chord length. The flow solution was obtained with an available node-centered flow solver using a Baldwin-Barth turbulence model at a Mach number of 0.2, an angle of attack of 16.2°, and a Reynolds number of 9×10^6. Excellent agreement with experimental data is shown in the figure for the surface pressure distributions.
(Shahyar Pirzadeh, 42245)
Aeronautics Directorate

Vortex-Flow Prediction With Unstructured-Grid Euler Methodology

The objective of this investigation was to assess the capability of an inviscid unstructured-grid method to predict flow fields with vortical-flow structures emanating from sharp edges. To accomplish the goal, the results from the unstructured-grid method were compared with results from an established structured-grid method. Both the structured- and unstructured-grid flow solvers employed in this investigation, known as CFL3D and USM3D respectively, were developed at NASA Langley Research Center. The configuration used for this study, the isolated fuselage of the Modular Transonic Vortex Interaction (MTVI) model, was selected because it is representative of future military aircraft fuselages and it has simple, analytically defined geometry. The structured and unstructured grids were generated to provide near-comparable resolution of the computational domain in order to minimize the effect of grid type on the solution. Computational results are shown for both inviscid methods at 19.8° angle of attack and a Mach number of 0.4. Turbulent, thin-layer, Navier-Stokes computations on the structured grid are also shown for reference. The figure presents the crossflow normalized total-pressure contours at three selected stations with an isometric view of the inviscid solutions and the corresponding surface grids. The crossflow total-pressure contours demonstrate excellent correlation between the structured- and unstructured-grid inviscid solutions. Additional analysis has also shown good correlations for the surface pressure distributions and total forces and moments.

(Farhad Ghaffari, 42856)
Aeronautics Directorate

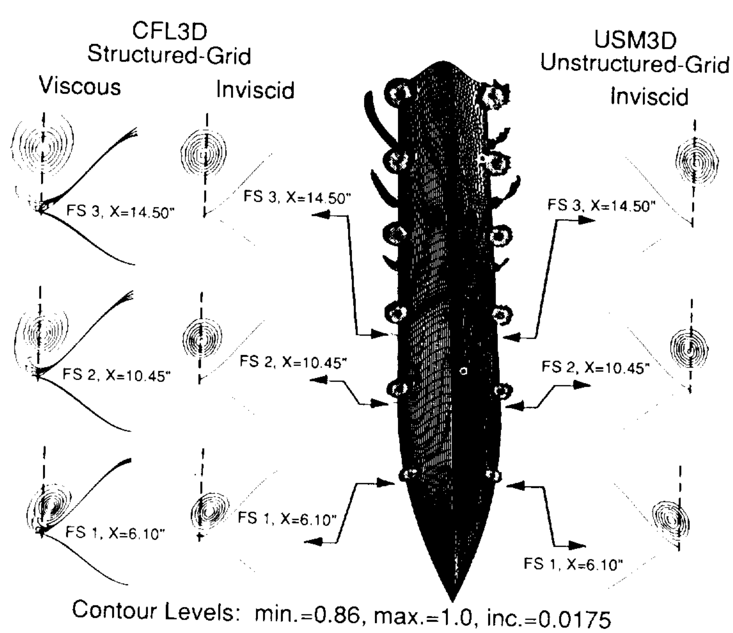

Comparison of structured- and unstructured-grid results.

Boundary-Layer Heat-Transfer Measurements on a Swept Semispan Wing

In a recent cooperative program with the Northrop Corporation, aerodynamic heat-transfer measurements were made on a swept semispan wing-body at various skin-temperature ratios and flow conditions. Also, the effects of skin heating and cooling on the extent of natural laminar flow were measured. The wing (semispan 36 in., tip chord 18 in.) and fuselage fairing were tested in the 8-Foot Transonic Pressure Tunnel. The model was mounted to a splitter plate located 8 in. from the tunnel wall to avoid tunnel-wall boundary-layer effects and the separated flow around the model support hardware. The wing upper-surface skin could be heated electrically, and the lower-surface skin could be heated or cooled with water from a closed-loop system. The model was instrumented with static pressure orifices, skin thermocouples, hot-film gauges, and heat-flux gauges. Mach number was varied from 0.20 to 0.80, Reynolds number from 1.1 to 3.8×10^6 per foot, tunnel stagnation temperature from 75 to 100°F, and angle of attack from 0° to 6°. The ratio of model skin temperature to the adiabatic skin temperature was varied from 0.85 to 1.10. The data will be used to validate computational fluid dynamics (CFD) meth-

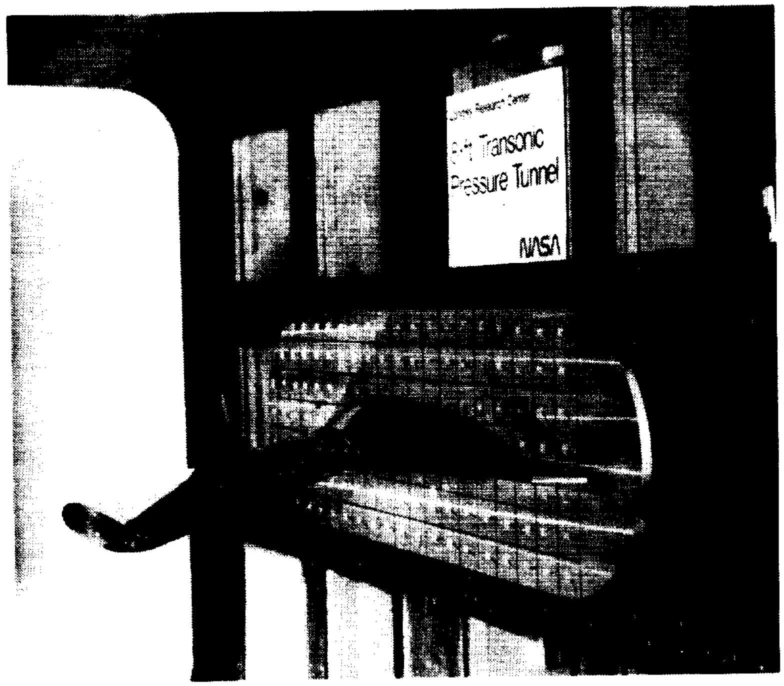

Northrop heat-transfer wing in 8-Foot Transonic Pressure Tunnel.
L-93-04220

ods for boundary-layer heat transfer and stability in the presence of temperature gradients.
(Cuyler Brooks, 41053, and Charles Harris)
Aeronautics Directorate

Volumetric Three-Dimensional Velocity-Field Measurements Using Holographic Particle Image Velocimetry

Three-dimensional velocity measurements have been successfully obtained using Holographic Particle Image Velocimetry (HPIV). The technique, which is a natural extension of traditional photographic PIV, uses two pulsed lasers fired in sequence to illuminate a probe volume seeded with tracer particles. Dual orthogonal, double-exposure holographic records were taken of tracer particles embedded in the flow, where the recorded image separation of each tracer particle was dependent on the laser pulse separation and the local flow velocity. Autocorrelation analysis of reconstructed real-image interrogation cells (approximately 2 mm^3 in size) provided three component velocity measurements over an extended measurement volume of 5 cm^3.

The system was demonstrated in the laboratory by obtaining HPIV measurements in the wake behind a cylinder in a low-speed wind tunnel and in the flow exiting a small 25-mm-diameter tube. An example of the velocity field exiting the 25-mm tube is shown in the figure on page 11. Overlaid x-y, y-z, and x-z cross sections of the flow are shown to help visualize the three-dimensional structure. A venting exhaust system placed to the left of the tube (in the negative x direction), and upstream approximately 250 mm, increased the three-dimensional nature of the flow. This resulted in a slight rotation of the flow as shown in the x-z top view and an asymmetric velocity profile in the x-y side view. An approximate parabolic profile can also be seen in the x-z side view. The availability of a technique like HPIV will help in the obtaining of instantaneous, volumetric data with which to validate computational fluid dynamics codes. It will also assist in experiments where an understanding of the full three-dimensional, three-component velocity field is required.
(William M. Humphreys, Jr., 44601, James L. Blackshire, and Scott M. Bartram)
Electronics Directorate

Velocity Measurements of Unsteady Flow Using Particle Image Velocimetry

Two-dimensional velocity measurements of the unsteady vortical flow downstream of a backward-facing step have been successfully obtained by using a Particle Image Velocimeter (PIV). The tunnel consisted of a 7.6-cm-tall step embedded in a 15.2-cm-tall channel. The step was approximately 122.0 cm wide, thereby ensuring two-dimensional flow near the tunnel centerline. The PIV system consisted of two frequency-doubled Nd:YAG lasers fired in sequence to generate a pulsed light sheet

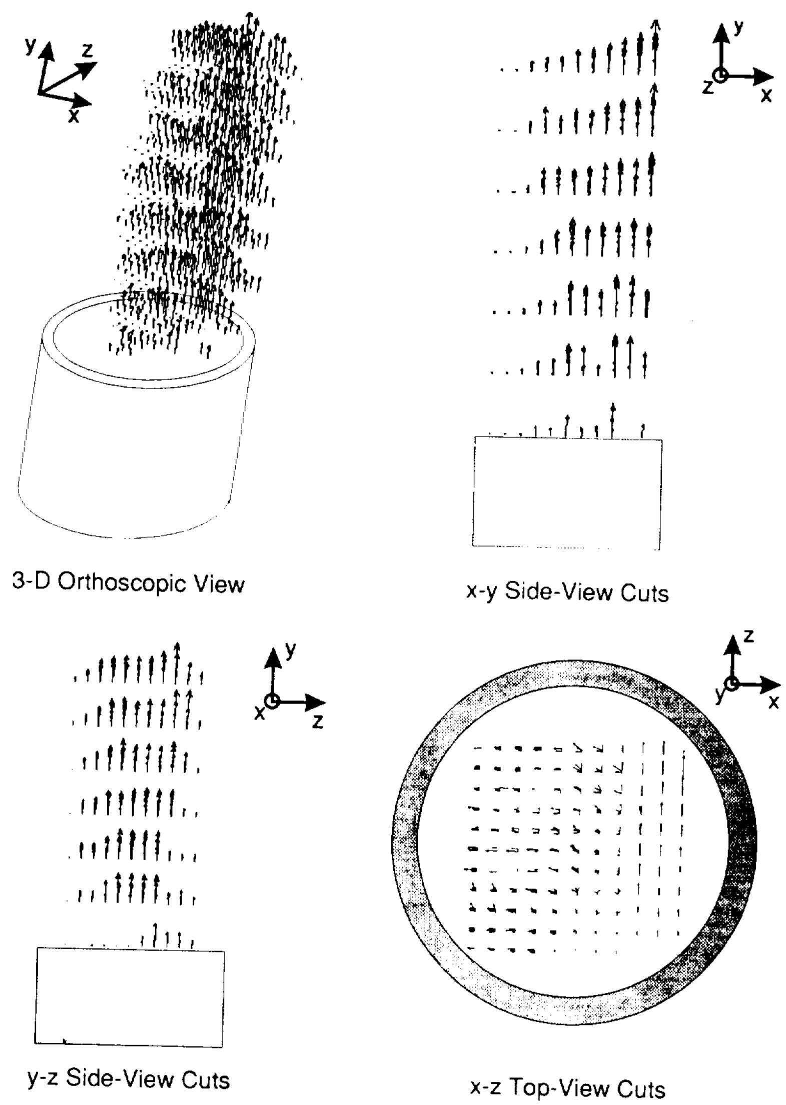

3-D velocity field of flow exiting a 25-mm-diameter tube obtained via dual holographic recordings.

100.0 mm wide and 1.0 m thick. This light sheet bisected the tunnel along its centerline immediately downstream of the step. A high-speed photographic camera was oriented normal to the plane of the light sheet and imaged 1.0-µm mineral-oil droplets in the airflow onto 70-mm film. The camera was coupled to the laser system to allow sequences of up to 55 frames of data to be taken with a maximum data-acquisition time of 3.5 sec and a frame-to-frame time separation of 66.7 msec. An electro-optical image shifter was attached to the camera to enable flow directionality to be obtained. Each double-exposure photograph was interrogated to track the movement of seed particles in adjacent 1.5- by 1.5-mm regions using auto-correlation analysis and resulting in the creation of two-dimensional velocity maps.

An investigation of the unsteady flow in the bottom corner of the step along the tunnel centerline was conducted by generating a sequence of 52 photographs taken at a sampling rate of 15 Hz. Examination of the individual velocity fields obtained from this sequence revealed fluctuating secondary and tertiary vortical structures. An example of a single frame of data is shown in the figure. Creation, dissipation, and movement of the vortical structures were evident. By averaging the sequence of photographs together, mean-flow structures were derived which agreed with Laser Doppler Velocimeter (LDV) surveys conducted in the facility. This test represents the first use of a time-resolved PIV system at Langley to examine the evolution of unsteady flow structures and shows the power of global velocity techniques to augment data obtained from traditional point measurement techniques such as LDV.
(William M. Humphreys, Jr., 44601, and Scott M. Bartram) Electronics Directorate

Determination of Measurement Uncertainties of Wind-Tunnel Balances

The multicomponent strain-gage balance is the standard transducer used to precisely measure aerodynamic force-and-moment loads on aircraft models during wind-tunnel tests. Prior to wind-tunnel application, each balance undergoes a rigorous calibration proce-

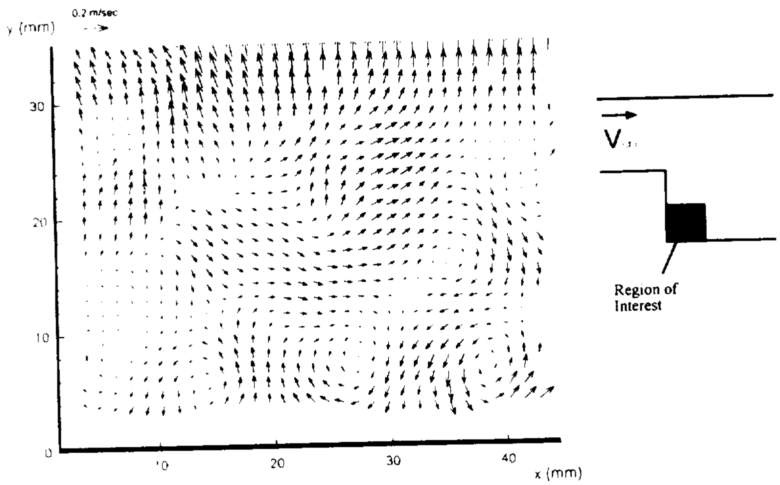

Velocity field obtained via PIV measurements downstream of backward-facing steps.

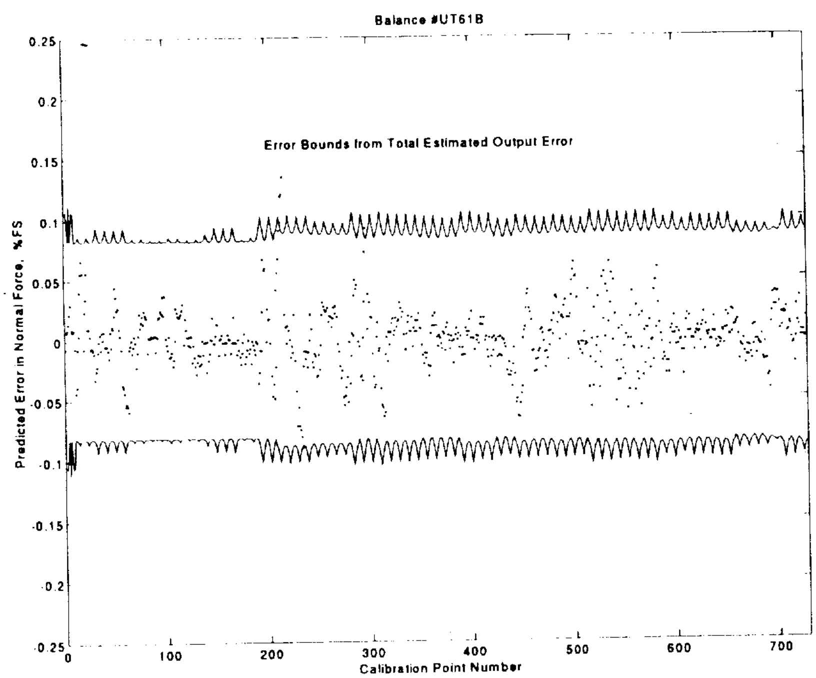

Predicted residuals and error bounds of force balance.

dure from which its calibration coefficients are determined and its performance accuracy is verified.

Balance accuracy has been customarily cited either as a worst-case proof load error or as a percentage of the full-scale balance load computed from calibration data. A method has now been developed to determine the 6 by 28 balance coefficient matrix, its uncertainty matrix, and the uncertainties of measured forces and moments as functions of the applied loads. A multivariate regression technique utilizes the 28 by 729 design matrix formed from the calibration data to obtain a minimum-variance estimate of the balance sensitivities, the interaction coefficients, and their unce-rtainties. Theses uncertainties are then employed to infer the uncertainties of forces and moments computed from observed balance outputs obtained during tests. It was shown that calibration coefficient uncertainties depend on both the measurement uncertainty and the structure of the experimental design.

During wind-tunnel testing, the total uncertainty of a single force-moment measurement inferred from the balance output voltages depends on both the coefficient uncertainty and the facility measurement uncertainty. With this new procedure, accuracies can be cited for each computed force and moment as functions of the actual balance output readings. The calibration uncertainties are bias errors, computed as functions of load, that are combined with random facility measurement precision errors to determine the total uncertainty during wind-tunnel tests. The new method has been verified using data obtained from balance calibrations.

(John S. Tripp, 44711,
Ping Tcheng, and Alice T. Ferris)
Electronics Directorate

Video Luminescent Imaging

Video luminescent imaging is a new technology based on the measured phosphorescence of an excited, aerodynamic surface coated with luminescent materials. Pressure sensitive paint (PSP) is a coating that, when excited with a wavelength-specific light source, luminesces. A linear relationship exists between the emission intensity of the excited luminophor and the pressure incident on the surface. The use of PSP is relatively nonintrusive, affecting the test by only the 25-mil-thickness coating on the model surface. Intensities are then sensed by an accurate camera and digitally stored by a personal computer. The processed PSP data provide accurate global mapping of surface pressure distributions and locations of shock, boundary-layer transition, and separation on the models for various aerodynamic configurations.

Langley Research Center and Ames Research Center conducted a cooperative test of a Navy double delta wing model in the Langley 7- by 10-Foot High-Speed Tunnel. The PSP used was a porphyrin compound, newly developed by the University of Washington, and was illuminated by UV lamps (365 nm). Langley researchers developed a separate data acquisition system consisting of a monochrome charged-coupled device (CCD) camera with a 650-nm band-pass filter, videocassette recorder/player (VCR), and a 486 personal computer with frame grabber and demonstrated real-time, color-enhanced, global surface flow visualization. The figure shows uncorrected graylevel mapping over the model surface during two test conditions. Data analysis consists of color-enhancing gray levels to aid visual interpretation, computational correction for model movement/deformation, and image processing to provide measurements of pressure distribution data.
(Lorelei Gibson, 44643, and Michael Mitchell)
Electronics Directorate

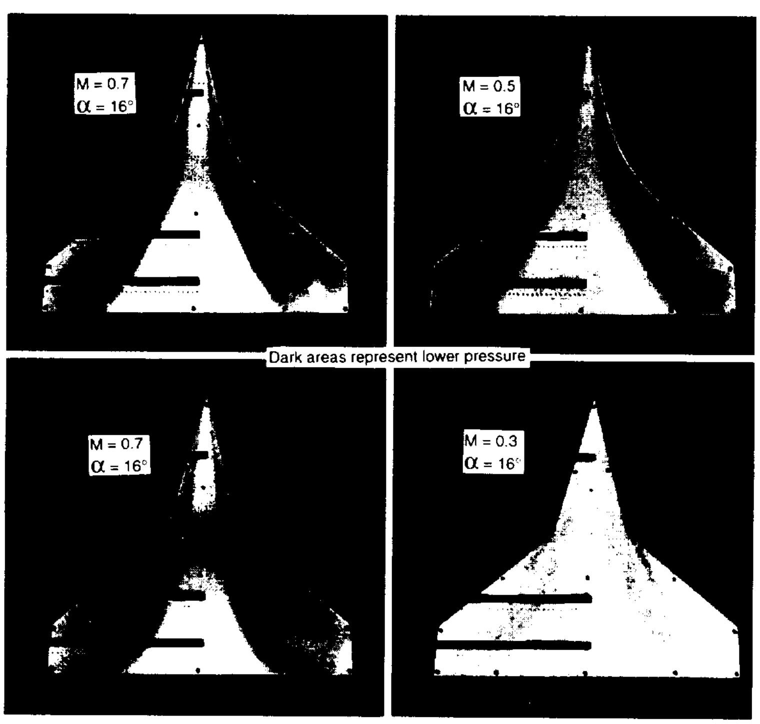

Global surface pressure distributions using PSP at Mach numbers (M) of 0.3, 0.5, and 0.7 and angle of attack (α) of 16°.

Supersonic Flow-Field Investigations Using Doppler Global Velocimetry

The first use of Doppler global velocimetry to measure supersonic flows about wind-tunnel models was conducted in the Unitary Plan Wind Tunnel. The investigation included measurements of the flow about an oblique shock generated by an inclined flat plate and measurements of the vortical flow above a 75° delta wing at various angles of attack. The measurement image, shown in the figure, of the oblique shock represents the average of ten frames of video data. These measurements of the vertical velocity component show a lag of 2 mm for the water condensation to match the gas velocity downstream of the shock. This exceptional measurement performance is primarily due to the ability of the technique to utilize seed particles far smaller than classic laser velocimetry techniques.

This new nonintrusive measurement technique uses the edge of an iodine absorption line as an optical

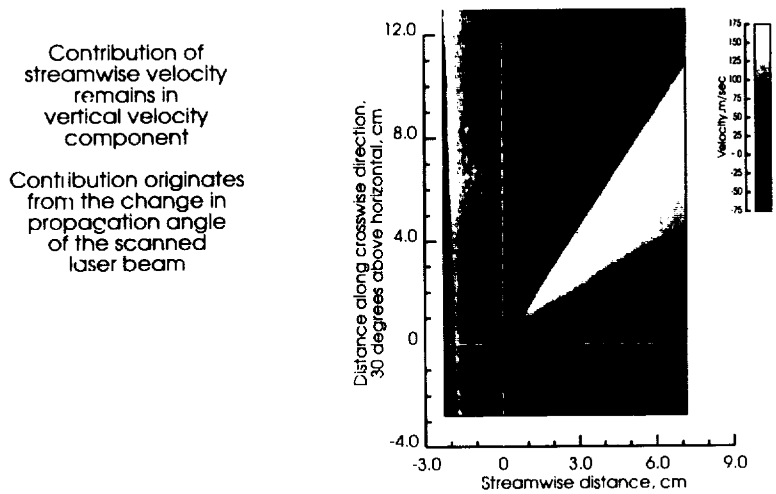

DGV measurements at Mach 2.5 about a flat plate inclined to −15°.

frequency-to-amplitude converter to determine the Doppler shifted frequency of scattered light from particles passing through a laser light sheet. The simplicity of the method is carried through to its implementation, requiring only a beam splitter, mirror, and two video cameras in addition to the iodine cell per measured velocity component. Using ordinary analog video electronics, three-component velocity images can be monitored during wind-tunnel operation as easily as standard light-sheet flow visualization.
(James F. Meyers, 44598)
Electronics Directorate

Effects of Type II De-icer Fluid on Aircraft Tire Friction Determined in ALDF Tests

Tests were conducted at the Aircraft Landing Dynamics Facility (ALDF) with financial support provided by the FAA under an existing Memorandum of Agreement. A conventional, 40 x 14 transport-aircraft main-gear tire was tested at speeds up to 160 knots ground speed on a non-grooved concrete test surface. Surface test conditions included dry, wet (water only), Type II chemical/water mixture, and 100 percent Type II chemical. Test tire operational modes included anti-skid controlled braking at zero yaw angle and yawed rolling at fixed 6° yaw angle. Initial ALDF tests to determine the variation of tire cornering friction performance with speed and surface condition have been completed. A typical example of the variation of tire/pavement side-force friction coefficient (μ_s) is shown in the figure for four different surface conditions—dry concrete, water-wet concrete, 3-parts water to 1-part de-icer wet concrete, and 100-percent de-icer wet concrete. These data were obtained during the same 100-knot test run. A section of dry concrete was provided between the liquid contaminated surfaces. The results indicate that for the 3-to-1 mixture the friction values are similar to the water-wet condition. The friction coefficient for 100-percent de-icer was about 30 percent lower than the water-wet value. The 3-to-1 mixture is probably more representative than the 100-percent mixture of what might be found in normal aircraft operations. Therefore, these results suggest that, in practice, the de-icer effects on friction will be similar to those of water. The information such as that shown in the figure will assist in establishing a national database on effects of aircraft Type II chemical de-icer depositions on

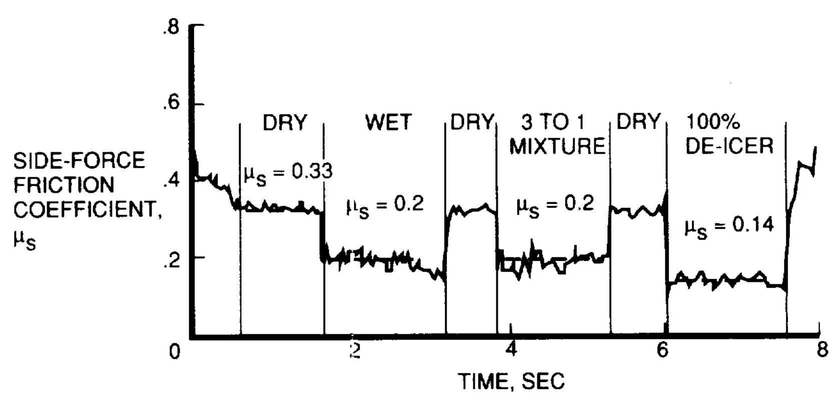

Aircraft de-icer fluid frictional properties. 40 x 14 tire; speed = 100 knots; yaw angle = 6°.

aircraft-tire/pavement friction performance. These data will also help improve the safety of aircraft ground operations during winter runway conditions.
(Thomas J. Yager, 41304, Sandy M. Stubbs, Granville L. Webb, and William E. Howell) Structures Directorate

New Tire-Contact-Friction Algorithm Correlated With Shuttle Nose-Gear Tire Experimental Results

The contact-friction algorithm is incorporated into a mixed formulation, two-dimensional shell finite-element model. The contact algorithm is based on a perturbed Lagrangian formulation and uses the preconditioned conjugate gradient iteration procedure. The contact algorithm incorporates a modified version of the Coulomb friction law, wherein the friction coefficient at the onset of sliding is different from that during sliding. The algorithm includes the effects of energy dissipated within the sliding portion of the contact zone. Numerical studies have demonstrated that the contact-friction algorithm is robust enough to handle the range of friction coefficients normally associated with aircraft tire applications. An illustrative result is shown in the figure, which presents measured and calculated lateral friction load intensity distributions and footprint shapes for the Space Shuttle nose-gear tire. The measured footprint and lateral friction loads data are shown at the top; the corresponding calculated results are shown at the bottom. The measured and calculated footprint shapes are similar. Both the measured and calculated lateral friction load intensities reach their respective maximum magnitudes in the lateral extremities of the tire footprint. Both measured and predicted lateral friction load intensities exhibit bands of alternating positive and negative friction values across the width of the tire footprint. The tire-contact-friction algorithm will be a valuable analysis tool for developing a fundamental understanding of the friction and wear mechanisms that exist in the tire-runway interface.
(John A. Tanner, 41305) Structures Directorate

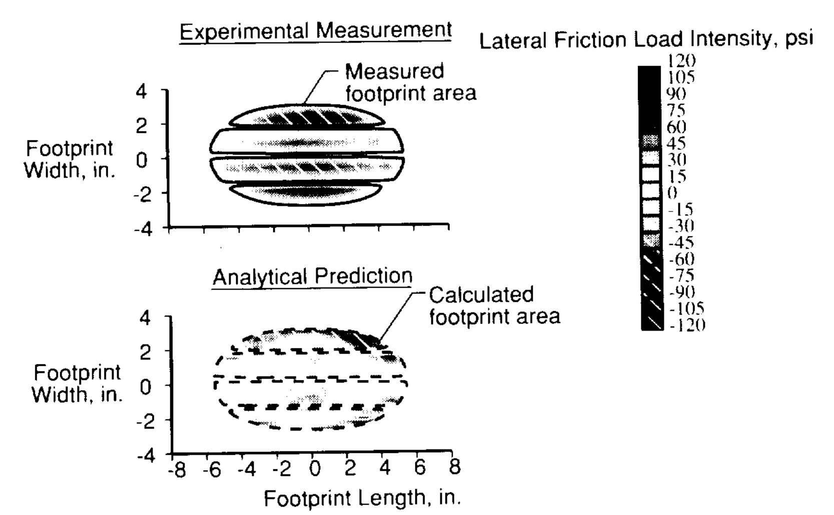

Measured and calculated lateral friction load intensity distributions. Tire load = 15 000 lb; Inflation pressure = 300 psi.

Stochastic and Nonlinear Response and Acoustic Radiation From a Panel-Stringer Structure Near a Supersonic Jet

The dynamic response and acoustic radiation of aluminum panel structures forced by the near field of a supersonic jet exhaust are being investigated experimentally and numerically. The objective is to enhance understanding of the nonlinear response of the structure and the resultant nonlinear acoustic radiation, as well as to control the response. The structures consist of six panels with stringers. For the experimental studies, the panel structures are mounted in a rigid frame near a model jet exhaust in an anechoic chamber. The structure is excited by the noise emanating from the jet as a result of instability, turbulence, and shock in the shear layer. Two types of nozzles are used: a conventional round convergent nozzle and a porous plug nozzle, both having the same mass flow and exit area. The plug nozzle remains shock-free at all pressure ratios. Control of the structural response is achieved by actively forcing the structure with an actuator at the shock frequency whose amplitude is locked in a

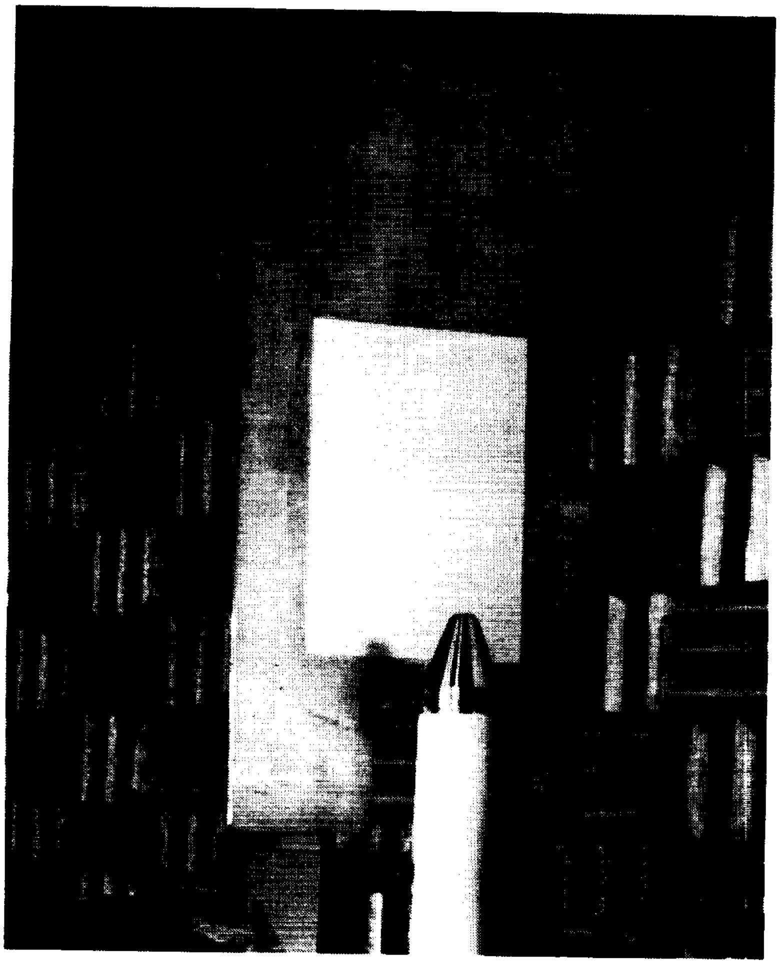

Panel-stringer structure excited acoustically by a high-speed jet.

L-91-13393

self-control cycle. Preliminary studies are made on the effects of jet noise and structural response at accelerated or decelerated speeds.

Experimental results of the standard jet at a pressure ratio of 3 indicate that the strain response of the structure is nonlinear and nonstationary, with periodic, chaotic, or random behavior. The time history of the pressure indicates rotation and flapping of the shock structure in the jet column, and the radiated acoustic pressure from the structure contains shocks and the formation of harmonics. Results from the active control of the structure show that the peak level of the vibration in the structure is reduced by the factor of 63, corresponding to a power-level reduction of 18 dB.

A significant reduction in response and radiation from the structure is also achieved with a newly developed high-performance-plug nozzle suppressor. At accelerated and decelerated speeds data show that the pressure exhibits a variety of behaviors different from those observed at constant speed **(Lucio Maestrello, 41067) Structures Directorate**

Composite Scaling Studies Provide Better Understanding of Composite Laminates

The size of a composite laminate can significantly influence the first ply failure stress and ultimate strength under tensile loading conditions with the magnitude of the size effect depending on several factors including laminate stacking sequence (blocked or dispersed plies), laminate type (fiber or matrix dominated), and the material itself. In one study, tensile tests were conducted on geometrically scaled angle ply laminates which were fabricated using two different scaling approaches. In the first approach plies of similar orientation were blocked together. In the second approach the ply orientations were distributed throughout the laminate thickness. Stress/strain data from scaled angle ply coupons loaded in tension to failure are shown in the upper figure. All scaled specimens exhibit the same initial modulus. However, a significant scale effect in strength is observed as size increases; the scaled coupons containing blocked plies exhibit a trend of decreasing strength. Thus, the baseline, or smallest specimen, appears twice as strong as the comparable full-scale specimen. For the distributed ply specimens, the trend is increasing strength with increasing specimen size. Also, the distributed ply

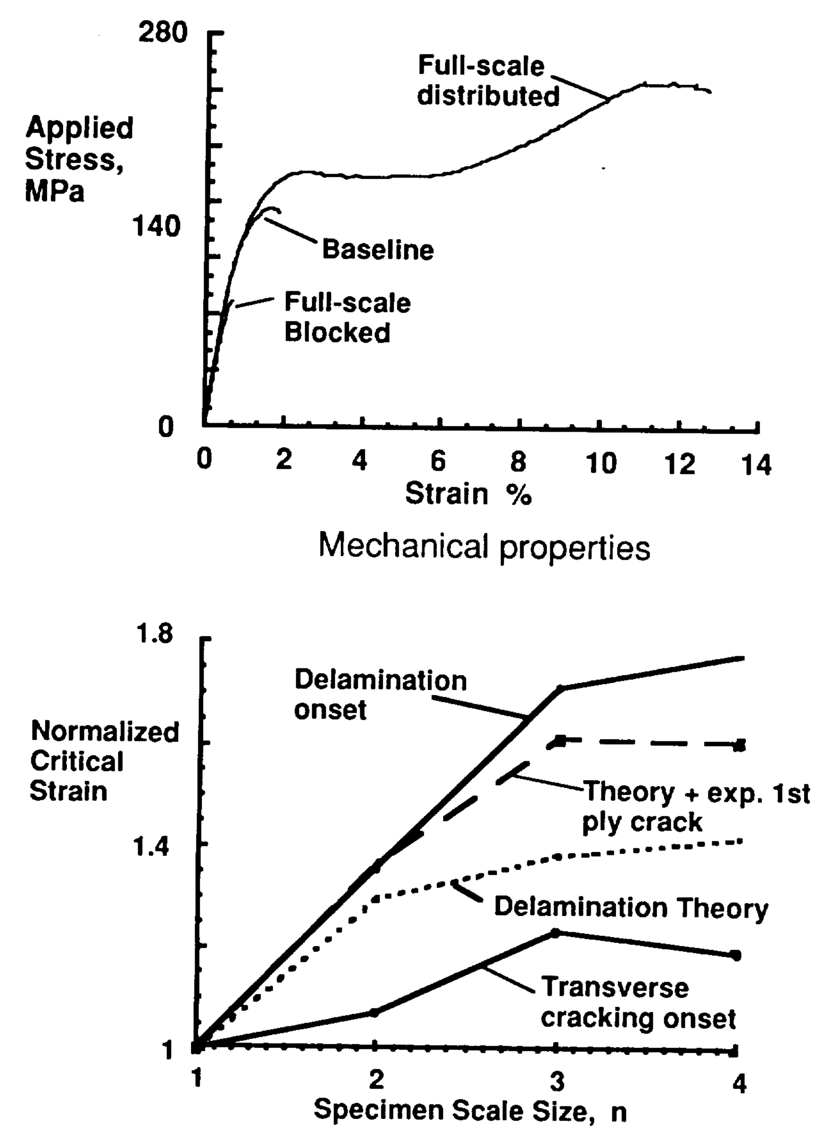

Failure theory evaluation.

lay-ups have a plastic, yielding behavior, while the blocked lay-ups exhibit a brittle response prior to failure. As a result of these findings, the ASTM D-3518 standard test method for determination of shear modulus and shear strength was changed to specify a minimum thickness and lay-up for the test specimens. A second study was conducted to investigate the effect of specimen size on the tensile response and ultimate failure in blocked and distributed scaled composite coupons. All lay-ups contained a core of 90° plies, which tend to develop transverse matrix cracks under tensile loading. These cracks act as stress risers in neighboring plies leading to premature fiber failure, or serve as sites of delamination initiation. The data in the lower figure show critical strains at the onset of transverse matrix cracking in the 90° plies and at the onset of delamination for quasi-isotropic laminates as a function of increasing size. Also shown are analysis results for delamination onset using a strain energy release rate approach which predicts a highly conservative failure strain magnitude compared to the experimental data. As a first approximation to account for matrix cracking, the experimental data for onset of transverse cracking were added to the delamination analysis. This response appears to more accurately represent strain at delamination onset with specimen size. These results are being used to develop accurate scaling laws for composite structures and to challenge current failure theories to account for size effects and the importance of transverse cracking in delamination onset.

(Karen E. Jackson, 44147)
Structures Directorate

Transonic Aeroelastic Phenomena Investigated for Transport Model in TDT

Modern high-speed transport aircraft operate near, and sometimes in, the transonic speed regime, where the aircraft's performance can be adversely affected by various aeroelastic phenomena such as flutter, limit cycle oscillations (LCO), and transonic buffet. Flutter is a diverging oscillation caused by interactions between the structural dynamic and aerodynamic characteristics of the aircraft. LCO, which is related to flutter, is a limited-amplitude, self-sustaining oscillation possibly

L-92-12102

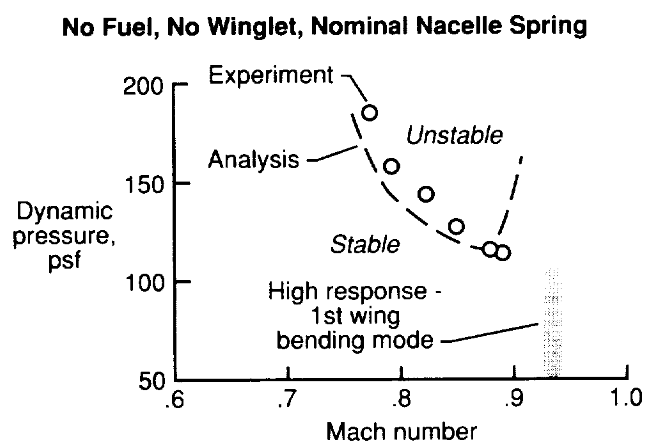

Experimental and predicted flutter boundary of a large transport aircraft.

caused by "classical" shock boundary-layer interactions or nonlinear engine nacelle strut stiffness. Transonic buffet is an irregular oscillation caused by shock-induced boundary-layer separation at transonic speeds. The study was a cooperative effort between NASA and Boeing to investigate and understand the various aeroelastic phenomena associated with advanced high-speed transport configurations and to provide a database to evaluate linear state-of-the-art and CFD unsteady aerodynamic and aeroelastic methods.

An aeroelastic model of a high-speed transport was tested in the Transonic Dynamics Tunnel (TDT). A photograph of the model mounted in the tunnel test section is presented in the figure. The wing had a supercritical airfoil, a removable winglet, and a flow-through engine nacelle. The rigid fuselage half-body provided realistic flow over the wing and removed the wing from the wind-tunnel wall boundary layer. In addition, wing internal fuel was simulated and could be varied remotely.

The aircraft parameters that were varied included fuel load, nacelle spring stiffness, nacelle flow blockage, winglet (on/off), and angle of attack. For each configuration tested, high buffeting response of the first wing bending mode was encountered in a narrow portion of the transonic region. Flutter boundaries obtained for several of the configurations tested were compared with 2-D strip theory (with corrections) predictions.
(Donald F. Keller, 41259, and Stanley R. Cole)
Structures Directorate

Micromechanics-Based Computer Code for Composites Stress Analysis

Microcracks in composites can grow to produce ply cracks and delaminations that seriously degrade these materials. Stress analyses of such microcracks must account for the local fiber-matrix configuration and material properties. The present micromechanics-based computer code (MICSTRAN) was developed for this purpose.

Airy's stress functions from the literature provided the analytical basis for this user-friendly computer code that runs on a personal computer. After a diamond or square arrangement is selected for the fibers, input involves elastic

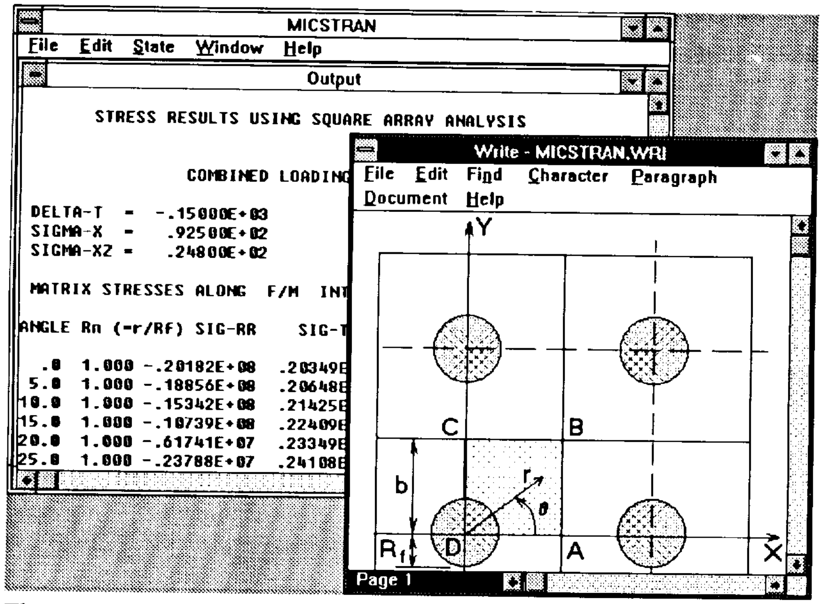

The MICSTRAN user interface under MS Windows™ environment.

and thermal properties for the fiber and matrix. In addition, any of the six components of applied stress, as well as thermal loading, can be specified. Output consists of composite elastic properties and all six components of local stress in the matrix and fiber or along the fiber-matrix interface. (See figure.)

MICSTRAN provides a micromechanics approach for developing composites with improved cracking resistance and also provides a computational basis for predicting the onset of cracking in composite structures. MICSTRAN is available through the Computer Software Management and Information Center (COSMIC).
(Rajiv A. Naik, 43457, and J. H. Crews, Jr.)
Structures Directorate

Flutter Study of Simple Business-Jet Wing Conducted in TDT

General-aviation companies often cannot afford to design and build a complex wind-tunnel flutter model for use in aircraft design and certification. Computer analysis using accurate flutter prediction codes can therefore play an important role, since many design parameters can be evaluated in a comparatively short time and at lower cost. The purpose of this program was to obtain experimental transonic flutter data on a simple and inexpensive flutter model. The data will be used to evaluate CFD aeroelastic codes, such as CAP-TSD (Computational Aeroelasticity Program - Transonic Small Disturbance) theory, that would be used in design and certification of future aircraft.

A simple semispan model of a typical business jet was fabricated and tested in the Transonic Dynamics Tunnel (TDT). A photograph of the model mounted in the TDT test section is shown in the figure. The wing consisted of an aluminum plate of varying thickness to which balsa wood was bonded and contoured to form a supercritical airfoil. A winglet was mounted at the wing tip, and a fairing was used to provide more realistic wing root aerodynamics. The baseline configuration consisted of the wing, root fairing, and winglet. The model was also tested without the winglet and with a tip boom intended to simulate the winglet mass with negligible aerodynamic effects.

Flutter boundaries for the three configurations presented in the figure are plotted as normalized flutter dynamic pressure (Q/Q*) versus Mach number, where Q* is the flutter dynamic pressure at Mach = 0.60 for the baseline configuration. The flutter boundary for the wing without the winglet was as much as 12 percent higher than for the baseline configuration. The flutter boundary for the winglet simulator, however, was less than 5 percent lower than that for the baseline. This small difference indicated that winglet mass affected the flutter characteristics of the wing much more than winglet aerodynamics.
(Donald F. Keller, 41259)
Structures Directorate

Gridless Solution Algorithm for Euler/Navier-Stokes Equations

Historically, computational fluid dynamics (CFD) methods for

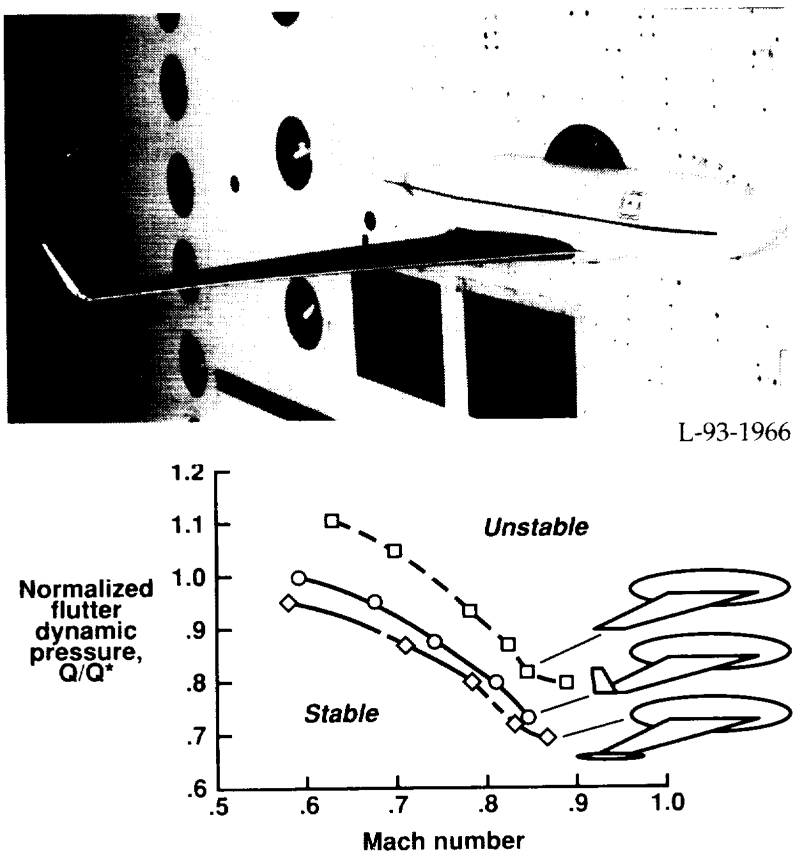

Effect of winglets on flutter characteristics of a transport wing.

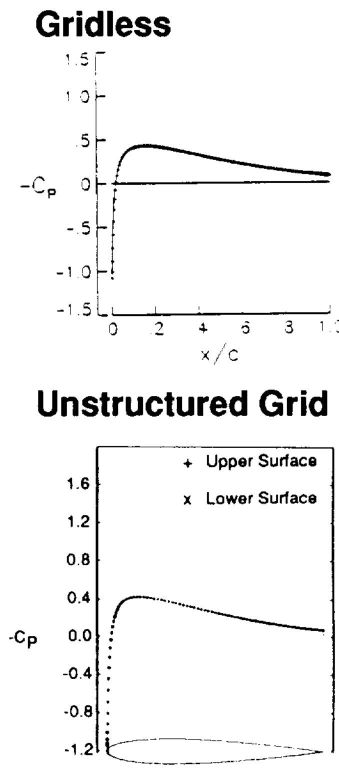

Navier-Stokes solutions for NACA 0012 airfoil. $M_\infty = 0.5$; $\alpha = 0°$; $Re = 5000$.

solving the Euler and Navier-Stokes equations have used either structured or unstructured grids. Since either type of grid has its advantages, no method has emerged superior to the other. A method that uses only clouds of points and does not require that the points be connected to form a grid was developed. The advantage of the gridless approach is that the points can be more appropriately located and clustered, leading to far fewer points being required to solve a given problem. The method can be used to analyze general geometries in a single-block computational domain and allows direct implementation of spatial adaptation. The governing partial differential equations (PDE's) are solved directly by first performing local least-squares curve fits in each cloud of points and then analytically differentiating the resulting curve-fit equations to approximate the derivatives of the PDE's. Since differences, metrics, lengths, areas, and volumes are not computed, the method is neither a finite-difference nor a finite-volume type approach. The gridless CFD approach has the potential to resolve the problems and inefficiencies associated with methods that require grid points to be connected. Consequently, it offers great potential for accurately and efficiently solving viscous flows about complex flight vehicle configurations.

Steady pressure coefficients (C_p) on the NACA 0012 airfoil were calculated using the Navier-Stokes equations for $M_\infty = 0.5$, $\alpha = 0°$, and $Re = 5000$. A comparison of gridless and published unstructured grid calculations shows very good agreement.
(John T. Batina, 42268)
Structures Directorate

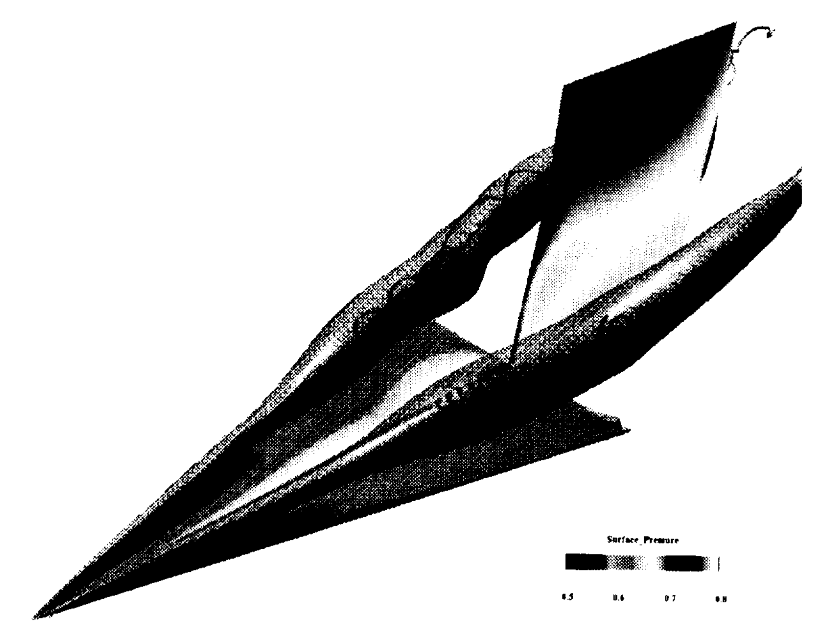

Flow-field and pressure contours for flow past a delta-wing/vertical surface at M = 0.4, α = 35°, and Re = 10 000.

Tail Buffet of a Delta-Wing/Vertical-Tail Configuration

A delta-wing/vertical-tail configuration was used to simulate, study, and control buffet of aircraft vertical tails. This multidisciplinary problem is solved in time using the compressible, unsteady full Navier-Stokes equations, the aeroelastic equations of motion for bending and torsional vibrations, and interpolation equations for the grid deformations due to the tail aeroelastic equations. The Navier-Stokes equations are solved using an implicit, upwind, flux-difference splitting method, and the aeroelastic equations are solved using the Galerkin method and a five-stage Runge-Kutta scheme.

Flow past the wing-tail configuration was calculated for a free-stream Mach number (M) of 0.4, a wing angle of attack (α) of 35°, and a Reynolds number (Re) of 10 000. The tail is modeled as a homogeneous, uniform, rectangular beam with a rectangular cross section. A grid of O-H type is used in the computational solutions. The figure shows surface pressure contours, total pressure isosurfaces, and vortex-breakdown critical points at an instant in time. **(Samuel R. Bland, 42272, Osama A. Kandil, and Steven J. Massey) Structures Directorate**

Flexible Swept Vertical-Surface Capability Added to CAP-TSD Aeroelasticity Code

The CAP-TSD (Computational Aeroelasticity Program - Transonic Small Disturbance) code was modified to allow aeroelastic calculations on aircraft with swept, flexible vertical surfaces. The major modifications include 1) adding terms to the TSD potential equation to account for swept shocks on the vertical surfaces, 2) devising a method to shear the grid vertically such that it conforms to the planform of the vertical surface, and 3) adding structural flexibility by computing the generalized aerodynamic forces in the structural equations of motion.

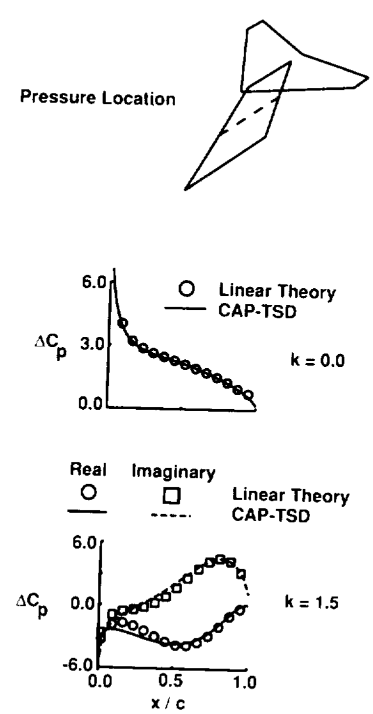

Lifting pressures on AGARD T-tail configuration.

To demonstrate the accuracy of the modifications, calculations were performed on an AGARD T-tail configuration shown at the top of the figure. The jump in surface pressure coefficient (ΔC_p) versus fraction of local chord (x/c) is shown for a fin twist mode shape at M = 0.8 and at reduced frequencies (k) of 0.0 (center of figure) and 1.5 (bottom of figure) near the midspan of the vertical fin. The unsteady results were computed by oscillating the vertical fin harmonically in twist for several cycles of motion. In order to compare the CAP-TSD results with linear aerodynamic theory, the linear equation coefficients were used. Comparisons show that for both the steady and unsteady cases, CAP-TSD is in excellent agreement with linear theory.
(John T. Batina, 42268, and Elizabeth M. Lee-Rausch) Structures Directorate

Multidisciplinary Design Optimization To Improve Aircraft Performance

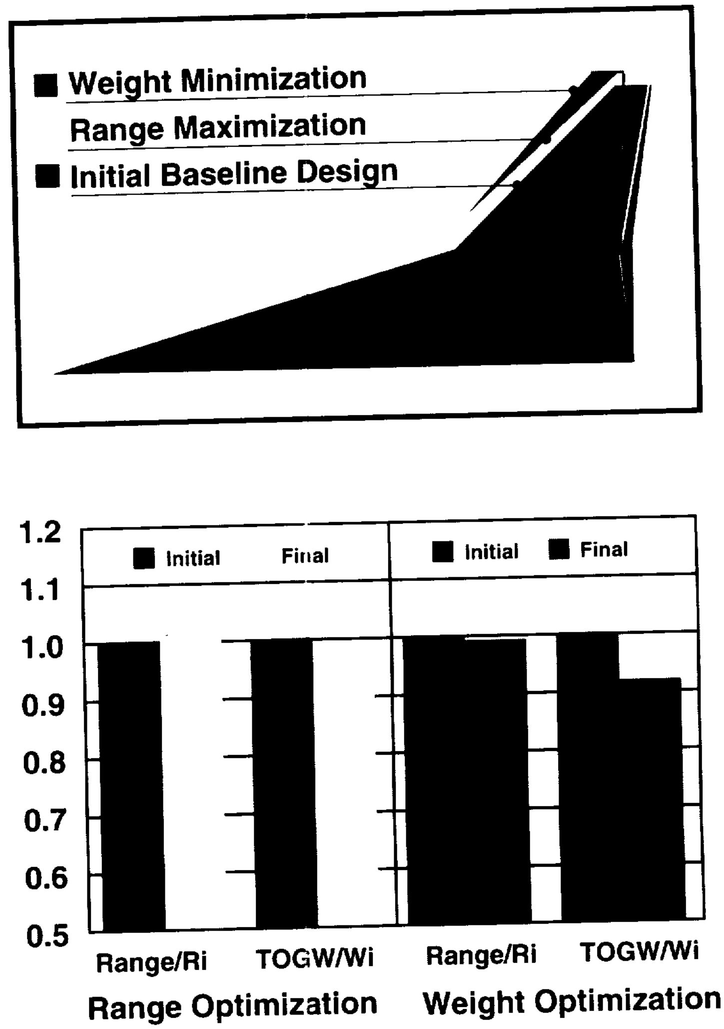

Effects of wing planform changes on performance characteristics of High-Speed Civil Transport.

The goal of multidisciplinary design optimization is to integrate the design of aircraft such that effects from various disciplines are accounted for simultaneously. In a design study, an optimizer is coupled to the analysis system, which consists of linear-theory aerodynamics codes, parametric weight analysis, and a complete mission evaluation that utilizes the rigid-wing drag polars. The optimization is a sequence of approximate problems where costly constraints and objectives are linearized with respect to the parametric description of the design problem. Since simple linearizations are generally valid only near the point at which they are calculated, limits are placed on the changes that can be made to the design parameters during a cycle.

The resulting integrated aerodynamic and performance design system was applied to the wing planform of the Langley High-Speed Civil Transport 2.4e configuration. Shape was optimized for either a maximum range objective or a minimum weight objective. Initial and final planforms are shown at the top of the figure, and aircraft performance is shown at the bottom. In the range maximization problem, the aircraft range was increased with a negligible change in take-off gross weight. For the weight minimization problem, take-off gross weight was

decreased with a negligible change in aircraft range.
(Jaroslaw Sobieski, 42799, Eric R. Unger, and Peter G. Coen)
Structures Directorate

Calculation of Wing Flutter Characteristics Using a Navier-Stokes Aerodynamic Method

The transonic speed range has been a main focus of recent computational developments, because flutter dynamic pressures are typically lower in this speed range. To meet the challenge of analyzing aeroelastic responses at transonic speeds, methods that use Euler and Navier-Stokes aerodynamics are being developed and validated.

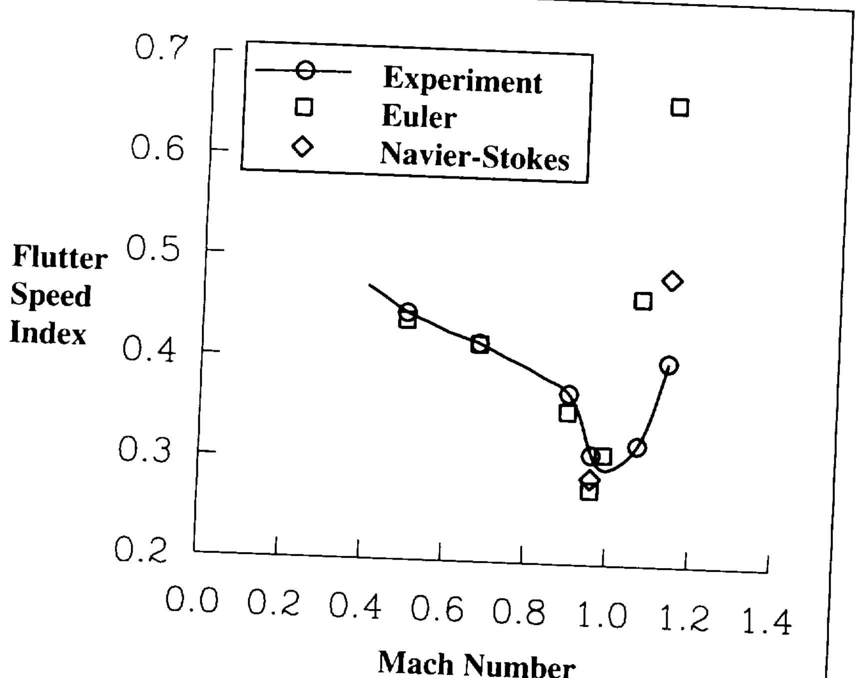

Comparison of computed flutter predictions with experimental data for 45° swept-back wing.

To allow for aeroelastic analysis, the structural dynamics equations of motion and a dynamic mesh capability were added to the CFL3D Euler/Navier-Stokes computational aerodynamics code. That code was developed in the NASA Langley Computational Aerodynamics Branch, Fluid Dynamics Division. The flow equations were integrated simultaneously with the structural dynamics equations, and the dynamic mesh was used to model wing motion. The resulting method was applied to a standard aeroelastic wing that was tested for dynamic response in the Langley Transonic Dynamics Tunnel (TDT). Flutter analyses were previously performed using Euler aerodynamics. The results in the figure show that at subsonic free-stream Mach numbers, the flutter speed index that was computed using Euler aerodynamics agrees well with the experimental values. However, at speeds above Mach one, the computed flutter boundary indicates an earlier rise than what was measured. The flutter characteristics were then recomputed at free-stream Mach numbers of 0.96 and 1.141 using Navier-Stokes aerodynamics. These results, which are included in the figure, indicate that the effect of including fluid viscosity on the flutter characteristics is to delay the rise in the flutter boundary for supersonic free-stream Mach numbers.
(Elizabeth M. Lee-Rausch, 42269, and John T. Batina)
Structures Directorate

Implicit Shear Deformation Model for Rotor-Blade Analysis

Analytical modeling of rotor blades as beams is an important part of comprehensive aeroelastic rotorcraft analyses. The introduction of composite materials and elastic couplings into rotor-blade design, however, reduces the accuracy of beam-based analyses, because classical beam modeling assumptions are violated. Improvements in beam modeling for these types of structures are gained by accounting for local cross-section deformations (warping) and shear-mode deformations.

A beam was recently studied that was both extension-twist and bending-shear coupled. The bending in one principal direction produced shear in the orthogonal direction; thus, the shear deformation had a significant effect on the beam bending stiffness. By including additional shear-related

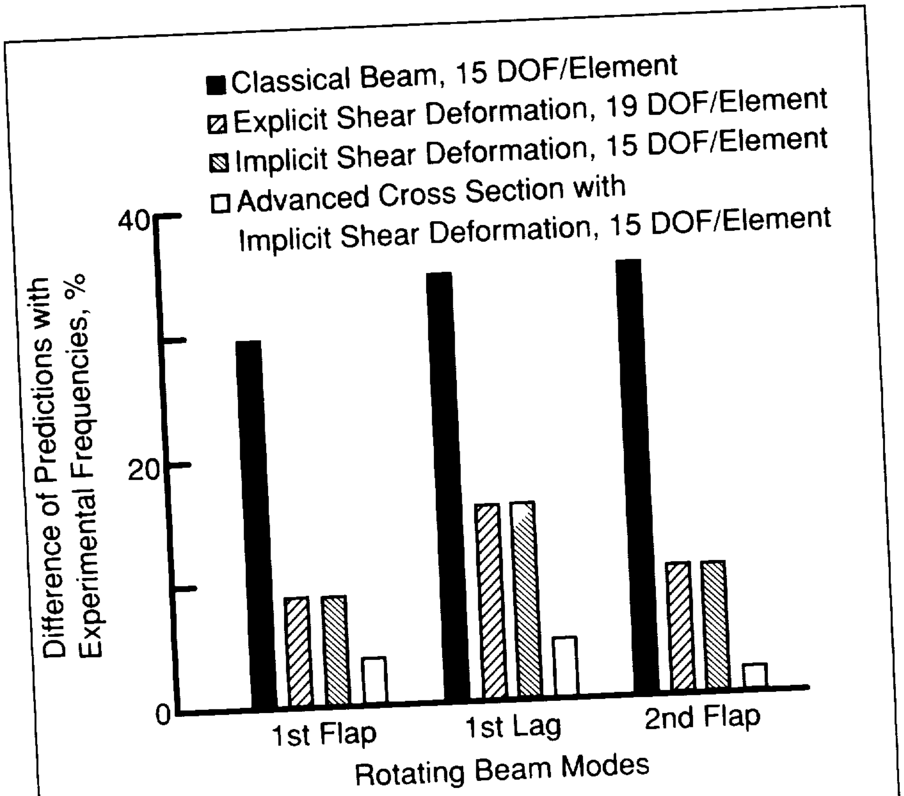

Frequency predictions of four beam models.

degrees of freedom (DOF) in a beam model, the effect of the shear deformation may be captured as shown in the figure (classical and explicit models). An implicit shear deformation model was developed in which the explicit shear-related degrees of freedom are statically condensed from the solution. The results show that the response obtained with the implicit model is identical to that obtained with the explicit model. Further, the implicit model decouples the local cross-section degrees of freedom from the global (spanwise) degrees of freedom, so that advanced cross-section analyses may be used in unison with the implicit beam model. The advanced cross-section analyses are generally finite-element based and account for nonclassical warping influences on cross-section stiffness properties. The improved results associated with coupling an advanced cross-section analysis with the implicit beam model are also illustrated in the figure. The implicit beam model has been successfully implemented in a rotorcraft comprehensive analysis known as UMARC (University of Maryland Advanced Rotor Code), which is available to and used by the rotorcraft industry.

(Mark W. Nixon, 41231)
Structures Directorate

Hypersonic Aeroelastic Analysis Method Using Steady CFD Aerodynamics

Computational fluid dynamics (CFD) methods offer the advantage of more accurate prediction of surface pressures compared with the more conventional linear aerodynamic methods, but at the expense of a significantly higher computational burden than the linear methods. For example, the computational burden increases when unsteady pressures are required for flutter analyses.

For very high-speed flight (typically Mach numbers at and above 5), a quasi-steady approximation may be made. This approximation assumes that the reduced frequencies associated with the important structural vibration modes that contribute to flutter are very much less than 1. Under these conditions, time constants of the unsteady flow are so small that the aerodynamics acting on the vehicle can be assumed to have "no memory," and certain steady CFD calculations should closely approximate the real and imaginary parts of certain other unsteady CFD calculations. If this is the case, then, for very high-speed flight, flutter analyses

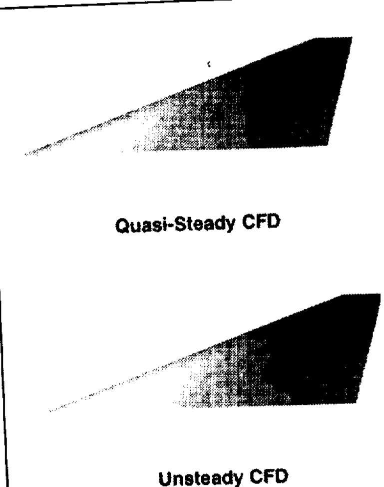

Comparison of imaginary parts of pressures obtained with quasi-steady and unsteady CFD methods.

shows the boundary defined by flutter points that were obtained with the tip mass. The measured flutter boundary agreed fairly well with preliminary analytical predictions for this configuration. The experimental flutter data obtained will be beneficial for validation of the analytical flutter codes that are used to define requirements necessary to verify that the aircraft will be free of flutter.
(Moses G. Farmer, 41263, and James R. Florance)
Structures Directorate

Cessna Citation X Flutter-Clearance Tests

Business-jet aircraft must be designed so that flutter will not occur within the flight envelope with a 20-percent safety margin. Traditionally, wind-tunnel model tests have played an important role in the flutter certification process of new designs. The objective of the present cooperative study with Cessna Aircraft was to provide wind-tunnel flutter data for use in ensuring that the wing of the Citation X will be safe from flutter.

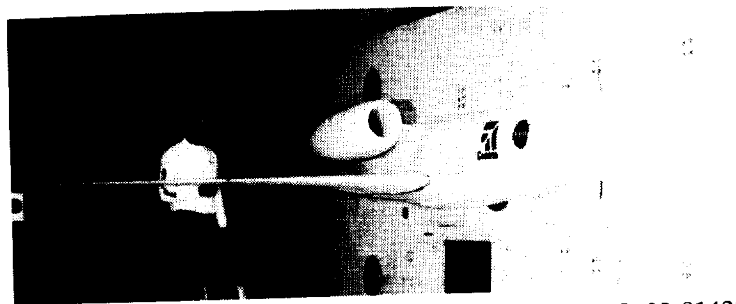

L-93-01432

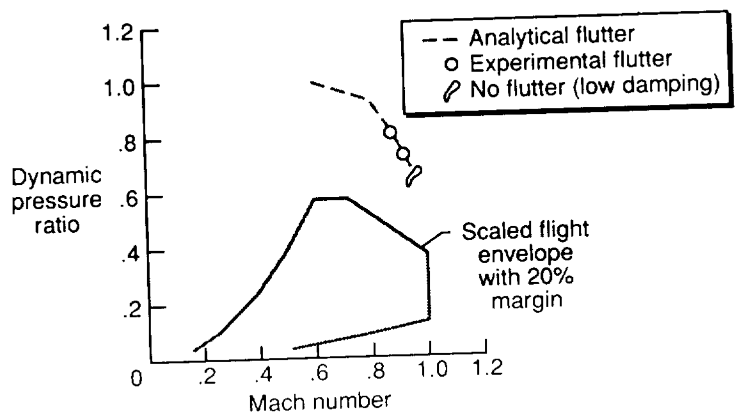

Flutter boundary for Cessna Citation X aircraft.

A 1/4-scale semispan aeroelastic model of the Citation X wing was tested in the Transonic Dynamics Tunnel (TDT). A photo of the model mounted in the TDT test section is shown in the figure. The rigid fuselage half-body and flow-through nacelle simulated the effect that the aircraft fuselage had on the flow over the wing. The wing model included an aileron that could be tested undeflected or at a deflection angle of 4°.

Eight configurations were tested to obtain data to correlate with flutter and aileron-reversal analyses. A wing-tip-mounted aerodynamic exciter was used extensively during the test to track frequencies and estimate damping as the flutter boundaries were approached. Flutter results are shown in the figure for the configuration with nominal aileron actuator stiffness. The flutter analysis (represented by the dashed line) predicted the flutter boundary to be outside of the scaled flight envelope with a 20-percent margin. The experimental flutter points (circular symbols) obtained for this configuration correlated well with the analysis and indicated that the Citation X wing will be safe from flutter.

Tests of this type ensure that flutter or aileron-reversal problems that may exist for a new design are identified early enough in the design/development cycle that a solution (fix) can be effected in a timely manner with minimum impact on cost and schedule. In addition, wind-tunnel tests such as those described here reduce the number of more costly flight flutter tests.
(José A. Rivera, Jr., 41207, and Moses G. Farmer)
Structures Directorate

Laser-Beam Welding of Aluminum-Lithium Structures

Significant cost and weight savings can be realized through the use of advanced materials and

employing this quasi-steady approximation would have the advantage of the accuracy associated with unsteady CFD calculations but without the associated disadvantage of increased computational burden.

Two calculations were performed for a cantilevered hypersonic wing. Imaginary surface pressure contours associated with the pitch mode are shown in the figure. The contour on the top was obtained with the quasi-steady method; the contour on the bottom was obtained with unsteady CFD calculations. These pressures compared very favorably and confirm the success of the method. These more accurate quasi-steady aerodynamics will result in a more realistic flutter sizing of hypersonic vehicles and could result in lighter structural weights.
(Robert C. Scott, 42838)
Structures Directorate

Boeing 777 Flutter Model Test Completed in TDT

Commercial transport aircraft must be designed so that flutter will not occur within the flight envelope that includes all conditions the aircraft may encounter. The objective of this program was to verify that the Boeing 777 wings will have the required flutter margin of safety throughout the aircraft flight envelope.

A dynamically scaled semispan aeroelastic model of the Boeing 777 wing was tested in the Langley Transonic Dynamics Tunnel (TDT) as part of the flutter clearance program. A photograph of the model installed in the TDT is shown in the figure. The rigid fuselage half-body simulated the effect that the aircraft fuselage will have on the flow over the wing. The model engine nacelle was designed to simulate air mass flow through the aircraft engine. The model was designed so that the amount of simulated fuel in the wing and the stiffness of the engine pylon could be changed remotely.

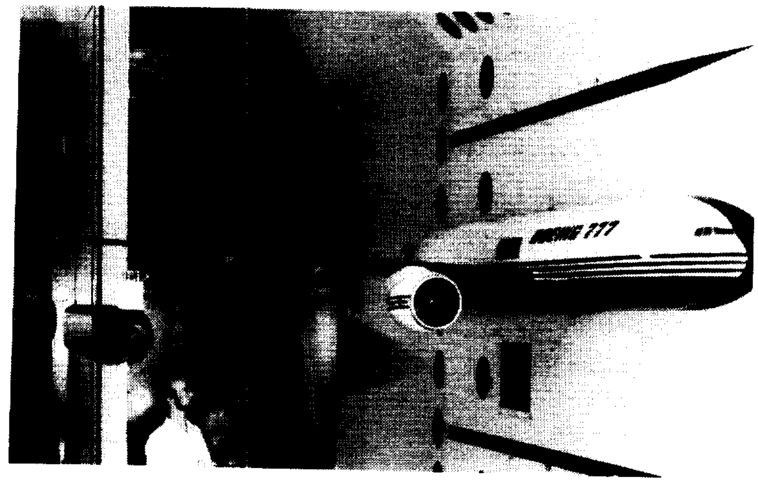

L-92-08248

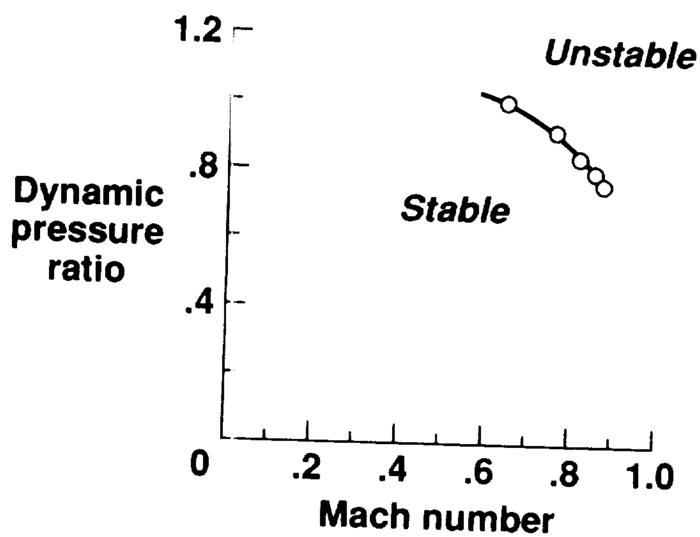

Configuration with wing-tip mass.

Ten configurations were tested throughout the simulated flight envelope of the aircraft without obtaining flutter. Parameters that were varied included wing fuel, engine pylon stiffness, and the stiffness of the structure that attached the wing to the fuselage. To create a configuration for which flutter would occur, a mass was installed in the wing tip. The figure

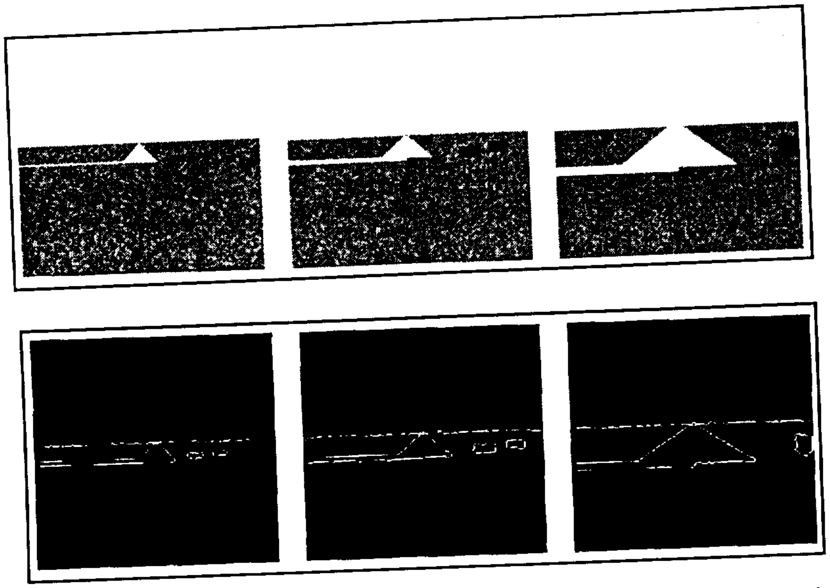

Detected edges: runway, taxiway, horizon, and buildings (lower portion of figure); from frames 1, 16, and 30 in the sequence of simulated images (upper portion of figure).

sors or replacement of a poor-resolution image with onboard high-resolution computer-generated imagery (CGI) to provide a much more effective "synthetic vision" display. The objective of this study was to develop methods for the analysis of images from passive millimeter wave (PMMW) imaging systems to delineate objects of interest. A sequence of simulated images as seen from an aircraft as it approaches a runway was obtained from a model of a passive millimeter wave sensor. Thirty frames from this sequence of images (200 × 200 pixels) were analyzed to identify and track objects in the image using the Cantata image processing package within the visual programming environment provided by the Khoros software system. An image analysis and object tracking system was implemented in Khoros and tested on the sequence of digitized images.

A number of different algorithms were evaluated and appropriate parameters were selected during the design of this analysis/tracking system. The final system consisted of the following stages: smoothing using a spatial averaging filter for noise reduction; detecting edge pixels using a recursive filter; bridging discontinuities in detected edges using an edge-linking operator; labeling objects in each image in this sequence; and comparing them with objects in subsequent frames to locate corresponding objects. The figure shows three of the thirty images and the corresponding detected edges of objects.

The preliminary results presented here using thirty simulated images clearly demonstrate the potential of image analysis methods for detection and tracking of objects in a dynamic scene. Analysis of real images is well-known to be a much more difficult task, particularly in real time. To realize a practical system, new vision algorithms for analyzing sensor-captured images and for fusing information from various sensors will be studied under an existing grant with Penn State University.

(Randall L. Harris, Sr., 46641, and Rangachar Kasturi)
Flight Systems Directorate

Effects of Historical and Predictive Information on the Ability To Predict Time to an Alert

The early detection of a subsystem problem that is developing during flight is potentially important, especially for twin-engine aircraft used in extended operations over water, because the extra time may allow the flight crew to consider and/or try more options for dealing with the failure. Some faults have the potential for such early detection, which may lessen the severity of the problem and thus enhance the safety of the flight. However, current automated monitoring systems do not alert the flight crew of a failure until a parameter value has exceeded an alert limit. To detect a failure before this limit is exceeded, the flight crew must monitor subsystem parameters and make predictions of their behavior. Recent parameter history or near-term parameter prediction may help the flight crew make long-term predictions. To analyze the benefits of such information, an experiment was conducted that evaluated the effects of recent historical and near-term predictive information

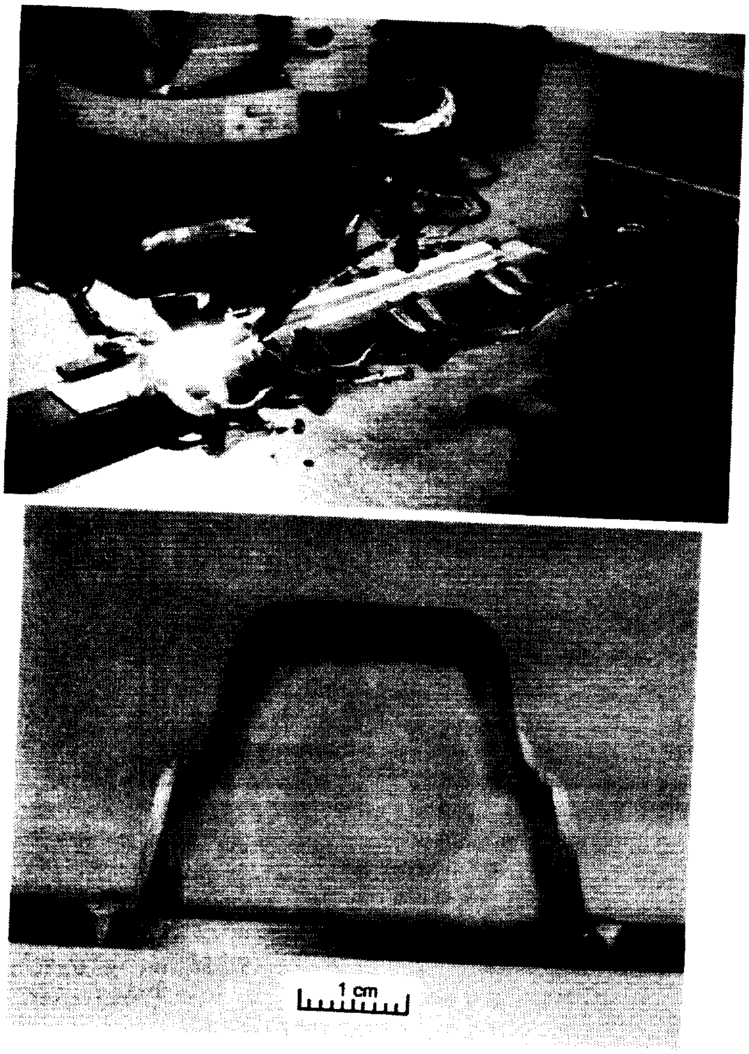

Laser welding of Al-Li built-up structures.

innovative processing methods. The addition of lithium to aluminum alloys decreases the density and increases the strength and elastic modulus; aluminum-lithium (Al-Li) alloys are therefore ideal candidates for aerospace structures. Laser welding is a candidate joining process for fabricating Al-Li built-up structures with applications in airframe components and cryogenic tanks and dry bay structures for space transportation systems. Studies on the Space Shuttle external tank have shown that using advanced materials and manufacturing methods yields a 20- to 30-percent structural weight savings and a 20- to 40-percent reduction in manufacturing costs.

An interagency agreement was established between NASA Langley Research Center and the Department of the Navy, Space and Warfare Systems Command (SPAWAR) to investigate the feasibility of laser-beam welding of Al-Li structural components at the Applied Research Laboratory of Pennsylvania State University. Initial results concluded that laser-beam welding was a feasible process to join Al-Li alloys using the built-up structure approach for aircraft structures. The figure shows a superplastically formed Al-Li stiffener being laser welded to a thin-gage sheet to form a skin-stiffened component. Because the laser-beam welding process exhibits very localized heating, structures can be welded so as to minimize the thermal distortions and the heat-effected zone; joint efficiencies are thereby increased. Laser-beam welding of Al-Li alloys compared with conventional welding processes offers significantly higher processing speeds (i.e., 200 in./min), elimination of the need for weld lands (facilitating the use of thin-sheet product), and the ability to automate.

(Cynthia L. Lach, 43133, and Dick M. Royster)
Structures Directorate

Methods for Detecting Objects Using Restricted Visibility Sensors

As part of the Advanced SenSor and Imaging Systems Technology (ASSIST) effort, imaging systems and display interface concepts are being evaluated to enhance a pilot's view of the outside environment under restricted visibility conditions. During the landing maneuver (the most critical phase of flight), a method of identifying important features (such as runways, taxiways, buildings, and other aircraft) within an imaging sensor's display is required. Such a capability could enable the "fusing" of multiple imaging sen-

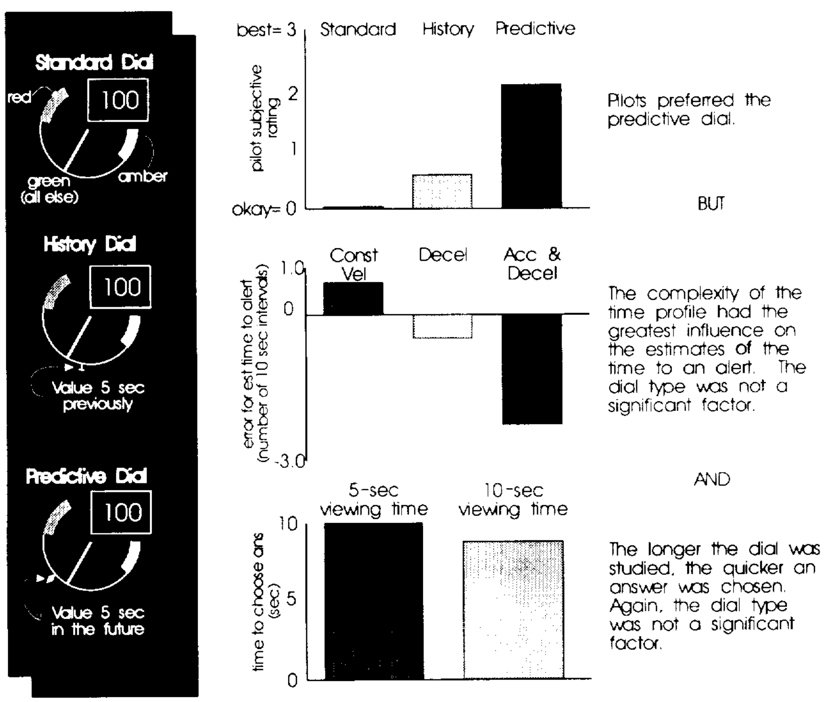

Displays and results from use of historical and predictive information in estimating the time to an alert.

on the pilot's ability to make long-term predictions of when a parameter will reach an alert range.

Eighteen current transport-line pilots participated as test subjects in a workstation study. Each subject estimated the time it would take for a parameter value to enter the alert range, that is, the amber or red area marked on a dial, using each of the three displays depicted in the figure. The history dial showed the parameter's value 5 seconds ago, and the predictive dial showed the parameter's value 5 seconds into the future. The subjects watched the dials in motion for either 5 or 10 seconds with a time profile that had either constant velocity, deceleration, or acceleration followed by deceleration. They then estimated the time that would be required for the parameter to reach an alert range. The experiment was designed so that neither the actual value nor the predictive bug entered an alert range during the evaluation time. Results were evaluated based on accuracy of response, time to respond, and pilot subjective ratings.

The primary results indicated that although pilots preferred the near-term predictive information, the predictive dial did not improve their ability to make long-term predictions. Instead, the time profiles greatly affected the pilots' estimate of the time to an alert (see figure). The constant-velocity time profiles had the least error. The pilots seemed to have difficulty accounting for the acceleration and the deceleration in the other two time profiles. Also, as the time to study the dial increased, pilots required less time to estimate the time to an alert; that is, performance with the 10-second viewing time was better than with the 5-second viewing time.

These results indicate that the simple solution of showing near-term predictive information in the history or predictive dial format does not necessarily improve a pilot's ability to make long-term predictions.
(Anna C. Trujillo, 48047)
Flight Systems Directorate

Pilot Cognitive Activities for Flight Deck Information Management

Increasing automation on modern commercial flight decks has resulted in flight tasks becoming less physically intensive and more cognitive in nature. This has focused attention on the need to consider the pilot's cognitive processing capabilities as part of the human engineering evaluation process. To accomplish this, techniques designed to examine the cognitive processes that individuals utilize in accomplishing tasks must be employed. One such method is "protocol analysis," requiring subjects to verbalize their thoughts while performing a task. To analyze such data, it is essential to have a taxonomy of cognitive terms, operationally defined and nonredundant, that an experimenter can use in scoring pilot protocols. The objective of the current project was to identify a concise listing of such cognitive activities regularly engaged in by individuals. All terms related to cognitive processes were identified

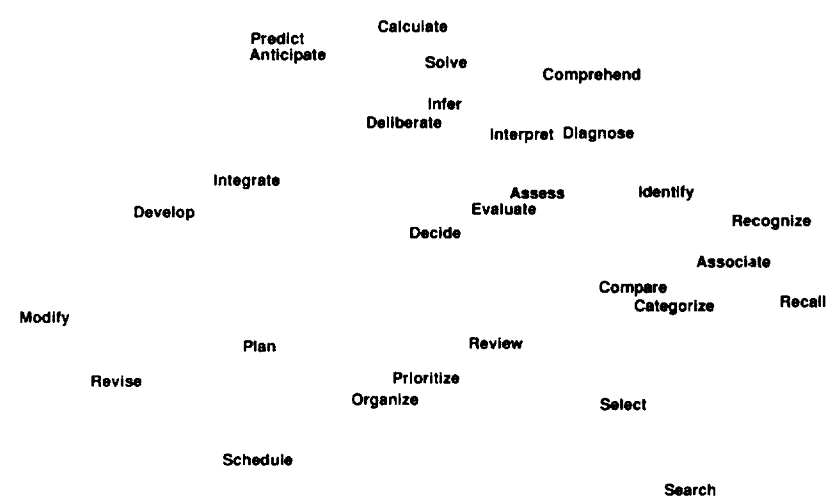

Multidimensional scaling analysis of cognitive activities.

through a dictionary search. Those items that were (1) synonymous or (2) of insufficient specificity for analysis (for example, "to think") were eliminated. This refined list consisted of 30 words. Seven subjects rated the similarity of each pair of terms (but not the term with itself). These data were analyzed using multidimensional scaling, a statistical technique that provides a visual representation of how subjects perceive items to be related. Terms located close to one another in the space are judged by subjects to be related, while terms lying far apart in the space are perceived to be unrelated.

Three important findings emerged from the results. First, "decide" was central to all other terms describing cognitive activities, underscoring the ubiquitous nature of decision making in the cognitive domain and the importance of the other cognitive processes in supporting decision making. Second, "diagnose" and "plan" occupied opposite ends of the spatial plot; each had different cognitive processes associated with it. This provides empirical evidence that planning and diagnosis represent fundamentally distinct cognitive activities, with each supported by different cognitive activities (i.e., those terms clustered around "plan" and "diagnosis"). A third finding concerns redundancies found in the original set of 30 terms. That is, subjects perceived several terms as being so similar to one another as to be virtually indistinguishable; for example, the words "analyze," "evaluate," and "assess" could be consolidated into a single term. These results constitute a taxonomy of cognitive processes that provide important information for use in flight deck experimentation and in understanding flight deck activities. Identification of the cognitive processes associated with planning and diagnostic tasks will aid researchers by focusing their efforts on examining how these processes are affected by design factors. The utility of these results was recently demonstrated in an experiment designed to examine how pilots make planning decisions related to in-flight weather diversions.

(Jon E. Jonsson, 42001, and Michael T. Palmer)
Flight Systems Directorate

Pilots' Cognitive Representations of Flight Deck Information Categories and Priorities

Increasing automation on modern commercial aircraft has made it more challenging for flight deck designers to determine what flight crews need to safely and efficiently perform their functions. Recent developments in cognitive research have shown the usefulness of psychological scaling techniques for representing human knowledge and processing structures. In applying these techniques to cognitive processes as they pertain to the flight deck, processes that are regularly engaged in by flight crews and which most directly affect the proper and safe use of flight deck systems should be targeted. Two such activities are information categorization and prioritization. The specific objective of this study was to establish, in an empirical fashion, how pilots categorize flight deck information and how they judge the relative importance of that information as they act upon it.

Two 20-element sets of experimental stimuli were randomly generated from a list of information elements enumerated in an information analysis of the Boeing 747-400. Each element in the list represented a piece or type of information found on the flight deck. Fifty-eight pilots then partic-

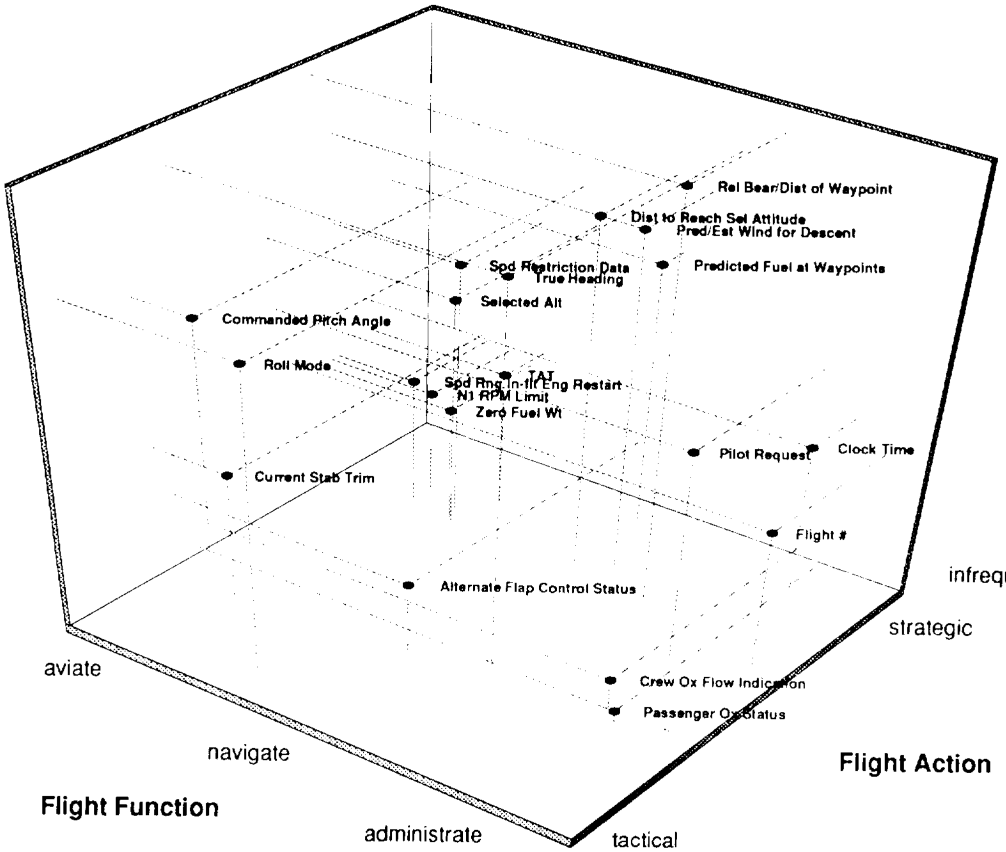

Spatial solution and interpretation of set A similarity rating.

ipated in the experiment. Each pilot used one of the two stimuli sets and did pairwise-comparison and rank-ordering tasks using their set of information elements. For the pairwise-comparison task, pilots rated the similarity of each pair of elements on a scale of one to nine. For the rank-ordering task, they ordered the information elements from most to least important. These prioritizations were performed under two separate conditions. The pilots first prioritized the elements independent of any context and then assumed the takeoff phase of flight. Under both of these conditions, the pilots were told to assume that all systems were operating normally. The data were analyzed using statistical methods that revealed common underlying groupings and dimensions of the data.

Analyses of the similarity data suggest that pilots mentally organize flight deck information along three dimensions (as shown in the figure). These three dimensions appeared to be related to the flight function (aviate, navigate, and communicate) that the information supports, the flight action (tactical and strategic) to which the information relates, and the sample rate (infrequent to frequent) at which the information is acquired. The rank-ordering analysis revealed that the pilots prioritize according to distinct clusters or categories. Based on the member elements of these clusters, the prioritization categories (in order of relative priority) were interpreted as flight control information, reference/navigation information, system information, communications information, and emergency information.

Results from this study provide a basis for understanding how pilots manage information. These results show how pilots categorize and prioritize the information with which they work. The dimensions resulting from both analyses can be used in a predictive fashion (during the design process) to evaluate a pilot's cognitive processing under different situations

and flight deck configurations. That is, the designer could infer cognitive loadings based upon each dimension, given the information that the pilot uses to perform a given task.
(Jon E. Jonsson, 42001, and Wendell R. Ricks)
Flight Systems Directorate

Method for Exploring Information Requirements Associated With Cognitive Processes

For a system to support humans in achieving the objectives for which they are responsible, it is necessary to first determine what information is required to support their tasks. Because of advanced automation, many operator tasks are becoming less physical and more cognitive. Recent developments in cognitive research have shown the utility of psychometric scaling techniques (e.g., multidimensional similarity scaling and multidimensional preference scaling) for determining human cognition and processing structures (e.g., categorization and prioritization). The data acquisition associated with these techniques is usually done in "sterile" environments (i.e., not in the domain). Using only a laboratory environment leaves questionable the applicability of the resulting cognitive models to the domain setting. The objective of the work described here was to develop a nonintrusive method for obtaining psychometric scaling data within the context of the task being analyzed and to assess the ability to compare the cognitive representations resulting from the "sterile" environment with those from the "context" environment.


Pilot with information acquisition interface. L-92-09570

The approach taken for this work was to combine existing psychometric scaling techniques with a new domain-specific, real-time method of assessing information use. With this approach, domain subjects participate in several laboratory psychometric scaling tasks that yield information regarding how the subjects perceive the information similarity (e.g., how they categorize information) and what criteria they use to determine the relative importance of the information. The domain-specific task then requires subjects to explicitly select items from the same set of information elements to perform a set of operational tasks in real time.

Data acquired during the domain tasks are then enhanced by retrospective verbal descriptions of why the subjects acquired the information. The domain-specific data acquisition was to require pilots to explicitly "select" information elements from an approach plate while flying various simulated approaches (as shown in the figure). Items on the approach plate were made illegible by a computer program, and the pilot made them legible in real time using the track ball to point at the target information and clicking the

track ball button. Multiple items could be selected at a time. Any item could be selected multiple times, and each time an item was selected it remained legible for 10 seconds. Acquisition data were formatted for analysis of what type of information was selected, when information was selected, how often it was selected, and with what it was selected.

The domain task for obtaining information in real time was demonstrated to be feasible and nonintrusive. The task was easy to administer, and the data collected allowed the examination of the relationship of cognitive processes identified by the laboratory tests (e.g., categorization and prioritization) and how information was acquired to support the domain task.
(Wendell R. Ricks, 46733,
Carl Feehrer, William H. Rogers, and John S. Barry)
Flight Systems Directorate

Compiler and Run-Time Techniques for Efficient Concurrent Object-Oriented Programming

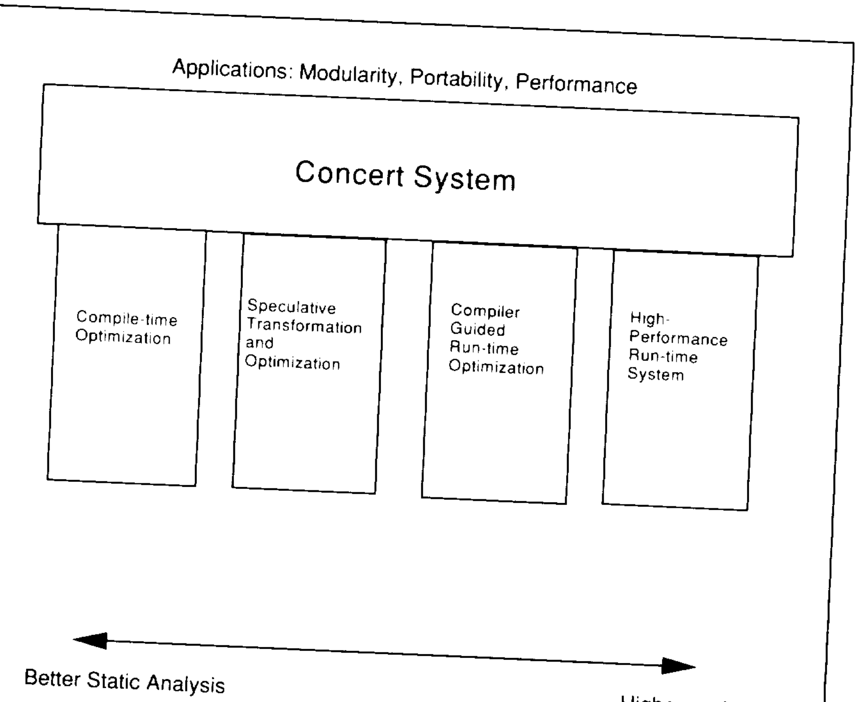

Levels of optimization in Concert system.

The introduction of concurrency complicates the task of large-scale programming. Concurrent object-oriented languages provide a mechanism for managing the increased complexity of large-scale concurrent programs. Fine-grained object-oriented approaches provide modularity through encapsulation while exposing large degrees of concurrency (i.e., exposing objects that can execute in parallel). The goal of the University of Illinois Concert project is to develop portable, efficient implementations of fine-grained concurrent object-oriented languages based on automatic grain-size tuning. A prototype Concert system has been developed, and it has been in operation on both sequential and parallel platforms. The system includes an optimizing compiler for an extended version of Concurrent Aggregates and a high-performance run-time system that runs on both Sun workstations and the Thinking Machine CM-5. Concert provides a framework for systematically extracting and exploiting the necessary information for grain-size tuning. The Concert system has four basic techniques for increasing execution grain size: compile-time optimization, speculative transformation and optimization, compiler-guided run-time optimization, and high-performance run-time systems.

This work was performed at the University of Illinois Urbana-Champaign, and it was funded in part by the Illinois Computer Laboratory for Aerospace Software and Systems block grant with the Langley Research Center.
(Kathryn A. Smith, 41699)
Flight Systems Directorate

PARADIGM Compiler for Distributed Memory Multicomputers

Distributed memory multiprocessors are increasingly being used to provide high levels of performance for scientific applications by connecting several thousand off-the-shelf microprocessors through simple low-cost interconnection networks. Distributed memory machines offer significant

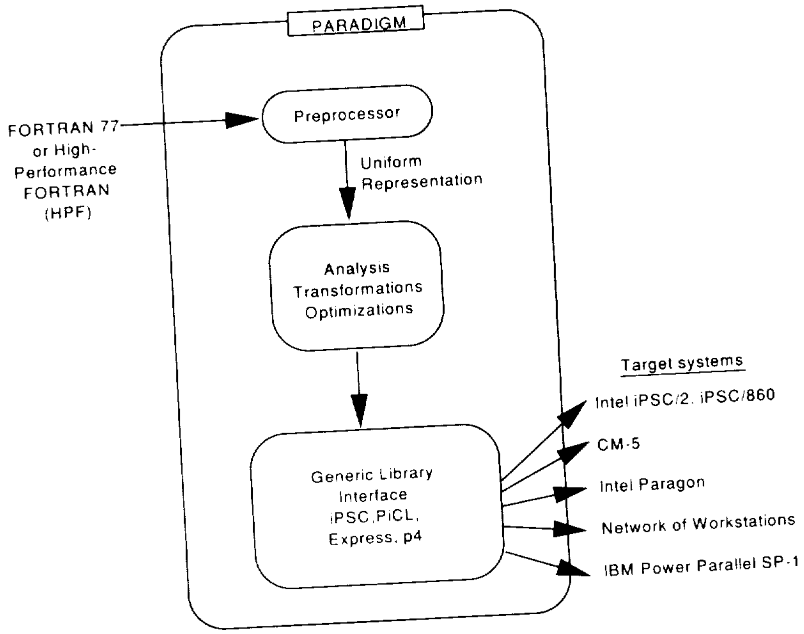

Application of PARADIGM compiler.

advantages over the shared memory multiprocessors, but they are more difficult to program. The goal of the PARADIGM project at the University of Illinois is to automate the mapping of sequential FORTRAN 77 and High-Performance FORTRAN programs to distributed memory multicomputers with little or no user intervention. A prototype PARADIGM compiler has been developed and evaluated. The PARADIGM compiler performs automated data partitioning using a constraint-based approach. Its capabilities include parallelization of sequential programs into Single Processor Multiple Data stream (SPMD) parallel programs, automated data partitioning, synthesis of high-level collective communication, multithreaded execution, and simultaneous exploitation of functional and data parallelism. The compiler currently outputs code for the Intel iPSC hypercube, the Intel Paragon, the Connection Machine CM-5, the IBM Power Parallel SP-1 systems, and the network of workstations.

This work was performed in the Coordinated Science Laboratory at the University of Illinois Urbana-Champaign, and it was funded by the Illinois Computer Laboratory for Aerospace Software and Systems block grant with the Langley Research Center, the National Science Foundation, the Office of Naval Research, and the Semiconductor Research Corporation.
(Kathryn A. Smith, 41699)
Flight Systems Directorate

Prototyping Environment for Real-Time Systems (PERTS)

Traditionally, real-time systems are built by first developing the application software and then by tuning the operating system and validating timing constraints using ad-hoc exhaustive techniques. This approach is time consuming. Exhaustive simulation and testing are reliable and feasible only for systems that use clock-driven or cyclic scheduling strategies. Consequently, almost all real-time systems that support critical applications are clock driven. Such a system is difficult to maintain and extend. The Prototyping Environment for Real-Time Systems (PERTS) is built on recent theoretical advances in real-time scheduling and validation, and it will facilitate new approaches in building real-time systems, thus resulting in systems that are responsive and robust and easy to modify and validate. The PERTS system has reusable software modules and tools for the design and development of time-critical systems. These software modules implement well-known and emerging real-time scheduling and resource management strategies that lead to robust and easy-to-maintain systems. The user can select and use a subset of them, and together with an operating system kernel that allows external schedulers and resource managers, assemble an effective run-time support system. The PERTS tools support reliable and efficient methods for the validation and performance profiling of systems built on these strategies.

This work was performed at the University of Illinois Urbana-Champaign, and it was funded in part by the Illinois Computer Laboratory for Aerospace Software and Systems block grant with the Langley Research Center.
(Kathryn A. Smith, 41699)
Flight Systems Directorate

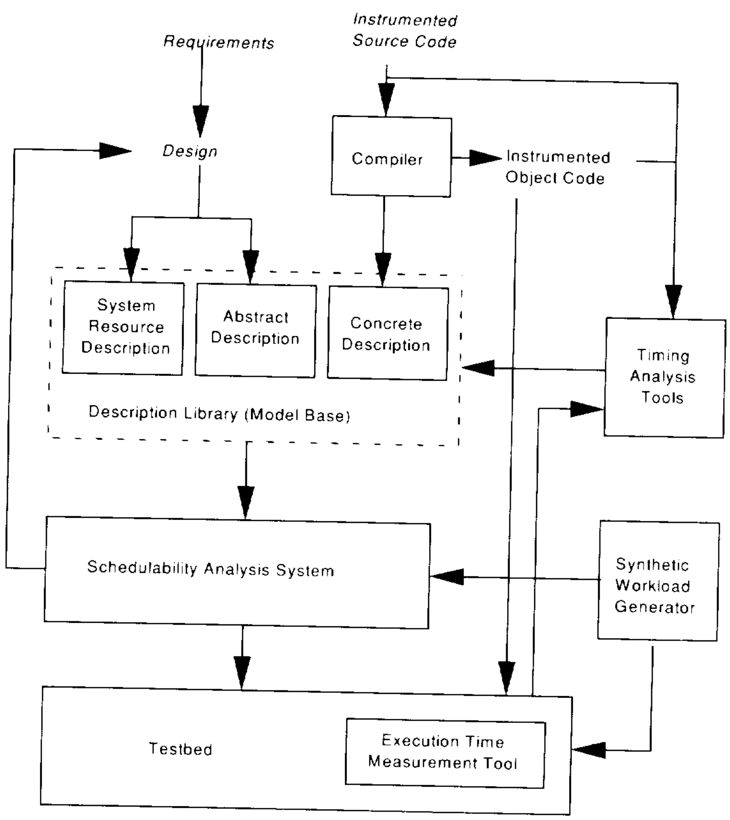

PERTS system architecture.

System for Automated Learning of Heuristics

Many application problems in real-time environments are controlled by heuristics that are difficult to adjust a priori. A prototype learning system, TEACHER, has been developed and evaluated. The goal of the TEACHER system is to automate the adaptation of these heuristics to the environment in real time with little user intervention. The system has been applied to learn better load migration policies in a distributed network of computers, new placement policies for tasks in massively parallel computing systems (these results can be applied to placing computational fluid dynamics computations on such systems), more accurate stereo vision algorithms for depth perception (these results can be applied in image recognition and understanding), faster search algorithms for scheduling and optimization, and circuit testing and logic synthesis.

This work was performed in the Coordinated Science Laboratory at the University of Illinois Urbana-Champaign, and it was funded in part by the Illinois Computer Laboratory for Aerospace Software and Systems block grant with the Langley Research Center.
(Kathryn A. Smith, 41699)
Flight Systems Directorate

Extended Cooperative Control Synthesis Methodology

Cooperative Control Synthesis addresses the problem of how to design control laws for piloted, high-order multivariate systems and/or nonconventional dynamic configurations in the absence of flying qualities specifications. This is accomplished by the simultaneous solution of two coupled optimal control problems. One optimal controller can be thought of as representing a pilot's control dynamics, and the other represents a vehicle's augmentation control law dynamics. This research focused on improving the process of Cooperative Control Synthesis by incorporating a more accurate representation of the pilot's control dynamics. The simplified pilot model in the original Cooperative Control Synthesis was superseded by the Modified Optimal Control Model. This model is based upon an optimal control model of a human operator as developed by Kleinman, Baron, and Levison (Bolt, Beranak, and Newman, Inc.). The improved process is primarily a result of enhancing representation of the pilot's dynamics through inclusion of the delay inherent in information acquisition and processing by the pilot. This delay is placed at each of the pilot's outputs, and it is treated as part of the plant dynamics for determination of pilot regulation and filter gains (as shown in the figure). The goal of this improved methodology, referred to as Extended Cooperative Control Synthesis, was to provide control laws with better pilot tracking performance and improved subjective rating.

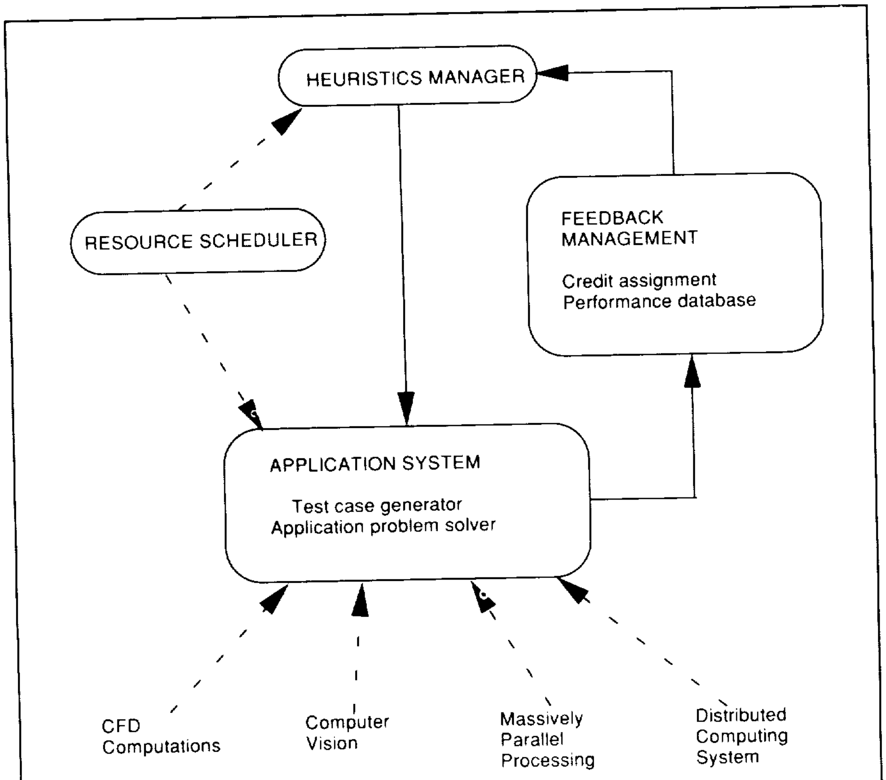

Overview of TEACHER system.

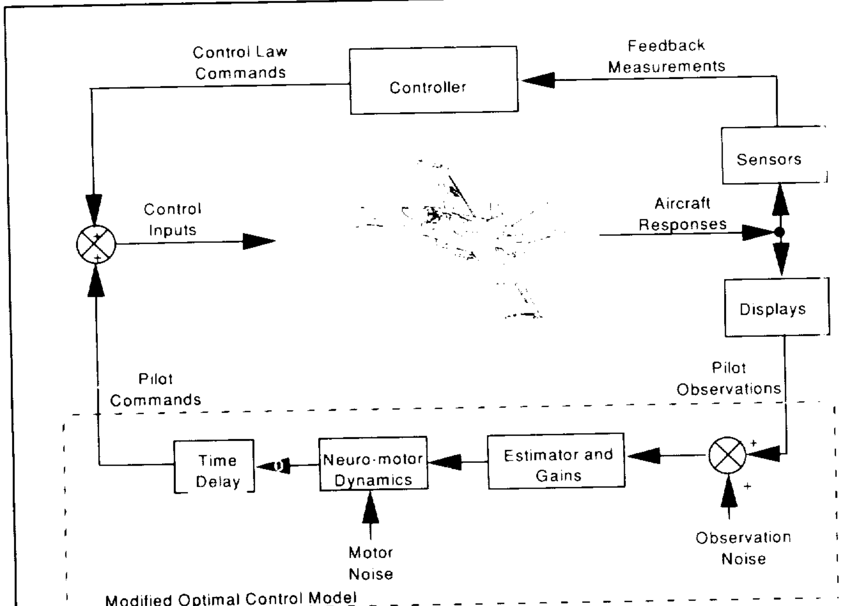

Extended Cooperative Control Synthesis block diagram.

Control laws were synthesized using the extended methodology for an acceleration command system in a compensatory tracking task. This design was then analyzed and compared with similar designs using the original methodology. Analysis results obtained with the extended method show more than a 20-percent reduction in predicted root mean square tracking error, and they significantly improved predicted Cooper-Harper ratings over those obtained from the original formulation.
(John B. Davidson, 44010)
Flight Systems Directorate

Total Reliability Modeling Interface for Fault-Tolerant Architectures

The Table-Oriented Translator to the ASSIST Language (TOTAL) is a computer program that enables the practicing design engineer to access the sophisticated mathematics of reliability analysis from a high-level system description without sacrificing the mathematical rigor that is vital for meaningful results. The TOTAL program, as its name implies, uses a spreadsheet style for system input. The system is described in terms of commonly used elements for fault-tolerant systems (such as processors, input/output devices, or sensors) and the strategies used to obtain high reliability (such as replicated redundancy, passive or active sparing, and pooled spares).

The TOTAL program constructs a more detailed reliability model in the Abstract Semi-Markov Specification Interface to the SURE Tool (ASSIST) language by enumerating the failure modes that are inherent in the high-level description. System failure criteria must also be supplied by the designer.

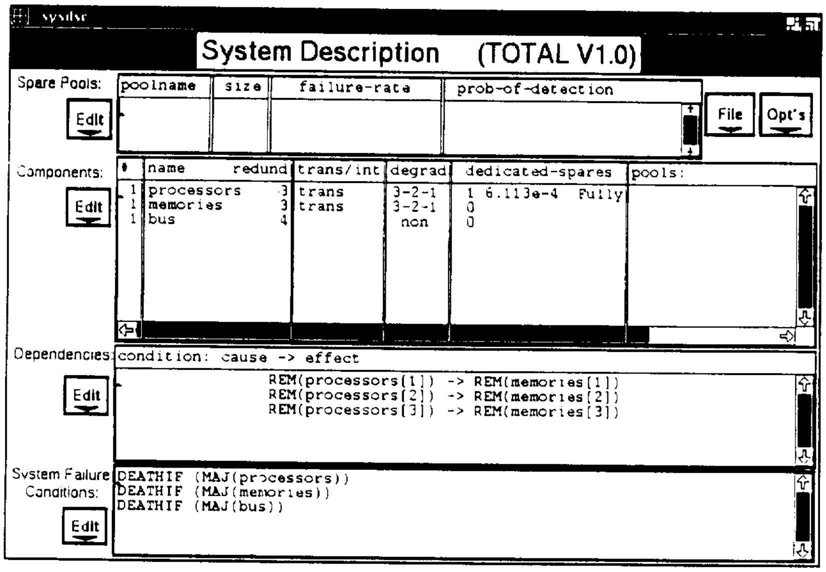

System description panel of example system.

The ASSIST model is then automatically solved by the Semi-Markov Unreliability Range Evaluator (SURE) program using designer-supplied component failure rates. Since a design-level description can result in reliability models that are far too large to be solved, the process includes model reduction techniques to enable many complex systems to be evaluated while providing the designer with rigorous error bounds on the results. The TOTAL program also includes a menu-driven input to guide infrequent users to correct system description. These menus are similar in concept to input forms for database data entry. The menu program was written using the Transportable Applications Environment (TAE). The TOTAL program is written in ANSI-standard "C". The entire package will run under DEC-Windows Motif on VAX/VMS systems and under Motif windows on Sun SPARCstations.

(Sally C. Johnson, 46204)
Flight Systems Directorate

Nonlinear Modeling Using Multivariate Orthogonal Functions

Aerodynamic forces and moments acting on aircraft at high angles of attack depend nonlinearly on the aircraft motion and control surface deflections. High-fidelity modeling of this multivariate dependence is required for studying the dynamics and the control of aircraft in this flight regime. Generally, determining which nonlinear terms should make up the model is very difficult, and current methods amount to sophisticated trial and error. The objective of this research was to develop a technique for accurately identifying nonlinear models, based only on experimental data. The model must include appropriate terms, have accurate values for the parameters multiplying each term, and possess good predictive capability.

The developed technique first generates multivariate orthogonal modeling functions from the data. Because of orthogonality, a model of the true multivariate nonlinear relationship can be found precisely and efficiently using an expansion of orthogonal modeling functions selected so as to minimize prediction error. Each included orthogonal modeling function is then decomposed into an exact expansion of ordinary polynomials, so that the final model can be interpreted as selectively retained terms from a multivariable power series expansion.

The approach was demonstrated by modeling a subsonic wind tunnel database for the F-18 aircraft. In the figure, aircraft motion variables and control surface deflections from a push-over pull-up flight test maneuver were input to both the wind tunnel database and the polynomial model for the vertical aerodynamic force C_Z. The polynomial model successfully captured the multivariate nonlinear relationship embodied in the wind tunnel database. The small mismatch from 16 to 22 sec was due to extrapolation by the polynomial model for unmodeled unsteady effects at high angles of attack in the wind tunnel data.

The technique described here is capable of generating an accurate polynomial representation of a multivariate nonlinear relationship based on experimental data alone. The resulting model has smooth derivatives, exhibits good predic-

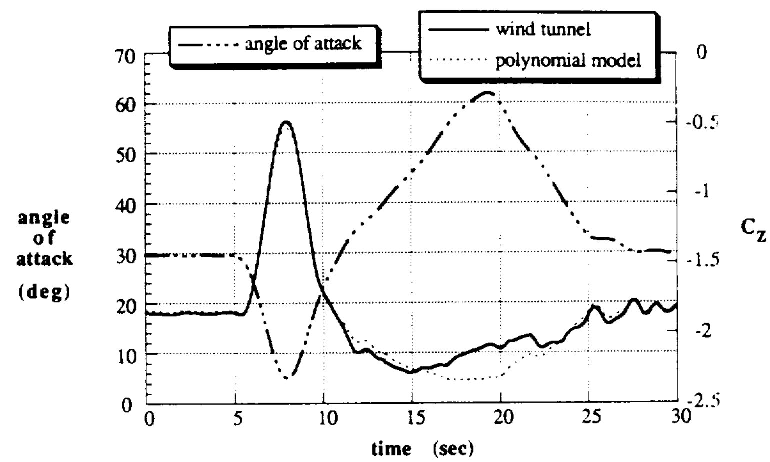

F-18 vertical aerodynamic force during push-over pull-up maneuver.

tive capability, and provides insight into the underlying nonlinear dependence. The method is general, and it can be used for other applications requiring accurate modeling of multivariate nonlinear relationships, such as biomedical modeling or economic forecasting.
(Eugene A. Morelli, 44078)
Flight Systems Directorate

Pad-Abort-to-Runway Maneuvers for Lifting Reentry Vehicles

In parallel with the development of low-cost vertically launched, horizontally landed manned spacecraft concepts, the feasibility of performing an abort from the launch pad to a landing at a nearby runway was investigated using engineering analysis, real-time piloted simulations, and maneuver optimization software tools. Based upon the HL-20 lifting-body simulation model, the effects of various abort motors, maneuver strategies, and thrust-vectoring capabilities were studied. Combinations of vehicle weight, lift-to-drag ratio, steady winds, and launch pad/ abort runway orientations were evaluated to develop manual and automatic control strategies for successful launch site aborts. Worst-case abort geometries (pad to runway) were identified, and necessary thrust levels were determined. Optimized maneuvers were generated.

Initial proposals for the launch pad abort scenario of these reentry vehicles included parachute descent to an ocean recovery; these "wet" aborts would necessarily require considerable rescue resources, and reuse of the vehicle would be questionable. The demonstrated capability of a "dry" abort makes these vehicles a more attractive and lower risk candidate for next-generation access to space.
(E. Bruce Jackson, 44060, and Robert A. Rivers)
Flight Systems Directorate

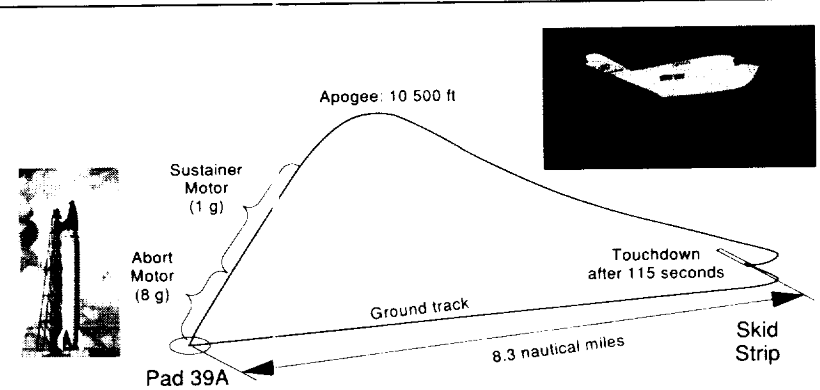

Typical pad-abort-to-runway maneuvers for lifting body vehicles with thrust-vectoring controls and sustainer rockets.

Elucidation of Phosphorescence Quenching in Photomagnetic Molecules by Positron Annihilation Spectroscopy

Platinum octaethyl porphyrin (Pt-OEP) is an efficient, room temperature phosphor under ultraviolet excitation. The phosphorescent triplet state (T_1*) is readily quenched by oxygen (O_2). This phenomenon is being utilized as the basis for global air pressure measurements in aerodynamic facilities at various laboratories. The exact

Atmospheric Environment	Doppler Broadening Parameter (S)	
	(Pt-OEP)	(Mg-OEP)
Pure Nitrogen	0.0893±0.0003	0.0891±0.0005
Pure Air	0.0931±0.0005	0.0900±0.0005
Pure Oxygen	0.0939±0.0004	0.0888±0.0007

Summary of Doppler broadening parameter (S) values in UV-irradiated (Pt-OEP) and (Mg-OEP) phosphors under different atmospheric conditions.

mechanism by which the O_2 molecule quenches the ($T_1^* \rightarrow S_0$) transition is still largely unknown. On the face of it, the diamagnetic excited singlet state S_n^*, which feeds the T_1^* state via internal conversion and intersystem crossings, would not be affected by O_2; only the magnetic T_1^* state, which can interact with the paramagnetic O_2 molecule, is affected.

To test this hypothesis, we compared the positron annihilation radiation Doppler broadening parameter (S) in UV-irradiated (Pt-OEP) and magnesium octaethyl porphyrin (Mg-OEP) porphyrins immersed in pure nitrogen, pure air, and pure O_2 media at atmospheric pressure. The (Mg-OEP) is not known to phosphoresce under UV excitation (i.e., no admixture of singlet and triplet states has been observed in this molecule). We should, therefore, expect no differences in the Doppler broadening parameter (S) in (Mg-OEP), but we expect increasing broadening in (Pt-OEP) under the same atmospheric conditions. Experimentally, it has been found that the Doppler broadening parameter (S) is constant in (Mg-OEP), but it increases with the mole fraction of O_2 in the surrounding medium in (Pt-OEP), thus indicating that the O_2 molecule quenches both the S_n^* and T_1^* excited states in (Pt-OEP). The experimental results of these measurements are summarized in the table.

(Jag J. Singh, 44760, Abe Eftekhari, and S. V. N. Naidu)
Electronics Directorate

Frequency Domain State-Space Identification Tools

Classical identification of linear systems for model verification and control design is commonly performed using concepts from spectral analysis. Computer-implemented fast Fourier transform algorithms have facilitated manipulation of large sets of data. Linear time-invariant systems are completely characterized in discrete-time analysis by their pulse responses. Measured pulse must be converted into a compact parametric form for use in analyses. Curve fitting algorithms have been used extensively for this purpose; in the algorithms a particular model structure is selected and the parameters are evaluated by minimizing the error between the model and estimated pulse responses.

Recently, a slightly different approach to obtain a state-space model from frequency response data was developed. The algorithm solves for a state-space model in two steps. First, the spectral estimates of the pulse responses are fitted with a model in matrix polynomial form. Then, smoothed pulse responses, computed from the polynomial parameters, are used with realization theory for order determination and a state-space realization. One advantage of this approach is the ability to recover state-space models from linked chains of transfer functions with minimum window distortions. Also, the algorithm, programmed using the commercial software program MATLAB, easily combines data obtained with different sampling rates into a single model.

Experimental validation used data from the Middeck Active Control Experiment (MACE), which is a NASA-sponsored Space Shuttle flight experiment being developed by the Massachusetts Institute of Technology. The first figure shows a sketch of the laboratory model. This model has gimbals, torque wheels, and an active member for actuation, and rate sensors and strain gages for response sensing. The available data record is limited to simulate down-linking of on-orbit data. The second figure shows a comparison of an experimental frequency response, using the torque wheels and a rate sensor, with the identified model obtained using 849 unevenly spaced spectral lines. Matching of the model with test is excellent except at low frequencies.

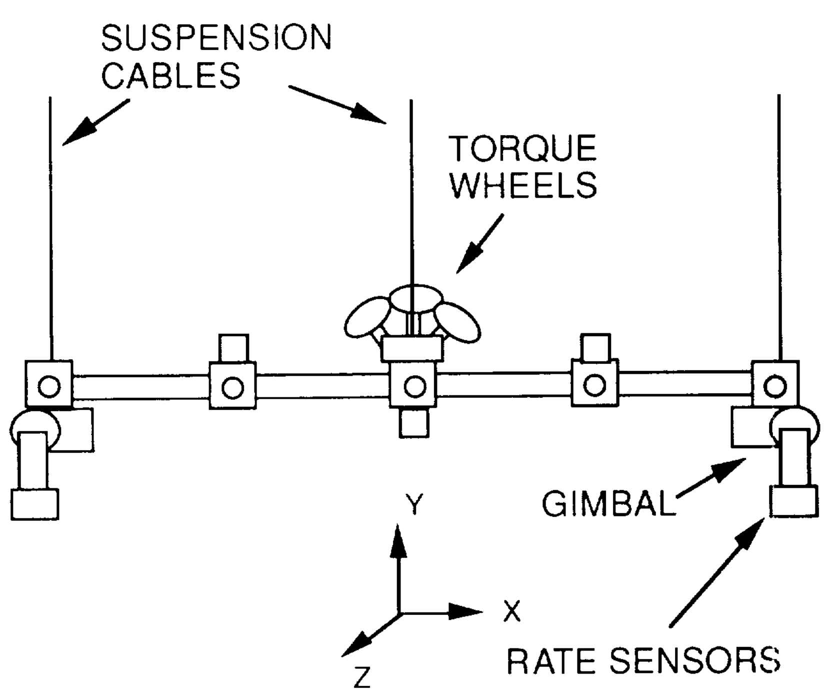

Middeck Active Control Experiment (MACE) laboratory model.

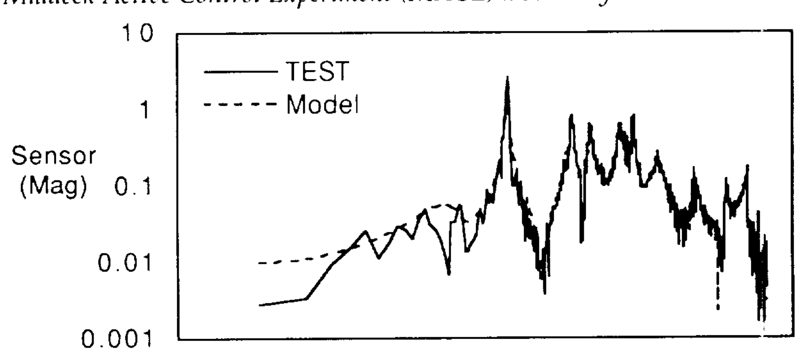

Comparison of identified MACE model with test.

The low-frequency matching can be improved by performing separate tests that target the low frequency, patch the frequency response function, and compute a unified model using this new approach.

(Lucas G. Horta, 44352, and Jer-Nan Juang)
Structures Directorate

Trajectory Optimization Based on Differential Inclusion

Methods for trajectory optimization can be divided into two different categories, namely direct and indirect approaches. Indirect approaches are based on the Pontryagin Minimum Principle. Their merits lie in high precision and the ability to identify subtle details of the trajectory. Major drawbacks are the involvement of artificial costates and the necessity to guess the optimal switching structure a priori. Direct approaches rely on a discretization of the infinite-dimensional optimal control problem into a finite-dimensional nonlinear programming problem. In practice, these approaches are very popular because of their usually robust convergence, even from bad initial guesses, and of the low level of expertise required by the use. A major stumbling block in the turnkey application of these approaches to general optimal control problems encountered in aerospace engineering is the convergence difficulty sometimes encountered for singular optimal control problems.

The achievement of the present work is to introduce a new discretization technique for optimal control problems. By employing a description of the dynamical system in terms of its attainable sets in favor of using differential equations, the controls are completely eliminated from the system model. Besides reducing the dimensionality of the discretized problem compared with state-of-the-art collocation methods, this approach also alleviates the search for initial guesses from where standard gradient search methods are able to converge. The new discretization shows robust convergence behavior, even for singular optimal control problems.

The figure gives a schematic representation of the differential inclusion concept. The equations of motion of the dynamical system are not enforced directly. Instead, for every i greater than 1, the states

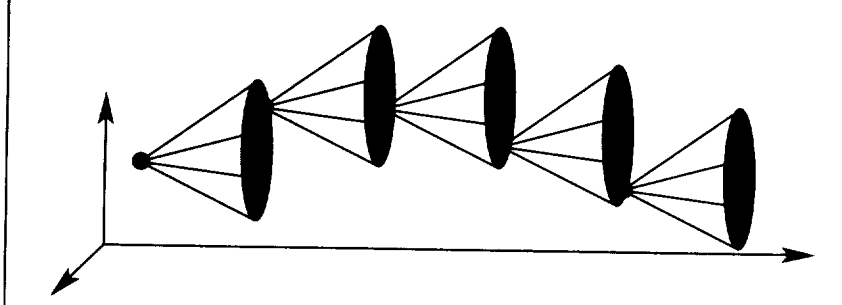

Schematic representation of differential inclusion concept.

at any node number i + 1 are prescribed to lie within the set of states that are attainable from the states at node i.
(Daniel D. Moerder, 46495)
Flight Systems Directorate)

Advanced Information Processing System

The Advanced Information Processing System (AIPS) is the result of a 10-year effort led by NASA with significant funding from the U. S. Army, the U. S. Air Force, and the Strategic Defense Office. The purpose of this effort was to develop digital systems that can support high-performance and critical real-time control tasks. The AIPS development was performed by Charles Stark Draper Laboratory under contract to NASA. The AIPS is not a single system. It is a group of building blocks and models from which a wide variety of systems can be designed to match applications that range from small undersea systems to the largest heavy space launch systems.

The AIPS building blocks are a set of fault-tolerant processors that can provide reliable computing power at distributed sites, with each site computer tailored to the performance and reliability requirements of that site. The sites can be connected through different types of networks, such as mesh, ring, and bus. Once a network is selected to provide, for example, the lowest cost alternative, the selected network can then be tailored to provide the required performance and reliability. An important feature of the AIPS is that the fault-handling mechanisms consume relatively little of the system throughput, and they are largely transparent to the user. Another important feature of the AIPS is that models are available that allow the designer to accurately assess the characteristics of a proposed AIPS configuration for a given requirement. The AIPS has been used by the U. S. Navy in its Unmanned Undersea Vehicle, and it has been selected for the ship control system on the Sea Wolf submarine.
(Felix L. Pitts, 46186)
Flight Systems Directorate

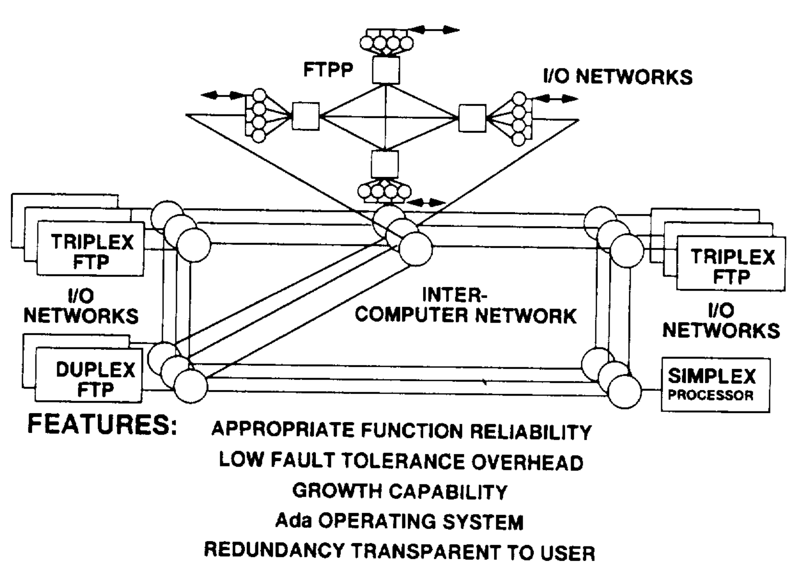

AIPS example configuration.

Nondescent Technique for Constrained Minimization

Practical systems are defined by systems of constraints. Techniques for optimizing these systems must, to be reasonably effective, be capable of accounting for these constraints in the optimization process. Another feature of practical

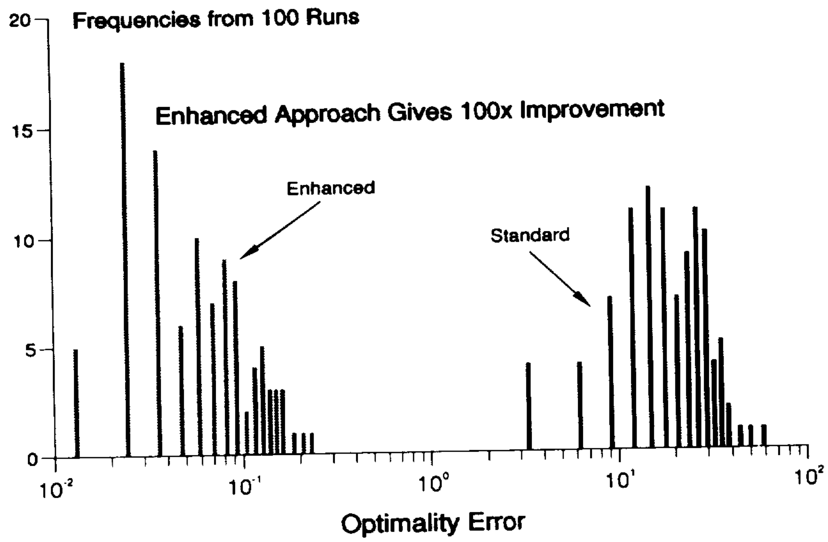

Enhanced algorithm performance from nondescent technique for constrained minimization.

systems is complexity. Very often, this results in the system's performance response to parameter selection being characterized by numerous local minima. Unfortunately, optimization procedures capable of rigorously treating constraints are typically based on local expansion theory, and they can get "caught" at local minima. These local minima, in turn, might yield significantly worse performance than the global optimum or other better local minima. Optimization algorithms based on local expansions are referred to as "descent algorithms" because they operate by calculating a sequence of search values, each of which returns increasingly good performance. Nondescent algorithms are an alternate approach to optimizing functions. These methods are not typically vulnerable to local minima, but they have not been capable of treating constraints, except through rather poor approximate means (such as penalty functions).

The achievement of this work was to reformulate a generic differentiable constrained optimization problem as an unconstrained problem, so that it could be solved by robust nondescent methods. The solution of the unconstrained problem solved by such methods satisfies the necessary conditions for optimality in the original constrained problem.

The figure shows the enhancement in algorithm performance from the use of this approach by displaying the distribution of optimality error (e.g., nonzero norm of the Kuhn-Tucker conditions) for the new approach and a standard penalty-based approach. A genetic algorithm was employed as a nondescent optimization engine in obtaining energy-optimal control settings for an aerospace plane model at a particular operating system. Trim, vertical acceleration, and dynamic pressure constraints were present. One hundred Monte Carlo experiments were conducted using the new approach. Results from these experiments were compared with a like number of runs for a number of penalty-based schemes, and then the best were chosen for comparison.
(Daniel D. Moerder, 46495)
Flight Systems Directorate)

Automatic Adaptive Finite-Element Mesh Refinement

The creation of adequate finite-element models for complex structural configurations is a time-consuming aspect of design trade-off studies and design optimization. To reduce engineering time expended in model development, automatic adaptive finite-element mesh capabilities have been developed. This capability continuously refines the mesh to improve accuracy where it is required.

Although considerable research on automatic adaptive mesh refinement techniques for in-plane two-dimensional and three-dimensional structural applications has been carried out, comparatively less research has been done for built-up shell structures, such as those found in aircraft, rockets, and automobile bodies. Automatic adaptive meshing involves when to remesh, where to remesh, and how to remesh. Error measures have been developed to indicate when solutions need improved accuracy and hence a finer mesh. Refinement indicators point to those regions that need finer mesh. Rule-based algorithms determine how the mesh is to be redivided. User-controlled options, with the

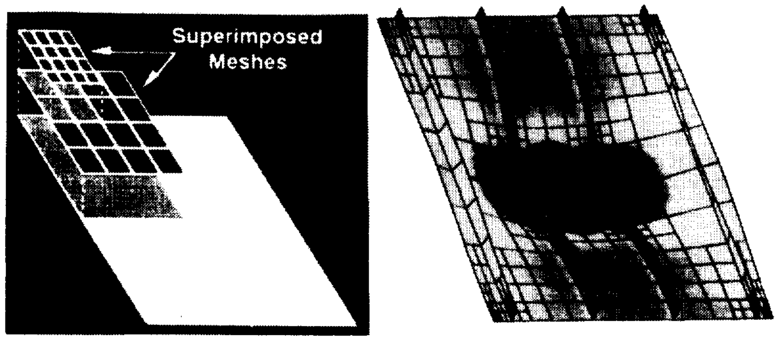

Automatic adaptive mesh superposition demonstrated on stiffened compression panel.

engineer in the loop, can be utilized for semiautomatic adaptivity.

The figure illustrates an automatic adaptive refinement using a superposition technique for remeshing an aluminum panel with discontinuous blade stiffeners. Such stiffener terminations are often required in practice, but their presence generates stress concentrations that can lead to failures. Because adaptive meshing techniques may lead to distorted finite-element meshes that introduce undesirable modeling error, a mesh superposition method has been developed and demonstrated. This method introduces little or no element distortion, provided the initial mesh is regular in shape. As depicted in the figure, refinement is done by superimposing a second (and subsequent) regular mesh over the first. (Here the total response is the sum of the responses of the superimposed meshes.) Refinement indicators identify the regions at the stiffener terminations as requiring fine-mesh superposition. Using this technique, the superposition-based meshes remain regular in shape.
(Jerrold M. Housner, 42907)
Structures Directorate

BVI Noise Prediction From Computed Rotor Aerodynamics

Blade-vortex interaction (BVI) noise is a highly impulsive helicopter noise source that occurs when rotor blades strike, or pass very close to, tip vortices previously shed into the rotor's wake. This noise occurs most often when the rotor is in descent.

A numerical prediction procedure, linking three independent prediction codes, was developed to predict the aerodynamics and acoustics of three-dimensional rotor BVI. The first code in the series is the Comprehensive Analytical Model of Rotorcraft Aerodynamics and Dynamics (CAMRAD/JA) code, which predicts the rotor performance, dynamics, and tip vortex wake trajectories and strengths. These predictions are utilized by the second code, the Full Potential Rotor code (FPRBVI), to predict the unsteady blade surface pressures. The FPRBVI code is an improved version of the NASA Ames Full Potential Rotor code (FPR). This improved version was developed by McDonnell Douglas Helicopter Company under a NASA Langley

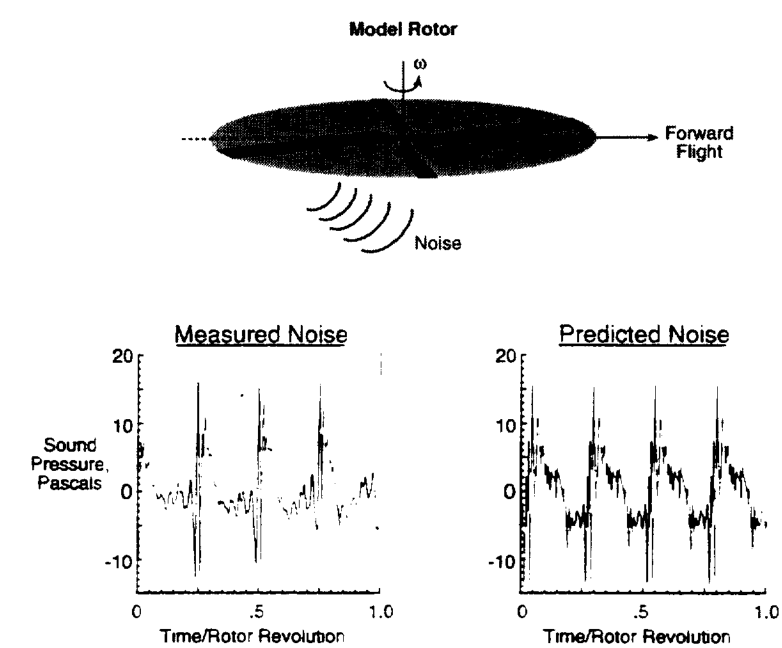

Comparison of measured and predicted noise for descent rotor condition.

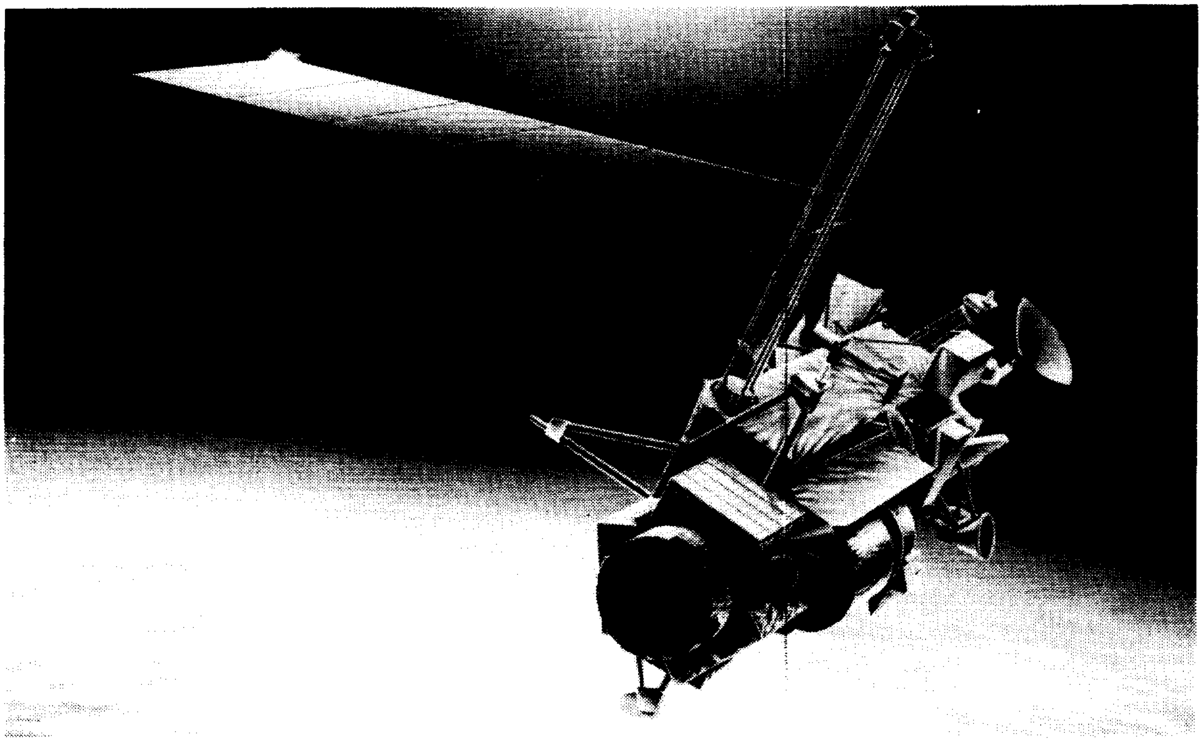

UARS global probe of Earth's upper atmosphere. L-91-07474

contract to include the entire tip vortex wake for a specified number of rotor revolutions. Previously, the code required the user to make a judgment on which vortex elements to include or exclude. This improvement has eliminated this decision, and it allows for all the wake to be included. The predicted unsteady blade surface pressures from the FPRBVI code are then input to the noise code, WOPWOP, to predict the noise.

The figure shows a comparison of acoustic predictions with the measured data for a 65-knot forward-speed case at an observer downstream and below the rotor disk. The measured acoustic data are from a model rotor test performed in 1989 by Sikorsky Aircraft, the United Technologies Research Center (UTRC), the NASA Langley and Ames Research Centers, and the U. S. Army Aeroflightdynamics Directorate (AFDD) in the German Dutch Wind Tunnel (DNW). The comparison is considered quite good in both amplitude and overall signal shape. The additional high-frequency "noise" in the predicted signal is partly caused by the numerics and interpolation algorithms used in the computations.

This prediction procedure, which uses publicly available codes, is compatible with the ROTONET system and will be available for industry or university use.
(C. L. Burley, 43659)
Structures Directorate

Upper Atmosphere Research Satellite (UARS) Disturbance Experiment

In space science platforms in which pointing of instruments is required, jitter can result from flexible appendages (such as solar arrays and booms) being excited by one or more disturbance sources. The Upper Atmosphere Research Satellite (UARS) has five gimballed instruments and a gimballed solar array that contribute to the spacecraft overall dynamics. The accuracy of methods used to predict UARS jitter during design and of other candidate methods is not well established. The UARS Disturbance Experiment was conducted to obtain data for evaluating methods and accuracy of ground analyses.

The on-orbit experiment was conducted to ascertain the pointing jitter contribution of each individual gimballed instrument. The controlled disturbance experiment on UARS was conducted during a spacecraft yaw attitude adjustment period when most instrument teams do not take atmospheric science data. To successfully isolate the effects of different disturbances, the normal continuous scanning operations of two instruments were altered. The Microwave Limb Sounder (MLS) Team at the Jet Propulsion Laboratory sent commands to their instrument, thus regulating the scan profiles of its 1.6-m antenna and switching mirror. The commands consisted of on/off sequences for its gimballed antenna and switching mirror. The High Resolution Doppler Images (HRDI) Team at the University of Michigan also altered their normal sequence of operations scheduled for the yaw adjustment period. The HRDI Team interrupted its calibration at the beginning of the experiment and began its normal scanning sequence such that it served as a second isolated disturbance source. The scan schedules of the MLS and HRDI instruments were interwoven with other routine disturbance sources, thus making it possible to have each instrument's disturbance both isolated and in combination with other disturbances.

The disturbance sequences were successfully executed onboard the UARS spacecraft. The experiment provided 13 isolated disturbance events, 24 multiple disturbance events, 3 sunrise solar array thermal snaps, 2 sunset solar array thermal snaps, and 33 min with all major disturbances removed. Every gimballed instrument onboard the satellite was moved both individually and with other instruments during the experiment. One of the first observations was an unexpected disturbance from the solar array drive mechanism, which causes near continuous excitation of a 0.23- to 0.26-Hz solar array elastic mode. Because of that, additional data were obtained in a later experiment for the "no disturbance" case taken when the solar array motor was off. The spacecraft developer is in the process of including the solar array drive as a disturbance source in the model.

(Stanley E. Woodard, 44346, and William L. Grantham)
Structures Directorate

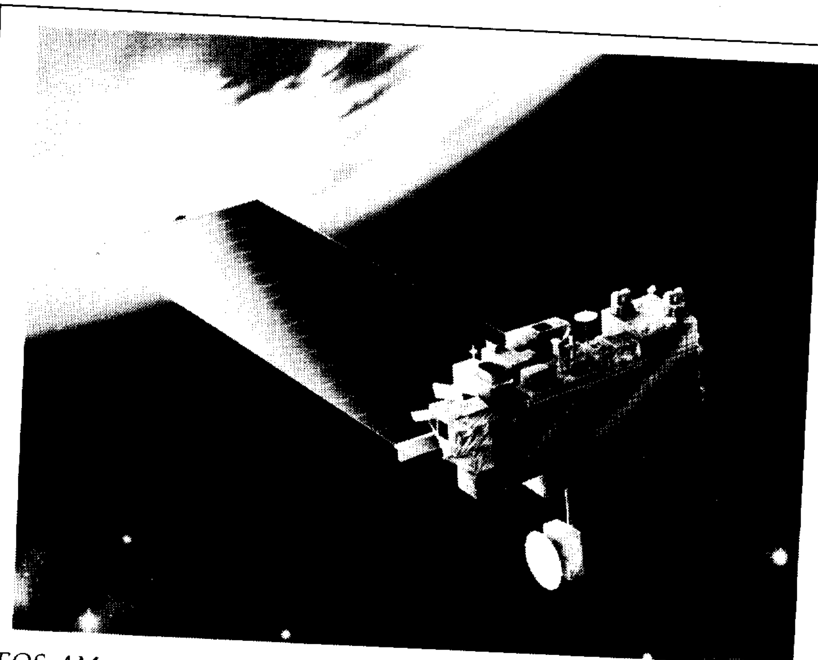

EOS-AM spacecraft.

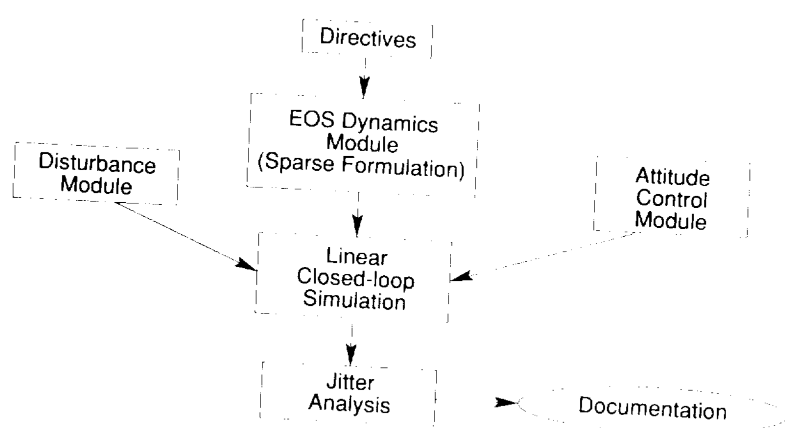

EOS simulation flow diagram.

Flexible Spacecraft Jitter Simulation and Analysis Tools

An efficient simulation and analysis software system has been developed for jitter simulation on flexible spacecraft, and it has been applied to the preliminary design of the EOS-AM spacecraft, shown in the first figure. Simulation of the spacecraft's open-loop/closed-loop response to both transient and steady-state disturbances can be performed in numerous ways. For this study, an efficient method is required because more than 500 flexible-body modes of vibrations were to be included in the closed-loop simulation. In addition, use of the MATLAB program was desired for ease of documentation and transfer of the results to Goddard Space Flight Center and Martin Marietta. An efficient MATLAB-based code was developed to meet these goals. The second figure shows an EOS simulation flow diagram for code (referred to as EOSSIM).

A sparse matrix formulation has been used to assemble the dynamic equations in first-order form. It is assumed that the attitude control system is implemented in a discrete form. Hence, the control torque computations are effectively treated as external forces on the right-hand side of the structural dynamics equations. This leads to a very sparse (tri-diagonal) structure for the plant equations. For the spacecraft dynamics model, it is only necessary to store and operate on N 2×2 blocks, where N is the number of rigid and flexible body modes included in the simulation. Once the time histories for the responses of interest have been computed, jitter analysis is performed. It would be prohibitively expensive to compute jitter using repeated "max" and "min" analyses within MATLAB because the number of time steps within the time history is usually of the order 10^5. Hence, an efficient code has been developed to compute jitter for multiple time windows. The code is written in FORTRAN, and it is linked to MATLAB with "mex" files.

(W. Keith Belvin, 44319)
Structures Directorate

RESEARCH AND TECHNOLOGY

Subsonic Aircraft

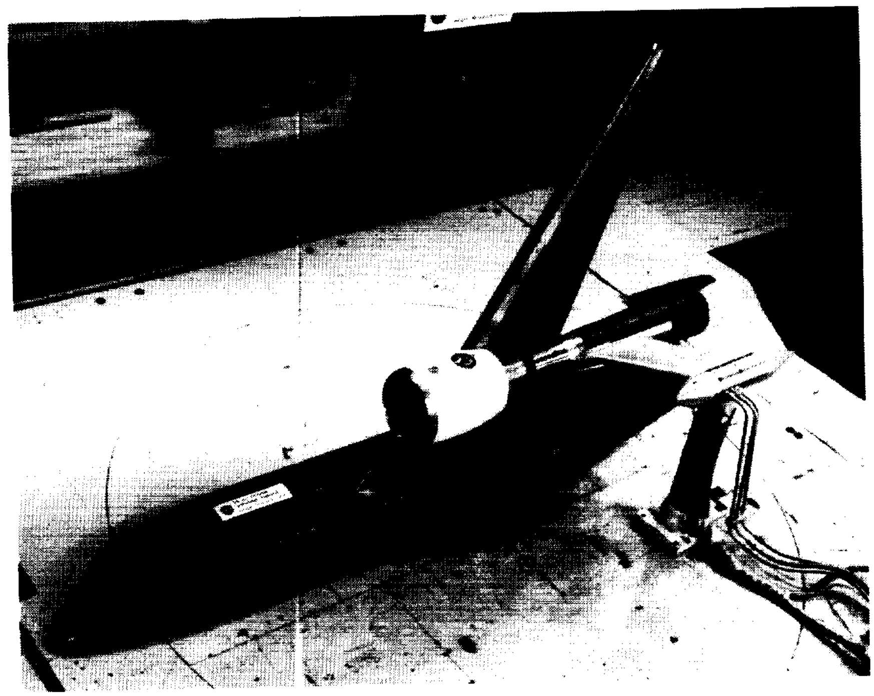

Develop technologies to ensure the competitiveness of U.S. subsonic aircraft and to enhance the safety and capacity of our national airspace system

Desulfurization of Ni-Based Superalloy Turbine Blades

Sulfur is a contaminant in all metal alloys that can cause severe effects on the strength of the material. At elevated temperatures, it can thermally diffuse to defects, grain boundaries, phase boundaries, coating interfaces, and ultimately, to free surfaces. In the case of Al_2O_3 protective coatings of Ni-based superalloys used for jet engine blades, the sulfur segregates to the coating interface, weakens the bond, and causes spallation of the oxide; thus, the oxidation protection of the underlying base alloy is reduced. The best solution to this problem is the complete removal of the sulfur. This can be done by simultaneous heating and ion sputtering of the alloy. The heating segregates the sulfur to the surface, and the simultaneous ion bombardment removes it from the surface. Specifically, the heating must be done in an ultrahigh vacuum chamber with very low oxygen and carbon backgrounds, so that the surface oxygen and carbon dissolve into the bulk and free up surface sites and permit the bulk sulfur to diffuse to and spread over the surface. When a high-purity inert gas, such as Ar, is backfilled into the system and stimulated to a glow discharge, the flowing plasma sputters the sulfur and convectively carries it away. In this way, sufficient processing of the metal can reduce the bulk sulfur to less than 10 percent of the original concentration and

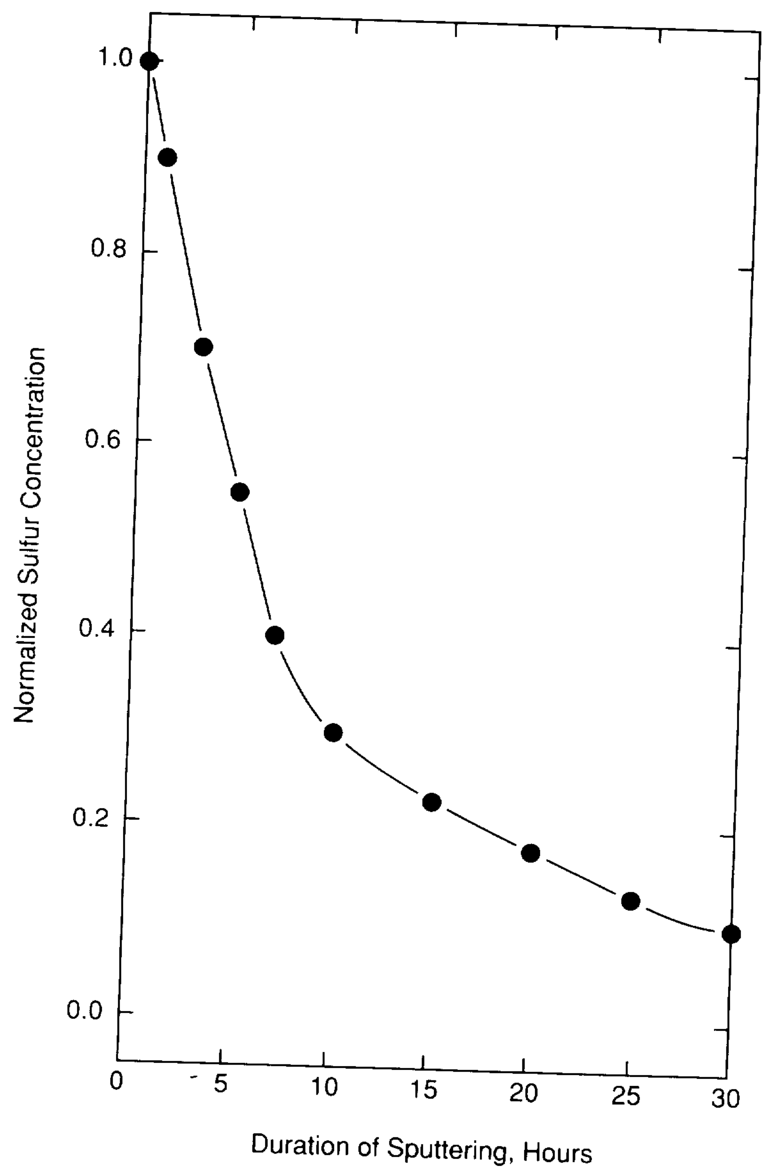

Decrease of sulfur from Ni-based superalloy with sputter annealing at 900°C.

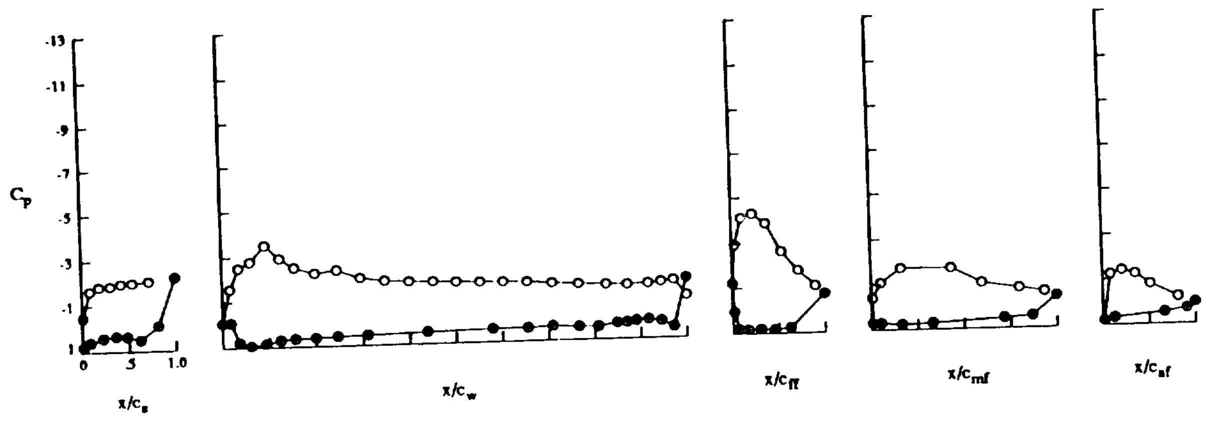

Typical pressure distribution results. "+" inside symbols indicates lower surface pressures.

thus substantially minimize the undesired spalling of the oxide coating. A proof-of-concept experiment for this process is shown in the figure.
(R. A. Outlaw, 41433)
Space Directorate

Boeing 737 Pressure-Instrumented Wing

A wind-tunnel investigation was performed in the Langley 14- by 22-Foot Subsonic Tunnel on a 1/8-scale Boeing 737-100 model instrumented with over 700 wing pressure orifices. The orifices were placed in chordwise rows at seven spanwise locations on the right-hand wing. An extensive pressure database was obtained for comparison with flight measurements and for verification of several computational fluid dynamic codes. The figure presents a typical pressure profile of the high-lift multielement wing. The contribution to the understanding of flow physics on a multielement wing could help industry manufacturers in their efforts to simplify flap systems without a decrease in performance.

Additional objectives of this investigation were to find the effect of a Gurney flap on the aircraft lift and drag and to obtain the effect of wing and tail leading-edge icing on the aerodynamic performance. Data for four various shapes of Gurney flaps were obtained and will be used to determine the cost effectiveness of employing a Gurney flap on a full-scale aircraft.

Through coordination with NASA Lewis Research Center, simulated ice was placed on the leading edges of the wing and tail to determine the effect on aerodynamic performance. These data will allow three-dimensional icing effects to be added to the existing Lewis two-dimensional B737 icing database.
(Brenda E. Gile, 45002)
Aeronautics Directorate

Computational Aerodynamics Applied to Transport High-Lift Flight Research

Computational aerodynamic codes are being used in support of NASA's Subsonic Transport High-Lift Flight Research Program. The current generation of multielement, high-lift codes offers capabilities not previously available to high-lift-system designers and researchers. These codes are relatively simple and fast, and are practical for engineering use. Flight data are being used to assess where these codes are applicable using "real-world" operating conditions.

A computational investigation of the NASA Transport Systems Research Vehicle (TSRV) B737-100 aircraft was conducted using production, two-dimensional, multielement computational methods. MCARF (Multi-Component Airfoil) uses a classical panel method along with an integral, confluent boundary-layer model to obtain a

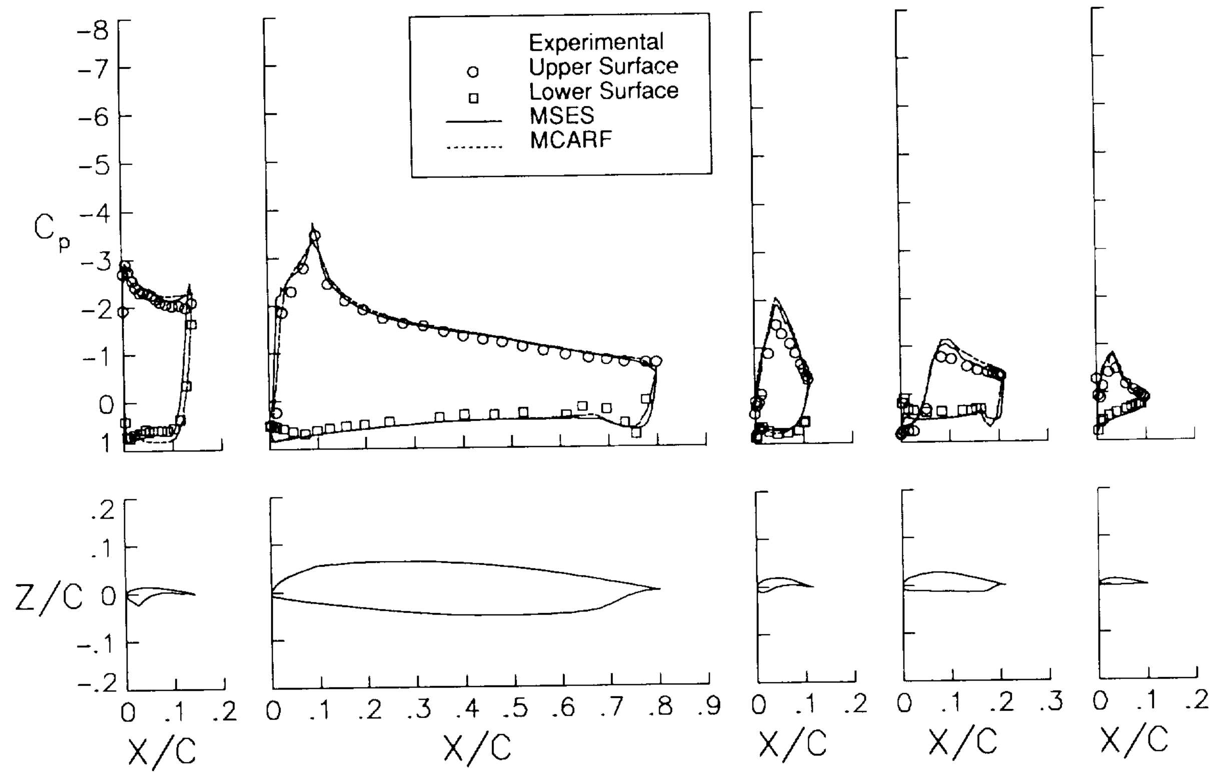

Comparison between flight data and computed pressure distributions for the takeoff configuration. 58 percent semispan station; $\alpha = 9.4°$; $R_c = 11.85 \times 10^6$; $M = 0.17$.

viscous solution over multielement high-lift systems, but does not predict the effects of flow separation. MSES (Multi-Surface Euler) couples an advanced Euler code with an integral, confluent boundary-layer model, allowing for the analysis of flows containing regions of locally supersonic flow as well as regions of limited flow separation. Both codes were modified using simple-sweep theory to account for three-dimensional inviscid flow effects on the TSRV high-lift system.

Comparisons between MCARF, MSES, and the three-dimensional flight-test results obtained from the TSRV five-element high-lift system were made for two high-lift configurations—one represents a takeoff configuration and one represents an approach configuration. Reasonable agreement with flight data was obtained with both codes under attached-flow conditions. Sensitivity studies performed using the MSES code showed a strong influence of the flap gaps and deflection angles on the aerodynamic loads. The sensitivity of the loads to relatively small changes in the flap system geometry indicated the importance of determining the in-flight structural deformation under high-lift conditions.

(Long P. Yip, 43866, Jay D. Hardin, and Julia H. Whitehead)
Aeronautics Directorate

Subsonic Flow Transition Detection Using an Infrared Imaging System

Infrared imaging is a nonintrusive, diagnostic technique that is capable of making quantitative, global temperature measurements.

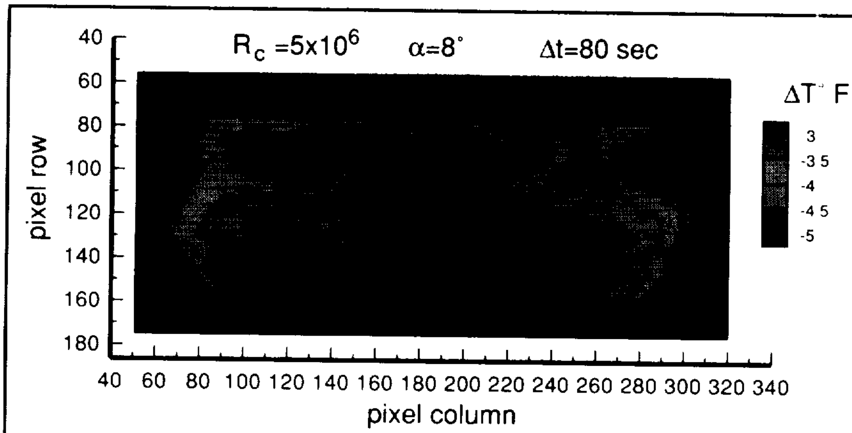

Boundary-layer transition on flap of 3-element airfoil by infrared thermography.

For this experiment, a commercially available infrared thermography system was used in a comparative study of techniques capable of detecting low-speed flow transition. This study was conducted in Langley's Low-Turbulence Pressure Tunnel on a multiple-element, stainless-steel, McDonnell Douglas airfoil in a Mach 0.2 flow with Reynolds numbers of 5×10^6 and 9×10^6.

The imaging system used in this experiment detected infrared radiation in the 8- to 12-μm region of the spectrum and generated real-time video data at 30 frames per second. The scanner was mounted in a pressurized canister and had optical access into the test section through a pair of antireflection coated zinc-sulfide windows. During testing, the imaging system provided a video signal of the small temperature gradient present on the surface of the airfoil as seen in the figure. This temperature gradient resulted from the change in heat-transfer coefficient caused by the transition from laminar to turbulent flow.

Temperature gradients as small as 0.2°C were detected by the system in this configuration. To preserve the small temperature gradients expected at these low Mach numbers and to improve the radiometric properties of the stainless-steel airfoil, the model was coated with a thin layer of black Kapton film. This insulating layer of film prevented the stainless steel from conducting away small surface-temperature gradients and increased the surface emissivity of the model to about 0.9.

As a result, the location of the transition region on this airfoil was successfully detected at angles of attack of 0°, 4°, 8°, 12°, and 16°. These results indicate that infrared thermography is an acceptable global-temperature measurement technique that can detect the region of flow transition in low-speed, subsonic test conditions. **(Stephen E. Borg, 44747, and Ralph D. Watson)**
Electronics Directorate

Advanced Rotor-Blade Technology Evaluated in TDT

In the fall of 1986, a Westland Helicopters, Ltd. Lynx, equipped with main rotor blades developed under the British Experimental Rotor Program (BERP), claimed the Class E-1 (helicopters without payload) speed record. Westland

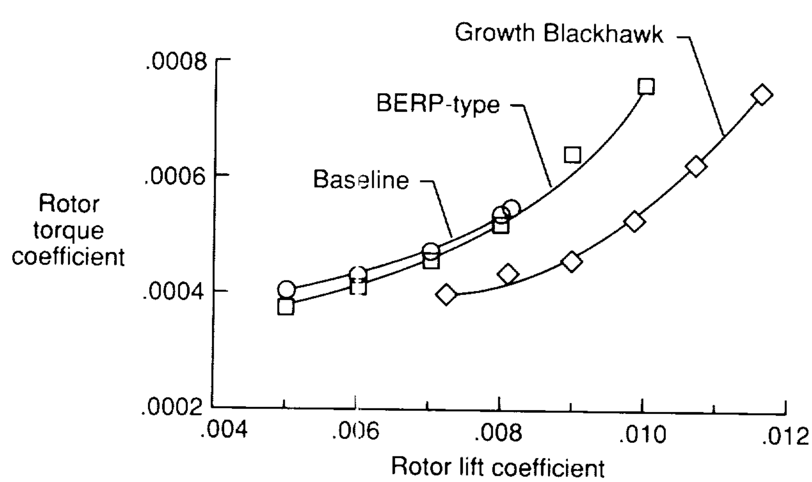

Comparison of rotor-blade performance.

has claimed that the BERP rotor blades can provide either an increase in aircraft speed for a constant thrust or an increase in load factor for a constant aircraft speed. For the next generation of U.S. Army helicopters, it is imperative that all rotor-blade design technology be evaluated as possible enhancements to current U.S. industry rotor design methods. Therefore, a test was conducted in the Langley Transonic Dynamics Tunnel (TDT) to acquire data to evaluate the BERP planform.

The test was conducted using baseline BERP-type model rotor blades mounted on a four-bladed articulated hub. The term "BERP-type" is used because of the difference in airfoil sections between the full-scale BERP blades and the model BERP-type blades. The performance improvements claimed for the BERP planform were evaluated by cross-plotting data to a nominal design condition of 4000 ft altitude and 95°F ambient temperature for a rotor task representative of the Army UG-60 Blackhawk helicopter at a gross weight of 18 500 lb. The data indicate that the BERP-type planform, compared with a baseline rectangular planform, provides increases in speed for a fixed rotor thrust (not shown). The figure is a plot of rotor torque coefficient, a measure of rotor power required, versus rotor lift coefficient, and it shows that the BERP-type blade also provides an increased load factor capability at a constant advance ratio of 0.30. In addition, data obtained from a previous TDT test are plotted for comparison purposes. These data indicate that a Langley-designed Growth Blackhawk tapered-blade planform provides performance improvements over the BERP planform in terms of power requirements and lifting capability. **(William T. Yeager, Jr., 41271, Kevin W. Noonan, Matthew L. Wilbur, Paul H. Mirick, and Jeffrey D. Singleton) Structures Directorate**

Combined Tension and Bending Testing of Tapered Laminates

Composite flexbeams in bearingless and hingeless rotor hubs are subjected to a combination of axial tension and bending loads. In order to study the durability of these flexbeam structures, tapered laminate coupons were designed and tested. A nonlinear beam element used at Bell Helicopter to evaluate composite flexbeam designs was incorporated in the computational mechanics testbed (COMET) code. This beam element includes additional terms in the element stiffness matrix to incorporate the nonlinear effects of a constant internal force on the flexural stiffness. Various tapered laminate configurations were modeled using the boundary conditions in an axial tension bending (ATB) testing machine that was designed and built at Langley Research Center.

The nonlinear-beam finite-element analysis yields the moment distribution in a tapered-beam configuration that is subjected to a combined axial load and bending load. Laminated plate theory was used to calculate the stresses and corresponding surface strains on the tapered laminate. The figure compares measured and predicted surface strains for an S2/E773 Glass/epoxy laminate with a nonlinear taper. Tapered laminate coupon tests will be conducted in the ATB test machine at Langley to evaluate composite rotor-hub flexbeam designs. This unique combination of testing and analysis will allow assessment of flexbeam failure modes, identification of optimum taper designs, and development of realistic accept/reject criteria for flexbeams with manufacturing flaws. Furthermore, because the tapered laminates tested are small coupons,

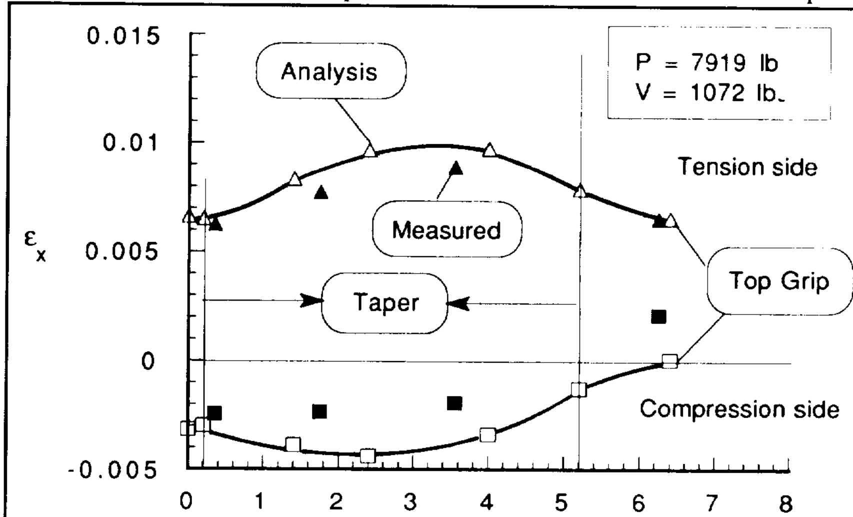

Surface strain distribution in S2/E773 nonlinear tapered laminate.

a database may be generated to evaluate the variability in the test data.
(T. K. O'Brien, 43465)
Structures Directorate

Wind-Shear Detection Performance of an Airborne Doppler Radar

Low-altitude microburst wind shear is a severe hazard to aircraft during takeoff and landing. According to National Transportation Safety Board records, wind shears have, directly or indirectly, contributed to approximately 50 percent of all commercial airline fatalities between 1974 and 1985 and over 600 fatalities since 1964. Recognizing this hazard, the FAA has required all commercial carriers to install some type of wind-shear hazard detection/avoidance system on their aircraft by 1995.

A pulsed Doppler radar has been developed that can detect the hazard, estimate its severity, and provide navigational information to a pilot concerning low-altitude wind shears. The primary obstacle for a radar system is the necessity of the system to look down into the ground clutter environment and extract wind estimates from relatively low-reflectivity weather targets. To assess the performance of airborne Doppler radar systems and demonstrate the feasibility of such systems to detect and provide guidance information to a pilot, a series of flight experiments were conducted near Denver, Colorado,

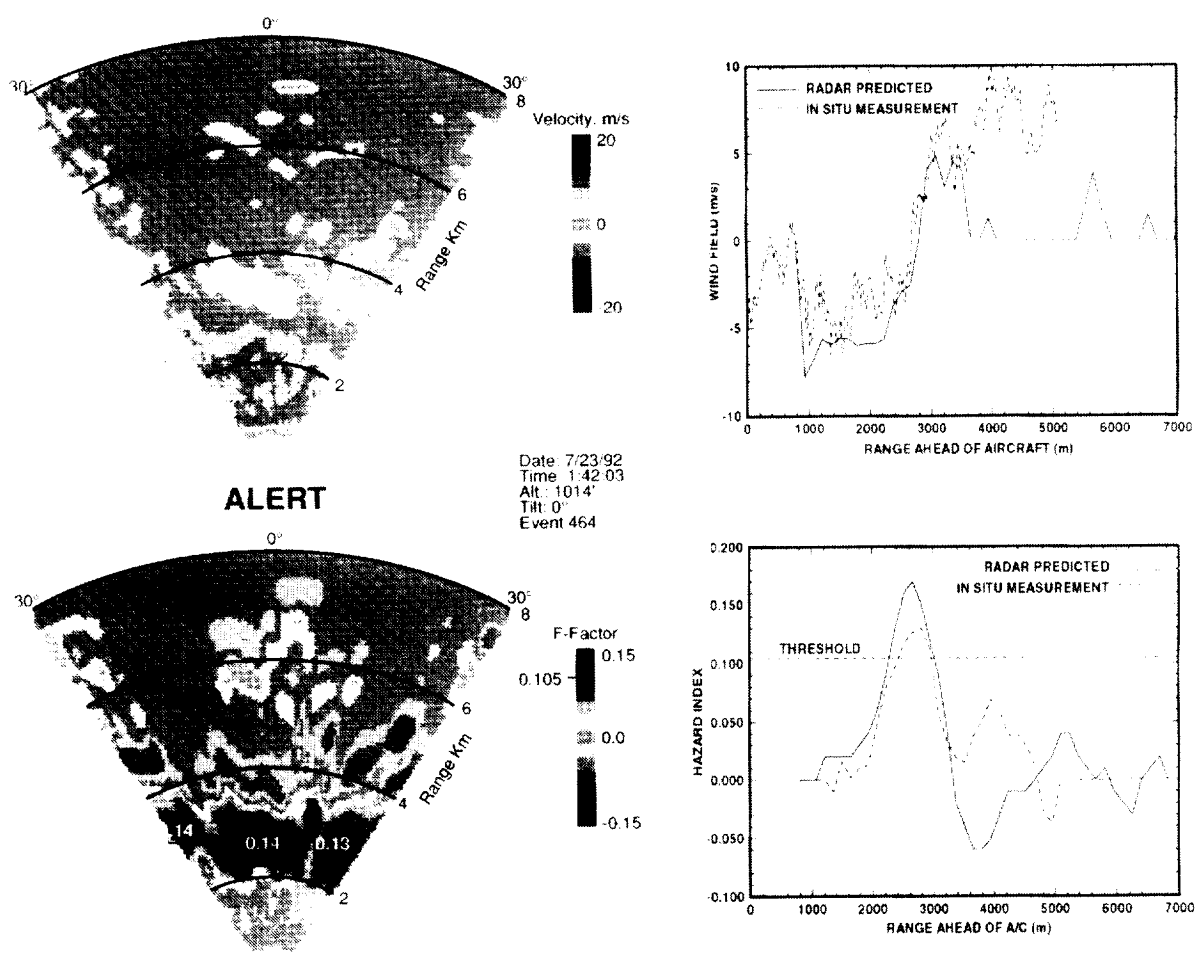

Airborne Doppler radar "DRY microburst" detection approximately 30 seconds prior to aircraft encounter and comparison with aircraft truth. (Original of figure in color; contact author for more information.)

and Orlando, Florida, during the summers of 1991 and 1992.

Over 100 microburst events were observed by the airborne radar, from which approximately 75, of varying degrees of severity, were penetrated by NASA's Boeing 737-100 research aircraft. The airborne radar predicted these encounters 15 to 90 seconds prior to the aircraft's penetration and showed excellent agreement with the onboard reactive system's measurements. The figure shows airborne radar PPI (planned position indicator) displays (and line plots that compare radar-predicted and aircraft in situ measurements) of the wind field and the associated wind-shear hazard index (F-factor) for a dry microburst encounter (the most stressing for the radar). Accurate and timely alerts were given when the hazardous threshold was exceeded. The ground clutter suppression techniques employed in the NASA-designed system eliminated the potential false/nuisance alerts produced by interfering ground clutter. The airborne radar's predictive capability was assessed by correlating the radar's predicted hazard index with that experienced by the aircraft. This analysis produced a 92-percent correlation coefficient.

The excellent agreement and near-perfect correlation of the airborne radar with the wind fields experienced by the aircraft demonstrate capability of the airborne Doppler radar to reliably detect and provide advance warning of hazardous wind shear, in the presence of severe ground clutter, even for low-reflectivity weather targets. The NASA wind-shear radar has been proven to be the primary instrument for providing detection, threat estimation, and navigation information associated with wind-shear microburst avoidance. Throughout this research program, NASA has transferred this technology directly to the aerospace industry, and specifically to avionics manufacturers interested in developing a next-generation airborne Doppler radar commercial product. NASA continues to provide technical guidance to the FAA on certification of airborne predictive wind-shear systems. A direct measure of this program's success and its ability to transfer this technology is the rapid development of the commercial product. Only 2 years after the first flight tests, three radar manufacturers are seeking certification and expect their product to be on commercial airlines by 1995.

(Steven Harrah, 41835)
Flight Systems Directorate

Vertical-Wind Estimation Technique Evaluated From Radar Simulation and Flight-Test Data

Doppler radar and lidar were two of the forward-looking sensor technologies for detecting hazardous wind shear that were flight-tested in the NASA Wind-Shear Program. An inherent limitation of these technologies is their inability to measure velocities perpendicular to the line of sight. Although these systems can detect the presence of a wind shear by measuring the divergence of the horizontal-wind profile, their inability to measure the vertical wind can result in a significant underestimation of the magnitude of the hazard. One method of overcoming this limitation is to estimate the vertical wind from the measured horizontal-wind profile through theoretical or empirical

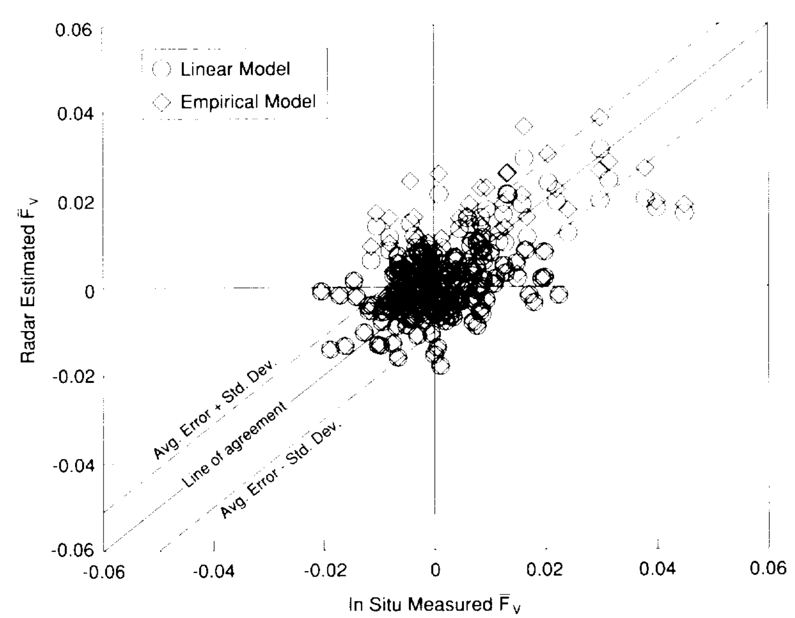

Comparison of the estimated and in situ measured vertical-hazard factors.

Case No.	Simulation Description	Model Simulation Time Slice (minutes)	Horizontal Grid Spacing in meters	Approximate Peak 1-kilometer FBAR @ 150 kts	Approximate Diameter of Outflow @ Peak ΔV (km)	Approximate Microburst Core Reflectivity (dBZ)	Intervening Rain in Model	Temp. Lapse Rate	Symmetry
1	DFW Accident Case-Wet Microburst Rain and Hail	11	50	0.2	3.5	55	NO	Adiabatic	Axisymmetric
2	06/20/91 Orlando, Florida - NASA Research Flight Wet Microburst	37	100	0.19	3.5	50	YES	Adiabatic	Rough Symmetry
3	7/11/88 Denver, Colorado - Incident Case, Multiple Microburst	49 51	100 100	0.08 0.2	3 1.5 - 3	35 20 - 40	LIGHT YES	Adiabatic	Varies between Microbursts
4	07/14/82 Denver, Colorado - Temperature Inversion Microburst	36	50	0.29	1.0	27	NO	Stable Layer	Axisymmetric
5	7/8/89 Denver, Colorado - Very Dry Microburst	40 45	100 100	0.18 0.16	3 3	17 - 20 5	NO	Adiabatic	Rough Symmetry Asymmetric
6	Derived Florida Sounding Highly Asymmetric Microburst	14	100	0.16	1	50	LIGHT	Adiabatic	Asymmetric
7	8/2/81 Adjusted Knowlton, Montana Sounding, Gust Front	27	100	0.14	N/A	20 (in area of largest FBAR)	NO	Adiabatic	Asymmetric

Characteristics of wind-shear data sets.

microburst models. The objective of this research was to evaluate the performance of a vertical-wind estimation technique with simulated radar and flight-test measurements. A high-fidelity, three-dimensional, asymmetric, microburst model was employed in conjunction with a Doppler radar simulation program to generate simulated radar measurements and to estimate the vertical wind and vertical component of the wind-shear hazard index $\bar{F}_v$. Two microburst downdraft models ("linear" and "empirical") were evaluated within the vertical-wind estimation routine. The radar simulation was used to study the effect of measurement error due to signal noise and ground clutter. The vertical-hazard estimates derived from radar flight-test measurements at a point 2 km in front of the airplane were compared with the onboard in situ measurements of that airspace. The performance of a vertical-wind estimation technique to complement Doppler based sensor measurements of hazardous wind shear has been evaluated and compared with flight-test measurements. Shown in the figure is the correlation between the estimated $\bar{F}_v$ derived from radar flight-test measurements and the onboard in situ measurements recorded as the test vehicle traversed the radar-sampled airspace. The results of this research can be directly applied to airborne Doppler based airborne forward-look systems to enhance their estimation of the wind-shear hazard potential and can provide a foundation for the development of new vertical-wind estimation techniques.
(Dan D. Vicroy, 42022)
Flight Systems Directorate

Wind-Shear Data Sets Delivered for Certification of Airborne Forward-Look Sensors

Federal Aviation Administration (FAA) certification of airborne forward-look wind-shear sensors will rely heavily on simulated wind-shear encounters. Simulation is required since the necessary range of environmental conditions would not likely be found within a feasible period of flight testing and because certain encounter scenarios would be too hazardous for flight testing. At the request of the FAA and industry, NASA developed and provided the required wind-shear models. Working meetings between NASA and FAA certification personnel were held to establish the certification objectives to be satisfied by simulation.

These objectives included evaluation of sensor performance in microbursts with extremely high and low precipitation (5 to 55 dBZ), unusual thermal signatures, very small scale lengths, various stages of growth, asymmetric shears, and a hazardous gust front. Critical scenarios included takeoffs with wind shear beyond the liftoff point, curved and straight-in approaches, wind shear obscured by intervening precipitation, and approaches with up to 25° of airplane drift angle. Having defined the scenarios, the NASA terminal-area simulation system (TASS) numeric wind-shear model was used to produce and iterate the required data sets. The iteration was performed to find data sets and trajectories that satisfied the scenario and precipitation/F-factor (wind-shear hazard index) characteristics that are required to show compliance with the sensor success criteria (also developed by NASA). The data sets were formatted to a standardized 3-D grid spacing for delivery to industry, and visualization graphics were produced. A definition of each of the required certification testing trajectories was derived and delivered to the FAA for incorporation into a systems-level requirements document. A total of nine TASS data sets, requiring approximately 1 gigabyte of storage, were derived for delivery, and 35 certification trajectories were defined and documented. The table summarizes the data set characteristics. Cases 3 and 5 are provided at two time slices each; there are nine total sets. Tapes containing the data sets have been delivered to three vendors (Westinghouse, Bendix, and Collins); Boeing and the three vendors are using the data sets in their radar certification activities and one vendor expects to achieve certification by the end of 1993. The NASA data sets are expected to form the standard for certification testing of any forward-look wind-shear sensor (radar, lidar, or infrared) for the foreseeable future.

(David A. Hinton, 42040)
Flight Systems Directorate

Feasibility of Airborne Use of Data Link of Terminal Doppler Weather Radar Information

The present ground-based terminal Doppler weather radar (TDWR) wind-shear sensor uses wind-change information to generate wind-shear and microburst alerts. During operational demonstrations, the TDWR proved effective in performing wind measurements, but the alerting algorithm provided overwarning to the Air Traffic Control (ATC) system in many circumstances. The transmission of TDWR data to flight crews via ATC has also been shown to introduce potentially hazardous delay. The FAA requested that NASA demonstrate the feasibility of generating airborne executive-level alerts using selected TDWR information provided directly to an aircraft by data link. Shaded components in the attached system architecture slide illustrate the required increments to the existing TDWR implementation. The approach taken was to identify the available TDWR products that are required to derive a shear-based wind-shear hazard index (F-factor), implement the necessary airborne F-factor and alerting algorithms, and evaluate this system during NASA multiple-sensor flight tests performed in 1991 at two locations served by TDWR sensors. The ground system locates and classi-

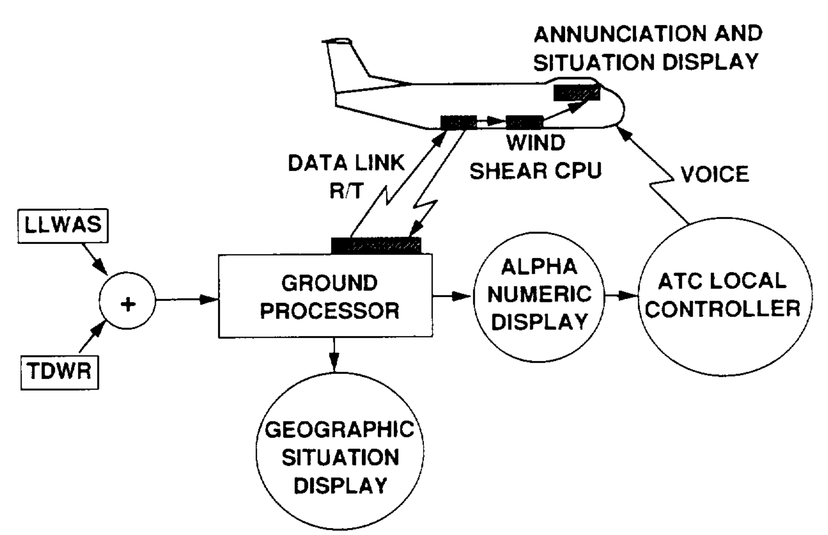

Existing ground and airsystem architecture. Data-link additions shown as shaded boxes.

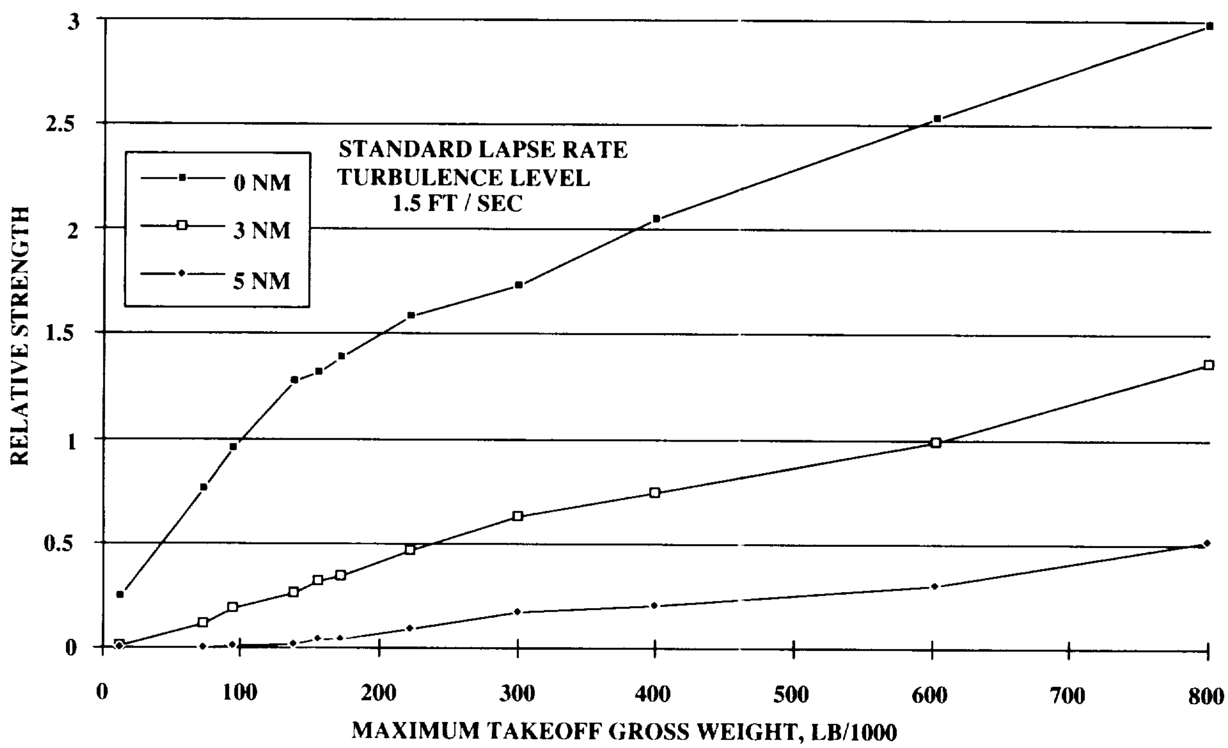

Predicted effects of atmospheric turbulence on wake strength decay as a function of generating aircraft weight and distance behind the generating aircraft.

fies weather events and provides the data to the aircraft. The airborne system quantifies the wind-shear threat, displays microburst locations on a cockpit moving-map display, and annunciates an alert if required. The practicality of airborne use of TDWR information was demonstrated, and the airborne display of microburst location and magnitude was used operationally to maneuver the aircraft for microburst penetrations and to ensure that microburst intensity did not violate flight safety criteria. Results indicate that the TDWR-produced microburst icons overestimate the areal extent of the wind-shear hazard; however, in the limited number of cases (5) where the aircraft penetrated the core of a microburst, the average absolute altitude-corrected F-factor error (TDWR predicted versus in situ measured) was only 0.018, or about 17 percent of the alert threshold of 0.105. This work has demonstrated the feasibility of providing ground-based TDWR information to aircraft via data link, adding value to that data through F-factor estimation, and providing situational information and alerts to the flight crew. Implementation of a data-link capability could provide forward-look wind-shear protection to those fleet aircraft that will not be equipped with airborne forward-look wind-shear systems.
(David A. Hinton, 42040)
Flight Systems Directorate

Wake-Vortex Research

The aircraft trailing-wake hazard is a primary factor in determining the minimum spacing that the FAA allows between aircraft operating from either single or closely spaced parallel runways. FAA experience has shown that current wake-vortex-imposed spacings are unduly conservative most of the time. Since spacing between aircraft has a direct effect on airport capacity, a cooperative research effort was initiated between NASA and the FAA to develop requirements for minimum safe spacings for both current and future aircraft. As part of that effort, an analytical study was undertaken to deter-

mine how weather conditions affect wake decay.

A representative sample of the commercial aircraft fleet was chosen for the study. The maximum range of takeoff gross weight for these aircraft included both Large (12 500 to 300 000 lb) and Heavy (>300 000 lb) category aircraft. Aircraft characteristics were taken from standard published sources, and calculations were performed for a wide range of atmospheric conditions. A key result of the study was the extremely strong effect that atmospheric turbulence was predicted to have on wake decay. For typical levels of atmospheric turbulence, wake decay occurred within a few miles behind the aircraft. For "light" turbulence, the vortices persisted much farther, especially for Heavy category aircraft. Thus, the vortices from Heavy category aircraft are stronger initially and last longer than those from smaller aircraft. In addition, there was a wide variation in wake strength within the Large category, and there was no obvious reason for using 300 000 lb as the dividing line between the Large and Heavy categories.
(George C. Greene, 45545)
Aeronautics Directorate

Organizing Principles for Presenting Systems Fault Information to Commercial Aircraft Flight Crews

Accident and incident reports indicate that flight crews occasionally mismanage or respond inappropriately to systems faults or do not understand how the automation manages these faults. Therefore, for automated fault-management aids to be effective, their design should account for how pilots think about and perform fault management. One way to accomplish this is to organize information for display to pilots based on their cognitive organization of that information. One dimension is based on high-level functional categories, such as flight control, flight guidance, and systems management. A second dimension is based on information-processing (IP) tasks (e.g., detection, identification, diagnosis, and response). There is some uncertainty concerning how pilots organize tasks within the IP dimension: IP models suggest tasks are ordered by logical processing dependencies (order of computation); a previous study suggested that pilots organize information by the order in which it is used (order of use). The objectives of this study were to determine whether the functional or IP task dimension is superordinate in the pilots' mental models and to assess how IP tasks are ordered within the pilots' models.

A workstation experiment was conducted that required each of 40 commercial pilots to perform an information retrieval task using one of four hierarchical menus. The menus were designed to correspond to hypothesized pilot cognitive organizations of systems fault information. Functional categories and IP tasks were represented in the top two tiers of these menus. Two of the menus contained functional categories as menu choices in the top tier and IP tasks as menu choices in the second tier, and the other two menus reversed the order of these tiers. One menu from each of these conditions had the IP task menu choices in the order in which information is computed and the other had them in the order in which information is typically used by pilots. Subjects' speed and accuracy of navigating through a menu to find specified information were measured. The

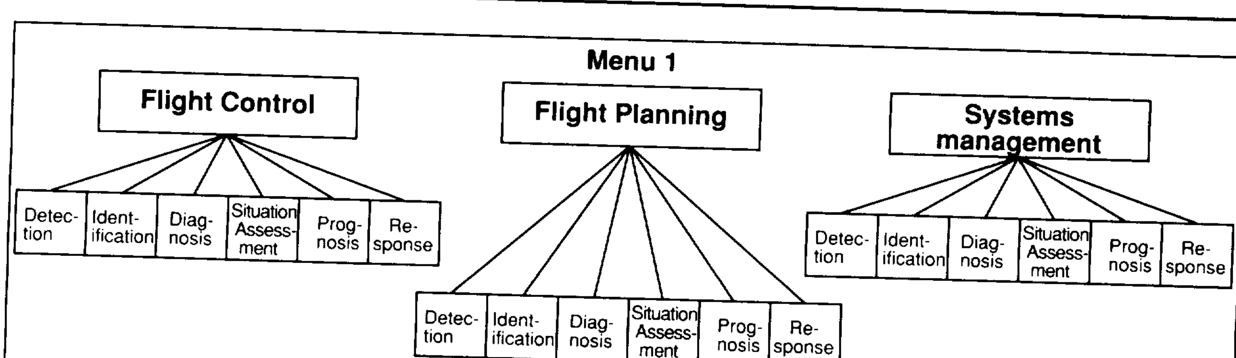

Example menu evaluated to determine pilot cognitive organization of fault-management information.

underlying assumption was that the closer the correspondence between a menu's structure and pilots' cognitive organization of systems fault information, the better pilots would perform.

There was evidence that pilots performed best with the menu with high-level functions as the top level and IP tasks in the order of computation (see figure), although the evidence was weak. The guarded conclusion drawn is that pilots' cognitive organization of fault-management information corresponds to the organization of this menu. Based on the assumption that pilots will more effectively use an automated aid if it organizes its information in a manner that corresponds to the way that pilots mentally organize the information, these results support an important design guideline: if a new aiding system that provides information relevant to several high-level functions is introduced on the flight deck, the information should either be distributed among existing function-based displays or, if a new display is required, it should be organized primarily by functional areas.
(Bill Rogers, 42045, and
Paul C. Schutte)
Flight Systems Directorate

Reduction of Spurious Symptoms in Aircraft Subsystems Fault Monitoring

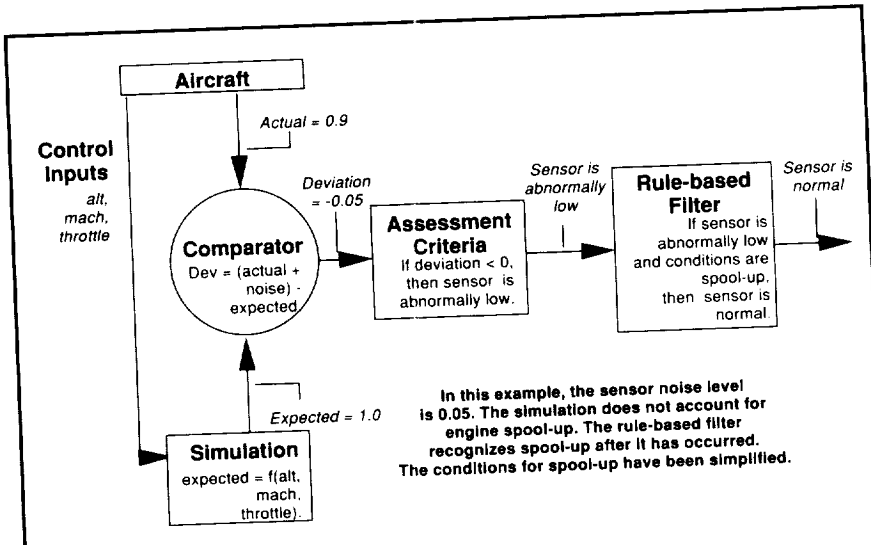

MONITAUR architecture.

Advanced aircraft fault-monitoring systems, such as MONITAUR, depend on computer simulation models of the subsystems they are monitoring to provide reliable data on how the subsystem should be behaving. If the models cannot produce accurate expectations of subsystem behavior, then the fault-monitoring system could produce spurious symptoms. From the pilot's perspective, spurious symptoms can manifest themselves as false alarms. This can lead to inappropriate actions and lack of trust in the monitoring system. An earlier study by Boeing demonstrated that MONITAUR would produce spurious symptoms when using "off-the-shelf" engine models. The objective of this research was to assess ways to reduce the number of spurious symptoms produced as a result of modeling errors.

MONITAUR was designed to use a rule-based filter to filter out spurious symptoms (see figure). In the previous Boeing study mentioned above, the rules for this filter were both sparse and primitive. One approach used in the current study was to examine the categories of symptoms produced and to develop a more robust set of rules. Another approach that was explored was the use of neural networks to enhance the engine models used by MONITAUR. Finally, a hybrid approach was used that combined the rule-based filter approach with the neural network approach. Both approaches were developed using one set of healthy engine data and were evaluated using a different set. The rule-based filter was also evaluated against fault data. The neural network approach could not be evaluated using fault data, because it is specific to an engine serial number and there was no fault data for the serial number used. The rule-based filter is specific only to engine type, and there was fault data for that type.

The enhanced knowledge in MONITAUR's rule-based filter was able to reduce spurious symptoms from 256 (unfiltered) to 35, a 70-percent reduction. The neural network approach was able to reduce the same number to 96, a 40-percent reduction. The hybrid approach reduced the number to 23, a 90-percent reduction. In the fault-data analysis, the rule-based filter approach did not miss any real symptoms; however, it did

add a delay of no more than 2 seconds before reporting the symptom.

MONITAUR was designed to provide early detection of abnormalities. Spurious symptoms could lead to either inappropriate action on the part of the flight crew and/or a lack of trust in the system. Finding cost-effective ways of reducing these spurious symptoms without reducing the sensitivity of their detection will add value to these symptoms. This study shows that a significant number of these symptoms can be reduced.

(William D. Shontz, 42019, Roger M. Records, and Paul C. Schutte)
Flight Systems Directorate

Formal Methods Applied to the Reliable Computing Platform

The reliable computing platform (RCP) is a fault-tolerant, digital computer design that can be validated in a rigorous fashion for flight-critical control applications on commercial aircraft. Although the RCP can be fabricated, its primary purpose is to develop and evaluate formal methods as an enabling technology for digital systems validation. Critical properties of the design have been verified using formal methods to give the strongest possible guarantee that the properties are true for all input conditions. If testing were used alone, it would not be feasible in an affordable test time to confirm correct operation for more than a small percentage of the input conditions. Formal methods using mathematical logic are the natural model for computer logic. By using the reasoning processes that are available to mathematical logic, design verifications can be performed that are the equivalent of exhaustive testing for the properties specified. Using properties that have been established with certainty through formal methods, mathematically sound reliability models of the RCP can be constructed that require only feasible amounts of testing to provide data on the physical processes that contribute to system reliability. For example, the property has been formally verified that a transient fault in one of the individual RCP computers will be corrected within a specified number of computing cycles. This property is inherent in the design, but the designer has control over parameters such as the number of cycles for recovery. This property permits the construction of a sound reliability model that includes transient recovery. Several projects using formal methods are underway or have been completed with U.S. airframe and avionics manufacturers. In these efforts, significant computational elements have been designed to formal specifications, and errors have been uncovered in proposed designs that were produced using

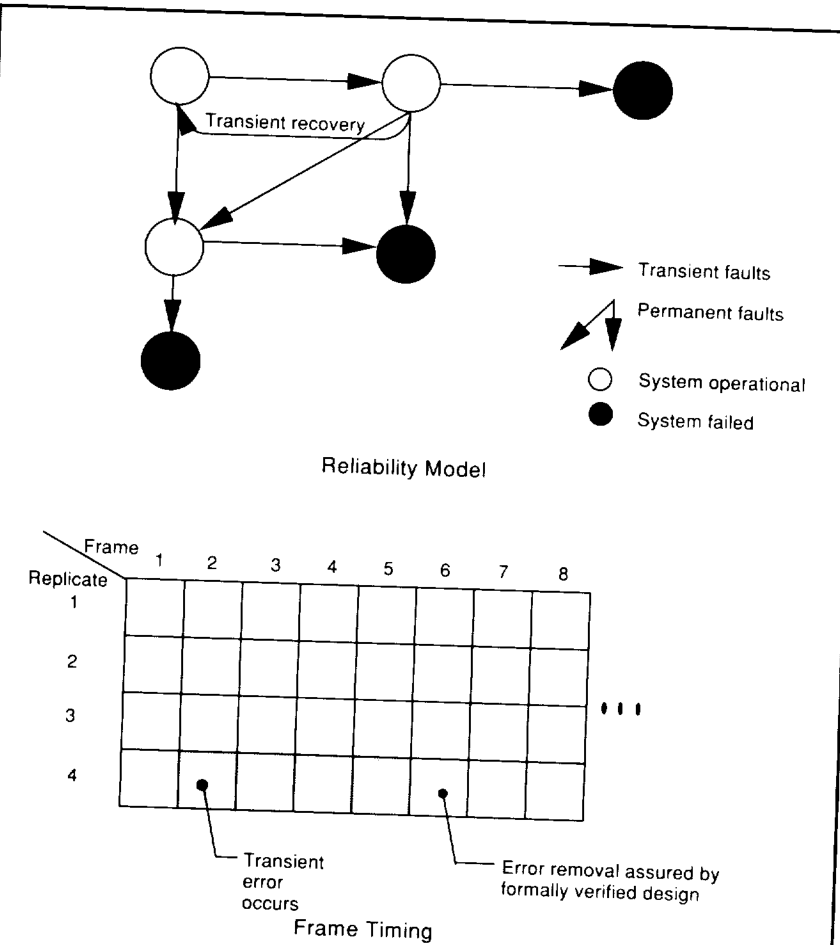

Transient recovery property.

traditional design techniques. As formal methods and supporting tools continue to evolve, they will provide an affordable means to produce digital systems that can be trusted in life-critical applications.
(Ricky W. Butler, 46198)
Flight Systems Directorate

Pictorial Flight Displays Provide Increased Traffic-Situation Awareness

Although modern flight decks have become more sophisticated in terms of computer-generated electronic displays, the display formats in use are largely electronic renditions of earlier electromechanical instruments. New computer-graphics capabilities make possible large-screen, integrated pictorial formats to provide gains in pilots' situation awareness, pilot/vehicle performance, and aircraft safety, with potential for significant operational benefits. The purpose of this research was to compare the spatial awareness of commercial airline pilots when flying simulated landing approaches with conventional flight displays to their awareness when flying advanced pictorial, "pathway-in-the-sky" displays. The specific aspects of spatial awareness addressed herein concern conflicting traffic assessments.

A simulation study was conducted that used sixteen commercial airline pilots repeatedly flying complex MLS-type approaches to closely spaced parallel runways with an extremely short final segment. Four separate display configurations were utilized in the simulated flights: (1) a conventional primary flight and navigation display with raw guidance data and TCAS (Traffic Alert and Collision Avoidance System) II; (2) the same conventional instruments with an active flight director; (3) a 40° field of view (FOV), integrated, pictorial pathway format with TCAS II symbology; and (4) a large-screen (70° FOV) version of the pictorial display.

Within any one of the nine approaches each pilot flew with each display, a single conflicting traffic scenario was encountered. TCAS II symbologies in each concept alerted the pilot to the conflict if he had not already detected the situation. The pictorial formats used the conventional resolution symbology set for traffic representation, but a resolution path was not indicated or required, as was the case with the conventional displays (climb or dive resolutions). As shown in the left portion of the figure, all the pilots detected each traffic incursion, and if a resolution path was indicated, it was initiated. However, with the pictorial formats, the pilots detected the conflict situation 8 or 9 seconds earlier (right portion of figure) than with the conventional displays, and the pilots often decided that no avoidance maneuver was required with the increased situation awareness reportedly available with the pictorial formats. No differences were detectable statistically between the two conventional displays or between the two pictorial concepts.
(Anthony M. Busquets, 46652, Russell V. Parrish, Steven P. Williams, and Dean E. Nold)
Flight Systems Directorate

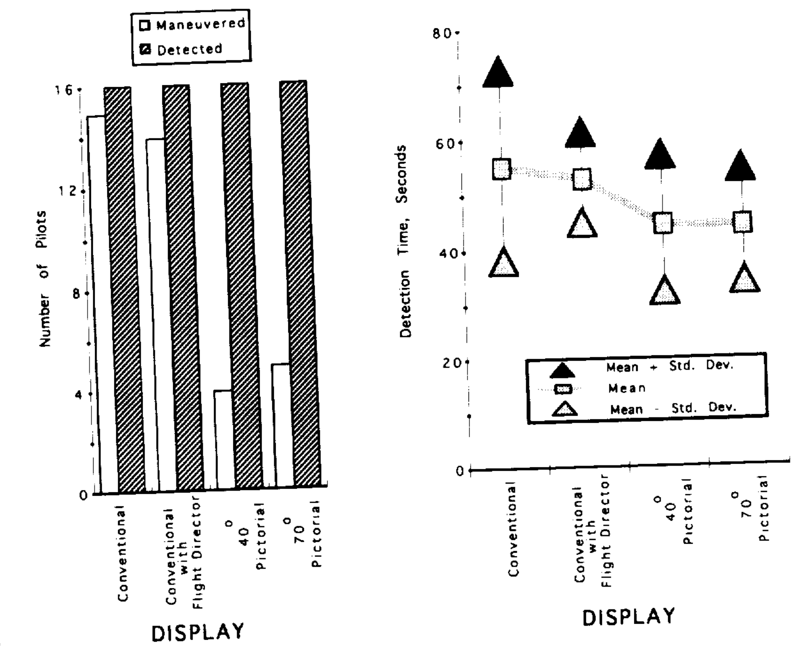

Traffic scenario results.

Flight-Deck Functional Requirements for 2005 High-Speed Transport

In order to accommodate the rapid growth in commercial aviation throughout the remainder of this century, the Federal Aviation Administration (FAA) is faced with a major challenge to upgrade and modernize the National Airspace System (NAS) without compromising safety or efficiency. Recurring themes in both the FAA Aviation System Capital Investment Plan and the FAA Plan for Research, Engineering, and Development are reliance on the application of new technologies and a greater use of automation. In addition, high-speed civil transport (HSCT) requirements may lead to flight-deck design and NAS-aircraft interactions that will be unique to this class of vehicle. Identifying the high-level functional and system impacts of future civil transport operational requirements, particularly in terms of HSCT flight-deck functionality and information requirements, was the objective of this study by the Boeing Commercial Airplane Group and NASA. A high-level analysis was conducted to identify and define the functions that must be accomplished to complete a high-speed commercial transport mission in a modernized NAS of the 2005 era. These required capabilities were then used to develop functional descriptions for the major aircraft systems, including system characterization, information sources and destinations, and intersystem relationships. A structured analysis of the functional requirements was defined based on aircraft flight phase (see figure for an example). The results of this analysis were documented as a comprehensively defined aircraft mission with both normal and non-normal components broken down into their associated flight-crew functions. The product of this study, documented in NASA CR-4479, was an initial step toward providing a requirements-driven approach, at a global level, to the efficient and effective transfer of information between the NAS operational environment and the advanced flight deck. Without an integrated and coherent understanding of these requirements, future design and development efforts for "human centered" automation will not be realized to their full potential.

(K. W. Alter, 42009, D. M. Regal, and Terence S. Abbott)
Flight Systems Directorate

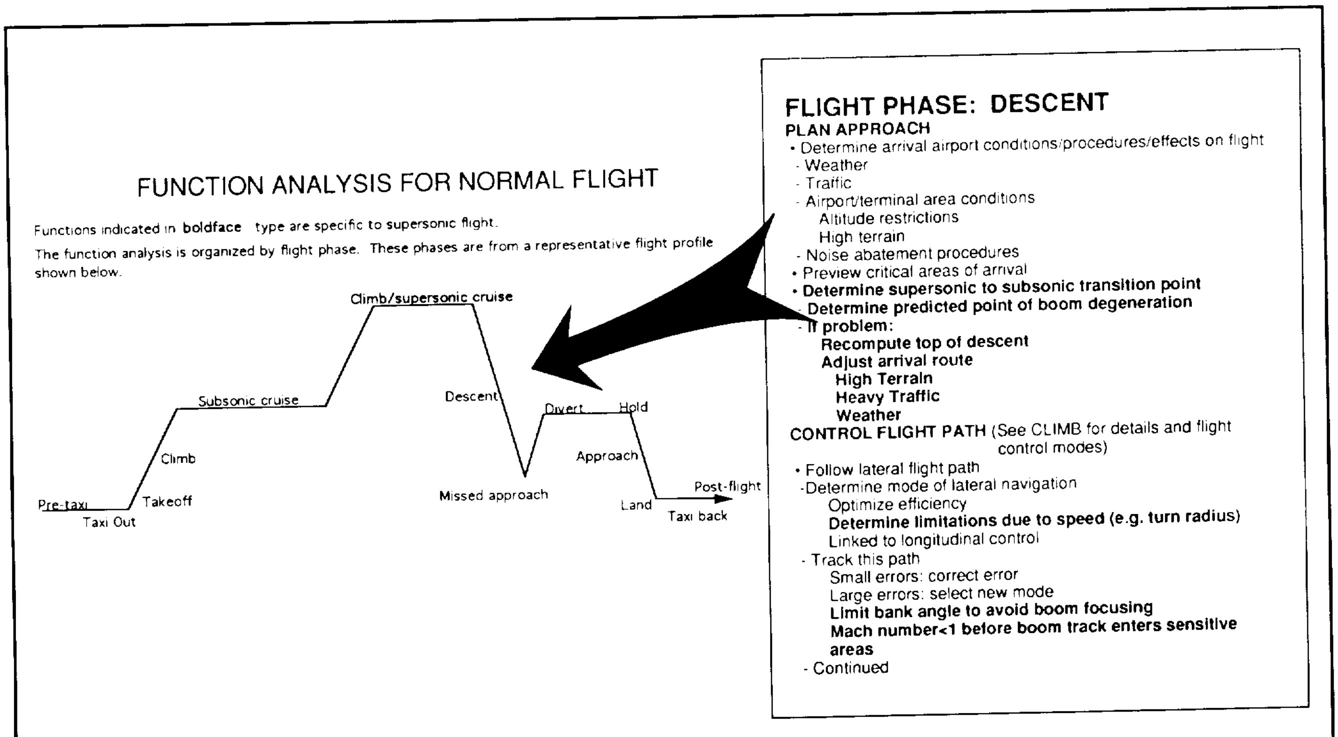

An example of the flight-deck functional requirements for HSCT operations.

Development of Transonic Area-Rule Methodology

The limiting subsonic speed at which high-performance transport and business jet aircraft fly is often set by drag rise due to compressibility effects. Delaying this transonic drag rise will potentially allow the design of more efficient and faster subsonic aircraft.

In the early 1950's, Dr. Richard T. Whitcomb showed that drag rise could be delayed using the sonic area rule. In sonic flow, changes in pressure are communicated with negligible dissipation between the fuselage and its external parts along Mach planes. As a result, drag becomes a strong function of the cross-sectional area of the aircraft, and this is the foundation of sonic area rule. When an aircraft is sonic area ruled, the fuselage is shaped to an optimal area distribution. The result is the well-known "Coke bottle" shaped fuselage. The sonic area-rule ideas were then expanded and validated for supersonic speeds, but little refinement has occurred in the transonic regime.

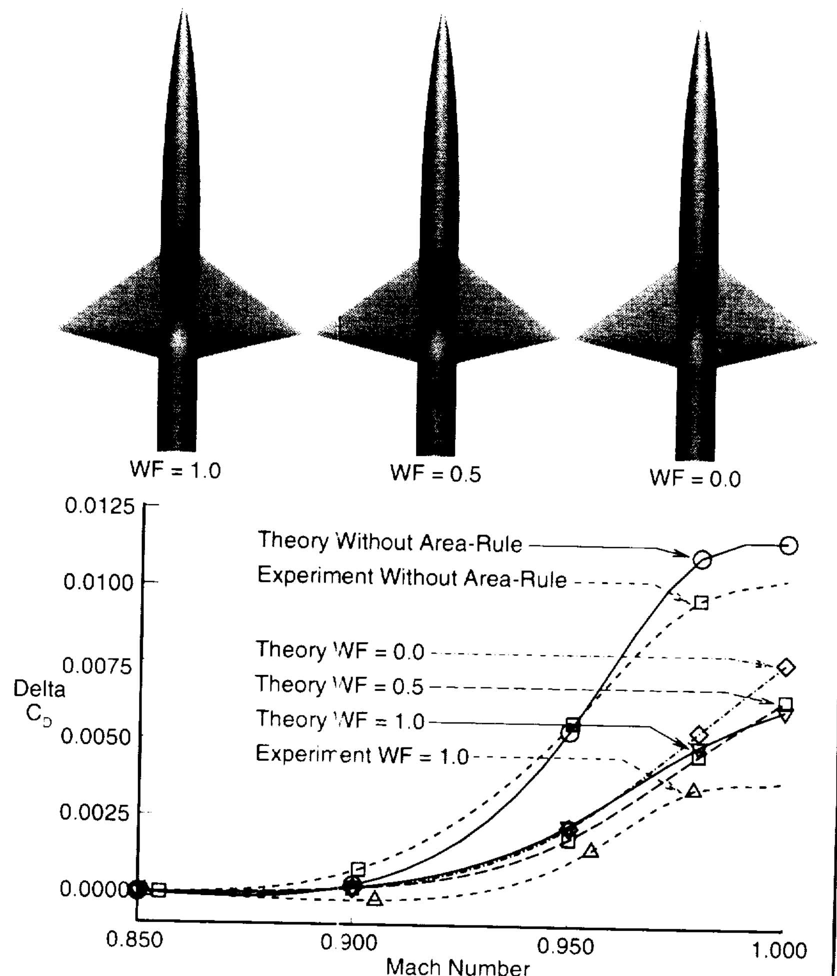

Drag-rise comparison of delta-wing/body geometries.

Transonic flow has the added complexity of mixed subsonic and supersonic regions. In this flow, the communication between the aircraft fuselage and its external parts has dissipation due to the subsonic regions. Therefore, the sonic area rule no longer strictly applies. The new transonic area-rule methodology utilizes a weighting function (WF) that accounts for the mixed flow. For example, WF equal to 1.0 corresponds to uniform sonic flow. The initial investigation has used an unstructured-grid Euler algorithm developed at Langley Research Center. This algorithm was compared with Whitcomb's original experimental work and showed good agreement for both the non-area-rule and sonic area-rule case (see figure). The sonic area-rule model was then theoretically re-area ruled with the new transonic technique (WF = 0.5 and 0.0). The numerical results showed equal or increased drag-rise delay (see figure). Also, the fuselage shaping methods used in this new technique are much less severe than the standard sonic area-ruling method. The combination of increased delay in drag rise and decreased body modification should lead to increased efficiency for transonic aircraft.

(Wayne D. Carlsen, 47741)
Aeronautics Directorate

Interface Technology for Structural Design and Analysis

Many industries are rapidly moving toward a concurrent engineering environment. A critical requirement of that environment is the ability to avoid costly design changes by examining the impact of design details concurrently with conceptual/ preliminary design. Computational tools that allow detail to be considered early in design are needed because so-called "details" are often failure-initiation sites and can become costly items if not addressed early in the design process. Interface technology provides a new set of computational tools for treating design details within the framework of finite-element codes now extensively used in industry. The full potential of these codes to treat detail at an early stage of the design process is unleashed by significantly reducing the engineering effort to treat details. Interface technology provides the insertion modeling computational tools to accomplish this. For example, the effect of damage on residual strength, or the effect of the integrity of a repaired area on the component's performance can be easily studied using insertion modeling tools that were developed from interface technology. These tools allow easy insertion of local models in the global models used for early design. Because they eliminate the need for coincidence of model grid points, no transition mesh is required to go from the fine local mesh to the global mesh. Instead, the inserted model attaches to the global model through interface elements that are derived from hybrid variational principles of mechanics and are employed by the user like any other finite element. Remarkably, these elements result in accurate prediction of stresses even at the interface. In the example shown in the figure, the local stress intensity at the tip

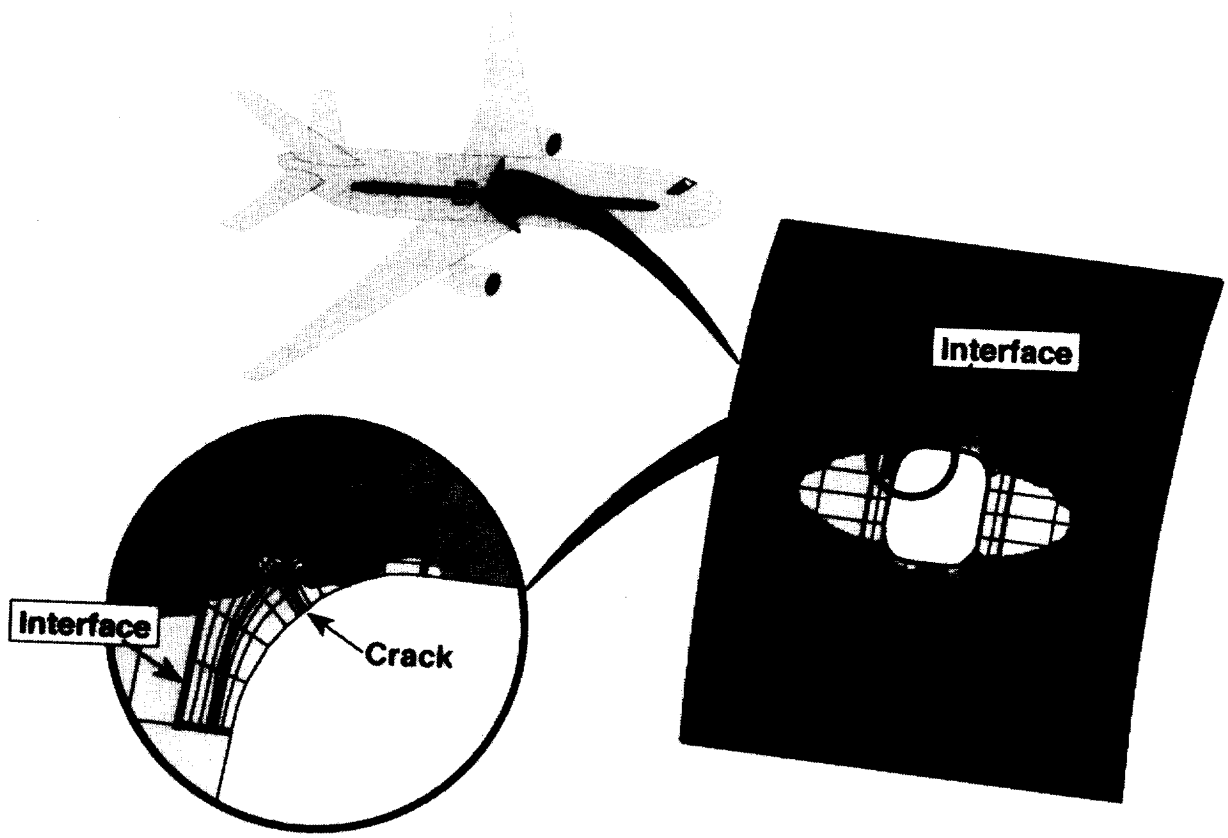

Interface technology used to insert crack in fuselage window panel model.

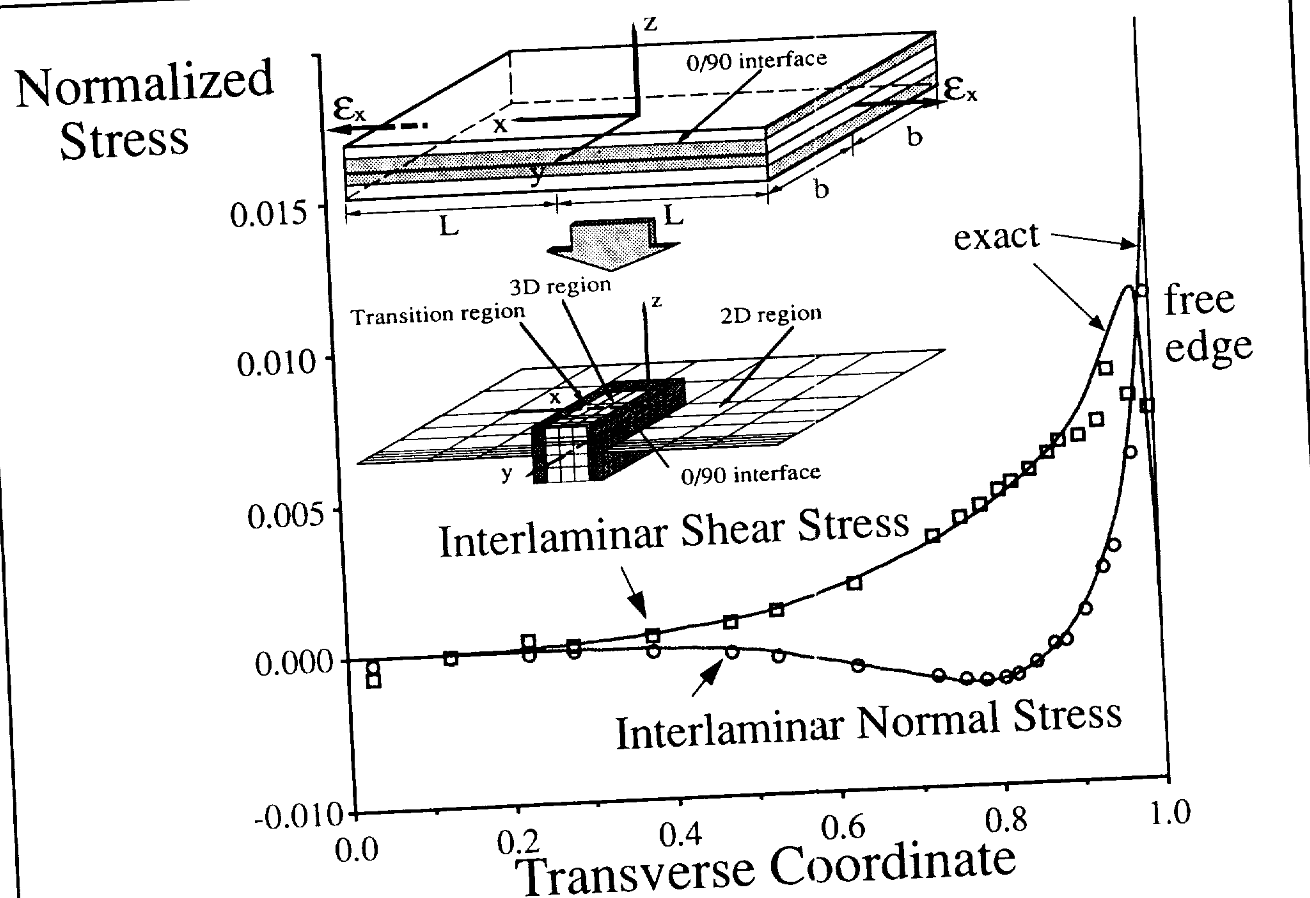

Transition-element technology verified in predicting edge delamination stresses.

of a crack emanating from a window in a curved composite fuselage panel is easily modeled by inserting a local crack model into a coarser model that may have been used in early design. Crack growth can be tracked by moving the local model within the global mesh. Computational tools based on interface technology have been developed within the COMET (COmputational MEchanics Test-bed) research code and are available for technology transfer.
(Jonathan B. Ransom, 42924)
Structures Directorate

Transition Elements for Laminated Composite Analysis

The strength of laminated composite structures is strongly influenced by local interlaminar normal and transverse shear stresses. Failure and life prediction of composite structural designs requires the accurate calculation of these stresses. Such calculations can be very expensive, because 3D brick finite-element modeling is often required. To enhance computational efficiency, it is desirable to use 3D finite elements only where they are necessary for modeling interlaminar behavior; 2D elements should be used everywhere else. To accomplish this goal, an interface technology-based computational tool has been developed to accurately join 2D and 3D regions together. To fit in the framework of conventional structural-analysis software, this tool takes the form of a transition element. The transition elements have two types of edges: edges that connect to a stack of brick elements and edges that connect to a plate or shell element. The edge(s) connected to plate or shell elements are constrained so that their membrane and bending deformations are

consistent with 2D plate and shell theory. Until recently, such elements tended to yield inaccurate interlaminar stresses in the vicinity of the transition element as the result of a boundary-layer pinching effect. Basing the transition element on a higher-order theory, the boundary effect is eliminated, thus providing accurate transition from 2D to 3D elements. The significant classical case of edge delamination in symmetrically laminated composite plates under uniaxial tension is used to demonstrate the performance of the higher-order transition element. The plate has laminae with fibers oriented in axial and transverse directions. Edge delamination can occur in such a plate because of the interlaminar stresses that arise near the plate edges as a result of the large stiffness-property differences between the laminae. The finite-element model uses a stack of 3D brick elements in the region of high interlaminar stress. Transition elements are placed on the three sides of the stack that join the 3D brick elements to the 2D plate elements. The results reveal that accurate interlaminar stresses are predicted throughout the plate, even within the transition elements.

(Alexander Tessler, 43178)
Structures Directorate

Test and Analysis of Stitched-RTM Wing Access-Door Panel

Advanced structural concepts for wing and fuselage structures are being developed to exploit the benefits of advanced composite materials. One structural concept under development for transport applications is a blade-stiffened panel made from layers of graphite materials that have been stitched together before the resin is applied to the part. Once the layers of graphite material are stitched together in the desired shape, the structural part is placed into fabrication tooling and epoxy resin is injected by using a resin transfer molding (RTM) procedure. The part is then cured by following the resin manufacturer's specifications. One advantage offered by stitching the graphite layers together is that the low-speed impact damage tolerance is improved.

To evaluate the stitched-RTM panel concept, a wing panel was designed and fabricated by Douglas Aircraft Company and was tested and analyzed at Langley Research Center. The panel design includes an access

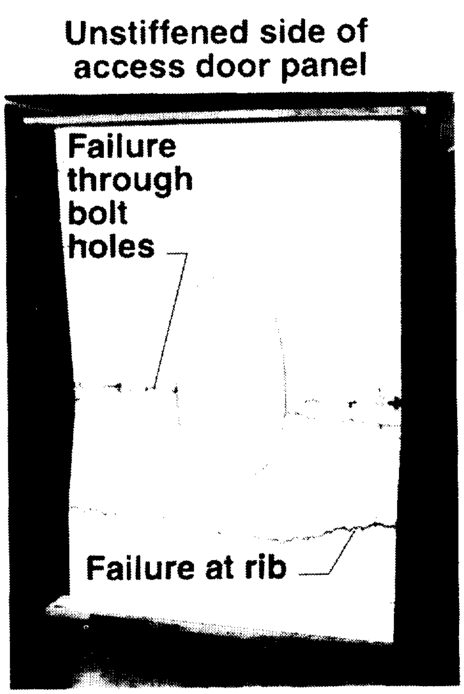

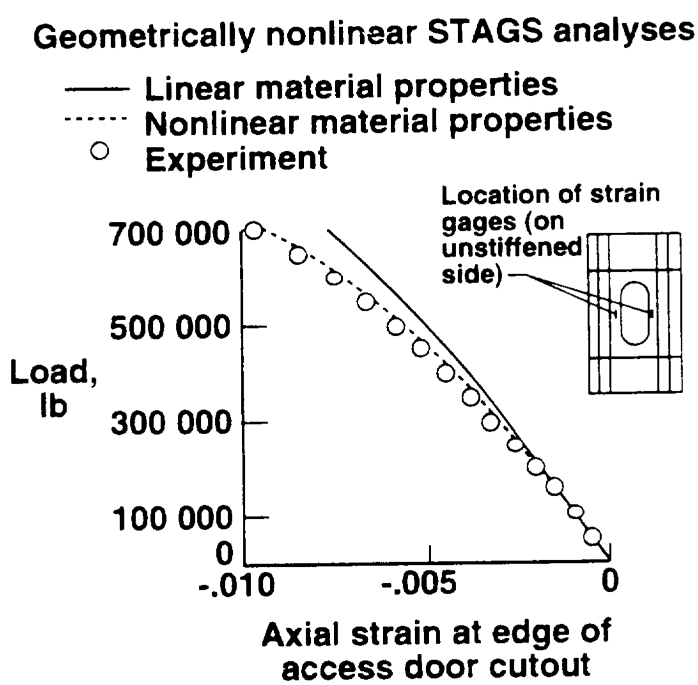

Comparison of test data with analysis for a stitched-RTM wing access-door panel.

door for assembly, inspection, and maintenance. The panel was subjected to low-speed impact damage and was tested to failure to determine the residual strength of the impact-damaged panel. Failure of this panel was caused by the stress concentrations at the fastener holes that were used to attach the access door to the stiffened panel, and not by the impact damage. These results indicate that this stitched-RTM design and structural concept is more sensitive to local design detail features than it is to low-speed impact damage; the results also indicate that highly-loaded graphite-epoxy wing panels can be designed for higher strain applications and can be damage tolerant.

The panel was analyzed by using the STAGS nonlinear structural analysis code, and the results indicate that both geometric and material nonlinear effects must be included in the analysis for the analytical results to correlate with the test results. The geometric nonlinear effects are a result of the eccentricities associated with the access-door cutout and a stiffener that is interrupted by the access door cutout. The material nonlinear effects are a result of the nonlinear characteristics of the material properties of this stitched-RTM material form.
(Dawn C. Jegley, 43185)
Structures Directorate

Analysis of Textile Preform Composites

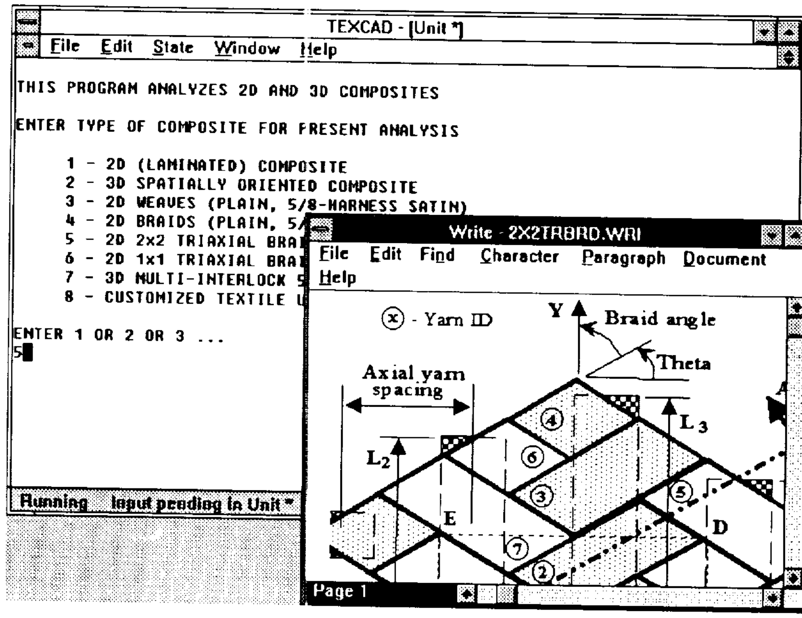

TEXCAD program graphical user interface under MS Windows™ environment.

A general-purpose micromechanics analysis tool to predict overall, three-dimensional (3-D), thermal and mechanical properties for a variety of fabric-reinforced composite materials was developed.

A simple 3-D geometric modeling technique was used to model the undulating yarn paths within each repeating unit cell (RUC) of the textile composite. Each yarn was modeled discretely. The yarns were assumed to have a constant cross section in the form of a flattened lenticular shape. Yarn undulations were assumed to follow sinusoidal paths. A stress-averaging scheme that assumed an iso-strain state was used to compute effective thermomechanical properties and internal stresses in the RUC. The calculated overall stiffnesses correlated well with available 3-D finite-element results and also with test results for a variety of textile preforms.

This analysis was implemented in the Textile Composites Analysis for Design (TEXCAD) program. Input to the TEXCAD program consists of architecture type (such as plain weave or braid), braid angle, yarn filament counts, yarn spacing, yarn fiber content, filament diameter, overall fiber volume fraction, and impregnated yarn and resin material properties. Output from the TEXCAD program consists of calculated yarn geometry, volume content, and yarn paths along with thermomechanical stiffness properties and thermal and mechanical stresses at locations along the yarn paths.

The TEXCAD program runs on a personal computer under the multitasking Microsoft (MS) Windows™ environment (shown in the figure). This program is capable of analyzing two-

dimensional (2-D) and 3-D composites, including tape laminates; spatially oriented composites; plain, 5-, and 8-harness satin weaves; 2-D braids; 2 × 2 triaxial braids; 1 × 1 triaxial braids; 3-D interlock braids; and even custom textile architectures. As shown in the figure, a generic graphical representation of each textile RUC is also included, and it may be viewed or printed at any time. Copies of the TEXCAD program have been distributed to users in industry and universities.
(Rajiv A. Naik, 43471, and C. C. Poe)
Structures Directorate

Cooperative NASA/Boeing/Pratt & Whitney Advanced Ducted Propeller Investigation

The advanced ducted propeller (ADP) offers significant performance and noise benefits (compared with current turbofan engines) for use on commercial transports. The large diameter of an ADP presents a challenge for aerodynamically efficient wing-mounted configurations. Ground clearance requirements force the engine nacelle closer to the wing, which makes physical integration of the engine and wing more difficult. Another benefit of the ADP is that it uses blade pitch changes to provide reverse thrust for airplane deceleration, thereby avoiding the weight penalties associated with current mechanisms in use on turbofan engines (such as cascades and buckets). However, as developed thus far, the ADP offers no mechanism for tailoring the reverse thrust flow field. Determination of the effects of the interaction of the ADP reverse flow field with the wing and the airframe, therefore, is of great importance to the development of the ADP as a viable engine for subsonic transports.

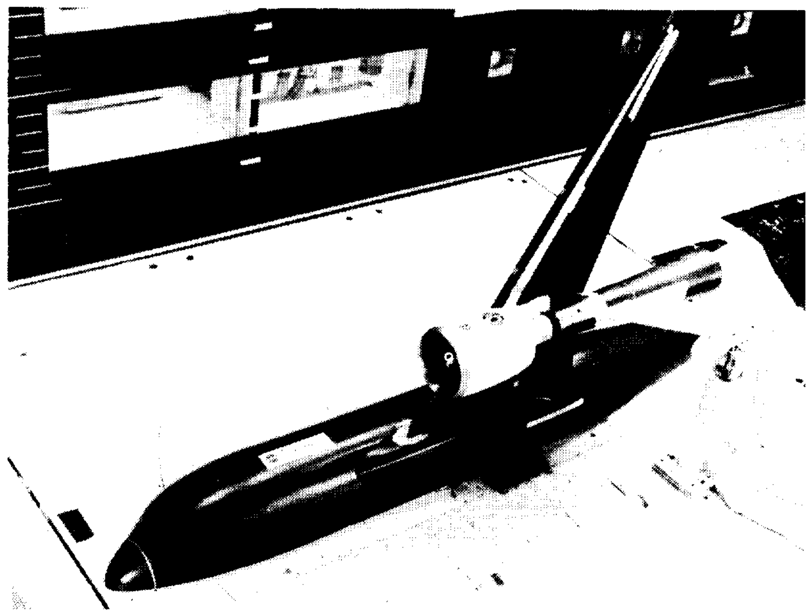

Boeing 757 with Pratt & Whitney advanced ducted propeller engine mounted in Langley 14- by 22-Foot Subsonic Tunnel. L-92-11358

A cooperative research program was initiated between NASA, Boeing, and Pratt & Whitney to enable testing of a large, semispan Boeing subsonic transport model and a Pratt & Whitney 17-in-diameter ADP in the Langley 14- by 22-Foot Subsonic Tunnel. A low-cost, temporary vertical wall was fabricated and installed in the tunnel for ground-effects testing.

Data were acquired for a range of ADP power settings and free-stream velocity conditions. The flow field created by the ADP operating in reverse thrust shielded a portion of the wing, and it resulted in an effective reduction in wing lift and drag for the configuration out-of-ground effect. Ground effect measurements were obtained, and they indicated no significant problems. There was a beneficial increase in drag and only a slight, undesirable lift increase in ground effect.
(Zachary T. Applin, 45062)
Aeronautics Directorate

Optimization of Actuator Arrays for Aircraft Interior Noise Control

Recent investigation of controlling noise from vibrating structures has demonstrated the potential of active structural acoustic control (ASAC) for effectively reducing aircraft interior noise. The ASAC relies on force inputs applied directly to a vibrating structure, instead of acoustic sources inside the structure, to

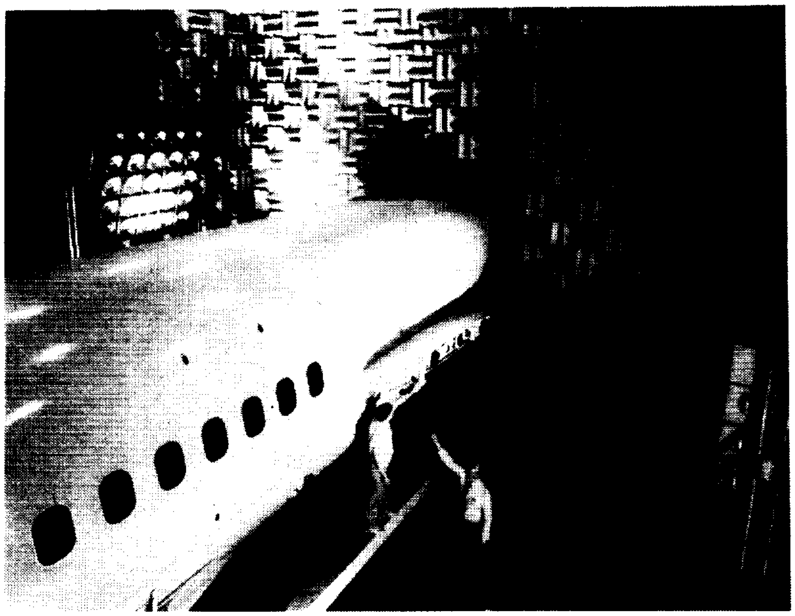

McDonnell Douglas Fuselage Acoustic Research Facility. L-87-2442

attenuate interior noise. As the ASAC concepts are integrated into practical aircraft noise control systems, some important issues arise. For example, an actuator that produces a localized force input to a structure, such as a small piezoelectric actuator, tends to excite a broad spectrum of structural modes. This behavior can significantly increase structural vibration levels, although the interior noise may still be reduced. Also, interior acoustic modes that are not present in the primary noise field may be excited. This spillover of control energy can limit the performance of a noise reduction system, and it can have possible fatigue implications for the fuselage structure. One approach to overcome these difficulties is through closely grouped actuators.

In an ongoing joint effort between Langley Research Center and McDonnell Douglas Aerospace, this actuator grouping concept was evaluated for a large number of piezoelectric actuators bonded to the exterior panels of the aft section of a DC-9 fuselage installed in the McDonnell Douglas Fuselage Acoustic Research Facility (shown in the figure). Measured data included the transfer functions between 34 piezoelectric actuators and 29 interior microphones, as well as the interior microphone responses caused by the primary noise produced by external speakers. These data were utilized to demonstrate a procedure for grouping the actuators such that their effectiveness in reducing the overall interior noise was enhanced while limiting the number of control degrees of freedom. This grouping procedure created actuator groups that improved overall interior noise reductions at four discrete frequencies by 5.3 to 15 dB compared with the baseline experimental configuration. The present work is the first evaluation of this grouping/clustering technique using experimental data from an actual aircraft fuselage.

(Harold C. Lester, 43592)
Structures Directorate

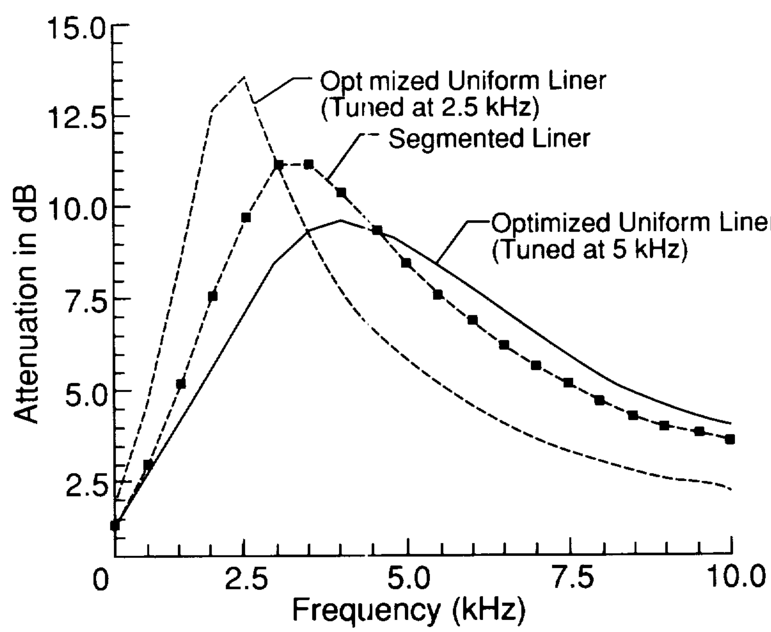

Improved broadband performance of two-segmented liner (unoptimized).

Finite-Element Algorithm for Optimizing Noise Suppression of Lined Ejectors

One component of the noise suppression system for the exhaust jet of a high-speed civil transport (HSCT) aircraft is expected to be a lined ejector. The liner of the ejector must provide significant broadband attenuation before the radiated noise will be within acceptable levels. A major challenge of HSCT technology is designing a broadband acoustic liner. An efficient finite-element model for predicting and optimizing the acoustic performance of a lined ejector with arbitrary flow and variable wall impedance properties has been developed. This finite-element model leads to a large matrix equation (consisting of several hundred thousand degrees of freedom), which is solved efficiently on one of Langley's supercomputers.

Results of a study on three different lining configurations at a Mach number of 1.5 are shown in the figure on the previous page. Two optimum uniform liners designed to achieve maximum suppression at 2.5 kHz and 5 kHz are compared with a two-segmented liner. Both optimized uniform liners perform well at their design frequencies, but their performance falls off rapidly to one side of their design frequencies. Although the segmented liner has not been optimized, it suppresses more broadband sound. These results show that an unoptimized lined ejector with variable impedance properties can attenuate more broadband sound than that of the optimized uniform liners. This gives credence to the variable wall impedance concept as a candidate for achieving broadband attenuation in HSCT. The finite-element algorithm allows even more innovative lining designs to be explored.
(Willie Watson, 45290)
Structures Directorate

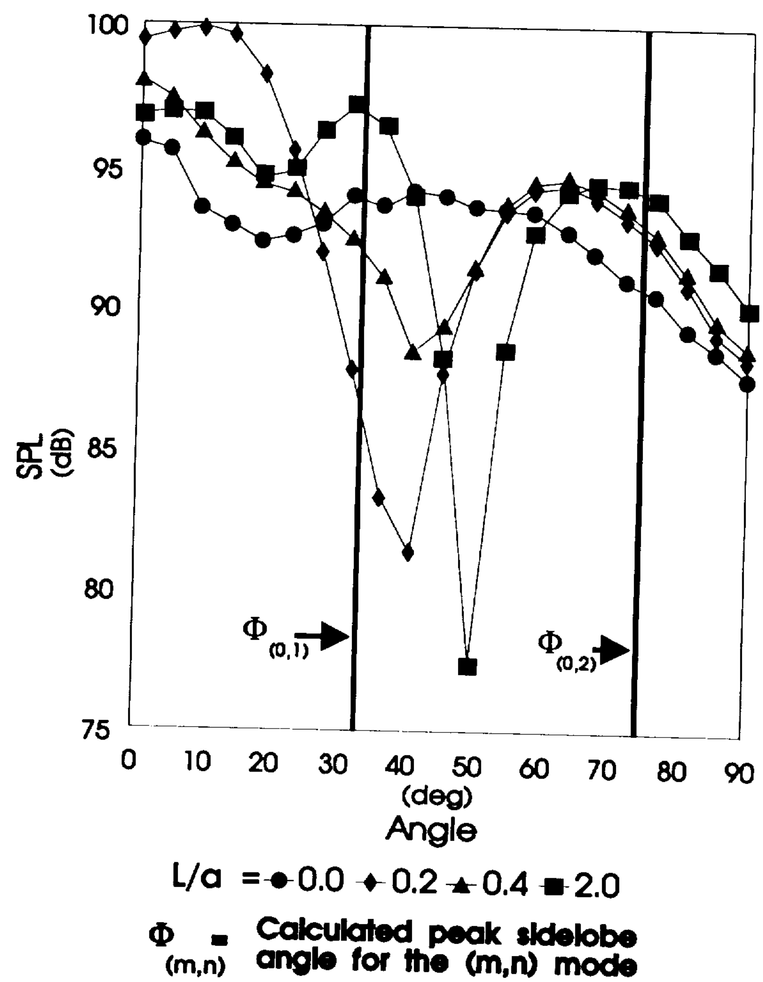

Variation of directivity with source location in duct.

Shroud Length Effect for Ducted Propellers

The ultra-high-bypass ratio propulsion system for future subsonic aircraft will have a fan diameter of approximately 12 ft and a nacelle length on the order of 1 diameter. This "short" nacelle design has led to studies into the effect of duct length on sound propagation and radiation. An acoustically long duct radiates only well-defined cut-on modes with characteristic lobes, while the radiation from a

source with no duct depends predominantly on the source directivity. An experiment, consisting of a point sound source mounted in the center of a plate which is movable in a duct, has been devised to investigate the region of transition from no duct to a long duct. The duct radiates into an anechoic room in which the directivity of the sound is measured in the far field.

A representative directivity plot is shown in the figure on the previous page for a frequency of 2620 Hz. Four different plate settings are shown: L/a = 0, 0.2, 0.4, and 2.0, where L is the distance from the plate to the end of the duct and a is the duct radius. When the source is at the end of the duct (L/a = 0), the directivity plot is relatively flat; this is expected for a point source in a flat plate radiating into free space. As L increases, a lobed pattern (indicating the presence of modes in the duct) becomes more distinct. The locations of the radiation peaks of the two modes that are expected to be cut on are shown, and the measured peaks are approaching the expected values of L/a = 2.0. The significance of this experiment is that, in order for noise control to be effective, the sound propagation in the duct must be well understood. This experiment shows that the effect of duct length can be quantified, and the results will be used to aid the development of analytical codes of sound propagation in finite-length ducts.
(Odilyn L. Santa Maria, 45104, Carl H. Gerhold, and William Nuckolls)
Structures Directorate

Mixer/Ejector Liner Performance

This experiment addresses the issue of whether the attenuation bandwidth of a mixer/ejector liner can be manipulated and enhanced over a desired frequency range by varying the surface impedance. The test model for the experiment was a 1/20-scale two-dimensional mixer/ejector with the primary nozzle operating at a Mach number of 1.5 and a temperature of 900°F. The ejector exit plane was located 0.5 in. in front of the nozzle exit plane. The figure shows far-field sound pressure spectra at 90° relative to the nozzle axis for four different liner configurations. The top curve shows the spectrum for a hardwall ejector, and it is taken as a reference condition. Three liner configurations were tested. One configuration was a conventional bulk absorber made from a synthetic fiber Kevlar™. The other two configurations were fabricated from a high-temperature glass ceramic with a microtubular structure.

Results for the two ceramic test liners show that the variable depth liner outperformed the constant depth configuration over a design target frequency range from approximately 5 kHz to about 12 kHz. Surprisingly, the constant depth configuration approaches the hard wall behavior at high frequencies. However, at lower frequencies, the results are encouraging.
(Tony L. Parrott, 45273)
Structures Directorate

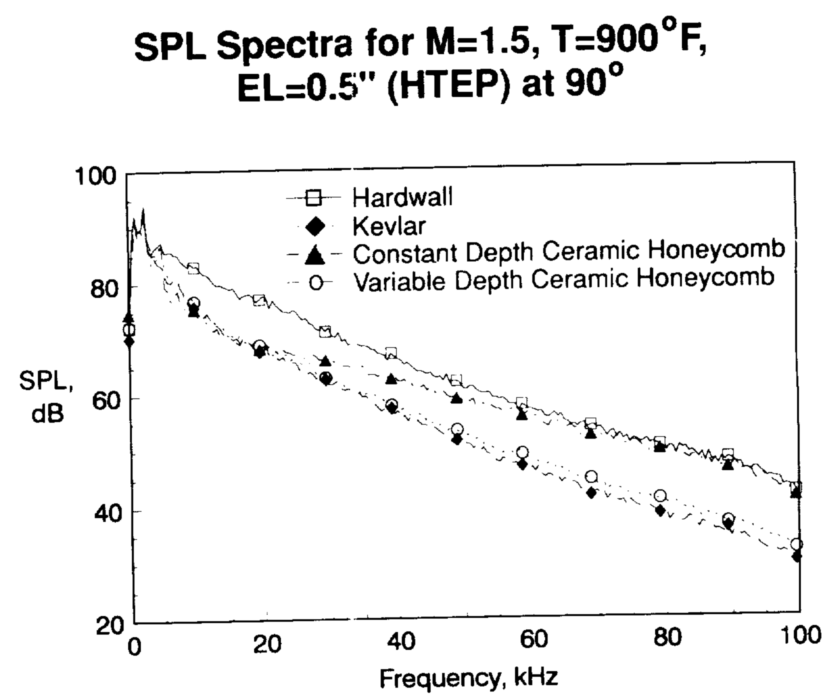

Comparisons of measured sound pressure spectra for three different liner configurations, with hardwall as reference, in scale model mixer/ejector.

Nonlinear Analysis of Stiffened Aluminum Fuselage Shells With Longitudinal Cracks

A number of aircraft in current service are nearing or exceeding their design service life. To ensure the structural integrity of these aircraft with a large number of service hours, a reliable and accurate structural analysis method is needed to determine the residual strength of aircraft with cracks in the fuselage skin, as well as other structural elements.

A hierarchical modeling strategy has been developed to analyze a stiffened fuselage shell that is subjected to an internal pressure loading and has a skin crack. Three levels of finite-element models are analyzed using the STAGS (STructural Analysis of General Shells) computer code.

The analysis is nonlinear to ensure that local stress and deflection gradients at the crack are predicted accurately. The analysis strategy includes a nonlinear analysis of a large stiffened fuselage section that is subjected to an internal pressure and bending moment loading. The model includes such structural details as frames, stringers, tear straps, shear clips, floor beams, and stanchions. In the crown of the fuselage, there is a longitudinal skin crack located midway between two stringers and two frames. The crack length is extended using a load relaxation technique while the shell is in a nonlinear equilibrium state. Displacements obtained from the analysis of this model with varying crack lengths are applied as boundary conditions to the second level of modeling, which represents a 6-bay × 6-bay crown section. This model is referred to as a local model, and it has a higher level of mesh refinement than the global model to characterize more accurately the structural response. Displacements obtained from the 6-bay × 6-bay model are applied as boundary conditions to a 2-bay × 2-bay model that is localized around the crack. This local model has an even higher level of mesh refinement to represent the behavior of the crack region.

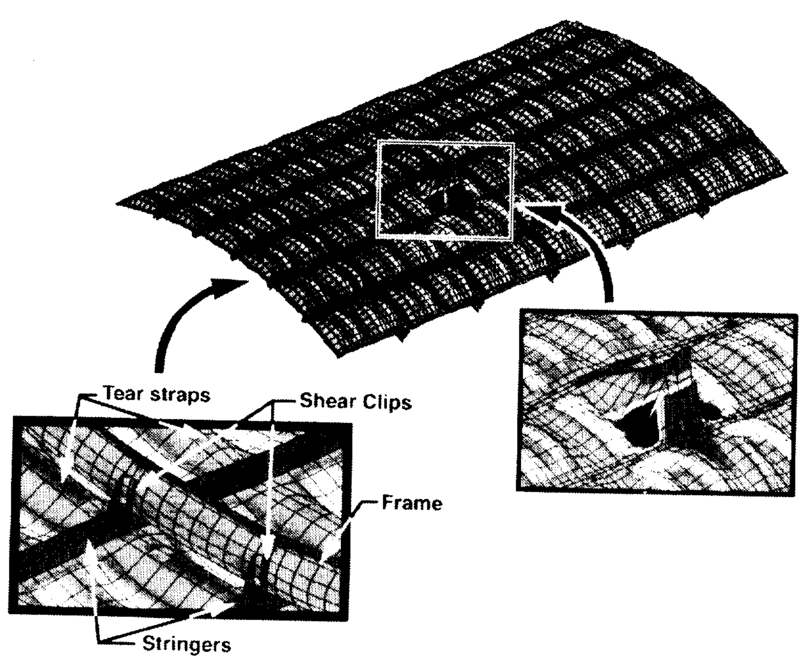

6-bay × 6-bay local model subjected to internal pressure and bending moment loads. (Original of figure in color; contact author for more information.)

This nonlinear structural analysis capability allows for an in-depth analysis of the stress and deflection gradients near a crack in a pressurized fuselage shell. Properties such as stress intensity factors at a crack tip can be determined by this analytical method, which can be used to determine the residual strength of the fuselage structure.
(Vickie O. Britt, 48030)
Structures Directorate

Fatigue-Life Prediction Methodology

Damage-tolerance design concepts based on fatigue-crack growth in aircraft structures are well established. The safe-life approach, using standard fatigue analyses, is also widely used in many designs. Fatigue analyses are slowly being replaced by durability analyses using smaller crack sizes than those used in damage-tolerant analyses. Studies on small-crack behavior have led to the realization that fatigue life of

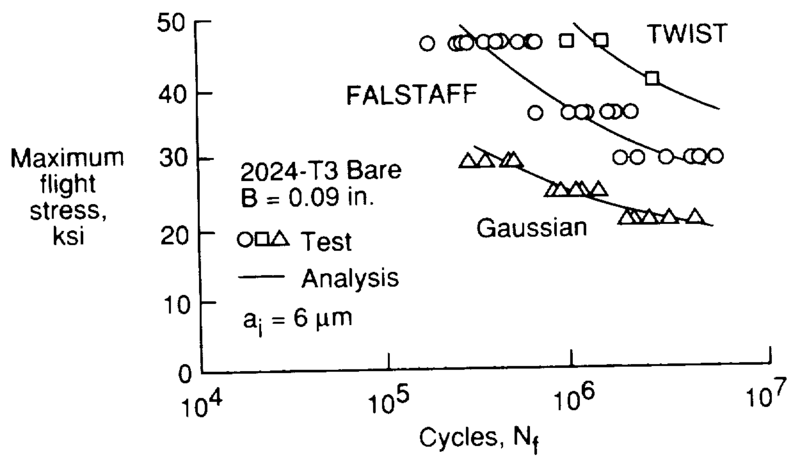

Fatigue lives for notched aluminum alloy under aircraft spectrum loading.

many materials is primarily "crack growth" from microstructural features, such as inclusion particles, voids, or slip-band formation. However, small cracks have been observed to grow much faster than large cracks. The improved fracture-mechanics analyses of some of the crack-tip shielding mechanisms, such as plasticity- and roughness-induced crack closure, and analyses of surface- or corner-crack configurations have led to more accurate crack-growth analysis methods for small and large cracks.

A typical comparison of experimental and predicted fatigue lives of notched specimens made of 2024-T3 aluminum alloy and tested under three aircraft spectrum load sequences is shown in the figure. The tests, conducted by several different laboratories, used a fighter wing spectrum (FALSTAFF), a transport wing spectrum (TWIST), or a Gaussian random (tension/compression) spectrum. The predictions were made using a crack-closure model with an initial defect size (a_i = 6 µm) that was based on an average inclusion particle or void size that initiated cracks. The predictions agreed well with the test data.
(J. C. Newman, Jr., 43487)
Structures Directorate

Verification of Fracture Criterion for Multiple-Site Damage

Structural integrity of aging commercial transport airplanes may be reduced by widespread fatigue damage (WFD) (i.e., cracks developing at several adjacent locations). The WFD problem is of concern because residual strength of a structure with a long lead crack may be greatly reduced by the existence of adjacent smaller cracks. Tests conducted by the Federal Aviation Administration (FAA) on panels with long lead cracks and multiple-site damage (MSD) are showing that residual strengths are strongly degraded (as shown in the figure) from single (lead) crack behavior. One of the objectives in the NASA Airframe Structural Integrity Program is to develop the methodology to predict failure of structures in the presence of MSD or multiple-element damage (MED). The approach is to use a finite-element (FE) analysis with adaptive mesh

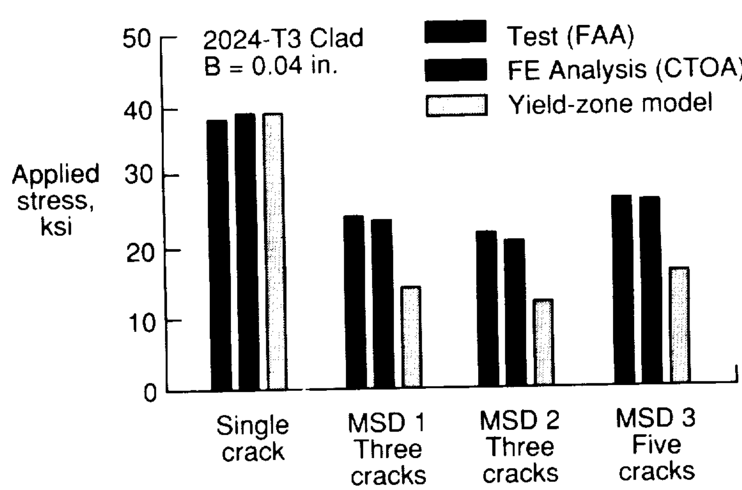

Comparison of failure stresses from tests and analyses of multiple-site damage (MSD) crack configurations.

capabilities and local fracture criteria to predict progressive failure in complex structures.

The critical crack-tip-opening angle (CTOA) fracture criterion has been verified for cracks tearing in thin-sheet 2024-T3 aluminum alloy material. An elastic-plastic FE analysis has also been successfully used to model the fracture process. Typical MSD crack configurations tested had a long lead crack with a various number of smaller MSD cracks near the lead crack. The simple plastic yield-zone linkup model greatly underpredicted the failure stresses in the presence of MSD, but the FE analysis using the CTOA criterion predicted failure stresses that agreed well with the tests.
(J. C. Newman, Jr., 43487, and D. S. Dawicke)
Structures Directorate

Self-Nulling Electromagnetic Flaw Detector

The Self-Nulling Electromagnetic Flaw Detector has been developed for the inspection of conducting materials for fatigue crack damage. It uses a ferromagnetic lens placed between concentric drive and pick-up coils to focus the flux of the probe. The unique coil configuration results in a zero, or null, voltage output when unflawed material is inspected. Changes in the path of the eddy-current flow caused by the presence of flaws in the material generate a time-varying magnetic field at the pick-up coil location. This magnetic field, in turn, produces an electromotive force across the pick-up coil leads, which is measured with an ac voltmeter. The first figure displays the flaw detection capabilities of the probe. This figure shows the relative insensitivity of the probe to lift-off changes and the large output of the probe in the presence of a fatigue crack. The device is extremely sensitive to fatigue cracks and small changes in material thickness caused by factors such as corrosion damage.

The simplicity of the design of the probe greatly reduces instrumentation requirements, and the unambiguous flaw signals can eliminate training time and operator errors. The device is extremely portable, and commercialized production is expected to produce a low-cost instrument. A portable

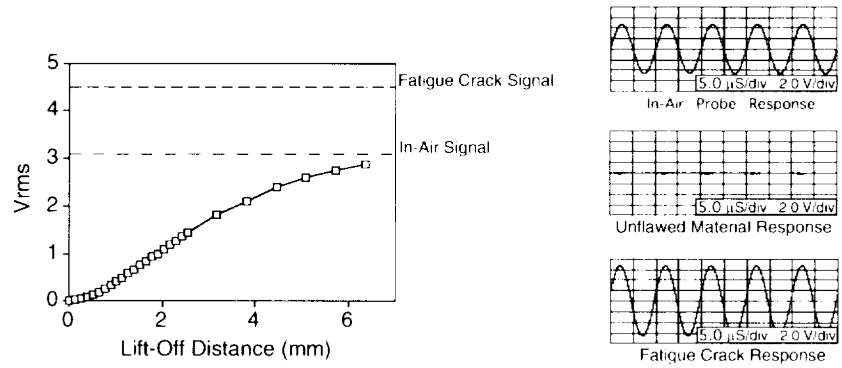

Flaw detection characteristics. Measurements are taken at 100 kHz with 1-mm-thick Al 6061 sample.

Portable field unit. L-93-07811

C-2.

field unit has been constructed, as displayed in the second figure. This figure shows an operator inspecting an airframe lap-joint sample.
(John Simpson, 44716, Buzz Wincheski, Min Namkung, Jim Fulton, Shridhar Nath, Ron Todhunter, and Jerry Clendenin)
Electronics Directorate

Portable Ultrasonic Instrument for Disbond and Corrosion Characterization in Aircraft

High-frequency mechanical vibrations, known as ultrasound, can penetrate into solid materials, interact with the internal structure, and carry information about that structure to a sensor. Langley researchers have been exploiting these phenomena to develop instrumentation for detecting and characterizing disbonds, corrosion, and cracks in aluminum aircraft structures. A number of ultrasonic approaches have been developed (normal-incidence compressional waves, angled shear waves, and plate or Lamb waves); these approaches exercise the stiffness properties of the material in different manners, thus allowing the instrumentation to access varied information about the material and exhibit sensitivity to different flaw types.

Through a combination of physical analysis and modeling, the science of the system tells us how to design the measurement probes and instrumentation. Artificial neural networks are trained using both actual measured signals and synthesized signals from physical modeling to provide robust interpretation of a wide range of possible conditions. Incorporation of arrays of multiple sensors can allow more rapid inspection and provide flexibility for multiple measurement approaches. This combination of modern technologies has great potential for aerospace and other engineering and industrial applications.

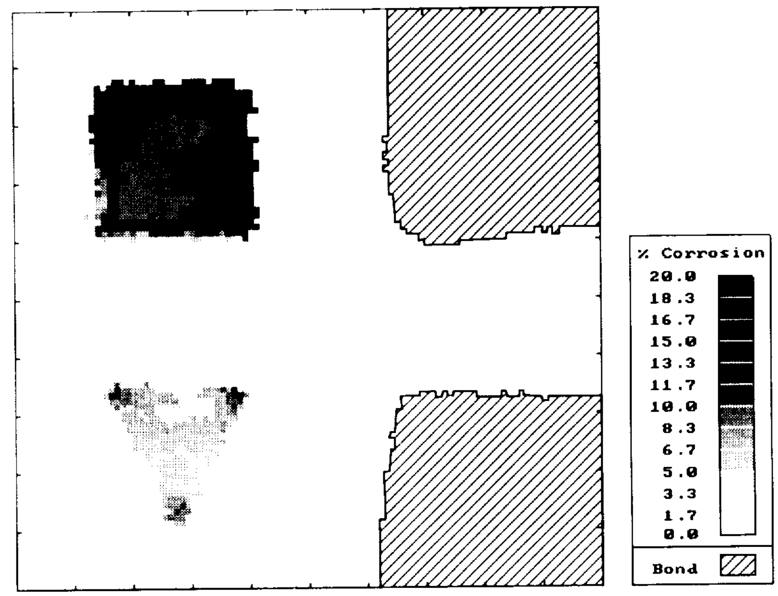

Ultrasonic determination of bond, disbond, and thinning caused by corrosion. Neural network interpretation identifies two bonded regions in upper and lower right of panel, and spectral analysis yields thickness of two electrochemically corroded patches on unbonded skin.

A portable PC-based instrument has been assembled using commercial board-level components and manual scanner. The system currently employs normal-incidence ultrasound, and it uses a trained software neural network to interpret the no-bond/bond condition and spectral analysis to determine the thickness. The results are expressed as an image in real time. Excellent accuracy has been achieved within the scope of the network training set. The figure shows the ultrasonic determination of bond, disbond, and thinning caused by corrosion in a test sample. Neural network interpretation identifies two bonded regions in the upper and lower right of the panel, and spectral analysis yields the thickness of two electrochemically corroded patches on the unbonded skin.
(P. H. Johnston, 44966, N. M. Abedin, D. R. Prabhu, and N. Nathan)
Electronics Directorate

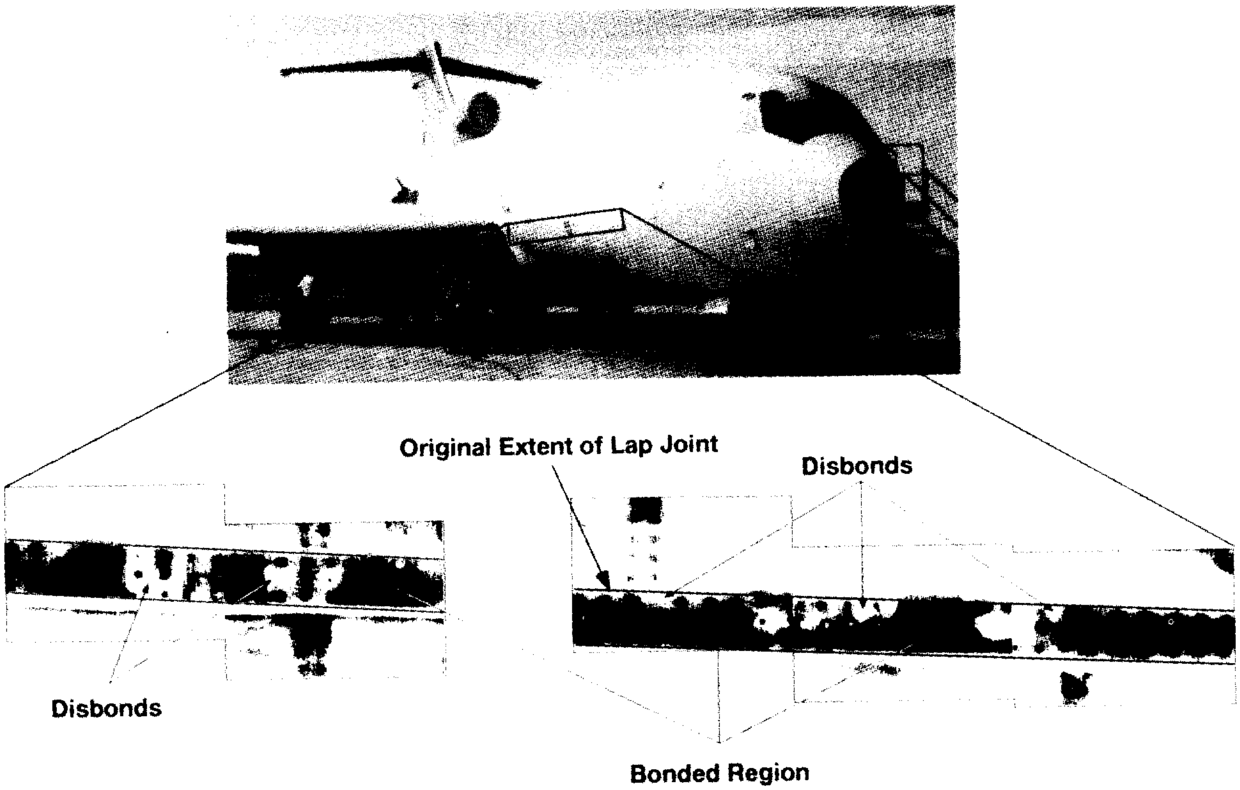

Application of thermal bond inspection system to commercial aircraft, which results in ability to image disbonding between two skins at lap joint.

Thermal Bond Inspection System for Aircraft Structural Integrity

The thermal bond inspection system (TBIS) uses thermal energy and infrared imaging to characterize the state of a bonded structure. A small amount of heat is applied to the surface of the structure; the time evolution of the surface temperature is then recorded using an infrared camera and a digital image processor. Various methods of data analysis then can be performed to transform the temperature images into images representative of physical features of the measured structure. By quantitatively analyzing the digitized images, the TBIS provides great improvements over simply measuring the surface temperature. This technology has the additional advantage of being completely noninvasive, noncontacting, and geometry insensitive, and rapid, large-area, archivable imaging is possible.

This technology, which has been successfully applied to characterizing both disbonding and material loss caused by corrosion in commercial aircraft skins, has a strong commercial potential for application to aging aircraft issues and numerous commercial applications outside the aerospace community.
(K. Elliott Cramer, 47945)
Electronics Directorate

Stress Imaging Via Differential Thermography

Dynamic stress imaging is a technology that has application and impact for a broad range of commercial needs. The commercial uses include stress imaging for aerospace materials and structures, industrial equipment and products, and civil structures, nondestructive material damage

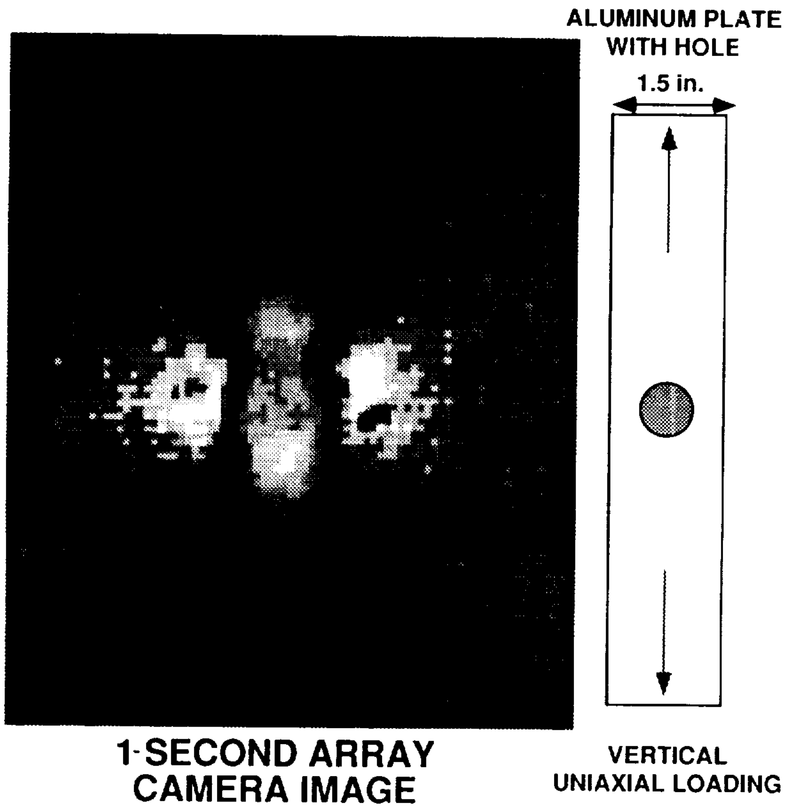

Stress field produced by tensile loading of aluminum plate with circular hole.

appraisal, and product and material development. Langley's Nondestructive Evaluation Sciences Branch has contracted Stress Photonics of Madison, Wisconsin, in a Phase II Small Business Innovation Research award to prototype an infrared camera optimized for differential thermography, stress imaging, and nondestructive evaluation.

The prototype instrument relies on the thermoelastic effect to permit direct observation of strains in materials that are being stressed. The thermoelastic effect produces small temperature changes when the structure is elastically loaded (i.e., a stress of 60 psi in aluminum produces 0.001°C temperature change). The technique images these small temperature changes with an infrared focal plane array (FPA) and sophisticated digital signal processing. The system produces an image of near-surface stresses by rapidly sampling the FPA and statistically correlating pixel data to the loading imposed on the target structure. Recent improvements in digital sampling, signal processing, and infrared detector array fabrication are combined into the portable, high-speed imager. The camera is capable of imaging the dynamic stresses in a structure in as little as 1 sec. The figure represents the stress field produced by tensile loading of an aluminum plate with a circular hole.

(K. Elliott Cramer, 47945)
Electronics Directorate

Tilt-Rotor Fountain Flow Noise

Studies have indicated that a civil tilt-rotor aircraft is a possible solution to the air capacity problem in the U.S., and it has a strong market potential by the year 2000. However, the reduction of noise levels in a vertiport environment can be a critical enabling technology for its development. Hover flight operations present the community with very severe noise signatures. The most dominant noise mechanism for the tilt rotor is a phenomenon called "fountain effect." Fountain-effect noise is generated when the rotors pass through the turbulent fountain flow created as the rotor downwash impacts the wing and is recirculated through the rotors over the inboard portion of the wing.

Langley and Ames Research Centers conducted a joint program of acoustic hover tests on the XV-15 tilt-rotor research aircraft. The flight experiment consisted of hovering the aircraft over a 500-ft-radius semicircular array of 12 ground plane microphones. Each flight condition was repeated for two reciprocal aircraft headings to provide a full 360° acoustic coverage. The figure presents A-weighted overall sound pressure

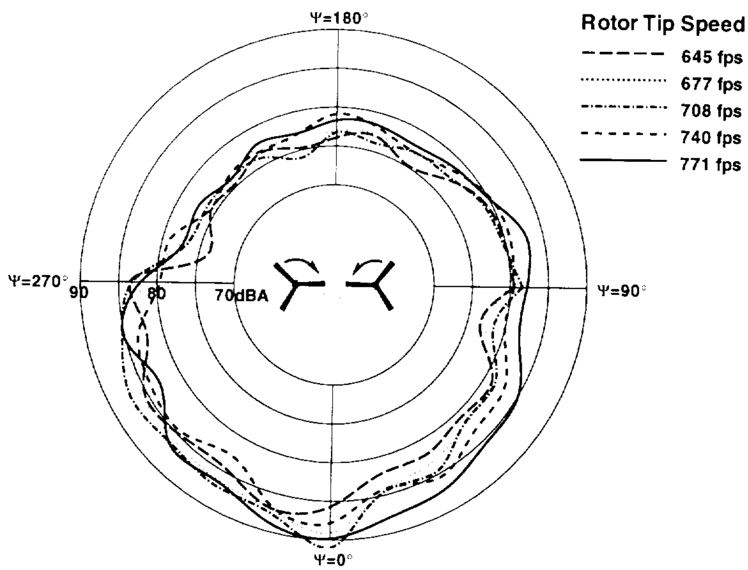

A-weighted overall sound pressure levels.

levels as a function of directivity angle for the 5 rotor tip speeds tested. Because of the aft directionality characteristics of "fountain effect" noise, A-weighted overall sound pressure levels measured aft of the aircraft ($\Psi = 0°$) were approximately 10 dB higher than the levels measured forward of the aircraft ($\Psi = 180°$). In addition, there is only a very weak correlation of noise level with rotor tip speed. (Noise levels typically decrease with decreasing rotor tip speed.) With improved understanding, it will be possible to model aerodynamically derived improvements to evaluate their noise reduction potential.
(David Conner, 45276, Ken Rutledge, and Mike Marcolini)
Structures Directorate

High-Speed Civil Transport

RESEARCH AND
TECHNOLOGY

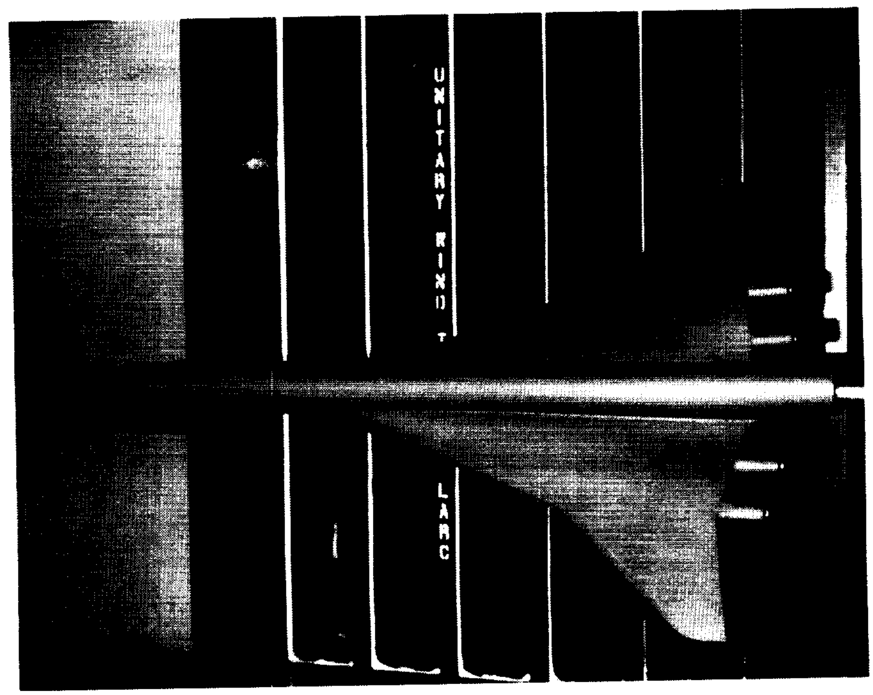

Resolve the critical environmental issues and provide the technology base for future high-speed air transportation

Supersonic Laminar Flow Control Swept Cylindrical Model

A cylindrical model was designed and fabricated for supersonic laminar flow control research that had adopted an unconventional approach to solve the challenging design criteria. The model was to have microperforated skin through which a nonuniform controlled level of suction would be applied. The variation in suction was provided by nine axial plenums under the porous skin, and each was controlled by metering holes through three primary plenums. The suction surface of the cylinder extended through 180° of circumference. Flow passages were designed to meet suction requirements by careful sizing of the perforated skin and the metering-hole diameters.

Multistaged electroforming was an approach employed in specific rocket-motor designs in the 1960's and appeared promising for this application. A machined core of high-strength stainless steel was filled with a conductive wax containing a fine dispersion of silver. Upon this filled core, electrodeposited nickel was applied and postmachined into nine axial plenums and drilled for metering holes into the three main chambers. Another layer of wax was laid, and the final skin of nickel was deposited around the entire circumference of the model. This layer was ground to a surface finish of 4 RMS. The model was then laser drilled to microperforate the outer skin and immersed in a hot-vapor degreasing bath to remove plating wax from the plenums. The model was completed by attaching connecting tubes to the base of the cylinder and through the support fixture for testing at the Supersonic Low-Disturbance Tunnel, building 1247D. The key fabrication elements of postmachining of electrodeposited nickel and wax removal were validated using trial specimens to identify potential difficulties. The model skin was perforated with 0.003-in-diameter holes whose shape and spacing were closely machined to meet the tight tolerances of the research objectives. Laser drilling samples using electrodeposited nickel were solicited from several vendors, and the best sample was selected. The final research article successfully validated a multistaged electroforming technique and has permitted design and fabrication of a more complex two-dimensional swept-wing model for related research.

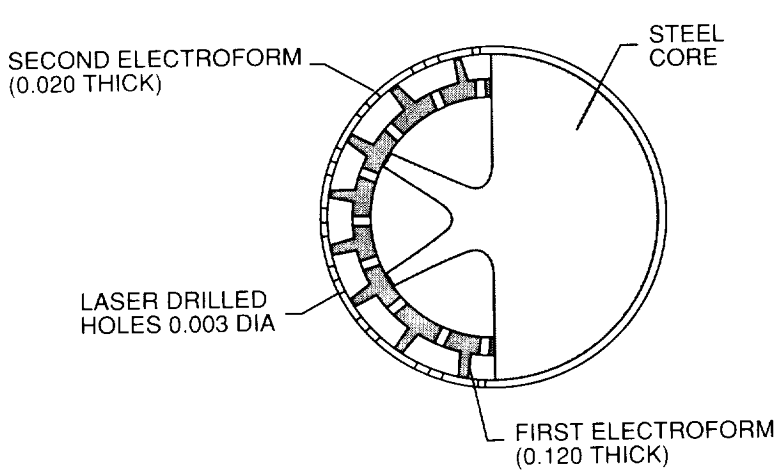

Supersonic swept cylindrical model. (Dimensions in inches.)

(William M. Kimmel, 47136)
Systems Engineering and Operations Directorate

Determination of Flow Quality in Unitary Plan Wind Tunnel

The effect of wind-tunnel flow quality on viscous flow characteristics, such as boundary-layer transition location, can have a significant impact on the aerodynamic perfor-

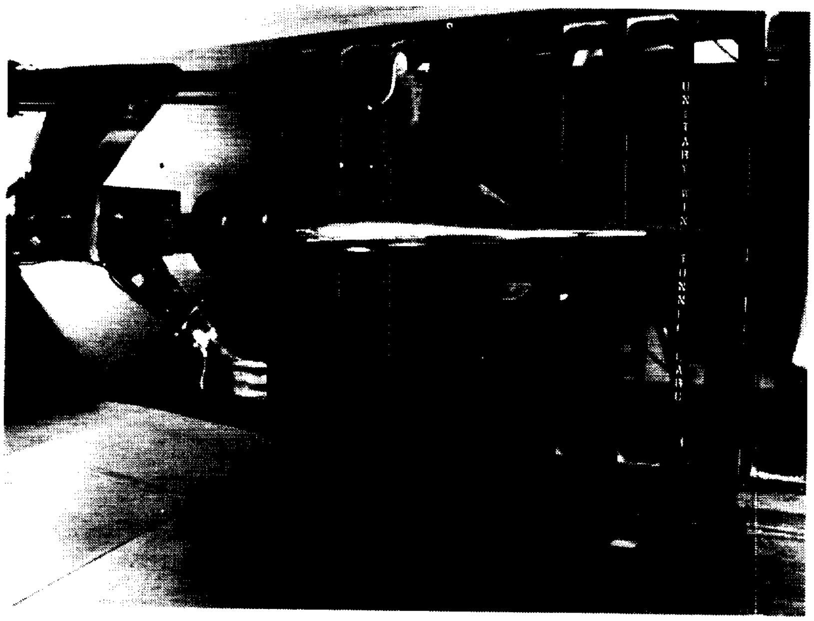

AEDC 10-degree transition cone mounted in Unitary Plan Wind Tunnel. L-91-14593

mance of slender supersonic configurations (e.g., the High-Speed Civil Transport). The Arnold Engineering and Development Center (AEDC) 10-degree transition cone has been tested in flight and in numerous wind tunnels around the world. The model provides a common reference to compare tunnel flow quality between facilities and was last tested in the Unitary Plan Wind Tunnel (UPWT) in 1974.

The AEDC 10-degree transition cone was tested in both UPWT test sections to determine any changes in cone transition Reynolds number that resulted from changes in tunnel flow quality since 1974. In addition, the tunnel free-stream turbulence levels were determined. Cone transition Reynolds numbers were obtained from transition location measurements by using boundary-layer pitot and hot-wire probes that translated longitudinally on the cone surface. Free-stream turbulence levels were measured by using a dynamic pitot-pressure transducer and a three-wire hot-wire probe. Static and unsteady data were obtained at Mach numbers from 1.6 to 4.6 over a Reynolds number range of 1.0×10^6 to 5.0×10^6 per foot. The results indicate a reduction of up to 28 percent in cone transition Reynolds number relative to the results obtained in 1974. This decrease in transition Reynolds number indicates that either the tunnel turbulence levels have increased, the model geometry has been altered, or transition location was interpreted differently since the 1974 test. In addition, the steady-state transition location indicated from pitot-probe results occurred significantly downstream of the location determined by the hot-wire probe. This database will provide information necessary to assess the effectiveness of future tunnel improvements.

(Jeffrey D. Flamm, 45955, Peter F. Covell, and Gregory S. Jones)
Aeronautics Directorate

Supersonic Wind-Tunnel Tests of Reference H Configuration

The Reference H high-speed civil transport (HSCT) configuration has been established as the baseline geometry for High-Speed Research (HSR) Program studies. This configuration was originally developed by the Boeing Aircraft Company and is representative of current state-of-the-art HSCT technology. Numerous experimental studies are being conducted to provide information necessary for design, code, and facility/test-technique verification. In addition, the Reference H will serve as a basis for evaluating aerodynamic technologies such as advanced wing and propulsion integration design methodologies.

Wind-tunnel tests were conducted in the Langley Unitary Plan Wind Tunnel on a 1.675-percent scale model of the Reference H configuration at Mach numbers ranging from 1.65 to 2.7. The objective of these studies was to determine the supersonic aerodynamic characteristics of the Reference H configuration and evaluate various nacelle diverter geometries. Because of the sensitivity of HSCT performance to drag, studies of the repeatability accuracy of the test measurements and detailed boundary-layer trip drag were also conducted. Force-

This test provided the first extensive low-speed data set for the Industry Reference Configuration. The data that were obtained are being used to evaluate this configuration and to identify areas that require additional testing. The data are also being used in flight simulation to develop advanced takeoff procedures aimed at reducing the noise near the airport.
(Guy T. Kemmerly, 45070)
Aeronautics Directorate

6-percent HSCT model mounted in Langley 14- by 22-Foot Subsonic Tunnel. L-93-04908

F-16XL High-Lift Flight Experiments

As part of a research program to reduce the risk of high-lift methods and concepts developed to improve performance of the high-speed civil transport, flight experiments are being conducted on an F-16XL aircraft. The objectives are to obtain detailed flow physics and performance measurements on the basic aircraft as well as a high-lift configuration. To optimize the flight instrumentation, several wind-tunnel and water-tunnel experiments have been conducted. The first test was conducted in the Langley Basic Aerodynamics Research Tunnel (BART) on a 4-percent scale model of the F-16XL. The primary objective of these tests was to obtain basic flow-field measurements using surface and off-surface flow visualization. A titanium-dioxide and kerosene mixture was used to determine the streamlines on the upper surface of the wing, while an upstream smoker and variable laser light sheet were used to visualize the vortex patterns in the flow field around the aircraft model. The tests were conducted at a dynamic pressure of 5 lb/ft^2, which yielded a unit Reynolds number of 400 000 per ft. Results showed a strong primary vortical flow field on the aircraft as well as secondary and crank vortices over the range of angle of attack (8° to 20°) of interest.

A second test was conducted in the Langley 16- by 24-Inch Water Tunnel using a 2.5-percent scale model and colored-dye injection for visualization of the wing vortices. The objective of these tests was to provide information on where to locate smoker exit ports on the flight vehicle. The model was tested at a speed of 0.25 ft/sec, a unit Reynolds number of 23 000 per ft, and a range of angle of attack of 5° to 20°. Several dye-injection ports were distributed along the fuselage and wing leading edge. The figure shows the vortex patterns at an angle of attack of 10°. Much of the dye from the fuselage and forward wing ports has entrained in the primary vortex. Ports farther

High-Speed Civil Transport Planform Tests

A series of flat-plate planform models were tested in the Langley 14- by 22-Foot Subsonic Tunnel to determine the effect of planform variations on promising high-speed civil transport technologies. These models vary in inboard leading-edge sweep from 68° to 74° and in outboard leading-edge sweep from 48° to 60°. A set of leading-edge vortex flaps were designed for the various planforms using a vortex-lattice design method. Although the vortex flap did not perform in the optimal manner with the vortex flow reattaching along the hinge line, the test results indicate that their effectiveness was only slightly influenced by leading-edge sweep for the range tested. It was also found that large increases in lift over drag were obtained when an attached-flow leading-edge flap was installed on the outer panel. Although the flap did not completely eliminate leading-edge separation on the outer panel, attached flow could be achieved by slotting the attached-flow flap.

Euler solutions on unstructured grids have been obtained for the planform models with deflected leading-edge vortex flaps and trailing-edge flaps. The grids were generated using an unstructured grid generator, VGRID3D, and calculations were obtained by using the unstructured grid Euler solver, USM3D. A typical surface-grid pattern and corresponding Euler solutions are shown in the figure. Initial comparisons between the computational and experimental results indicate reasonable correlation between the two near the design angle of attack but poor correlation at low angles of attack. Much of this discrepancy is because the Euler code overpredicts the expansion of the flow at the beveled trailing edge of the configurations. Although Euler solvers cannot model the secondary vortices that are typically present on these configurations, good agreement was obtained for the location of the primary vortex reattachment line.

(Kevin J. Kjerstad, 45022)
Aeronautics Directorate

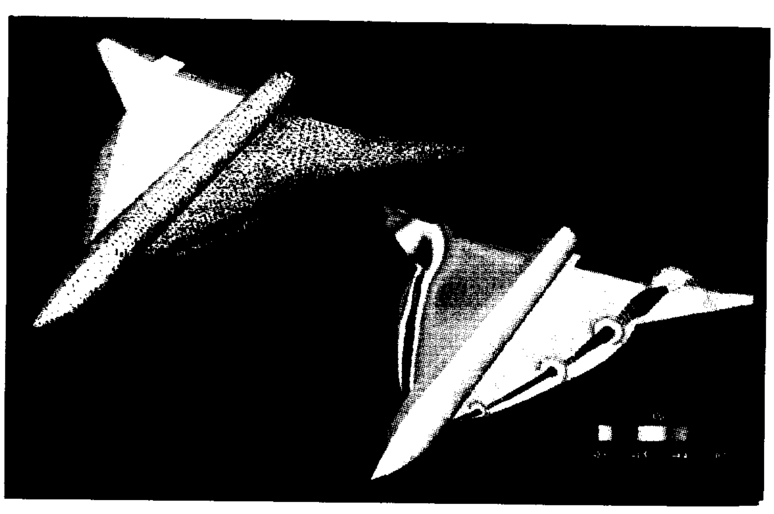

HSR planform study (USM3D). 68/48 planform with δ_{vf} = 30.0°, δ_f = 15.0°, Mach = 0.22, and α = 12.0°.

Low-Speed Tests of High-Speed Civil Transport

In an effort to generate a high-quality data set of the low-speed stability-and-control and ground-effect characteristics of the High-Speed Civil Transport (HSCT) Program's Industry Reference Configuration, a 6-percent scale model of the configuration was tested in the Langley 14- by 22-Foot Subsonic Tunnel. The model was configured with various leading- and trailing-edge high-lift systems. The primary customers of the results are the aircraft companies that work in the program and the NASA research team that compiles the simulator database.

The model was mounted on a blade-type support strut that was designed to enter the fuselage from both above and below. As shown in the figure, the model was first assembled with the blade penetrating the belly of the model. In this configuration, stability and control testing occurred with minimal interference to the flow into the vertical tail. To allow for ground-effect testing, the support was then inverted and penetrated the model from the top, just forward of the vertical tail.

distorted by propagation through the atmosphere. The study included idealized N-waves and signatures representing several distinct measured boom shapes. These were: N-waves, peaked waves, rounded waves, and U-shaped waves. Examples of measured N-waves, peaked waves, and U-shaped waves are shown on the right of the figure. Results are summarized on the left of the figure and show the linear regression lines relating the subjects' scores (the logarithm of the geometric means) to PL for each boom shape. The tight grouping of the regression lines indicates that no differences in subjective responses, for a given PL value, were observed. Thus, PL successfully accounted for loudness effects of both measured and idealized booms. This confirmed the previous recommendation of PL as the metric of choice for predicting loudness and/or annoyance of sonic booms.
(Jack D. Leatherwood, 43591, and Brenda M. Sullivan)
Structures Directorate

Absorption Theory Improves Prediction of Sonic-Boom Rise Time

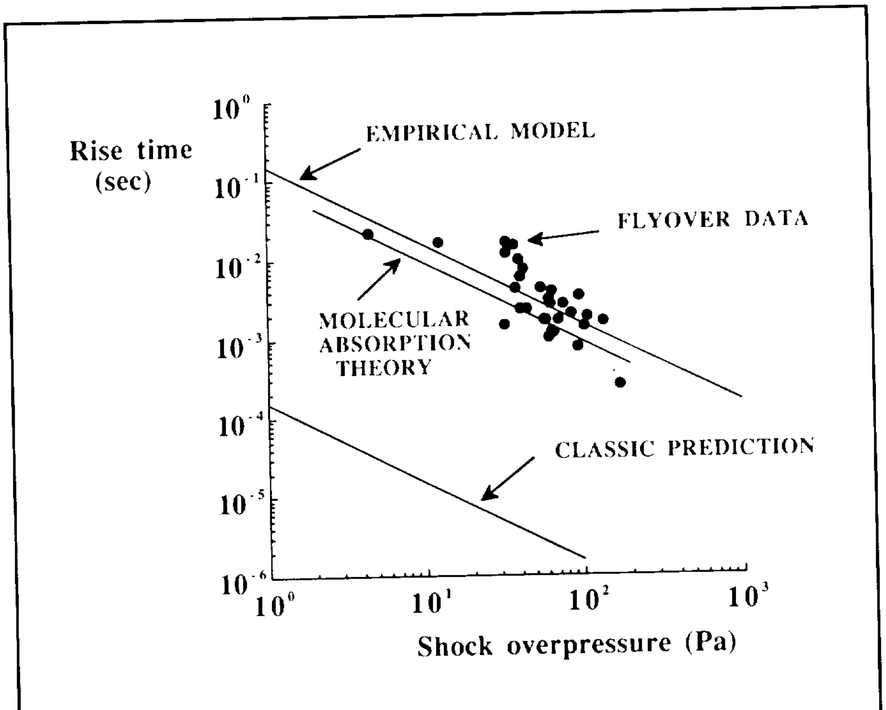

Prediction of sonic-boom rise time.

A goal of the NASA High-Speed Research Program is supersonic overland flight. A major stepping-stone to that goal is understanding the role played by the atmosphere in the distortion of the sonic-boom waveform. In general, the sonic-boom waveform has the shape of a letter N; that is, the pressure first rises, quite rapidly, from ambient atmospheric pressure to a peak value. This rapid rise is followed by a decrease in pressure to a value nearly as much below ambient as the initial rise was above ambient. This decrease in pressure occurs on a time scale that is on the order of several thousand times that of the initial pressure rise. Finally, the pressure is returned to ambient through another rapid pressure increase. The time span required for the initial pressure increase is referred to as the rise time, and this parameter is an important measure of the annoyance of the sonic-boom waveform. Ideally, this initial pressure rise should occur over as long a period of time as possible. However, the factors determining this rise time are not all at the disposal of the aircraft designer. The rise time is determined primarily by the total increase in pressure across the shock front. This increase is governed by the aircraft weight, Mach number, and shape, and a balance between the nonlinear propagation effects and the dissipation of the atmosphere. The tools initially available for prediction of sonic-boom rise time were based on nonlinear propagation of viscous and heat-conduction losses, plus an empirical fit to measured rise times. These two predictions are given in the figure, and they differ by several orders of magnitude. In an attempt to improve the prediction of rise time, a model was developed that incorporated absorption due to molecular relaxation effects of the various gases in the air. The predicted rise time of this improved model is displayed in the figure, and there is much better agreement than that obtained with the classical-theory prediction model.
(Gerry McAninch, 45269)
Structures Directorate

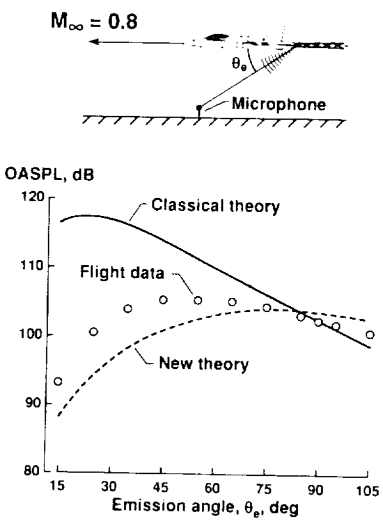

Comparison of measured and predicted jet noise levels from a high-speed aircraft flyover.

Research Center enabled a comparison to be made between high-speed flight data and predictions from the two theories. The figure shows the overall sound pressure level (OASPL) of the noise received by a ground microphone at various angles to the aircraft during a constant-altitude flyover at a Mach number of 0.8. The increase in measured noise level in the forward direction over that at 90° is significantly less than that predicted by the classical theory. Although the noise levels from the new theory are slightly lower than those that are measured, the frequency contents of the two are very similar and provide the direction to improvements to the new theory that should give even closer agreement with experiment.
(Thomas D. Norum, 43620)
Structures Directorate

Subjective Response to Recorded Sonic Booms

Langley Research Center has conducted a series of laboratory tests to quantify subjective loudness and/or annoyance of a wide range of simulated sonic-boom signatures. One result of these studies was the identification of perceived level (PL) as the best metric for predicting the subjective response to idealized sonic-boom signatures. However, validity of PL as a loudness estimator for more realistic signatures was not determined.

The sonic boom simulator at Langley Research Center was used to obtain subjective loudness judgments of actual sonic-boom signatures. The signatures were generated by supersonic aircraft at White Sands Missile Range and represented booms that were

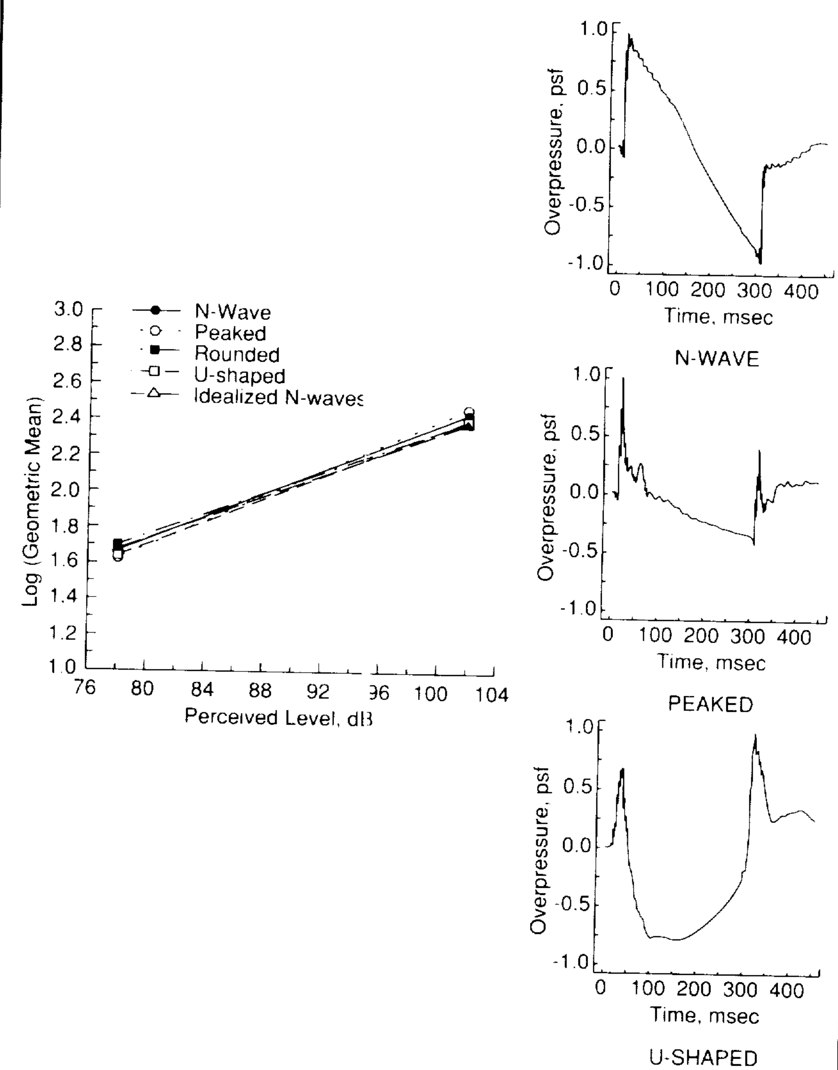

Subjective response to measured sonic booms.

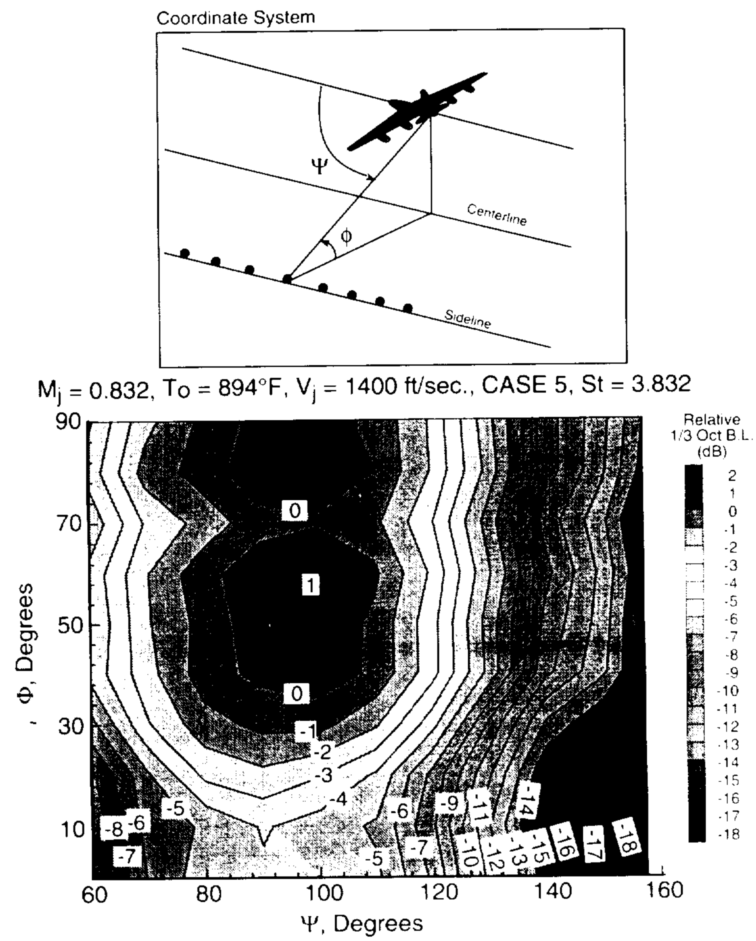

Relative acoustic levels in dB between four in-line engines and four equivalent noninteracting jets. (Original of lower figure in color; contact author for more information.)

planform configuration as the baseline, four nozzles were located in 13 alternate configurations to assess the importance of engine horizontal and vertical stagger, engine spacing, and outboard engine power setting on observed ground-based noise. The tests were designed to study the influence of shielding by using five jet exhaust velocities between 1000 and 1600 ft/sec at subsonic jet exhaust Mach numbers. These conditions are expected at the exit of a fully mixed HSCT-type ejector nozzle. One example of the results of this study is shown in the figure for the jet exhaust velocity of 1400 ft/sec. Relative acoustic levels, determined by the difference between four nozzles at equal power settings with a spacing of 2.5 jet exit diameters and no horizontal or vertical stagger from that of four equivalent noninteracting jets of equal power, are shown on a contour map in the figure. The angle ϕ is the azimuthal direction; $\phi = 0°$ is the sideline. The angle Ψ is the longitudinal direction; $\Psi = 0°$ is the engine inlet axis. The data are compared with those levels associated with the acoustic frequency that is expected to be most important to the ground-based observer in the perceived noise-level metric. As can be seen from the contour levels, significant reduction of noise can be achieved with this engine-airframe integration scheme. The most significant noise shielding is observed with 25° vertical stagger, where the outboard engine plume, operating with 10-percent power reduction, directly blocks noise radiation from inboard engines that are operating with a 10-percent increase in power setting.
(John M. Seiner, 46276, Bernard J. Jansen, and Michael K. Ponton) Structures Directorate

Flight Effects on Jet Shock Noise

The dominant forward-propagating noise from the High-Speed Civil Transport during its climb to cruise is projected to be the broadband shock noise that is produced by its supersonic exhaust jets. Classical acoustics theory predicts this noise to increase dramatically as the aircraft accelerates to high subsonic speed.

A newly developed theory of broadband shock noise predicts trends in flight that are radically different from those of the classical theory. Acoustic flyover measurements of an F-18A aircraft obtained during the 1991 climb-to-cruise experiments at NASA Dryden Flight

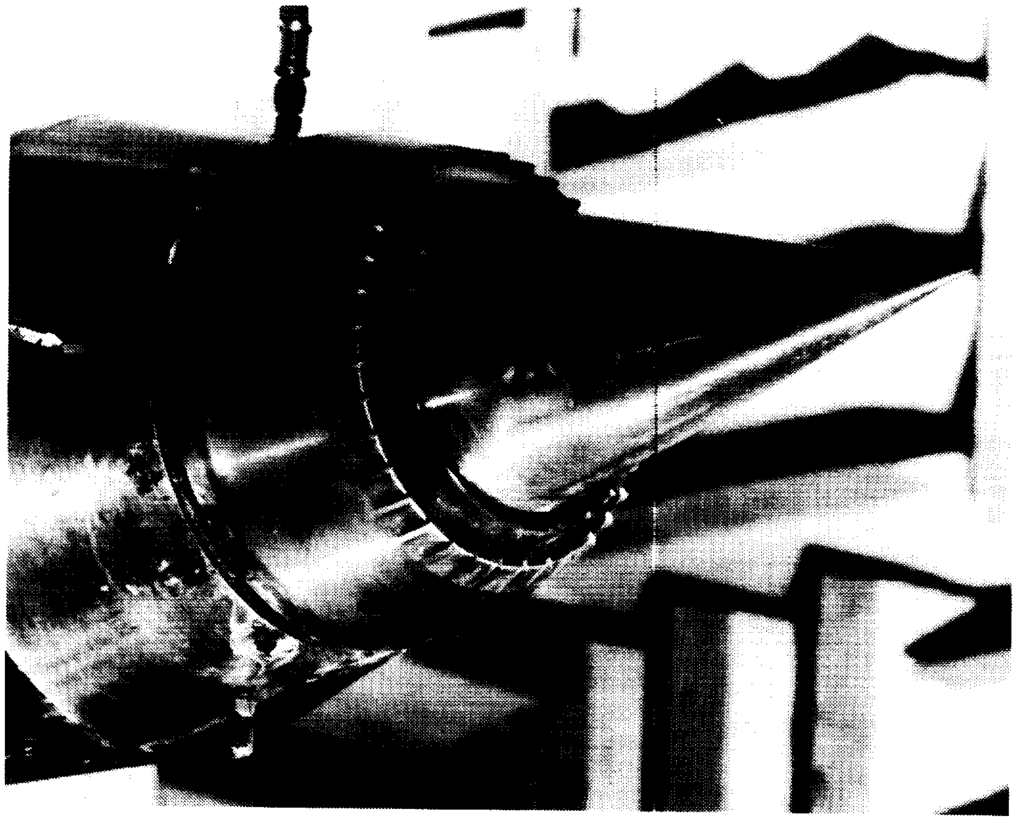

Langley Jet-Noise Laboratory 1/10th-scale high-temperature coannular supersonic jet nozzle with micromanipulators in primary stream. L-93-1917

A novel approach to reducing noise through enhanced supersonic turbulent mixing was examined in the Langley Jet-Noise Laboratory (JNL) by using small turbulence-generating devices that would have a minimum impact on propulsion performance. These devices, termed micromanipulators, are designed to introduce small-scale vorticity at the nozzle-exit lip at angles to the jet axis from streamwise to transverse. The injected vorticity, often introduced in counter-rotating pairs, is designed to have a scale (i.e., size) that matches the most highly amplified turbulent structure of the unforced jet mixing layer. Impressive noise reduction was observed with one class of micromanipulator, the wedge-shaped tab. Evaluation of this device was accomplished by operating the 1/10th-scale coannular jet nozzle shown in the figure over the entire engine-cycle operating line. In a subsequent study at Boeing, with a similar nozzle designed and constructed by NASA Langley, this device also showed good noise reduction with minimum impact on nozzle performance.

(John M. Seiner, 46276, Michael K. Ponton, and Henry H. Haskin) Structures Directorate

Noise Reduction Through Acoustic Shielding by Multiple Jet Arrays

Research was conducted using multiple jet nozzle arrays to determine how to best take advantage of the reduction of observed ground-based noise through jet-by-jet shielding. Jet acoustic shielding is expected to provide noise benefit due to refraction or absorption of sound waves from one jet by a nearby jet or by interaction of the jet flow fields. Using the Boeing standard HSCT (high-speed civil transport) engine

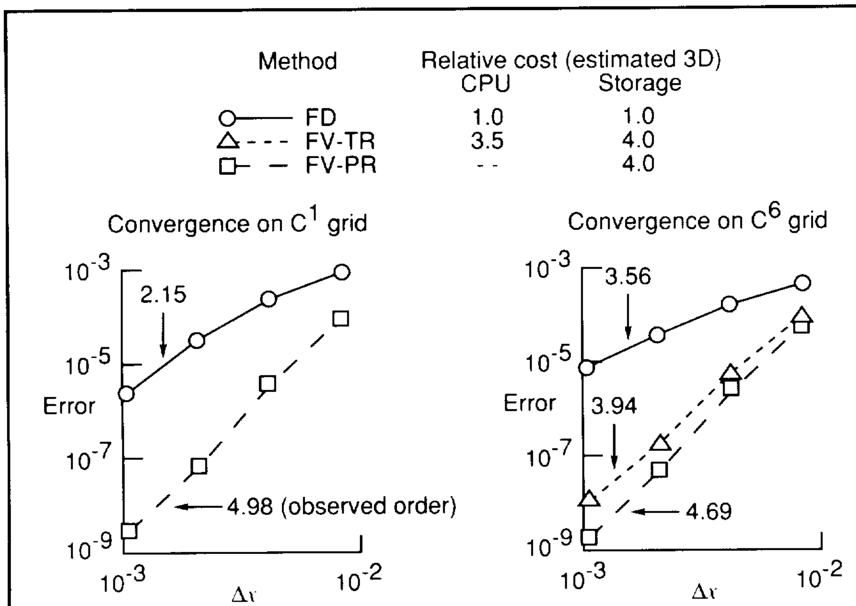

Grid-refinement study for fourth-order ENO schemes.

are relevant to problems in aeroacoustics and high-speed noise research. This work is performed in collaboration with Professor Shu of Brown University and Dr. Casper of ViGYAN, Inc.

The finite-difference method and two forms of the finite-volume method were tested on simple problems that isolated weaknesses. These weaknesses include grids that have a low order of smoothness, boundary contours that are not smooth, and flow discontinuities that are not aligned with the grid. Although the numerical test cases involved one- or two-dimensional cases, the cost assessments have been estimated where possible for three-dimensional computations.

All methods tested were accurate for smooth problems and free of oscillations near shocks and geometric discontinuities as expected. The finite-volume approach using a physical reconstruction (FV-PR) was the least sensitive to irregularities in the grid. However, this approach is prohibitively expensive when extended to three dimensions. A less expensive version of the finite-volume method, which uses a transformational reconstruction (FV-TR), was more sensitive to grid irregularities than FV-PR and less robust than either the finite-difference or FV-PR methods. The method failed entirely for a case in which the grid contained large discontinuities in the second derivatives. However, for grids with mild irregularities, the FV-TR method performed better than the finite-difference method in the sense of formal order properties. The finite-difference (FD) approach is the most cost-effective method; this method required only one-third to one-fourth of the computation time of FV-TR (the cost of FV-PR could not be reliably predicted). Although the finite-difference method was robust, its formal order property was more sensitive to the smoothness of the problem than either of the finite-volume methods. The figure illustrates the convergence properties just described for grids with continuity of the first derivatives (C^1) and with continuity of the sixth derivatives (C^6).

Current comparisons indicate that practical ENO-based high-order methods do well for smooth problems that contain isolated shocks but may not be suitable for problems that cannot be represented on a smooth grid. Further work is needed to improve the efficiency of schemes such as the FV-PR or to improve the accuracy and generality of the finite-difference method.
(Harold Atkins, 42308)
Aeronautics Directorate

Application of Micromanipulators for Suppression of Supersonic Jet Noise

For high-temperature supersonic jets, typical of those being investigated under the NASA High-Speed Research Program, the principal source of noise is associated with jet turbulent plume structures that convect supersonically relative to the ambient sound speed. This noise is termed eddy Mach wave emission. Reduction of this noise can be accomplished by minimizing the region of flow where turbulence is convected with these supersonic speeds. To achieve lower convection speeds requires application of a method that would enhance the mixing of the supersonic jet flow with ambient air or often a coflowing subsonic airstream.

study of the aerodynamic, structural, and packaging issues concerning the part-span NLF HSCT concept.
(Henri D. Fuhrmann, 45254)
Aeronautics Directorate

Automated Surface-Geometry Definition for a Complete High-Speed Civil Transport

The design and optimization of an aerospace vehicle using nonlinear Computational Fluid Dynamics (CFD) codes (Euler or Navier-Stokes) require the ability to generate smooth surface definitions and volume grids automatically as the design variables are changed from a baseline configuration. At the present time this process is time-consuming and is generally done interactively. The objective of the present work was to develop, for a complete high-speed civil transport (HSCT) class vehicle, an automated surface-geometry definition that is suitable for nonlinear CFD computations. The automated surface-geometry tool described herein is a prerequisite for imbedding an automated geometry/grid module in a design and optimization system for an HSCT.

The process starts with the Harris wave-drag geometry format, which is a familiar basic geometry description employed in preliminary design. Semianalytic methods are used to resolve the surface-to-surface intersections. The surface-geometry redefinition tools have been applied to supersonic transport configurations that consist of a wing, a fuselage, a horizontal tail, a vertical tail, a canard, a pylon, and a nacelle. The figure illustrates the complexity of the configuration that can now be handled. It shows bottom and top perspectives of the vehicle as well as close-up views of the wing-pylon-nacelle and the aft portion of the vehicle. Options that have been demonstrated include the insertion of fillets and adjustment of the fuselage area to maintain the original wave drag of the vehicle. The output surface-geometry definition is available in PLOT3D and Hess formats. The procedures run comfortably on workstations.

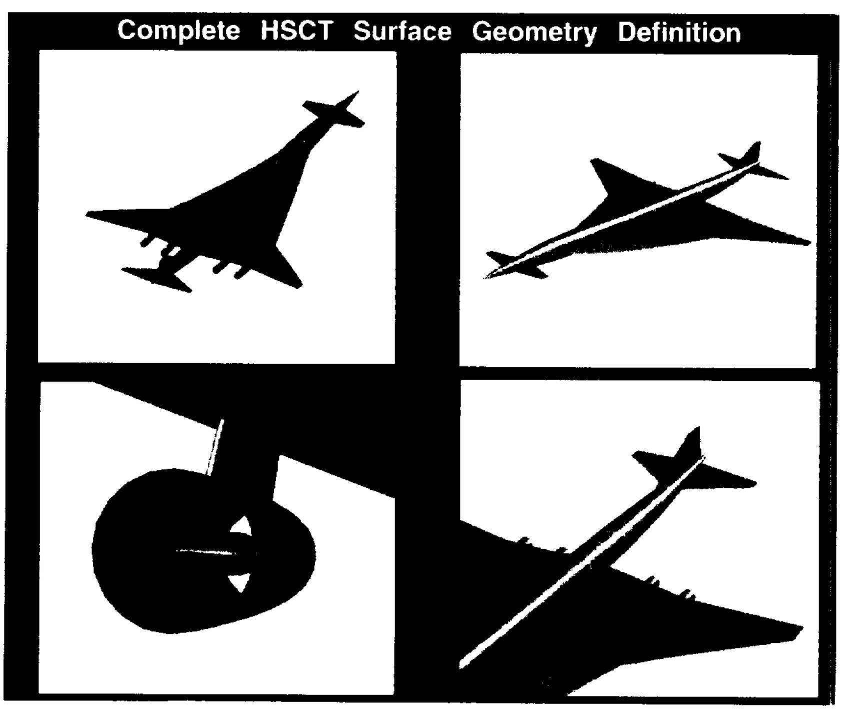

Four views of automated surface-geometry definition for a high-speed civil transport class vehicle.

Related efforts are underway to link this module with automated procedures for changing the geometry as design variables are changed and for generating a multiblock CFD grid.
(Raymond L. Barger, 42315, and Mary S. Adams)
Aeronautics Directorate

Assessment of High-Order-Accurate, Essentially Nonoscillatory Schemes

Numerical simulations in the fields of aeroacoustics and high-speed noise research demand a high degree of accuracy, but the capabilities to treat general geometries, capture shocks, and minimize costs are also important. To meet these requirements, the essentially nonoscillatory (ENO) approach has been implemented with both finite-difference and finite-volume interpretations. The purpose of this work is to compare the two approaches by using test cases that

the ease of changing fin angles, data can be obtained over a range of fin-deflection combinations that would be impractical if manual fin-angle changes were required.

The actual aerodynamic surface of the test model can be made of a thin shell that fits around the joined modular components shown in the figure. The system has been successfully used in two wind-tunnel tests recently conducted in the UPWT. During these tests, data were measured at rates that would have been impossible with the conventional discrete-fin-block-setting technique.

This model system was jointly funded by LaRC and several Department of Defense agencies. The versatility of the system allows it to be used for both point-design studies, of primary interest to the Department of Defense, and for exploration of missile technology issues, of primary interest to LaRC. **(Jerry M. Allen, 45592) Aeronautics Directorate**

Part-Span Natural Laminar Flow High-Speed Civil Transport Concept

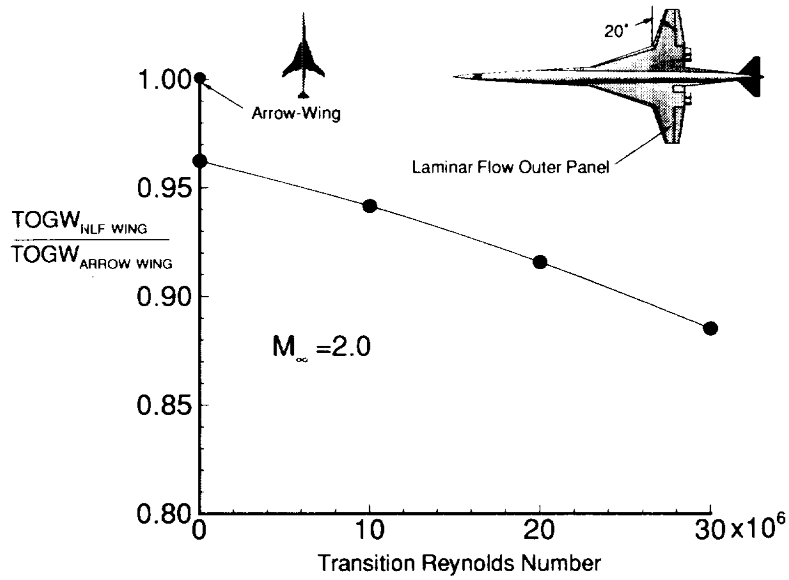

Supersonic natural laminar flow HSCT concept.

Current high-speed civil transport (HSCT) research includes the application of supersonic laminar flow to otherwise turbulent flow wings via active laminar flow control (LFC) devices. This method significantly reduces skin-friction drag but not without additional complexity and cost. Another method of obtaining laminar flow supersonic drag reduction is that of supersonic natural laminar flow (NLF). NLF, unlike LFC, uses no active means of boundary-layer control but rather, through airfoil geometry, creates a favorable pressure gradient that passively serves to prolong the extent of laminar flow on the wing. In this way, the benefits of laminar flow are obtained without the use of the suction devices that LFC requires.

To investigate the possible advantages of NLF for HSCT's, a study was conducted of a planform with leading-edge sweeps of 70° on the inboard section and 20° on the outboard low-sweep portion of the wing. Reducing the outboard wing sweep on what is typically referred to as a cranked arrow wing helps to attenuate the crossflow instability, which, in addition to airfoil geometries tailored for a favorable pressure gradient, results in increased laminar flow.

Flight experiments in 1958 demonstrated supersonic NLF at a transition Reynolds number of 9×10^6 on a wing with a leading-edge sweep of 26°. Based on this information and linear stability theory, the benefits associated with a range of NLF wetted areas thought to be attainable on the outboard wing panel were examined. The preliminary sizing and performance results shown in the figure demonstrate the possibility of improved efficiency and reduced takeoff gross weight when compared with a more conventional HSCT cranked arrow-wing design. Although some high-speed performance penalties do result from the reduction in wing sweep, overall the NLF HSCT shows both fuel savings and structural weight reductions that result from supersonic skin-friction drag reduction, subsonic aerodynamic performance, and a more efficient structural arrangement.

Currently, the Lockheed Aeronautical Systems Company is undertaking a more extensive

and-moment, pressure, and flow-visualization (laser vapor screens and mini tufts) data were obtained in the tests. The results of these studies have been compared with data obtained in the Boeing Supersonic Wind Tunnel and show very good agreement.
(Gloria Hernandez, 45572, and Peter F. Covell)
Aeronautics Directorate

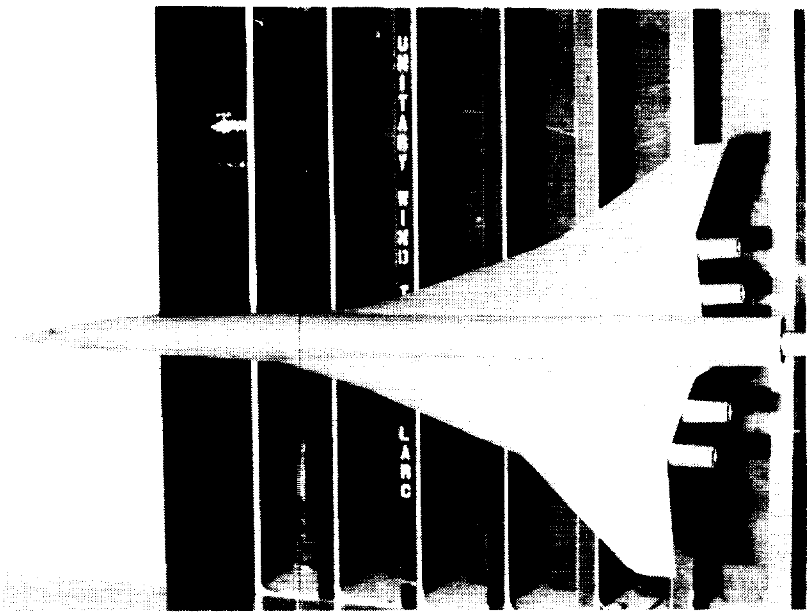

Reference H model installed in Unitary Plan Wind Tunnel. L-92-6360

A Modular, Remotely Actuated Missile Model System for Wind-Tunnel Testing

A new remote-control missile model system has been developed and experimentally tested. This new system evolved from an earlier version that has been used extensively for missile aerodynamic testing in the NASA Langley Research Center's (LaRC) Unitary Plan Wind Tunnel (UPWT) and other facilities. The self-contained modular components, shown in the figure, can be assembled in various ways to form the basis for the desired test configuration. When these components are connected, the resulting strong back model can be actuated by a small computer that allows very rapid positioning of the fin and model roll angles during testing.

The unique remote-actuation feature of this system allows up to eight fins to be deflected simultaneously. In addition, separate fin balances are used, so that individual loads on the fins can be measured simultaneously with the overall configuration loads that are measured by a conventional internally mounted balance. With

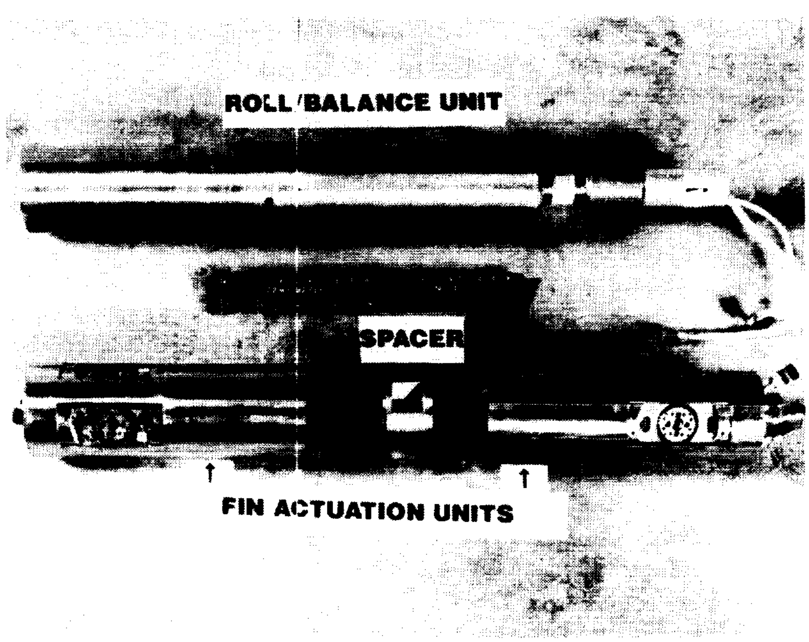

Modular components of remote-control missile model. L-93-06150

downstream on the wing are entrained in the secondary vortex. Based on the results from the tests, three exit locations were selected for the full-scale aircraft. These simple, low-cost wind-tunnel test techniques maximize the efficiency of flight tests by optimizing instrumentation location.
**(Clifford J. Obara, 43941, and Susan J. Rickard)
Aeronautics Directorate**

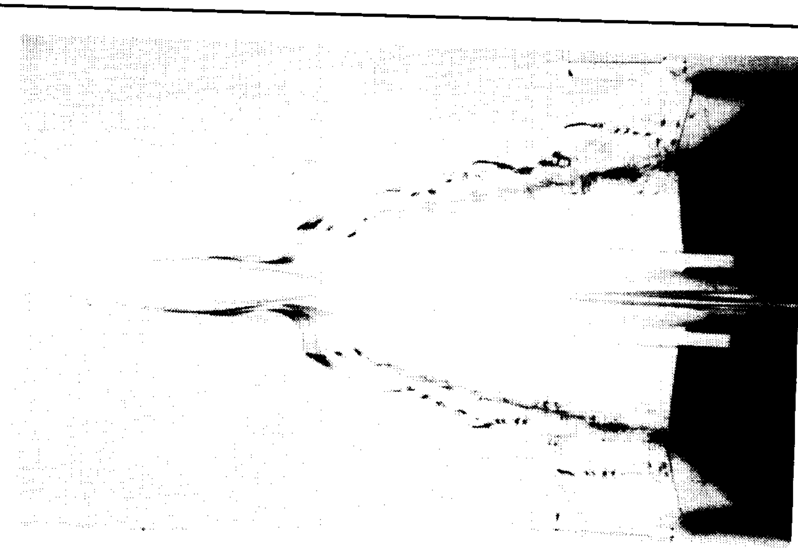

Vortex patterns on an F-16XL model in Langley 16- by 24-Inch Water Tunnel.

Low-Speed Wind-Tunnel Evaluation of Pressure-Sensitive Paint

Pressure-sensitive paints (PSP), previously only successful at high-subsonic, transonic, and supersonic speed regimes, were used to detect surface pressures at very low speeds in the Basic Aerodynamics Research Tunnel (BART). The tests were conducted to explore the use of PSP's for future application to low-speed ground and flight experiments. PSP's can provide a global quantitative pressure map over an entire aircraft surface with no modification to the geometry. Models are typically built with hundreds of flush pressure taps, or large arrays of pressure belts are installed on the aircraft wing to obtain the pressure measurements. This usually results in costly models or disturbed flow fields from the pressure belts.

The tests were conducted at a tunnel speed of 185 ft/sec, which resulted in a Mach number of 0.165. A PSP team from McDonnell Douglas Aerospace East used their patent-pending formula and techniques to make measurements over a 4-percent scale model of an F-16XL, a 76° delta wing, and a 76°

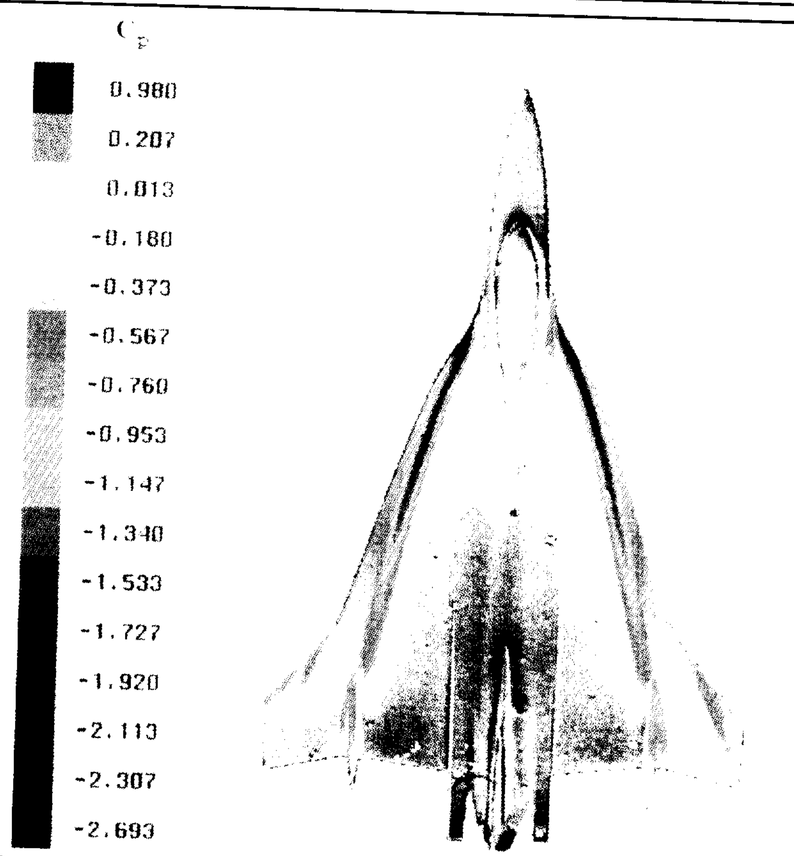

Pressure distribution on an F-16XL model in the Basic Aerodynamics Research Tunnel.

double delta wing. The figure shows a false-colored image of the pressure map over the upper wing of the F-16XL model. Initial results indicate that pressure differences greater than 0.1 psi could be resolved in atmospheric conditions. The results showed very good agreement with flush pressure taps located on the model surfaces. Maturity of the PSP technique will significantly enhance the ability to gather both ground and flight global pressure-distribution data through quantitative flow visualization.
(Susan J. Rickard, 48474, Anthony E. Washburn, and Clifford J. Obara)
Aeronautics Directorate

Visual/Motion Simulator cockpit and display panel. L-90-13683

Piloted Simulation Study of Airport/Community Noise

The high-speed civil transport (HSCT) simulation is part of an ongoing project designed to address critical issues involving Federal Aviation Administration (FAA) noise certification and public/industry acceptance of HSCT-type aircraft. The configuration simulated is the AST-105-1, which was designed to cruise at a Mach number of 2.62. Initially equipped with variable-stream control engines (VSCE), the simulation package was modified to incorporate turbine bypass engines (TBE), which are candidate engine cycles for the HSCT. The Langley-developed aircraft noise prediction program (ANOPP) estimates resulting ground noise levels for piloted takeoff trajectories that are performed in the Visual/Motion Simulator (VMS). The piloted simulation was retrieved from NASA Langley archives and updated to work with current system hardware. As a result, it was available for research work in a very short period of time.

To date, the piloted simulation has produced data that define benefits resulting from improved low-speed high-lift aerodynamic performance and advanced takeoff procedures for reducing the airport/community noise problem. The High-Speed Research (HSR) Program has been actively working towards developing aerodynamic concepts that would attain levels of performance simulated in this project. Advanced takeoff procedures that minimize airport/community noise have been developed and involve engine thrust levels under direct computer control. Combining improved low-speed high-lift aerodynamic performance with advanced operating procedures reduced the level of jet-engine noise suppression that was required by as much as 12 EPNdB (effective perceived noise in decibels) compared with full-thrust maximum-performance takeoffs with baseline aerodynamics.
(Louis J. Glaab, 41159, Donald R. Riley, and Robert A. Golub)
Aeronautics Directorate

CFD Inviscid Analysis of F-16XL Configuration

Recently a comprehensive program for using state-of-the-art computational fluid dynamic (CFD) methods has been initiated to aid in the design and analysis of complex aircraft configurations at

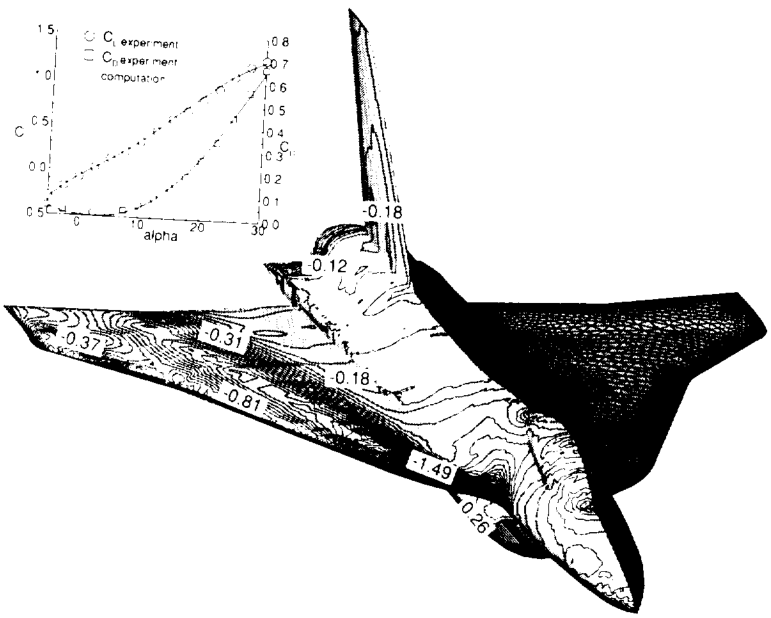

Computed surface pressure coefficient contours (left side) at M = 0.08, Re = 0.6 × 10^6, and α = 15° with triangular surface mesh (right side) for an F-16XL configuration. Force coefficient comparisons shown in insert.

high-lift low-speed conditions. More specifically, this work addresses the applicability of using an unstructured gridding approach (VGRID, USM3D) to solve the inviscid subsonic flow field about an F-16XL aircraft in terms of the force and moment coefficients and the overall flow characteristics. This method requires less gridding and run time than a structured Navier-Stokes method, which enables quick turnaround of CFD analyses. Fast solutions that provide an overall picture of the flow characteristics are important to the design process.

Computed force coefficients are compared with the experimental results obtained in the 30- by 60-Foot Tunnel at Mach 0.08 and Re = 0.6 × 10^6 for a range of angle of attack of −5° to 30° (insert of figure). As can be seen, very good comparisons are obtained between the experimental and computational results. Surface pressure coefficients are plotted as contours on the left side of the configuration (α = 15°) with some of the pressure values highlighted, and the triangular surface mesh is shown on the right.

Flight tests of an F-16XL aircraft are presently under way at Langley Research Center. These tests will provide performance data that are applicable to the development of the high-speed civil transport (HSCT), since they have similar wing aerodynamic characteristics. These tests will also provide data for validating the CFD codes and direct future wind-tunnel tests.
(Wendy B. Lessard, 41165)
Aeronautics Directorate

Correlation of Computed N-Factors and Experimental Transition Data on a Swept-Wing Leading Edge in Mach 3.5 Quiet Tunnel

Achieving large extents of laminar flow for highly swept supersonic wings is a challenging task because of boundary-layer instability that results from large crossflow near the wing leading edge and from amplification of first-mode instability waves farther downstream. A reliable and efficient prediction methodology is necessary to optimize wing design and suction distribution and to analyze off-design point performance. Linear stability analysis provides the growth rate of instability waves and corresponding N-factors. Validation with transition data from quiet-tunnel experiments yields a reliable computational prediction for laminar flow control (LFC) applications.

The experiment is conducted on a 77.1° swept-wing leading-edge model installed in the Mach 3.5 Quiet Tunnel. Surface-mounted thermocouples, pressure taps, and temperature-sensitive paint are used to detect transition. The free-stream Reynolds number, the angle of attack, and the suction distribution are the variables of the experiment.

The computational effort involves the calculation of the mean flow on the model by solving the thin-layer Navier-Stokes equations (using the code CFL3D). The results are interfaced to the temporal stability analysis code COSAL, which is modified for 3-D

boundary-layer profile inputs. Instability growth rates and N-factors are computed for the experimental data points. The temperature recovery factors that are derived from the experiment are used to locate the transition zone. The computed N-factors and the measured recovery factors are then compared. The figure shows one such comparison that involves variation in the free-stream Reynolds number. The computed N = 14 locations correlate well with the increase in recovery factor (indicating transition) in the Reynolds number range of 2×10^6/ft to 8×10^6/ft. Similar comparisons are in progress with changes in angle of attack, and in the near future with different suction distributions. This will eventually lead to a validated computational methodology that the industry can use for LFC wing and systems design.
(Venkit Iyer, 42319, Jamal A. Masad, and Louis N. Cattafesta, III)
Aeronautics Directorate

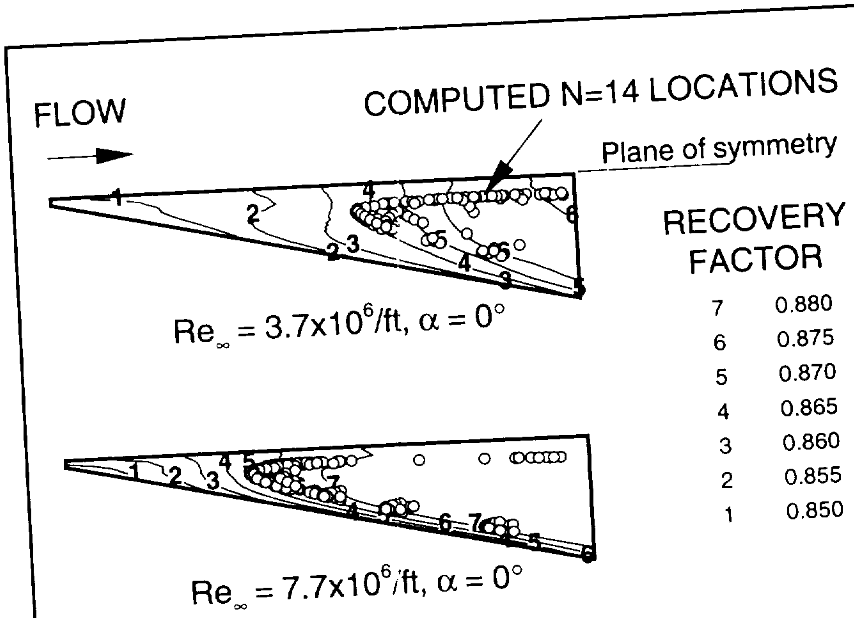

Correlation of computed N-factors and measured recovery factors on a Mach 3.5 swept-wing leading edge.

A New NASA LaRC Multipurpose Prepregging Unit

A multipurpose prepregging machine, capable of impregnating high-performance fibers (such as carbon and glass) with high-performance polymeric resins, was designed and built for the Polymeric Materials Branch at Langley Research Center. The machine is now installed and fully operational. A variety of impregnation methods are available to the operator, making the machine exceptionally versatile and capable of impregnating fibers with resin systems that differ in their processing characteristics. The machine is composed of a number of modules that can be used simultaneously or

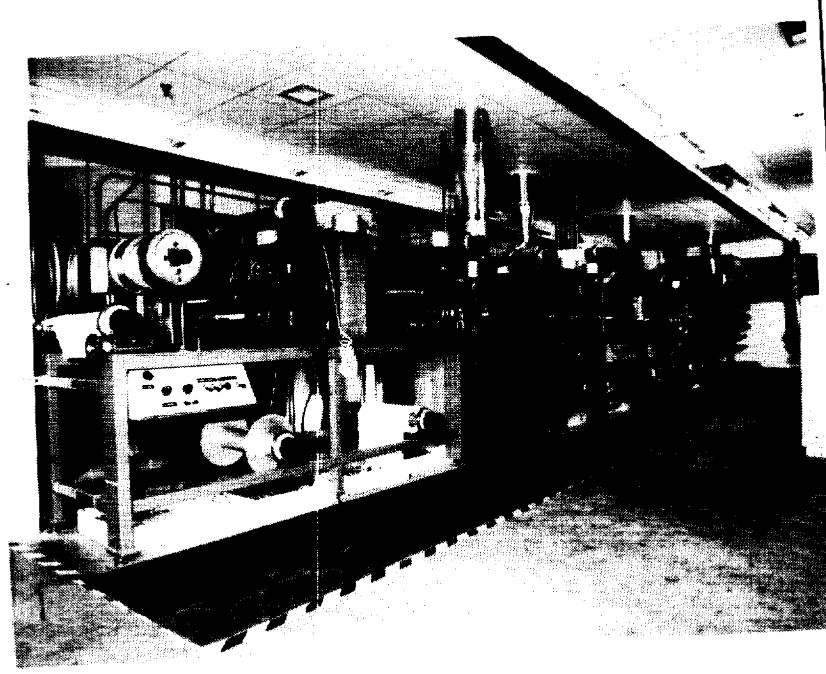

Twelve-inch prepregging machine.

L-92-10693

in a variety of combinations. The fiber creel can hold 144 spools, which ensures that the prepreg product can be made in widths that range from 1 to 12 inches. The impregnation module contains a reverse roll coater and a solution dip tank with metering bars. The reverse roll coater is used to prepare precast films that are then used to form a sandwich with the dry-fiber web to make prepreg. Alternatively, the impregnation can be performed directly at the coater gap if the fibers are drawn down between the rollers. The solution dip tank impregnates dry fibers with resins that have high melt viscosities but can be dissolved into a low-viscosity solution. Subsequent processing modules include two hot plates, four nip stations, a high-temperature oven, and a hot sled roller in the second hot plate. The nip rollers can be heated to a maximum temperature of 450°F; the hot plates and oven have a maximum temperature of 800°F. To date, a wide variety of polymers have been processed into prepreg material. Four NASA-developed polymers, LaRC CPI-2, LaRC IAX-10a, LaRC IAX-20b, and LaRC PETI have been scaled up and prepregged for Northrop Aircraft Corporation as part of the High-Speed Research (HSR) Program.

(R. Baucom, 44252, and
S. Wilkinson)
Structures Directorate

RESEARCH AND TECHNOLOGY

High-Performance Military Aircraft

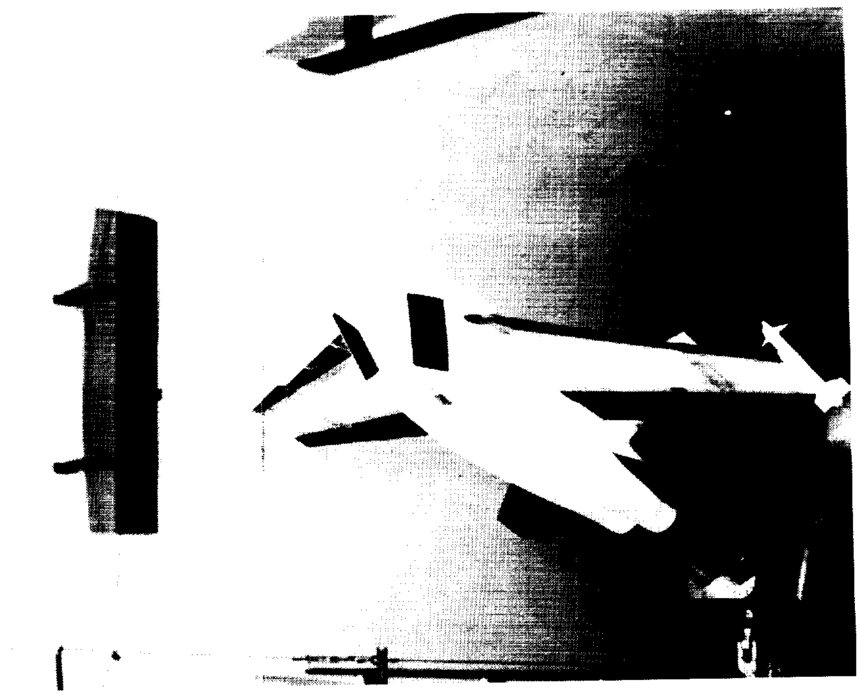

Provide technology options for revolutionary new capabilities in future high-performance military aircraft

Missile Base Pressure Drag

The base pressure drag of a gliding missile in free flight can be as much as 50 percent of the total missile drag. Although base pressure drag has been extensively studied for many years, very little experimental data exist that document the effect of fins on the base pressure drag of gliding missiles. Therefore, a cooperative program between NASA Langley Research Center and the Naval Surface Warfare Center Dahlgren Division (NSWCDD) was initiated to conduct an experimental investigation to determine the effect of fins on the base pressure of a generic missile. Using these data, an improved empirical method for determining the base pressure drag of gliding missiles was developed and incorporated into an NSWCDD missile aeroprediction code.

Wind-tunnel tests were conducted on a generic missile that consisted of an ogive cylinder 36 in. long and 5 in. in diameter. Three sets of fins were tested that had identical trapezoidal planforms and thickness-to-chord ratios of 0.05, 0.10, and 0.15. The fins were positioned at three longitudinal stations from the model base and were set at incidence angles of 0°, 10°, and 20°. The model base was instrumented with 89 pressure orifices that were arranged in concentric circles. These pressures were integrated over the entire base to determine the base pressure drag. The tests were conducted at angles of attack of 0°, 5°, and 10° and Mach numbers from 1.7 to 4.5. Results from this test showed that the effects of fins on the base pressure drag were generally linear with increasing fin incidence angle, fin thickness-to-chord ratio, and fin longitudinal position. However, as Mach number was increased, these effects became less pronounced.

(Floyd J. Wilcox, Jr., 45593)
Aeronautics Directorate

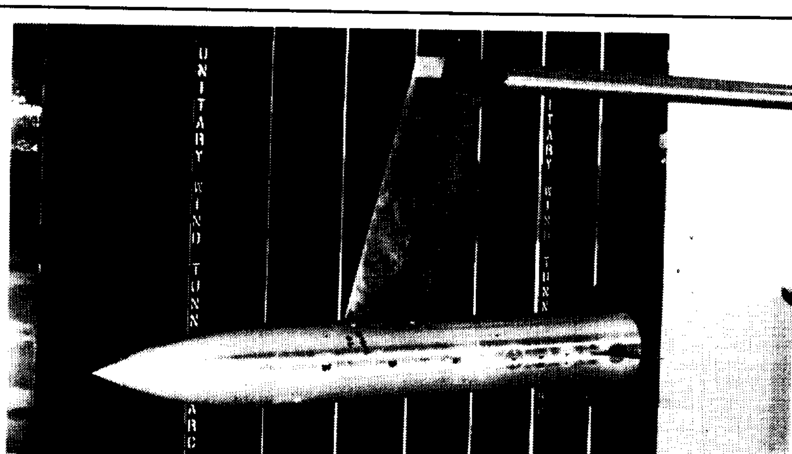

Base pressure drag missile model mounted in wind tunnel. L-92-03900

Supersonic Aerodynamic Characteristics of Sidewinder Missile Variant Configurations

Previous tail-span optimization studies at supersonic speeds on a modified Sidewinder-missile-type airframe indicate that this configuration may be a viable design for use with advanced fighter aircraft. Performance improvements associated with the modified configurations included lower stability levels accompanied by higher trim angles of attack and reductions in zero-lift drag.

A cooperative research effort between NASA Langley Research Center and the Naval Air Warfare Center, China Lake, California, was established to further investigate variations of the Sidewinder-missile-type airframe. As part of this cooperative effort, models of selected canard-controlled missile configurations designed by the U.S. Navy were fabricated with reduced tail-span geometries and were tested in the Unitary Plan Wind Tunnel to determine the longitudinal and lateral-directional aerodynamic characteristics. The test Mach numbers ranged from 1.75 to 2.86 at a Reynolds number

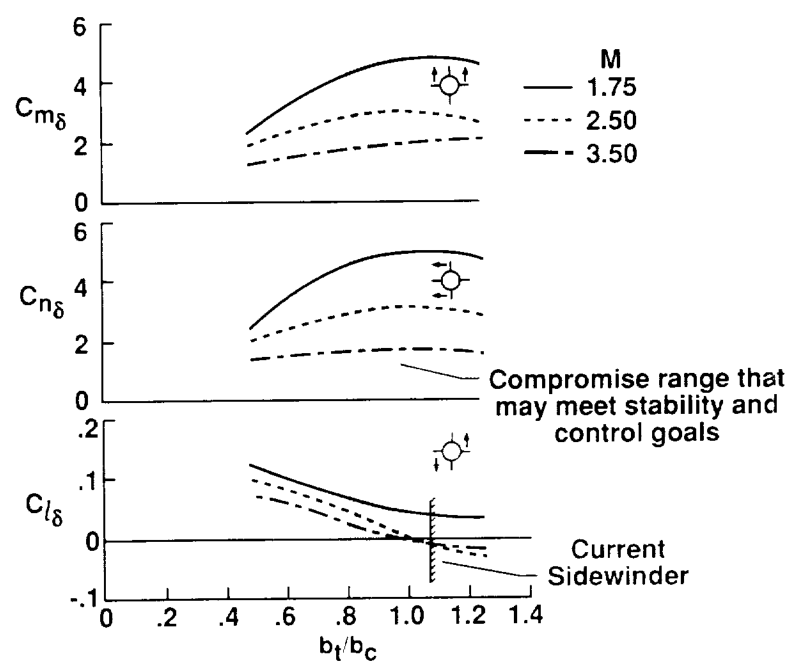

Variation of canard pitch, yaw, and roll-control effectiveness with tail-span/canard-span ratio for selected test Mach numbers.

of 2.0×10^6 per foot. Angles of attack ranged from −4° to 28° at model roll angles from 0° to 180°.

Results show that the reduced tail-span configurations exhibit favorable supersonic aerodynamic characteristics. Canards typically provide good pitch control ($C_{m\delta}$) and yaw control ($C_{n\delta}$) but adverse roll control ($C_{l\delta}$). A separate aileron-type control system is usually required for roll control. The summary figure shows that a range of tail-span/canard-span ratios is possible that gives near-maximum canard pitch control and yaw control and allows canard roll control at zero angle of attack. It appears that careful selection of tail-span/canard-span ratio can result in a canard aerodynamic control system that provides pitch, yaw, and roll/roll-rate control.
(A. B. Blair, Jr., 45735)
Aeronautics Directorate

Supersonic Characteristics of an Outboard Control-Surface Wing Concept

Experimental supersonic studies were conducted in the Langley Unitary Plan Wind Tunnel on a generic aircraft configuration with a modified trapezoidal wing planform that featured horizontal control surfaces integrated with the outboard region of the wing-tips. The wing arrangement is referred to as the outboard control-surface (OCS) wing planform. The investigation was a cooperative research effort between NASA and Northrop Corporation to identify potential aerodynamic technologies that can be incorporated into future high-performance aircraft.

The performance benefits of the OCS wing-planform concept were determined by comparison with a conventional trapezoidal wing planform that had the identical modified NACA 65-A004 airfoil section, exposed wing area, and leading-edge sweep angle (50°). Longitudinal and lateral-directional data were obtained over a Mach number range of 1.60 to 2.16 at a Reynolds number of 2×10^6 per foot.

A comparison of the untrimmed longitudinal aerodynamic characteristics indicated that the OCS wing planform has higher zero-lift

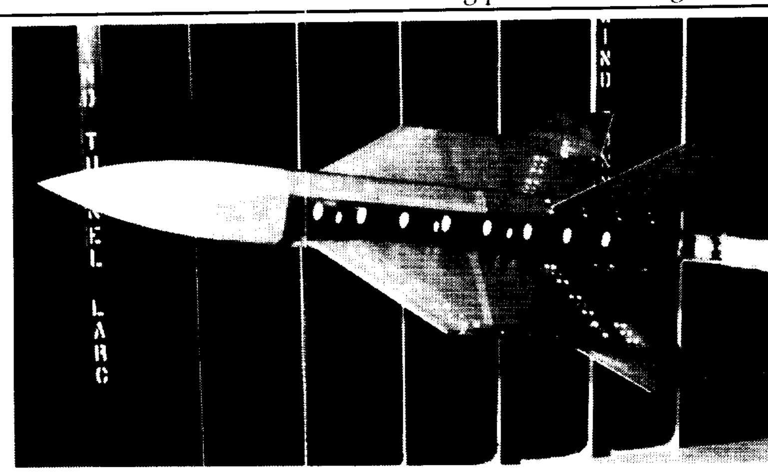

Outboard control-surface wing model in Unitary Plan Wind Tunnel.
L-91-16500

drag and drag due to lift than the trapezoidal wing planform. However, the OCS wing planform has very small values of trim drag at cruise lift conditions and no trim drag at maneuver lift conditions. Thus, at trimmed flight conditions, the OCS and trapezoidal wings have essentially the same drag because of favorable OCS trimmed drag characteristics. These results indicate that the upwash field at the wingtip efficiently loaded the deflected OCS panel to produce a thrust component that significantly reduced the drag due to lift of the OCS wing planform at trimmed conditions. Both wing planforms had good longitudinal and later-directional stability characteristics.

This investigation showed that the integration of an OCS to the tips of a wing is a viable concept that is competitive with more conventional control-surface integration concepts.
(Gaudy M. Bezos-O'Connor, 45083, and Peter F. Covell)
Aeronautics Directorate

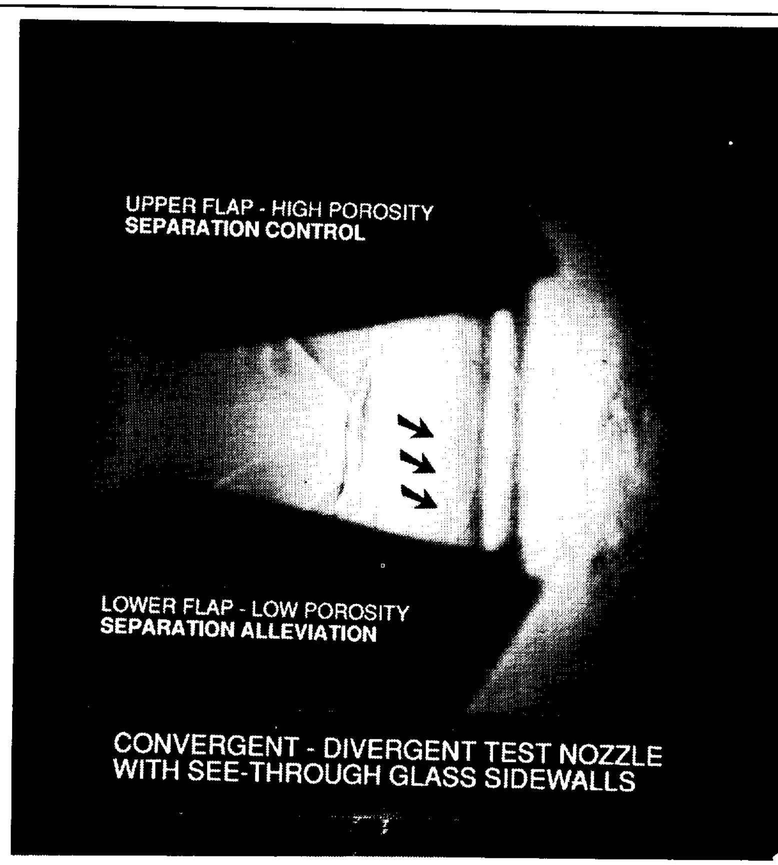

Focusing schlieren flow visualization showing passive shock/boundary-layer interaction control used for thrust vectoring in exhaust nozzles.

Passive Shock/Boundary-Layer Interaction Control in Exhaust Nozzles

Current high-performance aircraft use variable-geometry exhaust nozzles for operation over an extended flight regime. These systems configure the exhaust nozzle such that maximum propulsive efficiency can be obtained for any given flight condition or throttle setting. While effective in this respect, variable-geometry exhaust nozzles can be heavy, mechanically complex, and difficult to integrate into aerodynamic aircraft afterbodies with low-observable exhaust systems and other multifunction capabilities such as thrust vectoring and reversing. Thus, there is a tremendous potential for improving integrated aircraft system performance by developing an efficient fixed-geometry exhaust nozzle.

An experimental investigation was conducted at the static test facility of the Langley 16-Foot Transonic Tunnel through a grant with The George Washington University. In this study, novel concepts for passive shock/boundary-layer interaction (SBLI) control were tested in an effort to improve the off-design performance and extend the efficient operating range of fixed-geometry exhaust nozzles. Concepts included multidimensional convoluted contouring, which provides boundary-layer relief and generates streamwise vorticity, and a passive porous cavity.

Test results indicate that both concepts were highly successful for passive SBLI control. Convoluted configurations effectively alleviated shock-induced separation at off-design conditions. Depending on porous geometry, passive porous cavity configurations showed the ability to alternately alleviate or control shock-induced separation. This resulted in increases in off-design static-thrust efficiency by as much as 3 percent and allowed passive flow control

within the test nozzle. Through asymmetric application of this mechanism, thrust-vectoring angles of up to 11° were realized. **(Craig A. Hunter, 43020) Aeronautics Directorate**

Thrust-Vectoring Axisymmetric Ejector Nozzles

The renewed interest in ejector nozzles for commercial (reduced noise) and military applications (cooling air) was the driving force behind this investigation. Industry has extensive experience in the use of ejectors for cooling of nozzle parts; however, no data existed on ejector nozzles with thrust-vectoring capability. The purpose of this investigation was to provide a database for vectoring ejector nozzles.

A series of 24 unvectored and vectored axisymmetric ejector nozzles were designed and experimentally tested for internal performance and pumping characteristics at static (wind off) conditions. The model geometric variables investigated were primary nozzle throat area (A_t), primary nozzle expansion ratio (A_i/A_t), effective ejector expansion ratio (A_e/A_t), ratio of minimum ejector area to primary nozzle throat area (A_{ej}/A_t), and geometric thrust-vector angle (δ_p). The primary nozzle pressure ratio (NPR) was varied from 2.0 to 10.0. The corrected ejector-to-primary-nozzle weight-flow ratio was varied from 0 (no secondary flow) to approximately 0.21 (21 percent of primary weight-flow rate).

Results indicated that with no secondary flow, a discontinuity

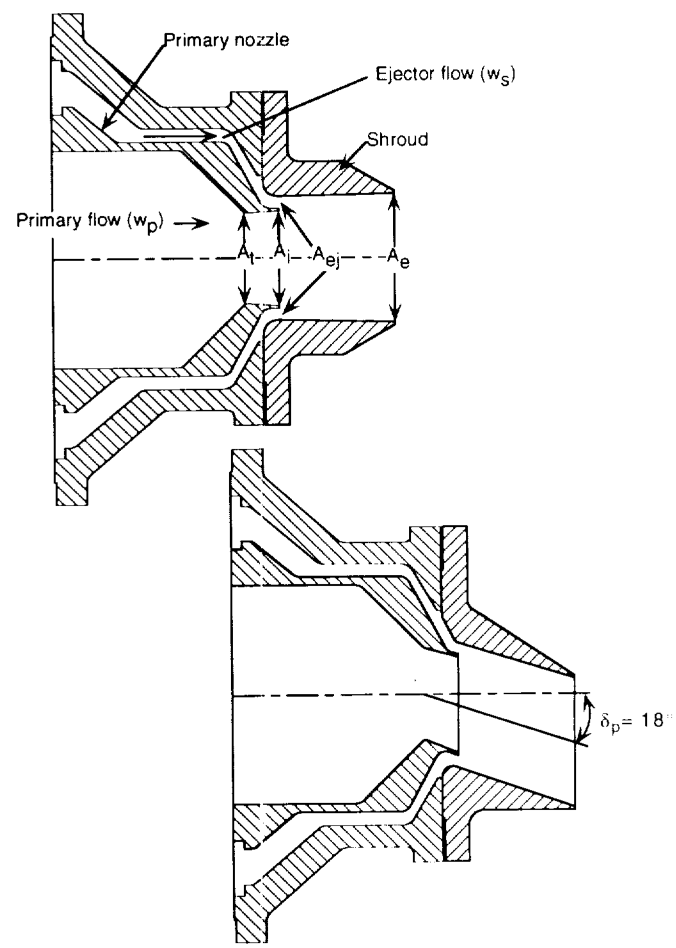

Sketches of axisymmetric ejector nozzles.

occurred in the gross thrust curve at NPR values well below design. Small amounts of secondary flow increased the gross thrust ratio and tended to eliminate the discontinuity in the thrust ratio. Additional secondary air did not necessarily improve the thrust ratio. It did tend to reduce the effective expansion ratio of the primary flow, which resulted in a shift in the NPR at which peak performance occurs. The pumping characteristics were similar for the unvectored and vectored configurations. Without secondary flow, resultant thrust-vector angles were greater than geometric turning angles. Adding secondary flow reduced measured thrust-vector angle; however, even at the highest secondary flow rate, measured thrust-vector angles were generally equal to geometric turning angles. **(Milton Lamb, 43021) Aerodynamics Directorate**

Tumbling Research

Contemporary aerodynamic design trends that incorporate high levels of relaxed static sta-

Tumble test of a dynamically scaled 50°-swept wing model in 20-Foot Vertical Spin Tunnel. L-91-10951

bility and unusual configuration features have stimulated research interest in the tumbling phenomenon as a flight-dynamics problem. Tumbling is defined as a continuous autorotation about an airplane's pitch axis, and it represents a severe out-of-control situation. The objective of this research was to define key parameters that determine susceptibility to tumbling and to develop configuration-design guidelines based on this information.

Research was conducted in the 20-Foot Vertical Spin Tunnel and in the 30- by 60-Foot Tunnel on a series of 12 generic flying-wing configurations to determine basic planform aerodynamic and mass-distribution effects on tumbling. Static and dynamic force-and-moment tests were conducted to provide aerodynamic data through a ±180° angle-of-attack range for implementation in 1- and 3-degree-of-freedom computer simulations. Two wind-tunnel test techniques that used dynamically scaled models were also used: (1) free-to-pitch testing on an instrumented apparatus that constrained the model to pitch rotation only and allowed a time history of the model attitude to be obtained; and (2) unconstrained free-tumble tests, in which the models were launched into the vertically rising airstream with prerotation in pitch.

Results indicate that high-aspect-ratio flying wings are more prone to tumble than low-aspect-ratio wings, but changes in relative mass distribution can modify these trends. Susceptibility to tumbling and maximum angular rates that were achieved both increase as aft movement of the center of gravity decreases the static margin, although high-aspect-ratio configurations can tumble even though they may be statically stable. Computer simulations using the 1- and 3-degree-of-freedom equations of motion predict developed tumbling motion that agrees well with the results of free-to-pitch and free-tumble tests, respectively.
(C. Michael Fremaux, 41193)
Aeronautics Directorate

Canard-Rotor-Wing

In response to a Navy requirement for an unmanned, high-speed, ship-based vertical take off and landing (VTOL), McDonnell Douglas Helicopter developed a concept called Canard-Rotor-Wing (CRW). The CRW would spin a

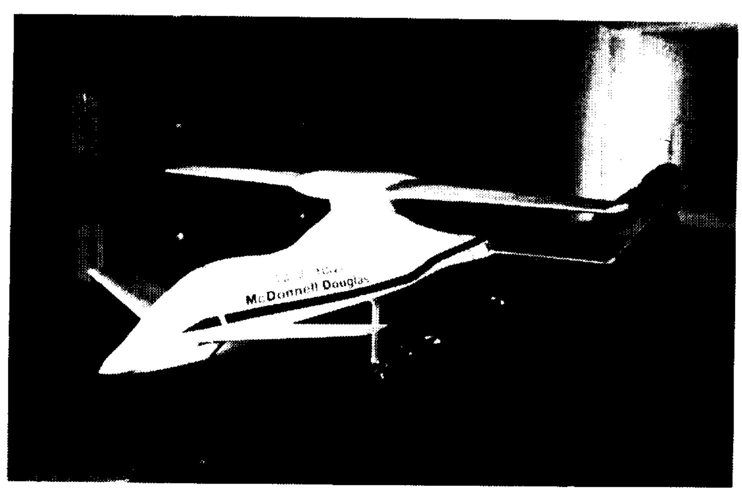

Canard-rotor-wing model mounted in the 14- by 22-Foot Subsonic Tunnel. L-93-02463

center wing to take off like a helicopter. The vehicle would then accelerate to about 120 knots when flaps would deploy from the front and rear wings. Flap deployment would off load the spinning center wing, which could then stop rotation and be locked into a position across the fuselage to perform as a third wing. The flaps on the other two wings would then be retraced and all three wings would share the lift loads in a fixed wing flight mode. A reverse of these events would transition the CRW back to its rotary wing—VTOL mode for landing on small landing areas.

Aerodynamic performance tests of the CRW configuration were conducted in the 14- by 22-Foot Subsonic Tunnel with the model controls in both symmetric and asymmetric positions. A drag buildup study was also performed, developing the resulting polar diagrams for the fixed wing mode.
(W. Todd Hodges, 44238)
Aeronautics Directorate

Commercial Turbofan Engine Exhaust Nozzle Flow

Achieving an aerodynamic contour design that meets performance specifications for turbofan engine installations involves complex, time-consuming, and expensive analysis and testing. The goal of the present investigation is to accurately predict static-pressure distributions, mass flow, and thrust quantities by using the recently developed three-dimensional Navier-Stokes code (PAB3D). The program is a cooperative effort with General Electric Aircraft Engines.

A relatively large number of analytical and computational methods for predicting the flow surrounding a turbofan engine exhaust system have been developed. Most of these methods use simple algebraic turbulence models. Because of the complexity of the exhaust flow field, a higher level turbulence model would improve the quality of flow and performance predictions. In the present investigation an improved version of the PAB3D code is tested and validated utilizing a k-ε turbulence model. In addition, a nozzle performance package is used within the PAB3D code to estimate nozzle performance.

The figure shows exhaust aerodynamic components for a typical commercial turbofan engine. The k-ε solutions accurately predicted the core and fan discharge coefficient (C_d) and thrust coefficient (C_{TX}) within 0.2 percent of the experimental data. The computed solutions provided significant insight into flow details, surface pressure distributions, and performance predictions by using a commercial turbofan engine exhaust nozzle as an example.
(Khaled S. Abdol-Hamid, 43049, and John R. Carlson)
Aeronautics Directorate

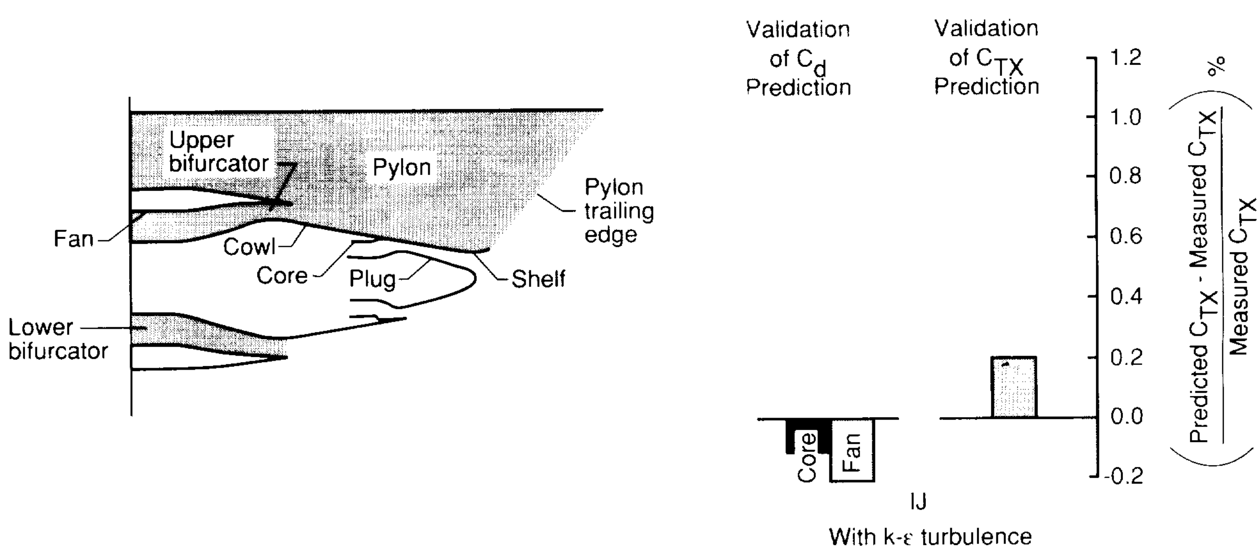

Exhaust aerodynamic components and comparisons between measured and predicted engine performance (separate flow configuration).

Computational Prediction of Isolated Performance of an Axisymmetric Nozzle at Mach 1.2

Accurate prediction of propulsion effects is an important factor of any aerodynamic design effort. A nozzle-performance module has been developed and incorporated into the Navier-Stokes method PAB3D for calculation of aerodynamic forces and moments. The present investigation demonstrates the accurate accounting of external aerodynamic effects, skin friction, and pressure drag on an axisymmetric nozzle at Mach 1.2 in thrust-minus-drag performance predictions.

The nozzle was a high-expansion-ratio axisymmetric convergent-divergent nozzle with an internal expansion ratio of 3.0 and a design nozzle pressure ratio (NPR) of 21.23. Experimental data could not be obtained above NPR = 10 because of limitations of the experimental apparatus. A 2-D wedge grid was used, and internal and external flow field regions were computed by using a two-equation k-ε turbulence viscous stress model.

Thrust-minus-drag ratios, $(F - D_n)/F_i$, were within 0.2 percent of the absolute level of experimental data, and the trends of data were predicted accurately. The predicted peak performance level was similar to the peak levels of other lower expansion ratio nozzles tested. PAB3D is an effective tool for the analysis of propulsion-system performance and has been used to extrapolate data beyond the experimental test results.
(John R. Carlson, 43047, and Kristina Alexander)
Aeronautics Directorate

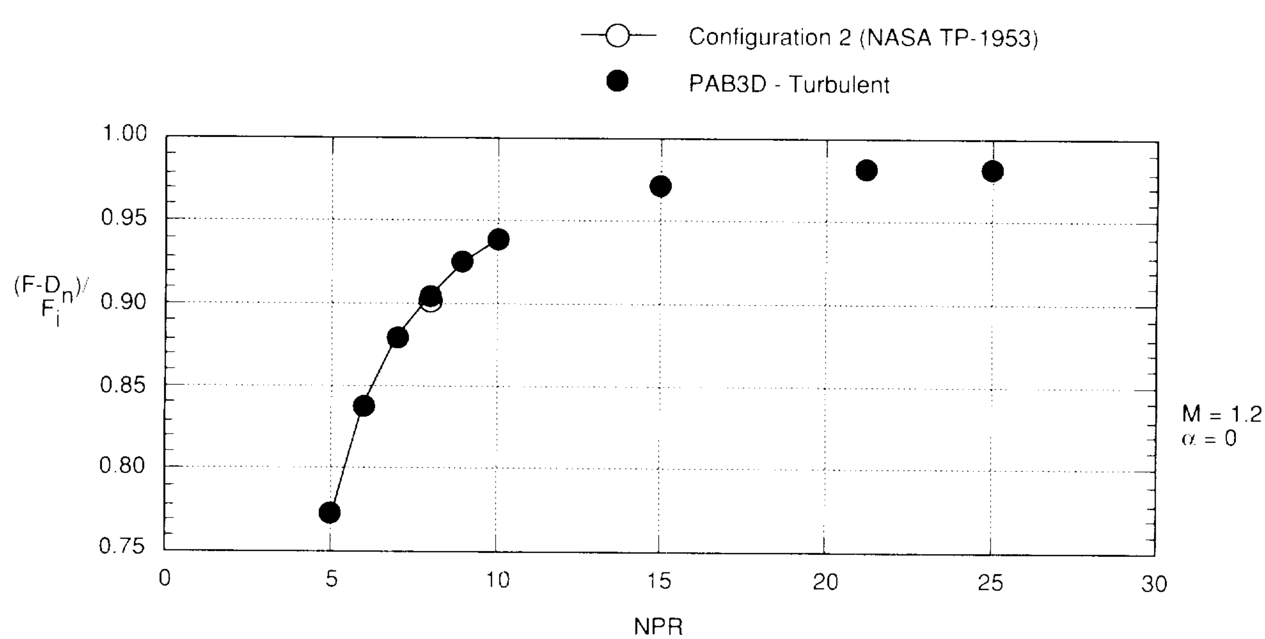

Axisymmetric supersonic cruise nozzle—prediction of isolated performance.

Supersonic Secondary Flows Using Nonlinear k-ε Model

A nonlinear k-ε model is used for investigating Reynolds-stress-driven secondary flows. Development of the nonlinear k-ε model is carried out by modifying a time-dependent three-dimensional Navier-Stokes code that employs the standard k-ε model. Since the additional nonlinear terms in the Reynolds stresses are not very large, they are treated as added-source terms in the original code.

Supersonic flow through a square duct is used as a model problem to show the improvements with the nonlinear k-ε model. Since the flow is symmetrical, only one-half of the duct flow was computed. The computations were carried out by using a 41 × 41 mesh in the crossflow direction and 251 points in the streamwise direction.

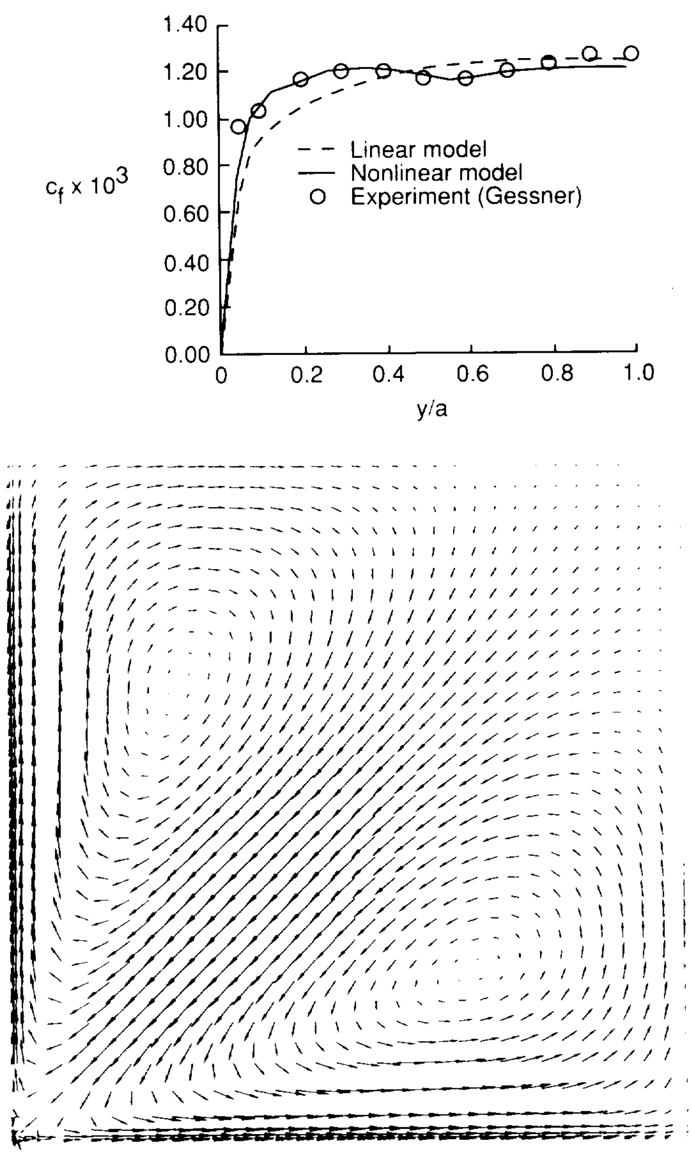

Spanwise skin-friction distribution and computed crossflow velocity vectors using nonlinear model.

The top figure shows the computed skin-friction distribution with the linear and nonlinear k-ε models and comparison with the experimental data as a function of the spanwise coordinate, where "a" is one-half duct width. The result obtained by using the nonlinear model is in excellent agreement with the data and clearly captures the undulations observed in the experiment. These undulations represent the convective influence of the secondary flow, which cannot be simulated with linear models. The bottom figure shows the computed crossflow velocity vectors with the nonlinear model. Computations with the linear model predict a unidirectional flow, while the nonlinear model clearly shows the two vortices symmetrical about the diagonal, which is in agreement with the experimental observations.

Highly accurate numerical validation of the nonlinear model was carried out in separated crossflows. This new model will improve the predictive capabilities of the computational fluid dynamics codes that are used for propulsion airframe integration.

(Balakrishnan Lakshmanan, 48057)
Aeronautics Directorate

Fluidic Thrust Vectoring of a Jet-Engine Exhaust Stream

Fluidic thrust vectoring is the deflection of the exhaust thrust vector of a jet engine through the influence of a secondary fluid stream. Advantages of this vectoring technique over mechanical thrust-vectoring systems are the reduction in nozzle weight and complexity from the elimination of mechanical actuators that are used in conventional thrust vectoring.

One such fluidic thrust-vectoring technique for convergent-divergent nozzles, known as shock-vector control, is the injection of a sheet of secondary air into the supersonic primary jet stream through a slot in the nozzle divergent flap. This injected flow presents an obstruction to the primary jet and results in the formation of an oblique shock in the primary jet flow field. The jet exhaust is then turned by the oblique shock, and the exhaust

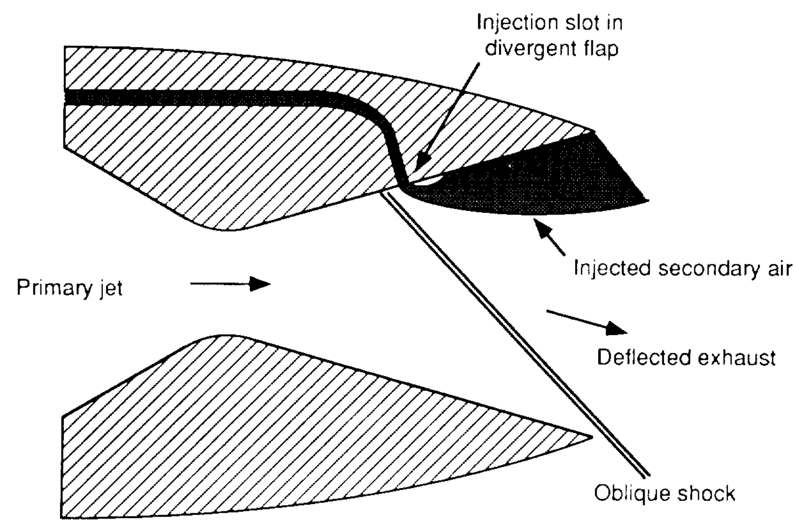

Fluidic thrust vectoring using shock-vector control.

thrust vector is deflected away from the slotted divergent flap.

A static test (no external flow) of this concept was conducted in the static test facility of the 16-Foot Transonic Tunnel. Results indicate that useful levels of thrust vectoring are produced (greater than 15°) by this technique. The amount of thrust vectoring is controlled by varying the weight flow rate of the secondary airstream. Moderate thrust losses at all but highly overexpanded primary jet conditions are incurred as a result of losses through the oblique shock, although the level of thrust produced is probably adequate for transitory vectoring operation. **(David J. Wing, 43006) Aeronautics Directorate**

F/A-18E/F Stability and Control Design Studies

Static wind-tunnel tests have been conducted in the 30- by 60-Foot Tunnel to determine the effect of leading-edge extension (LEX) geometry modifications to the McDonnell Douglas F/A-18E/F aircraft, which is currently under design as the latest version of the F/A-18. The photograph shows a 15-percent-scale model mounted for static force tests in the 30- by 60-Foot Tunnel. The LEX modifications were designed to allow the aircraft to maintain a specified level of maximum lift while improving the lateral stability (dihedral effect) and nose-down pitch-control capability at high angles of attack. Such characteristics are vital for good air-to-air combat effectiveness. The current tests were intended to study several LEX geometry concepts that were suggested by Langley researchers. In exploratory tests by McDonnell Douglas that preceded the Langley tests, some of these concepts appeared to have potential for improving the performance characteristics.

The results of the 30- by 60-Foot Tunnel tests showed the large positive impact of certain geometry parameters on the stability and

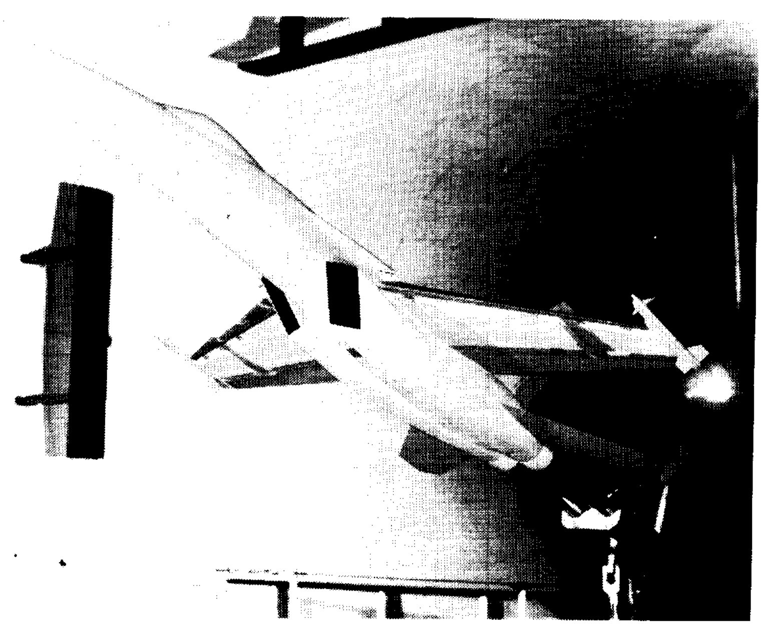

Model of F/A-18E/F design configuration mounted for static force tests in 30- by 60-Foot Tunnel. L-93-01944

control characteristics. The most significant impact was the addition of a slot that allows airflow between the LEX and the leading edge of the wing. This modification was then refined by McDonnell Douglas and incorporated into the final LEX design. In summary, the results of these tests helped validate concepts for performance enhancements to the F/A-18E/F and aided in design efforts to provide acceptable levels of maximum lift, lateral stability, and nose-down control capability.
(Gautam H. Shah, 41163, Sue B. Grafton, and Daniel G. Murri) Aeronautics Directorate

Surface Porosity Effects on Vortex Interactions

Experimental investigations were conducted in the Langley 7- by 10-Foot High-Speed Tunnel of the effects of surface porosity on vortex-vortex and vortex/vertical-tail interactions on a 65°-cropped delta-wing model. The model planform is sketched in the figure. Porous surfaces that were tested included the wing leading-edge extension (LEX) and the wing leading-edge flaps. Laser vapor screen (LVS) flow visualizations, wing upper surface static pressure distributions, and six-component forces and moments were obtained at Mach numbers of 0.2 to 0.5, angles of attack of 0° to 45°, sideslip angles of −5°, 0°, and 5°, and Reynolds numbers (based on chord) of 2.8 to 5.9 × 10^6. The LEX and wing flaps were flat plate with beveled leading edges and featured a uniform distribution of 0.05-in. diameter through holes. This hole arrangement provided a maximum porosity by area of 12 percent. The level of porosity was manually varied from 0 to 12 percent during the testing by covering selected regions of the LEX and flaps. Twin wing-mounted vertical tails and a centerline vertical tail were tested in the presence of all combinations of porous and nonporous LEX and wing flaps and with the LEX and flaps removed. The test data showed that surface

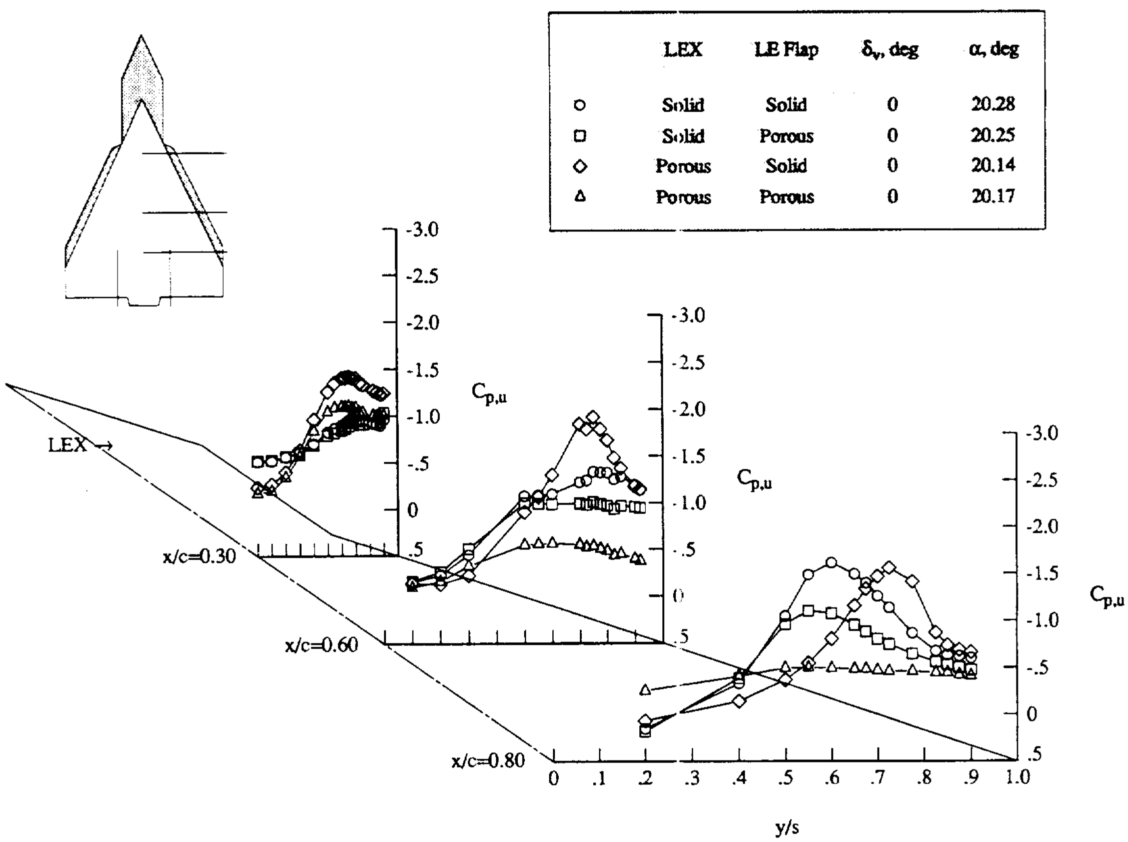

Porosity effect on wing surface pressures at Mach 0.50 and δ_{le} = 0°.

porosity was effective in suppressing vortex interactions by significantly reducing the vortex strengths. This effect could be achieved by applying porosity to the LEX or flaps or in combination. The surface pressure distributions on the right half of the model shown in the figure indicate that the location and magnitude of the wing leading-edge vortex pressure signature are highly sensitive to surface porosity. The LVS flow visualizations revealed a significant effect of porosity on the global flow field, including reduced interaction of the LEX and wing vortex flows and diminished vortex-tail interactions. The six-component force and moment data indicated that porosity decreased the longitudinal instability at high angles of attack at the expense of decreasing the maximum lift. Lateral-directional stability levels were sensitive to porosity and the tail arrangement, and the most favorable trends were obtained with the centerline tail.
(Gary E. Erickson, 42886)
Aeronautics Directorate

Actuated Nose Strakes for Enhanced Rolling (ANSER) Flight Experiment

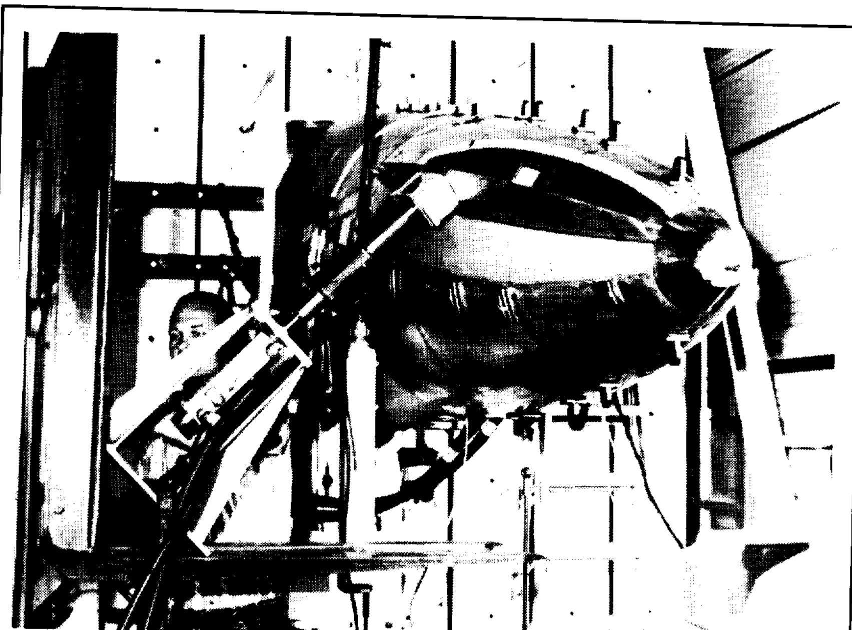

ANSER radome attached to F-18 forebody for static-loads testing.
L-93-07491

Rudder control for a conventional aircraft is markedly reduced as a result of the blanketing effect of the stalled-wing wake on the vertical tail as angle of attack is increased. As part of NASA's High-Angle-of-Attack Technology Program, extensive experimental and computational studies have indicated that the use of deployable nose strakes can favorably alter the basic aerodynamics and improve maneuverability of fighter-type aircraft at such flight conditions. Following exploratory and developmental testing, such a strake concept has been designed and fabricated at Langley Research Center. The flight hardware consists of a new radome that houses the hydraulically actuated strakes and is to be incorporated on the F-18 High-Alpha Research Vehicle (HARV). The design that provided the most practical aerodynamic benefit was a pair of conformal strakes, each capable of being deflected 90° and located at the 120° radial position from the bottom of the forebody. The term conformal refers to the configuration shape when both strakes are retracted, whereby the normal F-18 forebody contour is retained.

Static-loads tests were conducted after the radome was assembled (see figure). These tests established that the new design was able to meet and exceed the anticipated maximum flight loads. Further, the effect of these loads on the fuselage of the F-18 was analyzed by the airframe manufacturer and indicated that the resultant loads would not cause any structural limits to be exceeded.
(Daniel J. DiCarlo, 43870, Mark T. Lord, and Daniel G. Murri)
Aeronautics Directorate

RESEARCH AND TECHNOLOGY

Hypersonic and Transatmospheric Vehicles

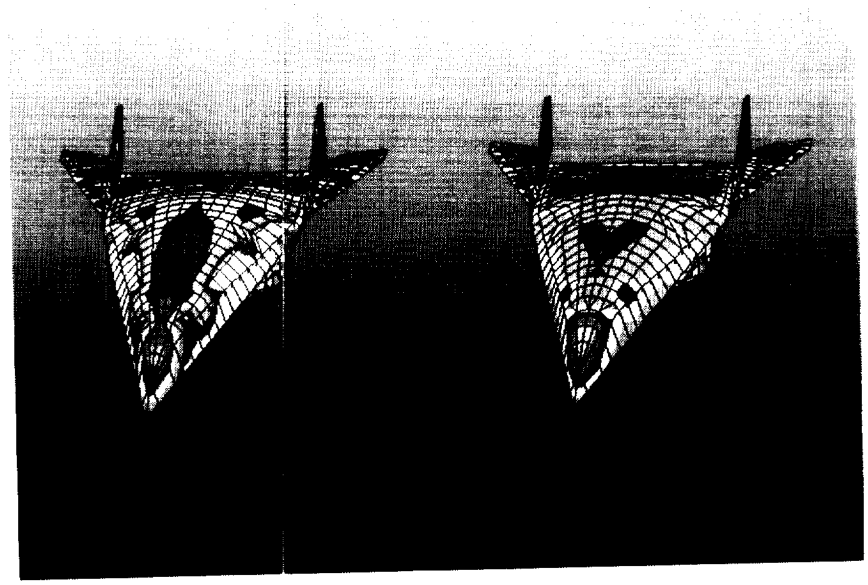

Develop the critical technologies for future hypersonic and transatmospheric vehicles

Numerical Simulation of Shock-Induced Combustion Past Blunt Projectiles Using Shock-Fitting Technique

For successful design of the hypersonic airbreathing propulsion system, it is essential to have a clear understanding of the physics of mixing and combustion at high speeds. Shock-induced combustion is one of the methods that is being investigated for hypervelocity propulsion where a shock is employed to initiate ignition in a premixed fuel-air mixture.

In the present study, a numerical investigation is being conducted to isolate and analyze the instabilities of shock-induced combustion in a hydrogen-air reacting system. Two-dimensional axisymmetric Navier-Stokes equations in conjunction with a detailed hydrogen-air reaction mechanism are used to simulate the ballistic range experiment in which blunt projectiles were fired in a premixed hydrogen-air mixture. A shock-fitting technique has been used here because previous studies of the same problem have shown that shock-capturing methods are overly dissipative.

Solutions have been obtained at Mach 5.11 and Mach 6.46. Mach 5.11 corresponds to the Chapman-Jouget velocity of the hydrogen-air mixture that is being considered here. Depending upon the projec-

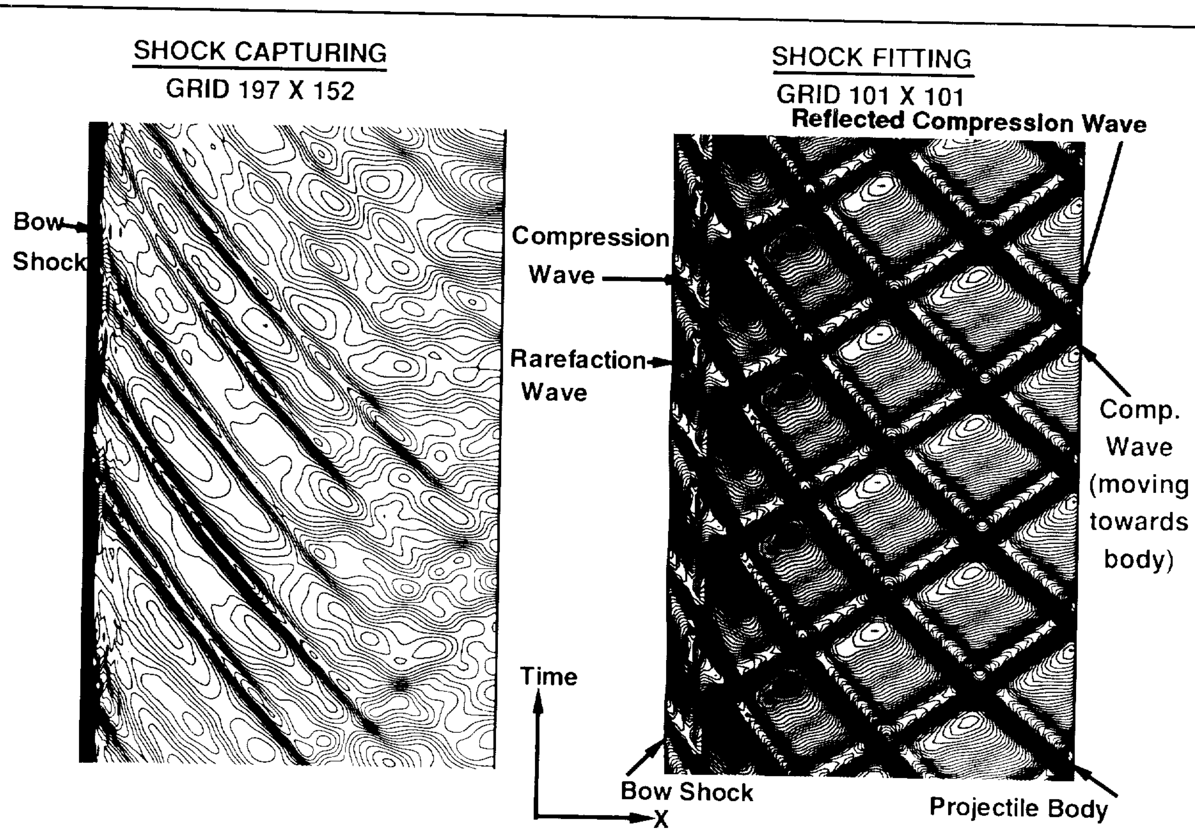

Contour plot for pressure along stagnation streamline for Mach 5.11 with shock-capturing and shock-fitting methods.

tile velocity, steady or unsteady flow field was observed. The figure shows the contour plot for pressure along the stagnation streamline for Mach 5.11 as a function of time. The unsteady flow field showed periodic oscillations of the reaction front. A comparison of the results shows that the shock-fitting technique has been able to capture the flow physics and the intrinsic details of the flow field more accurately than the shock-capturing method.

The results from the present study show that when the projectile velocity is close to the Chapman-Jouget velocity, the shock-induced reaction front is unstable. However, with sufficient overdrive (additional velocity), it was possible to stabilize the reaction front.
(J. K. Ahuja, 42285, A. Kumar, D. J. Singh, and S. N. Tiwari)
Aeronautics Directorate

Interpretation of Waverider Performance Data Using Computational Fluid Dynamics

A computational study was conducted to interpret wind-tunnel data from tests of a Mach 4.0 waverider model and a comparative reference model with a flat-top surface. The data indicated that the aerodynamic performance of the reference model was slightly better than that of the waverider model. These results contradict waverider design theory, which suggests that a waverider that is optimized for maximum lift-drag ratio should provide better performance than any other nonwaverider configuration at a given design point, especially at hypersonic speeds. It is important to determine the nature of this performance advantage, since the primary interest in waverider-derived configurations is their high lift-drag ratios, which are generated by an attached leading-edge shock at the design Mach number.

Computational fluid dynamic (CFD) solutions were obtained for each model at the design Mach number of 4.0 and at selected off-design Mach numbers. The solutions show that the lower surface-pressure values, and integrated lift and drag coefficients are much less for the reference model than for the waverider, because the reference-model lower surface is an expansion surface, in contrast to the waverider compression surface. The figure shows static-pressure contours that are nondimensionalized by free-stream pressure (P/P_{∞}). The darker shades represent higher pressure values. The lift-drag ratios of the reference model are higher because of a relatively low drag for a given amount of lift. A comparison of the base views of both models shows that the reference model exhibits the same shock-attachment properties as the waverider, because the planform shapes are identical. Therefore, the same effect that gives the waverider its high lift-drag ratio is present in the reference-model flow field. This suggests that the planform shape is the most important design parameter and that altering the lower surface of a waverider does

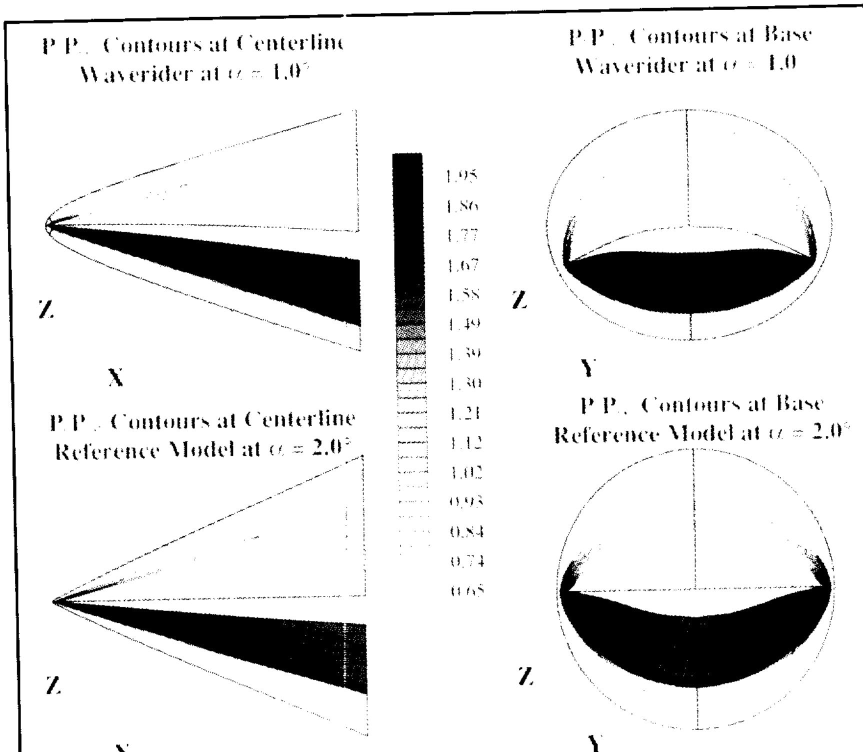

Comparison of waverider and reference-model flow-field solutions at angle of attack (α) where maximum lift-drag ratio occurs for each configuration at Mach 4.0 and Reynolds number of 2.0 × 10⁶ per foot.

not cause significant performance degradation. The highly uniform flow field shown in the base view of the waverider model indicates that this configuration has much better propulsion/airframe integration (PAI) characteristics. This work shows that the waverider concept remains a viable candidate for various hypersonic vehicle designs, including hypersonic cruise and single-stage-to-orbit concepts.
(Charles E. Cockrell, Jr., 45576)
Aeronautics Directorate

Scramjet Exhaust Simulation Modeling

It is impractical to test powered hypersonic configurations with actual combusting (hot) scramjet exhausts in most current wind tunnels. Instead, the "powered" effects are modeled by routing a cold simulant exhaust gas out the combustor nozzle. The simulant gas mixture is selected such that its thermodynamic properties at "cold" wind-tunnel temperatures are similar to the thermodynamic properties of "hot" scramjet combustion products. However, the simulant gases cannot completely model all the properties of the hot combustion products, and the resulting modeling errors need to be quantified.

A viscous computational study was performed to compare the forces and moments on the afterbody of a powered model for various simulant exhaust gases at both wind-tunnel and scramjet exhaust temperatures. The figure shows afterbody forces and moments for three exhaust gases across a range of static nozzle pressure ratio (SNPR) values. The combustor nozzle geometries were varied with the gases to produce consistent nozzle-exit Mach numbers. All forces and moments and SNPR's are normalized by the absolute values of results obtained by employing a hot simulant gas of steam (H_2O) and nitrogen at nominal Mach 10 conditions. These gases represent approximately 96 percent of the scramjet combustion products. The cold tetrafluoromethane-argon (CF_4-Ar) simulation agrees much better with that of the hot combustion products than does the cold-air exhaust simulation. Heating the air exhaust improves the simulation, but testing with hot air is no more practical than with hot steam. The hot steam and nitrogen results compare very well with the cold CF_4-Ar results for lift and pitching moment. The thrust values show a

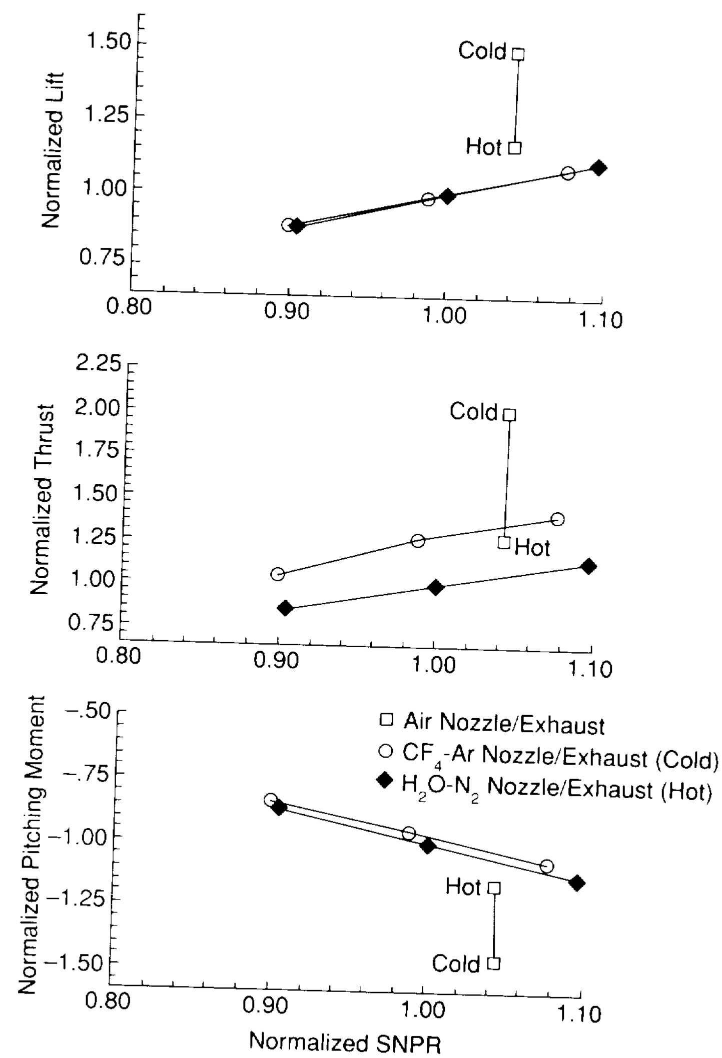

Computational afterbody force and moment comparisons versus SNPR for Mach 10 powered simulations.

small loss in linearity and a positive magnitude increment for the cold CF_4-Ar. However, the trends indicate that the afterbody forces and moments for a scramjet-powered vehicle can be approximated very well in wind-tunnel powered tests by employing a cold CF_4-Ar simulant gas if the appropriate nozzle geometry and pressure ratio are chosen.
(Kenneth E. Tatum, 45587, and Lawrence D. Huebner)
Aeronautics Directorate

Large-Eddy Simulation of High-Speed Transitional Boundary Layers

A central issue in large-eddy simulation (LES) is the development of models for the small subgrid scales. The main contribution of the model is to allow the transfer of the right amount of energy from the large to the subgrid scales, or vice versa near the wall. In all previous studies, the ad hoc manner in which the model constants or the model modifications have been treated (to satisfy certain physical conditions) is not satisfactory.

In this study, the subgrid scales are modeled dynamically in a large-eddy temporal simulation of a transitional boundary-layer flow along a cylinder at a Mach number of 4.5. The coefficients of the dynamic eddy-viscosity model are automatically tuned by using the spectral information of the smallest resolved scales with the aid of a test filter of a width that is larger than the grid filter.

The application of the dynamic model to a high-speed transitional boundary layer is successful. The model gives the proper asymptotic behavior of the modeled quantities near the wall and in the free stream. The model has no dissipative character like the standard Smagorinsky model. The LES with the dynamic model is able to capture the known "rope like" wave structure in the early stage of transition and the bulk of the flow-field structure during the entire transition region. A remarkable agreement exists between LES calculations and the direct numerical simulation (DNS) results concerning the resolved Reynolds stresses, heat flux, and time evolution of the skin friction. The LES of the transitional flow along a cylinder at a Mach number of 4.5 is achieved with nearly one-sixth of the grid resolution, one-sixth of the CPU Cray hours, and one-sixth of the central-memory requirements for DNS.

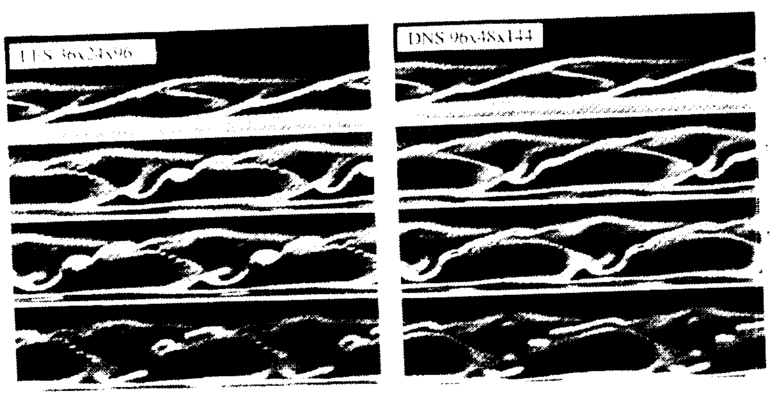

Comparison of flow structure in terms of spanwise vorticity in the middle of the skin-friction rise from DNS and LES.

The results from the present study show that simulation of temporal forced transition through laminar breakdown and beyond can be accomplished accurately and cheaply at high speeds. Location of transition onset (rise of skin friction), length of the transition zone, and peak skin friction can be predicted accurately by using dynamic modeling in a large-eddy simulation.
(Nabil M. El-Hady, 41072)
Aeronautics Directorate

Ramjet Performance Improvement Through Use of Bodyside Compression

High Mach number airbreathing propulsion systems generally focus on ramjet/scramjet concepts that employ the forebody of the vehicle to act as part of the engine inlet. Such systems require careful design of engine components to effectively exploit the potential of engine-airframe integration. The three-dimensional sidewall compression inlet is one ramjet/scramjet inlet concept that has been studied for many years.

The dominant feature found in the sidewall compression inlet flow field is a pair of glancing

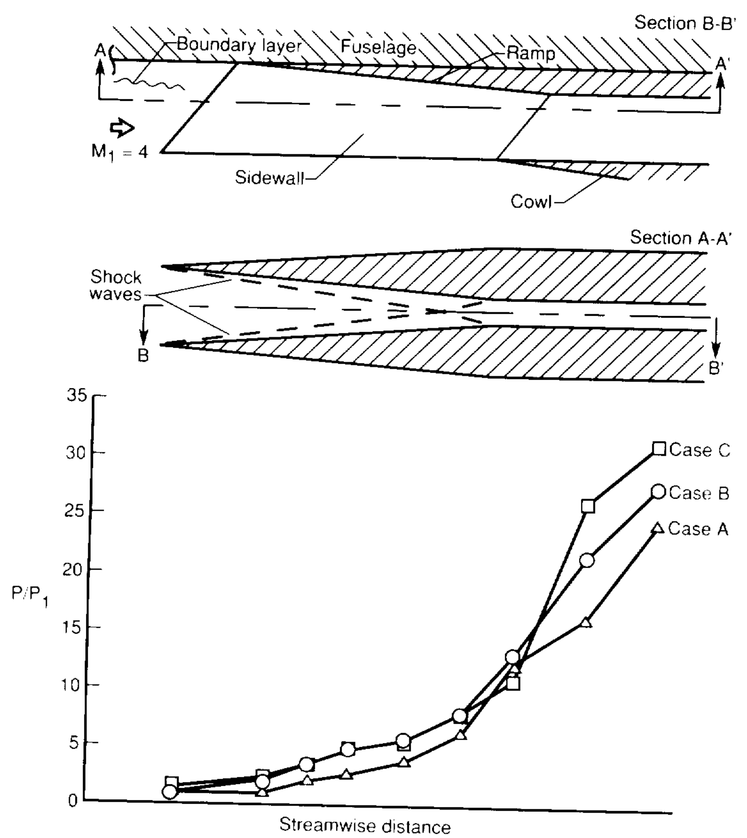

Inlet bodyside centerline wall-pressure distributions.

shock-wave/boundary-layer interactions caused by the sweeping of sidewall-induced shock waves across the incoming forebody boundary layer. A major result of these interactions is that the incoming boundary layer usually separates and rolls up into a strong streamwise vortex that is located near the root of each sidewall. As these vortices grow and reach the centerline, they interact with one another. In this vortex-vortex interaction, the vortices lift off of the surface and create a large core of low total-pressure fluid near the middle of the cross plane. Such a feature can inhibit inlet performance by limiting the amount of combustion-induced pressure increase that the inlet can tolerate (commonly referred to as the backpressure).

Compression surfaces (i.e., ramps) were placed on the bodyside between the sidewalls of the inlet. These ramps can be used to influence the local pressure field and to thereby modify the vortex-vortex interaction. The figure shows wind-tunnel data of the centerline wall-pressure distribution, normalized by the upstream static pressure (P_1), on the vehicle surface of a sidewall compression inlet with swept forward leading edges. The results from three inlet configurations are shown. The inlet without a ramp, case A, can achieve a backpressure of approximately 24.5 P_1. A straight ramp, case B, can increase this backpressure to 26.7 P_1, while a comparable convex ramp, case C, can permit the backpressure to reach 31.3 P_1. The convex ramp geometry is designed to reduce the streamwise pressure gradient in the region of the vortex-vortex interaction and to delay the vortex lift-off phenomenon. The result is a significant increase in inlet backpressure performance.
(Patrick E. Rodi, 46259, and Griffin Y. Anderson)
Aeronautics Directorate

Scramjet Fuel-Mixing Estimates in HYPULSE Expansion Tube Facility Using Mie Imaging

A series of generic scramjet fuel injectors were tested in the NASA HYPULSE facility at the General Applied Science Laboratories, Inc. (GASL). Test conditions at the fuel injectors are typical of what would be encountered at the entrance to a scramjet combustor on a single-stage-to-orbit (SSTO) vehicle flying at Mach 14. The prime objective of these tests was to measure the fuel-injector performance as indicated by the accomplished mixing and combustion of the hydrogen fuel. Typically, such information has been inferred from wall-pressure distributions or instream measurements of the fuel species concentrations. However, the short test times and severe flow conditions (low pressure and high temperature) of the HYPULSE facility at the hypervelocity flow simulations make mixing estimates difficult. Therefore, a technique was needed to ac-

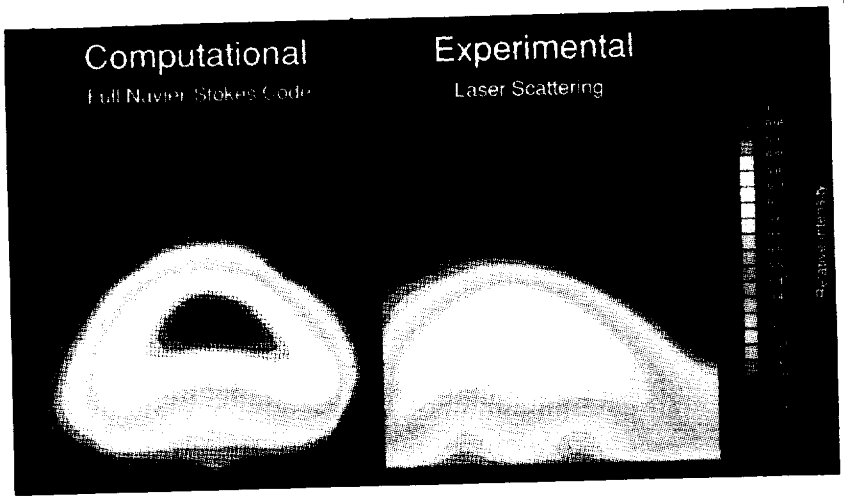

Comparison of fuel-plume imaging by laser light scattering with computed result.

quire time-mean, spatial distributions of the injected fuel plume during the short (0.30 msec) facility run time from which the integral mixing could be deduced.

The concept was to illuminate the injected fuel by scattering a laser sheet from solid silicon dioxide (SiO_2) particles that were contained in the fuel jet. The particles were produced in situ by burning a small amount of silane (SiH_4), which had been mixed with the hydrogen fuel, in the plenum of the fuel injector with enough oxygen to stoichiometrically react with the silane. The resulting fuel contained about 94 percent H_2 and 6 percent water in the gas phase, and had SiO_2 particles that were about 0.2 µm in scale. The laser sheet was generated from a flash-lamp pumped-dye laser with a pulse width of 50 µsec, which was sufficient to obtain time-mean images of the fuel plume. The images were collected with a CCD video camera and were corrected for background intensity, laser-beam variation, and view angle. The average image of two fuel plumes from a pair of swept-ramp injectors in scramjet model tests in HYPULSE is given on the right side of the figure. The image on the left was derived from a Navier-Stokes CFD solution of the combustor/injector flow field that considered only the gaseous part of the fuel jet. A procedure to analyze the images has been formulated and used to determine the fuel mixing. The analysis procedure is based on the flux of particles through the plane of the laser for the data image and the grid plane for the CFD solution, and on the assumption that this particle flux is proportional to the fuel mass flow. Both images in the figure have been scaled by the respective total particle flux. The CFD image appears to underpredict the data image, as is evident from the higher peak and narrower spreading. This observation is supported by the estimates of mixing efficiency, which were determined to be 52 and 46 percent for the data and CFD images, respectively. The computed mixing efficiency from the CFD solution is 44 percent. The use of this promising technique is continuing in hypervelocity tests of scramjet fuel injectors in HYPULSE. Improvements in the particle formation and imaging optics are under way.

(R. Clayton Rogers, 46239, Elizabeth H. Weidner, and Robert D. Bittner)
Aeronautics Directorate

High-Speed Scramjet Injector Design

Scramjet designers must understand complicated fuel-mixing processes to achieve useful engine thrust at flight Mach numbers above 10. Mixing control/enhancement mechanisms include fuel distribution, turbulent diffusion, axial vorticity, shock-wave interaction, and baroclinic torque. Computational fluid dynamics (CFD) is a useful tool for determining the relative contributions of the various mechanisms to the mixing process. As part of a parametric study of ramp, flush-wall, and strut fuel injectors, CFD was used to evaluate the relative impact of these mixing phenomena.

The figure illustrates the relative importance of two of the major drivers of the scramjet fuel-mixing process: turbulent diffusion and axial vorticity. This solution was performed for the swept-ramp geometry illustrated at flight Mach 14 conditions. The impact of axial vorticity generated by the ramp (evaluated by removal of all cross-flow from the ramp base plane) is less than the impact of turbulent diffusion (difference between laminar and turbulent solutions) on

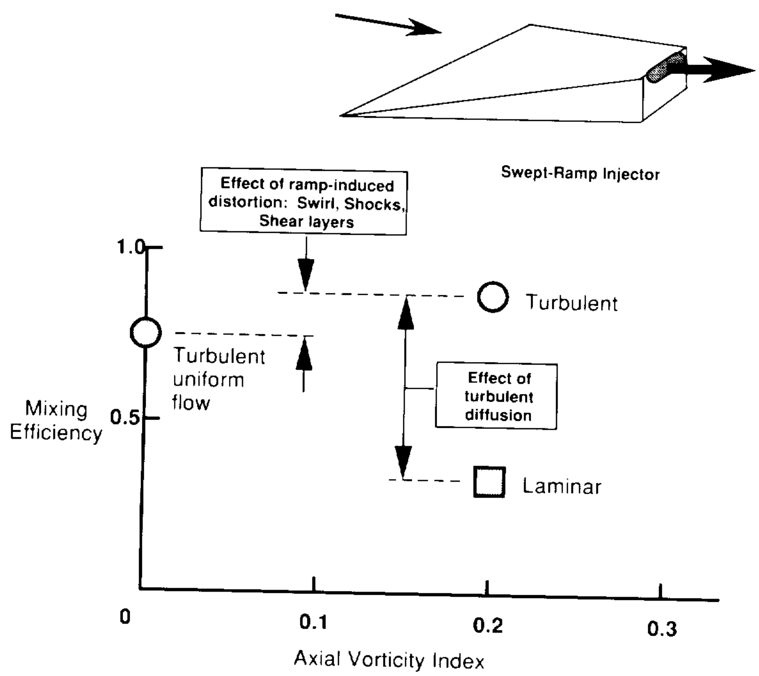

Contributions of turbulence and axial vorticity to scramjet fuel mixing.

mixing efficiency. Similar results for the three classes of fuel injectors are being evaluated and will enhance our understanding of the scramjet fuel-mixing process and lead to improved injector strategies.

This work was done in part under grant with the University of Missouri at Rolla.
(Charles R. McClinton, 46253, and David W. Riggins)
National Aero-Space Plane Office

Visualization of Mach 2 Vitiated Air Using Planar Laser-Induced Fluorescence

The nonintrusive optical diagnostic technique known as planar laser-induced fluorescence (PLIF) was used to study the vitiated-air component of a Mach 2 jet flame. Signals were obtained by probing the hydroxyl radical (OH) by using a tunable excimer laser near 32 441.8 cm^{-1}. The OH species is a chemical intermediate in all combustion flows and a convenient molecule for generating PLIF.

The laser is formed into a sheet that is 25 mm high and 0.08 mm thick and is parallel to the flow (X-axis in the figure). The resulting images are viewed at 90° to the direction of the laser sheet (Y-axis in the figure). Since the laser pulse duration is 20 nsec, the images represent "frozen" snapshots of the flow. Three instantaneous and temporally uncorrelated images are shown in the figure. The images show striation patterns or alternating regions of high and low OH signal along the Y-axis. This means that OH is being ejected

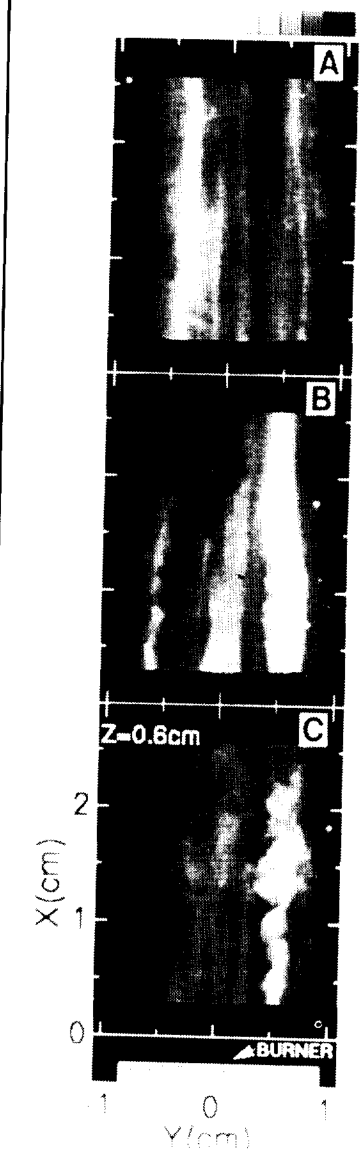

Instantaneous planar "snapshots" of vitiated-air component of a Mach 2 reacting flow obtained by using planar laser-induced fluorescence. Flow direction is along X-axis.

nonuniformly from the vitiated-air injector. The images also show vortical patterns in the vitiated air. Both results indicate that the flow

is unsteady. The images also illustrate the advantages of using planar nonintrusive optical techniques over probe measurements to study supersonic flow fields.
(R. Jeffrey Balla, 44608)
Electronics Directorate

Carborane-Based Oxidation Inhibitors for Carbon-Carbon Composites

Carbon-carbon (C-C) composites are a specialty class of materials with many unique properties that make them attractive for a variety of demanding engineering applications. A major factor that limits the wider use of these materials is their susceptibility to oxidation at temperatures above 400°C. The primary approach for protecting C-C composites from oxidation at high temperatures is to apply an oxidation-protective coating. However, conventional coatings typically develop microcracks and often suffer from other defects such as thin areas and pinholes; these defects make additional protection of the C-C substrate desirable. This additional protection can be afforded by adding inhibitor materials, typically as fine powders, to the matrix phase of the substrate during its fabrication. However, the use of these powdered inhibitors often results in nonuniformity of protection as well as fiber damage during molding, which reduces mechanical properties. In addition, inhibitors in the form of powders cannot be employed in the densification resins.

Langley Research Center has developed a solution to this problem based on the use of inhibitor compounds that are soluble in the matrix precursor resin (phenolic resin). The effectiveness of this inhibitor approach can be judged by the rate of mass loss in an oxidative environment. The figure shows oxidation data for a series of C-C composites oxidized at 832°C. The composites used both the molecular inhibitor vinyl-o-carborane and the particulate inhibitor boron carbide in the prepreg resin, as well as vinyl-o-carborane in the densification resin. Results indicate that the composites inhibited with vinyl-o-carborane have lower oxidation rates than the composites inhibited with the same level of particulate boron carbide; also, the addition of the vinyl-o-carborane to the densification resin results in a further decrease in the oxidation rates.

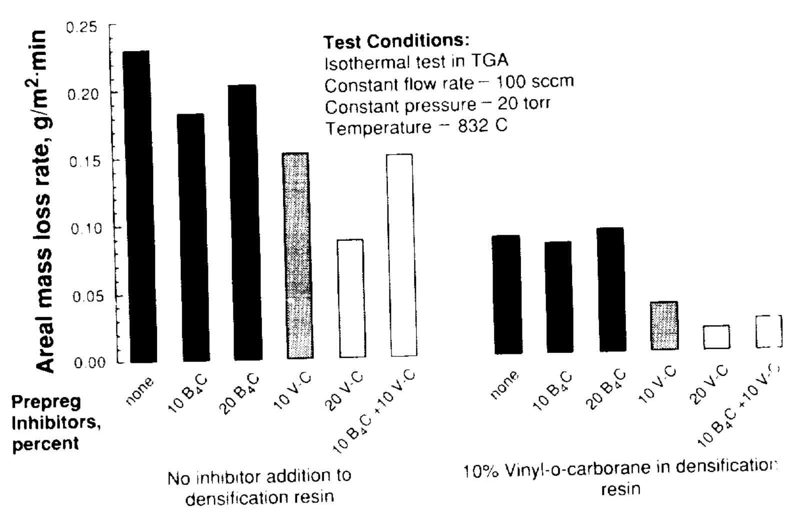

Vinyl-o-carborane (V-C) additions reduce the oxidation rate of carbon-carbon composites.

In addition to the research at Langley Research Center, Advanced Technology Materials, Danbury, CT, is conducting research under a Small Business Innovative Research Phase I contract to develop a moisture-resistant version of the carborane-modified phenolic resin system to improve performance in high-humidity environments.
(Wallace L. Vaughn, 43504)
Structures Directorate

Multilayer Lightweight Coating for Titanium-Based Materials

Titanium alloys and titanium matrix composite materials are attractive for many aerospace applications because of their high strength and low density. However, long-time use of titanium-based materials in air at temperatures above 500°C has been limited by their uptake of oxygen and nitrogen, which causes a severe loss in ductility of the materials. Also, titanium is subject to environmental attack when exposed to certain

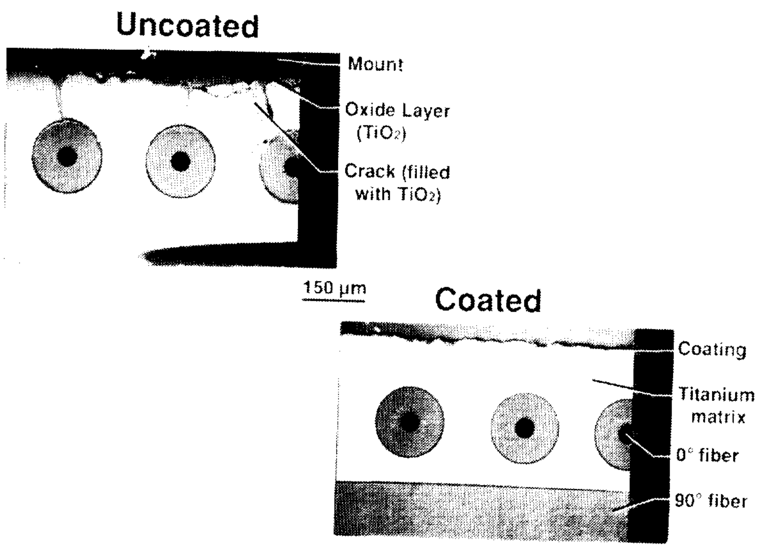

Microstructure of coated and uncoated SCS-6 silicon carbide fiber/Beta-21S titanium matrix composite samples after cyclic oxidation (144 cycles: 5 min, 800°C; 1 min, −196°C).

hydrocarbon-containing fluids at lower temperatures.

The multilayer lightweight coating is an effective means of shielding titanium-based materials from the environment and thus enabling their use at much higher temperatures. The coating is about 5 µm thick. It consists of an intermetallic reaction-barrier layer that separates the titanium from a two-phase glass layer. The two-phase glass is prepared by using sol-gel chemistry methods and functions as a diffusion barrier layer to block transport of oxygen and nitrogen to the titanium substrate. The two-phase glass consists of a silica-rich matrix plus a lower softening-point glass that is tailored to be soft at the use temperature. The soft phase promotes self-healing of defects and microcracks that may form in the coating.

The figure shows micrographs of coated and uncoated titanium matrix composite (SCS-6 silicon carbide fibers in Beta-21S titanium matrix) samples after 144 thermal cycles from 800°C to −196°C with 12 hours accumulated time at peak temperature. The uncoated sample has cracks from the surface to the first layer of fibers. Those cracks would cause failure in a structural application. The coated sample has no cracks.

The coating is currently being evaluated by Rohr, Inc. and NASA for coating the nozzle mixer of an advanced jet engine. Success will make production of the part possible from titanium with a weight savings of 25 percent and a cost savings of 10 percent. Other potential applications include the coating of valves and springs in automotive applications.
(R. K. Clark, 43513, and K. E. Wiedemann)
Structures Directorate

Effect of Aeropropulsive-Elastic Interactions on Hypersonic Vehicles

Current airbreathing hypersonic-vehicle configurations use an elongated fuselage forebody as the aerodynamic compression surface for the propulsion system. This type of airframe-integrated propulsion system results in an unprecedented form of aeropropulsive-elastic interaction, in which deflections of the fuselage produce propulsive force and moment perturbations that may appreciably impact the performance and control of the vehicle. The objectives of this research are to quantify the magnitudes of elastically induced propulsive perturbations for a representative hypersonic vehicle and to provide estimates of the impact of these perturbations on the vehicle's rigid-body flight dynamics.

Elastic mode shapes and in vacuo frequencies for a representative hypersonic configuration are shown in the portion of the figure entitled "Aeroelastic Model." From this model, fuselage deflections and angle-of-attack variations were obtained in response to atmospheric turbulence and aerodynamic control effector pulses. The fuselage deflections and angle-of-attack variations were used as inputs to a hypersonic propulsion code that analyzed the entire propulsion-system flow path, consisting of the undersurface of the fuselage forebody, the combustor module, and the undersurface of the fuselage afterbody. The code predicted variations in vehicle lift and pitching moment with angle-of-attack and fuselage deflection. Typical results are

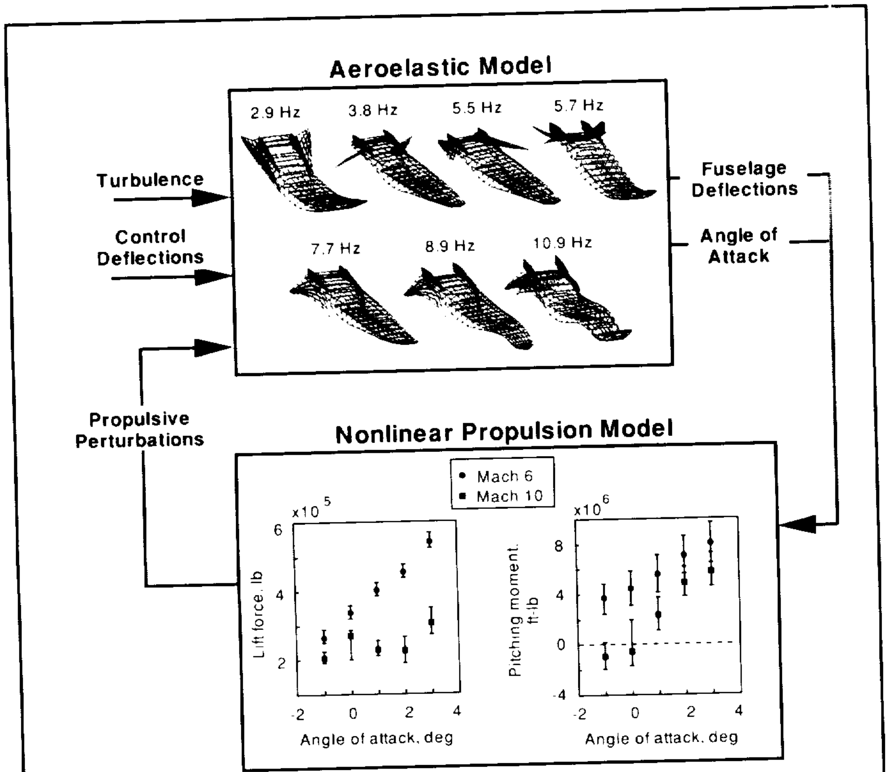

Block diagram of components used to model aeropropulsive-elastic interaction.

shown in the portion of the figure entitled "Nonlinear Propulsion Model." The symbols on these graphs indicate the data for the undeflected vehicle geometry, and the brackets indicate the magnitude of perturbations introduced by deformation of the fuselage forebody and afterbody. These perturbations were subsequently fed back into the aeroelastic model to assess their impact on the dynamics of the combined system. Inclusion of this effect significantly altered the frequency and damping of the vehicle's rigid-body modes. Nonlinearity of the propulsion-system sensitivities also introduced uncertainty into the prediction of the vehicle's rigid-body flight dynamics.

The analytical results show that significant propulsive lift, thrust, and moment perturbations may be produced by elastic deformation of the fuselage for this type of vehicle. These perturbations impact the vehicle's rigid-body flight dynamics and must be accounted for to accurately predict these modes. Furthermore, the results provide quantitative estimates of the sensitivity of the propulsion system to fuselage deflections and angle-of-attack variations for use in designing a robust control system for an airbreathing hypersonic vehicle.
(D. L. Raney, 44033, J. D. McMinn, and A. S. Pototzky)
Flight Systems Directorate

Hypersonic Airbreathing Vehicle Design/Optimization Code

A process for hypersonic vehicle design/optimization has been integrated into a workstation-based synthesis system on the Silicon Graphics IRIS workstation.

Airbreathing hypersonic vehicles require the airframe to be highly integrated with the main propulsion system. Interesting design trades result when attempting to find the combination of vehicle

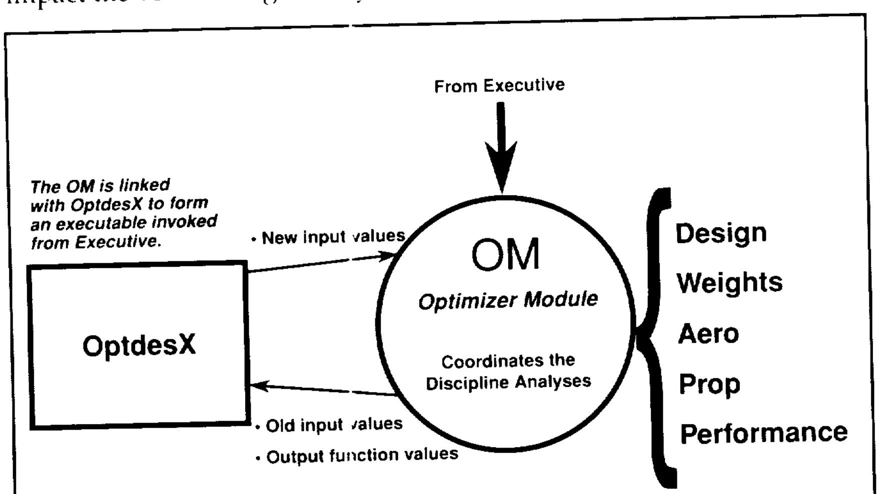

OptdesX drives optimization loop.

shape parameters and engine design parameters that best meet the mission requirements. The aerodynamic and propulsion forces and moments are particularly sensitive to many of these parameters.

The OptdesX optimization program has been integrated as a module of the interactive design/optimization program. The figure illustrates the basic architecture. Control of the discipline analyses required to compute the optimization objective function(s) is provided by the optimization module (OM).

To demonstrate the process, a parametric-geometry model was developed for a class of hypersonic vehicles. The model is designed such that the vehicle external moldline is defined by a small number of parameters (e.g., angles, coefficients, dimensions), and the shape is allowed to evolve during the optimization process. A 3D geometry display utility has been developed to provide visual feedback on current vehicle shape as the optimization proceeds.

Initial emphasis is on the flight regime for scramjet operation (Mach 6 to 15). The automated process employs the Supersonic/Hypersonic Arbitrary Body Program (S/HABP) for aerodynamic surfaces and the SRGULL program for the propulsion flow path.

Using energy method mission performance to determine the performance objective function, a 10-percent reduction in takeoff gross weight (TOGW) was achieved in just 4 iterations for this demonstration.

The long-term objective is to implement this system as the centerpiece in a multidisciplinary advanced design team. Meeting this objective will allow large-scale automation of the design process and will result in a substantial reduction in turnaround time.
(John G. Martin, 43755, and James L. Hunt)
National Aero-Space Plane Office

Vibrational Relaxation in Hypersonic Flow Fields

Vibrational relaxation times (τ) are critical parameters for modeling gases in thermochemical nonequilibrium. They strongly influence dissociation and chemical reaction rates, ionization and electronic excitation, shock standoff distances from hypersonic vehicles, and thus the radiative and convective heating of such vehicles. At the opposite extreme of low temperatures encountered in rapidly expanding flows, they dramatically affect the flow quality in test sections of hypersonic real-gas nozzles. Reliable laws are desperately needed to scale τ to these opposite temperature extremes (70 K to 40 000 K) from the experimental shock-tube range (2000 to 9000 K).

Theoretical models have been developed to provide these scaling laws. These models include comprehensive treatments of high-energy collisions that involve multiple quantum jumps, changes in the internal states of both molecules in a colliding pair, and corrections to first-order transition probabilities. The figure shows the dependence on temperature of the product of pressure and τ immediately behind a strong shock front in pure N_2, as compared with the straight line often used in computational fluid dynamics (CFD).

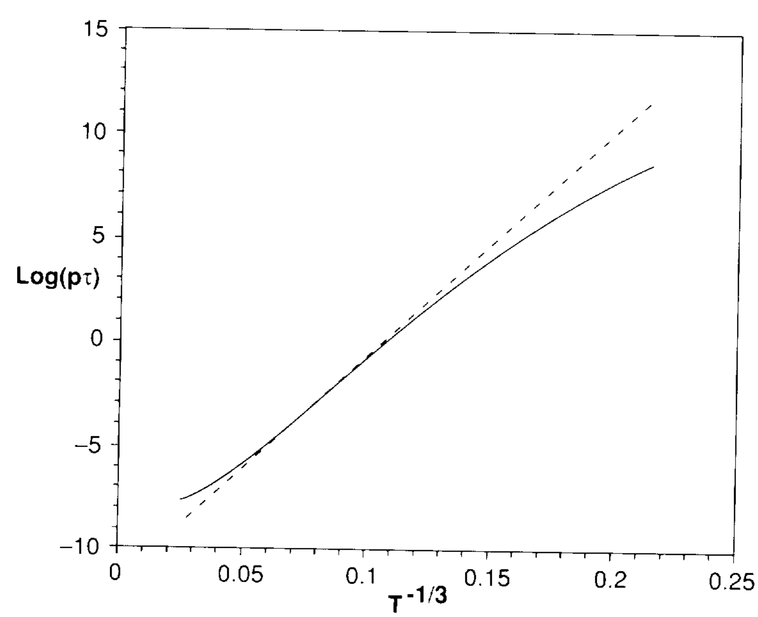

Temperature dependence of $p\tau$.

Farther downstream, as vibrational excitation increases, τ becomes a function also of the vibrational temperature to indicate a breakdown of the conventional assumption of a linear relation between cause (nonequilibrium) and effect (relaxation). Current CFD codes are being corrected for these and other deficiencies that relate to the relaxation process in highly nonequilibrium gas mixtures. The result will be an improved capability of CFD codes for predicting aerodynamic performances and heat loads of hypersonic vehicle designs. Commercial applications abound in the rapidly emerging fields of nonequilibrium chemistry and chemical synthesis, plasma, and laser technologies.
(W. E. Meador, 41434, M. D. Williams, and G. A. Miner) Space Directorate

Aerothermodynamics of a MESUR Mars Entry

The Mars Environmental Survey (MESUR) Pathfinder Mission proposes the landing of a probe on Mars to observe the planet's surface and atmosphere. The MESUR entry vehicle is envisioned to have a Viking-style forebody (70° sphere cone), 2.65 m in diameter, with a nose radius of 0.6625 m and a conical afterbody. Design of the thermal protection system for the MESUR vehicle requires an accurate definition of the entry aerothermal environment.

The computational code LAURA (Langley Aerothermodynamic Upwind Relaxation Algorithm) was modified to predict thermochemical nonequilibrium entry flows in Mars' CO_2-N_2 atmosphere. Flow fields have been computed for the MESUR trajectory's maximum stagnation heating point. These flow fields reveal the surface pressures and heating on the vehicle as well as the wake flow structure.

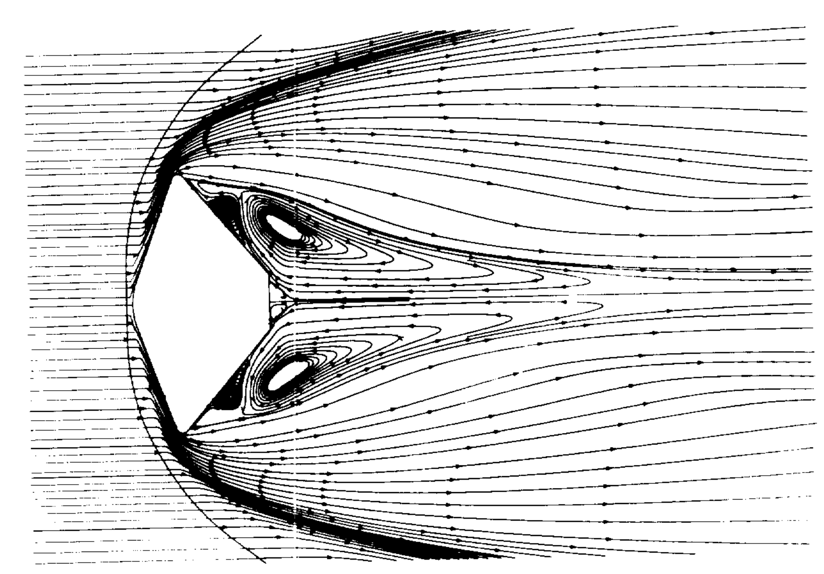

Flow-field streamlines about MESUR entry vehicle.

The figure displays streamlines about the vehicle for a zero-angle-of-attack case at 37 km altitude and 6.5 km/sec velocity. The wake is characterized by a system of recirculating vortices, the largest and strongest of which impinges on the vehicle's aftmost corner. This impingement results in a heat-transfer rate at that corner of 7 W/cm^2, which is three times greater than the prediction for the rest of the afterbody. The forebody stagnation-point heat-transfer rate, assuming a fully catalytic wall, is 118 W/cm^2.
(Robert A. Mitcheltree, 44382) Space Directorate

Nonequilibrium Flow Code Developed for Prediction of Flight Shock-Shock Interference Aerothermal Loads

A nonequilibrium flow code was developed for industry to predict shock-shock interference aerothermal loads for flight conditions. A second objective was to determine aerothermal heating on a 0.1-in-radius cylindrical body that represents a blunt leading edge caused by a type IV shock-shock interference at Mach 15 and a dynamic pressure of 2000 psf in chemical and thermal nonequilibrium flow.

The solver part of LARCNESS (Langley Adaptive Remeshing Code and NaviEr-Stokes Solver) was modified to account for chemical and thermal nonequilibrium flows typical of hypersonic flight. Air was modeled as a mixture of five chemical species (O_2, N_2, O,

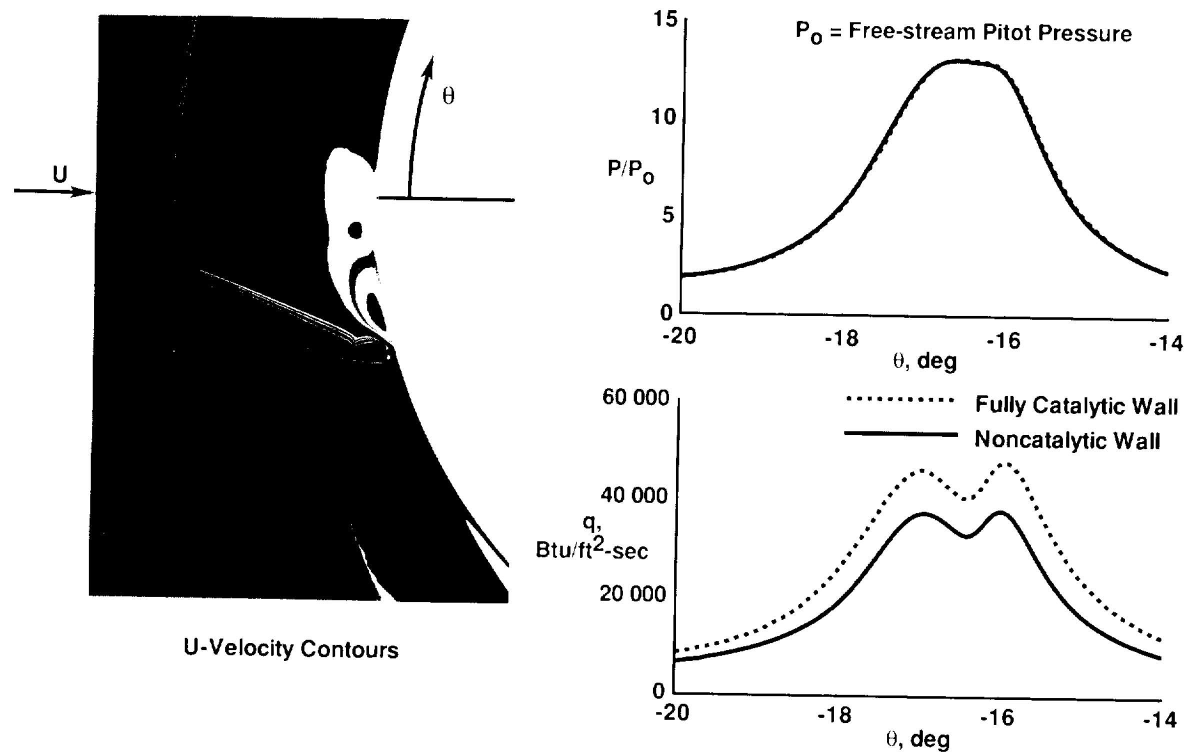

U-velocity contours and pressure and heat-flux distributions for a 0.1-in-radius cylinder in Mach 15 nonequilibrium flow.

NO, and N) and with two temperatures (translational and vibrational). Unstructured meshes of triangular and quadrilateral elements are used as they lend themselves to adaptation. The final mesh had over 155 000 elements with a spacing of about 0.05° on the body where the heat flux reached peak values. The mesh of quadrilateral elements on the body had a minimum thickness of 1.0E-7 in.

The type IV, supersonic-jet, shock-shock interference flow field is complex; it has two triple points, two shear layers, and a supersonic jet that undergoes repeated expansions and compressions before terminating in a normal shock close to the body. The supersonic jet, the surrounding shear layers, and the terminating normal shock are very clearly illustrated by the velocity contours. The pressure on the body behind the terminating normal shock is uniform over a 1° interval; the heat-flux distribution shows two peaks. The peak heat flux is about 48 000 Btu/ft^2-sec for a fully catalytic wall and 38 000 Btu/ft^2-sec for a noncatalytic wall (see figure). The code has been validated on existing equilibrium test data.

Such information is critical in the design of leading edges for hypersonic vehicles. The present study also demonstrates the need for highly refined meshes to capture the details of the flow features in this type of problem.
(Allan R. Wieting, 41359)
Structures Directorate

New Wing Concept for Reducing Supersonic Inviscid Drag

Aircraft that are designed to fly at supersonic speeds, such as advanced tactical fighters and the high-speed civil transport, generate a complex sequence of shocks that increase the drag of the aircraft. These shocks are unavoidable, but the drag they create can be reduced by modifying the geometry of the aircraft. One type of geometry modification to obtain drag reduction is the recontouring of the wing airfoil.

A new airfoil concept has been developed that takes advantage of the shocks that occur at supersonic speeds. For this new concept, the

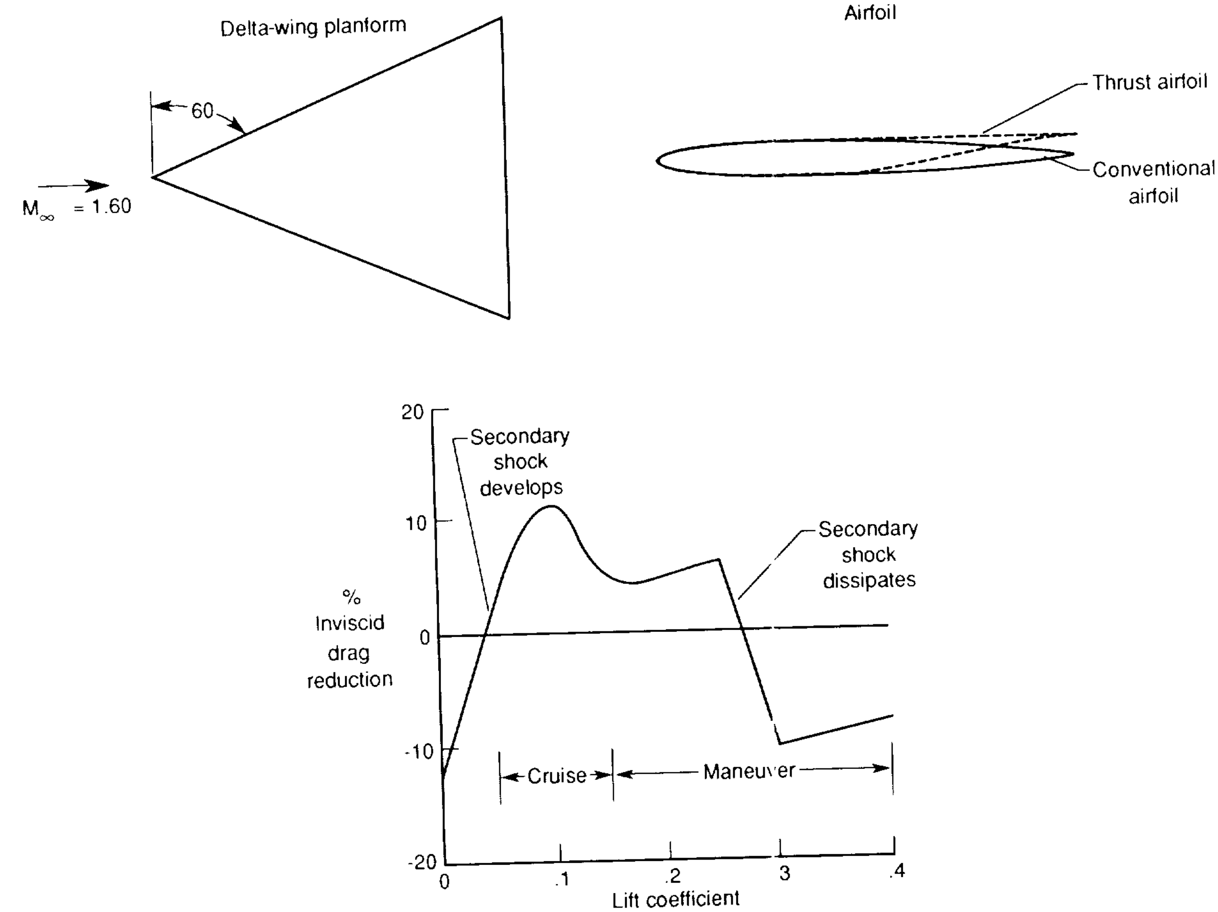

Drag reduction obtained from thrust airfoil on a delta wing at M = 1.60.

shape of a conventional airfoil aft of its maximum-thickness location is modified to account for the effect of a secondary shock that occurs on the wing surface. A more favorable orientation of the local airfoil surface is achieved which, in combination with the local surface pressures, creates a thrust force that directly decreases the drag force. The figure shows a delta-wing planform and the contours of a conventional airfoil and the new "thrust" airfoil. The effectiveness of the thrust airfoil for inviscid drag reduction is demonstrated by computing the drag on delta-wing planforms at a Mach number of 1.60 by using an inviscid computational method. One delta wing is composed of the conventional airfoil and another is composed of the thrust airfoil. In the presence of the secondary shock, the delta wing that is composed of the thrust airfoil yields an inviscid drag reduction of 5 to 10 percent compared to the delta wing that is composed of the conventional airfoil. This drag reduction is achieved over a wide range of lift that includes both cruise and maneuver conditions.

(James L. Pittman, 41359)
Structures Directorate

CFD Evaluation of Base-Pressurization Methods

Some scramjet engine designs utilize step expansions to minimize the variable-geometry requirements of the engine. The drawback of the step expansions is the high-pressure drag that they create, which reduces the efficiency of the engine. A numerical study of two-dimensional base flow fields was undertaken to investigate the effects of different types of base-pressurization methods. The computational fluid dynamics (CFD)

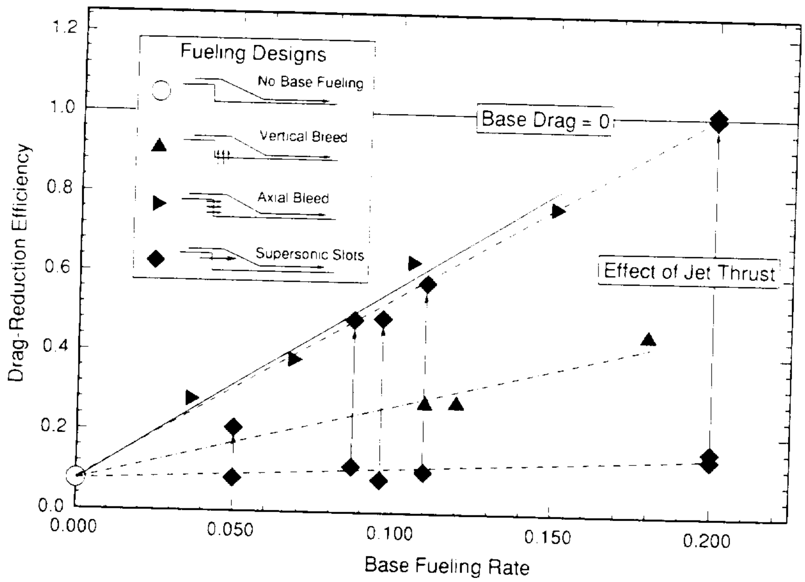

Computed base-pressurization results for various modes of fuel injection. Arrows indicate effect of adding jet thrust of supersonic slot injectors.

code used for this study was the General Aerodynamic Simulation Program (GASP) that was developed by Aerosoft, Inc.

Hydrogen fuel was injected from the base to add mass and heat (through combustion) to the flow in the low-pressure recirculation region that sets up just downstream of the step. With proper design, these additions can increase the pressure in the base region and reduce the overall base-pressure drag. The three different methods of injecting fuel into the base are illustrated in the figure: vertical subsonic transpiration, axial subsonic transpiration, and supersonic slots or ports. The results for these cases are summarized in the figure in terms of a drag-reduction efficiency, which is the ratio of the effective base pressure to throat pressure. The vertical-bleed cases, because diffusion of oxidizer down into the base region causes combustion in the low-Mach-number recirculation region, did not generate a large increase in the base pressure. The axial-bleed cases proved to have the best pressurization ability of the three designs, because the combustion region was confined to the high-Mach-number shear layer and because the large-total pressure losses that resulted increased the pressure in the base region considerably. The supersonic slot injection cases tended to scavenge mass from the base region, and these designs produced little base pressurization. However, the supersonic slots have significant streamwise momentum, which adds considerable thrust force; when this is factored in, the overall drag-reduction efficiencies of the axial-bleed and supersonic-injection methods become approximately equivalent. This work was done under contract with Analytical Services & Materials, Inc.
(Charles R. McClinton, 46253, and Paul H. Vitt)
National Aero-Space Plane Office

Structural Analysis of Hypersonic Vehicles

Analyses of a hypersonic vehicle demonstrate the improvement of a new structural panel formulation. The formulation is for airframe and engine surfaces designed as composite stiffened panels. Analyses of a hypersonic vehicle using this improved formulation and using traditional formulations were performed for Mach 10 in-plane and through-the-thickness temperature gradients. Visible in the figure are the differences between the correct analysis of the improved formulation and incorrect traditional analysis. Although not shown, comparable differences occur for computed thermal forces and computed mechanical forces and moments.

High-speed aircraft are frequently designed with fiber-reinforced composite-stiffened panels. Such panels are highly unsymmetric and orthotropic, therefore, the formulation of stiffness, thermal expansion, and thermal bending is complex. A hat-stiffened, fiber-reinforced, metal-matrix composite is used in this design. Metal-matrix composites are chosen for their high-temperature capability; some have a service use up to 1300°F. When allowing a stiffened panel to reach these high temperatures, its large membrane, bending, and membrane-bending coupling thermal response must be analytically quantified.

Differences in the displayed thermal moments are due to dissimilarities in the formulations of panel-stiffness terms and thermal coefficients. Traditional methods that are currently being practiced

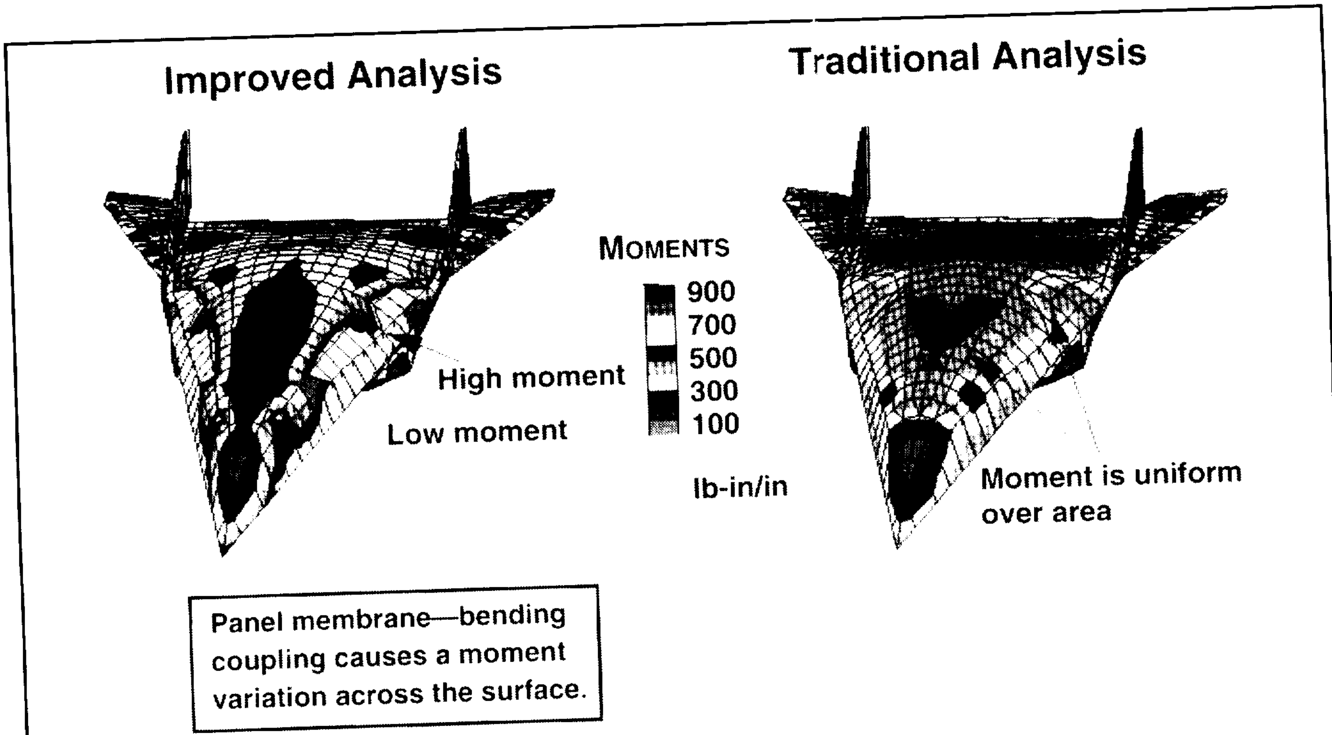

Calculation of thermal moment for a hypersonic vehicle flying at Mach 10. (Original of figure in color; contact author for more information.)

omit panel orthotropic compatibility, membrane-bending coupling of unsymmetric stiffness, and membrane-bending coupling of unsymmetric thermal expansion and bending. The improved formulation includes this data by extending classical lamination theory to the stiffened cross section and introducing additional thermal coefficients. It is robust enough to handle panels with general cross-sectional shapes. Special terms in the equations represent the actual shape of the stiffening member. By implementing this capability with a single plane of shell finite elements using the MSC/NASTRAN™ analysis program, the vehicle model can accurately solve thermal forces and moments.

(Craig S. Collier, 43767, and James L. Hunt)
National Aero-Space Plane Office

Symmetric Scramjet Free-Flight Experiment

The objective of this work was to design a "low cost," low-risk Mach-15 scramjet flight experiment as a candidate for the National Aero-Space Plane (NASP) HYFLITE program. The resultant configuration was a rocket-boosted, free-flying fin-stabilized symmetrical engine as depicted in the figure. Cycle analysis indicated that this configuration could produce sufficient thrust to accelerate, thus demonstrating scramjet performance at very high speeds Several potential problems associated with the small scale were addressed more rigorously. These included inlet combustor and nozzle heating, inlet mass capture, inlet boundary-layer transition, fuel mixing and finite-rate chemical kinetics, and scramjet nozzle flow interaction on the circular stabilizer fin. The design of the symmetric flight vehicle involved several component trade studies. The forebody trade study, using a viscous blunt-body flow solver, CFL3DE, with an engineering transition criterion for Gortler vortices, encompassed several vehicle scales, nose radii, and an inlet compression ramp radius of curvature to determine forebody contour shape requirements for providing turbulent flow at the inlet entrance. From this study, a suitable forebody contour shape was selected for a three-dimensional analysis to assess spanwise flow spillage along the compression-ramp surface and at the inlet shoulder. Results from that analysis indicate an acceptable mass capture of 79 percent for a full-span inlet

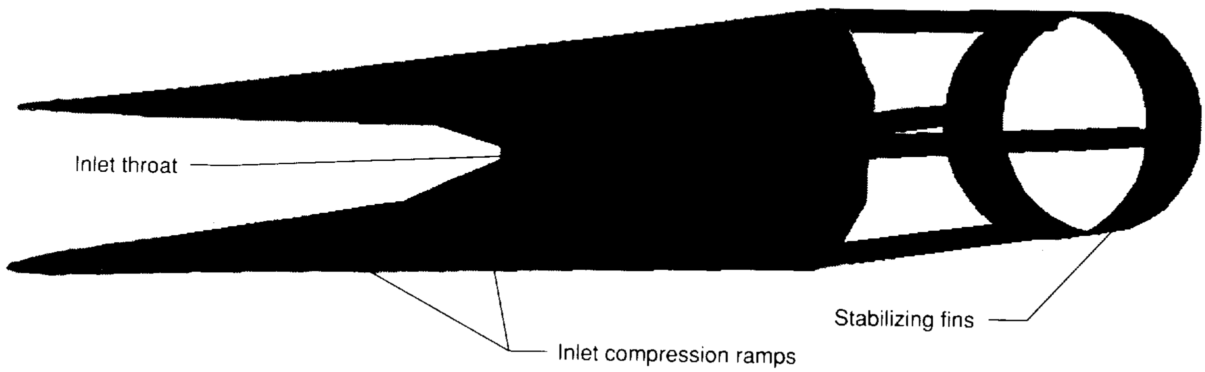

Symmetric scramjet free-flyer concept.

at the shoulder. The combustor, nozzle, and fin interaction studies were performed using a three-dimensional, parabolized Navier-Stokes solver, SHIP, and a one-dimensional (three temperature), finite-rate chemical kinetics analysis tool, SCRAM3. Analysis indicated a small positive effect of reduced combustor scale on mixing and combustion efficiencies. At the smaller scale, the mixing efficiencies actually increased slightly because of Reynolds number effects. Because the finite-rate chemical kinetics are fast at these high flight Mach numbers, the combustion efficiency also increased.

This work was done under contract with Analytical Services & Materials, Inc.
(C. R. McClinton, 46253, A. D. Dilley, and R. W. Hawkins) National Aero-Space Plane Office

Hypersonic Slender-Body Boundary-Layer Transition

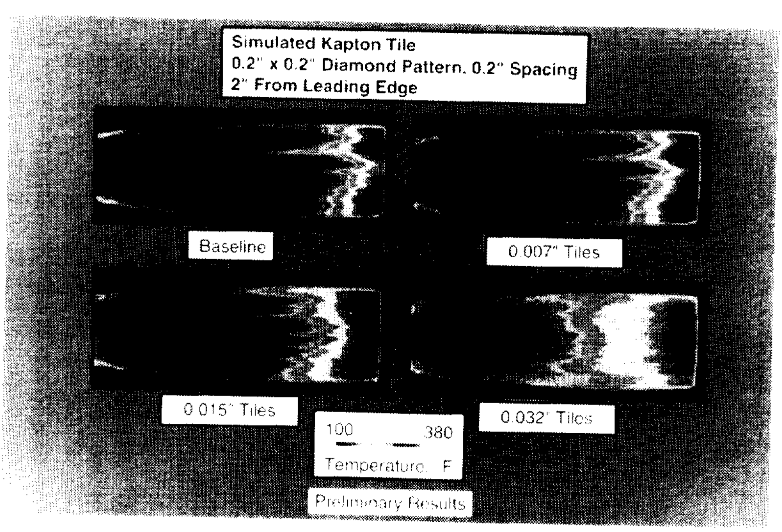

Effect of trip size on thermal mapping. (Original of figure in color; contact author for more information.)

Wind-tunnel tests have been conducted to determine the surface roughness criteria for hypersonic slender-body boundary-layer transition in the presence of a three-dimensional adverse pressure gradient in support of the Hypersonic Flight Test Experiment (HYFLITE), a proposed study within the National Aero-Space Plane (NASP) Program. HYFLITE represents the testing of subscale, unmanned flight vehicles to examine boundary-layer transition and scramjet performance at hypersonic speeds. The proposed thermal protection system (TPS) for the flight vehicles incorporates tiles similar to those used on the Space Shuttle orbiter, with the

associated roughness due to tile gaps and steps. The objective of the subject wind-tunnel tests is to determine the effects of various roughness heights, shapes, and locations relative to the leading edge on the transition process to assess the feasibility of using such a TPS system.

Phase I tests were performed in the Langley 31-Inch Mach 10 and 22-Inch Mach 20 Helium Tunnels with existing models to obtain initial estimates. A NASP configuration 202 forebody ($\alpha = 5°$, $Re_L = 3 \times 10^6$), a two-dimensional isentropic compression ramp, and a two-dimensional flat ramp were used with various transition trips to estimate the combined effect of roughness, adverse pressure gradient, and three-dimensional boundary-layers on transition. Global temperature distributions were measured using infrared thermography to determine regions that possibly correspond to boundary-layer transition to turbulence; heat-transfer data calculated from the thermal images for these regions were used to better define the onset of transition and the nature of the transition front as modified by the various transition strips. Hence, a viable testing technique was developed and demonstrated to study boundary-layer transition at hypersonic speeds. Phase I testing has been completed, and a detailed analysis of the extensive database, including comparison to computations, is under way. Preliminary findings indicate an unexpected sensitivity to small roughness that may limit the roughness criteria for the flight vehicle.

(Scott A. Berry, 45231)
Space Directorate

Hypersonic Shock-Shock Interactions

Experiments were performed to examine the effects of flow chemistry, geometry, and boundary-layer

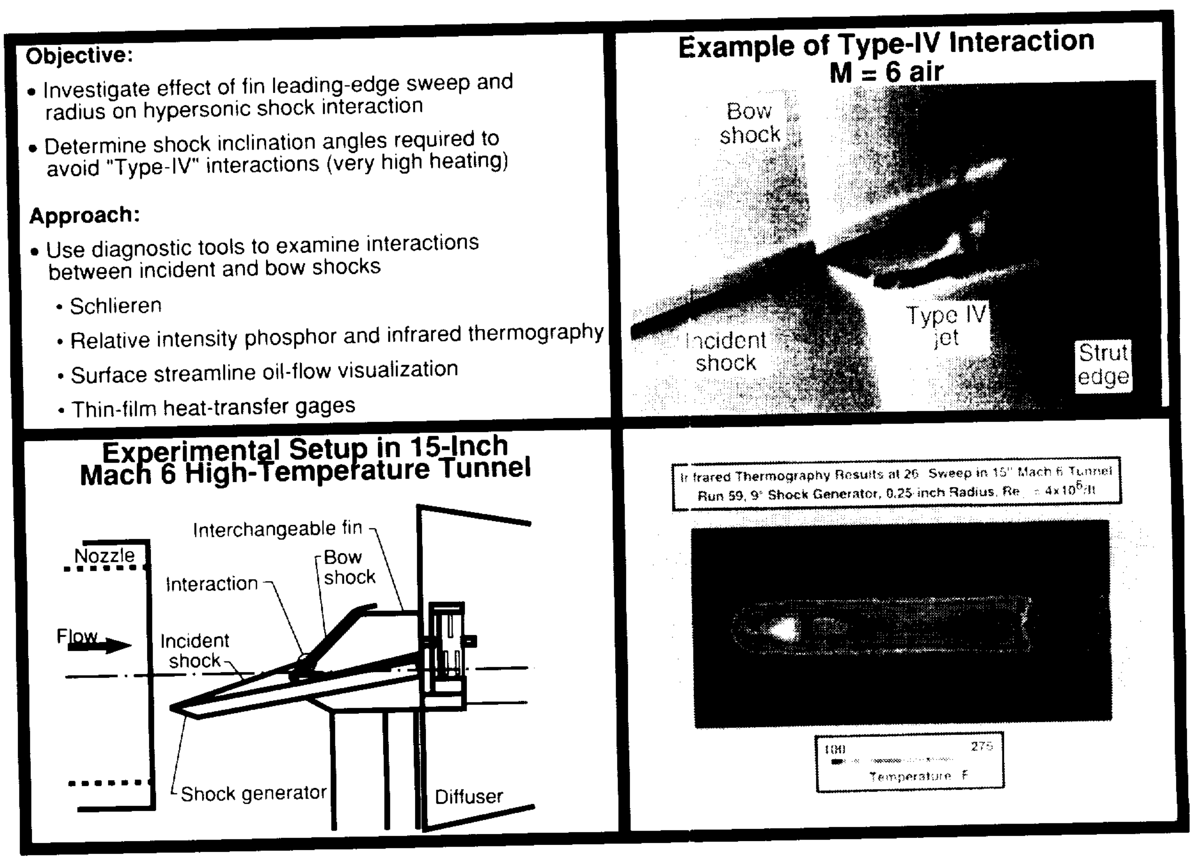

NASP government work packages—shock-shock interactions. (Original of figure in color; contact author for more information.)

state for a variety of shock interactions, including impinging shocks, glancing shocks, and compression corners for flight-relevant configurations. The class of interactions investigated are representative of the severe shock interactions that are expected on winged lifting-body concepts (e.g., the fuselage-wing shock interaction can cause high local heating on the wing leading edge) and with the inlet of hypersonic airbreathing vehicles. The results of these studies are therefore important for future aerospace vehicle component design, where it is necessary to accurately predict and, in many cases, attempt to minimize, the aerothermal loads.

Preliminary tests of generic shapes that provide shock-shock interactions in Langley conventional hypersonic wind tunnels and at hypervelocity test conditions in NASA HYPULSE at General Applied Sciences Laboratory (GASL) have been completed. Tests were conducted in a number of hypersonic facilities to achieve a wide range of flow conditions and used a number of measurement techniques to examine complex fluid-dynamic phenomena. These techniques include optical thermography, both infrared emission and two-color phosphor, to obtain global qualitative surface-temperature distributions, high spacial-density discrete thin-film gages to obtain high-frequency, quantitative heat-transfer data, steady and unsteady surface-pressure measurements, high-speed schlieren movies, focusing schlieren, and flow-field surveys. Data analysis has been initiated to examine size, nature, steadiness of interaction regions in hypersonic ideal and real-gas test conditions (i.e., to model the complex interaction), and the applicability of diagnostic techniques to each facility. Future plans include the completion of data reduction for the current phase and additional testing with increased instrumentation density through sensor miniaturization.

(Scott A. Berry, 45231)
Space Directorate

Fatigue of [0/90]2s SCS-6/ Ti-15-3 Composite Under Generic Hypersonic Vehicle Flight Simulation

Titanium matrix composites (TMC) are being evaluated for structural application on hypersonic vehicles. In such applications, TMC components will be subjected to a complex flight profile that consists of fatigue loading cycles, creep-fatigue loading cycles, and

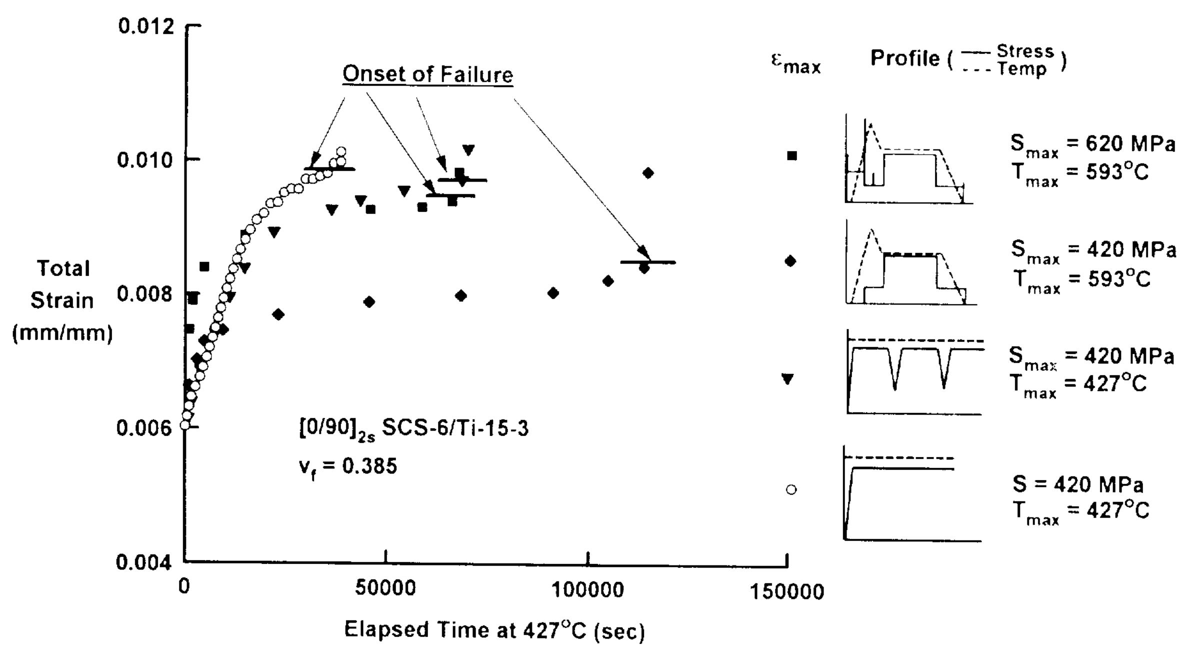

Variation of total accumulative strain with elapsed time at 427°C loaded to 420 MPa.

thermomechanical fatigue (TMF) loading at various elevated temperatures. It is essential that the life-limiting mechanisms be identified and incorporated into a life-prediction methodology. The objective of this research was to evaluate fatigue behavior of the $[0/90]_{2s}$ SCS-6/Ti-15-3 composite under a combination of load, time, and temperature that may occur during a generic hypersonic flight.

Several different load-temperature profiles were applied to the composite as illustrated in the figure. All profiles had the same sustained stress of 420 MPa applied at the sustained temperature of 427°C. The accumulative strain (both mechanical and thermal) for each test was recorded and plotted against elapsed time at 427°C (see figure). Somewhat surprisingly, the sustained-load/sustained-temperature test (the open circles) accumulated strain at the fastest rate and failed in the least time. This occurred in spite of the fact that the other profiles had cyclic loads and temperatures. The test data also indicate that the total strain to failure decreases with increased time at temperature under load. This implies an environmental attack on the fiber that reduces the fiber strength over time. For the flight profiles tested, the results indicate that holding load under elevated temperatures may be the most detrimental condition to apply to a titanium matrix composite. A failure criterion based on the failure strain in the 0° fiber can be used if it accounts for the appropriate environment degradation of the fiber strength.

(M. Mirdamadi, 43463, and W. S. Johnson)
Structures Directorate

Measurement and Prediction of High-Temperature Cyclic Deformation in Titanium Matrix Composites

Titanium matrix composites (TMC) reinforced with continuous silicon fibers are being considered as structural materials for elevated-temperature applications in future-generation hypersonic vehicles. The objective of this research is to experimentally determine the global stress-strain response of a $[0/90]_{2s}$ SCS-6/Timetal-21S (current NASP baseline material) composite that is subjected to a portion of a generic hypersonic flight profile and to analytically predict the laminate stress-strain response. The analysis will also include fiber-matrix interface failure.

A thermomechanical fatigue (TMF) test capability was developed to conduct a generic hypersonic flight profile (as shown in figure insert). A liquid-nitrogen cooling system and an induction heating system were required to achieve precise control of the cooling and heating rates. A two-dimensional micromechanical model (VISCOPLY) was used to predict the global stress-strain response of the composite subjected to the TMF flight profile. The VISCOPLY code is based on constituent properties and uses the vanishing fiber diameter (VFD) model to calculate the orthotropic properties of a ply. The ply properties are then used in a laminate analysis to predict the overall laminate stress-strain response. The fiber and the matrix can both be modeled as viscoplastic with temperature dependency. In the current analysis, the fibers were assumed to remain elastic with temperature-dependent properties, and the matrix was modeled as a thermoviscoplastic material. Tests were conducted on the Timetal-21S matrix at various temperatures (21°C to 760°C) to determine the

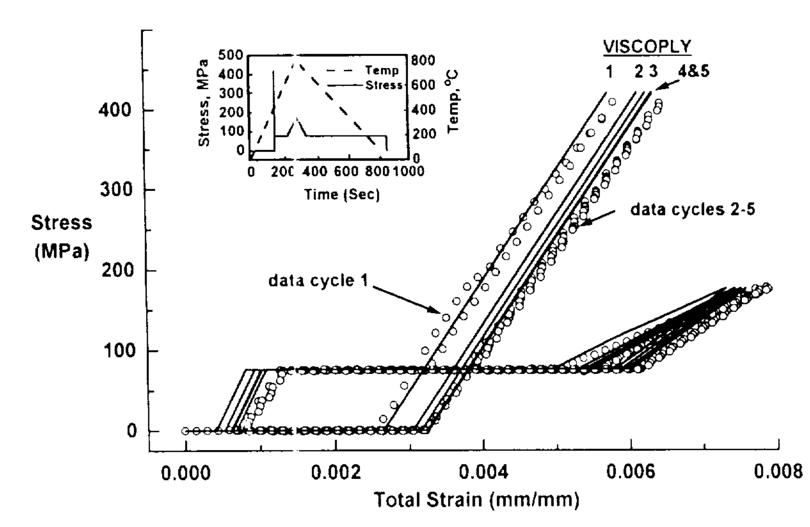

Measured and predicted stress-strain response of titanium matrix composite.

viscoplastic matrix material constants required by the material model in VISCOPLY. Temperature-dependent elastic material properties of the SCS-6 fibers were found in the literature. Fiber-matrix interface failure was accounted for in the analysis by multiplying the fiber transverse modulus of the 90° plies by 0.1. The measured and predicted responses of the composite when subjected to a portion of the TMF flight profile are shown in the figure. As seen in the figure, the experimental stress-strain response and the VISCOPLY prediction stabilized to the same stress-strain state (the prediction took four cycles to stabilize; the actual test took two cycles).
(M. Mirdamadi, 43463, and W. S. Johnson)
Structures Directorate

Nonlinear Thermoacoustic Response Method for MSC/NASTRAN

The equivalent linearization method of predicting the nonlinear response of structures was incorporated into the MSC/NASTRAN finite-element program. This method has been developed, verified, and enhanced over the past 20 years for combined thermo-acoustic mechanical loads, but it has not been widely used outside the research community.

The procedure was implemented as an iterative-solution sequence by the Direct Matrix Abstraction Programming (DMAP) language. The use of MSC/NASTRAN allowed the implementation of this method to be very general; hence, it is applicable not only to textbook-type problems, but also to complex structural configurations. The implementation of the equivalent linearization solution procedure has been verified with respect to a host of previously published textbook-type examples.

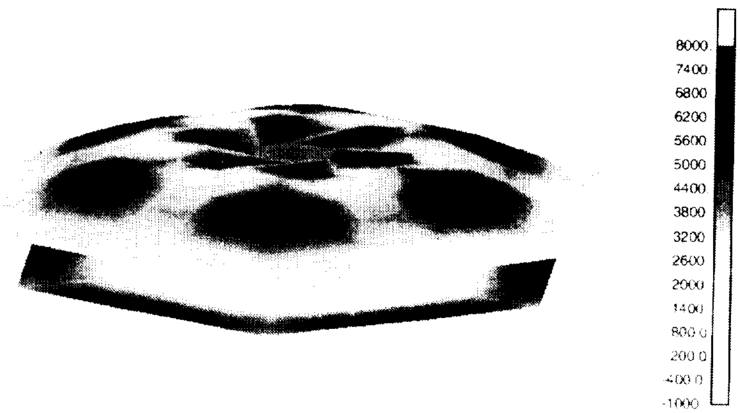

Deflected shape and stress contours for a typical TPS concept.

The figure depicts a hexagonal-shaped thermal-acoustic protection system (TPS) that covers an area of approximately 3.5 ft^2 and is 2.5 in. thick. This TPS concept is constructed from a carbon/carbon panel that is connected to a honeycomb backup structure with six titanium satellite posts around a center post. The figure shows the principal root-mean-square stresses on the carbon/carbon panel and backup structure for the anticipated thermoacoustic loads. The figure shows significant stress concentrations at the post-attachment locations and relatively lower stresses elsewhere. The reduction of these stress concentrations in the area of the post attachments has already been identified as a priority in the design of this type of thermal protection system. The high levels of stress in the backup structure arise from the high thermal expansion coefficient of the material and the rigid boundary condition that is imposed on the backup structure. The nonlinear dynamic analysis of this structure differs from linear dynamic analysis primarily in the frequency content of the response. The nonlinear analysis predicts higher frequencies in the response and subsequently shorter fatigue life.

This new capability will allow design engineers to predict the nonlinear thermoacoustic mechanical response of complicated structures. The immediate significance of the program is that it will assist in the evaluation of candidate thermal protection systems for hypersonic vehicles.
(Jay H. Robinson, 43601)
Structures Directorate

Flutter Characteristics of a NASP Model Determined in TDT

The proposed National Aero-space Plane (NASP) consists of a long, flexible, lifting-body fuselage

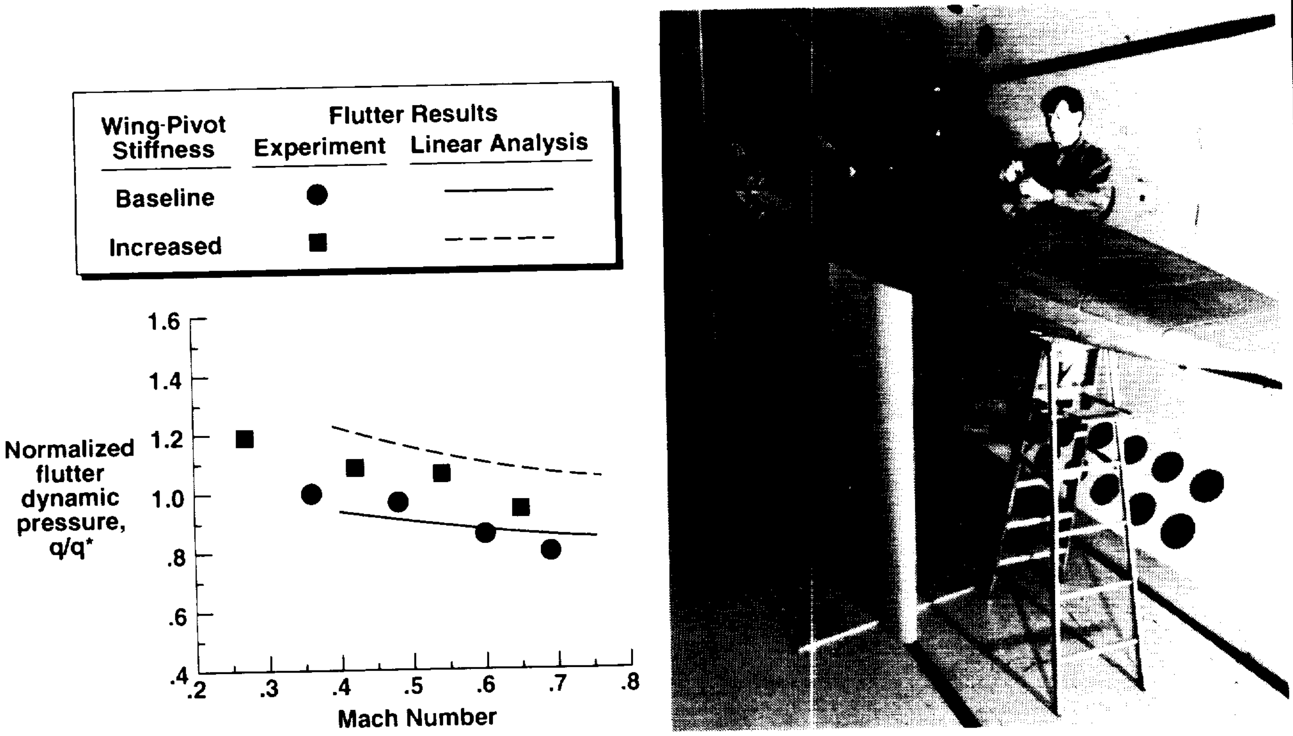

Comparison of wind-tunnel and flutter analysis results for NASP aeroelastic model. L-92-12800

and relatively small, highly swept, all-movable, clipped-delta wings. The fuselage flexibility and the all-movable feature of the clipped-delta wings may make the vehicle susceptible to aeroelastic instabilities throughout the flight envelope. A wind-tunnel test of a NASP model was conducted to meet three objectives: to measure the flutter mechanism inherent to this type of vehicle; to examine the effect of parametric variations on the flutter behavior of the model; and to correlate the experimental data with analysis.

A 1/10-scale representation of an unclassified version of the NASP vehicle was flutter tested in the Transonic Dynamics Tunnel (TDT). The model had all-movable, clipped-delta wings and cantilevered, clipped-delta vertical fins. A photo of the model mounted in the wind tunnel is shown in the figure. A flutter analysis of the model was performed using calculated linear, lifting-surface aerodynamics.

Analytical and experimental results for two configurations of the model are shown in the figure. The first configuration was the baseline model. The parametric variation for the second configuration involved an increase in the wing-pivot stiffness. The primary flutter mechanism was body-freedom flutter that involved the fuselage-pitch mode and the wing-pivot mode. The figure shows the experimental and analytical results in terms of normalized dynamic pressure versus Mach number.

The wind-tunnel test of this model showed that NASP-type vehicles that employ single-pivot, all-movable wings are susceptible to body-freedom flutter. The test results show that increasing the wing-actuator-pitch stiffness can make the body-freedom flutter instability less critical. The correlation of flutter analysis to the experimental data indicates that the mathematical tools used in this study were sufficient to predict the body-freedom flutter encountered in the wind tunnel.
(Stanley R. Cole, 41267)
Structures Directorate

Space Transportation

RESEARCH AND TECHNOLOGY

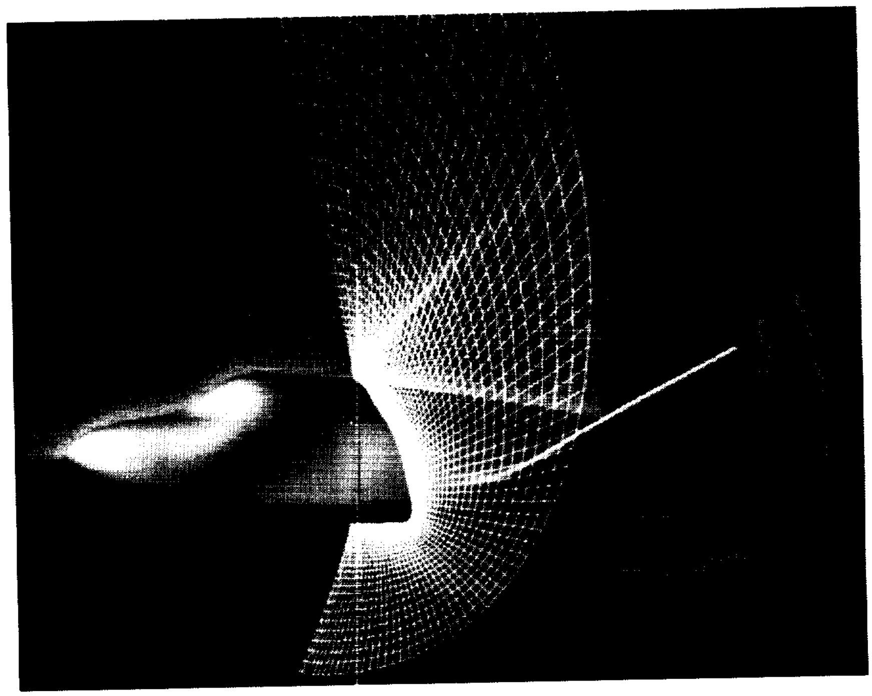

Provide technology for the current and evolutionary Space Transportation System (STS) and establish the technology base for future transportation system developments

Development of a Green's Function Code for Cosmic Radiation Protection

Astronauts and the crews of high-altitude aircraft are exposed to heavy-ion cosmic radiation that originates from the Sun and galactic sources. The shielding and exposure of these people are controlled by the transport of radiation through matter. Efficient space-radiation transport codes have been developed and applied to a wide range of missions, but the results of these codes could not be accurately validated in laboratory experiments. Now, the use of Green's function techniques has led to an efficient laboratory code (GRNTRN), which will be further developed for space-radiation transport calculations and will be validated with high-energy heavy-ion beam experiments.

Recent iron-beam transport measurements made at the Lawrence Berkeley Laboratory Bevalac accelerator by a team from the University of San Francisco provide an opportunity to validate the Green's function code. The iron beam had been accelerated to

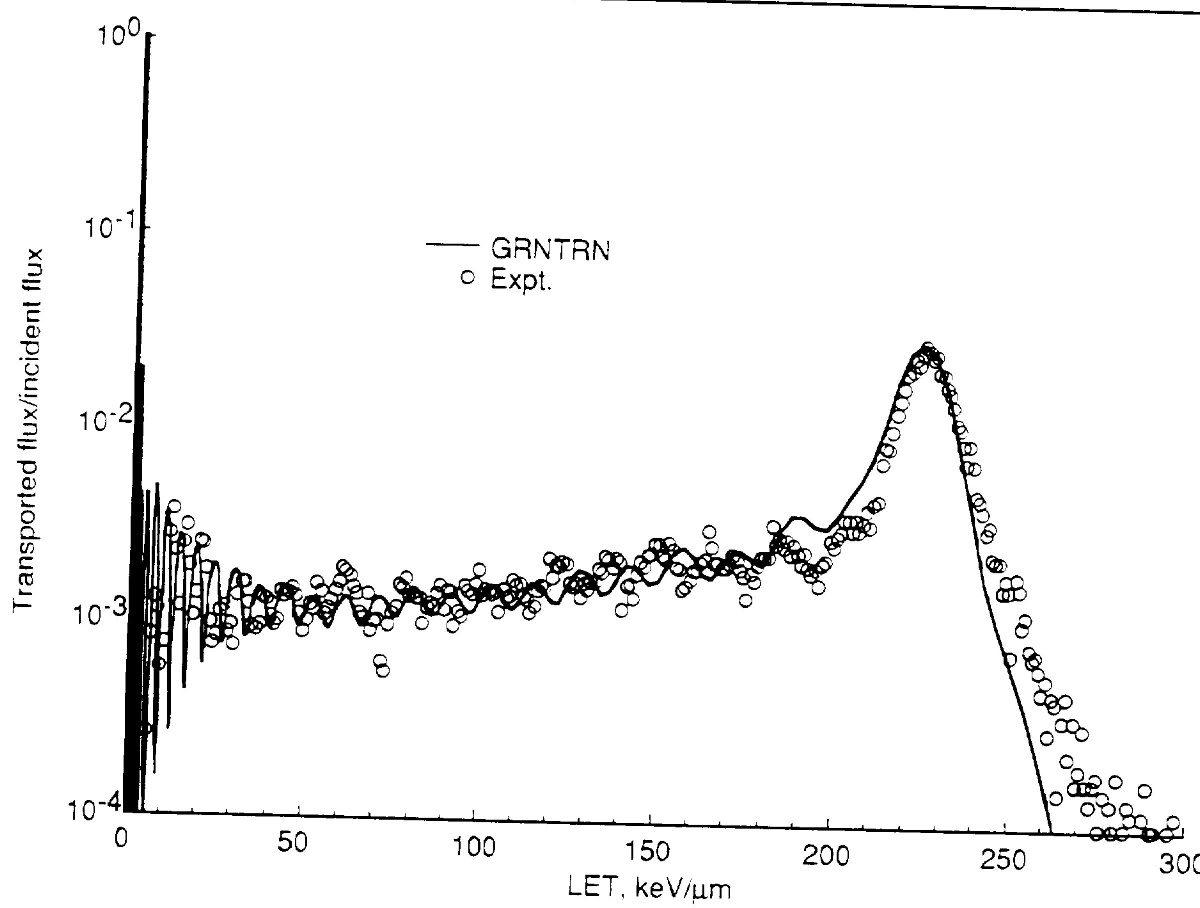

Comparison of GRNTRN results with iron-beam experiment.

600 million electron volts per atomic mass unit and passed through a series of beam transport elements, triggering devices, and a 2.24 g/cm^2 lead foil beam spreader prior to emerging from the beam tube and striking a layer of aluminum or polyethylene targets. The linear-energy transfer spectra of the degraded beam through the targets was measured by plastic nuclear track detectors. The data were compared with GRNTRN results as shown in the figure for a 4.6 g/cm^2 polyethylene target. The agreement was achieved only after accounting for effects due primarily to the lead foil for substantial beam-energy loss and ion fragmentation before striking the target.
(J. L. Shinn, 41427)
Space Directorate

Ground Facility Simulations of Shuttle Orbiter Hypersonic Aerodynamics

During the first flight of the Space Shuttle orbiter (STS-1), the body-flap deflection required for hypersonic trim was approximately two and one-half times that estimated from extensive wind-tunnel testing prior to the flight. This so-called "pitch-up anomaly", believed to be caused by mispredicting compressibility, viscous, and/or real-gas effects, was easily handled on subsequent flights by utilization of the elevons. Because the cause of the pitch-up anomaly was never really resolved, two existing high-fidelity orbiter models were refurbished and retested. These two orbiter models (0.004 and 0.0075 scale) were tested in five separate Langley facilities at Mach numbers from 6 to 18.5, at Reynolds numbers from 0.5 to 8×10^6 per foot, and most importantly, at ratios of specific heats (γ) of 1.22, 1.4, and 1.67.

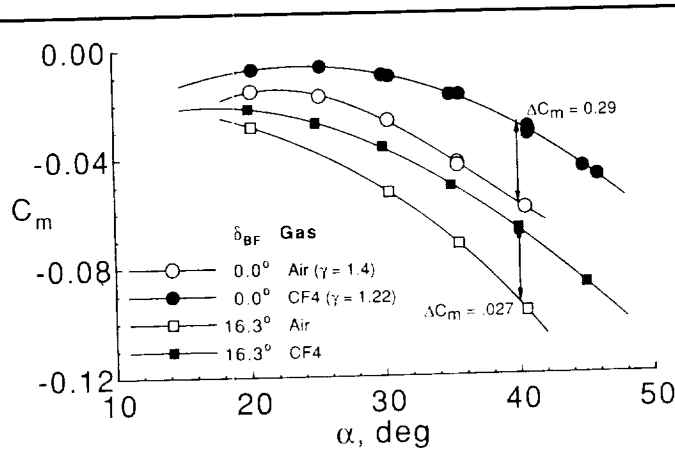

Effect of change in gamma on pitching-moment characteristics of 0.004-scale Space Shuttle orbiter obtained in 15-Inch Mach 6 High-Temperature Tunnel and 20-Inch Mach 6 CF_4 Tunnel. $M_\infty = 6$; $\delta_{BF} = 0°$ *and 16.3°. Moment center at 65%.*

This effort, though not complete to date, has provided significant insight into the cause of the anomaly by effectively eliminating several potential causes while focusing in on one specific cause. No significant support interference effects, which could be construed as having contributed to the anomaly, were observed for the range of models, supports, and test conditions investigated. The orbiter basic aerodynamics that were measured in the ideal-gas facilities agreed well with the 1977 Aerodynamic Design Data Book (ADDB), which was also based on ideal-gas results. Body-flap effectiveness increased with increasing Reynolds number as expected and agreed reasonably well with the 1977 ADDB. In addition, at low Reynolds numbers, the body-flap effectiveness did not change with either Mach number or γ. These results indicate that the cause of the anomaly was not a poor estimate of the body-flap effectiveness; real-gas effects caused the anomaly. As shown in the figure, testing in a heavy gas, in this case CF_4, to simulate the low-γ aspect of a real gas very closely approximates the nose-up increment in pitching moment of 0.03 that occurred during flight on STS-1. Lowering γ within the shock layer causes the flow to expand on the aft portion of the body to lower than ideal gas pressure levels and produces a loss in normal force and a significant nose-up increment in pitching moment.
(John W. Paulson, Jr., 45071, and Gregory J. Brauckmann)
Space Directorate

Orbiter Experiments (OEX) Aerothermodynamics Symposium

The Orbiter Experiments (OEX) Program, initiated in the mid-

1970's, provided a mechanism for utilization of the shuttle orbiter as an entry aerothermodynamic flight-research vehicle as an adjunct to its normal operational missions. Under the auspices of the OEX Program, elements of aerothermodynamic research instrumentation flew aboard the orbiters *Columbia* and *Challenger*. These OEX experiment instrumentation packages obtained in-flight measurements of the requisite parameters for: (1) determination of orbiter aerodynamic characteristics (both static and dynamic) over the entire entry flight regime, and (2) determination of the aerodynamic heating rates imposed upon the vehicle's thermal protection system during the hypersonic portion of atmospheric entry.

The data derived from the OEX complement of experiments represent benchmark hypersonic flight data heretofore unavailable for a lifting entry vehicle. These data are being used in a continual process of validation of state-of-the-art methods, both experimental and computational, for simulating/predicting the aerothermodynamic characteristics of advanced space transportation vehicles.

The *Orbiter Experiments (OEX) Aerothermodynamics Symposium*, held in April 1993, provided a forum for dissemination of OEX experiment flight data and for demonstration of the manner in which these data are being used for validation of advanced vehicle aerothermodynamic design tools.

The Symposium's invited speakers included OEX experiment principal investigators and other researchers who have been active users and analysts of the orbiter entry flight data. Proceedings of this symposium are being prepared for publication as NASA CP-3248.
(David A. Throckmorton, 44406)
Space Directorate

A Multiblock Analysis for Shuttle Orbiter Reentry Heating From Mach 24 to Mach 12

The Space Transportation System (STS) was designed in an era

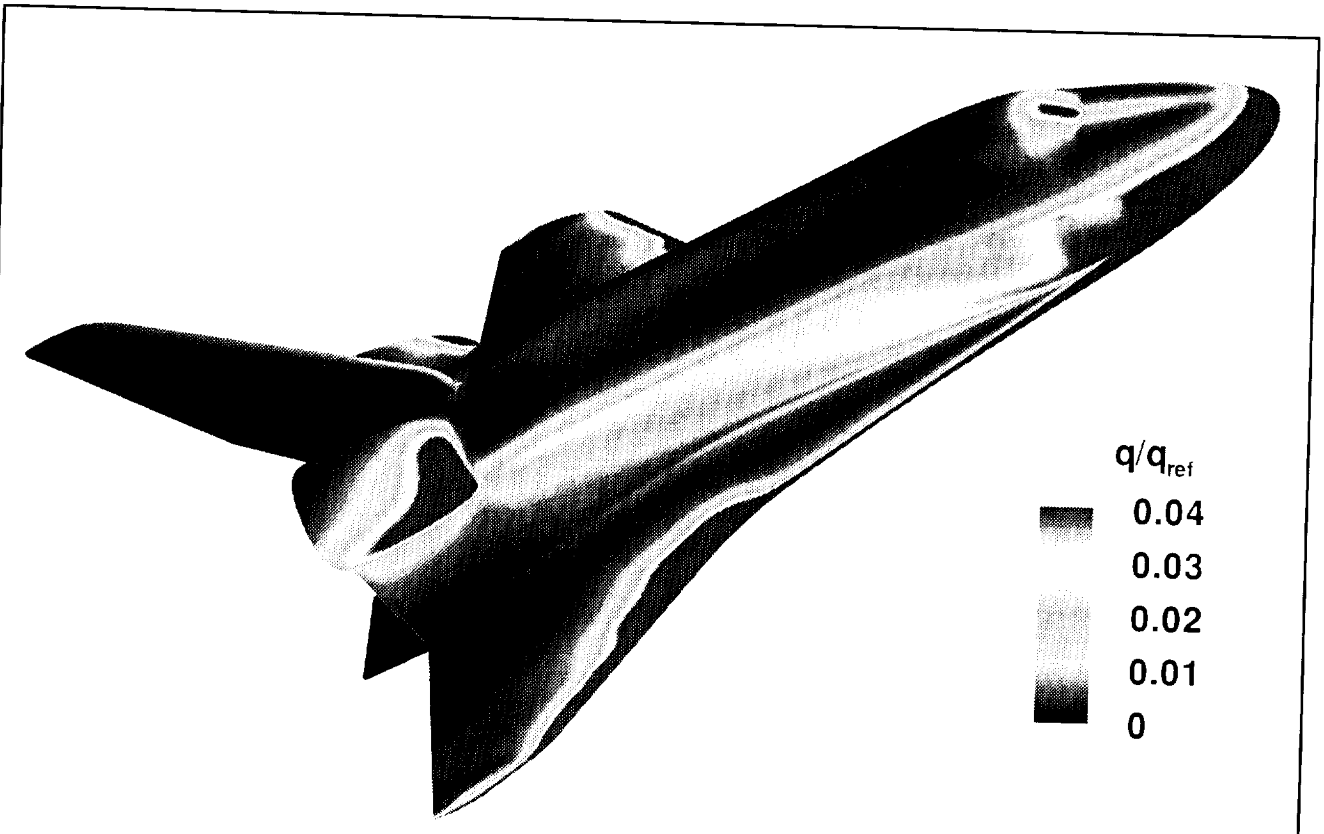

LAURA-computed surface heat-transfer results for complete orbiter configuration at Mach 18.

in which large-scale, computational fluid dynamic (CFD) analyses were unavailable to assist in the design process. Supercomputer technology has now progressed to the point where CFD has the resources (speed and memory) to make substantial contributions to future hypersonic vehicle design projects by providing flow-field solutions over complete, winged configurations. The solutions provide surface-pressure and heating predictions at selected design points; more importantly, they also provide insight into the flow structure about the vehicle, with powerful graphical analysis tools that show streamline traces, vorticity distributions, profile information, etc.

The capabilities and limitations of CFD simulations for hypersonic flow over winged vehicles must be periodically reevaluated to account for advances in algorithms and computational power, and to include updates to the database for code validation. The data provided by instrumentation that was flown onboard the shuttle orbiter *Columbia* comprise a crucial benchmark for such evaluations. The objective of this study was to perform this evaluation for the Langley Aerothermodynamic Upwind Relaxation Algorithm (LAURA) using the benchmark flight heat-transfer data from STS-2. A sample heating distribution at Mach 18, including the effects of thermochemical nonequilibrium, finite-rate wall catalysis, and a radiative-equilibrium boundary condition, is presented in the figure on the next page.

This work has demonstrated that a proven methodology is ready to be applied to the design of next-generation space transportation systems such as the single-stage-to-orbit vehicle.
(Peter A. Gnoffo, 44380, and K. James Weilmuenster)
Space Directorate

Navier-Stokes Analysis of Shuttle Orbiter Pitching-Moment Anomaly

On the entry phase of its first flight, STS-1, the hypersonic pitching-moment characteristics exhibited by the Shuttle orbiter were significantly different than pre-flight predictions. The body-flap deflection that was required to maintain vehicle longitudinal trim hypersonically was more than double that predicted prior to the flight. Although ample control power had been built into the system to overcome the underprediction of body-flap deflection requirements, the magnitude of the required deflection raised concerns about the structural and thermal integrity of the body flap. This "pitching moment anomaly" has been variously attributed to any one (or a combination) of several phenomena including viscous effects, diminished body-flap effectiveness, Mach number, and real-gas effects. While this question has been subjected to approximate analysis, there has been no previous definitive analysis of the pitching-moment anomaly.

A study was undertaken to analyze the hypersonic longitudinal aerodynamic characteristics of the Shuttle orbiter, and the phenomena that define those characteristics, through the application of state-of-the-art computational fluid dynamics. State-of-the-art flow solvers and computer hardware allow for Navier-Stokes solutions that employ complete gas chemistry models for complex configurations such as the Shuttle orbiter. The study consisted of defining the flow field about the orbiter at several points along the entry tra-

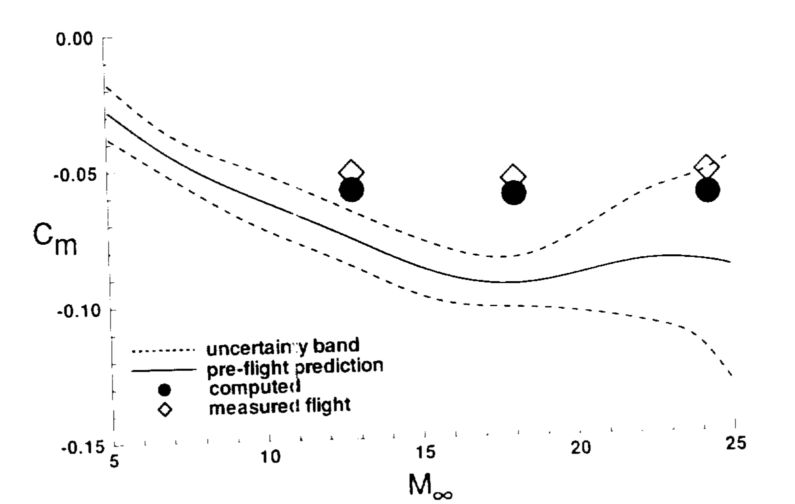

Comparison of computed Navier-Stokes orbiter pitching-moment results with preflight predictions and flight data.

jectory and comparing the computed vehicle aerodynamics with those measured in-flight as shown in the figure.

The primary finding of the study was that the STS-1 pitching-moment anomaly was a real-gas chemistry effect that was not duplicated in ground-based facilities (upon which the aerodynamics were based before STS-1), which used air as a test gas. In addition, CFD analyses indicated that at flight conditions, the body flap is more effective than predicted by tests in ground-based air facilities.
(K. James Weilmuenster, 44363)
Space Directorate

An Engineering Method for Calculating Heating on General Three-Dimensional Flight Vehicles

The design of advanced entry vehicles requires the accurate prediction of heating during entry. In the design process for such vehicles, it is useful to have both "benchmark" and "engineering" codes available. Benchmark codes model the flow processes as accurately as possible but require large computer run times. Engineering codes, on the other hand, model the flow processes approximately but can produce very fast results. These codes are very useful during the preliminary design phase, when results at many different conditions must be obtained. In the past, engineering codes were generally limited to relatively simple body shapes.

An engineering code, LATCH (Langley Aerothermodynamic Three-Dimensional Convective Heating), has been developed that can be used to make rapid and accurate heating predictions on the windward side of almost any entry-vehicle shape. It utilizes a generalized body-fitted coordinate system to describe the flow, similar to that used by most advanced benchmark codes. Heating calculations are performed using a combined inviscid and boundary-layer approach based on the axisymmetric analog for three-dimensional boundary layers. This code can produce heating predictions approximately one or two orders of magnitude faster than a typical benchmark Navier-Stokes code.

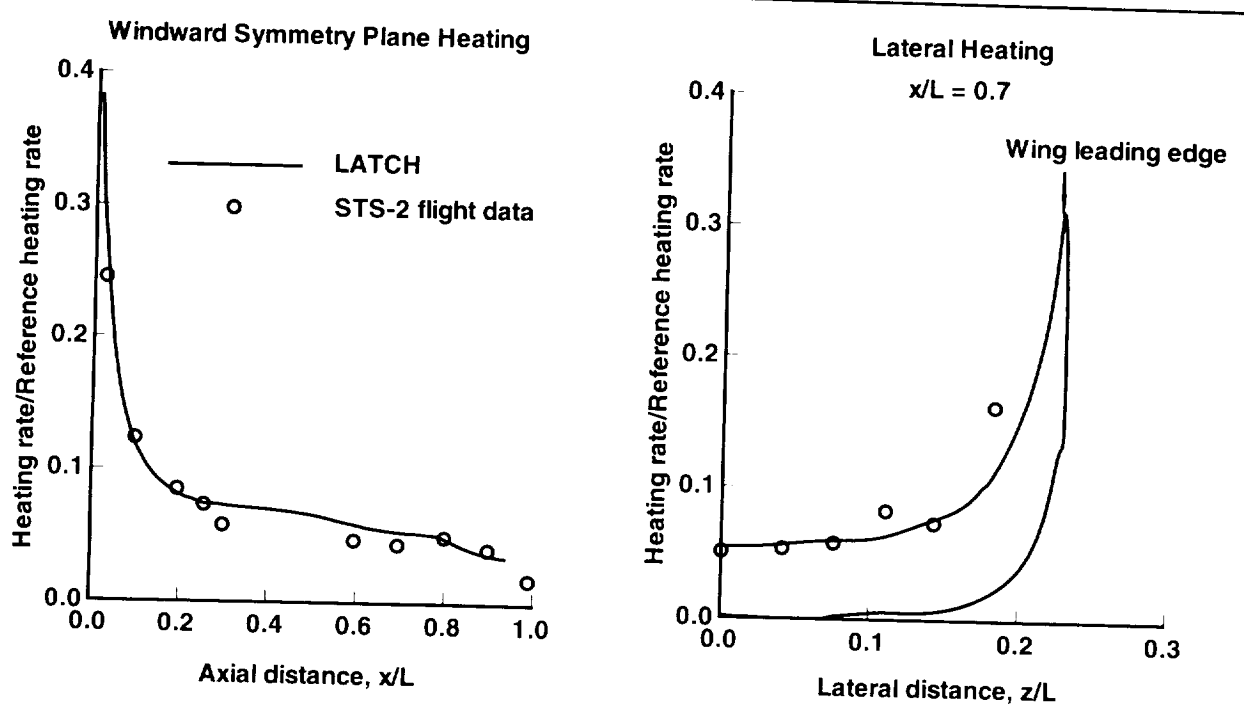

Heating comparison on Space Shuttle orbiter.

A study has been performed to assess the ability of the LATCH code to predict heating on complex vehicles in flight. Heating predictions on the Shuttle orbiter are shown compared with flight data at free-stream conditions of Mach number = 9.2 at an altitude of 46.7 km and at an angle of attack of 34.8°. The calculated results are in good agreement with the flight data. These and other similar comparisons demonstrate that the LATCH code can be used to accurately predict flight heating rates on the windward surface of winged entry vehicles such as the Shuttle orbiter.

(H. Harris Hamilton II, 44365, and Francis A. Greene)
Space Directorate

Blunt-Body Wake Flows

Determination of wake closure is a critical issue for aerobrakes, since the low lift-drag ratio aeroshell designs impose constraints on payload configuration/spacecraft design. The issue is that the payload should fit into the wake in such a manner as to avoid the shear-layer impingement and thus minimize heating. Rarefaction effects are one phenomenon that can significantly influence the features and development of aerobrake waves. Furthermore, if the rarefaction is significant (large Knudsen number), then continuum analyses become inadequate for describing the near-wake conditions.

A study has been conducted to provide an improved understanding of the effects of rarefaction on blunt-body wake structure and to clarify the boundaries for realistic application of the Navier-Stokes algorithms with respect to rarefaction effects. Calculations were made using a direct simulation Monte Carlo (DSMC) approach, the Navier-Stokes approach, and a recently developed zonally decoupled approach, for a 70° blunted-cone forebody with and without a sting/afterbody at wind-tunnel conditions. The freestream was Mach 20 nitrogen at three levels of rarefaction (freestream Knudsen numbers (Kn_∞) of 0.03, 0.01, and 0.001). This range of conditions includes both continuum (small Kn_∞) and transitional forebody flows. The zonally de-

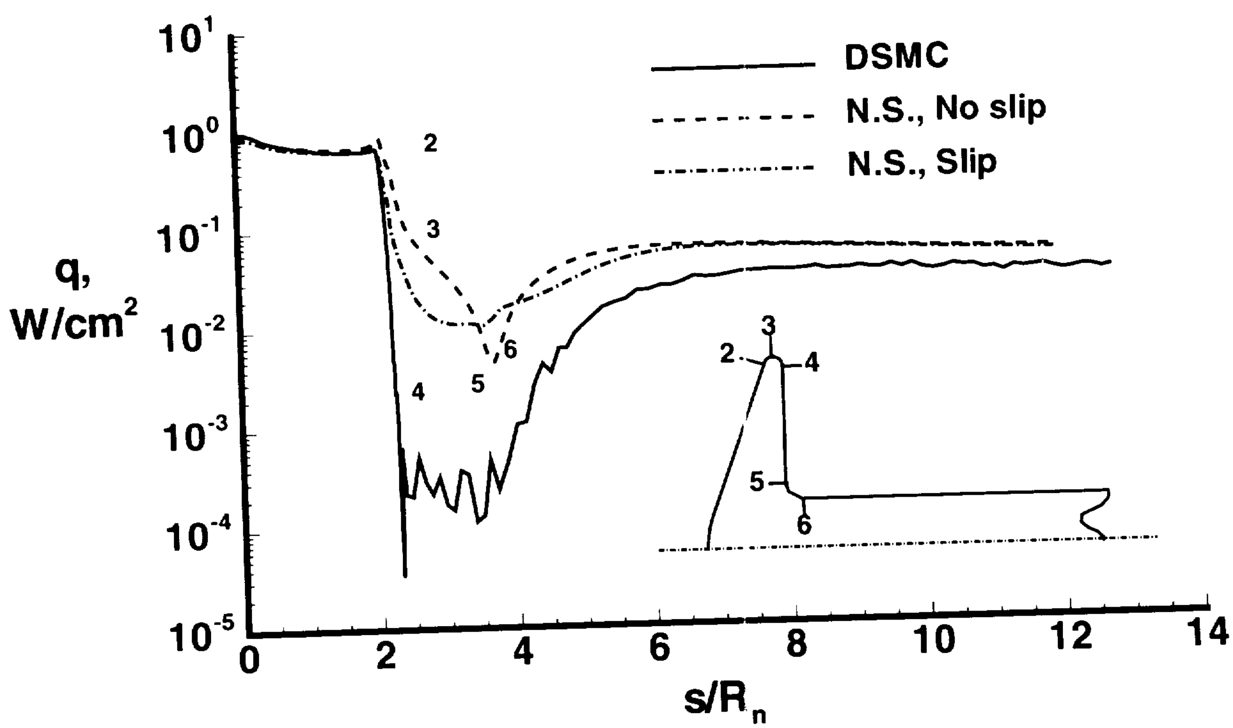

Comparison of DSMC and Navier-Stokes solutions for blunt-body surface heating. $Kn_\infty = 0.03$.

coupled methodology, whereby the forebody and wake regions are solved separately with no iterative feedback, was validated for these conditions by comparison with fully coupled solutions.

Rarefaction effects in the near wake persist to very low Knudsen numbers. Results of the calculations show that the location of maximum convective heating rate along the sting/afterbody is not coincident with the wake stagnation point but can be a considerable distance downstream of the wake stagnation point (larger payload volume). Including slip boundary conditions in the Navier-Stokes calculation provided improved agreement with the DSMC results. The zonally decoupled approach proved to be computationally efficient.

(James N. Moss, 44379, Richard G. Wilmoth, Robert A. Mitcheltree, and Virendra K. Dogra)
Space Directorate

Aerodynamics of Shuttle Orbiter at High Altitudes

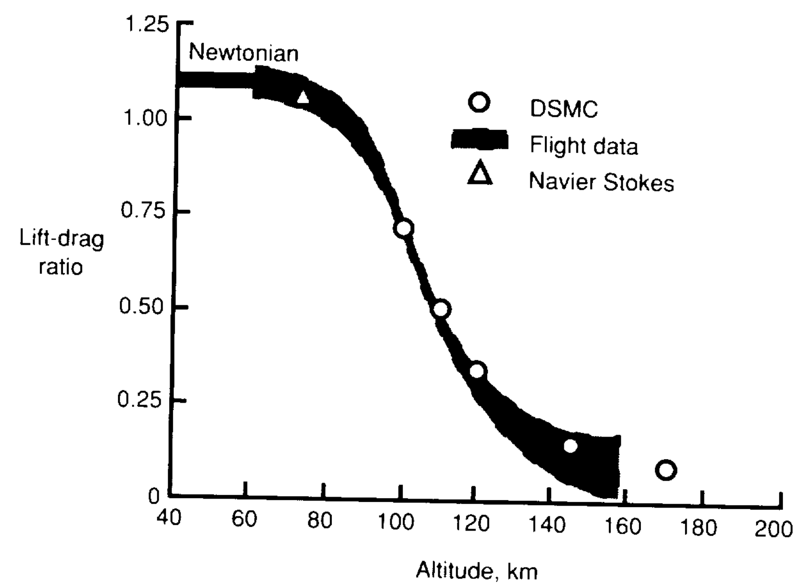

Comparison of high-altitude lift-drag ratio data for Shuttle orbiter.

The aerodynamic characteristics of a spacecraft in orbit and/or the early phase of atmospheric entry cannot be adequately studied in ground-based wind tunnels because of the low ambient density, low Reynolds number, high Knudsen number conditions prevailing at high altitudes. In recent years, computer simulation methods based on free molecular and direct simulation Monte Carlo algorithms have progressed to a point where high Knudsen number flow fields around vehicles of complex geometry can be simulated on engineering workstations, in three dimensions, and with relatively short turnaround times. This capability has been used to evaluate the aerodynamic forces and moments acting on the Shuttle orbiter in orbit and during atmospheric entry to 100-km altitude. Numerical simulation results have yielded values of the lift-drag and normal- to axial-force ratios that are comparable to those derived from accelerometer measurements made in flight. The simulations also revealed an unexpected characteristic of the normal-force coefficient variation with altitude, namely a nonmonotonic behavior with a maximum value at 110 km.

The present results have further validated the computer codes and simulation methods that will be used in the future to study advanced space transportation systems.

(Didier F. G. Rault, 44388)
Space Directorate

Flight Results of Orbital Acceleration Research Experiment (OARE)

The Orbital Acceleration Research Experiment (OARE) obtains measurements, in absolute terms, of the Shuttle orbiter's low-frequency, low-g acceleration environment in orbit and during reentry. OARE flight operations include in-flight instrument calibrations, and post-flight data processing enables identification of the steady-state aerodynamic contribution to the acceleration environment. The OARE is a joint endeavor of two NASA Centers: the OARE was conceived, and the principal investigator resides, at Langley Research Center; project and integration management are the responsibility of Johnson Space Center. The vendor for the sensor was Bell Aerospace, the vendor for the calibration table was Speedring, and Canopus Systems is

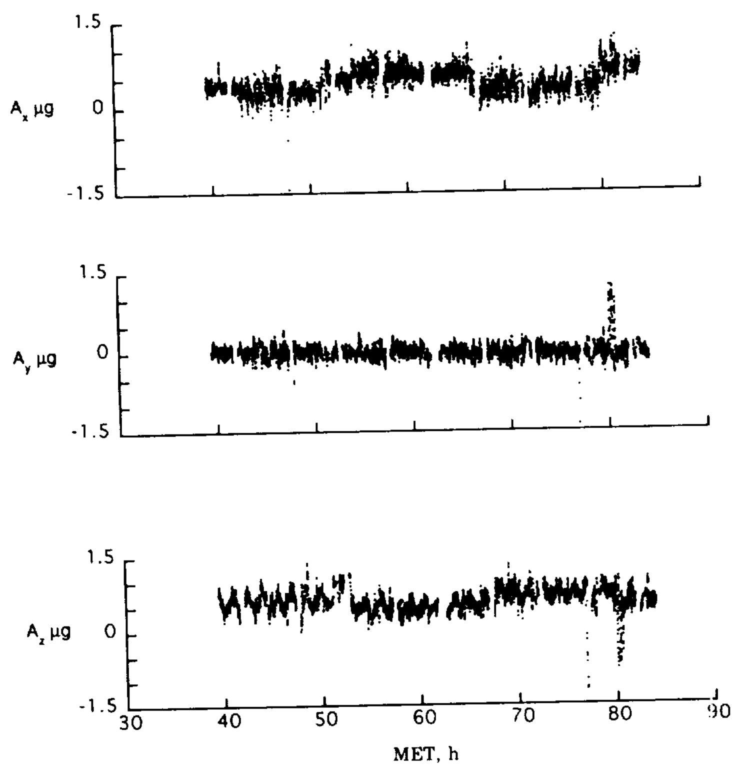

Three-axis orbiter acceleration measurements obtained on STS-50.

responsible for maintaining the flight equipment, the instrument simulator, and the ground support equipment.

The OARE has flown on two flights of the orbiter *Columbia*. Data from STS-40 confirmed the nano-g sensitivity of the system, and orbital acceleration variations were measured which correspond well with density models. Data from STS-50 were collected during the entire 14-day orbital segment of the flight and are of excellent quality. The sensor exhibited small biases on all three axes, while bias and scale-factor sensitivities to temperature were minimal. The OARE in situ calibrations provided the first set of absolute acceleration measurements of the orbiter on-orbit environment. A 60-hour portion of the flight data from STS-50 is shown on the figure. Analyses have been requested by and supplied to the microgravity community to support crystal growth experiments and other microgravity-dedicated accelerometry experiments. Small (but significant) forces were observed that will possibly impact the operation of future on-orbit experiments. Preparations are being made for the next OARE flight, which is on STS-58. This flight will include three separate sets of pitch, yaw, and roll maneuvers to verify the on-orbit calibrations.

(Robert C. Blanchard, 44391)
Space Directorate

Entry-Vehicle Configuration Optimization Using Response-Surface Methods

Reusable, rocket-powered, single-stage vehicles (SSV) are being studied because of their potential to greatly reduce Earth-to-orbit transportation costs. Advanced multidisciplinary design optimization methods are being used to obtain minimum-weight configurations with robust aerodynamic characteristics during entry. A response surface method (RSM) was utilized to determine the optimum values of the five configuration parameters shown in the figure for a circular-fuselage SSV to minimize the vehicle dry weight and maximize the aerosurface control margin during entry. A central composite design was utilized to efficiently determine the dry-weight response surface. The process required 27 configuration point designs, as opposed to 243 (3^5) required for a full-factorial analysis. A second-order regression fit was then performed, and an equation was obtained to relate dry weight to each of the five configuration variables. Constraint equations were also derived for landing speed and hypersonic, supersonic, and subsonic trim and stability levels. The dry-weight equation was then utilized as the objective function in a nonlinear optimizer that was subject to the seven constraint equations.

The dry weight of the SSV was reduced by 10 percent, and a robust aerodynamic entry configuration was obtained. The vehicle

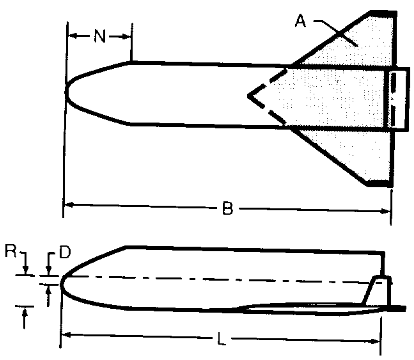

Variables		Range	Optimum values
Fineness ratio	= L/2R	4-6	5.02
Nose ratio	= N/L	0.2-0.4	0.2
Nose droop	= D/R	0-100%	26.9%
Wing area	= A/A_{ref}	75-100%	70.1%
Wing location	= B/L	85-105%	103%

Initial dry weight = 227,000 lb
Optimized dry weight = 205,000 lb

Single-stage vehicle configuration parameters.

was constrained to land at a speed of 205 knots. The resulting vehicle was also capable of being trimmed in the pitch plane at a subsonic, a supersonic, and a hypersonic entry condition at both payload-in and payload-out center-of-gravity (c.g.) conditions with minimal aerosurface deflections. The elevons and body flaps are only required to be deflected at a maximum of ±6°. Hence, large aerosurface margins are available to control the vehicle during off-nominal entry conditions. The RSM was also used to constrain the vehicle to be stable or neutrally stable in the pitch plane at a subsonic, a supersonic, and a hypersonic entry condition at both payload-in and payload-out c.g. conditions.

In this analysis and in previous applications, RSM has proven to be an efficient, flexible tool for multidisciplinary optimization and has the potential for broad application to industrial design and production.
(Douglas O. Stanley, 44518)
Space Directorate

Fuselage Internal Structural Modeling

Optimization of aerospace vehicle transportation systems requires the use of finite-element analysis (FEA) methods to investigate the impact of fuselage construction

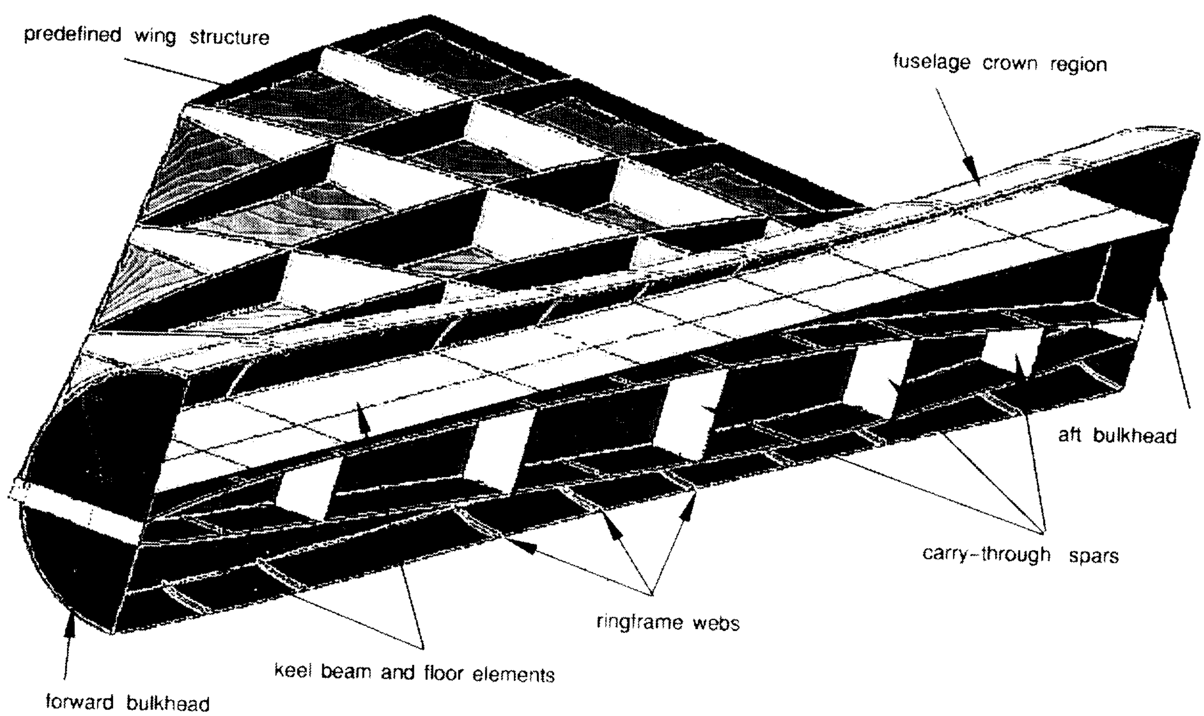

Fuselage internal structural modeling.

parameters, such as ringframe spacing, on total vehicle weight. Existing modeling practices are too labor intensive when design modifications, such as relocating a wing relative to the fuselage, produce topological changes in the analysis mesh. The purpose of this research was to provide internal fuselage structural modeling software to enable greater use, at an earlier stage, of FEA methods in the design process.

The development approach taken provides an appropriate mix of interactive and automated procedures. For example, a design engineer can graphically lay out structural arrangements of advanced vehicle concepts in an intuitive manner, while automated procedures simultaneously ensure that proper wing/fuselage integration constraints are met.

Internal structural elements that were generated include variable-width ringframes, longerons, bulkheads, keel beams, floors, and wing-box carry-through ribs and spars. The root rib of structurally modeled lifting surfaces, such as wings and tails, is automatically extruded through the fuselage, and ringframes are placed in the fuselage at the corresponding wing spar locations.

The figure shows the wing-body intersection of a typical supersonic transport design. The midsection of the outer fuselage surface was divided into crown, side, and subfloor regions. Additional ringframes were placed within the section by specifying the desired spacing. Keel-beam and floor structures were added by using the generic cutting-plane interface. The integrated wing carry-through and vehicle outer skin were automatically created in a manner consistent with FEA mesh-generation connectivity constraints.

This software has been interfaced to commercial FEA software, with mapped mesh areas and both membrane and bar- or rod-type elements. Initial testing has demonstrated a geometry modeling-time reduction factor of 10 to 20 over previous methods.
(Mark L. McMillin, 44521)
Space Directorate

Dual-Fuel Rocket Propulsion for Single-Stage Vehicles

For rocket-propelled, single-stage vehicles (SSV), the use of hydrocarbon fuel in addition to hydrogen fuel reduces vehicle size and empty weight by increasing propellant bulk density and propulsion-system thrust-to-weight ratio at the expense of overall propulsion-system specific impulse. For the same level of technical complexity, a reduction in vehicle empty weight potentially translates into a reduction in both development and production costs. Several dual-fuel propulsion options were investigated for a near-term technology SSV. Conceptual-level analysis methods were utilized to determine vehicle weight and size characteristics. To obtain the minimum empty weight, optimization of select propulsion-system and vehicle-design parameters was performed using a response surface methodology. With a four-parameter optimization, this process required 25 vehicle point designs, as

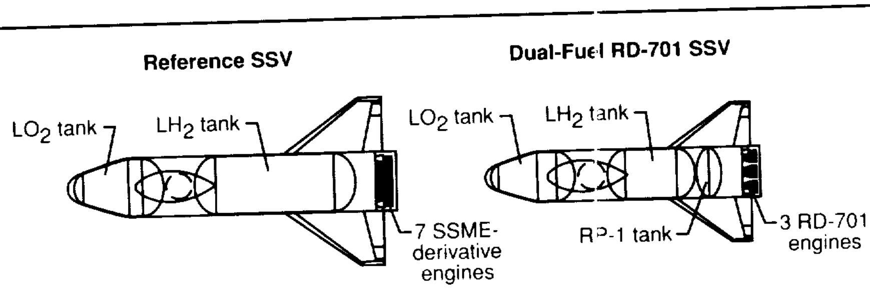

	Reference SSV	Dual-Fuel RD-701 SSV
Body length, ft	173	145
Wing span, ft	95	79
Empty weight, lb	244 000	161 000
Gross weight, lb	2 470 000	1 970 000

Effect of utilizing Russian RD-701 dual-fuel engine.

opposed to 81 (3^4) required for a full-factorial analysis. A second-order regression fit was utilized to relate empty weight to each of the propulsion-system and vehicle-design parameters. This empty-weight equation was then utilized as the objective function in a non-linear optimizer.

Three dual-fuel propulsion concepts were investigated. These were: a separate engine concept that combined existing Russian RD-170 kerosene-fueled engines with engines derived from the Space Shuttle Main Engine (SSME); the kerosene- and hydrogen-fueled Russian RD-701 engine concept; and a dual-fuel, dual-expander engine concept. Oxygen was the oxidizer in all vehicles. Parameters that were optimized included lift-off thrust-to-weight ratio, nozzle-area ratio, hydrocarbon-to-hydrogen thrust fraction, and dual-fuel to single-fuel transition Mach number. All dual-fuel concepts that were investigated reduced empty weight in comparison with a reference hydrogen-fueled SSV powered by SSME-derivative engines. After optimization, vehicle empty weight was reduced by 10 percent for the separate engine concept, 25 percent for the dual-expander concept, and 34 percent for the RD-701 concept. The figure illustrates the significant physical size difference between the reference concept and the RD-701 concept.
(Roger A. Lepsch, Jr., 44520)
Space Directorate

Single-Stage-to-Orbit Advanced Manned Launch System Concept

A fully reusable, rocket, single-stage-to-orbit (SSTO) Advanced Manned Launch System (AMLS) reference concept has been defined. Nominal and abort system performance, weights, and technologies that are required have been defined, and a number of trade studies and sensitivity analyses have been examined. Flow visualization, subsonic, and hypersonic wind-tunnel tests have been conducted for this configuration. The definition of low-cost operations for a fully reusable, two-stage concept developed previously has provided benchmark information for comparison with the single-stage concept. The SSTO concept that is defined was selected as one of three reference concepts in the NASA Access to Space study.

Although challenging from a performance viewpoint, an SSTO space transportation system offers the potential of significantly lower operations costs and faster turnaround than two-stage concepts. The concept that was examined utilizes a weight-efficient, optimized, circular body shape. A contractor, Rockwell International, conducted trade studies to determine structural and thermal protection system selections for reusable, cryogenic propellant tanks. Such tanks and the processes for their routine inspection are enabling technologies for SSTO. Propulsion-system trade studies examined the sensitivities of vehicle dry and gross weights to propulsion-system specific impulse and thrust-to-weight changes. These analyses have shown the increased benefits of propulsion-system weight improvements over specific impulse enhancements in reducing vehicle system weights and costs.
(Douglas O. Stanley, 44518)
Space Directorate

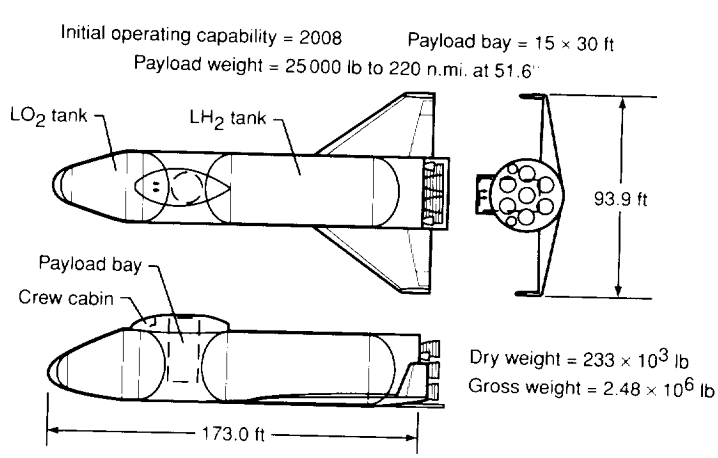

Access to Space study single-stage-to-orbit rocket.

Dataflow Design Tool for Multiprocessing Systems

Langley Research Center has developed a model of the multiprocessing execution of parallel computations or tasks with the participation of Old Dominion University

on Cooperative Agreement NCC1-136. The model is referred to as the Algorithm To Architecture Mapping Model (ATAMM) and is capable of predicting the multiprocessing performance and resource requirements of a class of algorithms. The algorithms are assumed to be executed iteratively and must be capable of being described by a directed graph, where nodes (vertices) represent algorithm tasks, and edges (arcs) impose a partial ordering on the tasks to assure correct results. Tokens, representing the presence of a signal on an edge, indicate the initial state of the algorithm. When the partial ordering is a result of inherent data dependencies within the algorithm, the directed graph is referred to as a dataflow graph. Dataflow graphs provide a graphical and mathematical model of computation in a way that inherent parallelism can be readily observed and exploited.

The Design Tool, a software program developed in-house to implement the ATAMM concepts, provides automatic and user-interactive graph-analysis capabilities that facilitate the design of a multiprocessing solution at compile time. Another program, referred to as the Graph Tool, developed by CTA Incorporated on Contract NAS1-18936, aids in the construction of the dataflow graph description of the algorithm. Once the problem has been graphically described and entered into the Design Tool as shown in the figure, speedup and computational performance bounds for a given number of processors are automatically determined along with run-time scheduling criteria and memory requirements. Also, the tool can provide optimizations to the algorithm schedule to increase processor utilization. The optimization is described by using artificial data dependencies called control edges, which impose additional precedence relationships between tasks. Control edges are also used to represent the appropriate iteration period (input injection delay), which assures that there are enough resources to support the exploitable parallelism. The dataflow graph, which implies the

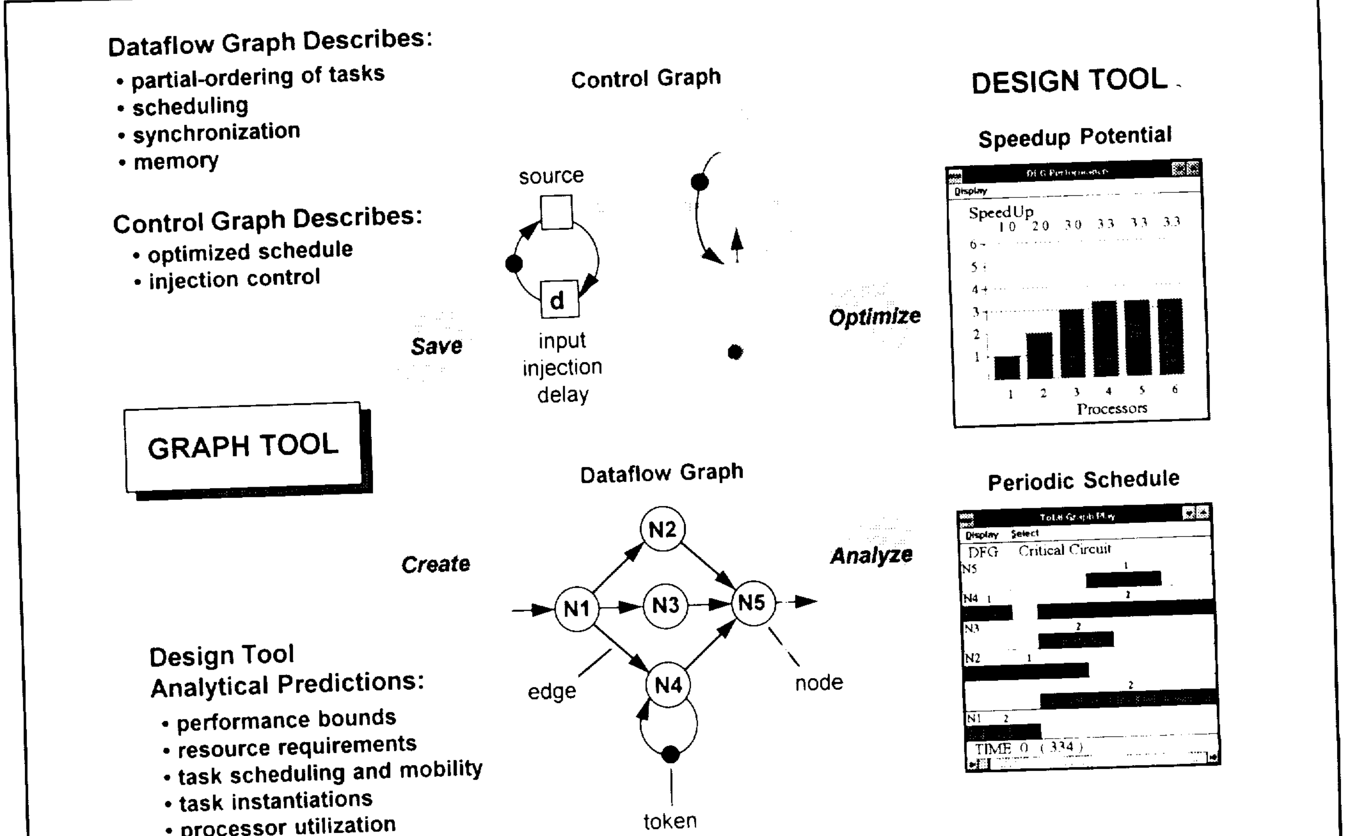

Dataflow graph analysis and design process using ATAMM toolset

scheduling solution as well as the memory requirements of shared data, is superimposed with the control graph and is automatically reconstructed for the user in the Graph Tool. Potential commercial uses include task scheduling of signal processing, control law, scientific, and medical applications. The dataflow/control-flow graph that is generated by the Design Tool also conveys the run-time criteria that are required of commercially developed real-time operating systems to assure predictable performance.
(Robert L. Jones, 41492, and Paul J. Hayes)
Flight Systems Directorate

Space Platforms

RESEARCH AND TECHNOLOGY

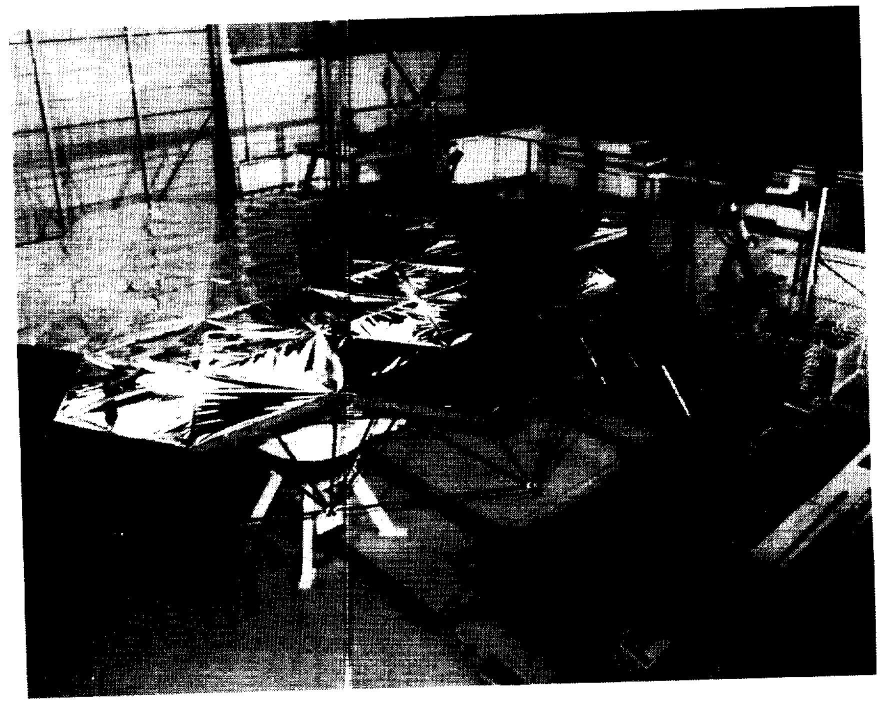

Provide technology for the current and evolutionary Space Station and space platforms and provide the technology base for future developments

Design and Fabrication of an Ultrastable Composite Optical Bench

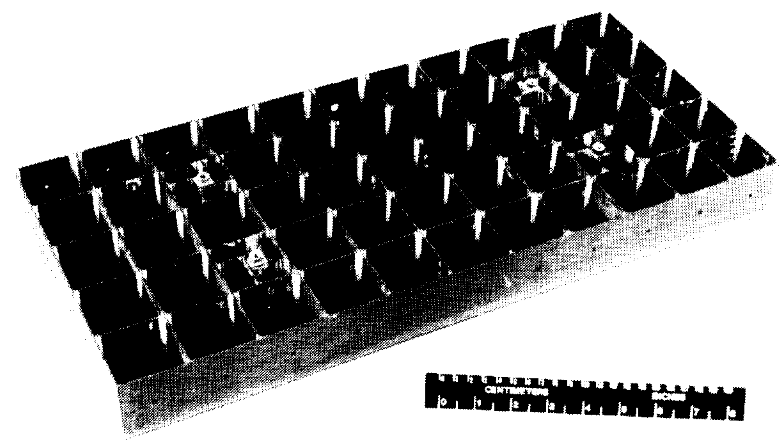

Composite optical bench prior to installation of facesheet (56 cm × 25 cm × 6 cm).
L-93-8211

Optical bench structures provide stable platforms on which to mount sensitive optical components with critical alignment tolerances. Future flight projects in astrophysics and atmospheric sensing place increasingly stringent demands on optical bench stabilities under both thermal and mechanical loads. High-stability optical bench structures with low weight can be attained through the use of carbon-fiber reinforced composite materials. The advancement of composite optical bench technologies to meet future mission needs is currently under way at NASA.

Amoco's P75/ERL1962 graphite/epoxy composite prepreg was utilized because it provides a "near zero" coefficient of thermal expansion (CTE) in a quasi-isotropic laminate and because data existed that demonstrated resistance to microcracking under thermal cycling for this material. The bench design was based on a composite "egg crate" core sandwich concept. This design is superior to conventional honeycomb sandwich construction in that the core material is identical to the facesheet material and therefore gives greater thermal/dimensional stability. Also, this concept allows optical mounting inserts to be installed into the rib structure with minimal use of potting compounds.

Processing conditions were determined for producing laminates with the proper fiber volume fraction required for a near-zero (±0.2 ppm/°C) CTE. A 56-cm × 25-cm × 6-cm demonstration bench incorporating several inserts was fabricated and is shown in the figure prior to installation of the facesheet. A chromium and gold moisture barrier was vapor deposited on the outside of the completed bench to avoid dimensional changes associated with the adsorption of ambient moisture by the graphite/epoxy composite. The completed bench weight was 3.3 kg.

Novel insert designs were developed for attaching heavily loaded or lightly loaded optical mounts. The high-load inserts were fabricated from composite and metallic components and bond directly into the optical bench core structure. They weigh only 45 grams, yet can withstand axial loads of 22 kN. In addition, threaded metallic inserts (not shown) have been developed that are capable of being installed in the optical bench after assembly by a single-side-access-only method. These inserts contain a double-locking mechanism and provide a threaded attachment point to the bench's composite facesheet.

(Timothy W. Towell, 44258)
Structures Directorate

Space Station Berthing

An analysis of nominal Space Shuttle berthing operations with the permanently crewed configuration (PCC) of Space Station *Freedom* was conducted. The end product was a 9-minute video animation spanning the entire 5-hour berthing scenario. All motions depicted represent the results of modeled dynamic forces and torques acting between the orbiter and station, as well as environmental perturbations acting on both vehicles.

Prior to berthing initialization, the PMC steady-state attitude, attitude rates, and control-moment gyro (CMG) angular momentum requirements were depicted. The following nine phases of the berthing operation were then simulated according to the nominal timeline sequence of events: 1) station reorientation from torque equilibrium attitude (TEA) to local vertical attitude, 2) solar-array rotation to a minimum plume impingement orientation, 3) orbiter remote manipulator system (RMS) grapple operation with both the station and orbiter in free drift, 4) RMS commanded rate null procedure and joint locking, 5) RMS vibration damping, 6) reaction control system (RCS) jet maneuver of combined stack to "parked" TEA attitude, 7) RCS to CMG control handover, 8) RMS retraction, whereby the orbiter and station are pulled together for mating, and 9) mating and subsequent CMG control steady-state operations.

RCS propellant usage, CMG control torque and momentum requirements, and RMS joint force and torque loads were computed throughout the nine mission phases as appropriate. Fuel requirements to hold local vertical attitude pre-grapple were minimal. The station attitude was determined to drift only a few degrees during the free-drift grapple operation. The rate null operation did not impose any excessive loads on the RMS joints for the berthing scenario simulated. Maximum joint loads occurred during the parked TEA maneuver phase.
(Richard A. Russell, 41935, and Michael Heck)
Space Directorate

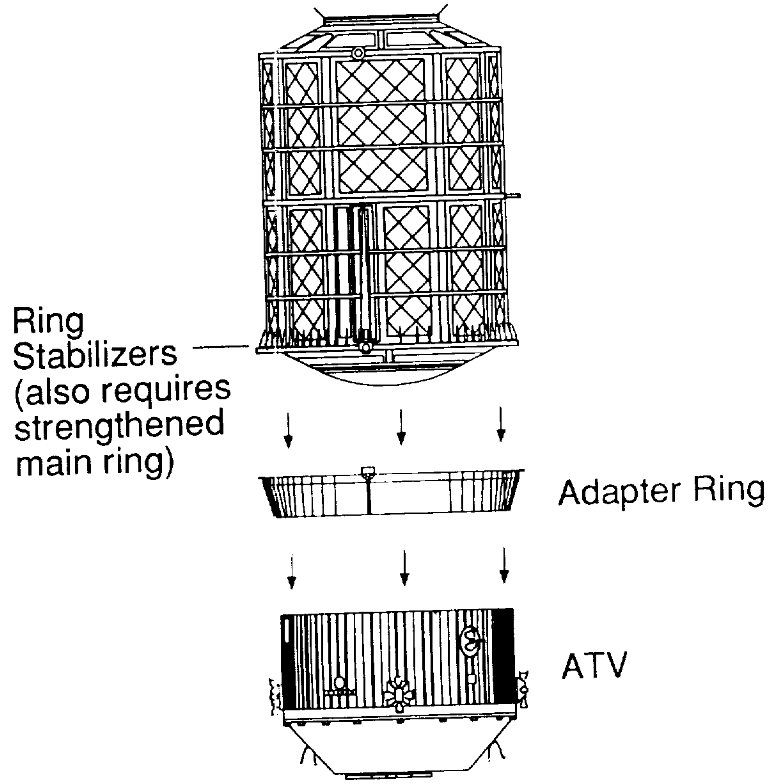

ESA automated transfer vehicle with attached pressurized payload.

Design Reference Mission Specifications for European Space Agency Automated Transfer Vehicle

The European Space Agency automated transfer vehicle (ATV) is a proposed orbital transfer stage that would provide automated rendezvous capability for the Ariane 5 launch vehicle. The primary Ariane 5/ATV mission under consideration is unmanned delivery of logistics resupply cargo to the space station. NASA has undertaken a feasibility assessment to define specific design and operational requirements for the ATV. The NASA LaRC portion of this study includes identifying,

evaluating, and prioritizing space station cargo options for ATV delivery. The space station resupply cargo options and associated delivery operations are referred to as ATV design reference missions. Preliminary prioritization of the ATV design reference missions was based on an unweighted set of evaluation criteria that consider Space Shuttle and Ariane 5/ATV flight operations, space station cargo-to-ATV integration requirements, and ground processing issues. Initial study results show that a single Ariane 5/ATV flight per year is an optimal flight rate for mixed-fleet transportation support as a result of shuttle cargo return limitations. For this single Ariane 5/ATV flight per year, the space station pressurized logistics module (PLM) is potentially the most desirable ATV cargo because of the resulting savings of a space shuttle flight needed for PLM delivery, minimal PLM modifications required for ATV compatibility, and minimal pre-flight cargo processing required at the Ariane 5 launch site in Kourou, French Guyana.
(William M. Cirillo, 41938)
Space Directorate

Accommodation of a Soyuz TM as an Assured Crew Return Vehicle

A study was conducted to determine the implications of accommodating two Soyuz TM spacecraft as assured crew return vehicles (ACRV) on the Space Station *Freedom* (SSF) at the permanently crewed capability stage. Operational as well as system issues associated with the accommodation of the Soyuz for several potential configuration options were examined. Operational issues considered include physical hardware clearances, worst-case Soyuz departure paths, and impacts to baseline operations such as pressurized logistics module exchange, space station remote manipulator system attachment, extravehicular activity (EVA), and autonomous rendezvous and docking. Systems analysis included the determinations of differences between Soyuz interface requirements and SSF capabilities for the electrical power system, thermal control system, communications and tracking, audio-video subsystem, data management system, and environmental control and life support system. Significant findings of this study have indicated that the current ΔV (difference in velocity between space station and Soyuz TM) capability of the Soyuz will need to be increased to provide adequate departure clearances for a worst-case escape from an uncontrolled SSF and that an interface element will be required to mate the Soyuz vehicles to station, to provide for autonomous rendezvous and docking structural loads, and to house Soyuz-to-SSF system interfaces. Of the options considered, the placement of the pair of Soyuz vehicles on the nadir port of node 1 and the zenith port of node 2 or on the nadir and zenith port of node 1 will have the fewest system interface modifications required for the SSF and the Soyuz and can provide for the autonomous rendezvous and docking and simultaneous departure of the Soyuz vehicles. However, since the option to use the nadir port of node 2 will impact elements currently under critical design review, the recommended configuration is to place the Soyuz vehicles on the nadir and zenith ports of node 1.
(Jonathan Cruz, 41951, Marston Gould, and Eric Dahlstrom)
Space Directorate

Configuration Analysis for Space Station Redesign

The Advanced Space Concepts Division provided configuration analysis for several space station redesign concepts. The configuration concepts (option A, option B, and a Russian participation configuration) were analyzed at some or all assembly sequence stages for flight characteristics. The configuration flight characteristics include attitude history, control moment gyro (CMG) and reaction control system sizing, orbit lifetime, fuel requirements, and microgravity environment determination.

Option A represented a significant departure from the baseline Space Station *Freedom* program. It had a shorter repackaged main-truss structure and a new radial pressurized module pattern. A new "arrow" flight mode was required in order to generate sufficient electrical power. The arrow flight mode aligns the main truss structure along the station velocity vector. Analysis determined that this flight mode was difficult to control and that it had a negative impact on the microgravity environment.

Option B incorporated some minor configuration and system changes from the baseline *Freedom* program. A small truss section was eliminated, and the third solar-power module was relocated

to the port side. These configuration changes resulted in slightly lower control requirements and a better microgravity environment than *Freedom*.

The Russian participation configuration incorporated some system changes from option A into the option B configuration. Russian pressurized elements were added to form a new module pattern. Each stage of the assembly buildup could be controlled with either the Russian complement of CMG's (15 000 N-m-sec) or the U.S. complement of CMG's (18 980 N-m-sec) for steady-state operations that assume partial feathering of one of the U.S. solar arrays in some cases.
(Patrick A. Troutman, 41954)
Space Directorate

Space Station Assembly and Operations at High Orbital Inclinations

This study examined the implications of assembling and operating the space station at a 51.6° inclination orbit utilizing an enhanced-lift space shuttle. Station assembly is currently baselined at a 220-n.mi-high, 28.8° inclination orbit. This study assumed that the shuttle is used exclusively for delivering the station to orbit, and that it can gain additional payload capability from design changes (e.g., a lighter external tank).

The high-inclination assembly manifest requires 19 flights to reach a permanently crewed capability (PCC) and one additional flight for the centrifuge accommodation node. PCC is achieved in September of the year 2000, a 3-month delay compared to the baseline sequence. Five advanced solid rocket motor (ASRM) flights are used during the later phase of the assembly sequence. An increase in the number of assembly flights and the use of more ASRM's are required, since the enhanced shuttle has almost 5000 lb less payload-to-orbit capability to a 51.6° inclination orbit compared with the baseline shuttle payload capability to a 28.8° inclination orbit. Design changes include accommodating the unpressurized berthing adapter and mobile transporter on the second assembly flight instead of the first, developing new carriers for off-loaded components, and modifying the first propulsion module and any associated software to provide reboost and attitude-control capability on the second assembly flight. Operational changes include restructuring extravehicular activity timelines on the first three assembly flights and grappling and berthing the first assembly flight with the S2 segment while attached to the unpressurized docking adapter.
(Patrick A. Troutman, 41954)
Space Directorate

Spacecraft Contamination Investigation by Direct-Simulation Monte Carlo Analysis—Application to UARS/HALOE

Space platforms and satellites create their own local artificial atmosphere, with gases emanating from surface outgassing, venting, and the operation of attitude-control thrusters. The Upper Atmosphere Research Satellite (UARS), which was launched into low-Earth orbit to study upper atmospheric chemistry, is equipped with several optical telescopes (including the Halogen Occultation Experiment, or HALOE) and other sensitive instruments that must remain free of contaminants. To ascertain the probable levels of contamination at the HALOE aperture, a three-dimensional direct-simulation Monte Carlo (DSMC) analysis is being performed for the complete satellite. The complex geometry of the 10-m UARS is modeled at a 5-cm spatial resolution, and each known source of contaminant gases is accounted for. The DSMC

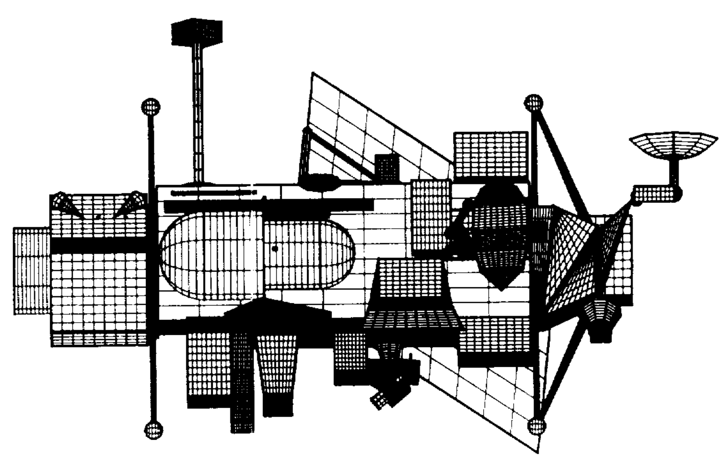

UARS configuration definition for DSMC analysis.

simulation is performed with two computer processors working in parallel to simulate both the near and far fields of the satellite. Results obtained for a series of satellite orientations and configurations, and several HALOE telescope pointing directions, indicate that contamination levels may be much lower than predicted from pre-flight design methodology.

This study, which is being run on engineering workstations, has also demonstrated the capability of the present 3D DSMC method to simulate flow fields about bodies of extremely complex geometry, in a parallel processing environment, with relatively short turnaround times.
(Didier F. G. Rault, 44388, and Michael Woronowicz)
Space Directorate

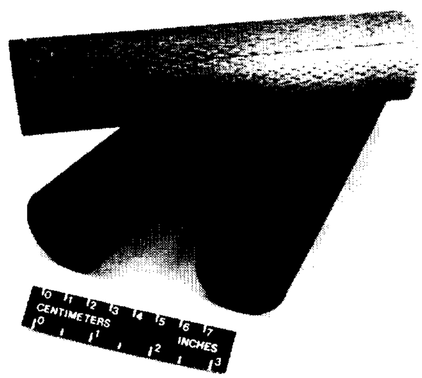

Carbon-carbon composite tubes fabricated by rapid densification process.

Rapid Processing of Carbon-Carbon Composite Materials

Carbon-carbon composites afford many engineering benefits as spacecraft structural materials. These benefits include low weight, high specific strength and modulus, zero moisture expansion, no outgassing, and insusceptibility to natural space radiation. Carbon-carbon composites are also attractive for a wide variety of high-temperature aerospace structural applications, including thermal-protection systems and hot structure. However, traditional fabrication methods are lengthy and the costs are high for parts. Under NASA sponsorship, Lockheed Missiles and Space Company and Textron Specialty Materials are developing an innovative liquid-phase chemical vapor infiltration process for densifying carbon-carbon composites; this process has a very high potential for reducing densification times from the weeks or months to only several hours. Fabrication costs are also expected to decrease markedly.

The liquid-phase densification process under development proceeds rapidly because of the virtually unlimited source of reactant (hydrocarbon liquid) and very high mass transport rates that are not achievable with conventional gas-phase processes. Four representative generic spacecraft components have been selected for demonstrating the potential of the rapid densification process: structural tubes, radiator panels, reflector panels, and aerobrake structural panels. Each of these four components poses a special geometry-related processing issue that must be addressed.

The figure illustrates the remarkable success that has been achieved in fabricating structural tubes. Excellent tube densities and mechanical properties were achieved in only 4 hours of densification time. Flat panels 6 in. by 12 in., not shown, have also been successfully densified. In addition, the process has been successfully modified to deposit silicon carbide oxidation protective coatings. Coating deposition rates approaching 1 mil/hr have been shown to be possible. Potential commercial applications for this new process include aircraft brakes, high-performance automotive pistons, and jet-engine exhaust-nozzle flaps and seals.
(Howard G. Maahs, 43084)
Structures Directorate

Low Earth Orbit Environmental Effects on Materials

The Long Duration Exposure Facility (LDEF) is an unmanned school-bus-sized satellite that accommodated a wide variety of technology and science experiments that require long-term exposure to a known low Earth orbit

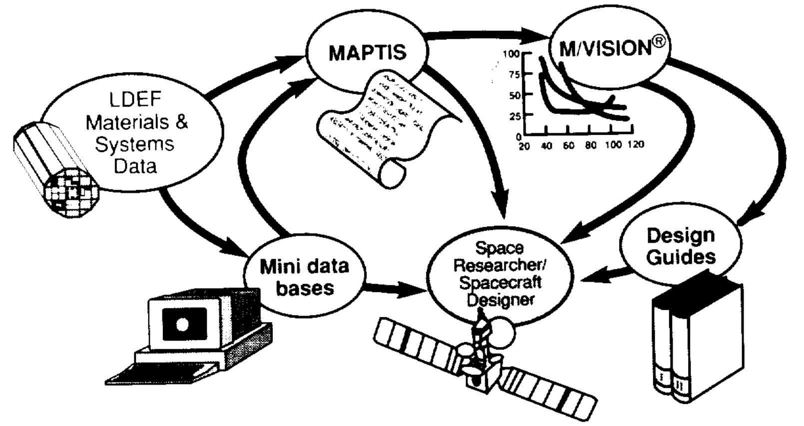

Databases for low Earth orbit environmental effects on materials.

environment. The LDEF was deployed by the Space Shuttle *Challenger* on April 7, 1984, in a nearly circular 257-n.mi. orbit with a 28.4° inclination. On January 29, 1990, after nearly 69 months in space, the LDEF was retrieved and returned to Earth by the Space Shuttle *Columbia*. The 57 experiments on LDEF involved over 300 U.S. and foreign investigators from private industry, universities, and government laboratories. The experiments, as well as the LDEF structure itself, provided an unprecedented opportunity to investigate the effects of the low Earth orbit environment on spacecraft.

To ensure that the materials and systems data from LDEF are available to current and future spacecraft designers, a set of databases, shown in the figure, have been developed. Initially, to provide the maximum amount of information to users in the shortest time possible, a series of mini-databases that run on Claris Corporation's Filemaker Pro® software for both IBM and Macintosh computer formats were developed under contract by Boeing Defense & Space Group. The databases have been developed on the following specific subjects: optical materials, silverized Teflon thermal blankets, treated aluminum hardware, thermal control paints, and the LDEF spacecraft environments. However, to capture all LDEF materials, including the data in the mini-databases, and in some cases, system data, Langley Research Center and Marshall Space Flight Center have jointly developed the LDEF Materials Data Base. The database is available in two versions. The first version utilizes a preexisting global-access database system, the Materials and Processes Technical Information System (MAPTIS), and can be accessed via a modem and an 800 phone number, or via telnet. The MAPTIS version of the database allows the user to search and retrieve tabular data. The second version of the database runs on PDA Engineering's M/VISION® software. Although this software system requires more sophisticated computer equipment, it has powerful query, spreadsheet, and graphical capabilities. All the databases are available free of charge to the user community.

To meet the needs of spacecraft designers, value is being added to the data collection, and "rules of thumb" based on the data are being developed. The rules of thumb are currently being developed under contract by TRW Inc. and will be compiled in handbook form and made available to the user community.
(J. G. Funk, 43092)
Structures Directorate

Improved Near-Earth Meteoroid Environment Model

Examination of 26 m^2 of aluminum that covered the surface of the Long Duration Exposure Facility (LDEF) during its 5.8 years in orbit about the Earth has revealed over 9000 craters that were caused by meteoroids and man-made orbital debris.

It was possible to determine the relative number of meteoroid impacts and man-made orbital-debris impacts on each of the 14 sides of the LDEF because of the unique, three-axis, gravity-gradient orientation of the LDEF. The huge difference between the number of craters on the space-facing end and the Earth-facing end provided the key by showing that essentially all the impacts on the space-facing end were from meteoroids. The meteoroid flux on the other 12 sides of the LDEF was then calculated, and the man-made orbital debris flux was obtained from the difference between the observed crater flux and the calculated meteoroid flux.

Some of the LDEF crater-flux data are shown in the figure. The

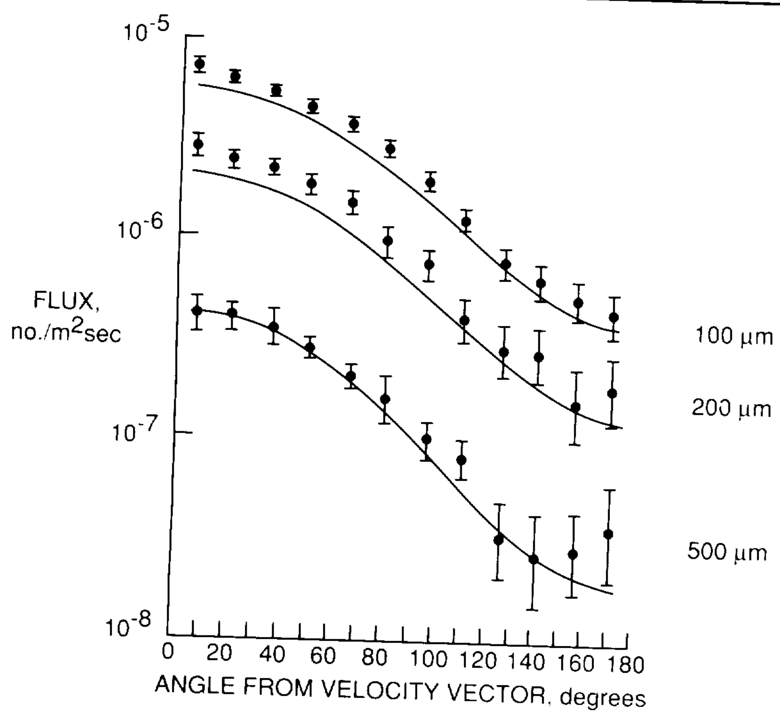

Distribution of craters around LDEF and meteoroid component of crater flux.

curves are the calculated meteoroid component. Essentially all the 500-µm craters were caused by meteoroids, while 25 to 30 percent of the smaller craters were caused by man-made orbital debris. There is evidence that man-made orbital debris dominates the impact flux both at much larger and much smaller particle sizes.

The improved near-Earth meteoroid environment model can be valuable in calculating the meteoroid hazard to commercial spacecraft, especially for spacecraft that are at an altitude above 2000 km. Radar observations suggest that the man-made debris hazard is not significant at these altitudes and that meteoroids therefore present the only impact hazard.
(Donald H. Humes, 41484)
Space Directorate

New Postlaunch Satellite Calibration Technique

It is well established that satellite instrument calibrations often shift as a result of launch vibrations and sometimes drift over their lifetimes because of sensor or optics degradation. It is generally agreed that absolute-calibration measurements from the NASA ER-2 aircraft are the most accurate method (±3 to 5 percent) of determining postlaunch calibration coefficients for narrowband satellite instruments at visible wavelengths. Historically, 1 to 3 ER-2 calibration experiments are conducted each year for only a few satellites because of high cost and operational complexities.

As a result of its support of the World Climate Research Program's (WCRP) Surface Radiation Budget

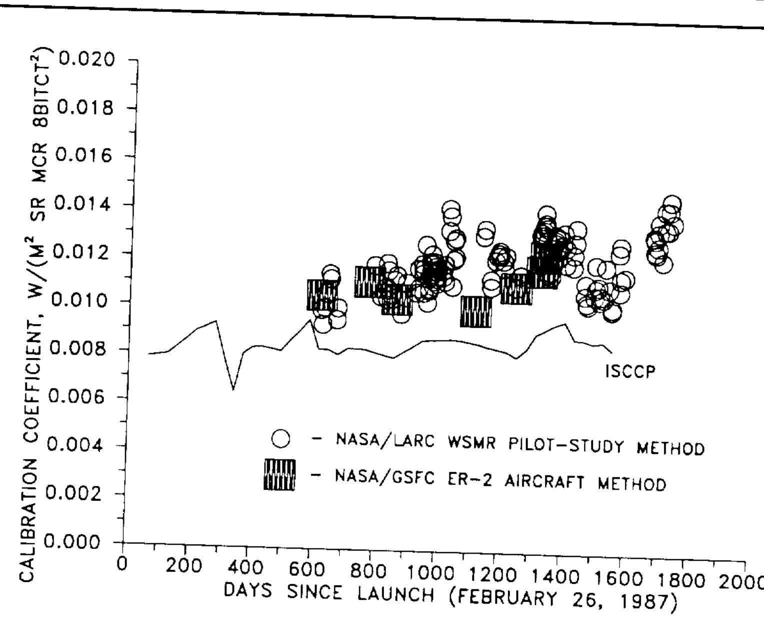

Langley Research Center pilot-study results for calibration of GOES-7 satellite visible channel compared with Goddard Space Flight Center (GSFC) ER-2 aircraft and ISCCP values.

(SRB) activity, Langley Research Center has jointly completed a 3-year pilot study of a simplified absolute-calibration technique with the U.S. Army at the White Sands Missile Range (WSMR). Objectives of the new technique were (1) low cost relative to other methods, (2) 50 to 80 calibration measurements per year, (3) capability for calibration of any overflying satellite with pixel sizes less than 2 km, (4) accuracy within ±7 percent, and (5) verification of erratic behavior for the GOES instruments as had been observed by the WCRP International Satellite Cloud Climatology Project (ISCCP). The technique is based on unmanned ground sites at WSMR with remote transmission of data back to Langley twice daily. For a yearly cost of $75,000 plus 1 man-year, all the above objectives were satisfied. Visible-wavelength instruments on the GOES-6, GOES-7, NOAA-9, NOAA-11, SPOT-1, and SPOT-2 satellites were calibrated and compared with values from other methods. In addition, it was determined that ISCCP values were low compared with both pilot-study and ER-2 results as shown in the figure. The pilot-study calibration results explain artifacts in ISCCP satellite cloud retrievals that have been detected by University of Washington scientists.

The pilot-study technique is useful for postlaunch cross calibration of narrowband instruments on the various EOS platforms. It is also useful for calibration of visible-wavelength instruments on foreign satellites and commercial instruments that may be launched on small platforms. Most importantly, it may be useful in detecting unstable instruments and the precise time of instrument deterioration.

(Charles H. Whitlock, 45675)
Space Directorate

EOSSIM: A Linear-Simulation and Jitter-Analysis Package

The EOSSIM software package is a linear-simulation and jitter-analysis tool that was developed to assess pointing performance of the Earth Observing System (EOS) AM-1 spacecraft. The package is written in MATLAB script language, with optional external interfaces to FORTRAN for some of the more computationally intensive operations. The software package is module based to enhance its versatility and portability. The five main modules that make up the basic package are as follows: the plant-definition module, the attitude-control-system module, the disturbance module, the simulation module, and the jitter-analysis module.

EOSSIM uses a sparse-matrix formulation for the spacecraft dynamics model which makes the discrete time simulations quite efficient, particularly when a large number of modes are required to capture the true dynamics of the spacecraft. Typically, EOS AM-1 jitter analysis is performed with more than 500 structural modes used to describe the spacecraft dynamics. EOSSIM requires finite-element-generated structural mode shape vectors and frequency data to form the open-loop plant models. In the development of EOSSIM, an efficient jitter-analysis procedure that determines jitter and stability values from time simulations in a very efficient manner was devised. The resulting jitter-analysis algorithms produced a speedup of more than 1600 over the brute-force approach of sweeping minima and maxima.

A graphical user interface (GUI) is also included in the EOSSIM software package. This interface uses MATLAB's Handle graphics to form a user-friendly environment that permits a convenient and intuitive way to set simulation parameters. The current version of the GUI allows the user to

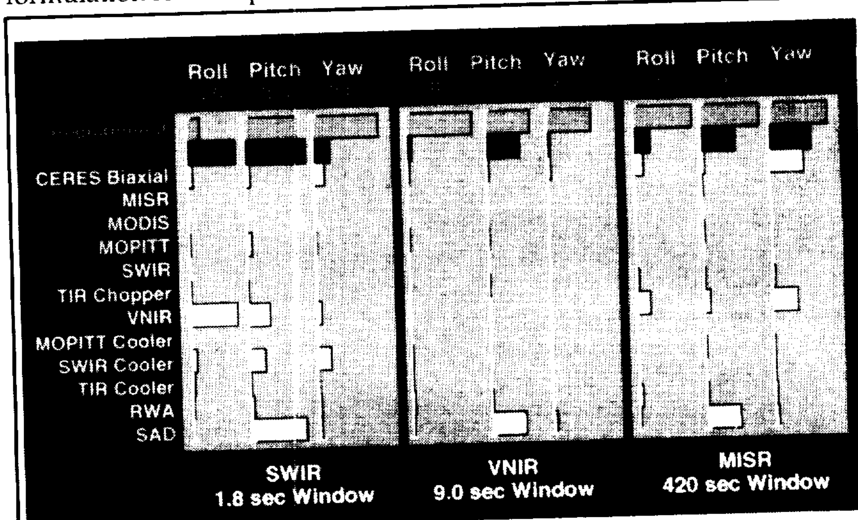

EOS AM-1 baseline jitter—phase 1.

interactively select the following jitter-analysis and simulation parameters: simulation type, problem size, disturbance model selection, performance output selection, and various levels of simulation and jitter-analysis documentation.

The EOSSIM software package has been transferred to and used by several aerospace corporations. EOSSIM will continue to be used by industry for jitter analysis and simulation of future EOS missions as well as in other missions that require simulation and jitter analysis for large-order systems.
(Peiman G. Maghami, 44039, Sean P. Kenny, and Daniel P. Giesy)
Flight Systems Directorate

Fluid Dynamics of Chemical Vapor Deposition

Chemical Vapor Deposition (CVD) is an important industrial process for the production of semiconductors, thin films, optical and corrosion-resistant coatings, paint pigments, drawing stock for optical fibers, and many other products. The quality of the finished product depends critically on the fluid dynamics of the process. However, it is difficult to quantify the fluid dynamics of CVD because of the complicated interaction of the fluid dynamics, heat transfer, nonequilibrium chemistry, and internal geometry that are normally involved. The mission of the Chemical Vapor Deposition Facility (CVDF) is to improve the understanding of the CVD process through development of laboratory instrumentation and numerical modeling tools that can be applied by NASA and coinvestigators in industry and academia.

A collaboration between CVDF personnel and University of Virginia (UVA) coinvestigators has produced a data set of three-dimensional flow-field measurements, growth-thickness experiments, and a three-dimensional numeric model of both the fluid dynamics and reactive chemistry associated with a horizontal CVD reactor. Correlations between the model and the experiments were used to validate the model, identify features of the reactor that were critical to its fluid-dynamic performance, and optimize the operating parameters for this process. The flow-field measurements and numeric model were performed on-site, while the growth data were obtained in UVA facilities. Laser velocimetry (LV) techniques, adapted from wind-tunnel applications, were used to measure the flow field inside the reactor (see figure). A CFD code, enhanced through the SBIR process specifically for CVD modeling, was used to develop the numeric model of this CVD reactor.
(Ivan O. Clark, 41500)
Flight Systems Directorate

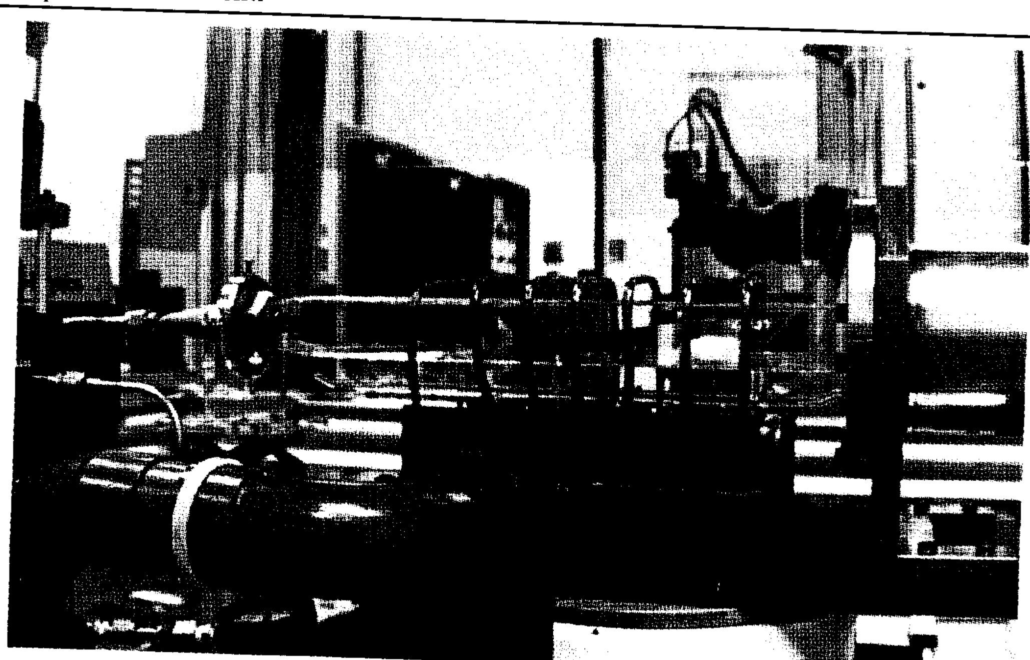

Chemical vapor deposition reactor installed in laser velocimetry lab.

Automated Structural Assembly Research Completed

In 1993, the Automated Structural Assembly Laboratory (ASAL) operations were concluded after successfully demonstrating robotic assembly of a 102-element tetrahedral truss structure and the installation of 7-foot-diameter panels on the planar surface of the truss structure. ASAL has been a joint program of the Structures and Flight Systems Directorates and has been the most autonomous telerobotic program in the agency. Automated structural assembly has been proposed for future missions, such as large spacecraft and planetary habitats. ASAL has demonstrated the ability to robotically assemble large structures under supervised autonomy. Technology that has been developed and integrated into the robotic assembly includes automated sequence planning for determining the optimum sequence for installation/removal of struts; automated path planning for determining collision-free trajectories for the robot arm and payload; interchangeable special-purpose end effectors with integrated sensors and microprocessors for monitoring and error detection; active compliance and load balancing using a wrist force/torque sensor; computer vision-based guidance for final alignment and closure; and an expert system-based executive for monitoring and replanning.
(Ralph W. Will, 46672)
Flight Systems Directorate

Truss structure assembled by robotic system. L-93-09366

Hydraulic Manipulator Testbed Controlled Remotely From JSC

Following the cancellation of the Flight Telerobotic Servicer (FTS) program, Langley Research Center (LaRC) and Johnson Space Center (JSC) have worked together to capture the telerobotics technology generated under the FTS program. The FTS Hydraulic Manipulator Testbed (HMTB) has been installed and placed in operation at LaRC, and one flight-qualifiable arm has been delivered to JSC. HMTB includes a hydraulically driven dexterous 7 degree-of-freedom robot arm, kinematically similar to the flight arm, and uses the FTS flight software, sensors, and control system. LaRC engineers have developed an interactive operator control station for HMTB that enables selection of control modes, control-system gains, motion commands, and sensor feedback. In August 1993, the software was installed on a workstation at JSC, and JSC personnel remotely controlled the HMTB in Cartesian and joint position moves. Commands from JSC and data from LaRC were transmitted over the Internet network, and video between the Centers was carried over the NASA teleconferencing network. Subsequent tests will use joysticks and rate control to simultaneously drive all seven joints of HMTB and will employ computer-generated graphics simulations to compensate for transmission time delays.
(Plesent W. Goode IV, 46685)
Flight Systems Directorate

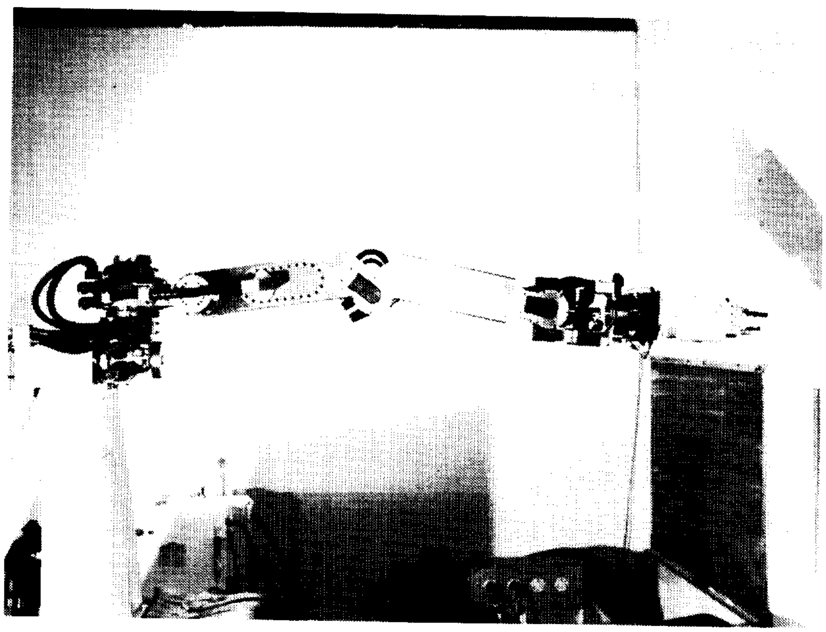

Hydraulic Manipulator Testbed for FTS program. L-93-00921

Semiconductor Laser for Free-Space Optical Communications

NASA Langley Research Center has been developing, for the Ballistic Missile Defense Organization, a high-power and high-modulation-rate semiconductor laser for free-space optical-communication applications. Current specific objectives call for a 1 W and 1 GHz modulation-rate laser.

A Monolithic Flared Amplifier-Master Oscillator Power Amplifier (MFA-MOPA) semiconductor laser has been fabricated for NASA Langley by Spectra Diode Laboratory and has been demonstrated in a laser transmitter design by NASA Langley. The MFA-MOPA semiconductor laser has been demonstrated to operate up to 3 W of power with direct modulation rates greater than 1 GHz. Currently, a 1-W version of the MFA-MOPA semiconductor laser is being offered for sale commercially by Spectra Diode Laboratory for optical communication, printing, recording, and medical applications.

(Herbert D. Hendricks, 41536)
Flight Systems Directorate

Radar and Antenna Tests of End-Mass Payload for Small Expendable Deployer Systems

The first Small Expendable Deployer System (SEDS) was a NASA experiment that flew as a secondary payload on a U.S. Air Force Delta II rocket on March 29, 1993. The SEDS-1 successfully deployed an instrumented end-mass payload (EMP) on a 20-km nonconducting tether from the second stage of the Delta II. The instrument measurements onboard the SEDS EMP were telemetered to U.S. Air Force and NASA ground stations using LaRC-developed antennas that were mounted on opposite sides of the EMP. The antennas were designed, fabricated, and tested at NASA Langley Research Center (LaRC). The antenna pattern and gain measurements for the EMP flight units were completed in the Langley Low-Frequency Antenna Test Facility. Volumetric pattern data were collected in 1° increments of theta (0° to 180°) and phi (0° to 360°). These data were used to calculate critical signal margins to ensure that all mission data would be received uncorrupted. Postmission analysis of the received signal strength at the ground stations indicated that the antennas and RF subsystem of the EMP exceeded all performance expectations. Data were collected that related to the rigid-body dynamics of the EMP, beginning at separation from the Delta II second stage through reentry and burnout by several onboard sensors. The EMP was also tracked by several ground-based radar and optical sensors.

In support of the experimental radar study of the EMP, volumetric radar cross-section measurements of a full-scale EMP model at 6 GHz were made in NASA Langley's Experimental Test Range (ETR). The ETR facility is a compact range that is designed for microwave scattering measurements in the 2- to 18-GHz range. The SEDS EMP model was placed near the center of a 6-ft by 8-ft test zone that provides a uniform plane wave to

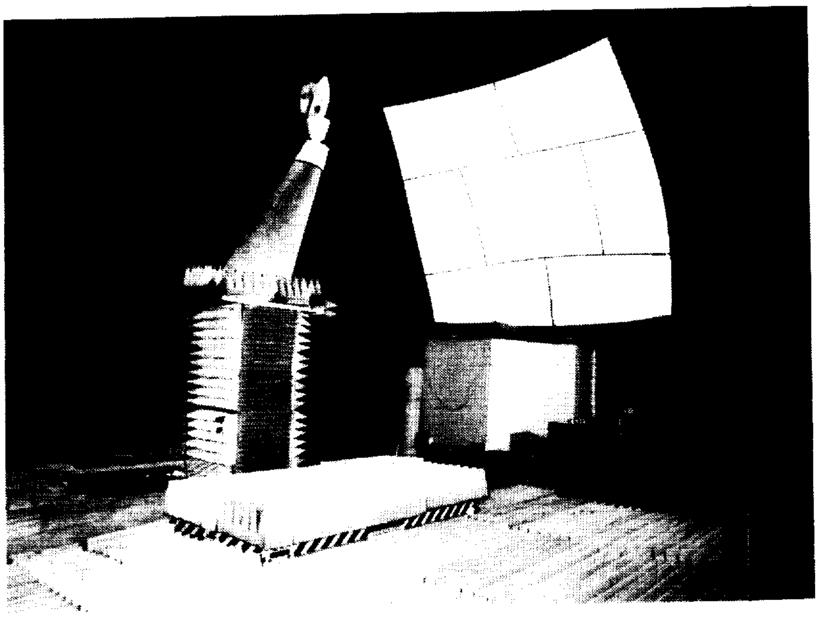

Radar measurements of end-mass payload (EMP) in Experimental Test Range. L-92-(6742

simulate the necessary far-field conditions. A low-cross-section pylon supported the model and included a computer-controlled 360° azimuth rotator for pattern measurements. A foam cradle was developed that allowed the model to be supported at various tilt angles while the 360° azimuth sweeps were performed (see figure). The tilt angles were changed in 5° increments. This resulted in a set of volumetric RCS data, with each tilt angle corresponding to a great-circle cut. These results provided verification, prior to launch, of the ability to track the EMP with a ground-based radar.
(Robin L. Cravey, 41819, Melvin Gilreath, and Erik Vedeler)
Flight Systems Directorate

Space Science

RESEARCH AND TECHNOLOGY

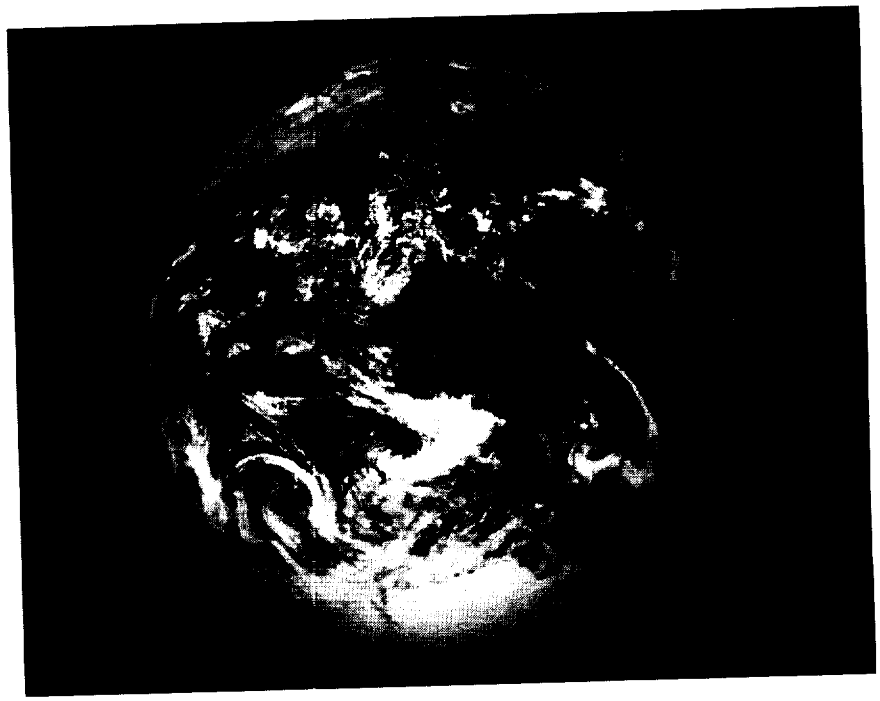

Provide technology for programs focused on Earth, the Solar System, and the Universe, and use the data as the basis for national and international policy making relating to changes to the global system

ESTAR Mission Analyses

Studies to design mission concepts for remote-sensing applications in Earth sciences using the Electronically Scanned Thinned Array Radiometer, ESTAR, have been conducted. Particular applications are the measurement of soil moisture over land, the measurement of sea surface salinity over the oceans, and measurements over the polar ice caps. Mission designs include spacecraft design, launch-vehicle configuration, and orbit analysis. A four-frequency ESTAR that implements one-dimensional aperture synthesis and a "small, low cost" single-frequency ESTAR that implements two-dimensional aperture synthesis have been studied.

Use of aperture synthesis methods in microwave radiometry is one approach to minimizing antenna mass and stowed volume in high-spatial-resolution measurements of soil moisture. Two-dimensional synthesis has been proposed as optimal in terms of these requirements. The objective of the Langley two-dimensional ESTAR study was to assess the feasibility of a soil moisture mission with a small spacecraft and to estimate the cost. An antenna in a symmetric cross configuration made up of two arms 8.75 m long and 0.30 m wide with 145 individual patch antenna elements was designed along with all other sensor hardware. A 535-kg spacecraft that delivers 177 W in payload power and is configured for a Taurus launch was designed. The system provided 10 km of spatial resolution at 1.4 GHz from a 400-km polar orbit with a 3-day revisit time. A 378-kg, Pegasus compatible, reduced-performance version that included a 4.5-m antenna was also defined. This system provided 19 km of spatial resolution, a 60° orbit inclination, and a reduced mission lifetime.

The four-frequency ESTAR was designed to provide measurements over land, oceans, and ice at 1.4, 6.8, 18.7, and 37 GHz. The design was driven by the 1.4-GHz antenna, which was a 9 m × 9 m array made up of 14 slotted waveguide "stick" elements. A 2500-kg spacecraft that delivers 670 W of payload power was designed and configured for a Titan II S-10 launch vehicle.

(J. W. Johnson, 41963, and W. A. Sasamoto)
Space Directorate

Gravity and Magnetic Earth Surveyor Subsatellite

The Gravity And Magnetic Earth Surveyor (GAMES) is a mission-to-planet-Earth spaceflight experiment with a projected 1998 launch. The experiment objective is to map the Earth's gravity and magnetic fields. The technique used to measure the high-order harmonics in the gravity field requires two co-orbiting satellites, a primary satellite and a passive, aerodynamically stabilized "subsatellite." The primary satellite carries a laser-ranging instrument that, when pointed at a corner cube reflector on the subsatellite, measures velocity variations between the two satellites. This relative velocity is a function of the spatial variation of the gravity field. The aerodynamically stabilized subsatellite is a new concept, and its flight characteristics are critical to the success of the GAMES mission. Langley was asked to conduct a performance analysis on the subsatellite as a part of the phase A study.

The objectives of the performance analysis were to define the deployment-rate damping time for the subsatellite, determine the magnitude of its steady-state oscillations, and estimate its orbit lifetime. The modeling approach required for the analysis included a high-fidelity aerodynamic model that simulated free molecular flow in the 250-km to 450-km altitude range and accounted for air-molecule accommodation, reemittance, and reflection effects. A surface finite-element mesh model of the subsatellite, with approximately 5000 elements, was developed for high-fidelity simulation of surface geometry, blockage, and shadowing. A solar-radiation pressure model and a global-winds

model were also included in the analysis. Magnetic hysteresis rods were used to provide deployment-rate damping for the subsatellite.

Analysis results show acceptable deployment-rate damping times and orbit lifetimes. Further, it was found that steady-state oscillations for 250 to 325 km in altitude were between 5° and 7°, respectively.
(J. W. Johnson, 41963, M. L. Heck, R. R. Kumar, and D. D. Mazanek)
Space Directorate

Eyesafe Ho:YAG Lidar for Cloud Monitoring

Although it is recognized that clouds play an important role in climate, reliable climatologies of even simple cloud properties such as base height are not yet available. Small, autonomous lidar systems (ceilometers) are currently used for continuous cloud base height monitoring at many airports. These systems must be inexpensive and eyesafe and, therefore, use very low-power visible-wavelength laser sources. Because of their low power, they have limited range and can detect only low-altitude clouds, so measurements by these systems are not useful for developing general cloud climatologies. Many high-power research lidars are available, but because of the laser power levels used, they are not eyesafe and require that an observer be present. This requirement makes it impractical to operate these systems on a continuous basis as required for climate research.

The human eye is much less susceptible to damage from laser radiation at near-infrared wavelengths in the 1.5- to 2.3-μm range. This allows operation at much higher pulse energies in situations where accidental human exposure to the transmitted laser beam is a safety concern. Until now, however, a high-power laser source that is suitable for lidar use has not been available in this spectral range. Schwartz Electrooptics and the University of South Florida have collaborated under Small Business Innovative Research (SBIR) contract NAS1-19300 to develop an eyesafe laser that is suitable for use in a cloud lidar system. The investigation showed that a Ho:YAG solid-state medium lasing at 2.1 μm was best able to produce the short, high-power pulses that are required for lidar. The laser produces 150 mJ in a 1-μsec Q-switched pulse at a 2-Hz repetition rate. This is about an order of magnitude more energy than has been obtained from existing lasers operating around 2 μm. The laser is now being integrated into an existing lidar system and will be used to explore application as an autonomous cloud-monitoring lidar.
(David M. Winker, 46747)
Space Directorate

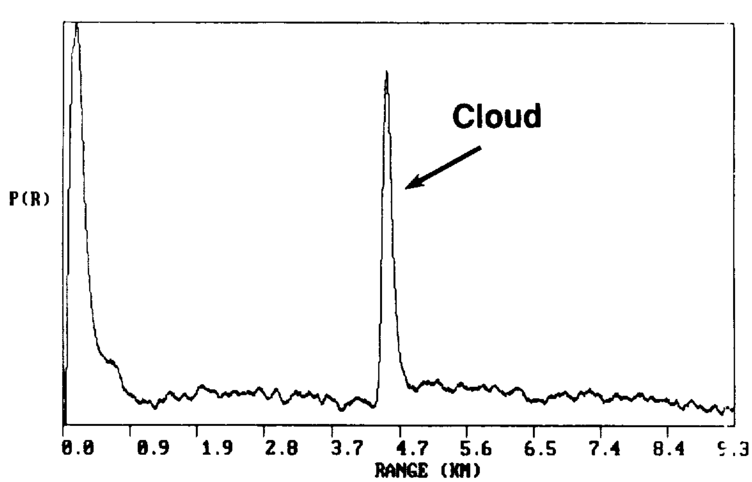

Sample 2.1-μm lidar return signal from a low-altitude cloud.

Remote Sensing of Multilevel Clouds

A multispectral, multiresolution (MSMR) method was developed to analyze complex cloud scenes that contain both single-layered and multilayered cloud decks. The MSMR method provides a framework for collocating AVHRR (Advanced Very High Resolution Radiometer) and HIRS/2 (High Resolution Infrared Radiometer Sounder) data and incorporates cloud-retrieval algorithms such as CO_2 slicing and spatial coherence. Automated atmospheric parameterization schemes were developed that were based upon rawinsonde profiles and analysis products such as ECMWF (European Center for Medium Range Weather Forecasting). The automated procedures were used to derive temperature and humidity profiles for

each HIRS/2 field of view, to estimate clear-sky and low-cloud radiances, and to dynamically determine the tropopause height. A unique new feature of the MSMR method was the development and implementation of an automated fuzzy-logic cloud-classification expert system. The expert system was trained and tested using AVHRR imagery that was collected during the FIRE (First ISCCP Regional Experiment; ISCCP refers to the International Satellite Cloud Climatology Program) Cirrus Intensive Field Operation (IFO II) held in Kansas during the fall of 1991. The expert system classifies the scene within a 32 × 32 AVHRR array (approximately 35 km × 35 km) as being composed of land, ocean, low cloud, middle cloud, or high cloud, either singly or in combination.

The MSMR method was applied to two daytime scenes from November 28, 1991, that were collected during the FIRE IFO II. The two cloud scenes consisted primarily of a cirrus veil overlying a stratus deck. Through the analysis of collocated AVHRR data, each HIRS/2 pixel was classified as being clear of clouds or containing up to two cloud layers. Cloud top heights for each layer present were determined by using a combination of the spatial coherence and CO_2 slicing algorithms. The cloud heights retrieved from satellite data compared well (within 1 km) with coincident lidar, radar, and aircraft data. Cloud analysis was performed for an ISCCP 2.5° grid cell that encompasses the FIRE IFO II experimental region. For both satellite overpasses, more than half the HIRS/2 pixels that fell within the ISCCP cell showed evidence of overlapping cloud layers. Overlapping cloud layers are not provided for in the ISCCP algorithm.

(Bryan A. Baum, 45670)
Space Directorate

First Measurements of Biogenic Emissions of Nitrogen Oxides Obtained From African Soils

Recent satellite measurements indicate that the continent of Africa is the world's center of burning. To assess the impact of African burning on the composition and chemistry of the global atmosphere and planetary climate, over 100 scientists from more than a dozen countries participated in the South African Fire-Atmosphere Research Initiative (SAFARI) in September and October 1992. As part of the Langley participation in SAFARI, we obtained measurements of emissions of oxides of nitrogen—nitric oxide and nitrous oxide—produced by microbial activities in African soils. Microbial activity is the major global source for both of these environmentally significant gases, which impact the chemistry of both the lower atmosphere (the troposphere) and the upper atmosphere (the stratosphere). The Langley measurements represent the first such measurements ever obtained for soils in Africa. Several years ago, Langley researchers discovered that burning significantly enhances the microbial production of these gases. We also obtained measurements of the emissions of these gases before and after

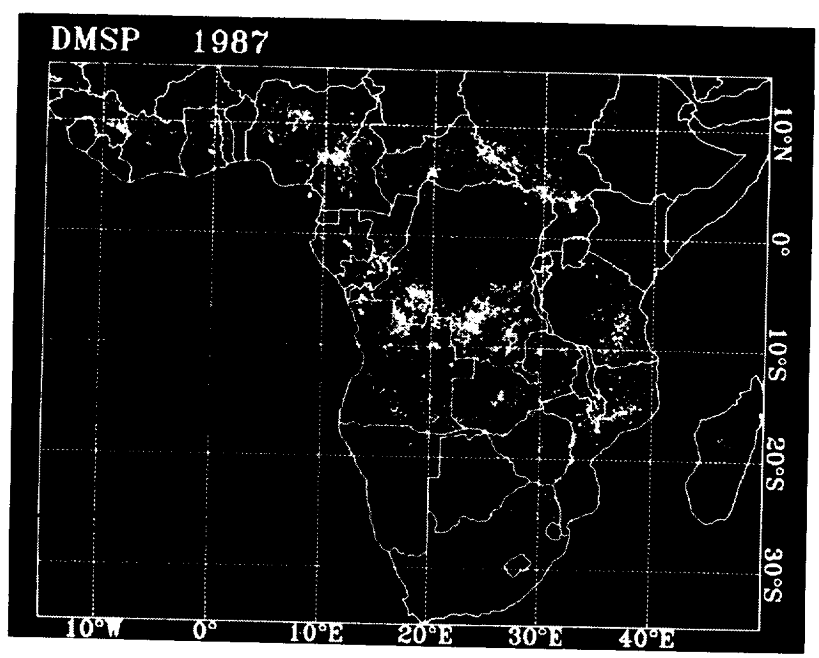

Distribution of burning in Africa in 1987 based on measurements obtained with Defense Meteorological Satellite Program. (Original of figure in color; contact author for more information.)

burning in Africa and found that burning has a very significant impact on the production of nitric oxide in soils. Following burning, the emissions of nitric oxide were much higher than they were before burning. Emissions of nitrous oxide were not detected, either before or after burning. We attribute the lack of nitrous oxide emissions to the severe and long-term drought in Africa.
(Joel S. Levine, 45692,
Wesley R. Cofer III, and
Donald R. Cahoon, Jr.)
Space Directorate

Measurements of Pressure Broadening and Shifts of Ozone Infrared Lines Near 3 μm

Knowledge of pressure broadening and line-shift coefficients for spectral lines of ozone is important for atmospheric remote-sensing studies. Accurate parameters are needed not only in the 9- to 11-μm region, which is usually used for ozone retrievals from passive infrared measurements, but also in other spectral regions, where ozone absorptions overlap the spectra of other trace gases such as methane. NASA Langley researchers, in collaboration with researchers at the College of William and Mary and a NASA Langley ASEE Summer Faculty Fellow, have conducted laboratory studies to determine room-temperature air-, N_2-, and O_2-broadening and shift coefficients for over 270 ozone lines in two absorption bands in the 3-μm spectral region.

The infrared absorption spectra of mixtures of ozone with the broadening gases at various pressures were recorded by using the high-resolution Fourier transform spectrometer at the McMath-Pierce telescope facility of the National Solar Observatory on Kitt Peak near Tucson, Arizona. The analysis was performed on microcomputers by using a nonlinear least-squares spectral-fitting technique developed at NASA Langley.

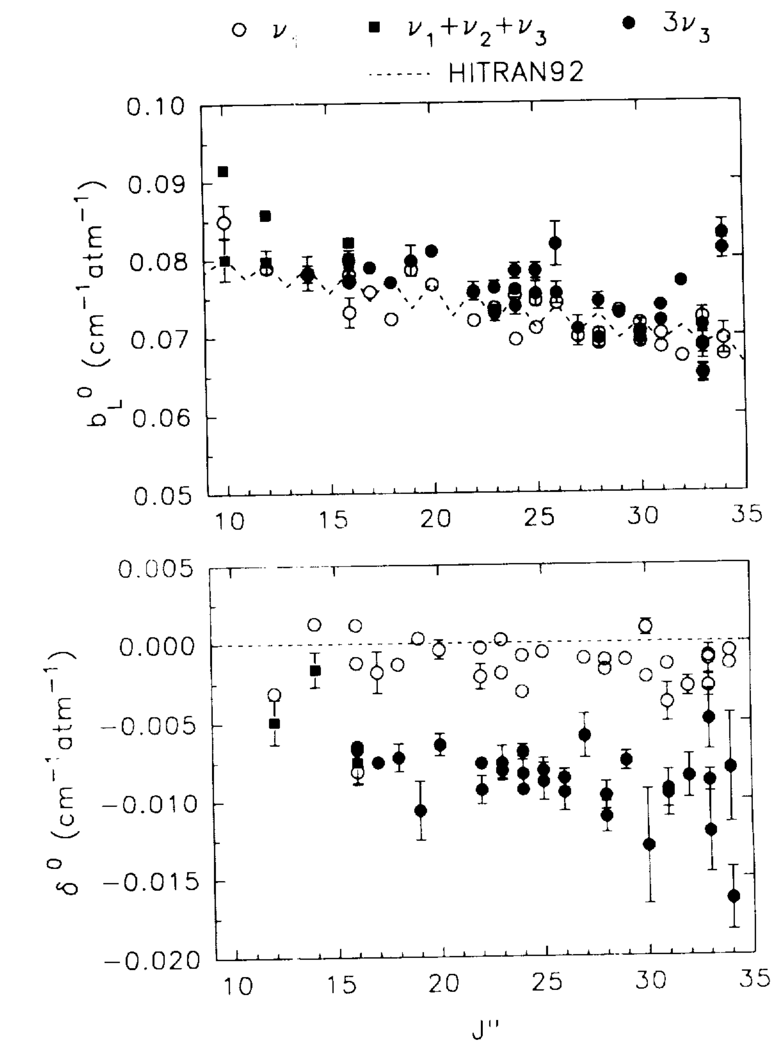

Observed air-broadening (b_L^0) and shift (δ^0) coefficients at 296 K for ozone lines with the same lower state rotational quantum numbers in the 3-μm and 9-μm bands. Error bars indicate standard error of each measured value.

The results of this study show some evidence for a small vibrational dependence of the broadening coefficients. The N_2- and air-broadening coefficients determined in the 3-μm ozone bands are, on average, 5 to 6 percent larger than the corresponding values measured in the 4.8-μm and 9-μm regions. For O_2-broadening coefficients, the differences are greater—

about 8 to 10 percent. The measured pressure-induced line shifts in the 3-µm region are significantly larger than those measured in the 9-µm and 4.8-µm regions; this difference indicates that the shifts depend on the upper vibrational level of the transition.
(Mary Ann H. Smith, 42701)
Space Directorate

Rapid Computation of Earth-Limb Emission in Non-LTE Environment

The capability to rapidly and accurately evaluate the equation of radiative transfer is essential to the interpretation of measurements of infrared Earth-limb emission in terms of the temperature and minor constituent concentrations in the middle atmosphere (10 to 100 km). In particular, many of the observable emissions from carbon dioxide, ozone, molecular oxygen, the hydroxyl radical, water vapor, and nitric oxide originate from radiative transitions that depart significantly from local thermodynamic equilibrium (LTE) in the mesosphere and lower thermosphere (50 to 100 km). Analysis of emission measurements from this region of the atmosphere must account for the nonequilibrium populations of the emitting species in both the radiation source term and the transmission term, which make up the equation of transfer. In principle, accurate calculations under the nonequilibrium conditions require time-consuming line-by-line calculations in which the properties of each spectral line are modeled at high spectral resolution.

Techniques that provide line-by-line accuracy with only a fraction of the computer time necessary to do the exact line-by-line calculation have been developed to evaluate the radiative-transfer equation under nonequilibrium conditions. The new technique involves redefining the absorption cross section and optical mass terms in the evaluation of the atmospheric opacity and is an extension of techniques used previously to analyze emission measurements in the LTE regime. Calculated radiances that employ the new technique and radiances that are calculated by using the exact line-by-line calculations agree to better than 0.5 percent. Less than 1 second of computer time on readily available desktop computer hardware is required to evaluate the limb radiance from 100 to 50 km, accounting for radiative transfer in over 1200 atmospheric layers. The time that is required is almost 3 orders of magnitude faster than needed for the line-by-line calculations. The new radiative-transfer techniques will be applied in the analysis of nonequilibrium emission to be measured by Langley's sounding of the atmosphere using broadband emission radiometry (SABER) experiment, which has recently been accepted for the definition phase by the NASA Office of Space Science for the thermosphere ionosphere mesosphere energetics and dynamics (TIMED) mission.
(Martin G. Mlynczak, 45695)
Space Directorate

TRACE-A

The TRACE-A(TRansport and Atmospheric Chemistry near the Equator—Atlantic) mission obtained more than 140 flight hours of data, which mapped the extent of high concentrations of tropospheric ozone that had previously been observed from satellite measurements and then confirmed from ozonesonde measurements in 1990 and 1991. The DC-8 measurements found very high levels of carbon monoxide, hydro-

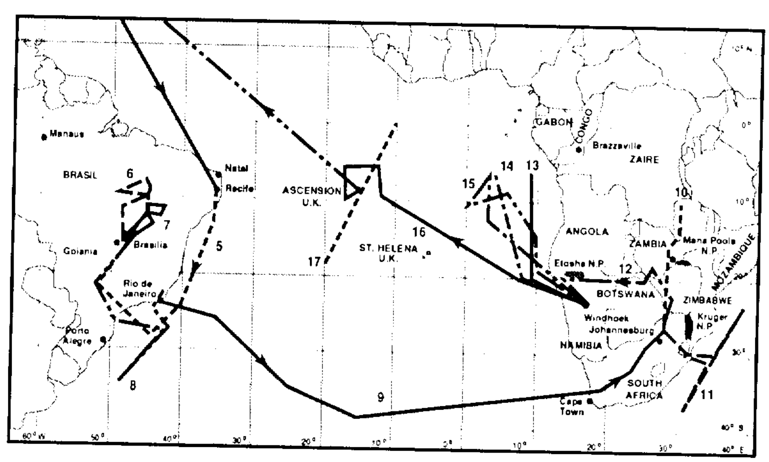

Flight tracks of DC-8 during TRACE-A field mission, September and October 1992.

carbons, peroxides, and reactive nitrogen species in support of an in situ source of tropospheric ozone formation. The precursors for this ozone generation are most likely the result of widespread biomass burning in southern Africa and in Brazil. More than 200 scientists and support personnel deployed in both continents to characterize the regional emissions of both source regions. During the measurement time period, September to October 1992, considerably higher emissions were found to emanate from southern Africa (in particular, northern Zambia) than from central Brazil. Preliminary analysis suggests that these high levels of ozone are correlated with the satellite observations of total ozone in this region. Measurements from the DC-8 also showed that the south tropical Atlantic is a region of strong subsidence, which would be conducive to downward transport of ozone from the upper troposphere and lower stratosphere. A special issue of the *Journal of Geophysical Research* will be devoted to the findings of TRACE-A.

(Jack Fishman, 42720, and James M. Hoell, Jr.)
Space Directorate

Airborne Measurements of Trace-Gas Emission/Deposition Rates

Uncertainties in the surface/atmosphere exchange rate of CH_4 and other climatically important trace species (e.g., O_3 and CO) severely impact the accuracy with which the global budgets of these species can be estimated. One source of uncertainty in current estimates of the CH_4 budget is the extrapolation of ground-enclosure measurements (with a measurement scale of $\approx 1\ m^2$) to represent large-scale CH_4 emission rates for entire ecosystems. Since large variations in methane flux have been observed over a very limited spatial domain, extrapolations of these flux measurements to larger scales make the resulting uncertainty in the large-scale flux estimate difficult to quantify.

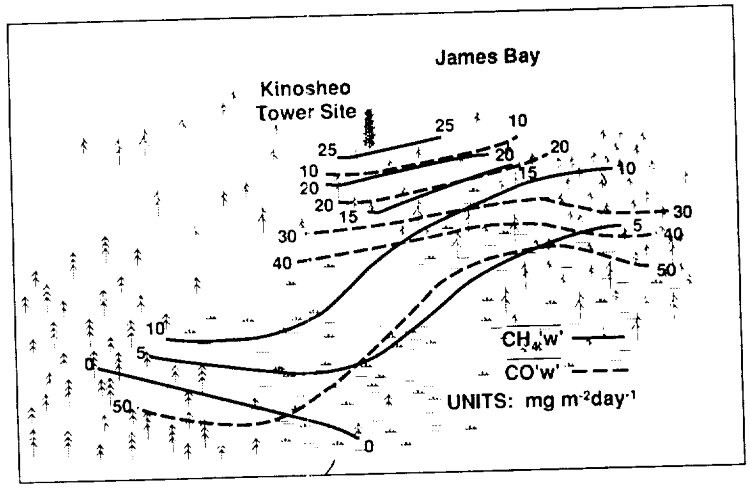

Airborne measurements of vertical flux (emission rate) of carbon monoxide and methane obtained during NASA ABLE-3B experiment over Hudson Bay Lowlands of Canada.

Airborne regional measurements of O_3, CO, and CH_4 emission/deposition rates were obtained over the Hudson Bay Lowlands (HBL) and northern boreal forest regions of Canada during July and August 1990 as a result of the National Aeronautics and Space Administration (NASA) Atmospheric Boundary Layer Experiment (ABLE-3B) program. Since the relative error of the airborne CH_4 flux measurements can be estimated, these data provide an excellent basis for estimating the associated uncertainty in large-scale flux estimates obtained from extrapolation procedures.

Regional measurements of the surface flux of CO and CH_4 obtained over the HBL during the ABLE-3B experiment are provided in the figure (units of the CO and CH_4 flux contours are mg m^{-2} day^{-1}). The data indicate that more productive CH_4 regions are located near the shore of the James Bay. Serendipitously, large CO fluxes were observed in the inland regions of the same study area in the HBL, as indicated in the figure. The explanation for these large CO fluxes is not currently well understood, but may be a result of either direct emission from the underlying vegetation or a product of the oxidation of naturally emitted hydrocarbons. Based on the results of this work and an extensive ground sampling network throughout the HBL, the role of the HBL in the global CH_4 budget had to be reassessed. Previous estimates, which were based on an extrapolation of CH_4 flux measure-

ments made in the peat fields of Minnesota, placed the contribution of the HBL to the global CH_4 budget at ≈7.5 Tg yr^{-1}. Current estimates indicate that the contribution is ≈0.5 Tg yr^{-1}. These results indicate that in situ airborne flux measurements provide valuable information on scales that are directly applicable for large-scale global climate change models. **(John A. Ritter, 45693, John D. W. Barrick, and Catherine Watson) Space Directorate**

Airborne Lidar Measurements of Ozone and Aerosols Over Tropical Atlantic

The Langley Research Center airborne differential absorption lidar (DIAL) system was operated from the Ames Research Center DC-8 aircraft to obtain distributions of ozone and aerosols in the troposphere over the tropical Atlantic during September and October 1992. This investigation was conducted as part of the NASA Global Tropospheric Experiment (GTE)/Transport and Atmospheric Chemistry near the Equator—Atlantic (TRACE-A) field experiment to determine the source of high ozone that occurs in the tropical Atlantic between Africa and Brazil during the burning season, which is primarily from June to October. The airborne DIAL system made simultaneous measurements of ozone and aerosol profiles above and below the DC-8 along the flight tracks. The DIAL-derived atmospheric cross sections of ozone and aerosol distributions from the surface to the tropopause level were used to provide the large-scale perspective on the state of the atmosphere and its composition.

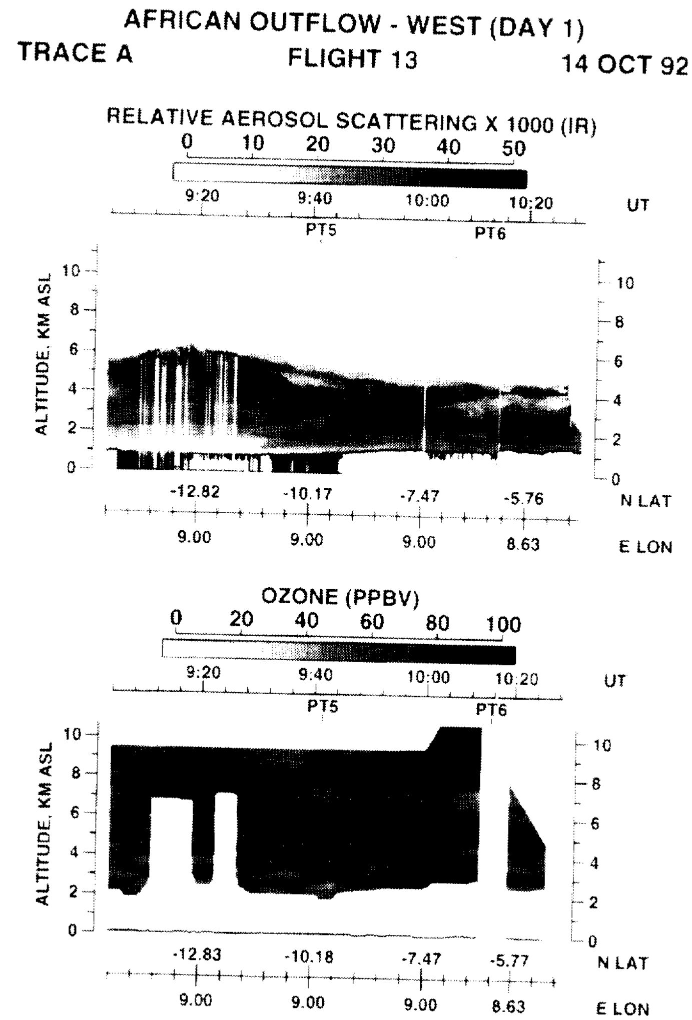

Airborne lidar measurements of aerosol (top) and ozone (bottom) distributions over the tropical Atlantic west of Angola on October 14, 1992. (Original of figure in color; contact author for more information.)

During TRACE-A, the airflow over the tropical Atlantic in the Southern Hemisphere was predominantly from the east (Africa) in the lower troposphere (below ≈8 km altitude) and from the west (Brazil) in the upper troposphere. The convective storms in Brazil transported gases in the extensive fire plumes from near the surface to the upper troposphere, where ozone was photochemically produced and advected eastward over the Atlantic. In central Africa, the fires were widespread, and in the absence of convective storms, the fire plumes were advected at low altitudes (below ≈6 km) over the Atlantic. Airborne DIAL measurements showed considerable variability in ozone and aerosol distributions and a strong dependence on the transport of air masses from

regions associated with biomass burning. There was a positive correlation between ozone and aerosols found downwind of biomass burning regions that were not involved in convection. The degree of photochemical ozone production in the plumes appeared to be dependent on the age of the plume. High ozone (>75 ppbv) was observed in the plumes below 6 km, and in the upper troposphere, ozone frequently exceeded 100 ppbv from photochemical ozone production in outflows from Brazil and from stratospheric air transported into the troposphere in intrusion events. The airborne DIAL data were used to help determine the relative contribution of the various processes to the buildup of high ozone over the tropical southern Atlantic.
(Edward V. Browell, 41273)
Space Directorate

Global Surface Albedos Estimated From ERBE Data

Knowledge of the surface albedo and its changes has important applications in the study of climate, ecology, land use, and agriculture. The only practical method for obtaining surface albedos at desired spatial and temporal scales over the entire globe is to estimate them from satellite measurements. Scattering and absorption by the intervening atmosphere can cause large differences between albedos at the surface and those measured at the top of the atmosphere by satellites; thus, atmospheric conditions must be accounted for as accurately as possible to convert top-of-the-atmosphere albedos to bottom-of-the-atmosphere (surface) albedos. Four atmospheric parameters were needed for this conversion. Water vapor and ozone burdens were obtained from the NOAA-9 Tiros Operational Vertical Sounder (TOVS), surface pressures were annual mean values (primarily a function of surface height), and aerosol properties were obtained from the World Climate Research Program (WCRP) estimates.

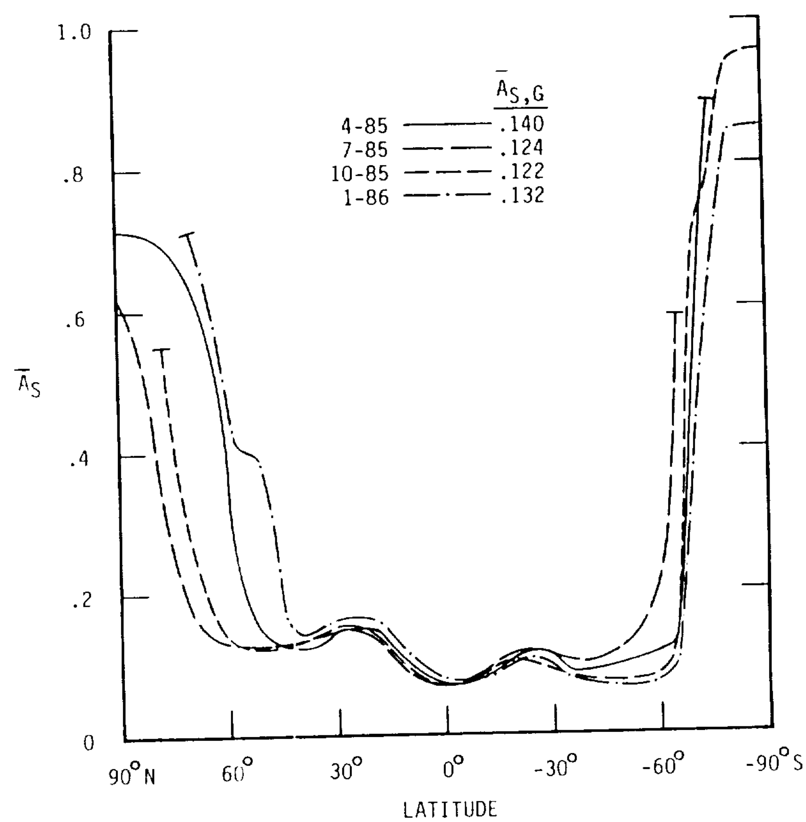

Zonal surface albedos.

The Earth Radiation Budget Experiment (ERBE) provided clear-sky, monthly averaged, broadband albedos for each of 10 368 global regions (2.5° latitude × 2.5° longitude). These albedos were converted into surface albedos, and the zonally averaged values for the midseason months are given in the figure. The north polar zones clearly illustrated the effect that seasonal ice/snow coverage has on surface albedos with winter-to-summer differences as large as 0.5 at 60° to 70°N latitudes. There is only a small seasonal effect from 40°N to 40°S. The "hump" at 15° to 35°N is caused by the high albedos of the Sahara and Arabian Deserts, and the one at 15° to 30°S is caused by deserts in Australia and southern Africa. Globally averaged surface albedos, shown in the figure, vary from 0.12 to 0.14, and the annual average is about 0.13.
(W. Frank Staylor, 45680)
Space Directorate

Effects of Mount Pinatubo Eruption on Earth's Radiation Budget

Measurements from the NASA Langley Research Center Earth Radiation Budget Experiment (ERBE) were analyzed to determine the radiative impact of the stratospheric aerosols produced by the Mount Pinatubo eruption during June 1991. Normal concentrations of stratospheric aerosols have little effect on the Earth's radiation balance. Increased levels can reduce the amount of sunlight that enters the Earth-atmosphere system, which leads to a cooling of the surface and diminished photosynthetically active radiation. Thus, large volcanic eruptions may affect power and fuel consumption and agriculture over many areas of the globe.

The wide-field-of-view radiometers on the Earth Radiation Budget Satellite (ERBS) have been monitoring reflected shortwave (solar), emitted longwave, and net radiative fluxes over the Tropics and midlatitudes since November 1984. Five-year averages of these quantities for 1985 to 1989 over the area between 40°S and 40°N define the normal or background conditions. The interannual variability of the monthly mean fluxes is approximately 1.5 Wm^{-2} for this zone. Following the Mount Pinatubo eruption, the reflected shortwave flux increased by almost 5 Wm^{-2} during August and September 1991 before gradually returning to background values by February 1993. Longwave fluxes diminished by approximately 1 Wm^{-2}, while the net flux, the amount of radiation absorbed by the planet, decreased by over 4 Wm^{-2}. The net flux was back at normal levels by March 1993. These flux anomalies are well correlated with aerosol measurements taken by National Oceanographic and Atmospheric Administration researchers. The ERBE data were used to validate climate model estimates of the radiative forcing caused by Mount Pinatubo. Additional analyses of the post-eruption flux anomalies indicated that during reentry into the troposphere, the volcanic aerosols alter the microphysical characteristics of cirrus clouds; this altering of characteristics induces a secondary radiative effect.

(Patrick Minnis, 45671)
Space Directorate

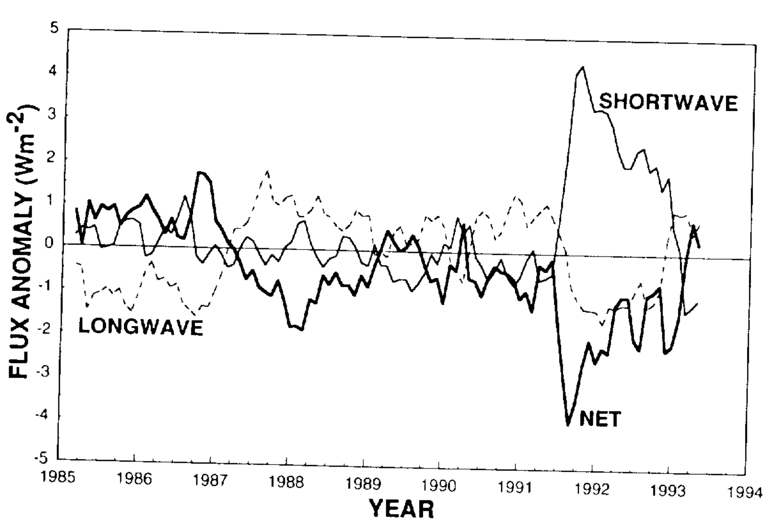

Smoothed monthly mean radiative flux anomalies over 40°S to 40°N from ERBS relative to 1985 to 1989 monthly averages.

Earth Radiation Budget Experiment Observations of Recent ENSO Events

The El Niño/Southern Oscillation (ENSO) is the most prominent large-scale climatological phenomenon on Earth. The region of primary interest in studying the ENSO is in the Tropics, extending from Indonesia to South America; the near-equatorial areas are the most important. ENSO events are associated with abnormal warming of the equatorial Pacific and are accompanied by significant changes in cloudiness and the Earth's radiation fields. ENSO events can cause dramatic climate changes, such as floods and droughts, in the United States and in other areas around the world. The Earth Radiation Budget Experiment (ERBE) solar-reflected and Earth-emitted radiation data were used to study the radiative characteristics of the 1987 and 1992 ENSO events.

The figure presents a time-series plot of the solar-reflected radiative anomaly in the equatorial Pacific relative to a 5-year (1985 to 1989) mean for each month. These data clearly show the strong radiative anomalies associated with both

the 1987 and 1992 El Niños as well as a large negative anomaly associated with the 1988 La Niña (cooling episode) event. Radiative features and variability are closely related to changes in the amount, type, and optical depth of clouds. Strong anomalies in Earth emitted radiation were also observed during the mature phase of the ENSO events. The Mount Pinatubo eruption in 1991 may have affected the development stages of the 1992 ENSO, but the major radiative effects of the volcanic aerosols were greatly diminished by May 1992 and should not interfere with the ERBE observations. The 1992 El Niño is similar in many respects to the 1987 event, but important differences are also evident. The 1992 El Niño is somewhat broader in its temporal extent (possibly because of the effects of volcanic aerosols), and there are indications that smaller anomaly patterns actually began in the previous year but then diminished and did not fully develop until 1992.
(Edwin F. Harrison, 45663)
Space Directorate

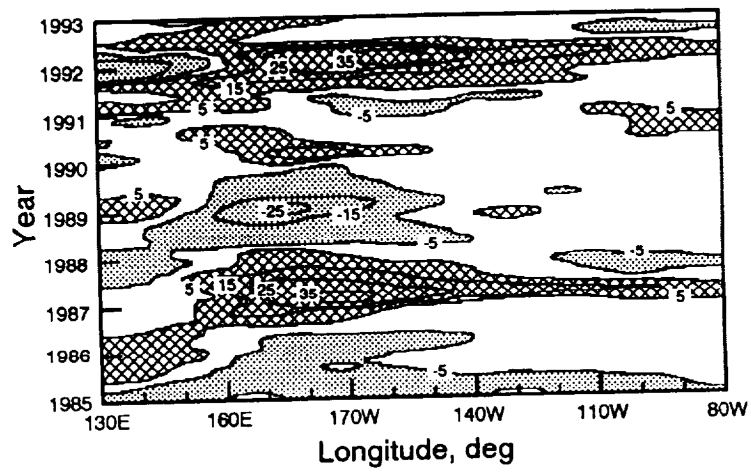

Time series of solar-reflected radiative anomaly from ERBE for 5°N to 5°S latitude. Crosshatched areas are greater than 5 Wm^{-2}; stippled areas are less than -5 Wm^{-2}.

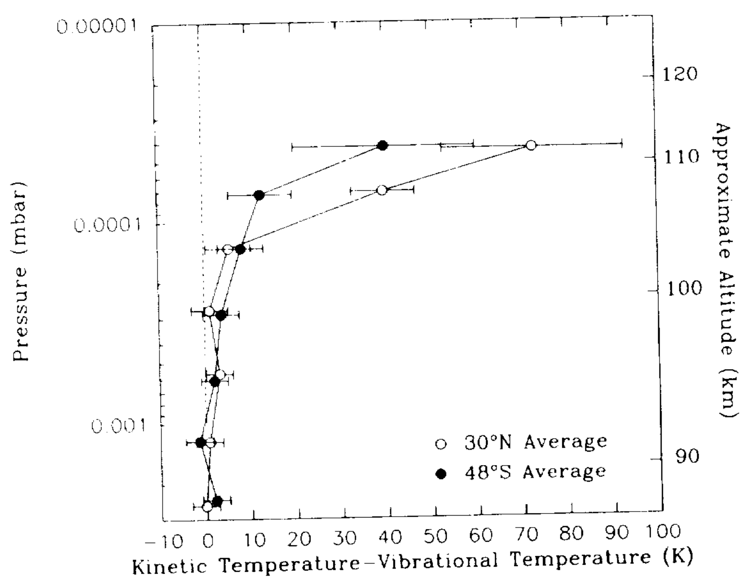

Difference between measured kinetic temperature and measured $CO_2(\upsilon_2)$ vibrational temperature plotted versus atmospheric pressure.

Nonlocal Thermodynamical Equilibrium in Upper Atmosphere Carbon Dioxide

A knowledge of the mechanisms responsible for populating the bending mode (υ_2) vibration of carbon dioxide (CO_2) in the upper atmospheric regions is important in several respects. First, infrared instruments flown on space platforms observe the 15-µm emission from this level in order to retrieve the atmospheric thermal structure. Therefore, departures of its population from that dictated from Boltzmann statistics should be known accurately to retrieve the kinetic temperature. Second, since CO_2 is a major species of not only the Earth's atmosphere, but also of Venus and Mars, determining the radiative cooling by the CO_2 15-µm bands is very important for understanding the energy balance and temperature structure of these terrestrial atmospheres.

Q-3.

The kinetic and CO_2 bending-mode vibrational temperatures shown in the figure have been deduced from analysis of high-resolution infrared solar-absorption spectra of the Earth's upper atmosphere. The spectra were recorded by the Jet Propulsion Laboratory Atmospheric Trace Molecule Spectroscopy (ATMOS) experiment onboard the Spacelab 3 shuttle mission in the spring of 1985. No evidence of deviations from local thermodynamic equilibrium (LTE) are found below 100 km. At higher altitudes, departures from LTE are observable, and the difference between the kinetic and CO_2 (υ_2) vibrational temperature increases to 40 K (48°S) and 70 K (30°N) at 112 km.

These results, obtained in collaboration with members of the ATMOS Science Team from JPL and the University of Liège, Belgium, have been interpreted with a non-LTE radiative-transfer model at the Instituto de Astrofisica de Andalucia, Granada, Spain. The calculations show that the observations can be explained by using a large value for the deactivation-rate constant of $CO_2(\upsilon_2)$ by atomic oxygen. The ATMOS observations lead to CO_2 15-μm-band cooling rates that are larger by a factor of 5 to 10 than those generally accepted until very recently.

(Curtis P. Rinsland, 42699)
Space Directorate

Global Effects of Mount Pinatubo Eruption

After some six centuries of dormancy, Mount Pinatubo in the Philippines (15°N, 121°E) erupted violently in mid-June 1991, resulting in perhaps the largest volcanic perturbation of the Earth's atmosphere since the 1883 eruption of Krakatau. The Pinatubo eruption produced a large quantity of micrometer-sized sulfuric acid aerosol particles in the stratosphere, particles which eventually dispersed over the globe. These particles had a significant impact on the global radiation budget and on stratospheric chemical cycles. For example, tropical stratospheric temperatures soon after the eruption were more than 3 standard deviations warmer than the 30-year mean, and global average surface temperatures decreased by about 1 K during the 18-month period after the eruption. Heterogeneous chemical reactions that were catalyzed by these volcanic aerosols have also been cited as the cause of unusually low ozone levels and high active chlorine levels that were recorded over Antarctica during 1991 and 1992.

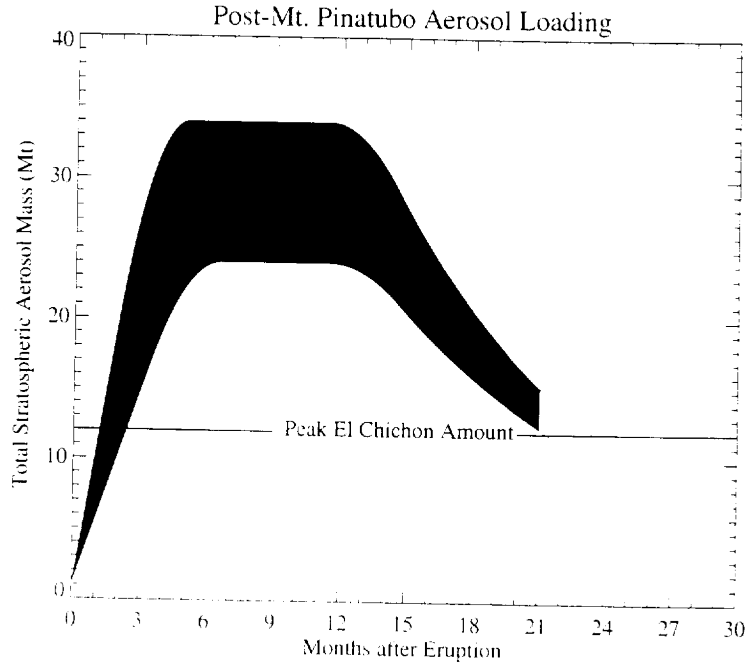

Evolution of global stratospheric aerosol mass (in megatons) following June 1991 eruption of Philippine volcano Mount Pinatubo.

The evolution of the Mount Pinatubo aerosol layer has been monitored globally by the SAGE II (Stratospheric Aerosol and Gas Experiment II) instrument aboard the Earth Radiation Budget Satellite. A quantity that succinctly captures the impact of the eruption is global stratospheric aerosol mass, which can be estimated by combining SAGE II aerosol extinction measurements at several wavelengths. The figure shows that global aerosol mass reached a peak near 30 megatons after the Pinatubo eruption and started to decline (with an e-folding time of approximately 1 year) by mid-1992 as significant numbers of particles began to sediment into the troposphere. By mid-1993, global mass had fallen to about 12 megatons,

which was the peak value observed following the 1982 eruption of the Mexican volcano El Chichon. Barring another major eruption, it is anticipated that the pre-Pinatubo level (less than 1 megaton) will be reached by late 1995 or early 1996.
(Lamont R. Poole, 42689)
Space Directorate

Antarctic Polar Vortex Processes

Field measurements in and theoretical studies of the Antarctic stratosphere have demonstrated that processes that occur in the wintertime polar vortex, such as the formation of polar stratospheric clouds (PSC's), engender chemical transformations that lead to the formation of the springtime ozone hole over the Antarctic continent. Recent analyses of Stratospheric Aerosol and Gas Experiment II (SAGE II) aerosol extinction data show that these same processes have significant effects on the global stratospheric sulfate aerosol budget and on rates at which these sulfate aerosols catalyze ozone destruction.

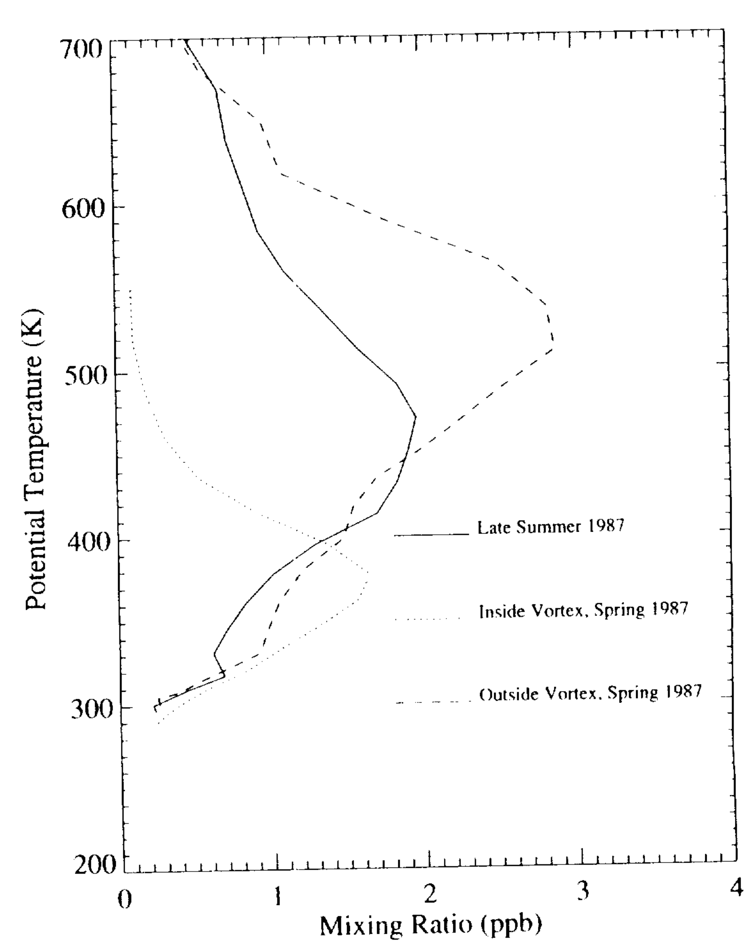

Average mass mixing-ratio profiles of Antarctic aerosol derived from SAGE II extinction measurements in late summer and following spring of 1987.

SAGE II data obtained over the Antarctic show an irreversible downward redistribution of aerosol inside the wintertime polar vortex through a combination of large-scale subsidence and the gravitational sedimentation of polar stratospheric cloud (PSC) particles. The figure compares average aerosol mass mixing-ratio profiles from the austral late summer and following spring periods of 1987. The peak in the springtime profile inside the vortex appears at a potential temperature about 80 K lower than that of the peak during the previous summer. This change corresponds to about a 5-km drop in altitude over the winter. On a yearly basis, it is estimated that some 5 to 7 percent of the total stratospheric aerosol mass is transported downward across the 400-K isentropic surface within the Antarctic vortex. Once below this level, the material can be freely advected to lower latitudes. Since some of the aerosol is transported to levels near the tropopause, exchange processes such as tropopause folds can then move the aerosol irreversibly into the troposphere. The Antarctic polar vortex thus plays a significant role in cleansing the stratosphere of particles during both ambient and postvolcanic periods.
(L. W. Thomason, 46842)
Space Directorate

Heterogeneous Chemistry on Stratospheric Aerosols

Eight years of nitrogen dioxide (NO_2) data collected by the spaceborne SAGE II (Stratospheric Aerosol and Gas Experiment II)

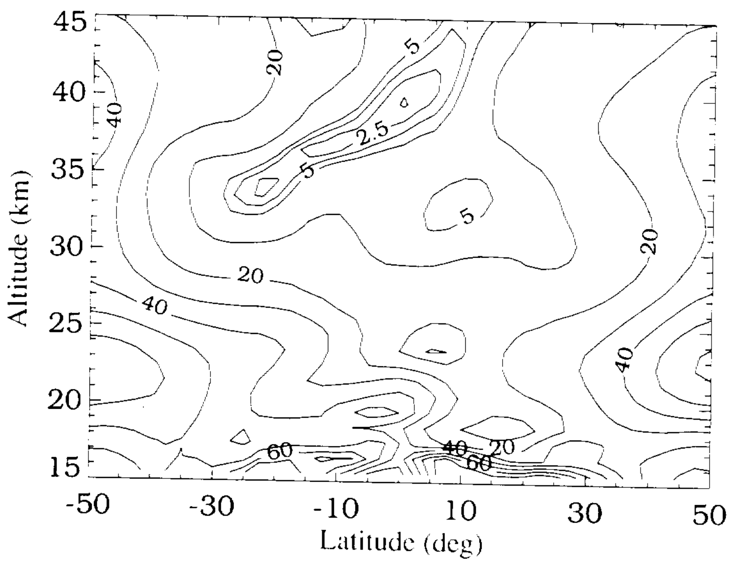

Annual cycle of NO_2 as observed by SAGE II expressed as a percentage of the mean as a function of latitude and altitude.

are being used to test the accuracy of photochemical models. Two-dimensional photochemical models are used worldwide in the assessment of man's impact on the chemistry of the atmosphere and Earth's climate. Recently, modelers under the auspices of the NASA High Speed Research Program were brought together to test the accuracy of their models against each other and actual observations. The SAGE II NO_2 data played a prominent role in this intercomparison and led to improvements in the models.

SAGE II provides the only long-term set of measurements of NO_2 in the stratosphere. These data were used to produce a seasonal climatology of stratospheric NO_2. The figure shows the amplitude of the annual cycle of NO_2 expressed as a percentage of the mean as a function of latitude and altitude. The hemispheric asymmetry near the equator in the 30- to 40-km region is due primarily to dynamics in this region. The large-amplitude seasonal variations in the lower high-latitude stratosphere are caused by seasonal changes in the photochemistry. Of the 10 models in the intercomparison, only 3 reproduced the observed hemispheric asymmetry, indicating that they have captured the subtleties of the dynamics in this region. All the models underestimated by about a factor of 2 the observed high-latitude amplitudes when only the normal-gas phase chemistry was included. However, when the models included heterogeneous-phase chemical reactions on stratospheric aerosols, the models and observations agreed well in the high-latitude lower stratosphere. The aerosol climatology used in the models was also based upon SAGE II data that were representative of a relatively clean stratosphere that was unenhanced by volcanic eruptions. This inclusion of heterogeneous chemistry also improved the model's agreement with nitric acid measurements. These heterogeneous reactions transformed the active nitrogen species, such as NO_2, into relatively inert species and were thought only to be important in the chemistry of the Antarctic ozone hole. This study demonstrated that these reactions are important and occur globally on the background stratospheric sulfate aerosols.
(Joseph M. Zawodny, 42681)
Space Directorate

SEDS End Mass Instrumentation

In March 1993, the Small Expendable Deployer System (SEDS) successfully deployed an instrumented End Mass at the end of a 20-km long tether. The End Mass instrumentation was a self-contained data system that was designed to measure the End Mass orbital dynamics, process and store these measurements, and transmit them to global receiving sites throughout the SEDS mission. This mission, which lasted about 1 1/2 orbits, included tether deployment, swing of the End Mass to local vertical, tether cut, and reentry into the Earth's atmosphere.

A three-axis load cell, three-axis accelerometer package, and three-axis magnetometer were incorporated as the primary sensors to measure tether tension, End Mass accelerations, and End Mass orientation with respect to the Earth's magnetic field. Circuits were developed to condition these sensor outputs to obtain the high-quality signals. This included electronic filtering and amplification (up to a gain factor of 40 000) of the sensor

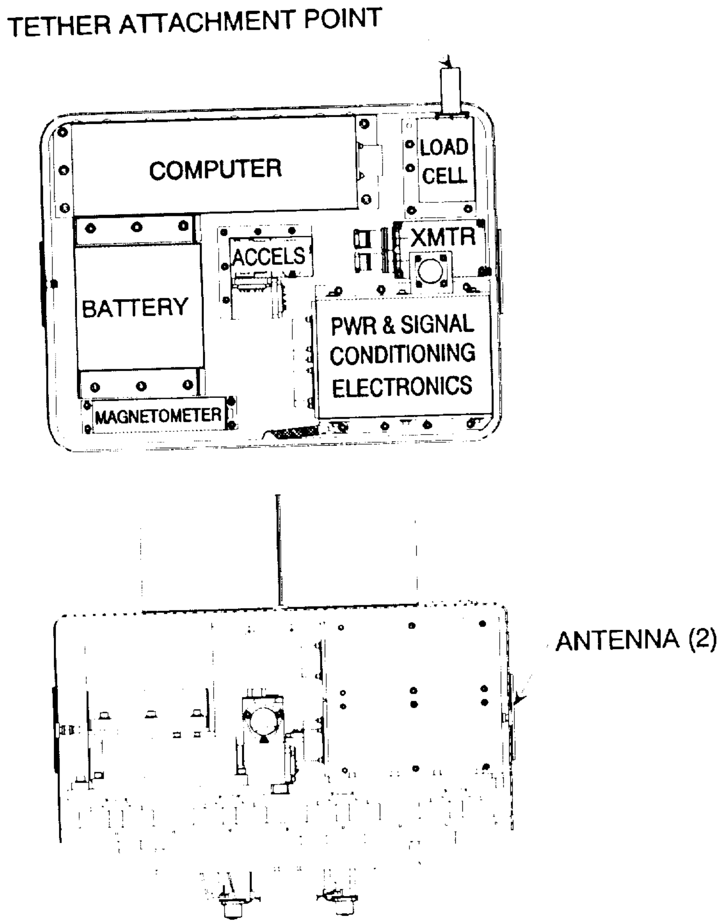

SEDS End Mass payload.

outputs with stability and linear response to within 0.004 percent of the full range. Firmware was developed for the onboard computer to sample these measurements, build data frames, and implement a pulse code modulation (PCM) stream for transmission of the data. The End Mass contained an S-Band transmitter and omnidirectional antennas for transmission of the PCM stream. The data-transmission scheme was developed to store the acquired flight data for periods of 6636 seconds before loss. These data were continuously sampled and retransmitted in a fashion that assured reception of all mission data, even though the End Mass telemetry signal was only intermittently received during the mission.

High-quality mission data were collected for 7791 seconds and are being analyzed. These data, combined with ground-based and deployer-derived data, will give a complete picture of the tether and the tethered End Mass dynamics. A second mission is scheduled for the spring of 1994.
(John K. Quinn, 41678)
Electronics Directorate

Facilities

RESEARCH AND
TECHNOLOGY

Develop, maintain, and operate national facilities for aerospace research and for industry and Department of Defense development support

Thermoelectric Devices for Thermal Instrumentation Enclosures

Electronically scanned pressure (ESP) sensors are used throughout NASA Langley Research Center in various wind tunnels to provide fast, reliable, and accurate pressure measurement. The ESP sensors have a thermal sensitivity of 0.04 percent FS/°C; therefore, a stable thermal environment is required for optimum performance. The National Transonic Facility (NTF) imposes unique temperature control challenges for the ESP sensors because of the tunnel's −150°C to 60°C and 9 atmospheres operating environment. No method currently in use provides for sensor cooling when tunnel conditions are above ambient temperature; they only provide for heating capabilities during the below-ambient tunnel runs. Because of these shortcomings, a thermal instrumentation enclosure to house an ESP sensor was designed using thermoelectric (TE) devices as heat pumps. The enclosure consists of an aluminum box encased in LAST-A-FOAM 9515 high-density insulation foam. To provide heat removal during the cooling function of the thermoelectrics, a finned aluminum heat sink was placed on the bottom of the packages. The thermoelectric device is a semiconductor-based electronic component that functions as a small heat pump. By applying a low-voltage dc power source, heat will be moved through the module from one side to the other. The phenomenon, known as the Peltier effect, is reversible; a change in polarity of the applied dc voltage causes heat to move in the opposite direction. Therefore, the device can be used for both heating and cooling. During cold runs, when the TE device operates as a heater, the I^2R effect of the current that is used to drive the TE elements adds to their ability to generate a temperature gradient. The added current causes the TE device to behave like a resistance heater and allows the TE elements to compensate for a temperature gradient of 180°C or more when the cold side is secured to a cryogenic surface. Extensive laboratory testing was conducted along a temperature range of −185°C to 60°C; this testing shows that the prototype enclosure provides ESP sensor thermal stability to within ±0.3°C and reduces thermal error to a negligible level. The prototype was installed into the existing NTF wall-pressure system and successfully operated for 5 weeks over the entire tunnel temperature and pressure range. Using TE devices for thermal-instrumentation-enclosure heat pumps will decrease the requirement for repeated re-zero calibrations of the ESP sensor; this decreased requirement will result in reduced tunnel operating costs and increased data accuracy.

(Mark Hutchinson, 44642)
Electronics Directorate

New Technique Used for Wing-Twist Measurements

A new single-camera technique has been used at the National Transonic Facility to measure the wing twist of a high-speed civil-transport model. An extensive series of wing-twist measurements were made at temperatures from −258°F to 120°F and at pressures from 15 psia to 101 psia. The Mach numbers for these tests ranged from 0.2 to 1.1. Measurements were made on both the baseline and high-lift configurations.

This new single-camera technique uses photogrammetry on digital images to determine 2-D object coordinates in the plane of twist. A 2-D conformal transformation between flow and no-flow object coordinates is then used to determine angle and displacement at various semispan stations. Compared with the previously used two-camera technique, the single-camera technique has less lighting requirements, has a shorter computation time, does not require precise timing synchronization, and is better suited to

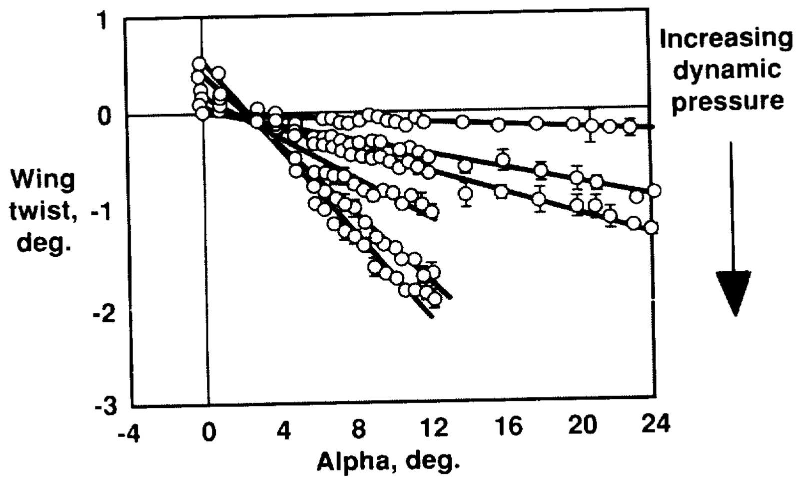

Example of wing twist versus angle of attack for runs at various dynamic pressures.

data reduction in a "semiautomated" mode. Laboratory and tunnel tests have shown that the uncertainty of the single-camera technique is comparable to the two-camera technique.
(A. W. Burner, 44635, and L. R. Owens)
Electronics Directorate and Aeronautics Directorate

Fuzzy-Logic Control of Wind-Tunnel Temperature

The high pressure air distribution system control room provides control of airflow to six research tunnels in the Hypersonic Blowdown Tunnels building. The air is supplied by a high-pressure bottle field, through a series of valves and an electric heater, to the tunnel in operation. A fuzzy-logic controller (FLC) has been developed and applied to the control of temperature processes during the operation of the air distribution system.

The FLC is a rule-based algorithm that provides control of designated temperature processes by using the error between a specified temperature setpoint and the process to be controlled and by using the rate of the controlled process. The feedback signals used by the FLC are processed based on their degree of membership in fuzzy sets. The control objective is to provide desired temperatures in a tunnel settling chamber or in an exhaust trench. The controller must also monitor temperature points between the heater and the settling-chamber temperature, or trench temperature. The temperature at these intermediate points must be kept within prescribed system constraints. The FLC accomplishes this by using feedback from the temperature points and rules that maintain the temperature within the constraints.

The FLC has been successfully applied to the control of temperature processes in the Mach 6 12-Inch High Reynolds Number Tunnel and the nozzle test chamber. Ultimately, it is desired to have the FLC control temperature

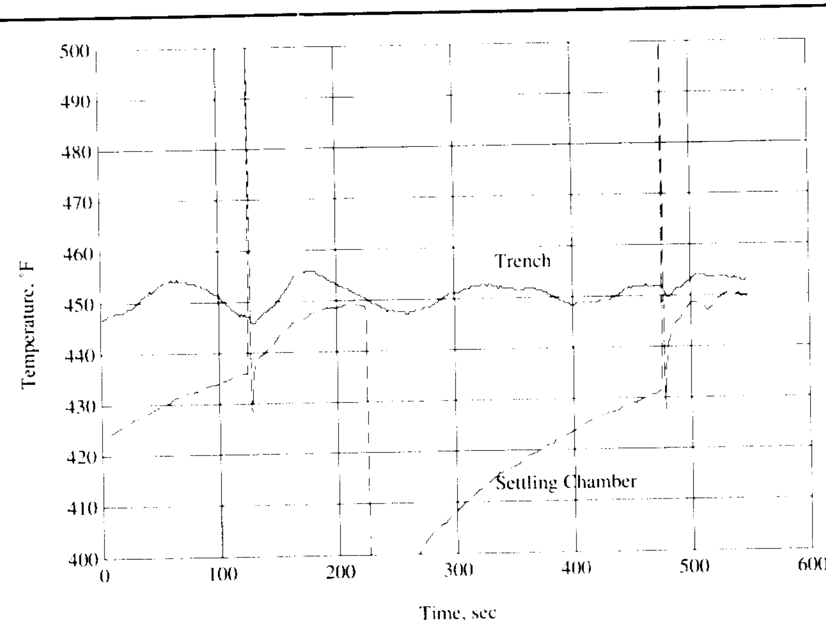

FLC of settling chamber and trench temperatures.

processes for all the tunnels in the Hypersonic Blowdown Tunnels building.
(David A. Gwaltney, 46977, and Gregory L. Humphreys)
Systems Engineering and Operations Directorate

Hypersonic Wind-Tunnel Nozzle Design

The flow quality of most hypersonic nozzles designed by using the classical method of characteristics (MOC)/boundary-layer technique deteriorates as the boundary layer becomes large relative to the inviscid core, which is typically at free-stream Mach numbers (M_∞) greater than 6 to 8. This necessitates using full Navier-Stokes and/or parabolized Navier-Stokes (PNS) computational fluid dynamics (CFD) solvers to determine if the flow uniformity of a MOC/BL designed nozzle is acceptable for performing experimental aerodynamic/aerothermodynamic benchmark studies. Such an approach was used to design a nozzle for the Langley 22-Inch Mach 20 Helium Tunnel that was precision machined, installed, and calibrated over a wide range of reservoir conditions by using a pitot-probe survey rake with previously unheard of resolution; the pitot-probe spacing was 0.125 in. over a 20-in. span to provide the details that were required to calibrate the PNS code. Once calibrated, by refining the grid and modifying the turbulent boundary-layer model, agreement between the PNS solutions and experimental data was excellent throughout the range of conditions analyzed. The figure represents the total pressure ratio across the shock at an axial location slightly downstream of the nozzle exit plane and shows excellent agreement between the experimental and computational results at a representative condition. The flow uniformity provided by this new nozzle was a drastic improvement over the previous nozzle, which was designed and built in the late fifties; however, even more uniform flow is required to perform benchmark experimental studies in the facility.

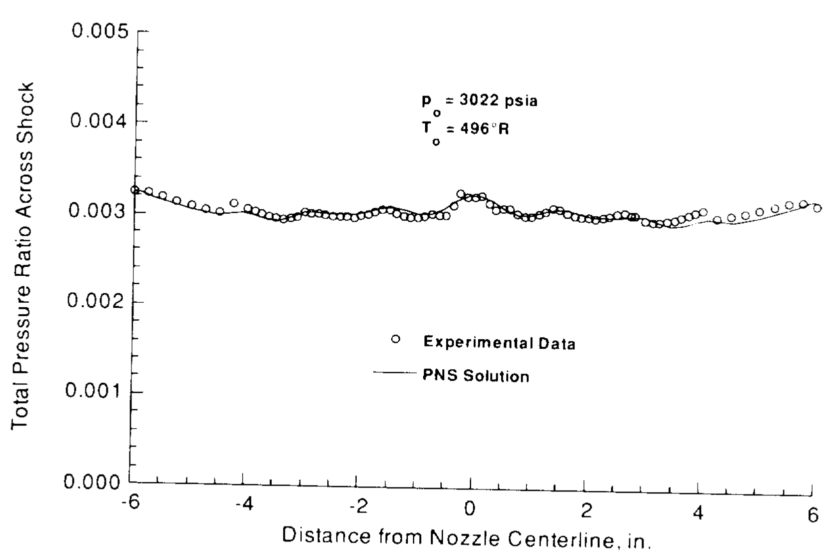

Comparison of experimental and computational data.

Dr. J. Korte (from Langley's Theoretical Flow Physics Branch) and others recently developed a nonlinear least-squares optimization procedure, coupled with a CFD PNS flow solver, that is used to develop an optimum design of the complete nozzle flow field. This new method was used to predict aerodynamic contours for two new nozzles (Mach 14.6 and 20) that are being fabricated for the helium tunnel. The new nozzles will be calibrated in early 1994 to provide the measurements to validate the CFD-based design procedure. The PNS predictions for the two new nozzles show improved expansion characteristics throughout the nozzle, which provides a more uniform flow field at the nozzle exit. If the predictions are proven to be accurate by the upcoming nozzle calibration, the CFD-based optimum design procedure will represent a quantum leap in the design of nozzles for hypersonic wind tunnels.
(Jeffrey S. Hodge, 45237, and John J. Korte)
Space Directorate

Flow-Quality Improvement Hardware for 8-Foot High-Temperature Tunnel

The 8-Foot High-Temperature Tunnel at NASA Langley Research Center (LaRC) is a combustion-driven blowdown wind tunnel.

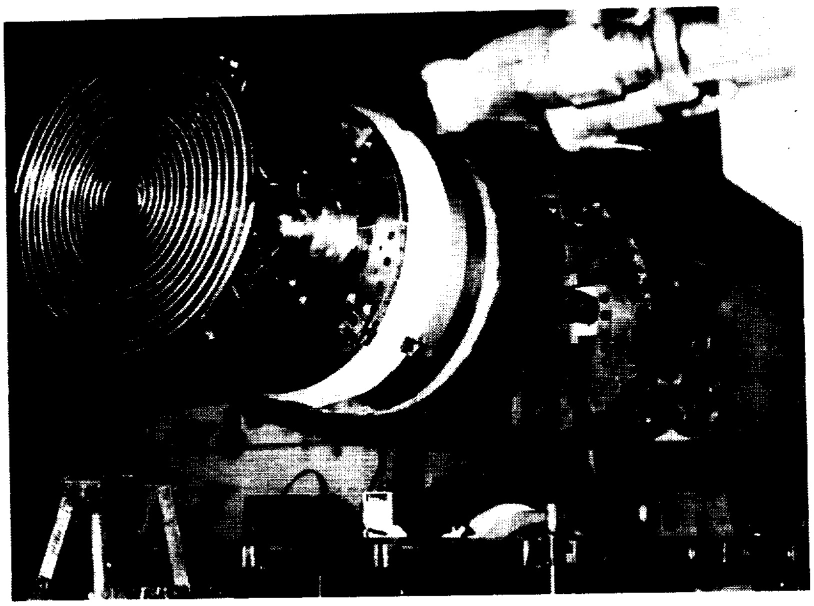

Internal components of 8-Foot High-Temperature Tunnel combustor.

The 8-ft-diameter by 12-ft-long free-jet section is designed to achieve Mach 4, 5, and 7 with true temperature simulation. The combustor has two primary modes of operation: (1) methane and air, and (2) methane and air with oxygen enrichment to raise the combustion-products oxygen content to 21 percent. The first mode of operation is used for aerothermal loads testing and flight weight structural concept verification. The second mode is used to test air-breathing scramjet and ramjet engines.

During checkout, to prepare for the testing of the concept demonstration engine, it was determined that temporal and spatial fluctuations of temperatures and pressure were unacceptable for testing hypersonic air-breathing propulsion systems. A flow-quality improvement team was organized that included members from LaRC and industry. The goal was to provide temperature and pressure variations within 5 percent of the mean flow. The two major recommendations from the team were to install a baffle plate and a resonator plate within the combustor

The main goal for the baffle plate is to provide a more uniform flow of oxygen-enriched air to the spray bar by providing a pressure drop approximately 2 ft upstream of the spray bar. A secondary goal for the baffle plate in combination with the resonator plate is to act as a Helmholtz resonator to absorb temporal oscillations. The goal of the resonator plate is to act as a Helmholtz resonator and dampen out oscillations in the air feed system that are currently at approximately 30 Hz. By removing these oscillations, the combustion process should become stabilized.

A team was then established across Division levels to design, analyze, fabricate, and install the baffle plate and resonator less than 4 months from when they were conceptualized. Concurrent engineering was used to meet the tight schedule. The baffle plate and resonator were delivered within budget and on schedule. After several adjustments to the baffle plate and spray bar, the flow quality fell within acceptable limits.

(Peyton B. Gregory, 47242)
Systems Engineering and Operations Directorate

Expansion of Research Aircraft Ground Station Facility

The need arose for near-real-time processing of data taken by the Orbital Acceleration Research Experiment (OARE) instrument during shuttle flight STS-58 to enable Langley's principal investigator to determine instrument modes, success of on-orbit calibrations, and the general health of the instrument. Timely assessment of specific instrument parameters allows modifications to the mission timeline to enhance the planned measurements (or make them possible).

Two additions/modifications were made to the Research Aircraft Ground Station (RAGS) facility to make near-real-time OARE data processing possible. (1) Interface circuits that can handle the required pulse code modulation (PCM) format and bit rates between the flight control center (which receives the tracking and data relay satellite system (TDRSS) downlink from the White Sands

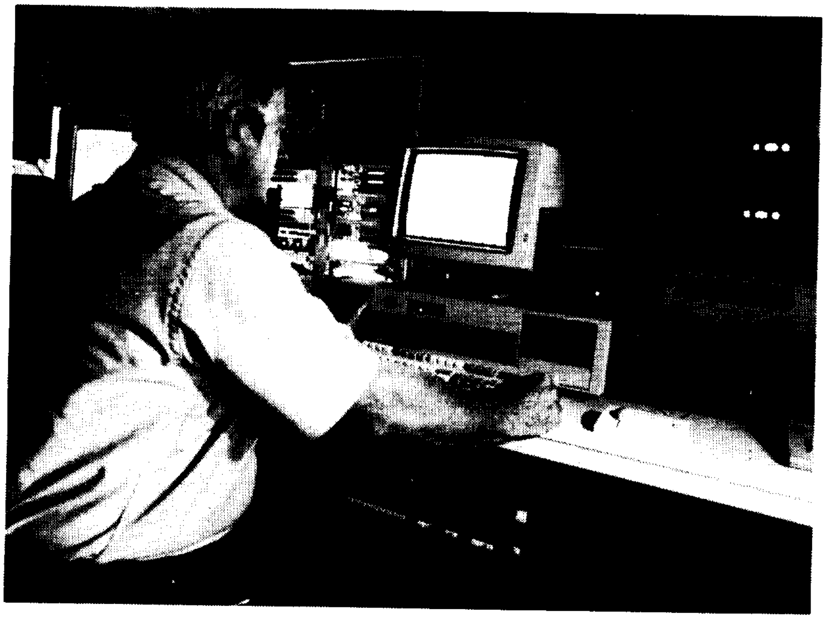

RAGS enhancements in use during STS-58. L-93-12054

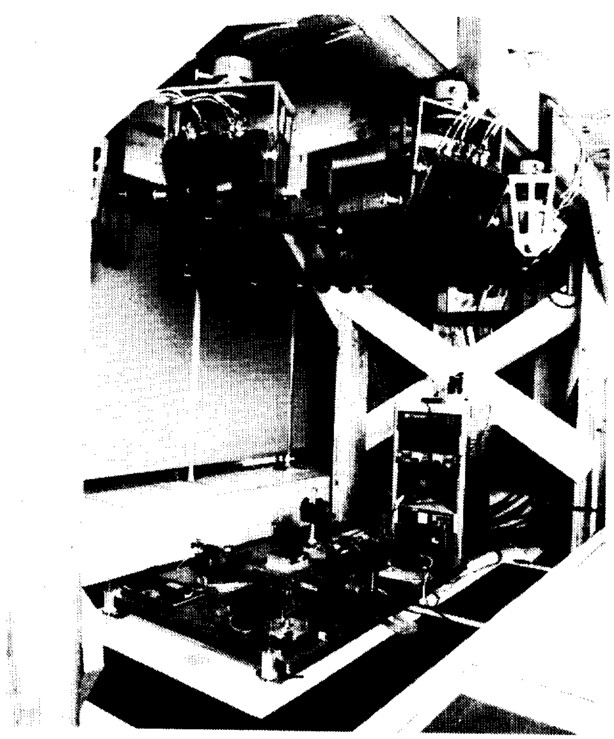

Optical measurement system (OMS) showing laboratory setup for measuring point-tracking accuracy.

Missile Range via satellite) and the RAGS were designed, fabricated, installed, and tested. (2) A PC-based system was developed to read the PCM bit stream and process the data in accordance with OARE formats. This capability enhancement was tested end-to-end in premission validation tests to demonstrate the near-real-time processing capability and provide valuable personnel training prior to the mission. In addition, operational procedures were established that facilitate STS-58 operations and enhance OARE mission success. This capability is a step toward achieving a capability at Langley that could be used for real-time monitoring and control of a broad range of shuttle experiments and space station payloads. This work was done in part under contract with Lockheed Engineering & Sciences Co.
(Herbert R. Kowitz, 41962)
(Electronics Directorate

Optical Measurement System

An optical measurement system (OMS) based on linear charge-coupled-device (CCD) sensors has been designed to determine the position and attitude of a levitated cylinder in six degrees of freedom and to supply this information to the control system of a large gap magnetic suspension system (LGMSS). In the LGMSS, several large electromagnets arranged in a planar configuration levitate a cylindrically shaped element that contains a permanent magnet core. The cylinder is levitated at a distance of 91 mm (36 in.) above the magnets. In order to stabilize levi-

tation and control motion in six degrees of freedom, information on the position and attitude of the suspended element is required. In the OMS, multiple one-dimensional imaging sensors are used to detect small infrared light-emitting diode (LED) targets that are embedded in the surface of the levitated element (see figure). The position and attitude of the cylindrical element are determined from the measured locations of the images in the sensors and transformation equations, which relate the coordinates of the target images in the reference frames of the sensors to the position and orientation of the levitated element in the laboratory reference frame. Rigid body motion has been assumed.

The OMS has been calibrated and experiments have been conducted on the system to evaluate its accuracy. Experiments designed to determine the accuracy of point tracking revealed that the system is capable of determining the x, y, and z location of an individual target within a volume of 10.16 cm × 10.16 cm × 5.08 cm to better than 0.001 cm (0.0005 in.). Results of initial experiments using a model of the levitated cylinder showed the accuracy of the system with a 1°/second yaw rate to be 0.002 cm (0.001 in.) in x_{cm}, y_{cm}, 0.001 cm (0.0005 in.) in z_{cm}, 0.005° in pitch and yaw, and 0.1° in roll. The decreased accuracy of the roll measurement results from the short moment arm or diameter of the cylindrical element. The final system configuration has been designed to operate at a sample rate of 40 samples/second.
(Sharon S. Welch, 46611)
Flight Systems Directorate

RESEARCH AND TECHNOLOGY

Technology Transfer and Commercial Development

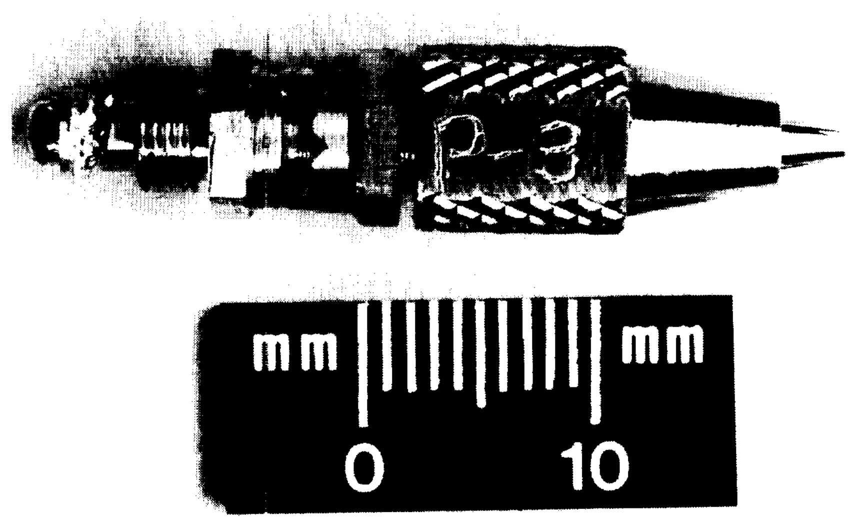

Facilitate the transfer of aerospace-generated technology to the public domain

Surgical Force Detection Probe

A wind-tunnel balance is not the kind of instrument a patient would expect to find in the hands of his or her surgeon in an operating room. Dr. Richard Prass, M.D., of Eastern Virginia Medical School, however, may soon add new meaning to cutting-edge technology. Dr. Prass desired to measure the amount of force that he was applying to human tissue during surgery. A balance is an electromechanical transducer that converts applied forces and moments into electrical signals. A small lightweight balance was designed and fabricated and was then placed within a hand-held cylindrical housing. Various surgical implements can be attached to the balance through one end of the probe housing. The probe is 1/2 inch in diameter and 6 inches in length. Like its wind-tunnel counterparts, this balance is instrumented with standard strain gages.

The strain-gage signals are electrically isolated by signal-conditioning electronics, which also amplify each of the signals. The user is able to perform gain and offset adjustments via front-panel controls, and bar-graph displays provide amplitude information for each of four channels. A personal computer is incorporated into the system for data acquisition, display, and storage.

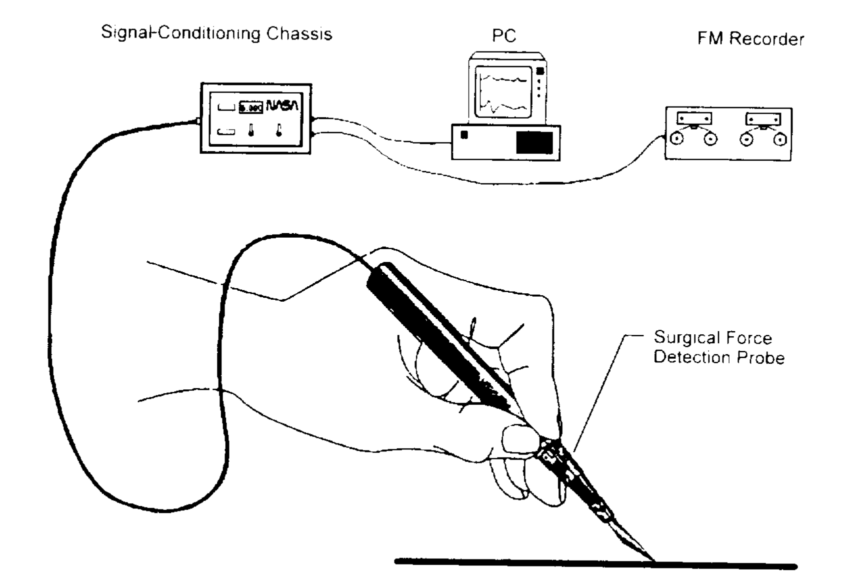

Surgical force detection probe system.

This instrument would allow the documentation of the usual forces that are applied during routine surgical procedures. This type of documentation has never been reported. A comparison among experienced surgeons and those in training would then be possible. Such data may provide feedback that may be effectively used during residency training. When used in conjunction with interoperative neurological monitoring, the instrument would allow correlation of specifically applied forces to monitored nerves that are responsible for nerve injury. These data may lead to new concepts in nerve dissection that will improve surgical outcome.
(Ping Tcheng, 44717, Paul Roberts, Regina Courts, and Taumi Daniels)
Electronics Directorate

Remote-Data-Logging Groundwater Seepage Meter

The Coastal Groundwater Research Program at Virginia Polytechnic Institute and State University (VPI&SU) is investigating the importance of groundwater discharge and its associated solute load to estuarine and marine environments. Research suggests that groundwater transport of

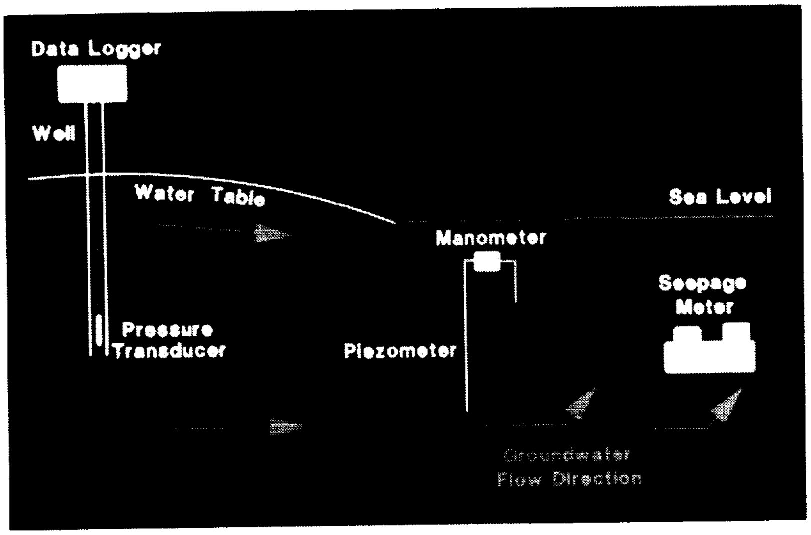

Instrument sampling locations.

contaminants is significant in many coastal regions. Ongoing research for the Environmental Protection Agency Chesapeake Bay Program is aimed at defining and reducing contaminant loadings from groundwater to the Chesapeake Bay system. In order to more accurately measure groundwater discharge volumes and temporal patterns, new methodology was required. Researchers at VPI&SU requested support in the design and fabrication of a remote-sensing instrument to directly measure subaqueous groundwater discharge.

The remote groundwater seepage meter incorporates an onboard data logger and a developed flow-metering and control system. This instrument provides greater time-series data collection and analysis and minimizes problems associated with manual methods, while remaining cost effective. Presently, the remote seepage meter is being utilized by researchers at VPI&SU to investigate groundwater discharge rates in relation to upland and tidal surface water hydrodynamics.
(Harry G. Walthall, 45194)
Systems Engineering and Operations Directorate

Design of Low-Thermal-Conductance Cryogenic Support

A common problem in many designs that are concerned with thermal transfer is limiting the thermal conductance of a structure while maintaining structural integrity. A recent project designed a thermally critical support by using the following methodology. The intent was to design a structure to bridge a 200°C thermal gradient with minimum thermal transfer but adequate structural properties. First, materials were ranked by plotting the ratio of thermal conductivity to strength as a function of temperature (75 to 300 K). The best materials from this ranking were evaluated for availability, cost, and low-temperature fracture properties. The material selected was an Epon 828 epoxy with a balanced-weave glass-fiber cloth. Several shape concepts were developed, with the purpose being a long thermal path length and a small cross-sectional area. Six shapes were evaluated, four of which are shown in the figure on the next page. These were analyzed by designing them to be thermally equivalent and evaluating failure stress due to static loads, critical buckling stress, and normal modes.

The shape chosen was a tapered circular cone. This shape was then optimized by using NASTRAN to adjust the wall and flange thicknesses to their ideal values. The cone was laid up, and the methods for curing with a machined metal mold were perfected. The fabricated part has survived a thermal soak to 77 K.

This same methodology could be used to design any commercial part that must meet both thermal and structural criteria.
(Ruth M. Amundsen, 47044, and Jill M. Marlowe)
Systems Engineering and Operations Directorate

Evaluative Testing of Adhesives for Cryogenic Applications

Bonding materials for cryogenic use is difficult when the two materials have highly different coefficients of thermal expansion (CTE's). On the Material in

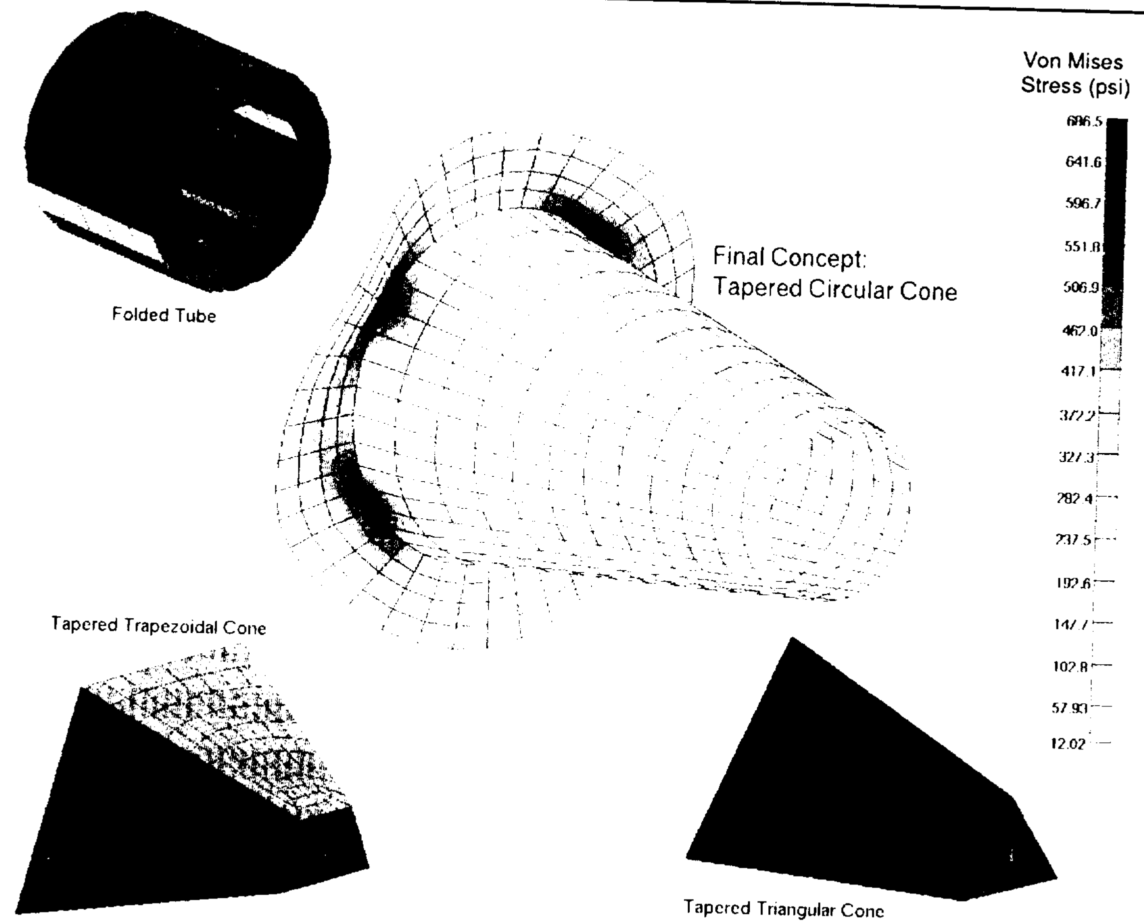

Candidate support designs.

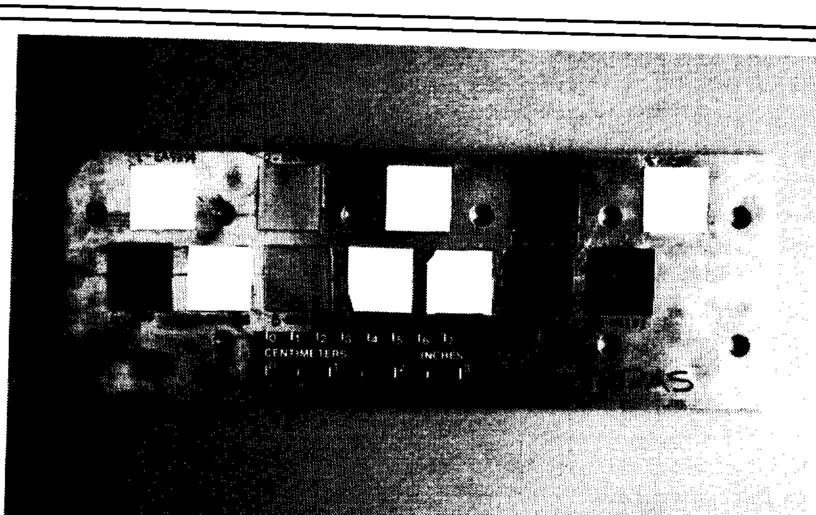

Sample test fixture for epoxy evaluation. L-93-4384

Devices as Superconductors (MIDAS) project, thin ceramic boards are to be bonded to a metal fixture. There are superconductor samples on the boards, thus the fixture must withstand cryogenic temperatures (80 K) without damaging the boards. Evaluation testing was performed on several adhesives to assess their performance in bonding ceramic boards to two different metals. Silicon dioxide (SiO_2), with a CTE of 0.5×10^{-6}/K, and Yttria Stabilized Zirconia (YSZ), with a higher CTE, were bonded to aluminum 6061 (CTE = 23×10^{-6}/K) and copper (CTE = 17×10^{-6}/K). Seven

different adhesives were used: Hysol EA 9394 and XEA 9361, Eccobond 285, Epon 828, Scotchweld 2216, Stycast 2850FT, and Tra-bond 2151.

The bonded and cured samples were soaked at 77 K for 3 days. On the aluminum fixture, the only successful adhesive was XEA 9361; the bonds for both ceramic types survived. On the copper fixture, XEA 9361, Epon 828, and Stycast 2850FT all bonded both ceramics successfully; however, Epon 828 stressed the SiO ceramic to failure. The EA 9394 and Tra-bond 2216 successfully bonded the YSZ ceramic on copper.

For general use, the XEA 9361 was most successful in maintaining bonds across high CTE mismatches during exposure to cryogenic temperatures. The Stycast 2850FT is currently preferable for aerospace use, since it passes the NASA outgassing requirements. Either of these adhesives could be used for commercial applications that require bonds of high-CTE to low-CTE materials at cryogenic temperatures.
(Ruth M. Amundsen, 47044, and Charles E. Jenkins, Jr.)
Systems Engineering and Operations Directorate

A Novel Multiphase Fluid Monitor

A gauging system has been developed for monitoring the quantity and flow rate of slush hydrogen (SLH_2) onboard the National Aero-Space Plane (NASP). It is based on the fact that the mass-attenuation coefficient of an absorbing medium for electromagnetic radiation is independent of the phase of the absorbing medium. We selected Cd^{109}/Ag^{109} X rays (22.6 keV) as the radiation whose attenuation and mass-attenuation coefficient would provide the desired information about the quantity and composition of SLH_2 fuel at any time.

Actually, Ag^{109} radionuclide produces two close-lying X rays ($K\alpha$ at 22.1 keV and $K\beta$ at 25.0 keV) whose relative intensity ratio (R) is 100/19. Since attenuation coefficients of X rays are strongly dependent on their energies, it is expected that the value of R will change as the X rays penetrate through an absorber. Furthermore, the value of R will be different for different phases of an absorber. For example, the value of R after passing through a certain thickness of ice will be higher than its value after passing through the same thickness of water, because the density of ice is lower than that of water. These results are illustrated in the figure. Obvious technical spin-offs of these results lie in cardiovascular monitoring and agricultural frost-damage monitoring technologies.

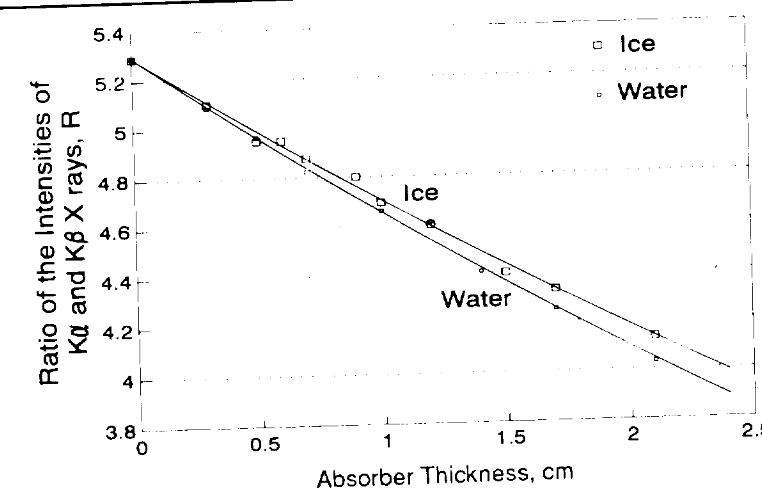

Comparison of R values for ice and water.

(Jag J. Singh, 44760, Danny R. Sprinkle, S. V. N. Naidu, and Abe Eftekhari)
Electronics Directorate

Interactive Surface Grid Quality Analysis

A surface analysis code (SurfACe) has been developed to help researchers assess surface grid quality of computational grids used in CFD analyses. Anomalies in grids used in these analyses can result in flow solutions that are not consistent with the true flow-field characteristics of the vehicle. SurfACe can be used to highlight grid generation errors that are not easily detected in wireframe or shaded representations of a grid and can thereby increase the cost effectiveness of CFD as an aircraft design tool.

V22 surface and unstructured surface grid displayed within SurfACe. (Original of figure in color; contact author for more information.)

SurfACe can be used to evaluate both structured and unstructured surface grids on a number of grid quality parameters that indicate changes in surface curvature and changes in surface grid quality. Surface curvature parameters related to grid smoothness are: the magnitudes of the x-, y-, and z-components of the surface normal vectors, first and second derivatives of these vectors, and the normal, Gaussian, and mean curvatures. Grid quality parameters related to grid resolution are: surface grid cell area, orthogonality, and aspect ratio. Each parameter is displayed on the geometry by using a variable-color map. The displays can be viewed dynamically with the rotation, translation, and scaling controlled either by the keyboard or by the mouse. Wireframe, hidden-line, and shaded views of the surface grid are also available.

SurfACe is an interactive surface grid analysis program with a graphical interface written in ANSI standard C that runs on Silicon Graphics Iris 4D workstations. SurfACe accepts both binary and formatted PLOT3D, GRIDGEN, LAWGS, and unstructured FAST surface grid files.

This work has been done under contract with Computer Sciences Corporation.
(P. A. Kerr, 45782)
Electronics Directorate

Proposed Design for Carriage Wheels of Aircraft Landing Dynamics Facility

The existing wheels of the high-speed carriage at the Aircraft Landing Dynamics Facility (ALDF) contain a rubber insert in the outer rim. After considerable use, the rubber tends to squeeze out of the sides of the wheel, increasing the effort needed to maintain the wheels at operational levels. To eliminate this problem, a new solid wheel design was proposed by the ALDF Project Office. The objective of this analysis was to compare the performance of the existing carriage wheel with the proposed design.

The basic approach of the study was to analyze both wheels under similar loading conditions. The results were then compared to evaluate the relative performance of the new design. Finite-element modeling (FEM) techniques were used to construct detailed analytical models of both wheel designs. Closed-form solutions were used to verify the analytical methods. Because some closed-form methods cannot be applied to complex cross sections, a simple annular disk was also modeled and was used to help interpret the FEM results.

The load cases were selected to represent the various loading conditions that the actual wheel can experience during a carriage run. These conditions included spin loading, static and dynamic loading, slipping during launch, and misalignments from the rails or bearings. A modified Goodman diagram was used to address fatigue. The analysis showed that the proposed new design meets all criteria.

The driving factor behind the rubber insert in the existing wheels is the flexibility. A rigid wheel, such as the proposed design, develops contact stresses that exceed the ultimate strength of the material when misaligned. However, this stress is quantified by the surface strength of the material, which is based on the Brinell hardness. Allowable contact stress calculations predicted the life criteria would be met.

From the analysis, it was concluded that the wheels can be fabricated from the proposed design. Experiments should be performed to assess the amount of vibration that is transferred to the carriage by each of the wheels and to confirm that the change in design does not interfere with the research being performed on the carriage.

(Regina L. Spellman, 47244)
Systems Engineering and Operations Directorate

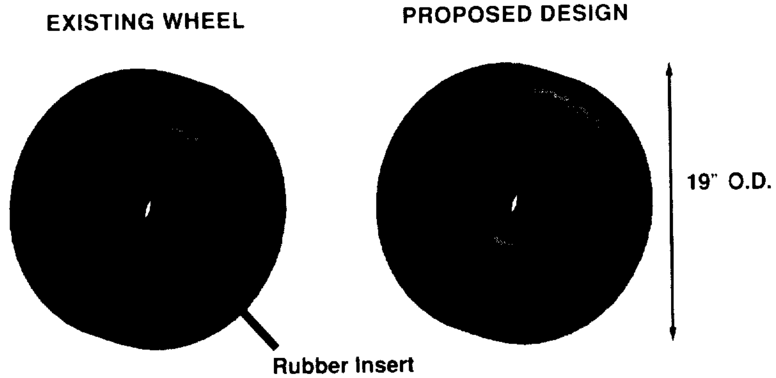

Existing and proposed designs of ALDF carriage wheel.

Structural Modeling and Analysis of Aortic Aneurysm From CAT Scan Data

The feasibility of utilizing patient CAT scan data to generate structural finite-element models with which to predict the stresses, and potential failure sites, within aortic aneurysms was studied. Aortic aneurysms are abnormally enlarged areas of the main blood vessel that supplies blood to the body and legs. Medical-community interest in this research is motivated by the fact that rupture of aortic aneurysms is the 13th leading cause of death in the United States—over 15 000 deaths per year. Because even corrective surgery entails risk to patients, a diagnostic tool that would predict the risk of uncorrected aneurysms is desired. In the present study, a margin-of-safety indicator that was developed from the locally computed, maximum principle stress and the failure stress of typical aortic tissue is investigated as a possible risk indicator for an uncorrected aneurysm.

The CAT scan data of a patient who was examined prior to a suc-

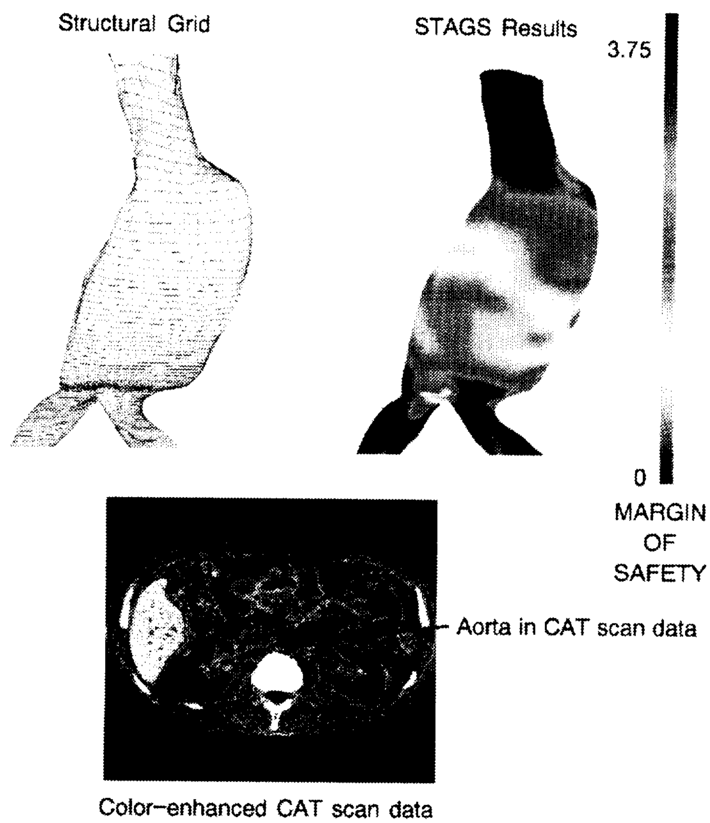

Stress analysis of an aortic aneurysm using CAT scan generated surface geometry.

cessful repair of an aortic aneurysm were obtained as a series of image slices through the patient's body at 5-mm intervals. The contents of each slice is a representation of the local density within the patient's body. Because the structure of the aorta is only identified by its contrasting density with neighboring tissue, image processing techniques were utilized to detect the edges of the aorta cross sections. To help assure the accuracy of the data, a medical doctor helped identify the structures within the CAT scans. The cross-section data generated were then used to develop a structural model grid. The grid was utilized within a finite-element structural-analysis computer code to determine the stresses due to internal pressurization in a geometrically nonlinear manner. The margin of safety indicated in the figure shows the computed results where zero margin corresponds to predicted failure. Because of the sparseness of CAT scan data in the region, the area with the low margin of safety near the branching of the two iliac arteries is not considered significant. However, the areas with the smallest margin on the upper left side of the aneurysm are probable failure sites.
(Stephen J. Scotti, 45431)
Structures Directorate

Externally Accessible Pressure Instrumentation Insert

The purpose of this device is to provide a means of installing a dynamic pressure measurement sensor into a closed composite structure with external accessibility. This design produces minimal surface disturbance and requires a small internal volume. The designated application is for wind-tunnel testing of a dynamically scaled wing. Current methods of installing this sensor require internal accessibility. Since the pressure sensors may get damaged during testing or handling, they should be easily replaceable without disassembly of a complex structure. For many applications, it may be impossible to disassemble the structure without modification of dynamic characteristics. This new design provides a means of replacing defective sensors with no structural disassembly and with minimal aerodynamic surface disturbance.

Excluding the transducer, there are four components to this assembly. The encapsulated disk (–1) is captured in the composite layup. After the composite is cured, the skin is through drilled and counter-bored using a predrilled hole in the disk for location. The 1/4-turn holder (–2) is permanently bonded into (–1) with epoxy in the desired orientation. The pressure sensor (–5) is bonded into the Kulite holder (–4) with room-temperature-vulcanizing (RTV) rubber. This assembly is inserted into (–2), passing lead wires and a calibration tube through preexisting conduit under the aerodynamic surface. The 1/4-turn orifice

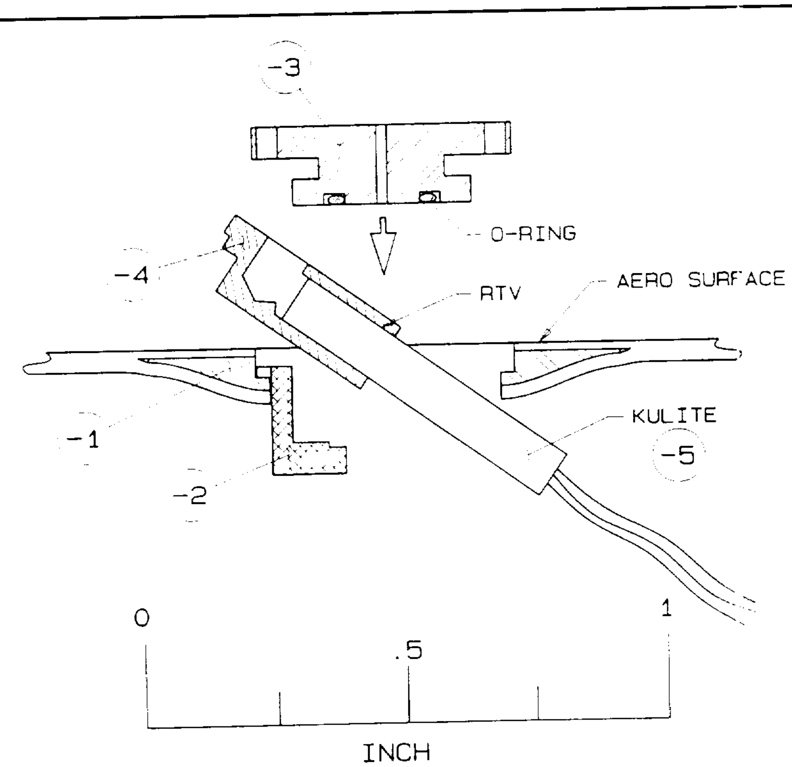

Instrumentation insert assembly.


Wing-tip boom for OV-10A research aircraft. L-93-01272

(−3) is installed and rotated 90° into position by using a spanner-type tool. A commercial O-ring seal between (−3) and (−4) prevents leakage at this interface. Item (−3) is locally contoured to the external surface.

Replacement of damaged sensors will consist of removing (−3) with the installation tool, installing a working sensor into (−4), and re-installation of the parts as before. Little or no additional work will be required to return the apparatus to "as new" condition.
(Christopher M. Cagle, 47140)
Systems Engineering and Operations Directorate

Wing-Tip Boom for Flight Application on OV-10A Research Aircraft

The Research Aircraft Support Section at Langley Research Center required a lightweight, high-strength, wing-tip boom for flight application on the OV-10A research aircraft. The boom's geometry and stiffness had to be such that it did not cause amplification of any aircraft- or velocity-generated vibrations, since it was to be used in the study of aircraft-wake vortices. The Composites and Models Development Section constructed a hollow graphite-epoxy boom, approximately 8-ft long, with an outside diameter of 4.5 in. that tapered down to 2.25 in. The boom was laid up on an aluminum mandrel by using 36 plies of graphite-epoxy material that was precut to conform to each ply geometry. The geometry was a 0°, +60° layup with a vacuum debulking process between each second

ply. This process netted a smooth outside diameter with no post-cure machine work. After the prepreg layup operation was completed, a shrink tape was applied circumferentially to increase molding pressure to the vacuum-bag autoclave pressure cure cycle. The process that was developed by the technician allowed for producing a tapered structure with unique variations on accepted layup techniques.
(William D. Lupton, 45484)
Systems Engineering and Operations Directorate

Vibratory Stress Relief Welding Technology

Vibratory stress relief welding technology was used when doing extensive full-penetration welding of 1.5-in-thick reinforcement bars for the model injection system of the 8-Foot High-Temperature Tunnel (8-Foot HTT) test facility. Critical alignment of support rails in the tunnel mandated that a retrofit be accomplished that would maintain the critical straightness without having the real system removed for welding or stress-relieving processes.

The use of strategically placed welds during assembly helped to provide accurate alignment and integrity. Vibratory weld conditioning and subsequent stress relief of all parts provided for sound structural members throughout the fabrication process. The vibratory conditioning as weld metal was deposited enhanced the bead contour and eliminated porosity, resulting in a reduction of residual weld stresses.

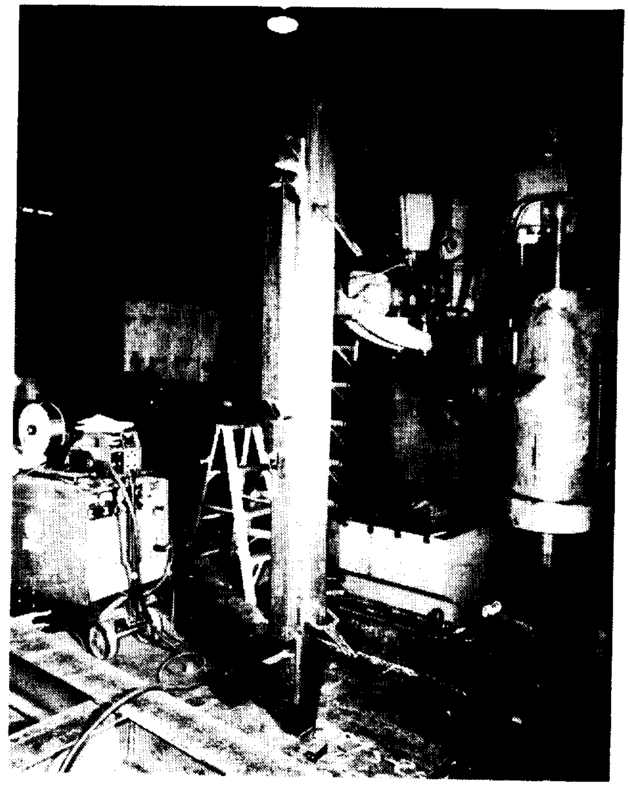

Vibratory relief welding technology used on 8-Foot HTT components.
L-93-01815

A tolerance of ±0.020 from the original shape was maintained over a length of 96 in. throughout the retrofitting of the tunnel.
(Gerald Miller, 44536)
Systems Engineering and Operations Directorate

Boresight—A Two-Axis Alignment System for Lidar In-Space Technology Experiment (LITE)

The boresight is a two-axis gimbaled alignment system that is used on LITE to maintain colinearity between the instrument's outgoing laser beam and the telescope that is used to collect the return energy. This is accomplished by moving a prism that is positioned in the path of the outgoing laser beam. The boresight provides an adjustment range of ±1° in both axes, can be commanded to move in steps as small as 1.54 arc seconds, and is mechanically stiffened through zero-backlash couplings to maintain its position during shuttle launch.

During the mission, the boresight can be commanded to check the instrument's alignment and, if necessary, to automatically reposi-

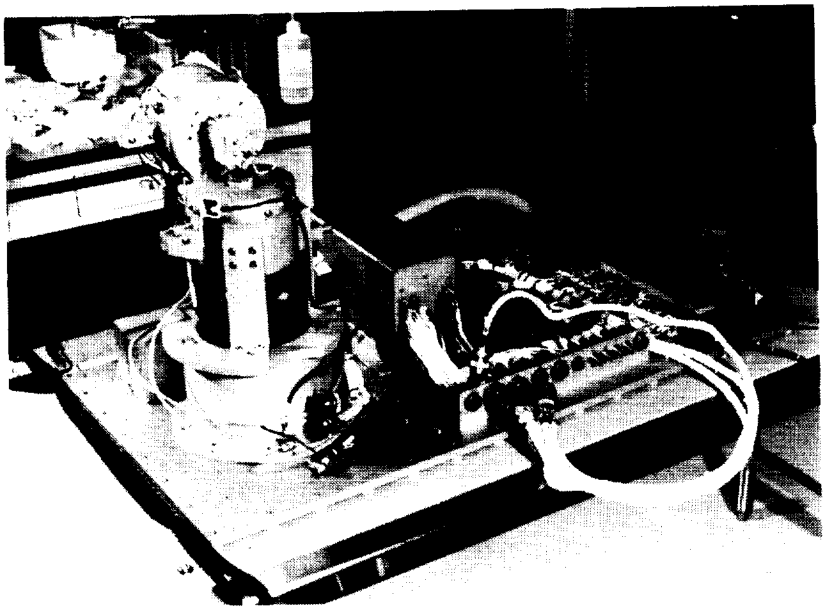

LITE boresight two-axis alignment system during subsystem functional testing. L-92-08672

tion the prism so that the instrument is aligned. This check is accomplished by using a beam splitter in the telescope aft optics to redirect 5 percent of the laser return energy from the instrument's science channels to a quad detector. The output signals from the quad detector are used by the boresight to calculate the correction that is required to maintain instrument alignment. If the instrument is not aligned properly, the boresight calculates the direction and magnitude of the correction that is required to align the instrument and moves accordingly. Once this adjustment has been completed, the boresight reports to the instrument controller that the instrument is aligned. If the instrument is grossly misaligned and the return signal does not fall on the quad detector, the boresight can be commanded to go into a search mode. In this mode of operation, the boresight will search for the return, starting at the current position, in an outward squared spiral pattern. Once the return signal has been detected, the boresight can be commanded to align the instrument.

The boresight subsystem has successfully completed functional, environmental, integration, and instrument-level testing.
(Ruben G. Remus, 47106, James E. Wells, and Clayton P. Turner)
Systems Engineering and Operations Directorate

A Space-Qualified Laser Transmitter

A high-energy, space-qualified laser transmitter was developed for the Lidar In-space Technology Experiment (LITE). The LITE instrument will be launched on the Space Shuttle in 1994 to study aerosols in the Earth's upper atmosphere.

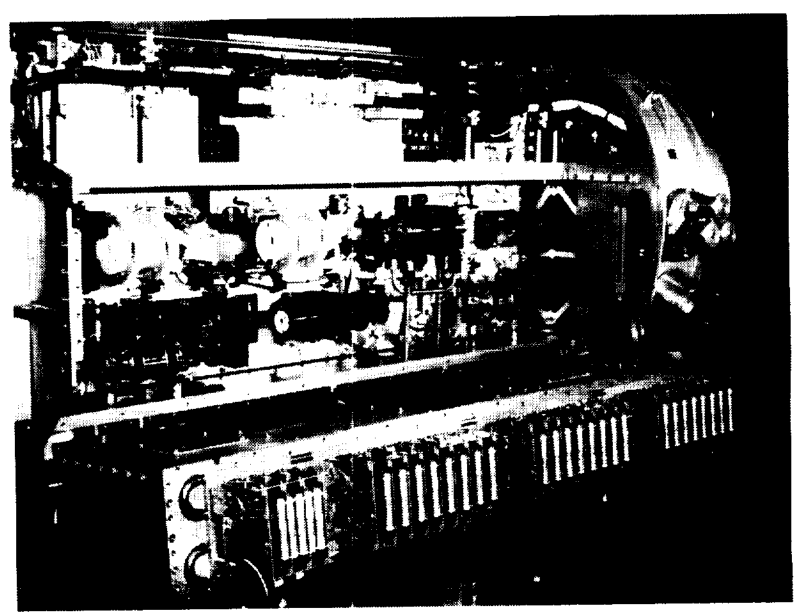

LITE laser transmitter module. L-92-06143

The Laser Transmitter Module (LTM) contains two independent Nd:YAG laser oscillators and their associated optics and electronics. The flashlamp-pumped, Q-switched oscillator generates a fundamental wavelength of 1064 nm. The fundamental wavelength is frequency doubled and tripled to obtain wavelengths of 532 nm and 355 nm. All three wavelengths are output simultaneously. The laser beam is amplified twice to produce a total energy output of 1100 mJ per pulse. The pulse rate is 10 Hz, and the pulse width is 30 nsec.

The LTM is enclosed in an aluminum canister that is pressurized with dry nitrogen. The canister is 60-in. long and 24 in. in diameter. The LTM weighs 590 lb and requires 2.2 kW of electrical power. A thermal control system maintains a constant operating temperature inside the canister. A deionized water-coolant loop removes excess heat from the laser oscillators and various electronic components. Heat from the LTM's water-coolant loop is rejected to the shuttle's Freon coolant loop through an external heat exchanger.

The LTM was subjected to extensive environmental testing to qualify for spaceflight. A thermal-vacuum test demonstrated that the LTM can maintain constant laser energy output when it is exposed to the temperature extremes that it will experience in orbit. A vibration test proved that the LTM will survive lift-off accelerations up to 10 g's. An electromagnetic interference test verified that the LTM will not adversely affect shuttle operations with radiated or conducted emissions. The optical performance of the LTM was characterized in atmospheric testing of the LITE instrument. The LTM successfully met all mission and science requirements. **(Christopher L. Moore, 47172) Systems Engineering and Operations Directorate**

Damage Tolerance of Braided Composites

Impacts from hail, debris, tools, etc. can delaminate conventionally laminated composites because of the relatively weak resin interface between laminae. The through-the-thickness, or interlacing, reinforcement in textile composites has the potential to eliminate delaminations or reduce their size and thus eliminate or reduce strength degradation due to accidental damage. Thus, an investigation was conducted to compare the damage tolerance of braided composites and laminates made conventionally with prepreg tapes. Accordingly, 1/4"-thick carbon/epoxy composite plates made of 2D and 3D braided preforms and prepreg tapes were impacted by falling weights, were then C-scanned to measure damage size, and were finally loaded in compression to measure residual strengths. The prepreg tapes were AS4/3501-6 and IM7/8551-7. The modified 8551-7 epoxy is much tougher than all the other epoxies.

Values of damage resistance and postimpact failing strain for equal damage size are plotted in the figure for each material. Damage resistance is the transverse shear stress per unit length to advance the impact damage, which consists primarily of matrix cracks and disbonds between yarns or laminae. The results are normalized by those for the AS4/3501-6 laminates made from prepreg tape. Both damage resistance and postimpact failing strain for the braids were essentially equal to those for the AS4/3501-6

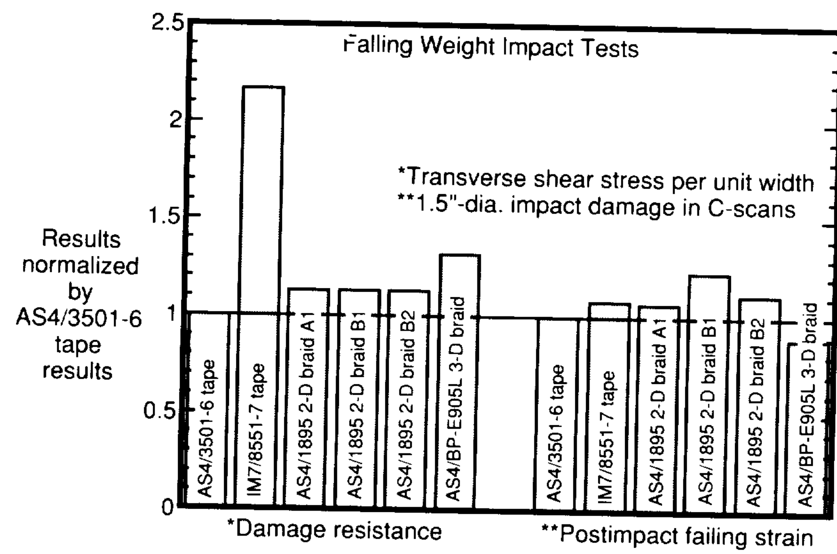

Damage tolerance of composites made from prepreg tape and braided preforms.

tape laminates. Postimpact failing strains for the AS4/3501-6 and IM7/8551-7 tape laminates were also nearly equal, but damage resistance for the IM7/8551-7 tape laminates was more than twice that of the AS4/3501-6 tape laminates. Thus, the damage tolerances of laminates and braids made with conventional epoxies were essentially equal. However, damage resistance increased remarkably with increasing resin toughness, but postimpact failing strains did not increase.
(C. C. Poe, Jr., 43467,
W. C. Jackson, M. A. Portanova,
and John E. Masters)
Structures Directorate

Experimental Methods and Stress-Analysis Models for Time- and Temperature-Dependent Behavior of Polymer Composites

A potential difficulty associated with using polymeric composites in supersonic aircraft is the task of predicting the changes in material properties due to aging of the composite after long-term exposure at elevated temperatures. These changes in the composite-material strength and stiffness will be primarily caused by changes in the mechanical properties of the polymer matrix material alone. Physical aging, considered to be a thermoreversible process, will cause changes in a polymer's mechanical properties that are brought about by the volume recovery upon cooling from above the glass transition temperature (T_g). During aging, the polymer moves towards a state of equilibrium. This state of equilibrium is defined as the point of minimum volume change and is approached asymptotically.

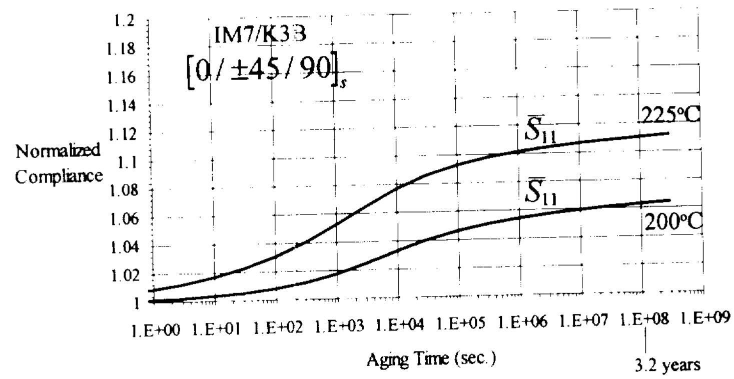

Effects of temperature on long-term compliance of a quasi-isotropic laminate under constant load.

To address this problem, several complimentary studies have been performed to determine the effects of stress and physical aging on the matrix-dominated time-dependent properties of a high-temperature, continuous-carbon-fiber-reinforced, thermoplastic composite. Several of these studies utilized isothermal tensile creep/aging test and analysis techniques that were developed for polymers and adapted for the composite material. From the test results, the time-dependent transverse (S_{22}) and shear (S_{66}) compliances for an orthotropic plate were found from short-term creep compliance measurements at constant temperatures below T_g. These compliance terms were shown to be affected by physical aging. Time-temperature superposition was employed to generate momentary isothermal master curves from the short-term test data. The associated aging time-shift factors and shift rates were found to be a function of temperature and applied stress. These test parameters were then used in conjunction with the effective time theory and classical lamination theory to predict the long-term changes in compliance of general laminates under constant in-plane loads and isothermal conditions. The figure shows a prediction of long-term compliance changes (normalized against the initial value) for a quasi-isotropic laminate at two different test temperatures and with a constant axial load. Results such as those shown in the figure imply that the effects of physical aging over extended periods may have a significant impact on the durability and the long-term effective stiffness of the composite.
(Tom Gates, 43400)
Structures Directorate

FRANC: FRacture ANalysis Code

FRANC is a workstation-based, two-dimensional, finite-element analysis code that was designed specifically for analyzing cracked structures. The program was developed by Cornell University and Kansas State University under sponsorship of the NASA Langley

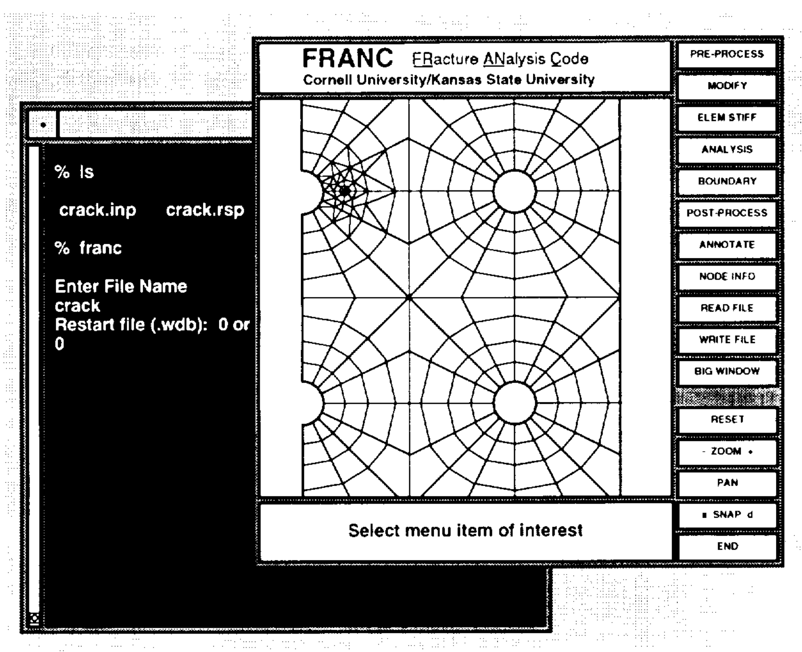

Stress analysis of crack extending from rivet in lap-splice joint.

Research Center (user's manual published as NASA CR-4572). The program is developed around "user friendly" window concepts, allowing a structural analyst to efficiently create a finite-element mesh, analyze the problem, and visualize the results. The code is unique in the ability to interactively introduce cracks into a structure, predict the direction of crack growth, and automatically remesh to model a growing crack.

The FRANC system consists of a preprocessor, a solver, and a postprocessor. The preprocessor is used to create the uncracked finite-element mesh. The structural analyst interactively defines the geometric boundaries and the mesh gradient, and FRANC automatically creates a mesh of 8-noded quadrilateral and 6-noded triangular elements. The boundary and loading conditions can then be defined graphically.

The solver is an elastic, two-dimensional, finite-element analysis code that calculates the local stresses and displacements. The postprocessor will graphically display contour stress plots, stresses along a line or circle, and displacements. The stress contour plot can be used to determine regions of high local stresses, where cracks are likely to develop. The structural analyst can then interactively introduce a crack (or multiple cracks) into the model, and FRANC automatically performs the remeshing, calculates the crack-tip stress intensity factor, and predicts the direction of crack propagation. The crack (or cracks) can be grown with FRANC performing the automatic remeshing.

The FRANC system is uniquely suited to analyzing complicated cracked structures. The automatic mesh generation, crack-growth direction prediction, and crack-tip remeshing capabilities allow for efficient modeling of nearly any two-dimensional configuration.

The FRANC system has recently been expanded to include the ability to model layered structures and contact problems. Using these new capabilities, the code has been experimentally verified for cracks that propagate from interference-fit rivets in thin-sheet, lap-splice joints.
(C. E. Harris, 43449,
A. R. Ingraffea, D. V. Swenson, and D. S. Dawicke)
Structures Directorate

Quantitative Experimental Stress Tomography

QUEST (Quantitative Experimental Stress Tomography) is the world's first microfocus X-ray tomography system capable of imaging a specimen during mechanical loading. QUEST permits imaging of variations in the internal structure as a function of stress. Analysis of the images obtained from QUEST can provide precise measurements of object shapes and how they change under stress. This system has been applied to the characterization of a wide variety of specimens. Typical of these is a measurement of the expansion of a rivet hole following riveting. The extent of expansion significantly affects the fatigue life of a riveted panel. The microfocus tomography system enabled measurement of the expansion to within 2 μm at different positions along the rivet. This information is used to confirm destructive methods for determining the hole expansion.

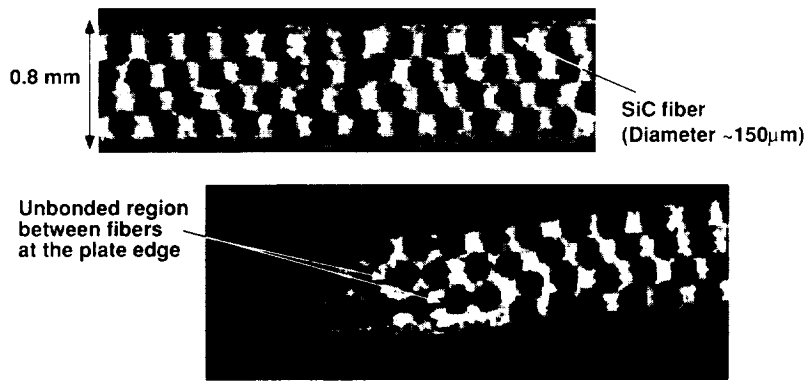

Microfocus X-ray tomography image of $[0]_4$ SCS-6/Ti-1100 metal-matrix composite.

The system has potential for reducing the time required for product development in industry. By nondestructively cross sectioning the sample, the effects of variations in processing procedures can be more exactly determined. Viewing the internal structure during the application of stress also allows quick assessment of the structural integrity of a proposed structure and an assessment of the degradation of the structure as a result of internal flaws.
(William P. Winfree, 44963)
Electronics Directorate

Electronic Shearography

Electronic shearography is a laser-based digital interferometry system that is used to detect areas of stress concentration caused by anomalies in materials. The technique senses out-of-plane surface displacement of an object in response to an applied load. Data are presented in the form of a fringe pattern produced by comparing two states of the test sample, one before and the other after a load is applied. Electronic shearography incorporates a CCD camera and frame grabber for image acquisition at video frame rates. Fringe patterns are produced by real-time digital subtraction of the deformed object image from the reference object image. Shearography also uses a "common path" optical arrangement that provides reasonable immunity to environmental disturbances such as room vibrations and thermal air currents. As a result, shearographic testing can be implemented without the need for sophisticated vibration isolation that is required for conventional holographic interferometry. This capability represents a significant advantage for many industrial applications that require large-area, real-time NDE inspection.
(Robert S. Rogowski, 44990, Leland D. Melvin, and John B. Deaton)
Electronics Directorate

High-Temperature Fiber-Optic Microphone

A fiber-optic microphone has been developed for measuring fluctuating pressures in high-temperature environments that exceed 1000°F. An optical fiber probe with at least one transmitting fiber for transmitting light to a pressure-sensing membrane and at least one receiving fiber for receiving light reflected from a

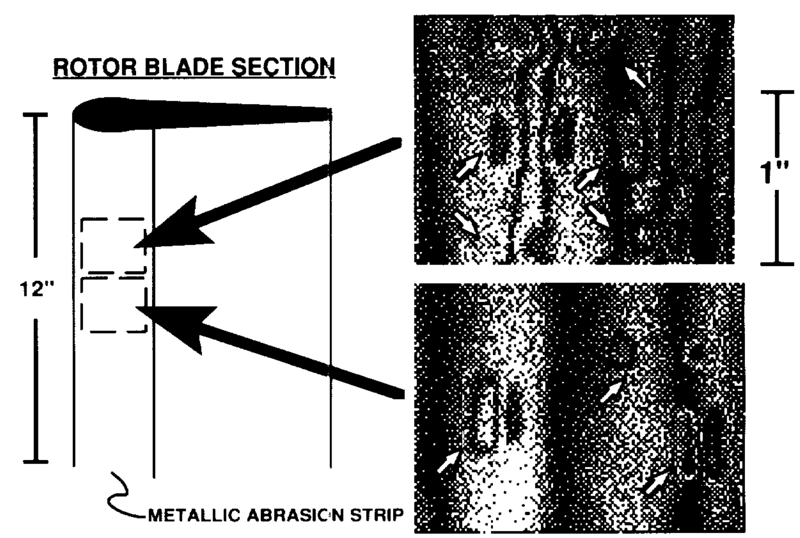

Shearographic images, generated using thermal stressing, of several defects (marked with arrows) behind a metallic abrasion strip at leading edge of a composite rotor blade.

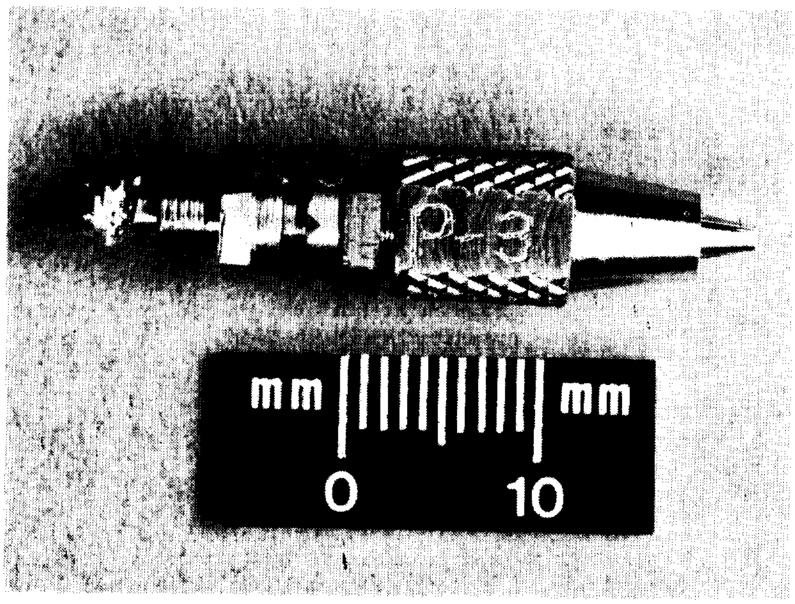

High-temperature fiber-optic microphone. L-92-10050

stretched membrane is provided. The pressure-sensing membrane may be stretched for high-frequency response. Further, a reflecting surface of the pressure-sensing membrane may have dimensions that substantially correspond to dimensions of a cross section of the optical fiber probe. U. S. Patent No. 5,146,083 has been issued to the inventors. A fiber-optic probe is also provided with a backplate for damping membrane motion. The backplate also provides a means for on-line calibration of the microphone.
(William E. Robbins, 42733, and Allan J. Zuckerwar)
Systems Engineering and Operations Directorate

NASSTAR: An Instructional Link Between MSC/NASTRAN and STAR

Correlating structural models with modal survey test data has become an increasingly more complicated and computationally intensive task for the structural analyst working on any type of structure. NASSTAR is a menu-driven FORTRAN77 program that was written to answer the need for simplifying the data manipulation in the correlation process. NASSTAR automates the modal-survey-test/analysis-correlation process by providing a translator between MSC/NASTRAN V66, the structural analyst's finite-element code, and STAR V3.0, the test engineer's data-processing code. It is an aid to the structural analyst who must supply a test-verified finite-element model; specifically, the program addresses correlations that use a cross-orthogonality criterion.

As shown in the figure, NASSTAR is organized into three main sections, which correspond to the three main parts of a testing program: test-procedure support, pre-test support, and post-test support. The test-procedure support section of NASSTAR helps the analyst determine acceptable accelerometer locations by using the pre-test finite-element model. The pre-test support section automates translation of pre-test results from MSC/NASTRAN into STAR. The last section, post-test correlation, automates the transference of test results from STAR into MSC/NASTRAN for the cross-orthogonality check, or into PATRAN pre-processing or post-processing software for viewing test-mode shapes. NASSTAR provides tutorial messages that guide the analyst for all phases of the testing process. The usefulness of the program has been demonstrated through a case history of a modal survey test program that used NASSTAR.
(Jill M. Marlowe, 47027)
Systems Engineering and Operations Directorate

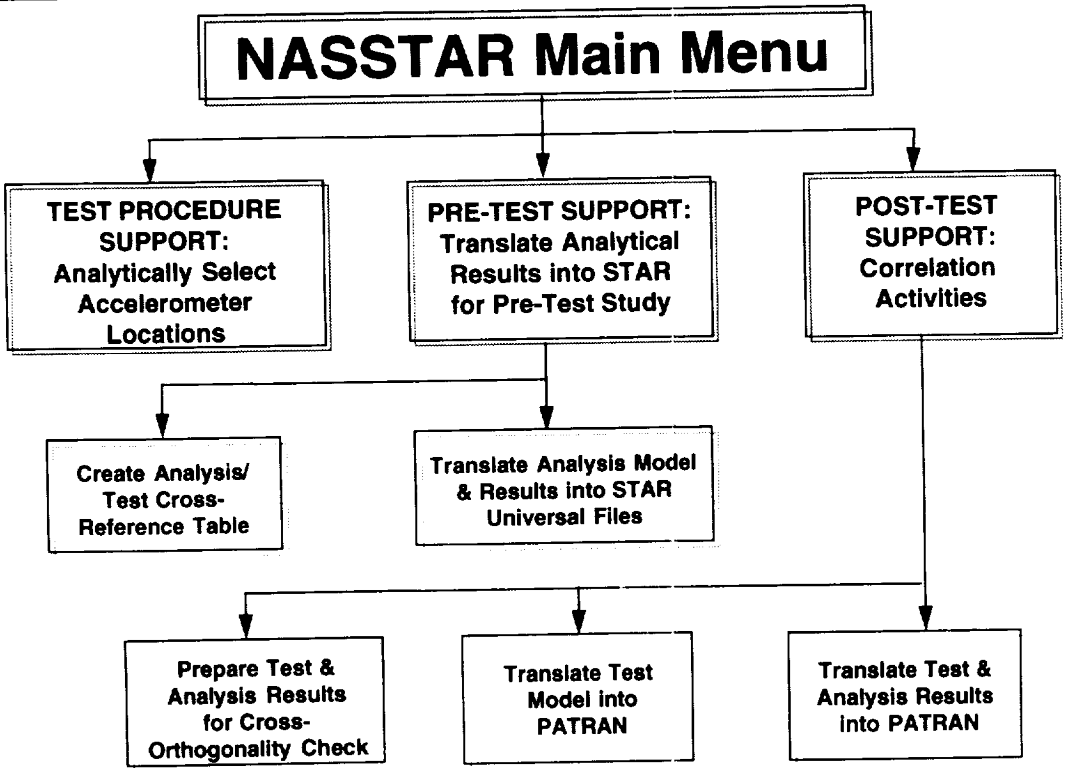

NASSTAR program menus and organization.

Aerospace Test Facilities

RESEARCH AND TECHNOLOGY

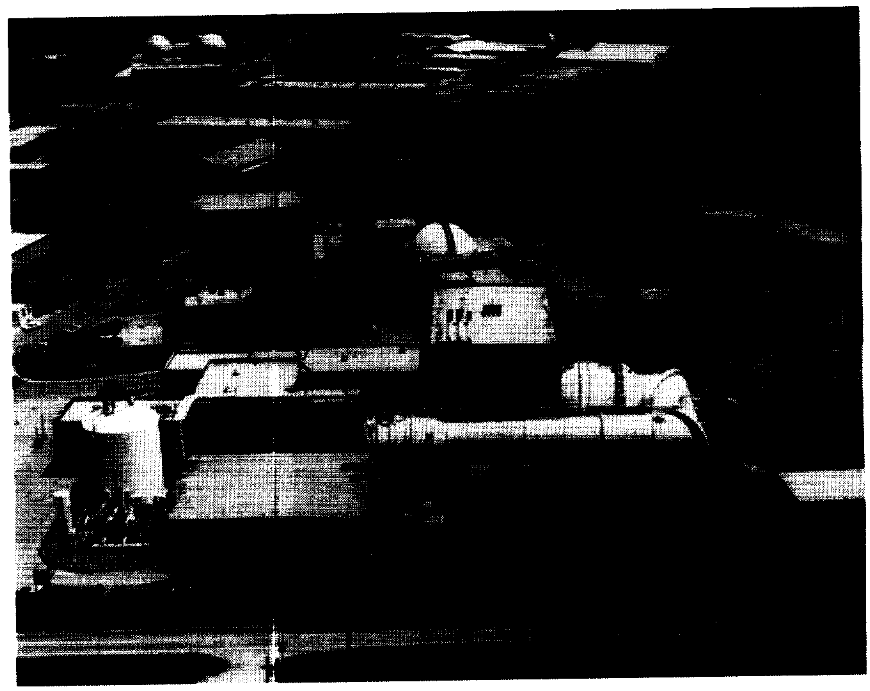

This section includes brief descriptions of many of Langley's major aerospace test facilities; for more detailed information, including availability, please contact the individual identified after each description

30- by 60-Foot Tunnel

The Langley 30- by 60-Foot Tunnel is a continuous-flow, open-throat, double-return tunnel powered by two 4000-hp electric motors, each driving a four-blade 35.5-ft-diameter fan. The tunnel test section is 30 ft high and 60 ft wide and is capable of speeds to 100 mph. The tunnel was first put into operation in 1931 and has been used continuously since then to study the low-speed aerodynamics of commercial and military aircraft. The large open-throat test section lends itself readily to tests of large-scale models and to unique test methods with small-scale models. Large-scale and full-scale aircraft tests are conducted with the strut mounting system. This test method can handle airplanes to the size of present-day light twin-engine airplanes. Such tests provide static aerodynamic performance and stability and control data, including the measurement of power effects, wing pressure distributions, and flow visualization.

Small-scale models can be tested to determine both static and dynamic aerodynamics. The captive test methods include conventional static tests for stability and control, performance, and forced-oscillation tests for aerodynamic damping. Dynamically scaled subscale models, properly instrumented, are also freely flown in the large test section with a simple tether to study their dynamic stability characteristics at low speeds and at high angles of attack.
(Frank L. Jordan, 41136)

L-79-7344

Low-Turbulence Pressure Tunnel

The Langley Low-Turbulence Pressure Tunnel (LTPT) is a single-return, closed-circuit tunnel that can be operated at pressures from near vacuum to 10 atm. The test section is rectangular (3 ft wide and 7.5 ft high and long), and the contraction ratio is 17.6:1. The LTPT is capable of testing at Mach numbers from 0.05 to 0.50 and Reynolds numbers from 0.1×10^6 to 15×10^6 per foot. The chord length for a typical two-dimensional multielement airfoil tested in the facility is approximately 2 ft. A high-lift model support and force balance system is provided to handle both single-element and multiple-element airfoils. Recent flow-quality measurements in the LTPT indicate that the velocity fluctuations in the test section range from 0.025 percent at Mach 0.05 to 0.30 percent at Mach 0.20. The LTPT is a unique facility that provides flight Reynolds number testing capability for airfoil testing and a low turbulence environment for laminar flow control and transition studies.
(Michael J. Walsh, 45541)

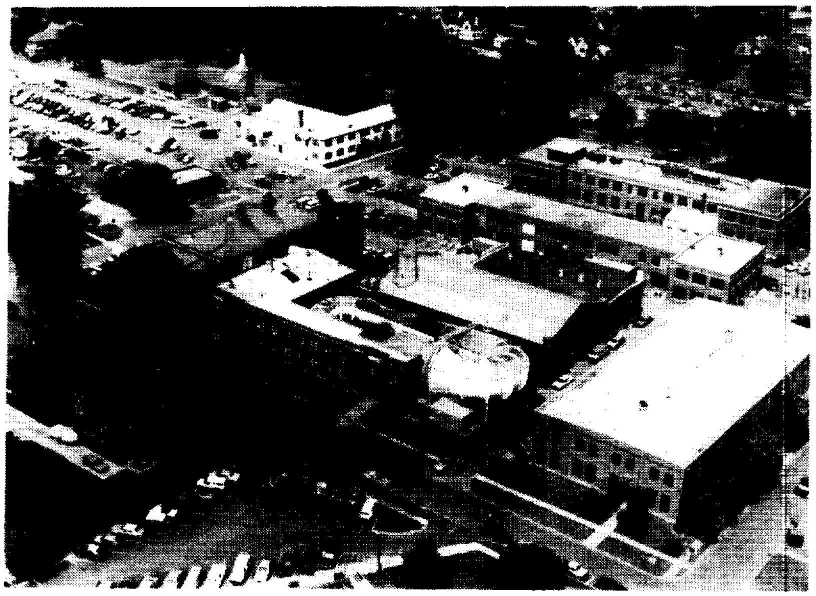

LTPT L-86-6751

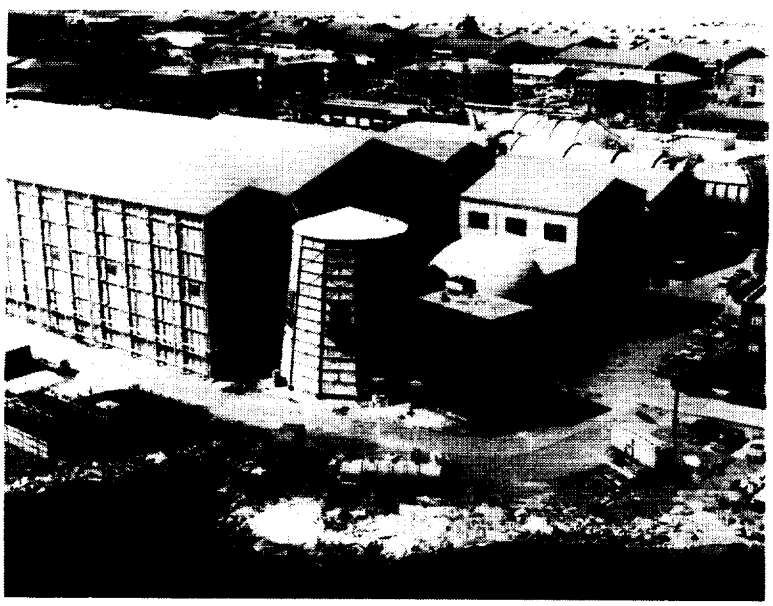

L-85-3590

20-Foot Vertical Spin Tunnel

The Langley 20-Foot Vertical Spin Tunnel is the only operational spin tunnel in the Western Hemisphere. The present facility was built in 1941 and has been in essentially continuous operation since that time. All U.S. military fighters, attack airplanes, primary trainers, bombers, and most experimental airplanes are tested. General-aviation airplanes and many foreign designs are also evaluated when required.

The tunnel, which is used to conduct spin research and tumbling research on aerospace vehicles, is a vertical tunnel with a closed-circuit annular return passage. The test section has 12 sides and is 20 ft across by 25 ft high.

Dynamically scaled models are used to investigate the spinning and tumbling characteristics of airplane configurations. Spin recovery is studied by remote actuation of the models' aerodynamic controls to predetermined positions. Tests are recorded on high-resolution color video. A rotary balance apparatus supported by a swinging boom is used to conduct force-and-moment testing and pressure testing of models under spinning conditions.
(Raymond D. Whipple, 41194)

14- by 22-Foot Subsonic Tunnel

The Langley 14- by 22-Foot Subsonic Tunnel is used for low-speed testing of powered and unpowered models of various fixed- and rotary-wing civil and military aircraft. The tunnel can reach a maximum speed of 318 ft/sec and has a test section 14.5 ft high, 21.75 ft wide, and 50 ft long. The tunnel can be operated as a closed test section with slotted walls or as one or more open configurations when the sidewalls and ceiling are removed to allow extra test capabilities, such as flow visualization and acoustics testing. Boundary-layer suction on the floor at the entrance to the test sec-

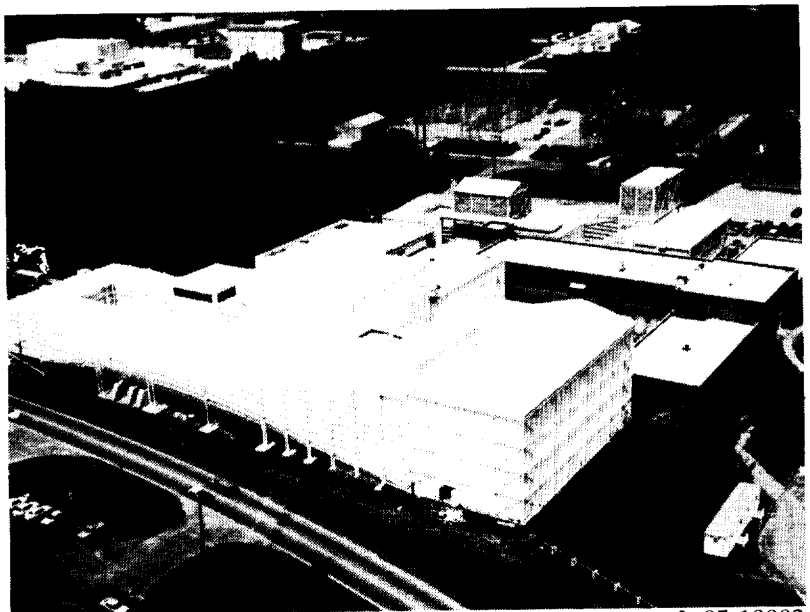

L-85-10002

tion and a moving-belt ground board for operation at test-section flow velocities of 111 ft/sec can be installed for ground-effects testing. The tunnel is equipped with a three-component laser velocimeter for laser-light-sheet flow visualization and detailed flow-field velocity measurements.
(Harry L. Morgan, Jr., 41069)

8-Foot Transonic Pressure Tunnel

The Langley 8-Foot Transonic Pressure Tunnel (8-Foot TPT) is a variable-pressure slotted-throat wind tunnel with controls that permit independent variations of Mach number, stagnation pressure and temperature, and dew point. The test section is square, with filleted corners, and has a cross-sectional area equivalent to that of an 8-ft-diameter circle. The floor and the ceiling of the test section are axially slotted to permit continuous operation through the transonic speed range.

The Mach number range of the facility is from 0.2 to 1.2, and the stagnation-pressure range is from 0.25 to 2.0 atmospheres. Temperature is controlled by water circulating through cooling coils, and the tunnel air is dried to prevent condensation in the flow.

The 8-Foot TPT is a very versatile wind tunnel capable of supporting basic fluid-dynamics research as well as a wide range of applied aerodynamics research. With screens and honeycomb in the upstream settling chamber, the quality of the flow in the test section is suitable for performing reliable code-validation experiments and laminar-flow research.
(James M. Luckring, 42847)

Transonic Dynamics Tunnel

The Transonic Dynamics Tunnel (TDT) is a continuous-flow variable-pressure wind tunnel with a 16-ft by 16-ft test section; it normally uses air or a heavy gas as the test medium. The maximum

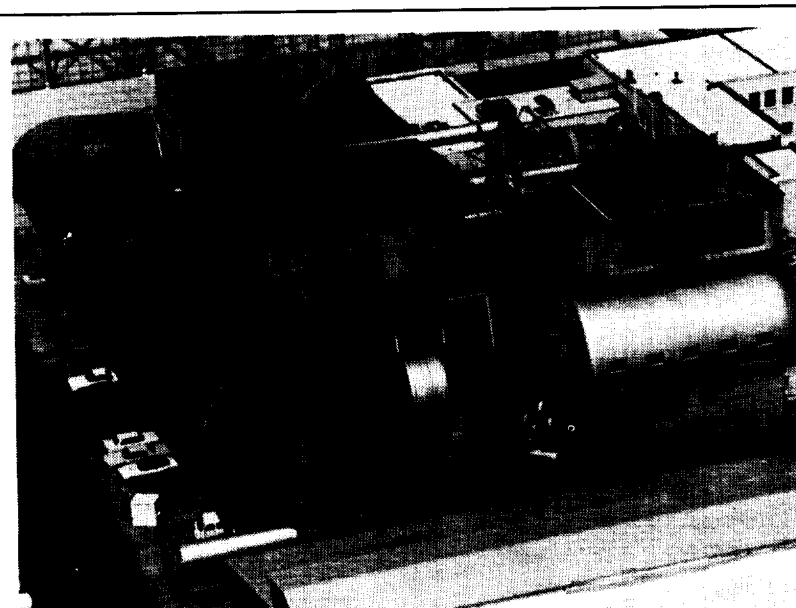

L-71-3976

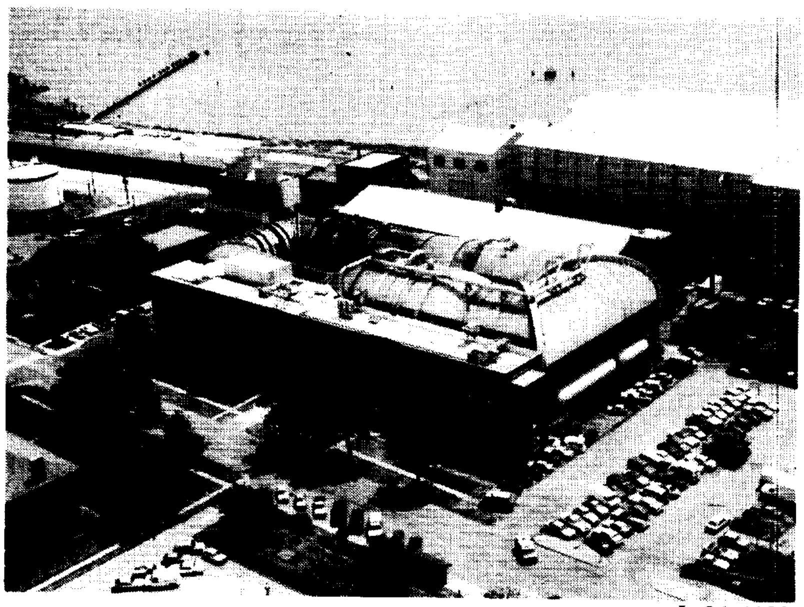

L-86-6183

Mach number is 1.2, and the maximum Reynolds number obtainable is approximately 10×10^6 ft^{-1} in heavy gas and 3×10^6 ft^{-1} in air. The TDT is a unique "national" facility that is used almost exclusively for testing of aeroelastic phenomena. Semispan sidewall-mounted models and full-span sting-mounted or cable-mounted models are used for aeroelastic studies of fixed-wing aircraft. In addition, the Aeroelastic Rotor Experimental System (ARES) test stand is used in the TDT to study the aeroelastic characteristics of rotor systems. The Helicopter Hover Facility (HHF), located in an adjacent building, is used to set up the ARES test stand in preparation for entry into the TDT and for rotorcraft studies in hover. The TDT Data Acquisition System is capable of simultaneous support of tunnel tests, HHF tests, and model checkout in the Calibration Lab. A major facility upgrade to replace the present heavy gas is planned in the spring of 1995, at which time the tunnel will be unavailable for about 1 year.
(Bryce M. Kepley, 41244)

16-Foot Transonic Tunnel

The Langley 16-Foot Transonic Tunnel is a closed-circuit, single-return, continuous-flow, atmospheric tunnel with a Mach number capability from 0.20 to 1.30. The slotted octagonal test section measures 15.5 ft across the flats. The tunnel is equipped with an air exchanger with adjustable intake and exit vanes to provide some temperature control. This facility has a main-drive power system consisting of two 30 000-hp motors driving counter-rotating fans. A 36 000-hp compressor provides test-section plenum suction.

The tunnel is used for force, moment, pressure, flow visualization, and propulsion-airframe integration studies. Model mounting consists of sting, sting-strut, and semispan support arrangements; propulsion simulation studies are made with dry, cold, high-pressure

L-86-4496

air or with turbine-powered engine simulators.
(Bobby L. Berrier, 43001)

National Transonic Facility

The National Transonic Facility (NTF) is a fan-driven , closed-circuit, continuous-flow, pressurized wind tunnel. The test section is 8.2 ft by 8.2 ft and approximately 25 ft long, with a slotted-wall configuration. The test gas may be dry air or nitrogen. For the air mode of operation, heat removal is by a water-cooled heat exchanger (cooling coil) located at the upstream end of the settling chamber. For the cryogenic mode of operation, heat removal is by evaporation of liquid nitrogen, which is sprayed into the circuit upstream of the fan. The tunnel design Mach number range is from 0.2 to 1.2, and the test-temperature range is from 150°F to –320°F. The design total pressure range for the NTF is from 15 to 130 psia.

The combination of pressure and cold test gas can provide a maximum Reynolds number of 120×10^6 at a Mach number of 1.0 based on a chord length of 9.75 in. By using the cryogenic approach to generate high Reynolds numbers, the NTF achieves its performance of near-full-scale conditions at lower cost and at lower model loads than concepts based on ambient temperature operation. In addition, with both temperature and pressure as test variables, three types of investigations are possible; these include Reynolds number effects at constant Mach number and dynamic pressure, model aeroelastic effects at constant Reynolds number and Mach number, and Mach number effects at constant dynamic pressure and Reynolds number.
(Dennis E. Fuller, 45129)

L-90-6542

0.3-Meter Transonic Cryogenic Tunnel

The 0.3-Meter Transonic Cryogenic Tunnel (0.3-m TCT) is used for testing two-dimensional airfoil

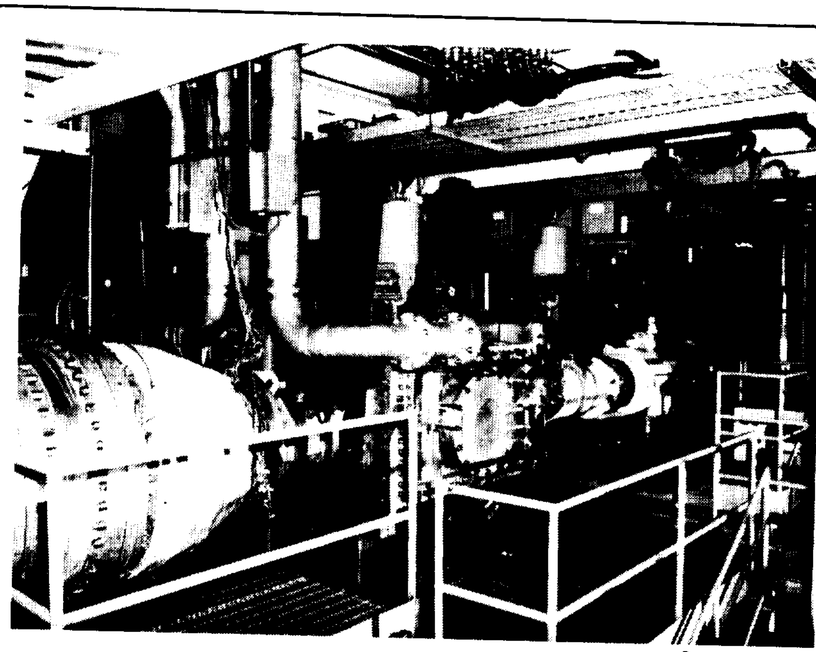

L-85-09893

sections and other models at high Reynolds numbers. The tunnel can operate continuously over a range of Mach numbers from about 0.1 to above 1.2, with a stagnation pressure from 14.7 to 88.0 psia (1 to 6 atmospheres) and a stagnation temperature from −320°F to 130°F (78 K to 328 K). This results in a maximum Reynolds number capability in excess of 100×10^6 per foot. The adaptive walls, floor, and ceiling in the 13-in. by 13-in. (33-cm by 33-cm) test section can be moved to the free-stream streamline shape, eliminating or reducing the wall effects on the model. The combination of flight Reynolds number capability and minimal wall interference makes the 0.3-m TCT a powerful tool for aeronautical research at transonic speeds. The Mach number, pressure, temperature, and adaptive wall shape are automatically controlled. The test section has computer-controlled angle of attack and traversing wake survey-probe systems. A heat exchanger and alternate gas supply unit have recently been added to the facility, adding the capability of using alternate test media—a heavy gas, sulfur hexafluoride (SF_6), or air.
(Stuart G. Flechner, 46360)

Unitary Plan Wind Tunnel

Immediately following World War II, the need for supersonic wind-tunnel facilities to develop advanced airplanes and missiles was recognized. The Department of Defense and the National Advisory Committee for Aeronautics (NACA) developed a plan for a

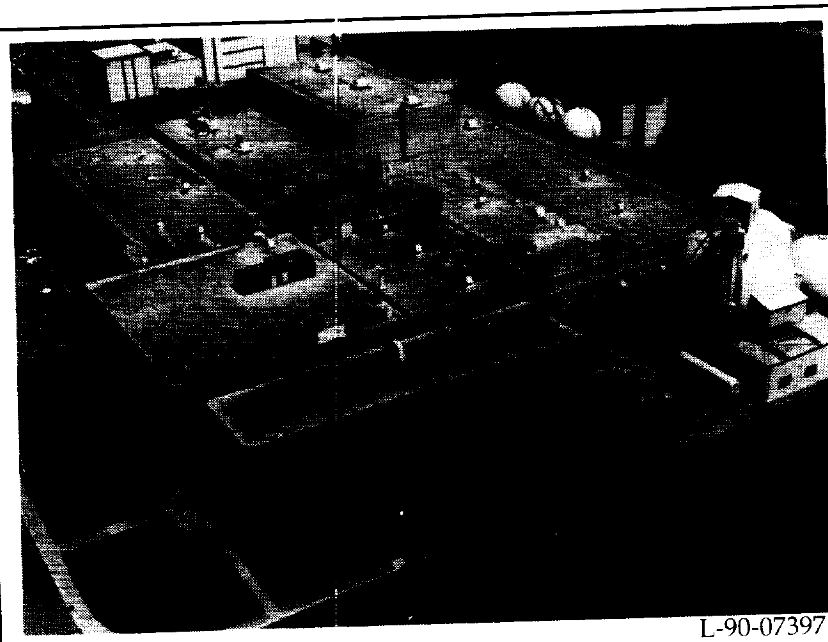

L-90-07397

series of facilities that was approved by the United States Congress in the Unitary Plan Wind Tunnel Act of 1949. This plan included five wind-tunnel facilities, three at NACA laboratories and two at the Arnold Engineering Development Center. The Langley Unitary Plan Wind Tunnel (UPWT) was one of the three built by NACA. The UPWT is a closed-circuit, continuous-flow, variable-density tunnel with two 4-ft by 4-ft by 7-ft test sections. One test section has a design Mach number range from 1.5 to 2.9, and the other has a Mach number range from 2.3 to 4.6. The tunnel has sliding-block-type nozzles that allow continuous variation in Mach number while the facility is in operation. The maximum Reynolds number per foot varies from 6×10^6 to 11×10^6, depending on Mach number. Types of tests include force and moment, pressure distribution, jet effects, dynamic stability, and heat transfer. Flow visualization capabilities in both test sections include schlieren, oil flow, vapor screen, and mini tufts.
(William A. Corlett, 45911)

Hypersonic Facilities Complex

The Hypersonic Facilities Complex consists of nine hypersonic wind tunnels located at three Langley sites. These facilities are considered a complex because together they represent a major unique national resource for wind-tunnel testing. The complex currently includes the following: 15-Inch Mach 6 High-Temperature Tunnel, 12-Inch Mach 6 High Reynolds Number Tunnel, 20-Inch Mach 6 Tunnel, 20-Inch Mach 6 CF_4 Tunnel, 18-Inch Mach 8 Tunnel, 31-Inch Mach 10 Tunnel, 20-Inch Mach 17 N_2 Tunnel, 60-Inch Mach 18 Helium Tunnel, and 22-Inch Mach 20 Helium Tunnel. These facilities are used to study and to assess the aero-

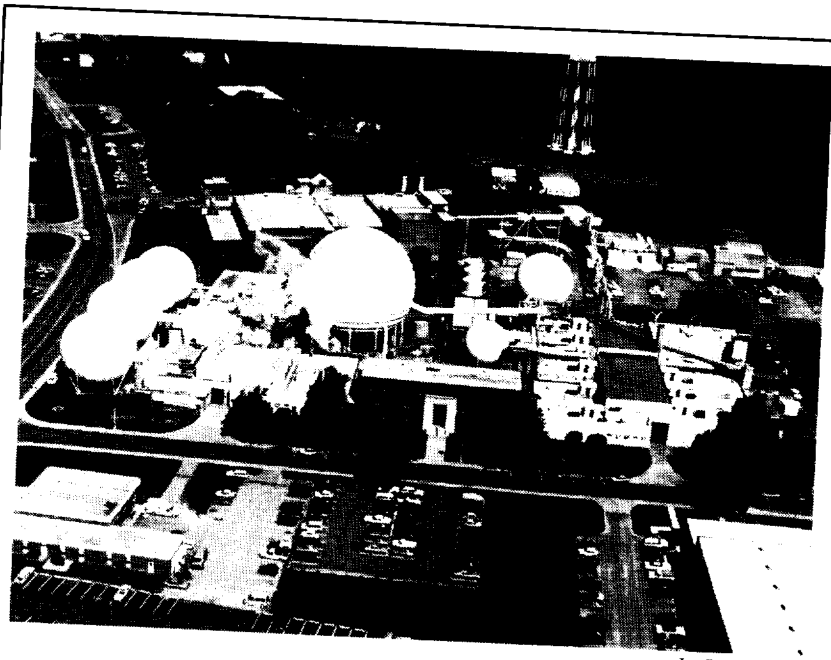

L-89-11615

dynamic, aerothermodynamic, and fluid dynamic phenomena associated with advanced manned space transportation systems, such as Personnel Launch System vehicles, Assured Crew Return Vehicle concepts, and Advanced Manned Launch System concepts; to support the development of the National Aero-Space Plane technology, lunar return and Mars entry and return vehicles, and hypersonic missiles and transports; to perform basic fluid dynamics studies of complex flow phenomena such as shock-shock interactions and shock impingements; to establish data bases for calibration of computational fluid dynamics (CFD) codes; and to develop measurement and testing techniques.

This complex of facilities provides an unparalleled capability at a single installation to study aerodynamic, aerothermodynamic, and fluid dynamic phenomena for advanced aerospace vehicle concepts over wide ranges of hypersonic simulation parameters, namely Mach number, Reynolds number, density ratio or ratio of specific heats, and thermal driver potential (wall-temperature ratio). Several modifications have recently been made and are continuing to be made to the facilities to improve their flow quality, reliability, productivity, and capability.
(C. G. Miller, 45221)

Scramjet Test Complex

The Langley Scramjet Test Complex consists of five test facilities and a diagnostics laboratory that offer a complete spectrum of supersonic combustion ramjet (scramjet) test capabilities. The complex includes the Direct-Connect Supersonic Combustion Test Facility (DCSCTF), the HYPULSE expansion tube, the Combustion-Heated Scramjet Test Facility (CHSTF), the Arc-Heated Scramjet Test Facility (AHSTF), the 8-Foot High-Temperature Tunnel (8-Foot HTT), and the Nonintrusive Diagnostics Laboratory (NDL). Scramjet inlet models are tested in air or nitrogen from Mach 1.6 to 17 in various Langley aero-

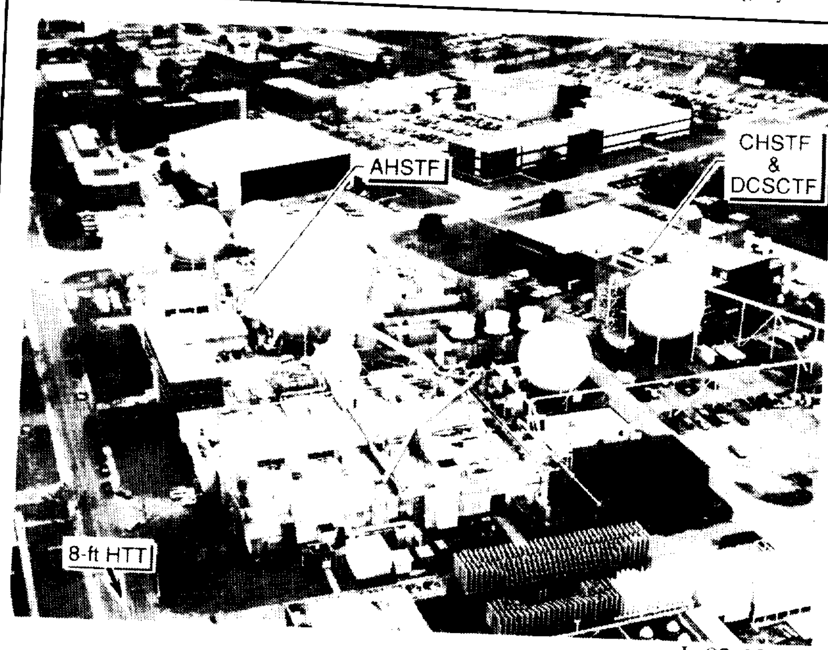

L-92-12685

dynamic wind tunnels to study inlet flow phenomena and to validate computational fluid dynamics codes. Scramjet combustors are tested in the DCSCTF and the HYPULSE expansion tube to provide basic research data on fuel-air mixing and combustion processes. The hydrogen-air-oxygen combustion heater of the DCSCTF supplies simulated air to the combustor entrance at total enthalpy levels up to Mach 8 flight speeds (total temperatures to 5000°R). The HYPULSE expansion tube, a pulse facility with a 500-μsec test time, is located at the General Applied Sciences Laboratory in Ronkonkoma, New York. HYPULSE provides clean, undissociated air to the combustor entrance at total enthalpy levels duplicating Mach 13.5, 15, and 17 flight (total temperatures to 15 000°R). Designs from the individual scramjet component tests are assembled to form component integration engines that are tested in two subscale engine test facilities, the CHSTF and the AHSTF. A hydrogen-air-oxygen combustion heater in the CHSTF produces simulated air that duplicates Mach 3.4 to 6 flight total enthalpies, and an electric arc in the AHSTF heats air to total enthalpy levels corresponding to flight speeds up to Mach 8. Scramjet model size in both of these facilities is approximately 6 in. by 8 in. in frontal area by 6 ft in length. The 8-Foot HTT is capable of testing injectable scramjet models up to 12 ft in length. These models can be single or multiple engines of the size tested in the subscale facilities mounted on aircraft-type forebody-afterbody structures or larger scale single scramjets with frontal areas of approximately 20 in. by 28 in. Test gases with total enthalpy levels duplicating Mach 4, 5, and 7 flight are produced in the 8-Foot HTT by methane-air-oxygen combustion. The NDL is used to develop various optical diagnostic techniques for supersonic reacting flow. Laboratory-scale combustion devices provide air total temperatures to 4000°R and a speed range to Mach 2. This laboratory has been used to develop the hardened Coherent Antistokes Raman Spectroscopy (CARS) system, to demonstrate the application of ultraviolet Raman scattering to measure temperature and O_2, N_2, H_2, H_2O, and OH mole fractions simultaneously, and to develop laser-induced fluorescence of OH in supersonic reacting flow. A velocity measurement technique based on molecular tagging of oxygen is currently being developed in the NDL. These facilities comprise a Scramjet Test Complex unequaled in its capability to investigate engine flow fields, scale effects, speed effects, and engine-airframe integration.
(R. Wayne Guy, 46272)

Aerothermal Loads Complex

The Aerothermal Loads Complex consists of four facilities that are used to carry out research in aerothermal loads, propulsion, high-temperature structures, and thermal protection systems. The 8-Foot High-Temperature Tunnel (8-Foot HTT) is a Mach 5, 6, and 7 blowdown-type facility in which methane is burned in oxygen-enriched air under pressure; the resulting combustion products are used as the test medium, with a maximum stagnation temperature of approximately 3800°R available in order to reach the required energy level for flight simulation. The nozzle is an axisymmetrical conical contoured design with an exit diameter of 8 ft. Model mounting is semispan or sting, with insertion after the tunnel is started. The Reynolds number ranges from 0.3 to 2.2×10^6 ft^{-1}, with nominal Mach numbers of 5, 6, and 7, and the run

L-91-3594

time ranges from 20 to 180 sec. The tunnel is used for studying detailed thermal-loads flow phenomena as well as for evaluating the performance of air-breathing propulsion systems and high-speed and entry-vehicle structural components. A major effort was recently completed to provide alternate Mach number capability as well as O_2 enrichment for the test medium. This was done primarily to allow models that have hypersonic air-breathing propulsion applications to be tested.

The three other facilities are a smaller scale HTT and two arc tunnels. The 7-Inch High-Temperature Tunnel (7-Inch HTT) is a 1/12-scale version of the 8-Foot HTT with basically the same capabilities as the larger tunnel. It is used primarily as an aid in the design of larger models for the 8-Foot HTT and for aerothermal loads tests on subscale models. The 20-MW and 5-MW Aerothermal Arc Tunnels are used to test models in an environment that simulates the flight reentry envelope for high-speed vehicles such as the Space Shuttle. The arc tunnels are currently on standby status.
(Allan R. Wieting, 41359)

Acoustics Research Laboratory

The Langley Acoustics Research Laboratory (ARL) provides the principal focus for acoustics research at Langley Research Center. The ARL consists of the anechoic quiet flow facility, the reverberation chamber, the transmission loss apparatus, and the human-response-to-noise laboratories. The human-response laboratories consist of the exterior effects room, the anechoic listening room, and the sonic boom simulator. The ARL is used to conduct aeroacoustic studies of aircraft components and models as well as subjective acoustic studies involving actual test subjects.
(Lorenzo R. Clark, 43637)

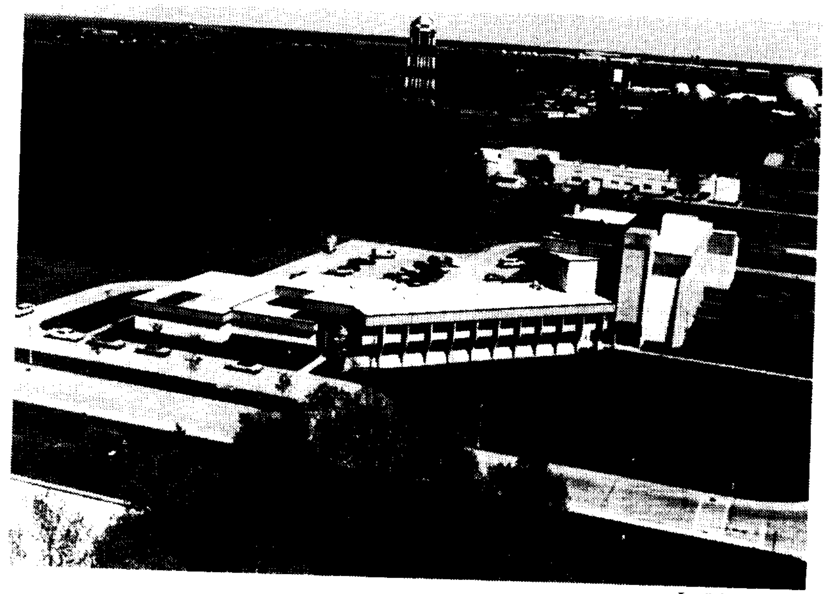

L-80-03126

Avionics Integration Research Laboratory (AIRLAB)

AIRLAB is an environmentally controlled structure located in the high-bay area at 1 South Wright Street. AIRLAB houses several specialized resources for testing avionics systems response to high intensity radiated fields (HIRF). One such resource is a Gigahertz Transverse Electromagnetic cell that can be used for anechoic testing. Three mode-stirred reverberating chambers are also available. Radio frequency sources, measurement devices, and data collection and storage equipment complement the test cells to support various tests and experiments. Test specimens such as flight-control computers and specialized fault-tolerant digital systems are available for experimental use. Alternatively, experimenters can provide their own systems as test specimens. In support of the test facility, there are workstations where highly reliable digital avionics systems can be modeled to assess upset response, reliability, performance, and other system characteristics that are important to system validation. Modeling and experimental capabilities are developed by in-house staff based on in-house research. AIRLAB addresses issues in the conception, design, and assessment of systems that can dramatically improve performance and lower production and maintenance costs while providing a high, measurable level of safety

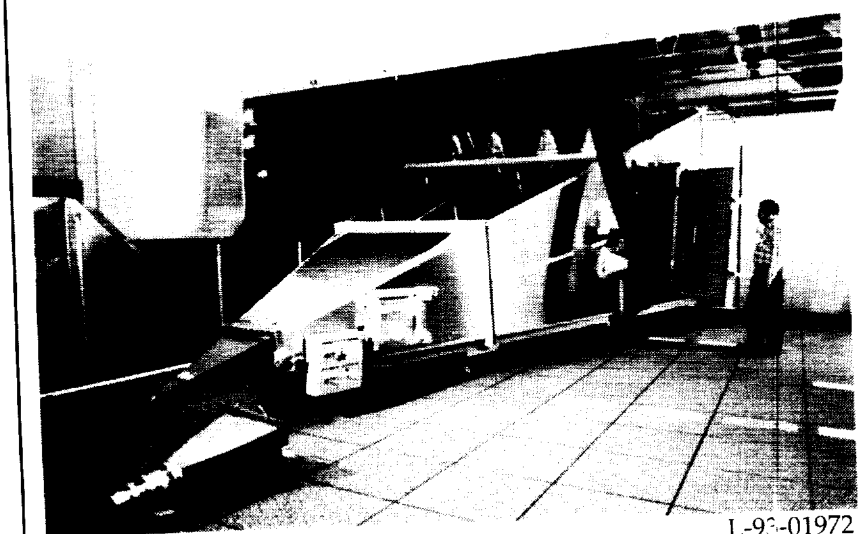

AIRLAB L-93-01972

for passengers and flight crews. It serves as a focal point for U.S. Government, industry, and university personnel to identify and develop methods for systematically validating and evaluating highly reliable digital control and guidance systems for aerospace vehicles.
(Charles W. Meissner, Jr., 46218)

Aerospace Controls Research Laboratory

The purpose of the Aerospace Controls Research Laboratory (ACRL) is to conduct research and testing of spacecraft control systems. The ACRL is equipped with modern microcomputer facilities for simulations, data acquisition, and real-time control-system testing. Both control-law testing using experimental test articles and advanced control-system component development are supported by the laboratory. The ACRL provides the controls community with facilities on which the performance of competing control laws may be compared.

An example of a test facility in the ACRL is a large-angle magnetic suspension test fixture (LAMSTF). The LAMSTF (shown in figure) consists of a planar array of five room-temperature electromagnets arranged in a circular configuration with associated sensors, control electronics, and power amplifiers. The LAMSTF levitates and controls a cylindrical suspended element that contains a core composed of neodymium-iron-boron permanent magnet material that is magnetized along the long axis of the cylinder. The core is controlled in five degrees of freedom, with roll being the uncontrolled axis.

The LAMSTF can be used in the development of the technology for future large-gap magnetic suspension systems by providing the experimental validation of design concepts in the areas of electromagnets, control, sensing, and electronics as well as by providing insight into the requirements and challenges introduced by large-scale systems.

The ACRL also includes advanced sensor and processor facilities that support research in control-system components for

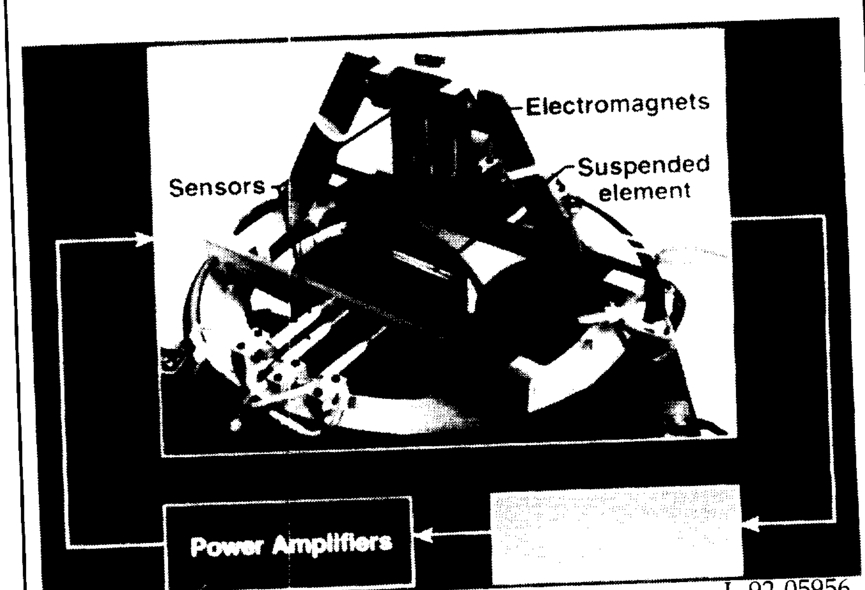

L-92-05956

space systems. Component development currently focuses on optical sensing and computing devices. Two different photogrammetric position tracking systems and an optical processor for a controls experiment are being developed. The facility includes equipment for performing experiments in optics, two stable tables, optical mounts, lenses, mirrors, polarizers, beam splitters, photomultiplier tubes, acousto-optic modulators, HeNe and Ar lasers, computer-controlled precision stages, and laser-beam steering systems. **(Douglas Price, 46605)**

Transport Systems Research Vehicle (TSRV) and TSRV Simulator

The Transport Systems Research Vehicle (TSRV) and TSRV Simulator are primary research tools used by the Terminal Area Productivity (TAP) program. The goal of the TAP program is to increase capacity during instrument weather conditions for the National Airspace System. The TSRV has two flight decks: a conventional Boeing 737 flight deck provides operational support and safety backup, and the fully operational research flight deck, positioned in the aircraft cabin, provides the capability to explore innovations in advancing technologies, including avionics, displays, and systems integration.

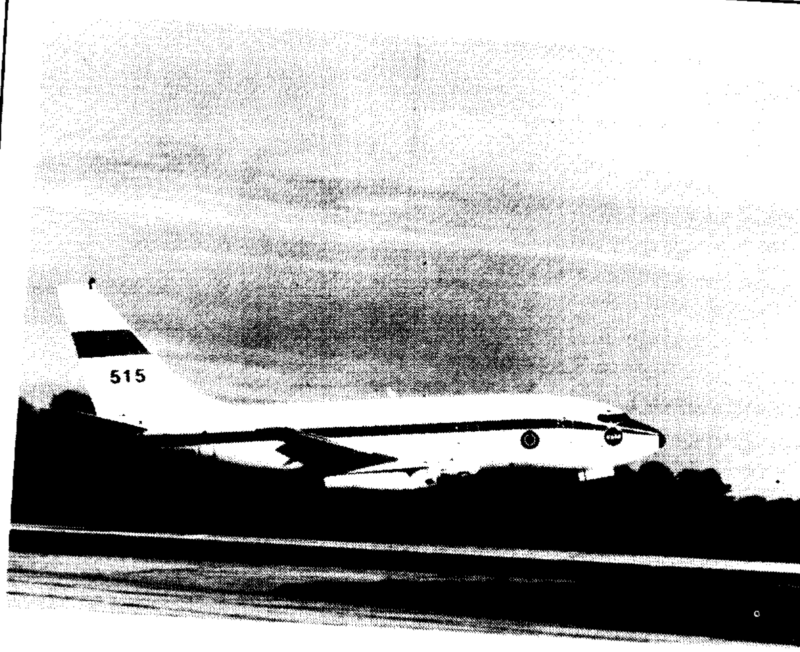

L-85-827

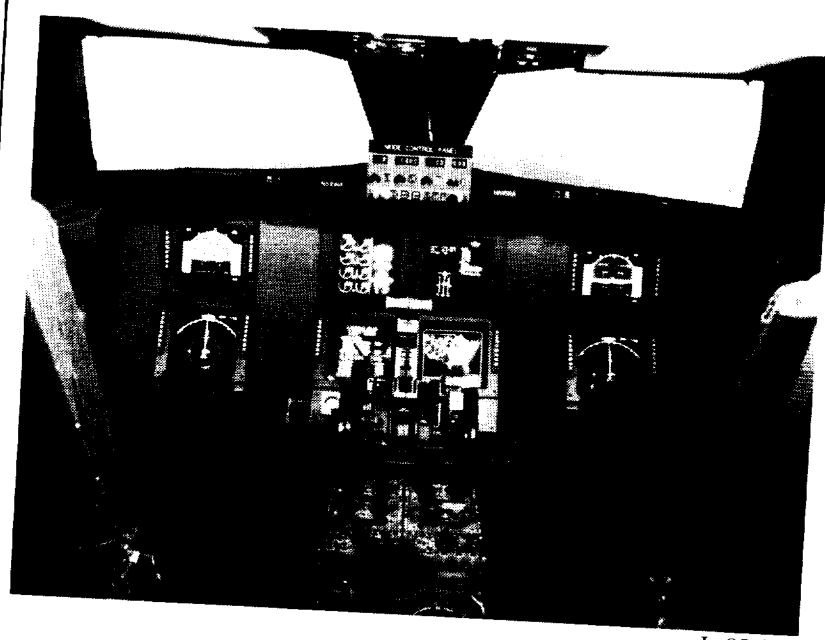

L-93-505

The TSRV simulator provides the means for ground-based simulation in support of the TAP research program. Four out-the-window display systems (driven by an Evans and Sutherland CT-6 Computer-Generated Imagery System) allow realistic real-world scenes to be presented to the crew. The simulator has recently been upgraded to a full complement of eight electronic displays and two side-arm controllers representative of the technology available in commercial transports of the 1990's. The simulator is fully integrated with a realistic air traffic control facility to provide an environment for systems-level studies. **(George Steinmetz, 43842, Billy Ashworth, and Jacob A. Houck)**

Enhanced/Synthetic Vision & Spatial Displays Laboratory

The Enhanced/Synthetic Vision & Spatial Displays Laboratory (ESVSDL) serves as a primary testing facility for the candidate flight display concepts, systems-subsystems, and devices emerging from the Crew Station Technology and Low-Visibility Landing/Surface Operations research efforts. The laboratory provides a unique capability to conduct iterative development and pilot-vehicle experimental evaluation research for advanced cockpit technologies in a highly realistic flight simulation environment. Major elements of the ESVSDL are the following: (1) the Advanced Display Evaluation Cockpit (ADEC), which is a reconfigurable transport aircraft research cab; (2) the Aircraft Cockpit Ambient Lighting and Solar Simulator (ACALSS), which provides real-world ambient and solar lighting conditions to the ADEC; (3) the Visual Imaging Simulator for Transport Aircraft Systems (VISTAS), which is a highly flexible, rapidly reconfigurable, large-screen flight display workstation for evaluation of a wide variety of enhanced/synthetic vision and spatial display formats; and (4) the Collimated Flight Display Workstation (CFDWS), which provides the capability for pilot evaluation of collimated flight displays. Other major elements include a general-purpose digital processor, which handles system input/output and vehicle math model simulation; three high-performance raster graphics display generators, which provide sophisticated graphics formats (in

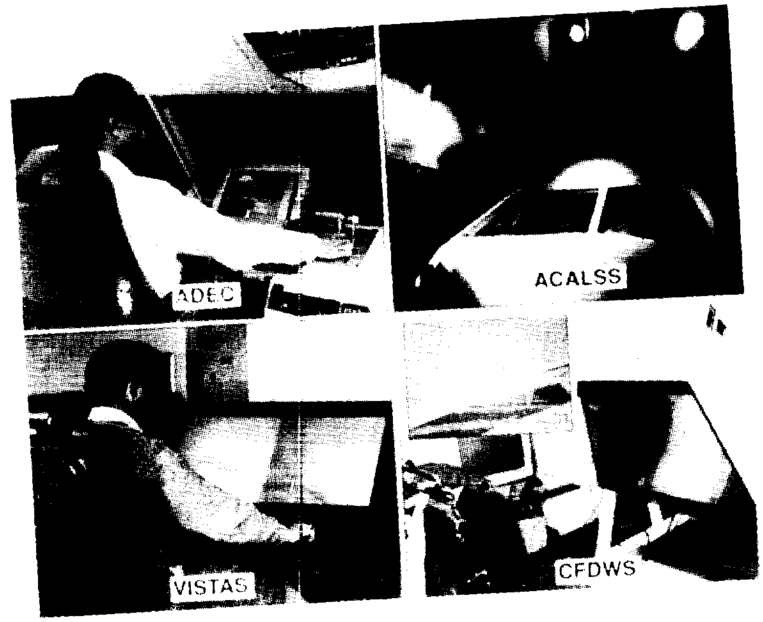

2-D, 3-D, and stereo 3-D modes) to the displays within the facility; and a fiber-optic link to the Langley central computing facility for research requiring more complex vehicle simulation.
(Jack Hatfield, 42012)

Human Engineering Methods Research Laboratory

The Human Engineering Methods (HEM) Research Labora-

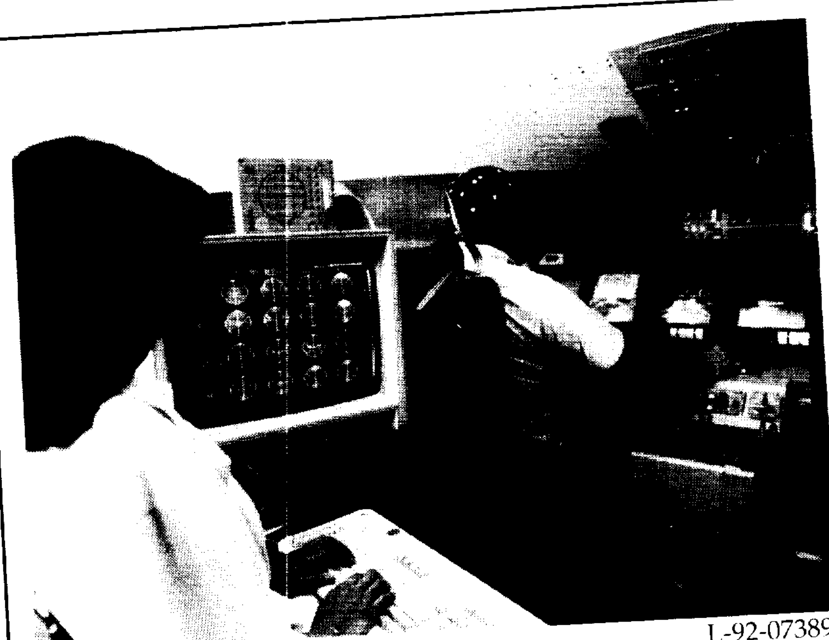

L-92-07389

tory is utilized for the development of human-response measurement technologies to assess the effects of advanced crew station concepts on the crew's ability to perform flight-management tasks effectively. Behavioral response and psychophysiological response measurement systems have been developed to assess mental loading, stress, task engagement, and situation awareness. Measurement capabilities include topographic brainmapping (EEG and evoked responses), monitoring of pulse, heart and muscle electrical activity (EKG and EMG), skin temperature and conductance, respiration, and tracking of eye lookpoint (oculometry) and overt behavior (video analysis). A real-time multi-attribute task (MAT) battery has been developed to recreate flight-management task conditions in the laboratory setting for initial testing of advanced human-response measurement concepts. Mobile physiological monitoring and behavioral response capture-stations are located at simulator sites to refine these measurement concepts for flight-management research.
(Alan Pope, 46642)

General Aviation Simulator

The General Aviation Simulator (GAS) consists of a general-aviation aircraft cockpit mounted on a three-degree-of-freedom motion platform. The cockpit is a reproduction of a twin-engine, propeller-driven, general-aviation aircraft with a full complement of instruments, controls, and switches, including radio navigation equipment. Programmable control-force feel is provided by a "through-the-panel" two-axis controller that can be removed and replaced with a two-axis side-arm controller that can be mounted in the pilot's left-hand, center, or right-hand position. A variable-force-feel system is also provided for the rudder pedals. The pilot's instrument panel can be configured with various combinations of cathode-ray tube (CRT) displays and conventional instruments to represent aircraft such as the Cessna 172, Cherokee 180, and Cessna 402B. A collimated-image visual system provides a nominal 40° horizontal-view by 23° vertical-view out-the-window color display. The visual system accepts inputs from a Computer-Generated Image (CGI) system. A Calligraphic-Raster Display System (CRDS) is used to generate the head-down displays and to mix with the CGI for the head-up display. The simulator is flown in real time, and a host computer simulates aircraft dynamics.

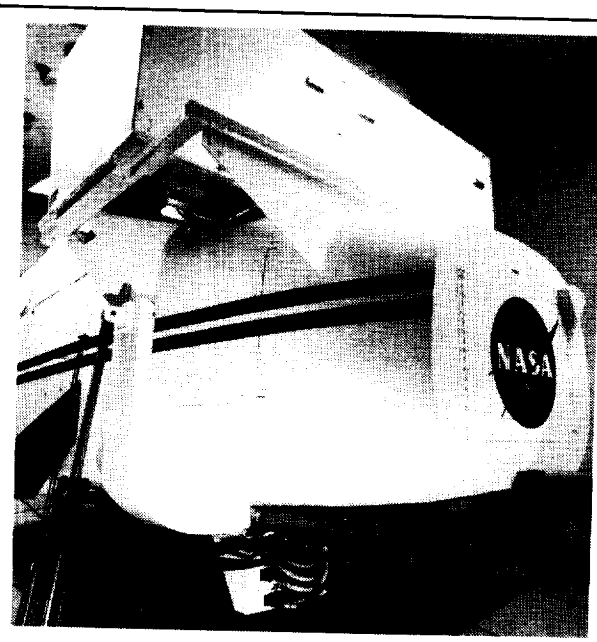

L-83-4,586

Research has been conducted to improve the ride quality of general-aviation aircraft by deveoping gust-alleviation control laws to reduce the aircraft response to turbulence while generally good flying characteristics are maintained. A research study recently completed is the General Aviation E-Z Fly, a program to investigate ways of making general-aviation airplanes easier to fly, especially for low-time pilots or nonpilots.
(Lemuel E. Meetze, 46452)

Differential Maneuvering Simulator

The Langley Differential Maneuvering Simulator (DMS) provides a means of simulating two piloted aircraft operating in a differential mode with a realistic cockpit environment and a wide-angle external visual scene for each of the two pilots. The system

L-90-10308

consists of two identical fixed-based cockpits and projection systems, each based in a 40-ft-diameter projection sphere. Each projection system consists of two terrain projectors to provide a realistic terrain scene, a target image generator and projector, a laser target projector, and an area-of-interest projector. The terrain scene, driven by a Computer-Generated Image (CGI) system, provides reference in all six degrees of freedom in a manner that allows unrestricted aircraft motions. The resulting sky-Earth scene provides full translational and rotational cues. The internal visual scene also provides continuous rotational and bounded (300 ft to 45 000 ft) translational reference to the other (target) vehicle in six degrees of freedom. The target image, a computer-generated model, is presented to each pilot and represents the aircraft being flown by the other pilot. This dual simulator can be tied to a third dome (the General Purpose Fighter Simulator) and thus provide three-aircraft interactions when required. The image for the second aircraft is generated by a digital laser projector. For a higher resolution visual scene, an area-of-interest projector system is available in each sphere to provide a 30° vertical by 40° horizontal display.

Each cockpit provides three color displays with a 6.5-in-square viewing area and a wide-angle head-up display. Kinesthetic cues in the form of a g-suit pressurization system, helmet loader system, g-seat system, cockpit buffet, and programmable control forces are provided to the pilots consistent with the motions of their aircraft. Other controls include a side-arm controller, dual throttles, and a rotorcraft collective. Simulated engine sounds and wind noise add realism.

Research applications include studies of advanced flight control laws, helmet-mounted display concepts, and performance evaluation of new aircraft design concepts for development programs such as F-18 E/F, AX, and F-22. **(Lemuel E. Meetze, 46452)**

Visual/Motion Simulator

The Visual/Motion Simulator (VMS) is a general-purpose simulator consisting of a two-person cockpit mounted on a six-degree-of-freedom synergistic motion base. Four collimated visual displays, compatible with the Computer-Generated Image (CGI) system, provide out-the-window scenes for the left- and right-seat front and side windows. Six electronic displays mounted on the left- and right-side instrument panels provide for displays generated by a graphics computer. A programmable hydraulic-controlled two-axis side arm and rudder pedals provide for roll, pitch, and yaw controls in the left seat. Another programmable hydraulic-controlled loading system for the right seat provides roll and pitch controls for either a fighter-type control stick or a helicopter cyclic controller. Right-side rudder control is an extension of the left-side rudder control system. A friction-type collective control is provided for both the left and right seats. An observer's seat allows a third person to be in the cockpit during motion operation.

A realistic center control stand, in addition to providing transport-type control features, provides autothrottle capability for both the forward and reverse thrust mode. A cockpit display unit (CDU) is provided in the forward electronics panel of the center control stand. Motion cues are provided in the simulator by the relative extension

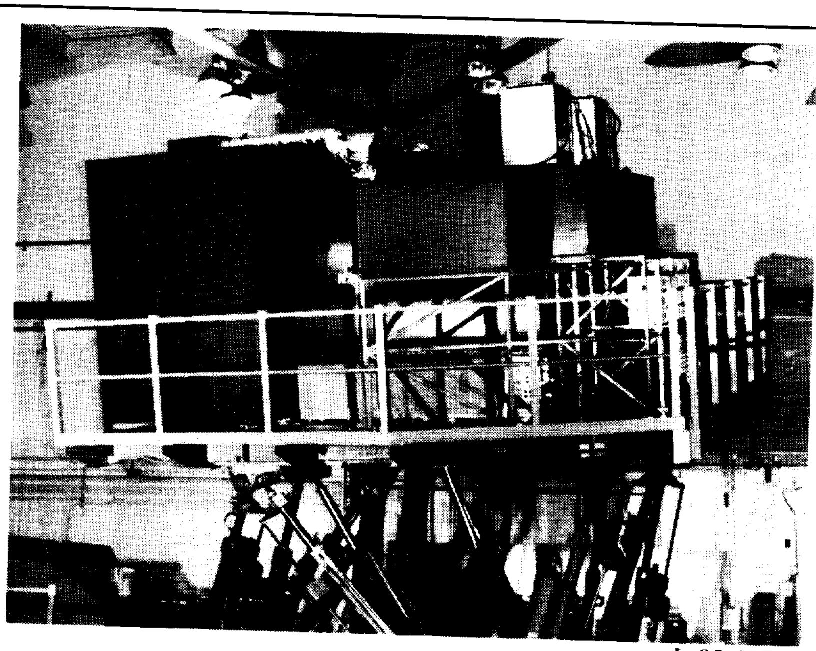

L-90-13717

or retraction of the six hydraulic actuators of the motion base. Washout techniques are used to return the motion base to the neutral point once the onset motion cues have been commanded.

Research applications have included studies for transport, fighter, and helicopter aircraft, including the National Aero-Space Plane (NASP), Personnel Launch System (PLS), and High-Speed Civil Transport (HSCT). These studies addressed phenomena associated with wake vortices, high-speed turnoffs, microwave landing systems, energy management, noise abatement, multibody transports, maneuvering stability flight characteristics, wind-shear recovery guidance, vortex flaps, and stereographic displays. Numerous simulation technology studies have also been conducted to evaluate the generation and usefulness of motion cues.
(John D. Rollins, 46448)

Space Simulation and Environmental Test Complex

The Space Simulation and Environmental Test Complex consists of facilities and equipment used to evaluate and qualify space-flight experiments and components. These facilities include a 60-ft vacuum sphere, an 8- by 15-ft thermal vacuum chamber, two 5- by 5-ft thermal vacuum chambers, two dynamic shaker systems, several thermal vacuum bell jars, and mass-properties measurement equipment.

Vacuum spheres and chambers are used to simulate high-altitude and space environments by providing vacuum pressures to 1×10^{-7} mm Hg and temperatures from −300°F to 300°F. A 60-ft vacuum sphere is used to simulate altitudes to 200 000 ft operating at ambient temperatures. Thermal vacuum chambers are equipped with cryogenic pumps and cold traps to avoid contamination to payloads, which can result from oil migrating from diffusion or turbomolecular pumps. The thermal vacuum chambers are also equipped with residual gas analyzers (RGA's) to continuously moni-

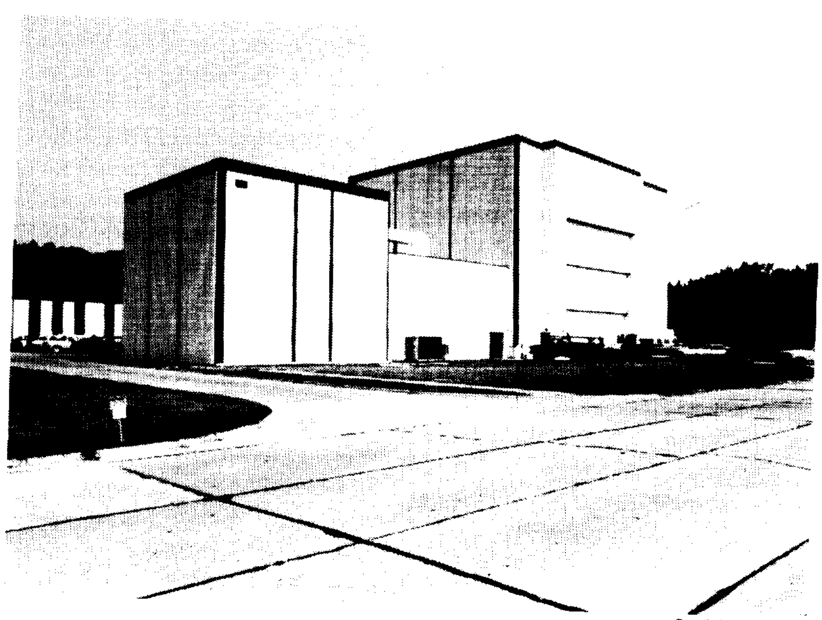

L-89-09325

tor and identify molecular contamination within the chambers.

The vibration test facility is equipped to perform vibration testing, modal analysis, and center-of-gravity and moment-of-inertia characterization of aerospace components, subsystems, and small payloads. Vibration capability consists of three dynamic shakers that share a common control and data-acquisition system. Dynamic shakers (2000, 17 000, and 24 000 force-lb) are used to verify payload performance by simulating expected mission acceleration forces.
(Thomas J. Lash, 45644)

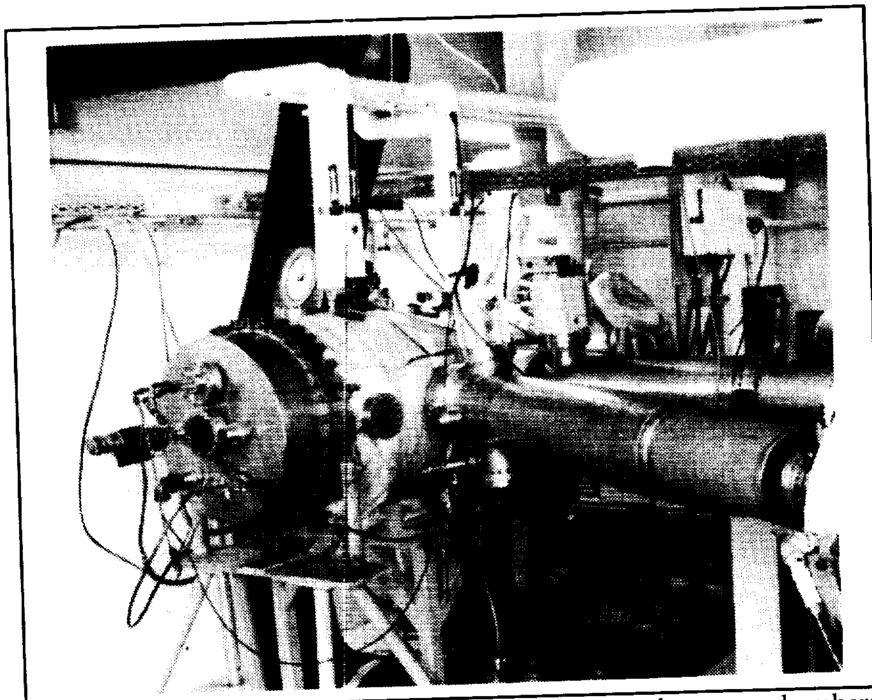

Space Environmental Effects Laboratory

The Space Environmental Effects Laboratory houses state-of-the-art research equipment to simulate the effects of the space environment on spacecraft materials and coatings. The research conducted in this laboratory includes studies of the durability of materials and coatings for specific space missions, studies of space environmental damage mechanisms, and techniques for improved laboratory simulation of the space environment for more reliable materials testing. The laboratory features a space-radiation simulation capability with 1-MeV electrons, 2-MeV protons, and solar ultraviolet radiation independently or simultaneously projected upon a 10-in-diameter target area in a clean, ultrahigh vacuum chamber. The target area can be maintained at any temperature from −100°C to 100°C or cycled over this temperature range during irradiation. These electron, proton, and ultraviolet radiation sources are uniquely designed for unattended, 24-hr-per-day continuous operation to provide cost-effective long-term testing.

Another ultrahigh vacuum chamber is equipped to expose materials to simulated solar ultraviolet (UV) radiation with two UV sources. A xenon source with quartz optics covers the wavelength range of 180 to 400 nm, and the second source is a deuterium lamp with a magnesium fluoride window to cover the vacuum UV and near-UV ranges of 115 to 400 nm. The test materials can be exposed at any temperature from −150°C to 100°C. This laboratory also has an atomic oxygen simulation system with a 2-in. × 3-in. exposure area and a vacuum ultraviolet radiation source. Another test facility is a specially designed ultraviolet exposure system that allows the simultaneous exposure of six coating specimens in individual ion-pumped vacuum chambers. These chambers mate to a spectrophotometer to allow *in situ* measurement of the solar absorptance under conditions simulating the high vacuum of space.
(Wayne S. Slemp, 41334)

Advanced Technology Research Laboratory

The Advanced Technology Research Laboratory was dedicated in 1989 in support of the Space Research and Technology Program. The laboratory has facilities that are used to perform a wide range of research activities to further both space and aeronautics technologies. The Aerothermodynamic Physics Laboratory provides the capability to understand the thermal radiation process of hypervelocity gases interacting with spacecraft and aircraft. The Low Pressure Physics Research Laboratory supports the study of

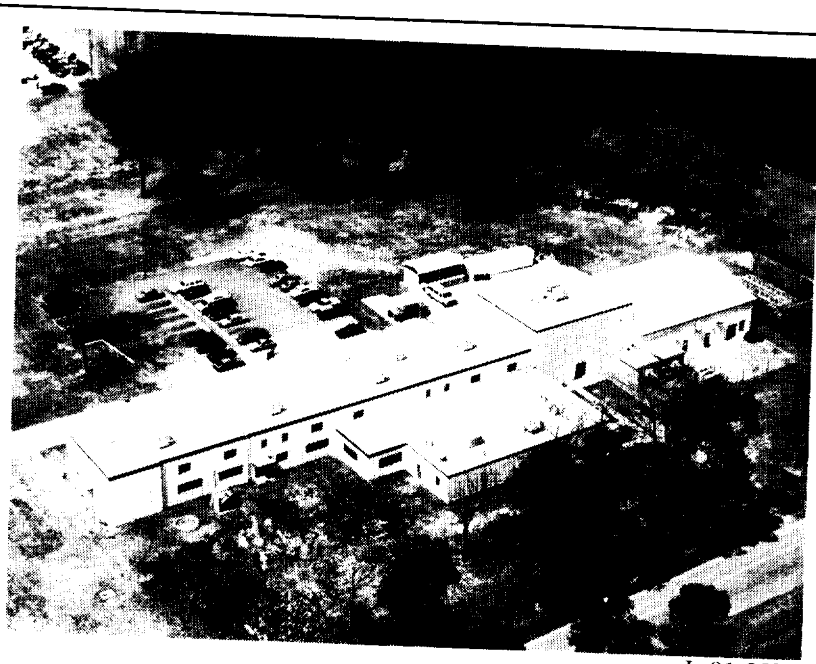

L-91-3852

gas-surface interactions critical to space and aeronautical vehicles. The Radiation Physics Computer Laboratory is used to perform world-class theoretical research dealing with human radiation exposure and shielding in high-flying aircraft as well as research on advanced space missions. The Micrometeoroid Analysis Laboratory contains equipment to analyze panels returned from space to model the micrometeoroid-debris environment of the Earth and the effects of that environment on NASA and commercial spacecraft.

Ultrahigh-vacuum and other equipment simulate the space environment and specialized conditions associated with advanced spacecraft. The focus is on the study of reaction cross sections at kinetic energies between 0.5 and 5 electron volts; the transport of hydrogen through National Aero-Space Plane surfaces; the establishment of high-purity, high-energy atomic oxygen beams; the development of high-purity molecular oxygen for medical purposes; and the development of methods to extract oxygen from the Martian atmosphere or from other gases.

Laboratory equipment includes: (1) the latest computer technology, which is fully integrated into the Center's high-speed data network; (2) a large bank of capacitors; (3) solar simulators; (4) optical spectrometers; (5) an 85-m^3 vacuum tank with a high-capacity vacuum pump; and (6) surface analysis equipment.
(E. J. Conway, 41435)

Spacecraft Dynamics Laboratory

The Spacecraft Dynamics Laboratory is a group of facilities designed for structural dynamics, vibration isolation, and pointing controls research on aerospace structures and equipment. Testing at low frequencies, 0 to 300 Hz, is emphasized for characterizing structural systems and high-gain pointing control systems. The individual laboratories are described herein.

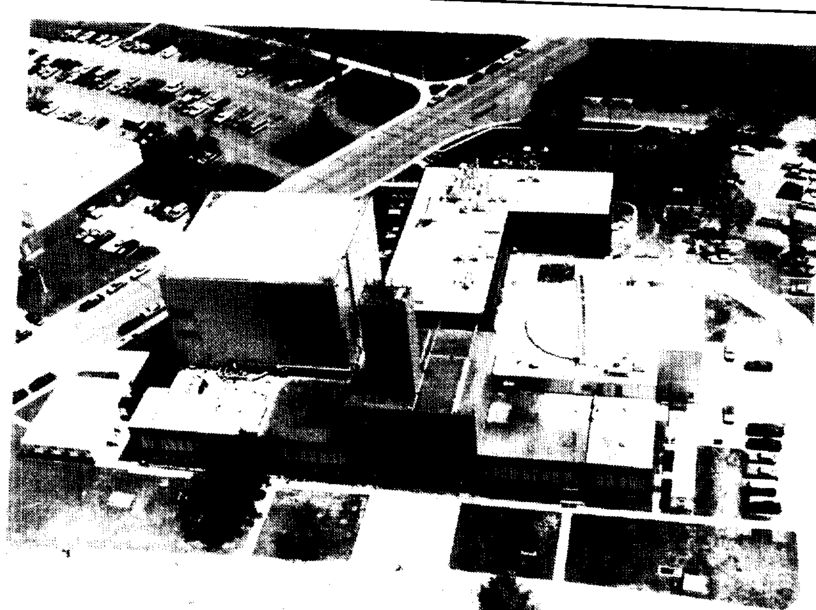

L-87-4626

The 16-m Thermal Vacuum Chamber has a 55-ft diameter cylinder, a 64-ft-high hemispherical dome peak, a flat floor, and a rotation option of a centrifuge arm or table. The centrifuge is rated at 20 000 lb to 100 g with a 50 000 force-lb capacity and a maximum allowable specimen weight of 2000 lb. Access is by two doors; one door is 20 × 20 ft. A vacuum of 100 μm Hg can be achieved in 160 minutes. Temperature gradients of 100°F can be obtained from portable radiant heaters and liquid-nitrogen-cooled plates. The laboratory is serviced by a control room that features video monitoring and 138 channels of data acquisition.

The Space Structures Research Laboratory is an open room with an area of 5200 ft^2. There is a work platform 73 ft above the floor with removable decking, a 20- × 30- × 40-ft freestanding gantry for isolated suspension, and a vertical 12- × 12-ft backstop. The laboratory is serviced by a control room that can support several simultaneous test setups. The control room features video monitoring, 784 channels of data acquisition, a 384-channel structural test and analysis system, a distributed control system, and an environmental monitoring system.

The Structural Dynamics Research Laboratory is dominated by a 38-ft-high backstop. Test areas around this backstop are 15 × 35 × 38 ft and 12 × 12 × 95 ft with spiral stairs, ladders, and platforms for high access. The laboratory is supported by a control room that features video monitoring and 416 channels of data acquisition.

A variety of dynamic test and signal processing equipment is available to support these laboratories, including 10-in-stroke shakers, near-zero spring-rate suspension systems, and an arc-second attitude and jitter measurement system.
(Robert Miserentino, 44318)

Intravehicular Automation and Robotics (IVAR) Laboratory

The Intravehicular Automation and Robotics (IVAR) Laboratory contains a full-size mock-up of a space laboratory module, which houses simulated space science and materials processing experiments, with remote control and monitoring capabilities for principal investigators. Full-size mock-ups of flight-qualifiable systems can be installed in laboratory racks, and simulated microgravity experiments can be controlled remotely by using supervised autonomy. A mobile telerobotic logistics system will support sample changing and resource sharing for multiple experiments. Expert system-based executive software supports automated planning and error detection. Computer graphics supports task planning and operator interface development. Increased automatic functions, dedicated experiment robotics, and resource sharing using an onboard logistics system are being investigated. Currently, the laboratory contains a full-size mock-up of a microgravity protein crystal growth experiment, a vapor deposit furnace experiment, and a logistics support system.
(Ralph W. Will, 46672)

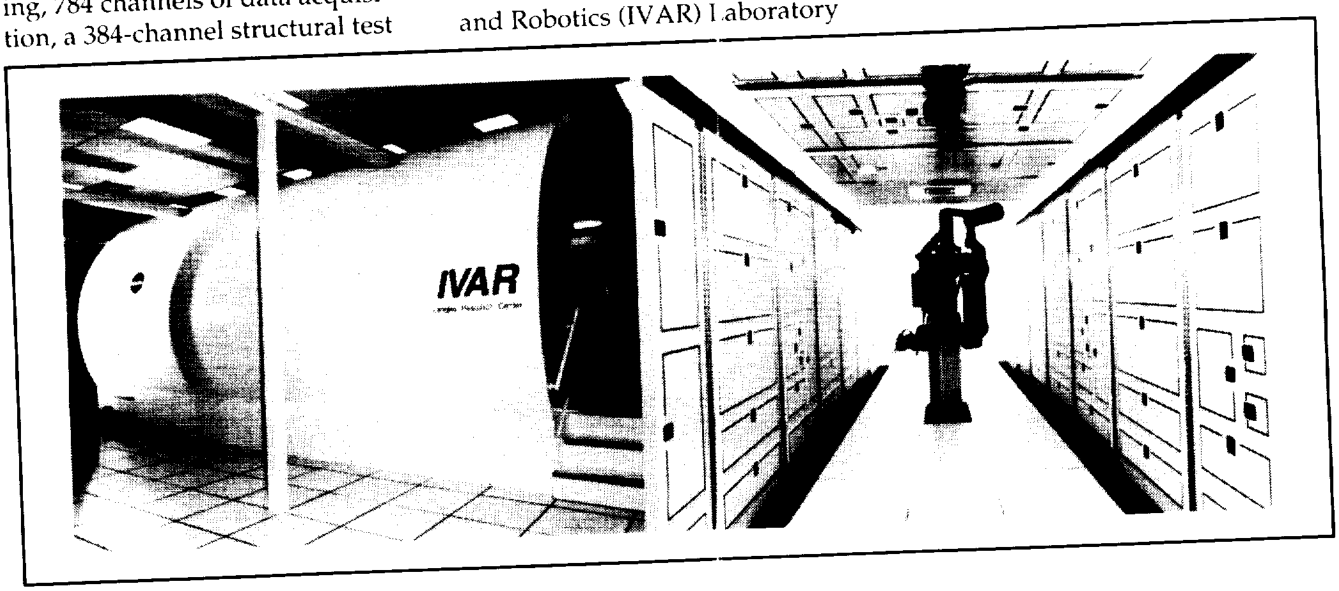

Materials Research Laboratory

The Materials Research Laboratory houses experimental facilities for conducting a wide range of research to characterize the behavior of advanced structural materials under the application of mechanical and thermal loads. This research encompasses the study of deformation characteristics and damage mechanisms leading to the development of nonlinear constitutive models, strength criteria, and durability and damage tolerance criteria. A high-bay area surrounded by 8 enclosed laboratories houses 49 servohydraulic testing systems (1 kip to 400 kips), a scanning electron microscope, 3 X-ray radiography systems, 13 high-temperature creep frames, and 3 multiparameter test facilities. The multiparameter facility permits the simultaneous testing of up to six coupons under combined temperature (to 3000°F), cyclic mechanical loads, and partial pressures. An environmental fatigue laboratory has dedicated test facilities for aqueous environments, inert gases, and ultrahigh vacuum. A long-term durability facility has 20 load frames and temperature chambers for testing composite panels under synchronized cyclic thermal and mechanical loads to simulate supersonic flight conditions.

The new light-alloy laboratory complex is also part of the Materials Research Laboratory. This laboratory provides integrated research facilities to conduct alloy synthesis and development, innovative processing and joining, coatings technology, and complex characterization using electron optics and surface analysis techiques. Equipment and instrumentation are available to conduct surface analysis, thermal analysis, metallurgy, microscopy, X-ray, and dimensional stability studies. The complex is divided into separate and enclosed discipline-oriented laboratories. Each laboratory has an independent environmental control and a distribution system for laboratory gases and liquid nitrogen. A separate laboratory is also available for the development of thin-gage metal-matrix materials.
(Charles E. Harris, 43449)

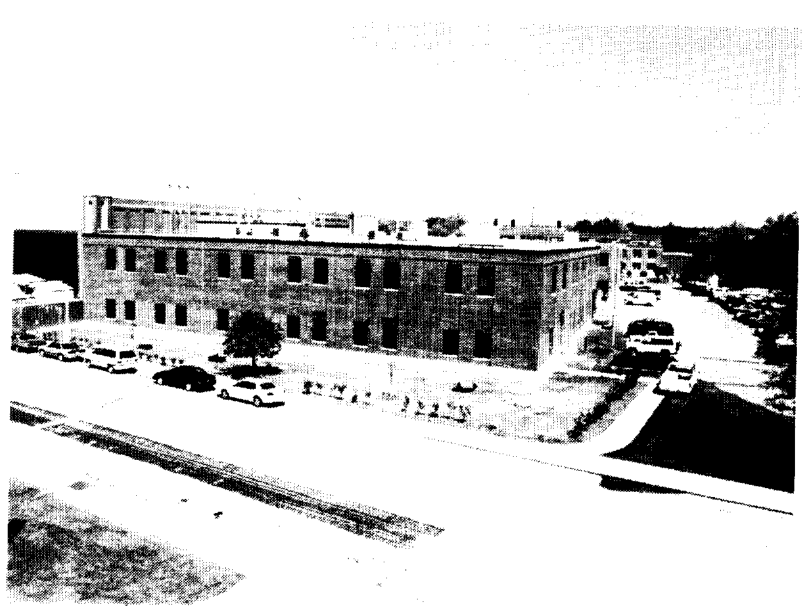
L-93-4414

Structures and Materials Research Laboratory

Built in 1939 to contribute to the development and validation of aircraft structural designs during World War II, this laboratory currently supports a broad range of structural and materials development activities for advanced aircraft, aerospace vehicles, and space platform and antenna structures. Research includes the development, fabrication, and characterization of advanced materials and the development of novel structural concepts. Static testing, environmental testing, and material fabrication and analysis are performed. Emphasis is on the development of structural mechanics technology and advanced structural concepts enabling the verified design of efficient, cost-effective, damage-tolerant, advanced-composite airframe structural components subjected to complex loading and demanding environmental conditions. This research also emphasizes advanced space-durable materials and structural designs for future large space systems that afford significant improvements in performance and economy. A significant feature of the laboratory is its static testing equipment, which has capabilities up

Polymeric Materials Laboratory

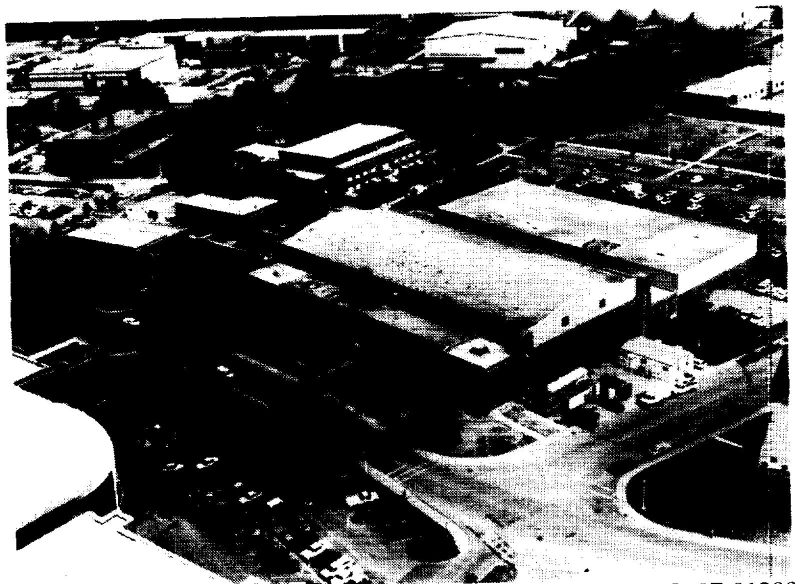

L-87-01200

to 1 200 000 lb (specimens 6 ft wide by 18 ft long) and down to 10 000 lb (smaller specimens).

This complex also houses the Langley state-of-the-art analytical and metallurgical laboratory, which features all aspects of material specimen preparation and examination. Complete automated metallographic preparation equipment is available for research on light alloys as well as metal-matrix and resin-matrix composites. Optical microscopy includes quantitative image analysis and regular microscopy. Current-technology electron microscopy is available, including scanning electron microscopy, scanning transmission electron microscopy, and electron microprobe X-ray analysis. Also included in the laboratory complex is the Carbon-Carbon Research Laboratory. This laboratory is dedicated to the development, fabrication, testing, and analysis of carbon-carbon and refractory composite materials for use as thermal protection and hot structural materials for advanced hypersonic vehicles to temperatures up to 3000°F.
(James H. Starnes, 43168)

The Polymeric Materials Laboratory complex provides 25 000 ft^2 of floor space for the synthesis and characterization of high-performance polymers as well as the development of processing technology and composite fabrication. The complex contains seven synthesis laboratories and a bench-scale laboratory designed for synthesis of large batches of polymeric materials. The facility also contains a film-casting laboratory with environmentally controlled film-casting boxes and a chemical storage area that is protected by an automatic CO_2 extinguisher system.

Much of the work of this laboratory is directed toward the synthesis of processible, tough, durable, high-performance matrices and the development of relationships between molecular structure, neat

L-86-8407

resin properties, and composite properties. Classes of polymers being analyzed include amorphous, semi-crystalline, and lightly cross-linked thermoplastics; semi-interpenetrating networks; toughened thermosets; and piezoelectric polymers. Extensive characterization equipment is housed in the instrument laboratories and is used for performing chromatography; thermal analyses; X-ray, rheological, rheometric, and spectroscopic characterizations; and mechanical strength determinations of adhesives, polymer moldings, films, fibers, and composites.

The Composites Processing Laboratory is the focal point at Langley for research and development of advanced polymer composite systems. Its primary function is to determine the potential of new polymers for use as matrix systems for the fabrication of advanced fiber-reinforced composites. Unique dry-powder-coating-melt-fusion equipment is employed to fabricate prepreg from advanced, difficult-to-process polymer matrix materials. A new modular tape prepreg machine that is capable of making high-quality prepreg by solution coating, film casting, and direct fiber impregnation is now in operation. **(R. Baucom, 44252)**

Low-Frequency Antenna Test Facility

The Low-Frequency Antenna Test Facility is an indoor far-field measurement facility that provides a simulated free-space environment for performing antenna measurements to support the analysis and design of advanced antenna systems for NASA's current and future research programs.

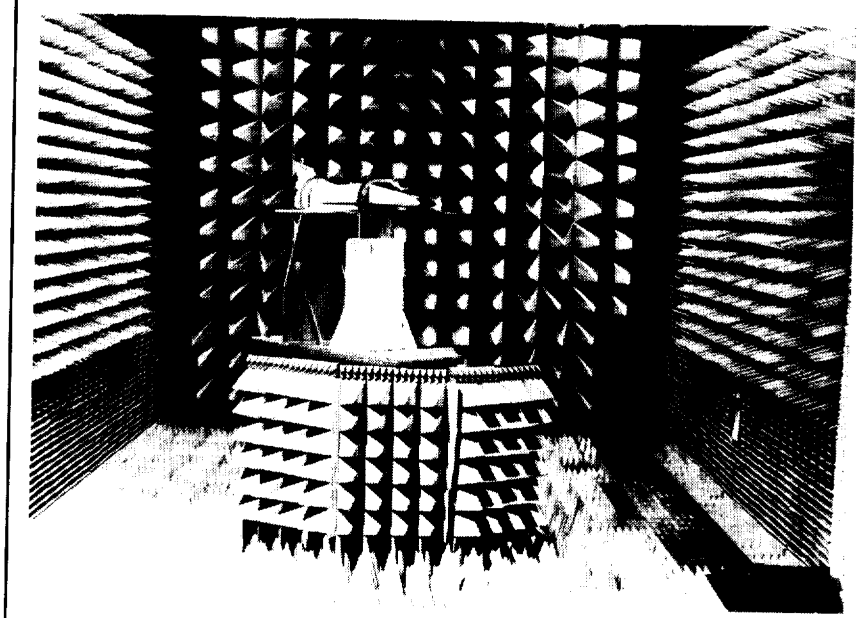

L-91-00627

Antenna measurements can be conducted over the 0.10- to 40-GHz frequency range. Test models or antennas up to 12 ft in length and 2000 lb or less in weight can be measured as long as the far-field criteria are satisfied. Instrumentation includes a Hewlett Packard (HP) Model 85301B antenna measurement system, a Flam and Russell Model FR959 workstation, an HP Model 8720C network analyzer, and a Scientific Atlanta precision antenna/model positioning system. Test-chamber size is 30 ft high by 32 ft wide by 105 ft long. Measured data stored on disk can be processed to prove antenna directivity, polar or rectangular plots of the radiation patterns, and three-dimensional contour plots of the antenna radiation characteristics.
(Thomas Campbell, 41772)

Compact Range Facility

The Compact Range Facility is an indoor facility that utilizes a commercially available reflector that was modified by adding an elliptical rolled edge to improve the quality and size of the quiet zone. The facility provides a simulated free-space environment for performing antenna and electromagnetic scattering measurements in support of NASA aerospace research programs.

Antenna or scattering measurements can be conducted over the 2- to 18-GHz frequency range. The quiet zone is approximately 4 ft high by 8 ft wide by 8 ft long. Model handling is accomplished with a 2000-lb-capacity bridge crane. Model supports include metal pylons and foam columns. Instrumentation is a Hewlett Packard Model 8530 network-analyzer-based system. The test chamber

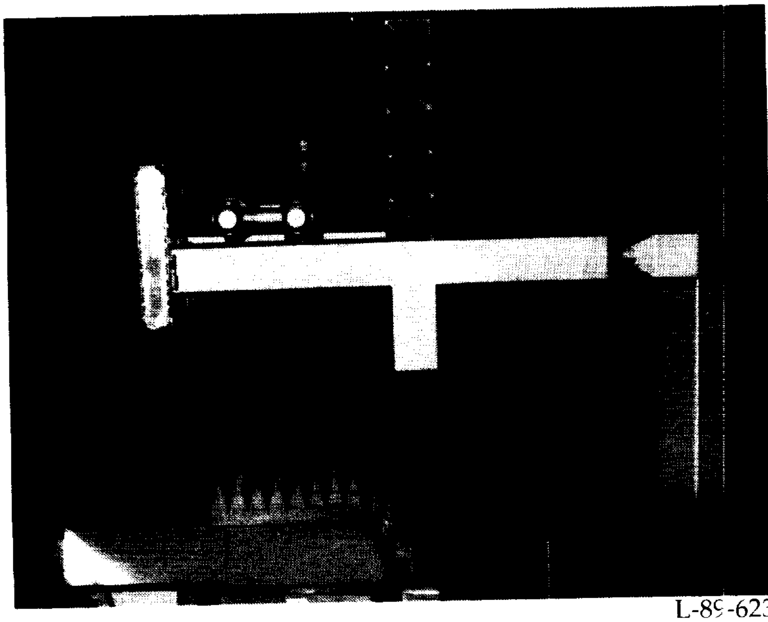

L-89-6234

is 30 ft high by 28 ft wide by 65 ft long.
(Thomas Campbell, 41772)

Experimental Test Range

The Experimental Test Range (ETR) is an indoor radio-frequency (RF) anechoic test facility that utilizes a dual Gregorian compact-range, blended-edge reflector system to perform antenna and electromagnetic scattering measurements. The facility provides an RF shielded, simulated free-space environment for performing electromagnetic measurements in support of NASA aerospace research programs and compact-range technology advancement.

Antenna or scattering measurements can be conducted over the 2- to 18-GHz frequency range. The quiet zone is approximately 6 ft high by 8 ft wide by 8 ft long. Model handling is accomplished with a 4000-lb-capacity bridge crane. Instrumentation includes a pulsed/CW radar and a Tektronix XD 88/30 workstation for data processing. The test chamber is 40 ft high by 40 ft wide by 65 ft long.
(Thomas Campbell, 41772)

Impact Dynamics Research Facility

The Impact Dynamics Research Facility (IDRF) is used to conduct crash testing of full-scale aircraft under controlled conditions. The aircraft are swung by cables from an A-frame structure that is approximately 400 ft long and 230 ft high. The impact runway can be modified to simulate other ground crash environments, such as packed dirt, to meet a specific test requirement.

Each aircraft is suspended by cables from two pivot points 217 ft off the ground and allowed to swing pendulum-style into the ground. The swing cables are separated from the aircraft by pyrotechnics just prior to impact. The length of the swing cables regulates the aircraft impact angle from 0° (level) to approximately 60°. Impact velocity can be varied to approximately 65 mph (governed

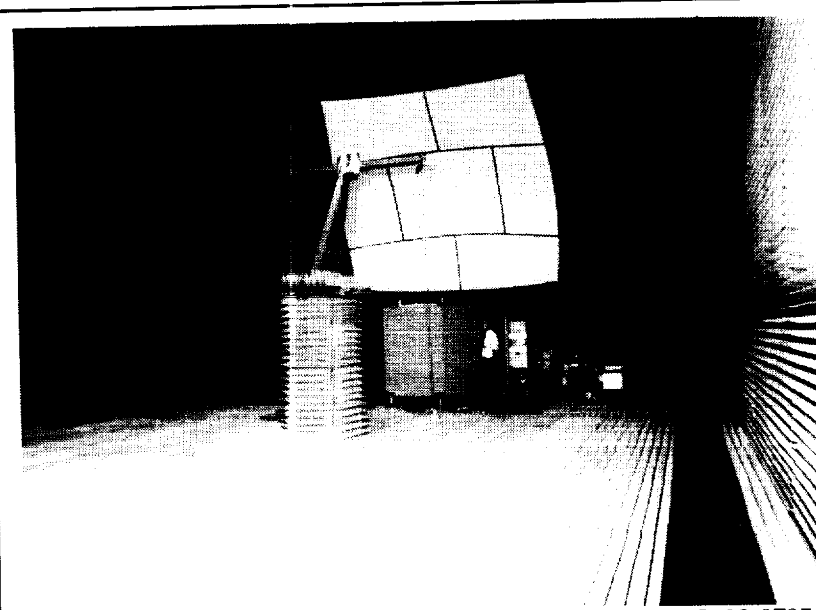

L-90-07956

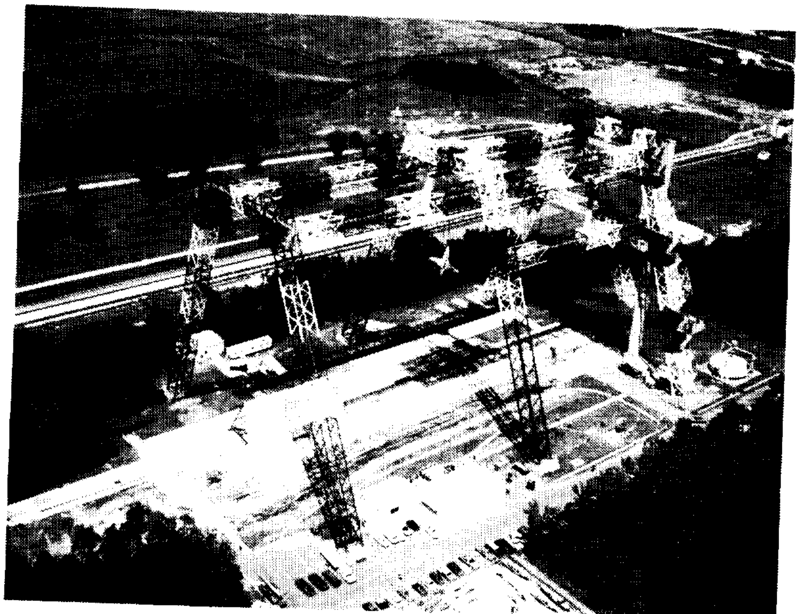

L-74-2505

by the pullback height). Variations of aircraft pitch, roll, and yaw can be obtained by changing the aircraft suspension harness attached to the swing cables. Onboard instrumentation data are obtained through an umbilical cable that is hard wired to the control room at the base of the A-frame. Photographic data are obtained by onboard, ground-mounted, and A-frame-mounted cameras. Maximum allowable weight of the aircraft is 30 000 lb.
(Granville Webb, 41303)

Aircraft Landing Dynamics Facility

The Aircraft Landing Dynamics Facility (ALDF) is a test track primarily used for landing-gear research activities. The ALDF uses a high-pressure water-jet system to propel the test carriage along the 2800-ft track. The propulsion system consists of an L-shaped vessel that holds 28 000 gal of water pressurized up to 3150 lb/in^2 by an air-supply system. A timed quick-opening shutter valve is mounted on the end of the L-shaped vessel and releases a high-energy water jet, which catapults the carriage to the desired speed. The propulsion system produces a thrust in excess of 2 000 000 lb, which is capable of accelerating the 54-ton test carriage to 220 knots within 400 ft. This thrust creates a peak acceleration of approximately 20g. The carriage coasts through the 1800-ft test section and decelerates to a velocity of 175 knots or less before it intercepts the five arresting cables that span the track at the end of the test section. The arresting system brings the test carriage to a stop in 600 ft or less. Essentially, any landing gear can be mounted on the test carriage, including those exhibiting new or novel concepts, and virtually any runway surface and weather condition can be duplicated on the track.
(Granville Webb, 41303)

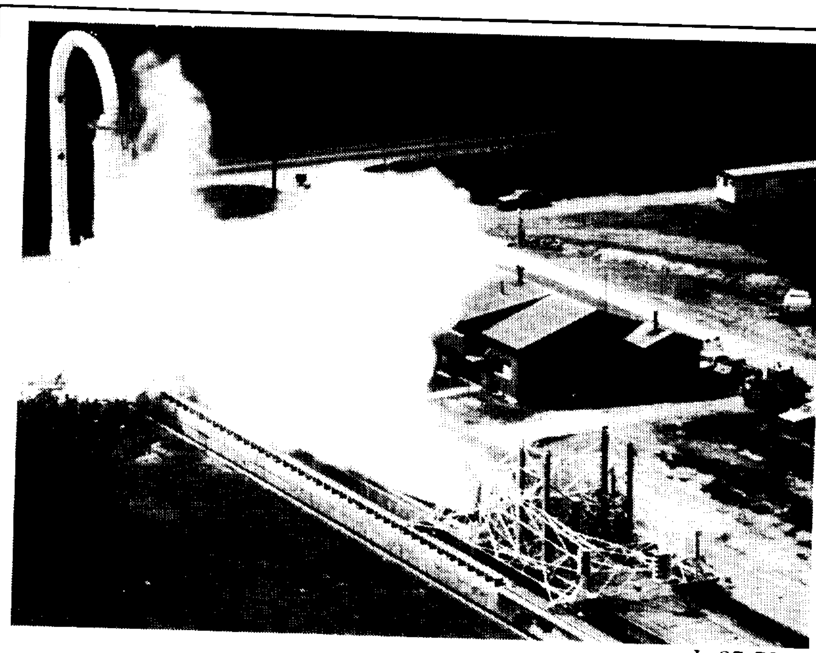

L-85-5341

Flight Research Facility

The hangar is the centerpiece of the Flight Research Facility. It provides a clear floor space of approximately 87 000 ft^2. Door dimensions will allow entry of a Boeing 747 or any other non-T-tail, commercial or military transport-class aircraft. Features such as floor air and electrical power services, radiant floor heating to minimize corrosion-causing moisture, a deluge fire-suppression system, energy-saving lighting, modern maintenance facilities, and entry doors and taxiways on either side of the building make this structure an effective and versatile facility. Surrounding the hangar are ramp areas and a high-power engine run-up stand with load-bearing capabilities sufficient to handle a wide variety of aircraft. Extensive and modern maintenance equipment makes it possible to repair, maintain, and modify a wide range of aircraft including modern metal and composite airliners and business-class aircraft, fighters, and helicopters.

The inventory of research and program support aircraft enables research to be performed over a wide range of flight conditions, from hover to supersonic speeds and from ground level to altitudes over 50 000 ft. The current research fleet includes a B-737-100, an F-16XL, an OV-10A, an LR-28, and a UH-1H. Present research topics include terminal-area traffic-flow studies, microwave-landing-system (MLS) approach optimization, global-positioning-system (GPS) navigation and approach optimization , handling qualities, aircraft performance, engine noise, wake-vortex detection and quantification, and high-lift performance definition and optimization, all of which make use of the fixed-wing aircraft. The UH-1H has been modified with the addition of tall skids to create a centerline drop capability for powered and unpowered remotely controlled scale models of high-performance airplanes. These research activities are conducted at the Radio-Controlled Drop Model Facility, which is located remotely from the primary Flight Research Facility. This complex is used to study the low-speed dynamic behavior of aerospace vehicles, with particular emphasis on high angle-of-attack characteristics of combat aircraft.

L-90-7025

Some Langley aeronautical research experiments are flight-tested at Dryden Flight Research Facility and Wallops Flight Facility. Within the (Langley) Flight Research Facility, a Flight Control Center has been created to allow the full monitoring of flight tests at any NASA site and to allow the control of flights originating at Langley on a real-time basis. Via satellite or the Langley tracking antenna system, these facilities enable researchers at Langley to receive test data, voice transmissions, and video and allow the researchers to assess the effectiveness of a particular maneuver, to review the quality of data acquired, and to evaluate experiments in near real time. This system uses the satellite-based NASA Communications System (NASCOM) Time Division Multiple Access (TDMA) System and the Langley multi-frequency tracking antenna system (MTAS).

(Harry Verstynen, 43875)

16- by 24-Inch Water Tunnel

The Langley 16- by 24-Inch Water Tunnel is used for flow-visualization studies at low Reynolds numbers. The tunnel

L-87-3479

has a vertical test section with an effective working length of approximately 4.5 ft. The test section is 16 in. high by 24 in. wide. All four sidewalls are Plexiglas to provide optical access. A pump transfers the water from the test-section exit to the reservoir upstream of the test section. The test-section velocity can be varied from 0 ft/sec to 0.75 ft/sec. The unit Reynolds number range for water at 78°F for this velocity range is 0 to 7.7×10^4 ft^{-1}. The normal test velocity that produces smooth flow is 0.25 ft/sec.

A sting-type model support system positions the model. The model attitude can be varied in two planes over angle ranges of about 33° and 15°. Ordinary food coloring is used as a dye to visualize the flow. Dye may be ejected from small orifices on the model surface or injected upstream of the test section. A laser fluorescence anemometer is available to provide more quantitative flow information.

(Bobby L. Berrier, 43001)

Scientific Visualization System

A Scientific Visualization System has been brought on-line in the Analysis and Computation Division's Animation Laboratory to support videotape recording of computer graphics generated on the Supercomputing Network Subsystem or on high-performance graphics workstations. Dynamic video displays are essential for accessing, understanding, analyzing, documenting, and displaying the vast numerical databases resulting from computer simulations of time-dependent physical phenomena or from detailed measurements in ground-based or in-flight experimental facilities.

The central component of the system is the DF/X Composium, a digital-component video-editing suite. The Composium menu-driven software offers a fully

L-92-08444

featured video-processing and special-effects capability, including three-dimensional fonts, paint box, layering, and compositing. The Composium provides centralized control of all ancillary equipment, including the ability to handle multiple video sources. Two Abekas real-time digital video disk recorders provide on-line storage for a total of 75 seconds of video. One Abekas is on the Langley Ethernet network and can accept raster image files in multiple formats directly from a remote workstation. Two digital videotape recorders are used for archive storage and as high-capacity working stores. A Silicon Graphics IRIS 4D/340 high-performance graphics workstation running the FAST data visualizer and WAVEFRONT modeling-animation software is also available. The system includes analog tape recorders in VHS, S/VHS, Umatic, Umatic/SP, BetaCam, and BetaCam/SP formats that may be used as either sources of video input or as a means of recording a completed video for distribution.

This system makes it possible to create professional, self-contained video technical reports to document and explain the results of Langley's theoretical or experimental research. Two representative videos that use the system are the "Visualization of Earth Radiation Budget Experiment (ERBE) Data" and "HL-20 as a Personnel Launch System", which demonstrate the system's advanced capabilities.
(Bill von Ofenheim, 46712)

Geometry Laboratory (GEOLAB)

A geometry laboratory, GEOLAB, has been established in the Analysis and Computation Division to provide advanced capabilities to support research applications that require surfaces and grids for numerical simulations in computational fluid dynamics (CFD) and computational structural mechanics (CSM). The laboratory consists of high-speed workstations, advanced software geometry tools, and a staff skilled in the production of surface representations and computational grids for complex aerospace configurations.

The GEOLAB hardware includes nine Silicon Graphics, Inc., high-performance workstations, four X-terminals, and a Cyberware color 3D laser digitizer. The software includes computer-aided design (CAD), grid generation, and visualization tools that have been developed or acquired to facilitate the generation and analysis of surface representations, surface grids, and volume grids for both structured and unstructured techniques. Among the tools currently being used in the GEOLAB are: GRIDGEN, ICEM-CFD, VGRID, GridTool, SurfACe, and Volume.

The GEOLAB staff is available to assist researchers to develop the necessary skills to use the hardware and software or to perform specific tasks when requested. Surfaces and grids have been generated for configurations such as the Space Shuttle, HSCT, F-18, and the F-16XL. The digitizer has been used to scan the X-15, F-22, and Waverider to create surface grids. Office space is available for guest researchers to temporarily colocate, on a space-available basis, in GEOLAB while using the laboratory.
(Eric L. Everton, 45778)

L-91-14599

Supersonic Low-Disturbance Pilot Tunnel

The Supersonic Low-Disturbance Pilot Tunnel, which has been in operation since 1981, uses high-pressure air from a 4200-psia tank field dehydrated to a dew-point temperature of −52°F. The air, filtered to remove all particles larger than 1 μm in size, is reduced in pressure by control valves located upstream of the settling chamber. The tunnel flow exhausts to a vacuum sphere complex that provides run times up to approximately 1 hour for stagnation pressures from 25 psia to 100 psia and Reynolds numbers from 1.8 to 18×10^6 per ft at a free-stream Mach number of 3.5. The settling chamber contains seven antiturbulence screens along with a number of dense, porous plates that function as acoustic baffles to attenuate incoming pressure fluctuations from approximately 0.2 percent of stagnation pressure to approximately 0.01 percent. In addition, the radiated noise is reduced by making the nozzle wall boundary layers laminar through the use of boundary-layer removal slots just upstream of the nozzle throat and a properly tailored expansion nozzle with highly polished walls. The quiet test core is approximately 6 in. long, 2 in. wide, and 4 in. high.

The low-disturbance environment of this tunnel makes the tunnel a unique facility for high-speed transition research that cannot be done in conventional tunnels.
(Michael J. Walsh, 45542)

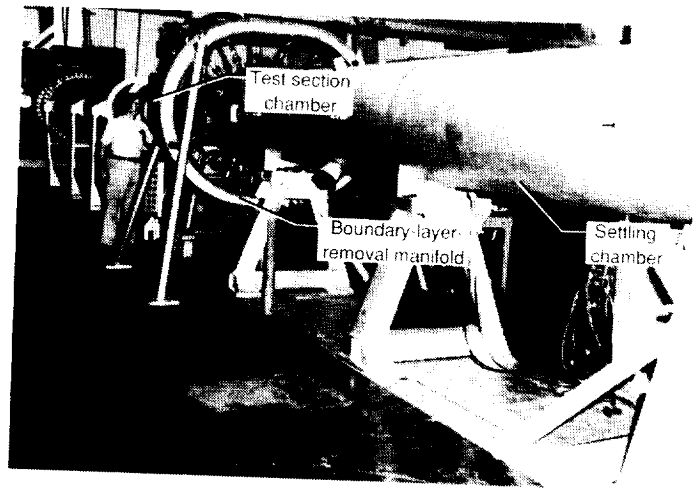

L-81-4419

Pyrotechnic Test Facility

The Pyrotechnic Test Facility contains the Langley Research Center aerospace environmental and functional simulation equipment used for the handling and testing of small-scale potentially hazardous materials, including explosive and pyrotechnic materials, devices, and systems. The facility contains three 12- by 18-ft test cells, which are used for assembly and checkout, environmental testing, and test firing. A 30- by 60-ft general-purpose, high-bay, open work area is used for

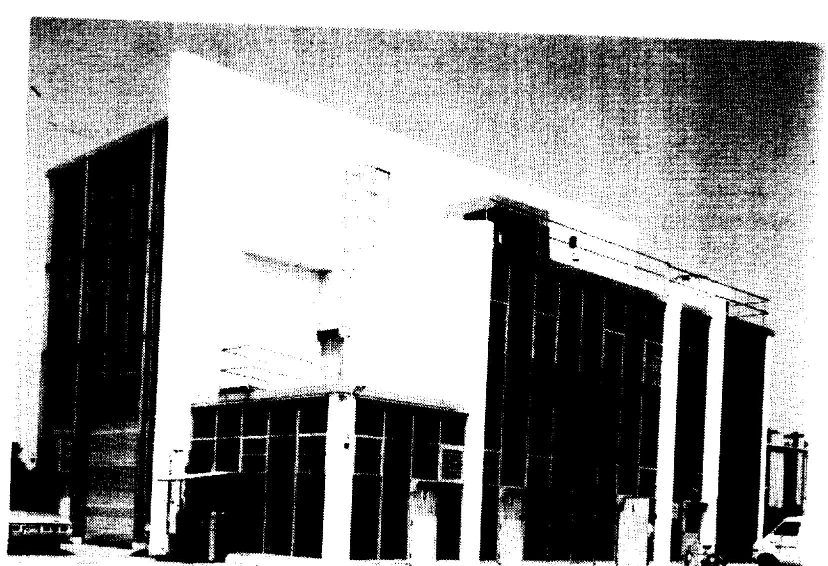
L-80-5749

system testing and contains control systems for environmental and functional testing. These test capabilities include remotely operated vibration, mechanical-shock, constant-acceleration, thermal, thermal vacuum, electrostatic-discharge systems, and electrical and mechanical firing systems. High-speed measurements of acceleration, force, pressure, temperature, and explosive performance monitoring systems are also available.
(Laurence J. Bement, 47084)

Probe Calibration Tunnel

The Langley Probe Calibration Tunnel (PCT) is an open-jet pressure tunnel with a capability to independently control velocity, density, and total temperature. The primary purpose of this unique facility is to economically calibrate probes for the major NASA aerospace test facilities. Typical operational cost for the PCT is 1 percent of the cost to operate a major facility. The PCT has two interchangeable nozzles that give it a continuous-flow capability over a Mach number range of 0.05 to 1.0. The operational envelope shown in the figure illustrates the PCT mass-flow requirements for an equivalent stream tube for several of NASA Langley's major research facilities. The subsonic nozzle and transonic nozzle both maintain a 15:1 ratio of probe diameter to nozzle-exit diameter to assure flow uniformity. The combination of the staged pressure system and the low mass-flow requirements of the PCT enables economic and accurate probe calibration for hot-wire probes, flow-angularity probes, thermocouples, and other miscellaneous aerodynamic probes. Tunnel stagnation pressure and temperature can be varied from a minimum of 0.20 atm to a maximum of 10 atm and from 500°R to 600°R, respectively. This corresponds to a Reynolds number range of 1×10^6 to 51×10^6 per foot for a Mach number of 1.
(Gregory S. Jones, 41065)

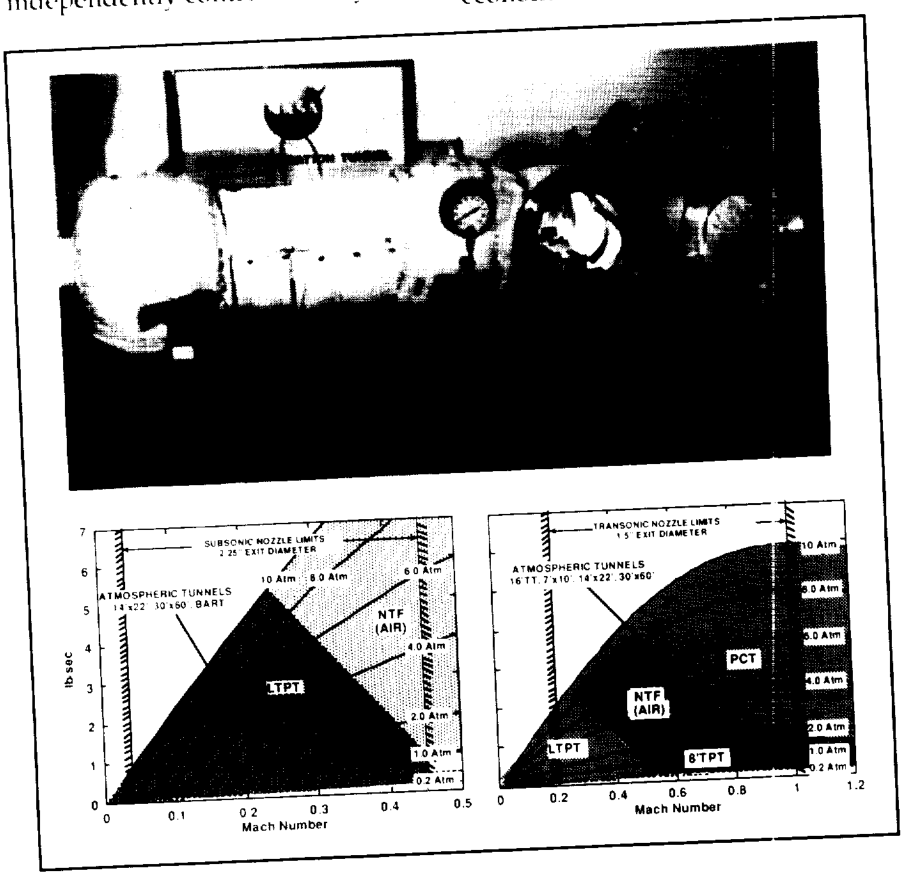

Aerospace Test Facilities

Contributing Organizations

RESEARCH AND TECHNOLOGY

Aeronautics Directorate

The Aeronautics Directorate was composed of approximately 350 scientists and engineers who led the Center's programs in basic and applied research in various aeronautics disciplines, utilizing research wind tunnels, aircraft, and computers that have a replacement value exceeding $1 billion. The Directorate was organized into four research divisions, which conducted aeronautical research to advance the state of the art throughout the complete aerodynamic speed range. The Advanced Vehicles Division conducted multidisciplinary advanced aeronautical vehicle studies to assess the benefits of discipline research advances and to identify potential new research thrusts. The Applied Aerodynamics Division conducted research on subsonic through hypersonic aerodynamics including propulsion integration using computational fluid dynamics techniques and a variety of wind tunnels. The Flight Applications Division conducted experiments that complement the ground-based research efforts of other organizations at the Center with an emphasis on flight experiments, flight dynamics, and aviation safety. The Fluid Mechanics Division conducted theoretical, computational, and experimental research to advance the state of knowledge in fluid mechanics as it applies to the design of advanced aircraft and missiles across the speed range and to hypersonic propulsion systems.

This past year a number of significant research efforts were accomplished, including an intensive effort to analyze the flow about the McDonnell Douglas MD-11 engine pylon in the presence of the wing. This effort resulted in the prediction of a 0.5- to 0.75-percent reduction in aircraft drag. The predictions were verified by McDonnell Douglas in flight tests, and the new pylon design was incorporated into the production MD-11 airplane.

Wing trailing-edge modifications that would reduce the drag of the McDonnell Douglas C-17 by 2 percent were evaluated in the 0.3-Meter Transonic Cryogenic Tunnel. Modifications to the winglet that also resulted in additional drag reductions were developed in the National Transonic Facility. Both of these modifications will be flight-tested on the C-17. In addition, tests in the Low-Turbulence Pressure Tunnel indicated that properly placed microvortex generators could eliminate a severe flow separation on the deflected flaps at certain approach conditions; thus, the lift coefficient was increased by about 0.3 and the section drag coefficient was reduced by about 50 percent.

The NASA/General Electric (GE) Hybrid Laminar Flow Control (HLFC) Nacelle Flight Program demonstrated, for the first time, the feasibility of laminar flow control applied to engine nacelles. As a result, GE is considering the incorporation of HLFC on future production nacelles.

Electromagnetic analysis programs (such as moment method techniques) have the capability to furnish detailed information about the surface currents on a body due to an electric plane wave excitation or the electric near-field response of the body, but the only results used are usually the monostatic or bistatic radar-cross-section returns. These results are presented in an integrated fashion and do not show the mechanisms that produced these results . Therefore, a need existed to visualize the basic quantities of electromagnetic scattering. A specialized computer program, EM-ANIMATE, was developed in-house to visualize and animate the surface currents and electric near-field data from the MOM3D electromagnetic scattering code developed under contract. EM-ANIMATE (LAR-15075) and MOM3D (LAR-15074) are available from COSMIC.

Significant progress has been made in the High-Speed Research Program toward a down-select of high-lift systems by the end of fiscal year 1994. NASA/industry wind-tunnel activities were conducted to assess several candidate high-lift concepts. Computational

REPORT DOCUMENTATION PAGE

Form Approved
OMB No. 0704-0188

1. AGENCY USE ONLY *(Leave blank)*

2. REPORT DATE
August 1994

3. REPORT TYPE AND DATES COVERED
Technical Memorandum

4. TITLE AND SUBTITLE
Research and Technology Highlights 1993

5. FUNDING NUMBERS

6. AUTHOR(S)

7. PERFORMING ORGANIZATION NAME(S) AND ADDRESS(ES)
NASA Langley Research Center
Hampton, VA 23681-0001

8. PERFORMING ORGANIZATION REPORT NUMBER
L-17397

9. SPONSORING/MONITORING AGENCY NAME(S) AND ADDRESS(ES)
National Aeronautics and Space Administration
Washington, DC 20546-0001

10. SPONSORING/MONITORING AGENCY REPORT NUMBER
NASA TM-4575

11. SUPPLEMENTARY NOTES

12a. DISTRIBUTION/AVAILABILITY STATEMENT

Unclassified–Unlimited

Subject Category 99

12b. DISTRIBUTION CODE

13. ABSTRACT *(Maximum 200 words)*

The mission of the NASA Langley Research Center is to increase the knowledge and capability of the United States in a full range of aeronautics disciplines and in selected space disciplines. This mission will be accomplished by performing innovative research relevant to national needs and Agency goals, transferring technology to users in a timely manner, and providing development support to other United States Government agencies, industry, and other NASA centers. This report contains highlights of the major accomplishments and applications that have been made by Langley researchers and by our university and industry colleagues during the past year. The highlights illustrate both the broad range of the research and technology (R&T) activities supported by NASA Langley Research Center and the contributions of this work toward maintaining United States leadership in aeronautics and space research. The report also describes some of the Center's most important research and testing facilities. For further information concerning the report, contact Dr. Michael F. Card, Chief Scientist, Mail Stop 110, NASA Langley Research Center, Hampton, Virginia 23681, (804) 864-8985.

14. SUBJECT TERMS
Research and technology; Aeronautics; Space; Structures; Materials; Electronics; Flight systems; Technology transfer; Technology commercialization; Engineering; Aerodynamics; Wind tunnels; Facilities; Tests

15. NUMBER OF PAGES
263

16. PRICE CODE
A12

17. SECURITY CLASSIFICATION OF REPORT
Unclassified

18. SECURITY CLASSIFICATION OF THIS PAGE
Unclassified

19. SECURITY CLASSIFICATION OF ABSTRACT

20. LIMITATION OF ABSTRACT

functions and what type of information should be provided to crews in advanced aircraft flight decks.

The FSD space-related research accomplishments include the following: the development and validation of an optical measurement system that determines the position and attitude of a magnetically levitated cylinder and provides this information to the control system of a large-gap magnetic suspension system; the development of a linear simulation and jitter analysis tool to assess pointing performance of the EOS AM-1 spacecraft; the successful design, fabrication, and laboratory testing of antennas for the End Mass Payload on the first Small Expendable Deployer System (SEDS)—the antennae worked better than predicted in the SEDS flight; and the development and operation of an interactive operator control station for the Flight Telerobotic Servicer Program's Hydraulic Manipulator Testbed (HMTB). The HMTB now resides at LaRC and was recently controlled remotely from JSC by using the LaRC control station software.

National Aero-Space Plane Office

The National Aero-Space Plane (NASP) Office oversees all NASP technical activity in NASA as a part of Langley's duties as NASA Lead Center for NASP. The office also coordinates a broad-scope hypersonic vehicle research and technology program at Langley and conducts vehicle systems analyses for airbreathing space launch vehicles and hypersonic aircraft. The NASP Office is made up of the Systems Analysis Office, the Flight Research Office, the NASP Technology Office, and the Numerical Applications Office.

Significant accomplishments for the NASP Office over the past year include the following: (1) met all requirements for the NASP Government Work Packages, including performance, cost, schedule, reporting, and documentation; (2) investigated high-speed scramjet mixing processes to benefit mixer designs; (3) developed the first version of a hypersonic airbreathing vehicle design-optimization code that will greatly shorten the design cycle for this class of vehicle; (4) evaluated methods to minimize base-pressure drag in scramjet combustors; (5) developed a new, more accurate method for the structural analysis of vehicles constructed of composite stiffened panels; and (6) contributed significantly to the design of vehicles and instrumentation for the proposed NASP HYFLITE flight experiments.

Space Directorate

The Space Directorate had primary responsibility for Langley's research programs in aerothermodynamics, advanced transportation, atmospheric sciences, and systems analysis. The directorate was organized into the Advanced Space Concepts Division, the Atmospheric Sciences Division, the Space Systems Division, and the Space Technology Initiatives Office.

The Advanced Space Concepts Division (ASCD) conducted systems analysis of advanced spacecraft and instrument analysis of advanced remote sensors for the Mission to Planet Earth program. The analyses included the identification of critical technologies, mission architecture studies, and technology assessments. The ASCD provided independent systems analysis for the Microgravity Science and Applications Program and provided technical support to the Office of Advanced Concepts and Technology (OACT) in Space Station *Freedom* utilization and in-space technology experiment development (e.g., Middeck 0-Gravity Dynamics Experiment and Modal Identification Experiment). ASCD also supported the Space Station *Freedom* program with independent systems analysis and advanced studies and contributed substantially to the redesign of the Space Station *Freedom* and the transition of the program to the host Center.

The Atmospheric Sciences Division (ASD) was involved in programs focused on global-change issues with particular emphasis on climatic effects of radiation balance, clouds, and aerosols and on understanding middle and lower atmospheric chemistry. Efforts included research in Earth radiation sciences, stratospheric sciences, and tropospheric sciences; remote sensing from space for global-scale examination of the Earth; modeling and data analysis to provide a conceptual and predictive understanding of Earth as a system; and advanced technology development in remote-sensing systems. Research highlights included techniques for remote sensing of multilevel clouds, measurements of ozone and aerosols over the tropical Atlantic, determination of the global effects of the Mt. Pinatubo eruption, determination of global surface albedo values, and study

of polar vortex processes. Six operational space instruments continued to provide key data on radiation processes and stratospheric chemistry. These instruments included three Earth Radiation Budget Experiment (ERBE) instruments, the Stratospheric Aerosol Measurements (SAM II) experiment, the Stratospheric Aerosol and Gas Experiment (SAGE II), and the Halogen Occultation Experiment (HALOE). Preparations continued for the third shuttle flight of the Measurement of Air Pollution from Satellites (MAPS) experiment and an initial flight of the Lidar In-space Technology Experiment (LITE). The ASD was involved in development of the Earth Observing System with the Clouds and the Earth's Radiant Energy System (CERES) and SAGE II experiments, interdisciplinary investigations focusing on the radiant energy system and stratospheric modeling, and a Distributed Active Archive Center for Earth science data. Management of the Global Tropospheric Experiment to examine tropospheric chemistry focused on implementation of the Transport and Atmospheric Chemistry near the Equator-Atlantic experiment. The division continued management of the First ISCCP Regional Experiment for improved parameterization of clouds and radiation for use in climate models.

The Space Systems Division (SSD) continued to provide systems analyses and configuration assessments for the Agency Access to Space study. Previously completed work on the HL-20 Personnel Launch System was used as a point of departure for an expendable-launch-vehicle-based personnel and small logistics transport for Space Station *Freedom*. This concept, designated HL-42 (42 percent larger than the HL-20), was included in the recommended architecture for the expendable-based system. Most of the effort devoted to Access to Space has focused on the rocket SSV (single-stage vehicle). The previous SSD work on the single-stage-to-orbit concept has provided a unique SSV design that has shown the viability of a cost-effective single-stage-to-orbit (SSTO) vehicle design with the appropriate investment in technology. Space Systems Division studies have shown that a rocket SSTO vehicle is a realistic option with maturation of lightweight structure, reusable cryogenic tanks, and advanced rocket-propulsion technologies.

The Space Exploration Initiative Office completed the design of a unique teleoperated lunar rover and developed a process for technology development and transfer. A pilot program with John Deere, Inc., was initiated to evaluate this process.

Structures Directorate

The Structures Directorate led the Center's research programs in the technical areas of materials, structures, and acoustics. Both applied research and technology development programs were conducted, with emphasis on advanced aircraft, spacecraft, and launch-vehicle systems. The directorate had more than 250 scientists and engineers in four divisions that performed research in the technical areas of materials, structural mechanics, structural dynamics, and acoustics. Each division maintained a complement of modern research facilities as well as technical support functions. In addition, each division had a cooperative, university, and industry research program to assure that the best talents were available to solve today's research challenges.

Recent technical accomplishments in the materials area include the development of a new crack-tip opening-angle fracture criterion that accurately predicts stable crack growth in thin-gage aluminum alloys typical of aircraft structures, the development and demonstration of a new sol-gel coating for titanium alloys that provides oxidation protection up to 1200°F, and the further development of textile composites made from powder-coated towpreg that show an outstanding balance of mechanical properties. For the structural mechanics area, recent technical accomplishments include the successful shakedown at Mach 7 of the 8-Foot High-Temperature Tunnel following a major facility renovation, testing and analyses of the first Advanced Composites Technology (ACT) stiffened fuselage panels, and the development of interfacing techniques for structural finite-element analysis codes. In the structural dynamics area, recent technical accomplishments include the completion in the Transonic Dynamics Tunnel (TDT) of a series of wind-tunnel tests on transport and business jet aeroelastic models and the development and astronaut evaluation of an Active Damping Augmentation (ADA) system for the Space Shuttle Remote Manipulator System (RMS); in the CFD area, the accomplishments include the initial development and reporting on a gridless solution algorithm

2D N/S. In the acoustics area, recent technical accomplishments include noise reduction for HSR through shielding by multiple jet arrays, application of micromanipulators for suppression of supersonic jet noise, and completion of tests to determine subjective responses to a range of simulated sonic-boom signatures.

Systems Engineering and Operations Directorate

The Systems Engineering and Operations Directorate's prime function was to provide engineering and technical support for the institutional and research needs of the Center's ongoing aeronautic and space programs. Its 1013-person complement provided a wide variety of engineering and technical disciplines to design and fabricate hardware components and develop software codes for the unique experimental systems requested by the researchers. Its five divisions and two offices had specific support functions. The Systems Engineering Division was responsible for the design, development, analysis, and testing of aerospace hardware and wind-tunnel models; the Facilities Engineering Division was responsible for the design, construction, and modification of facilities and hardware; the Fabrication Division produced hardware, components, and systems for aerospace projects and research facilities; the Operations Support Division provided maintenance services and support for the operation of the wind tunnels, facilities, and research equipment; the Systems Safety, Quality, and Reliability Division managed safety, quality assurance, and environmental compatibility programs; the Facilities Program Development Office coordinated the Langley Construction of Facilities Program with NASA Headquarters; and the 8-Foot High-Temperature Tunnel Shakedown Project Office managed performance verification testing for this recently modified high-performance facility.

This year the Directorate made major strides in utilizing concurrent engineering and fabrication techniques to develop flow-quality-improvement hardware for the 8-Foot High-Temperature Tunnel. The Lidar In-space Technology Experiment (LITE) completed all space-qualification testing and is awaiting shipment to the Kennedy Space Center. Several devices were designed and fabricated to assist in the collection of fluctuating pressures in high-temperature environments, dynamic pressures in wind-tunnel models, and groundwater seepage rates for contaminant discharge studies. A methodology to optimize the design of low-conductance cryogenic supports was utilized, and evaluative testing of adhesives for cryogenic applications was performed. An analytical assessment of a new solid wheel design for the Aircraft Landing Dynamics Facility carriage was completed. A multistaged electroforming technique has permitted the design and fabrication of complex porous-skin wind-tunnel models. A fuzzy-logic controller has been developed and applied to the control of temperature processes in the Hypersonic Blowdown Tunnels Complex. An instructional computer program linking MSC/NASTRAN and STAR to aid in the test correlation of finite-element models was successfully demonstrated.

Technology Utilization and Applications Office

One of the responsibilities of NASA, mandated by Congress, is to promote economic and productivity benefits to the nation by facilitating the transfer of aerospace-generated technology to the public domain. NASA meets this objective through its Technology Utilization Program, which provides a link between the developers of aerospace technology and those in either the public or private sectors who might be able to employ the technology productively. The *NASA Tech Briefs Journal*, which has more than 200 000 subscribers, has been an effective method of announcing new technology generated by NASA. The Technology Utilization and Applications Office assisted industry by providing available technology that can meet their needs, arranging visits to the Center to discuss NASA technology with the developers, coordinating a Space Act Agreement that allows for joint development of technology for the company needs, and assisted in arrangements for the use of NASA facilities.

Another important facet of the NASA Technology Utilization Program is its applications engineering projects, which involve the use of NASA expertise to redesign and reengineer aerospace technology to solve the problems delineated by Federal agencies or other public-sector institutions. Applications engineering projects originate in various ways; some stem from requests for NASA assistance from other government agencies, and some are generated by NASA engineers and scientists who

perceive possible solutions to public-sector problems through the adaptation of NASA technology. Additionally, NASA employs a multidisciplinary applications team that maintains a liaison with public-sector agencies, medical and public-health institutions, professional organizations, and academia to uncover significant problems in diverse fields such as health care, public safety, transportation, environmental protection, and industrial processes that might be amenable to solution by the application of NASA technology. A Technology Utilization applications engineering project is considered to be successful when the technology developed under the project is used or is manufactured for the market.

To help obtain secondary uses of Langley technology, public awareness of Langley innovations was promoted by the Technology Utilization and Applications Office. Two such methods are the submission of Langley candidate items for induction into the Space Foundation Hall of Fame and the submission of candidate items to the Research and Development (R&D) 100 Award competition. Awards are presented annually to the 100 most significant technological advancements selected from candidate items received worldwide. Langley received two R&D 100 Awards in 1993, one for the Airborne In Situ Wind-Shear Detection Algorithm and one for the Hyperthermal Oxygen Atom Generator (HOAG). The wind-shear detection algorithm was developed as a measurement standard for evaluation of predictive (forward look) wind-shear detection systems in actual research microburst encounters and as an advancement over available in situ wind-shear detection algorithms. The HOAG is a small, ultrahigh-vacuum-compatible, hyperthermal, atomic-oxygen generator that provides a flux of pure, energetic, ground-state oxygen atoms. In 1993, the Space Foundation inducted NASA-developed cooling garments into the Hall of Fame. Langley was instrumental in getting children with hypohidrotic ectodermal dysplasia (HED) to obtain access to cooling garments and assisted in the establishment of the HED Foundation.

Contributing Organizations

REPORT DOCUMENTATION PAGE

Form Approved
OMB No. 0704 0188

1. AGENCY USE ONLY *(Leave blank)*	2. REPORT DATE	3. REPORT TYPE AND DATES COVERED
	August 1994	Technical Memorandum

4. TITLE AND SUBTITLE
Research and Technology Highlights 1993

5. FUNDING NUMBERS

6. AUTHOR(S)

7. PERFORMING ORGANIZATION NAME(S) AND ADDRESS(ES)
NASA Langley Research Center
Hampton, VA 23681-0001

8. PERFORMING ORGANIZATION REPORT NUMBER
L-17397

9. SPONSORING/MONITORING AGENCY NAME(S) AND ADDRESS(ES)
National Aeronautics and Space Administration
Washington, DC 20546-0001

10. SPONSORING/MONITORING AGENCY REPORT NUMBER
NASA TM-4575

11. SUPPLEMENTARY NOTES

12a. DISTRIBUTION/AVAILABILITY STATEMENT

Unclassified Unlimited

Subject Category 99

12b. DISTRIBUTION CODE

13. ABSTRACT *(Maximum 200 words)*

The mission of the NASA Langley Research Center is to increase the knowledge and capability of the United States in a full range of aeronautics disciplines and in selected space disciplines. This mission will be accomplished by performing innovative research relevant to national needs and Agency goals, transferring technology to users in a timely manner, and providing development support to other United States Government agencies, industry, and other NASA centers. This report contains highlights of the major accomplishments and applications that have been made by Langley researchers and by our university and industry colleagues during the past year. The highlights illustrate both the broad range of the research and technology (R&T) activities supported by NASA Langley Research Center and the contributions of this work toward maintaining United States leadership in aeronautics and space research. The report also describes some of the Center's most important research and testing facilities. For further information concerning the report, contact Dr. Michael F. Card, Chief Scientist, Mail Stop 110, NASA Langley Research Center, Hampton, Virginia 23681, (804) 864-8985.

14. SUBJECT TERMS
Research and technology; Aeronautics; Space; Structures; Materials; Electronics; Flight systems; Technology transfer; Technology commercialization; Engineering; Aerodynamics; Wind tunnels; Facilities; Tests

15. NUMBER OF PAGES
263

16. PRICE CODE
A12

17. SECURITY CLASSIFICATION OF REPORT	18. SECURITY CLASSIFICATION OF THIS PAGE	19. SECURITY CLASSIFICATION OF ABSTRACT	20. LIMITATION OF ABSTRACT
Unclassified	Unclassified		

NSN 7540-01-280-5500

Standard Form 298 (Rev. 2-89)
Prescribed by ANSI Std. Z39-18
298-102